THE BELL SYSTEM

Technical Journal

Volume 50 September 1971 Number 7

TH-3 MICROWAVE RADIO SYSTEM

(General Articles listed on inside back cover)

THE BELL SYSTEM TECHNICAL JOURNAL

THE BELL SYSTEM TECHNICAL JOURNAL is published ten times a year by the American Telephone and Telegraph Company, H. I. Romnes, Chairman and President, J. J. Scanlon, Vice President and Treasurer, R. W. Ehrlich, Secretary. Checks for subscriptions should be made payable to American Telephone and Telegraph Company and should be addressed to the Treasury Department, Room 2312C, 195 Broadway, New York, N. Y. 10007. Subscriptions $10.00 per year; single copies $1.25 each. Foreign postage $1.00 per year; 15 cents per copy. Printed in U.S.A.

THE BELL SYSTEM
TECHNICAL JOURNAL

DEVOTED TO THE SCIENTIFIC AND ENGINEERING
ASPECTS OF ELECTRICAL COMMUNICATION

Volume 50 September 1971 Number 7

TH-3 Microwave Radio System:

System Considerations

By R. M. JANSEN and R. C. PRIME

(Manuscript received February 23, 1971)

This paper gives a general description of the TH-3 long-haul microwave radio system which operates in the 6 GHz common carrier band. Performance objectives are expressed, and the allocation of noise to the various contributors is developed. Particular attention is given to the balance between intermodulation noise and tertiary interference. In conclusion, the predicted performance is compared with measurements made on the initial installation.

I. INTRODUCTION

The TH-3 microwave radio relay system is a new long-haul facility designed to provide modern solid state equipment with improved performance for use in the 6 GHz band. When work began on the project in 1966, most of the Bell System radio traffic was carried on the 4 GHz TD-2 system. Also, at that time the first TD-3[1] radio route was being installed. Since TH-3 routes can be installed most economically as an "overbuild" on existing TD-2 and TD-3 (TD radio) routes, it was clear that TH-3 must be compatible with TD-2, and as much like the new TD-3 as possible. The features of TH-3 which differentiate it from its predecessor in the 6 GHz band, the TH-1

radio system,[2] and make it more like TD radio are the individual transmitter-receiver bays, and the 70 MHz IF. The latter increases certain difficulties with interchannel interference but allows TH-3 to use the FM terminals, switching systems, and some of the IF circuits developed for TD-3. Also, by adopting the 70 MHz IF, a combined TD and TH-3 facility with crossband protection switching looks feasible at this time.

Although TH-3 was originally conceived as a long-haul, multichannel system with a 4000-mile capability, the need to adapt it to shorter routes with a smaller cross section of circuits was quickly recognized. The so-called medium-haul TH-3 then came into being. It is discussed in later articles of this issue.[3,4]

Many of the design techniques which were assimilated during the TD-3 development were directly applicable to TH-3. Thus the designers of TH-3 had a headstart with regard to available circuit designs and to understanding how superior transmission performance could be achieved. However, TH-3 did bring significant advances to the art of radio repeater design. In particular, microwave integrated circuits, microwave envelope delay equalizers, and a means of preventing adjacent channel interference called RF squelch are key features of the TH-3 repeater.

The measuring capabilities and analysis tools that were available at the start of the project were a valuable asset. For example, the computer-operated transmission measuring set[5] was invaluable for its precise measurements of amplitude and delay distortion. Theory relating distortions to intermodulation noise was already available,[6–9] and computer programs developed for TD-3 were used initially to determine the distortion requirements. However, these programs could not conveniently handle some commonly occurring distortions (such as fourth and higher-order envelope delay distortion). As an important step in the TH-3 development, a computer program was written based on new mathematical techniques[10] which gave the designers adequate means to relate system distortion to intermodulation noise.

II. SYSTEM OBJECTIVES

The circuit objectives for noise, tones, and reliability are consistent with the current Bell System objectives for long-haul facilities.

(*i*) *"Worst circuit" noise of 41 dBrnc0 for a 4000-mile system during periods of nonfaded transmission.* The noise may increase to 55 dBrnc0 during fading, after which the channel will be switched automatically to a protection channel.

(*ii*) *Single-tone interference of −68 dBm0 maximum in any voice circuit of a 4000-mile (41 dBrnc0) system during nonfaded transmission.* Subjective tests have shown that if the noise-to-tone-power ratio in a message circuit is constant, the tone is less discernible when the noise power increases. The result is that the requirement for those baseband tones which increase dB for dB with fading is −47 dBm0 when the noise in the circuit is 55 dBrnc0 (during a 40 dB fade). Under normal conditions this corresponds to a −87 dBm0 requirement.

(*iii*) *Reliability of 0.02 percent per year for a two-way, 4000-mile system, as measured by accumulated yearly outage.*

The following are particular design objectives for TH-3:

(*iv*) *1800 message circuits per channel.*

(*v*) *10 MHz baseband.* The bandwidth is adequate to transmit 1800 message circuits or high-definition TV.

(*vi*) *Baseband response of ±0.25 dB flatness over the message band from about 5 kHz to 8.5 MHz for each radio channel on an IF protection switching section. Also, no more than 30 degrees phase difference (at baseband) between the radio channels of a protection switching section.* These objectives prevent hits on data transmission and disturbance to TV when the signal is transferred between regular and protection channels. To meet the above phase objective, the absolute delay of all radio channels in a switching section must be equal to within 10 ns, which corresponds to 6.5 feet of IF cable.

(*vii*) *75 ±20°F Operating Temperature Range.* In long-haul radio stations the temperature in the vicinity of the TH-3 radio bays will be maintained within these limits. As a safeguard against loss of temperature control, the system should continue to operate with little degradation at ambient temperatures between 40°F and 120°F. The latter temperature range is specified as the operating temperature range for medium-haul TH-3.

III. SYSTEM MODEL AND NOISE ALLOCATIONS

Besides the actual T-R bays, the components of the TH-3 and TD-3 systems are almost identical. Figure 1 is a block diagram of a TH-3 system. The number and sequence of the various components in the transmission path of a 4000-mile system has a first-order effect on the performance. Therefore to make system calculations, a system model was constructed which in the best judgment of the designers would

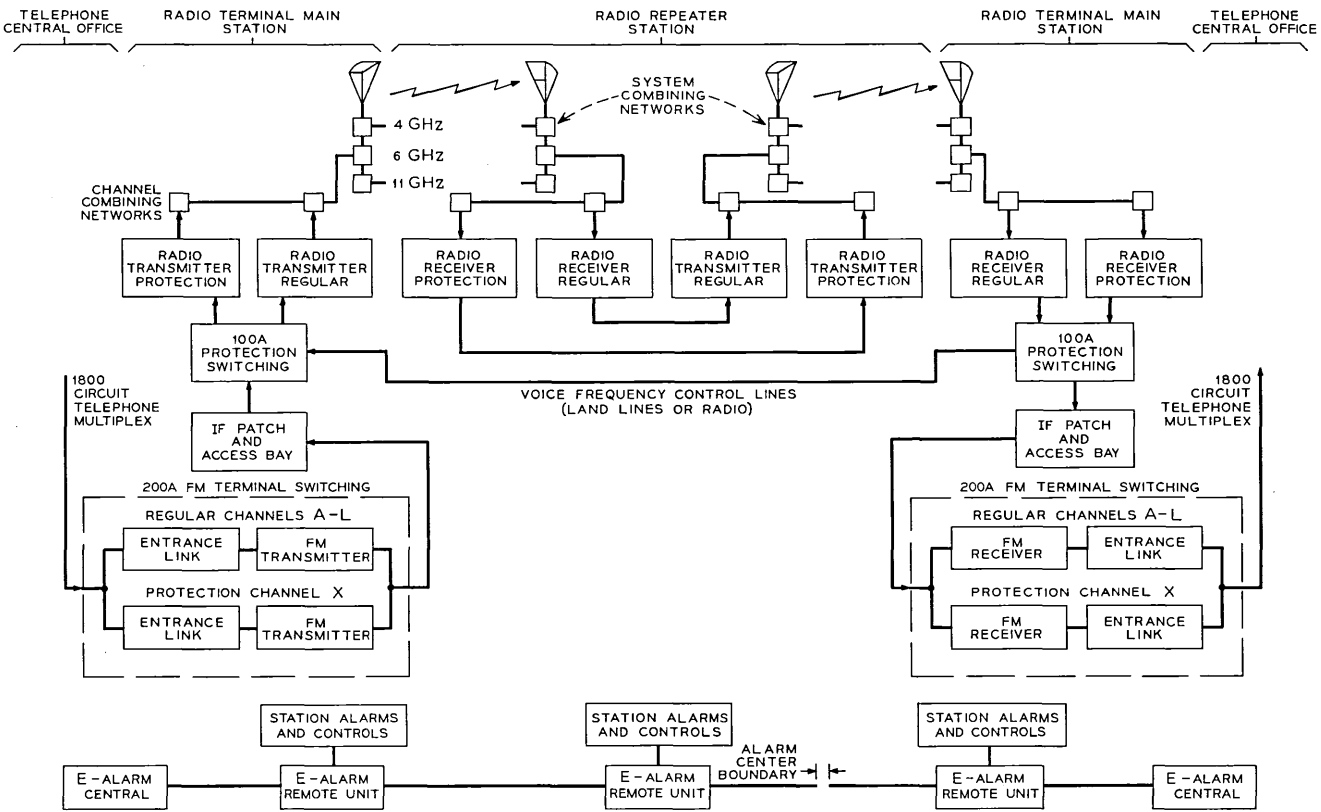

Fig. 1—Block diagram of TH-3 system.

represent the nominal TH-3 system. The principal assumptions made in the model were based on the conditions existing in the field.

(*i*) 150 hops in 4000 miles.
(*ii*) 51 main stations with IF switching, and 100 repeater stations.
(*iii*) 17 of the 51 switching main stations will also have L-Multiplex terminals. These stations, called terminal main stations, have by necessity FM terminals and wire line entrance links. Thus, the model 4000-mile system is divided into 16 parts and they are assumed to be connected at the channel, group, or supergroup level.
(*iv*) The path loss of a nominal hop is 63.2 dB from the transmitter test access on the TH-3 T-R bay to the receiver test access. (The locations of these access points in the T-R bay are explained in the following article.)[11]

During the course of the development the 41 dBrnc0 allocated to the total system was divided between the system components in several different ways. The final allocation is shown in Fig. 2.

3.1 *Multiplex*

MMX-2R mastergroup multiplex and LMX-2 multiplex terminals provide the 1800-message circuit load. The baseband signal extends from 564 kHz to 8.524 MHz.

3.2 *Wire Line Entrance Link*

The 3A entrance link was described in Ref. 1. Since that writing the link has been improved to handle 1800 circuits. Also, the maximum length of the entrance line has been increased to eight miles by employing an intermediate repeater.

3.3 *FM Terminals*

Before the advent of the 4A FM transmitter, 35 dBrnc0 had been allocated to the sixteen 3A FM transmitter-4A FM receiver pairs. The

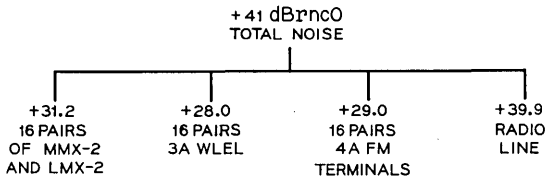

Fig. 2—Allocation of total noise objective.

4A FM terminals[12] have improved noise performance and sixteen pairs are allocated only 29 dBrnc0.

3.4 *Protection Switching*

The 200A protection switching system protects the FM terminals and WLELs but need not be dedicated to TH-3. The twelve working channels may be divided between TD-2, TD-3, and TH-3 systems and the single protection channel is provided with switched pads to match its transmission levels to those of the system it is protecting. The 100A protection switching system[13] protects three hops on the average, although ten-hop switching sections are not uncommon. Minor modifications were made to the 100A system to adapt it to TH-3, as explained in Section 4.1.4.

3.5 *IF Patch and Access Bay*

The terminal main stations have an IF patch and access bay. This bay is common to all heterodyne radio systems in the station which have a 70 MHz IF. In a typical large station, the IF trunks from several TH-3, TD-2, and TD-3 radio lines will fan into the IF patch and access bay where they will be assigned to FM terminal equipment within one of several 200A protection switching systems or, in the case of through channels, routed to outgoing radio lines. The purpose of the bay is to provide an easy means to reassign IF trunks and to have a common location to monitor all the IF trunks in the station. IF trunks carrying TV are also brought through the patch bay and, where necessary, connections are made to the television operating center through an FM terminal and special WLELs.

3.6 *Alarm System*

The C1 alarm system may still be used with TH-3, but the E-type alarm is now recommended. The E alarm uses rugged digital coding and has the potential to monitor remotely the meter readings on the T-R bays.

3.7 *Power*

Most of the subsystems which compose TH-3 are operated from a −24 volt power plant. However, there is a need for + 130V and +24V in some alarm and switching circuits. In particular, both −24V and +24V plants are used with the 100A protection switching system. Other subsystems needing +130V and +24V may be supplied from the −24V supply by means of dc-to-dc converters.

3.8 *Radio Line*

The radio line is that part of the system from the first microwave radio transmitter to the last radio receiver inclusive. Thus, it includes all of the radio T-R bays and the antenna systems. Also, when considering the total noise allocation for the radio line, interference picked off the air by the receiving antennas must be taken into account. The noise allocations for the radio line are shown in Fig. 3 and are discussed below.

(*i*) *Co-channel interference* is the same as for TD-3 and has been dealt with adequately.[14]

(*ii*) *Intersystem interference* has been included because of the high usage of the 6 GHz band. The allocation is of the same order as co-channel interference.

(*iii*) *RF echoes in the antenna systems* were allocated only 6 dBrnc0 per hop. The allocation is nevertheless realistic as a result of the antenna improvement program[15] which was started in 1964. This effort was directed mainly at reducing echoes due to mode conversion.

(*iv*) *Echoes in IF trunks* were given essentially the same allocation as in TD-3.

(*v*) *Tertiary interference and noise from the microwave T-R bays* are dealt with in the following sections.

IV. DESIGN ASPECTS OF THE TH-3 RADIO LINE

4.1 *General*

The first step in designing the system was to choose the basic frequencies: RF, IF, and baseband, on which the TH-3 design was founded. The factors involved in the decision-making process are discussed in the following paragraphs.

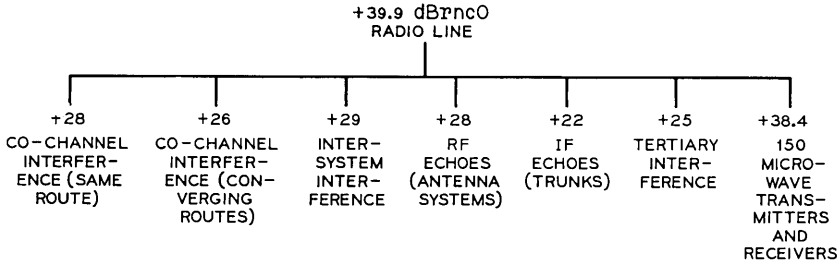

Fig. 3—Noise allocations for the radio line.

4.1.1 *RF Channel Assignments*

The TH-3 system was designed initially to operate on sixteen channel frequencies. These frequencies are consistent with the TH-1 channel assignments[2] because of the obvious need to coordinate with TH-1 and other users of the 6 GHz common carrier band.* However, the TH-1 auxiliary channel frequencies are not used since for most long-haul applications 4 GHz auxiliary channels will be available for order wire, switching, and alarm purposes. Later in the TH-3 development the need for TH-3 on the so-called staggered frequencies (which are interleaved with the CCIR recommended frequencies) was recognized, and the design was augmented with sixteen alternate channel frequencies. The staggered frequency plan will be used on routes where it is necessary to coordinate with systems already operating on the staggered frequency plan. Both of the RF frequency plans are shown in Fig. 4. The use of the staggered frequencies is not without some disadvantage. Channel 28S† cannot be squeezed into the common carrier band and consequently the route may grow to only seven instead of eight radio channels. It is some consolation that there is a channel 20S which, along with 18S, can be substituted for another channel in the event that this other channel is blocked. Unfortunately a channel cannot be made up from alternate hops of 18S and 20S because they are so close together in frequency that the mutual interference would be intolerable.

4.1.2 *Microwave Carrier Frequencies*

All of the microwave carrier‡ frequencies in TH-3 are generated below the RF signal frequency. This action was taken to avoid stability problems with the lower sideband upconverter. With the chosen microwave carrier arrangement it was computed that the RF selectivity was adequate to prevent image interference from radars below the common carrier band. Another matter requiring attention was the need to shield components sufficiently so that near-end image interference at high-low repeater stations would not be caused by RF leakage between bays.

---

* The TH-1 broadband channel assignments are recommended by the CCIR (REC 383-1, Documents of the XIIth Plenary Assembly, New Delhi, 1970, Vol. IV, Part I, p. 84) and they are an accepted standard within the United States.

† Staggered channels are denoted by the letter S, and regular channels by the letter T.

‡ The microwave carriers are generated by the microwave generators and shift oscillators in the T-R bays. These carriers convert IF to RF in the transmitter modulator and RF to IF in the receiver modulator.

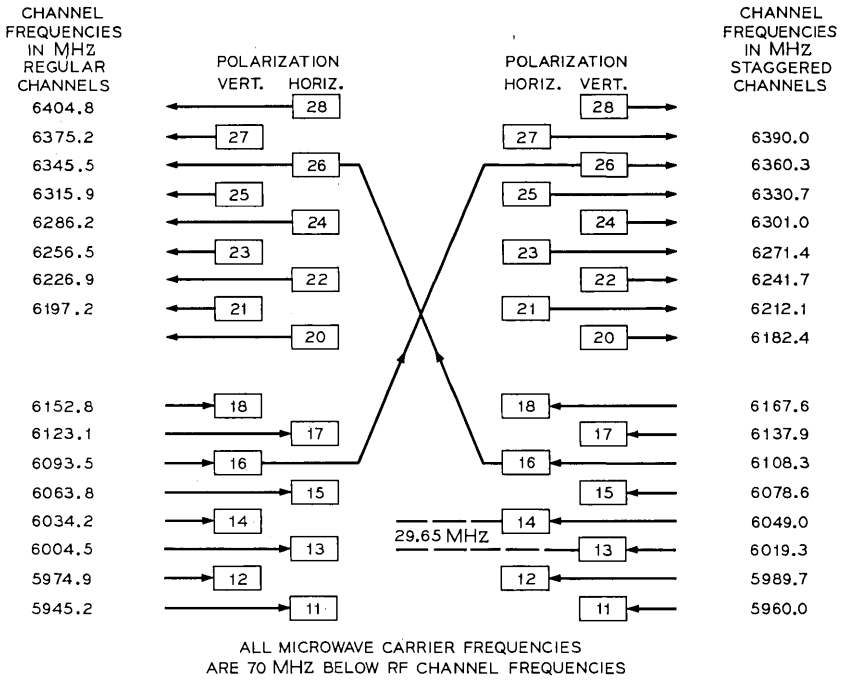

Fig. 4—TH-3 regular and staggered frequency assignments (low-high station).

4.1.3 *Growth Sequence of Radio Channels*

The standard growth sequence for the regular channels is 4T,† 8T, 2T, 6T, 3T, 7T, 1T, 5T. This sequence is the same as for TH-1. It was chosen because the preferred order of growth for TM-1 is the reverse of that for TH-1 and therefore conflicts with short-haul systems are more likely to be postponed. The even channels are on one polarization, with channel 4T nearest the antenna, and the odd channels are on the other polarization with channel 3T nearest the antenna. Four antennas are required at a repeater station, and each antenna is connected exclusively to either receivers or transmitters. Normally channels 8T and 1T will be the protection channels, although any two channels can be used. If the staggered frequency plan is used, the standard growth sequence will be 1S, 5S, 3S, 7S, 2S, 6S, 4S. The even channels are equipped last because there is no channel 8S.

† Channel 4T is short for 14T or 24T.

4.1.4 *Switching System Parameters*

The original 100A designed for TD systems has a protection pilot at 7 MHz and a noise monitoring slot at 9 MHz. Both of these frequencies were changed in TH-3 because the TH-3 baseband extends to 10 MHz. The noise slot was moved to 10.2 MHz to be above the signal, but well below a 10.7 MHz tone which will be present on most TH-3 channels. The protection pilot was placed at 11.88 MHz, well above the tone. The pilot frequency was chosen so that the second-order sidebands of the pilot would fall nominally between the second and third mastergroups on the adjacent channels. However, the level of the sidebands is such that it should not matter if the sidebands do fall into mastergroup 2 or 3.

4.1.5 *Modulation Parameters*

In the preliminary calculations of thermal noise it was assumed that TH-3 would use the same peak frequency deviation as TD-3. Experience with the system has shown no reason to change this parameter. The average busy hour speech load produces an rms frequency deviation of 798 kHz or the per circuit rms frequency deviation is 118 kHz. In Bell System terminology the equivalent sine wave power (explained in Ref. 16) of the 1800-message circuit load is +27.6 dBm0.

The TD-3 pre-emphasis (see Fig. 4 of Ref. 1) is widely used by TD-2 now that the capacity of that system has been expanded to 900 and 1200 message circuits. The same characteristic was chosen for TH-3 to simplify the 200A protection channels. (The pre-emphasis and de-emphasis networks are located within the 200A switching system, and a particular 200A system might include TD-2, TD-3, and TH-3 channels within the same switching group.) This pre-emphasis has a 3 dB advantage at the top message circuit (8.524 MHz) relative to the 4.6 MHz reference (or crossover) frequency.

4.2 *Thermal Noise*

The allocation for the 150 microwave transmitters and receivers was originally lower than specified in Fig. 3. As the development progressed it became evident that the thermal noise would exceed its portion of the allocation, principally because an optimistic view had been taken of the losses in waveguide networks and antenna systems. Relief came from two directions. Firstly, the improved performance of the 4A FMT permitted the bay allocation to be raised to 38.4 dBrnc0. Secondly, the improvements in the IF filter design made it possible to reduce the allocation for intermodulation noise, and as a

consequence the allocation for thermal noise could be raised to 36.9 dBrnc0 (or 15.1 dBrnc0 per hop). This was a reasonable objective, still low enough to assure a 40 dB fade range.

4.3 *Intermodulation Noise*

Excellent intermodulation noise performance was achieved by adhering to the following principles in the design of the T–R bay:

(*i*) Using wideband active devices and achieving the required selectivity with passive networks;
(*ii*) controlling carefully the distortion of all networks and equalizing as close as possible to the source of the distortion. This minimizes the effects of AM-to-PM conversion and the need for mop-up equalization;
(*iii*) maintaining return losses above 30 dB in almost all cases; and
(*iv*) blocking harmonics of the IF where they could give rise to echolike distortions.

It was found that the RF channel combining and separating networks in the T-R bays caused significant envelope delay distortion (EDD) to those thru-channels on the same polarization which were closest in frequency. The total EDD introduced into a channel by the channel combining and separating networks of the channels 59.3 MHz above and below is shown in Fig. 5. This EDD is very well controlled and is essentially the same for all channels. Therefore, it was

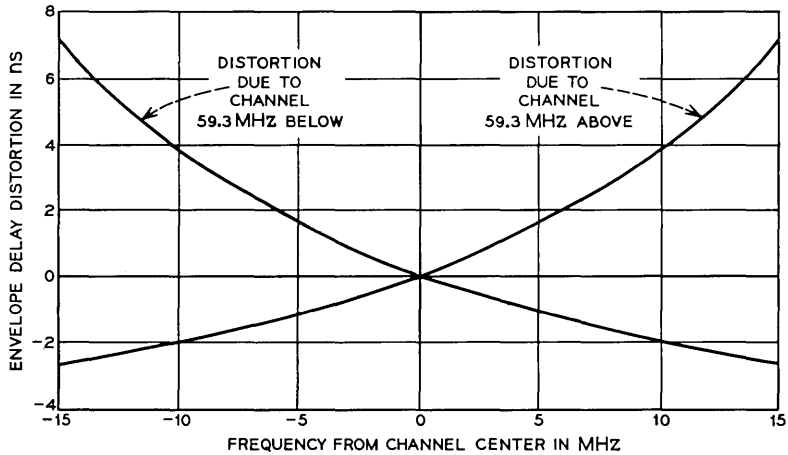

Fig. 5—Envelope delay distortion due to channel networks in channels 59.3 MHz above and below channel of interest.

possible to equalize it almost exactly at IF in every radio receiver. There are different situations according to which other channel networks are in the path of the channel of interest. The alternatives are: no equalization, equalizers to match either one of the EDD characteristics in Fig. 5, or an equalizer to compensate for both adjacent channels in which case the slope components cancel and only parabolic equalization is required.

As a consequence of these design techniques only a small amount of EDD slope is necessary to mop up TH-3 switching sections. No parabolic or other shape of EDD mop-up equalizer is required.

In the TH-3 system model it is assumed that a 4000-mile circuit is demodulated to baseband sixteen times. Since the reason for demodulating to baseband is to drop and pick up circuits, it was assumed that the composition of the circuit load is sufficiently different on each of the sixteen sections that intermodulation noise contributions from the individual sections add on a 10 log law* (power addition). Early measurements on preproduction T-R bays in the laboratory indicated that the intermodulation noise of a simulated multihop section was accumulating on an almost systematic 19 log law. Thus, a 14 log law represented the equivalent smooth accumulation of intermodulation noise for the overall system.

It was discovered that the 1009A† IF bandpass filter in the radio receiver was mainly responsible for the near systematic addition. Actually, the noise contribution of one filter was small compared to the thermal noise of a hop, but on long systems the noise from the filters was dominant. Further, it was clear that the original allocation of 34.2 dBrnc0 for the intermodulation noise of the T-R bays could not be met. The requirements for the filter were carefully reviewed and the conclusion was that too much selectivity was being specified at the expense of inband distortion to the transmitted signal.

The design of a new IF bandpass filter, designated the 1044A, was then undertaken. Its specifications were carefully related to intermodulation noise with the aid of the computer program referred to earlier. The filter was made as broad as possible so that the inband distortion was minimized. The objective was to hold the noise contribution of an individual filter to 0 dBrnc0 so that it would be satisfactory even if it caused systematic addition. However, the wide

---

* A 10 log law means that the total noise from N hops is 10 log N dB greater than the noise from one hop.

† The amplitude versus frequency characteristics of the 1009A and 1044A IF filters are shown in the following article.[11]

bandwidth of the filter gave rise to an additional source of noise by a mechanism known as tertiary interference.

The new filter was successful and the noise allocation for the intermodulation noise of the T-R bays was reduced to 33 dBrnc0 with confidence. However, tertiary interference, which had been negligible before, was allocated 25 dBrnc0. Although the net change in the allocations was small, the ability of the system to operate within them was vastly improved by the introduction of the 1044A filter.

4.4 *Tertiary Interference*

The mechanism of tertiary interference is well known. Ref. 2 explains how tertiary interference gave potential tone problems in the TH-1 system. In TH-3 the problem was not that of transferring a single tone from one channel to another, but of directly superimposing the message modulation of one channel onto the message sidebands of the next-to-adjacent channel. In previous systems the selectivity of the channels has been so great that the center channel greatly attenuates the tertiary path. However, in TH-3 a repeater will transmit some of the first-order sidebands of the adjacent channels, as shown in Fig. 6. Consequently, tertiary interference appears as a low level of noise in the disturbed channel. In the future, as more and more circuits are transmitted over systems using the established frequency plans, tertiary interference will be an increasingly important consideration. It is shown in the Appendix how the 25 dBrnc0 allocation was derived for tertiary interference.

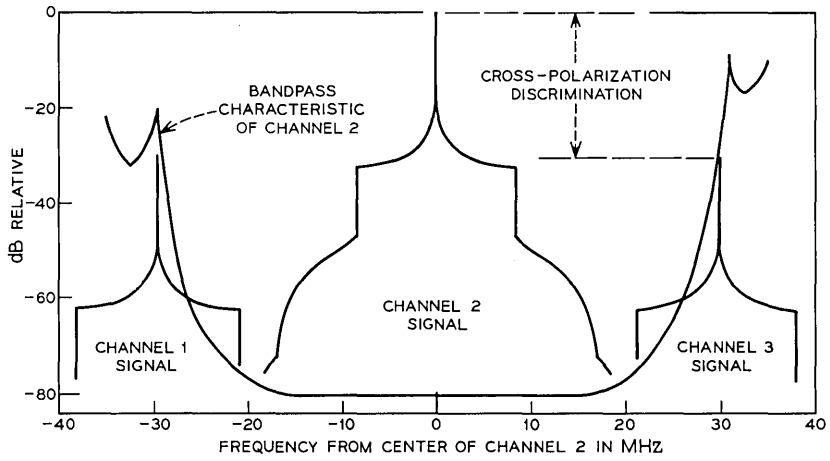

Fig. 6—Bandpass characteristic shown relative to spectra of adjacent channels.

4.5 *RF Squelch*

RF squelch is a technique for suppressing interference from a noisy channel into an adjacent channel. The principle of the squelch scheme is to monitor the IF at 86 MHz and attenuate the transmitted power by 29 dB when the noise is equivalent to a fade of 47 dB or greater. Briefly, the squelch initiator circuit detects high noise in the IF by monitoring the output of the limiter in the radio transmitter. During a deep fade or an open channel the squelch initiator changes the bias on the diode in the transmitter modulator so that the conversion efficiency is reduced by 29 dB. In most other systems a carrier resupply is used to quiet the channel by inserting a clean carrier. The resupply method has a disadvantage which the RF squelch was specifically designed to overcome; that is, when the carrier resupply operates, the channel is dead. On the other hand, when the squelch operates, it is equivalent to a 29 dB fade in the following hop. Thus, if the units operate inadvertently, the channel is completely disabled by the resupply, but it is still usable in the case of RF squelch. Also, it is argued that when a channel fades beyond about 50 dB, but cannot get protection, it is better to make the circuits unacceptably noisy for a fraction of a second than to have a break in the connection while the resupply is operated. Further, the carrier resupply quiets the message circuits, simulating the off-hook condition for all the idle circuits and consequently a massive seizure may occur in the tandem switching machine. In contrast, when the squelch is operated, the message circuits will be noisy and the off-hook condition will not be recognized by the terminal signaling equipment.

The tertiary noise interference described earlier will become much greater if the gain of a radio repeater in the center channel is increased. This would happen if the center channel suffered a selective fade, or the previous transmitter failed or was down for maintenance. To prevent excessive tertiary interference under these circumstances it is necessary that the RF squelch be operated in the first radio repeater following the fade or failure. Therefore, since the excess gain of the TH-3 repeater (which is actually due to the AGC amplifier and limiter) is approximately 50 dB, the RF squelch has to operate on less than a 50 dB fade.

If strong adjacent channel carriers are transmitted through the AGC amplifier and limiter, the repeater will not go to full gain when the desired RF signal is lost. The selectivity of the IF bandpass filter in the radio receiver was chosen to prevent the adjacent channel car-

riers from reducing significantly the excess gain of the repeater and thereby changing the trip point of the RF squelch by more than 0.3 dB. As already mentioned, the new IF filter was designed with minimum selectivity consistent with good intermodulation noise performance. Based on the minimum antenna cross-polarization discrimination (XPD) of 25 dB, and the receiver RF selectivity of 9 dB, the IF filter had to provide 25 dB of selectivity at ±29.65 MHz.

4.6 *Tone Problems*

The interference-to-carrier (I/C) requirements for tones at IF are shown in Fig. 7. Two requirements curves are given, one for tones where the I/C ratio does not change with fading, and one for tones where the I/C ratio increases dB for dB with the fade. The former is similar to the requirement specified for TD-3.[1] Generally there is a 19 dB difference between the two requirements curves as explained in the tone objectives in Section II. Below about 17 MHz the requirement is determined by interference into the channel under consideration, and above about 17 MHz by interference into the adjacent channels when the tone is retransmitted. The most severe requirements are imposed by tones which fall into the baseband regions occupied by the message circuit load and the 11.09 to 11.67 MHz auxiliary channel.[3] The 1800 circuits occupy the band 0.564 to 8.524 MHz, but the requirement shows this region extending to 0.312 MHz in recognition that an extra 60 circuits may be added at the low-frequency end if desired.

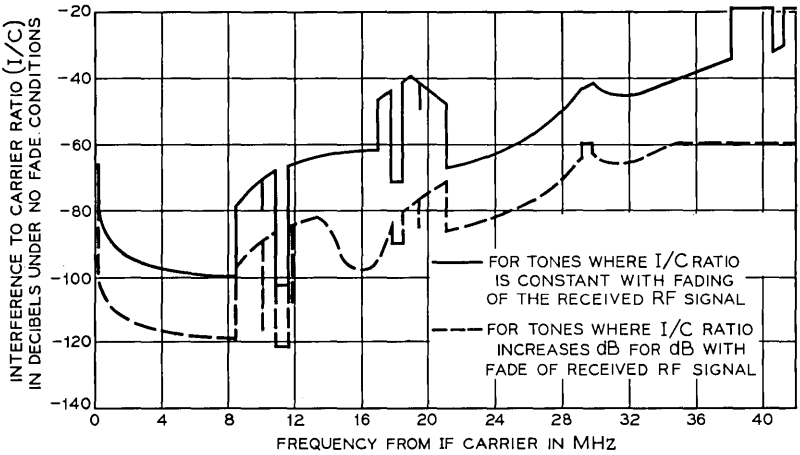

Fig. 7—Requirement for tone interference to carrier ratio at microwave receiver output.

There are special requirements at the 10.2 and 11.88 MHz to prevent malfunction of the 100A and 300A switching systems.[4] Also, the squelch initiator could be operated by interfering tones instead of noise, and at around 16 MHz the requirement for tones whose I/C ratio increases with fading is controlled by RF squelch considerations.

Some tones, such as those introduced by the dc-to-dc converter in the TWT power supply, are introduced at every repeater in the system. For these tones a multiple exposure factor was applied which decreased the permissible level of the tones. The factor was computed as 10 log of the number of tones expected to fall in a 3 kHz message circuit. However, if there were many tones the factor was computed so that the combined power of the tones plus thermal noise would not be more than 0.1 dB greater than the thermal noise alone. For the TWT power supply tones, the multiple exposure factor was calculated to be 13 dB based on either the tone or noise criteria, except in the auxiliary channel (because the auxiliary channel is limited to only ten hops) where the factor is 3 dB.

4.6.1 *Co-Channel Interference*

A carrier-to-interference (C/I) requirement of 66 dB is placed on co-channel interference consistent with what can be achieved with the front-to-back coupling loss of the horn antenna. A much more severe C/I requirement would be necessary if the beat frequency between the carriers of the co-channel signal and the desired signal exceeded the baseband frequency of the lowest message circuit. Although the multiplex normally used with TH-3 will put the lowest message circuit at 564 kHz, the system was engineered for a lowest circuit of 312 kHz so that an extra supergroup can be carried if desired. By carefully controlling the frequency of the transmitted signals the beat frequencies on long systems are held below 312 kHz. This is achieved by putting frequency stability requirements of ± 100 kHz on the FM transmitter, 5 ppm (± 30 kHz at 6 GHz) on the microwave generators, and ± 4 kHz on the shift oscillators. If the repeater station bays did not use a shift oscillator, the stability requirements for the FM transmitter and microwave generator would be much more severe.

4.6.2 *RF Selectivity and Interchannel Tone Interference*

The RF selectivity of the T-R bay was determined by the need to suppress interchannel tone interference and direct adjacent channel interference (DACI). The amplitude response of the RF networks is

presented in Fig. 9 of Ref. 11. Field measurements of DACI are recorded later in this paper. Based on early measurements it was determined that about 10 dB of receiver RF selectivity at ±29.65 MHz was adequate to avoid DACI problems with the adjacent channels. The actual selectivity is approximately 9 dB.

For the purpose of calculating tone interferences certain minimum characteristics of the antenna system were assumed.

(*i*) The minimum XPD is 25 dB.
(*ii*) The minimum side-to-side coupling loss between antennas is 80 dB for the same polarization, and 83 dB for opposite polarizations.

As explained in Ref. 2, 74.13 MHz is the natural IF for TH-1 channel assignments. If a 74.13 MHz IF had been used, the interchannel tone interferences would have fallen nominally at zero and 14.83 MHz in the baseband. As a consequence of using the 70 MHz IF, similar interferences fall at 4.13, 6.57, 8.26, and 10.70 MHz. Three of these tones fall into the message portion of the baseband and therefore they must be very low in level. Nevertheless, the RF selectivity needed to suppress these tones is not considered excessive.

4.6.2.1 *The 4.13 MHz Tones.* Tones at 4.13 MHz are caused by near-end interference between transmitters and receivers of channels 16* and 20, 17 and 21, or 18 and 22. The coupling path from transmitter to receiver may be via the side-to-side coupling of the antennas or leakage between the bays. Certain tone mechanisms of this type control the transmitter RF selectivity with a requirement of 93 dB at ±70 MHz. Other mechanisms involving the transmitted signal itself put RF selectivity requirements of 45 dB at −74.1 MHz on the disturbed channel receiver. In the latter case, the RF selectivity is more than adequate. Also, there must be 160 dB loss in the leakage path between the transmitted and the received signals.

4.6.2.2 *The 6.57 MHz Tones.* Tones at 6.57 MHz in the baseband also are caused by near-end interference. The image interference from channels 14 through 18 into channels 20 through 24, respectively, falls into this category and is potentially the most serious in the system. This tone puts a requirement of 97 dB on the RF selectivity of the receiver at −133 MHz which again is achieved comfortably. However, the loss in the leakage path must be 180 dB which is by far the toughest

* In this description of tone interferences, the channel number, *N*, can refer to either the regular channel frequencies or the staggered frequencies, where appropriate.

leakage requirement. This requirement is met by designing the TWT to prevent excessive leakage and carefully sealing the receiver modulator.

4.6.2.3 *The 8.26 MHz Tones.* Tones at 8.26 MHz in the baseband are caused by far-end image interference from channels 11, 12, 13, 20, 21, 22, and 23 into 16, 17, 18, 25, 26, 27, and 28, respectively. This type of interference requires slightly less RF selectivity in the receiver (94 dB at 148 MHz) than the previous case and is of little concern.

4.6.2.4 *The 10.70 MHz Tones.* Tones at 10.70 MHz in the baseband are caused by both far- and near-end interference between adjacent channels (29.65 MHz apart) and next-to-adjacent channels (59.3 MHz apart). The most important interference is the far-end interference between next-to-adjacent channels. This mechanism sets a requirement of 47 dB on the RF selectivity of the receiver at ± 59.3 MHz for hops with nominal received signal power (-23 dBm). For those few hops with the highest allowed received signal level (-15 dBm), the requirement is 55 dB, which is missed typically by about 2 dB. As far as near-end interference is concerned, the worst case is due to beat oscillator leakage. The path loss requirement for the leakage is 131 dB which is small compared to other leakage requirements referred to above.

V. RESULTS OF LABORATORY AND FIELD TESTS

5.1 *Description of Laboratory and Field Facilities*

5.1.1 *Laboratory*

The first prototype bay was constructed in 1967 from preproduction models of the bay components. Three additional bays made according to the production drawings were added in early 1968. Four laboratory bays (two main station and two repeater station) were then available for system testing.

The four laboratory models were used extensively before the field testing began. Particular attention was given to laws of addition of intermodulation noise, echolike noise generated by harmonics of the IF, and tones associated with the TWT power supply.

5.1.2 *Field Trial Route*

The initial installation of TH-3 was a nine-hop route between Vega, Texas, and Dodge City, Kansas. Testing was originally scheduled for the period May through December 1969. Since the 1044A filter was not available until December 1969, some further testing was performed in 1970 to evaluate the system equipped with this filter.

The route consisted of two switching sections with an intermediate main station at Hooker, Oklahoma. The first switching section, Vega to Hooker, was the primary trial section.

The channels on the first switching section were chosen to examine the most important intrasystem interferences. At least three adjacent channels were necessary to check third-order interferences* and tertiary interference. Also channels were needed to check the special tone interferences (see Section 4.6.2). To accomplish these ends, channels 1T, 2T, and 3T were installed from Vega to Hooker and channels 3T, 7T, and 8T from Hooker to Vega. Channels 3T and 7T were installed in both directions on the second switching section to provide one regular and one protection channel. By interconnecting at IF, any number of hops up to thirty could be connected in tandem in the first switching section.

One new building and tower were constructed for the initial installation. The remaining stations were existing TD-2 stations and required only additions to the existing buildings. The antennas were re-oriented using the latest technique to reduce multimoding, and the cross-polarization discrimination was optimized at 4 GHz as is common practice for routes carrying both 4 and 6 GHz signals. The first switching section was 139.4 miles long or an average of 27.9 miles per hop. This conforms reasonably well with the system model which assumes 26.7 miles per hop. Also, since in the system model FM terminals are placed approximately every ten hops, measurements on ten hops (a loop from Vega to Hooker to Vega) can be extrapolated to the full system length on a power basis.

5.2 *Antenna System Performance*

A knowledge of the antenna coupling losses[1] that actually existed on the field trial route was necessary to properly evaluate the results of interference tests.

Swept measurements were made of the side-to-side and back-to-back coupling losses at all possible locations on the route. Generally, the measured coupling losses varied rapidly with frequency. The side-to-side coupling versus frequency response had a very fine grain, almost noiselike, structure which is attributed to energy coupling via many modes. The back-to-back coupling response also showed rapid variations although the structure was much coarser than for side-to-side coupling. The minimum side-to-side coupling losses followed an approximate normal distribution. For the same polarization, the mean was 92 dB and the standard deviation was 5.5 dB. For opposite polarization, the mean was 102 dB and the standard deviation was 8 dB.

---

* Third-order interferences are caused by $2A - B$ and $A + B - C$ type products between the RF signals of adjacent radio channels.

A distribution for back-to-back coupling could not be obtained because the test equipment lacked the necessary sensitivity. The minimum value measured was 115 dB.

Swept cross-polarization discrimination measurements were made on each hop of the first switching section. A signal was swept in 20 MHz increments over as much of the 6 GHz band as intersystem interference considerations would allow. It was found that the XPD of two antennas was less than 25 dB at 6 GHz. These two antennas were readjusted to meet the 25 dB system requirement. A typical measured XPD is shown in Fig. 8. The peak-to-peak variation was typically 1 to 6 dB within a 20 MHz band although larger variations were observed. The broad variation over a 250 MHz band is shown in Fig. 9. Figure 10 shows the cumulative distribution curve for lowest values of XPD measured in each 20 MHz band for every antenna. The inverse linear average needed for tertiary interference (see Appendix) is 29.4 dB.

Co-channel interference is dependent on the front-to-back coupling loss of the antennas. This ratio was spot-checked at a few stations and the lowest ratio measured was 67 dB, which is 1 dB better than the co-channel interference objective.

Swept envelope delay distortion measurements were made on each of the hops of the Vega-Dodge City route. The EDD test signal was applied to the antenna system at the 6 GHz system combining networks and received at the far-end combining network. A typical EDD measurement is shown in Fig. 11. The ripple observed in Fig. 11 can be attributed to the following two phenomena:

(*i*) dominant-mode echoes in the circular waveguide,
(*ii*) echoes due to mode conversion in a multimode medium such as the circular waveguide.

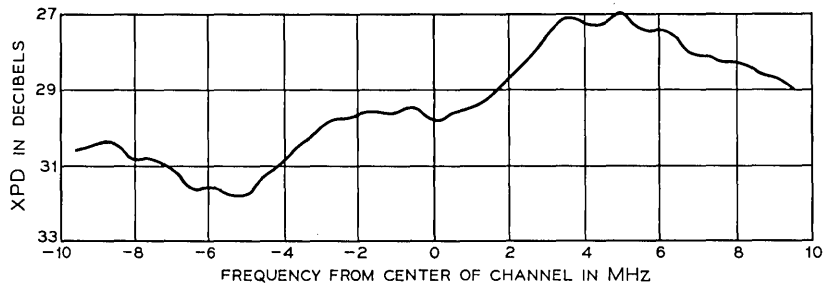

Fig. 8—Typical XPD as measured on the field trial route.

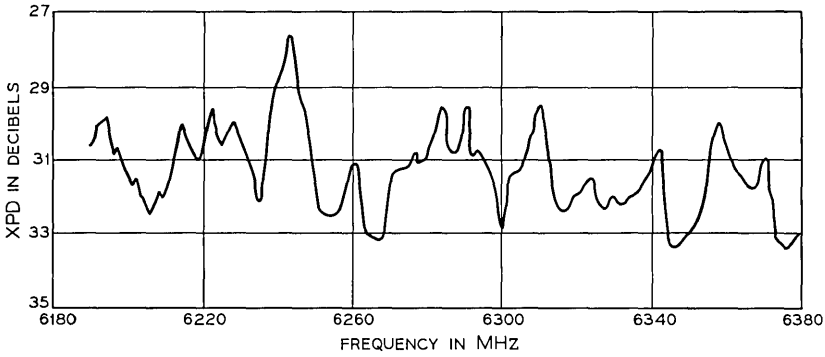

Fig. 9—Typical broadband XPD variation as measured on the field trial route.

To reduce multimoding, the first switching section was equipped with an improved circular flex (KS-20104) connecting the antenna to the rigid circular waveguide run. As a control, the second section was left with the original flex (KS-15690). The measurements indicated that the improved flex reduced the peak-to-peak ripple by a factor of two. The EDD ripples on the first section corresponded to antenna echoes

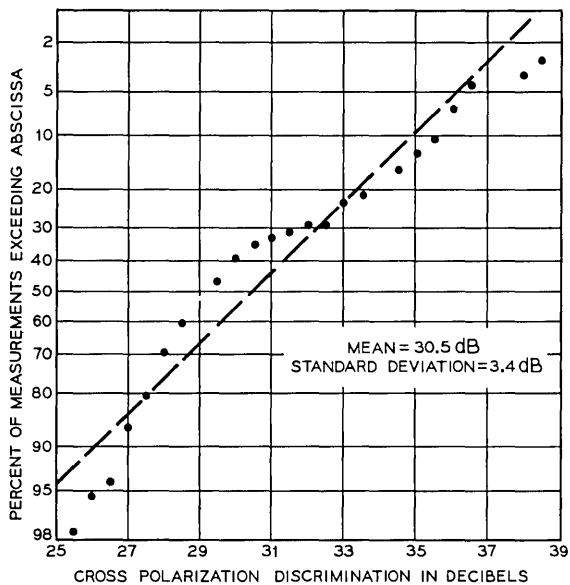

Fig. 10—Distribution of antenna system cross-polarization discrimination as measured on the field trial route.

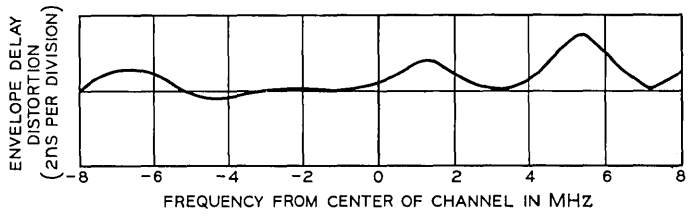

Fig. 11—Typical envelope delay distortion of antenna system equipped with KS-20104 circular flex.

which are typically 55–60 dB below the desired signal. The noise contributed by echoes of this level is computed to be less than 6 dBrnc0 per hop in the top channel, which will meet the antenna system allocation.

5.3 *Multihop Performance*

5.3.1 *Envelope Delay Distortion*

Since the 1044A filter was not available until December 1969, most of the field trial measurements were made on bays equipped with the 1009A filter. The envelope delay distortion measurements showed a systematic increase with the number of hops. After a few hops, a coarse (W-shaped) ripple became the dominant feature of the measurements. A ten-hop measurement typically had 6 ns peak-to-peak ripple over the center portion of the band. Little difference could be seen in the one- or two-hop results using either 1009A or 1044A filters. However, the ten-hop results with the 1044A filter, shown in Fig. 12,

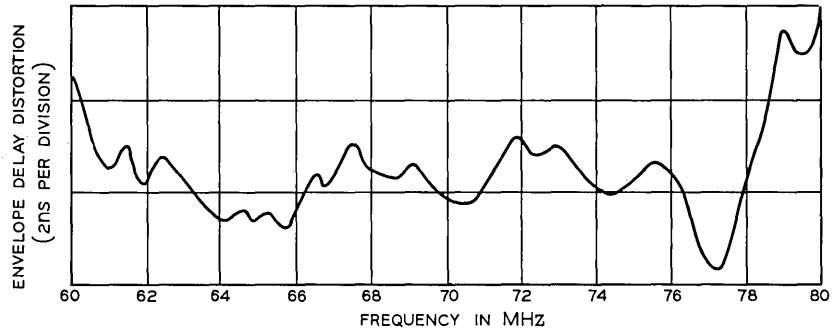

Fig. 12—Envelope delay distortion measured on a ten-hop loop equipped with 1044A IF filters. (The test set receiver had a 1.4 kHz lowpass filter before the oscilloscope and a sweep rate of 100 Hz.)

were markedly different. Although a W shape is still discernible, the peak-to-peak ripple is less than 3 ns. To achieve the EDD shown in Fig. 12, it was necessary to use a 0.25 ns/MHz sloper on every other hop. Most of the ripple is attributable to the antenna systems although the W shape is caused by the equalized RF networks.

5.3.2 *Noise Loading*

For all noise loading measurements the noise generator output was bandlimited from 0.3 to 8.204 MHz to simulate the 1800-circuit load that the system was designed to carry. This signal was then shaped by the pre-emphasis network.

The noise loading measurements showed that the intermodulation noise of the system related very closely to the measured EDD. When the new IF filter became available, a significant reduction in the system intermodulation noise was observed, as shown in Table I below, even though the law of addition was still high. A set of noise load "V-curves" obtained with the 1044A filter installed is shown in Fig. 13. These data were recorded on ten hops of the field trial route by looping channels at IF. The contribution of the FM terminals has been subtracted out so that the curves represent the noise due to the radio line portion of the system.

The noise of ten hops of the radio line is presented in Fig. 14 as a function of baseband frequency. The total noise at reference drive is shown along with the thermal and intermodulation noise components which were derived from the V-curves.

The thermal noise objective for ten hops of the radio line is 25 dBrnc0. As can be seen from Fig. 14, the requirement is exceeded by about 1 dB at 8.5 MHz. This is partially due to the baseband rolloff of the system. Since the ten hops exhibited about 0.6 dB rolloff, this would increase the thermal noise by 0.3 dB over what would be expected from a system with no rolloff. In addition, some of the first production components had noise figures slightly above normal.

The objective for cross-modulation noise caused by transmission

TABLE I—INTERMODULATION NOISE (AT 8.0 MHz) OF THE SYSTEM EQUIPPED WITH 1009A OR 1044A IF FILTERS (dBrnc0)

No. of Hops	With 1009A Filter	With 1044A Filter
2	16.0	9.0
6	23.5	15.4
10	26.0	19.2

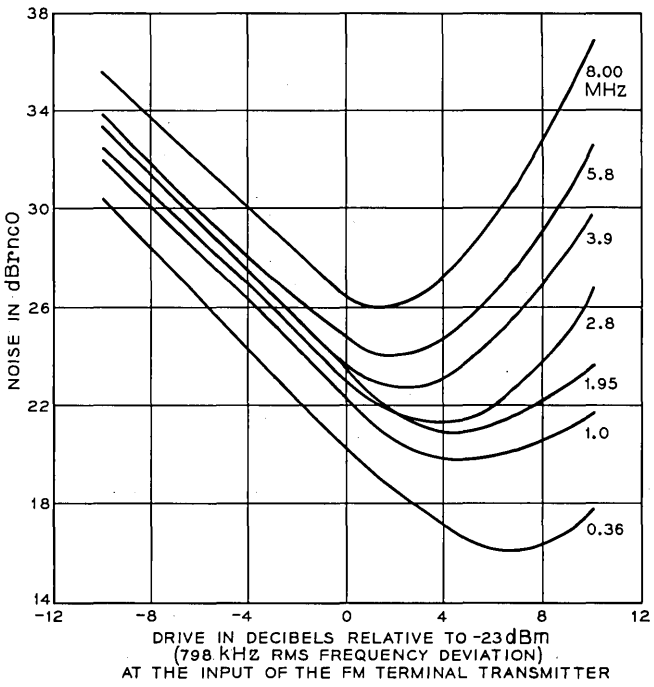

Fig. 13—Noise load V-curves measured on a ten-hop loop equipped with 1044A IF filters.

deviations and antenna system noise is 22.4 dBrnc0 for the radio line portion of a ten-hop system. As can be seen from Fig. 14, the measured cross-modulation noise meets the objective with 3 dB margin which is sufficient to allow the system to meet the total noise objective of 27.2 dBrnc0, even though the thermal noise objective was exceeded by about 1 dB.

Tests were also made comparing the chosen pre-emphasis and the pre-emphasis recommended by the CCIR for 1800-circuit loading.* The results of these tests indicate that the CCIR network gives about 1 dB less noise at low and high baseband frequencies, but about 1 dB more noise over the center of the baseband. On the whole, the performance of the two networks is about the same.

* CCIR REC 275-2, Documents of the XIIth Plenary Assembly, New Delhi, 1970, Vol. IV, p. 139.

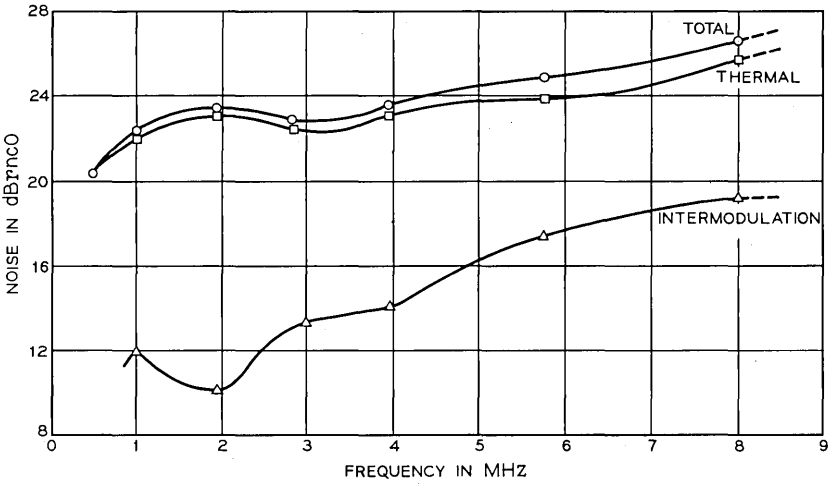

Fig. 14—Thermal and intermodulation noise versus baseband frequency as derived from noise load measurements on a ten-hop loop.

5.3.3 *Baseband Response*

The radio line exhibits a characteristic 0.06 dB/hop rolloff at 8.5 MHz and 0.12 dB/hop rolloff at 11.88 MHz. The rolloff is so consistent that the difference between any two radio channels will be less than 0.25 dB, so the wideband signals can be switched from regular to protection channels without significant level changes.

5.4 *Intrasystem Interference*

5.4.1 *Tertiary Interference*

The tertiary interference (see Section 4.4 and the Appendix) was measured by fading the center channel while one of the adjacent channels was carrying a noise load signal. Typical results of a measurement are shown in Fig. 15. The noise increases linearly with the fade depth* up to about 40 dB. Above this value, the total noise power approaches the carrier power and the amount of transfer in the limiter is reduced. This leads to the increase of the double adjacent noise at the same time that the transfer tertiary is beginning to roll off. At about a 47 dB fade, the squelch operates and the gain of the center channel repeater is reduced by 29 dB, thus reducing the tertiary noise by the same amount.

* Assuming a selective fade which affects only the center channel.

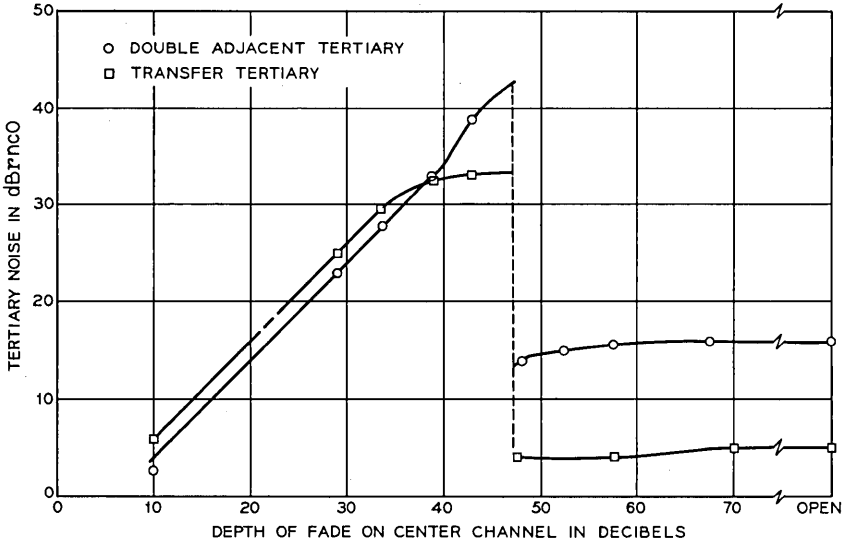

Fig. 15—Typical tertiary interference versus fade on center channel as measured on the field trial route.

Figure 16 shows a plot of the first- and third-order tertiary noise versus baseband frequency. The shape of the first-order noise is due to the selectivity of the center channel repeater (see Fig. 6). The shape of the third-order noise is sharper because it has the additional selectivity of two more repeaters. It can be seen that the difference between the two orders is not very large at the top baseband frequency as this is where the adjacent channel has the least selectivity.

Figure 17 shows the measured first- and third-order tertiary interference at 8 MHz after the noise was adjusted for XPDs of 30 dB.* Second-order noise is not shown because the XPDs involved in the path were very high. It was observed that with very high XPDs large variations in the value of the XPD were common. The predicted noise is also shown. The slope of the curves beyond the second-order path is due to selectivity of the center channel repeater at 21.7 MHz which is 5 dB per hop. When the center channel is open, the first repeater after the open channel is at full excess gain, and the noise power at the output is 38 dB below normal signal power (29 dB of loss is due to the squelch). The next repeater provides the additional 9 dB of gain to provide a squelched output, 29 dB below normal. As a result, the

*The XPDs were adjusted to 30 dB, the approximate mean of the measured XPD data.

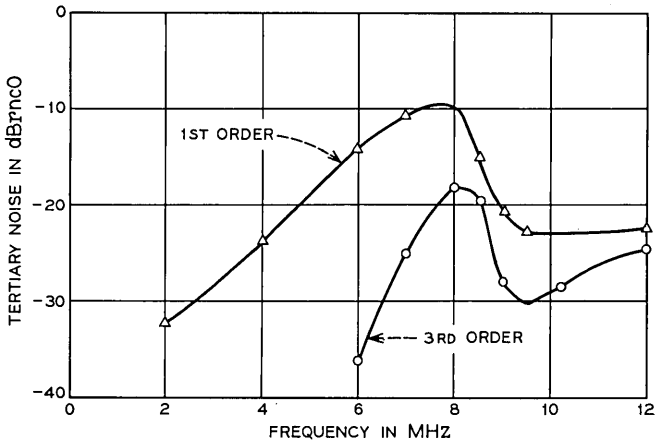

Fig. 16—Tertiary noise at a 0 dB fade versus baseband frequency as measured on the field trial route (XPD adjusted to 30 dB).

second-order tertiary noise is greater than the first-order noise. The measured values are in reasonable agreement with the values predicted from the model. The variation in the measured values is due to variations in the XPD with time and measurement error.

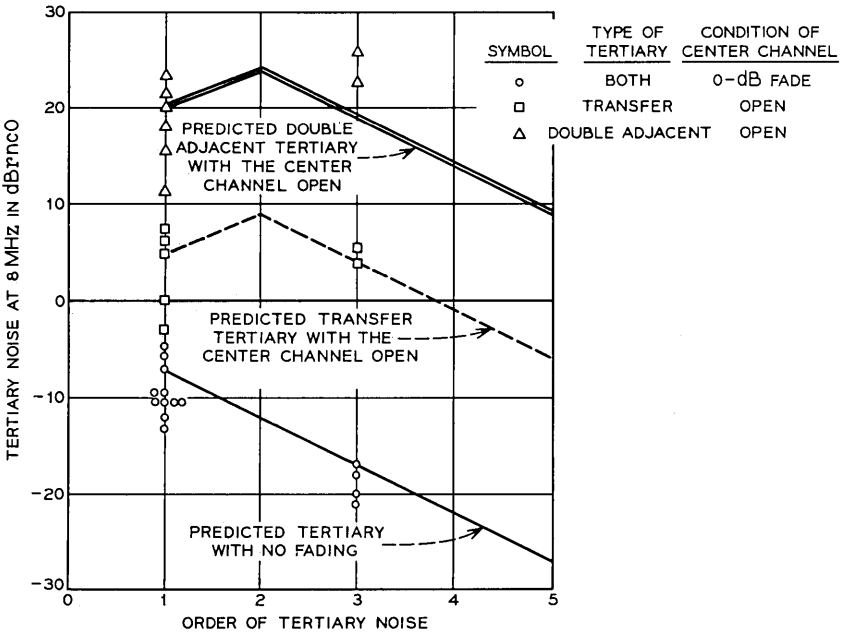

Fig. 17—Comparison of measured and predicted tertiary interference.

5.4.2 *Tone Interference*

Leakage measurements were a major part of the field tests. The results of tone measurements indicate that the bay meets the leakage requirements when correctly assembled; i.e., all covers in place and screws properly tightened.

Early measurements on the trial route showed that tones generated in the TWT power supply converter were out of limits both at the low end and the top end of the baseband. These tones fell at harmonics of the 24 kHz converter frequency. They were particularly strong in the auxiliary channel region. More filtering was added to the power supply and the tones were brought down to the objectives, except in the auxiliary channel region where they were about 7 dB above the objectives (which includes a 3 dB multiple exposure factor). A new power supply is being introduced into manufacture; one of its features is improved tone performance.

5.4.3 *Adjacent Channel Interference*

Adjacent channel interference was measured as a function of the depth of fade on the disturbed channel. The results of these measurements are shown in Fig. 18. The data has been adjusted to correspond to an XPD of 30 dB. If the faded hop had a lower XPD, the noise for deep fades would increase about 2 dB for every dB decrease in the XPD. Thus a combination of a 40 dB differential fade on a hop with minimum XPD would result in some circuits exceeding 55 dBrnc0. The increase in noise at 10.2 MHz would not be sufficient to cause the 100A system to switch the channel before a 40 dB fade. However, the likelihood of a 40 dB fade with no fade of the adjacent channels is extremely low.

The primary purpose of the RF squelch was to prevent the noise from an open channel from "spilling" into the adjacent channels centered 29.65 MHz away. When a channel was opened, causing the squelch to operate in every transmitter, it was found that the noise spillover into the adjacent channels increased their noise by less than 1 dB. Thus, even though a channel may be open, the effect on the adjacent channels is small.

VI. ACKNOWLEDGMENTS

The work of many individuals is reported in this article. In particular the authors acknowledge the accomplishments of T. G. Cross, W. D. Hutcheson, J. S. Torres, and D. S. Williams.

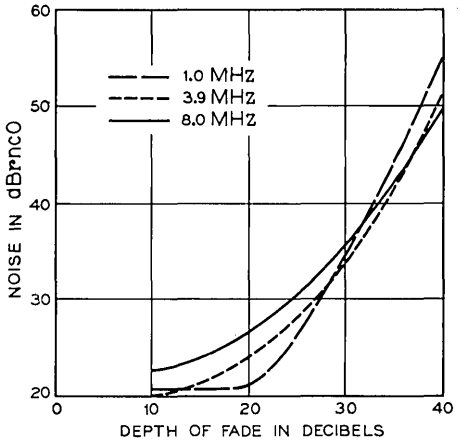

Fig. 18—Adjacent channel interference measured as a function of fade on disturbed carrier (XPD adjusted to 30 dB).

APPENDIX

Reference 2 described two types of tertiary mechanism which will be called first-order transfer tertiary and first-order double adjacent tertiary interference, respectively. These interferences are defined as first-order paths in Fig. 19, along with second- and third-order paths, etc. The figure shows the interference being introduced into channel 2 from channel 1 on the first hop. In practice, additional sets of paths will exist for interferences introduced into channel 2 from channels 1 and 3 on all hops but the last. It is clear from Fig. 19 that the interference will be transmitted by channel 2 and transfer back into channels 1 and 3 at every following hop. If channel 2 has a selectivity of a few dB to the outermost first-order sidebands of channel 1, the interference due to the second- and higher-order paths will rapidly decrease. However, if there is no selectivity in the center channel, there will be a vast increase in tertiary interference because the nth-order interferences will be no less than the first order.

It follows from the shape of the amplitude characteristic of the center channel (see Fig. 6) that the tertiary interference will be greatest in the top message circuit. The interference into the top message circuit due to transfer tertiary and double adjacent interference is expressed below in terms of the signal-to-noise ratios at baseband. In deriving these equations it was assumed that the signal-to-noise ratio in the first-order sideband regions (after a limiter) is the same as the signal-to-noise at baseband.

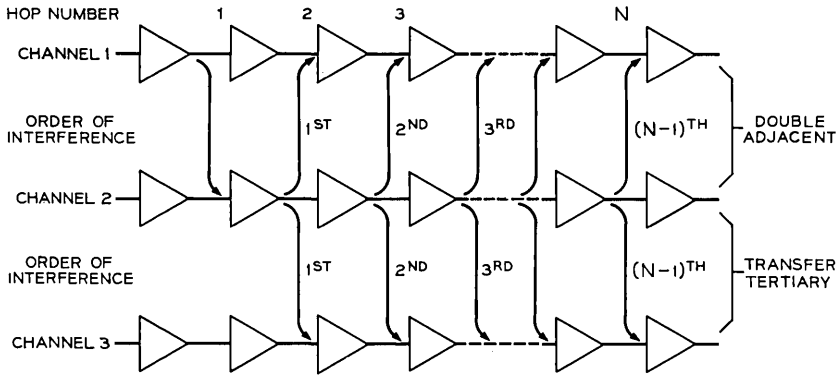

Fig. 19—Kth-order tertiary interference paths.

$$(S/N)_{\text{total}} = -10 \log \left\{ \sum_{k=1}^{N-1} (N - k) 10^{-(S/N)_k/10} \right\} - M \text{ dB} \qquad (1)$$

where

N = number of hops in the system,
M = 6 dB due to the fact that the disturbed channel can be exposed to a transfer tertiary and a double adjacent interference on both sides amounting to four interference paths in all.

The term $(S/N)_k$ is the signal-to-noise ratio due to a kth transfer tertiary (or double adjacent) path, given by:

$$(S/N)_k = 2(\overline{XPD}) + kL + T + C + B \text{ dB} \qquad (2)$$

where

$\overline{XPD}$ = cross polarization between channels in dB,
L = selectivity of the repeater at the frequency of the top message circuit in the adjacent channel in dB,
T = 6 dB due to limiter transfer in the channel adjacent to the disturbed channel,
C = 6 dB due to the advantage of the correlated sidebands in the disturbed channel over the interference,
B = 10 log 4/3 = 1.2 dB which is a factor for spreading interfering 3 kHz talkers over 4 kHz (1 kHz guard band and 3 kHz for talker) in the disturbed channel.

Power addition is assumed in this equation because there is several kHz change in the frequency difference between adjacent channels on successive hops. The equation is written as though the XPD were a constant

value for all hops. In practice of course this is not true, but it can be shown that for a large number of hops $\overline{XPD}$ is the inverse linear average given by:

$$\overline{XPD} = -10 \log \left\{ \frac{\sum_{n=1}^{N} 10^{-X/10}}{N} \right\} \tag{3}$$

where X is the XPD of the individual hops in dB.

In equation (3), X (dB) is a random variable and if it is assumed that the XPD distribution measured on the field trial route is representative (see Fig. 10), then

$$\overline{XPD} = 29.4 \text{ dB}.$$

The RF selectivity of the repeater at 21.13 MHz (which is the frequency of the top message circuit in the adjacent channel) is approximately 5.0 dB; i.e., L in equation (2) is 5.0 dB. Substituting these values into equations (1) and (2) results in a signal-to-noise ratio of 47.6 dB for a 150-hop system which is equivalent to 24.4 dBrnc0.

REFERENCES

1. Hathaway, S. D., Hensel, W. G., Jordan, D. R., and Prime, R. C., "TD-3 Microwave Radio Relay System," B.S.T.J., *47,* No. 7 (September 1968), pp. 1143–1188.
2. Kinzer, J. P., and Laidig, J. F., "Engineering Aspects of the TH Microwave Radio Relay System," B.S.T.J., *40,* No. 6 (November 1961), pp. 1459–1494.
3. Seastrand, K. L., and Williams, D. S., "TH-3 Medium-Haul Application: System Considerations," B.S.T.J., this issue, pp. 2271–2285.
4. Cooney, R. T., Griffiths, H. D., and Lanigan, F. H., "TH-3 Medium-Haul Application: Protection Switching," B.S.T.J., this issue, pp. 2315–2343.
5. Geldart, W. J., Haynie, G. D. and Schleich, R. G., "A 50 Hz to 250 MHz Computer-Operated Transmission Measuring Set," B.S.T.J., *48,* No. 5 (May–June 1969), pp. 1339–1381.
6. Bennett, W. R., Curtis, H. E., and Rice, S. O., "Interchannel Interference in FM and PM Systems Under Noise Loading Conditions," B.S.T.J., *34,* No. 3 (May 1955), pp. 601–636.
7. Rice, S. O., "Distortion Produced in a Noise Modulated FM Signal by Nonlinear Attenuation and Phase Shift," B.S.T.J., *36,* No. 4 (July 1957), pp. 879–889.
8. Liou, M. L., "Noise in an FM System Due to an Imperfect Linear Transducer," B.S.T.J., *45,* No. 9 (November 1966), pp. 1537–1561.
9. Cross, T. G., "Intermodulation Noise in FM Systems Due to Transmission Deviations and AM/PM Conversion," B.S.T.J., *45,* No. 10 (December 1966), pp. 1749–1773.
10. Rice, S. O., "Second and Third Order Modulation Terms in the Distortion Produced When Noise Modulated FM Waves are Filtered," B.S.T.J., *48,* No. 1 (January 1969), pp. 87–142.
11. Hamori, A., and Jensen, R. M., "TH-3 Microwave Radio System: Microwave Transmitter and Receiver," B.S.T.J., this issue, pp. 2117–2135.
12. Androski, F. J., Lentz, N. E., and Salvage, R. C., "TH-3 Microwave Radio System: 4A FM Transmitter and Receiver," B.S.T.J., this issue, pp. 2249–2269.

13. Griffiths, H. D., and Nedelka, J., "100A Protection Switching System," B.S.T.J., *44,* No. 10 (December 1965), pp. 2295–2336.
14. Curtis, H. E., "Radio Frequency Interference Considerations in the TD-2 Radio Relay System," B.S.T.J., *39,* No. 2 (March 1960), pp. 369–387.
15. Grady, R. R., Longton, A. C., and Slade, R. P., "Higher Order Mode Effects in the Horn Reflector Antenna System," Proc. Nat. Elec. Conf., *26,* 1970, pp. 354–359.
16. Members of the Technical Staff, Bell Telephone Laboratories, *Transmission Systems for Communications,* 4th Ed., Winston-Salem, N. C.: Western Electric Co., Inc., 1970, Chap. 20.

THE BELL SYSTEM TECHNICAL JOURNAL
Vol. 50, No. 7, September, 1971
Printed in U.S.A.

TH-3 Microwave Radio System:

Microwave Transmitter and Receiver

By A. HAMORI and R. M. JENSEN

(Manuscript received February 8, 1971)

The features and performance of a 6-GHz transmitter and receiver are described in this paper. The system objectives of 41 dBrnc0 for 4000 miles at 1800-circuit loading derived in the previous paper are applied to the design. With the exception of the 10-watt traveling-wave tube, the equipment is all solid state.

I. INTRODUCTION AND FEATURES

The microwave transmitter and receiver constitute the basic units of a radio system. They provide the gain necessary to compensate for the transmission loss of the station-to-station air path and the selectivity required to keep the radio channels properly separated. Since many of these units may be connected in tandem, each must meet stringent thermal noise, cross-modulation noise, selectivity, and equalization requirements in order to satisfy the overall system objectives.[1]

All the equipment required for transmitting and receiving a frequency-modulated 6-GHz signal is contained in one bay, including the channel separating and combining circuits, as shown in Fig. 1. The radio bays are mounted side-by-side with direct waveguide connections at the top of each bay; the waveguide used throughout is WR-159. With the exception of the traveling-wave tube, all circuits are solid state; only a −24-volt supply is required for primary dc power.

Two types of bays, main station and repeater, are made. The main station bay contains independent transmitter and receiver units. The reason for this is illustrated in Fig. 2. In main station A the transmitter serves the W-E direction while the receiver in the same radio bay serves E-W. An equipment outage or maintenance work on the transmitter requires the use of a protection channel only in the W-E

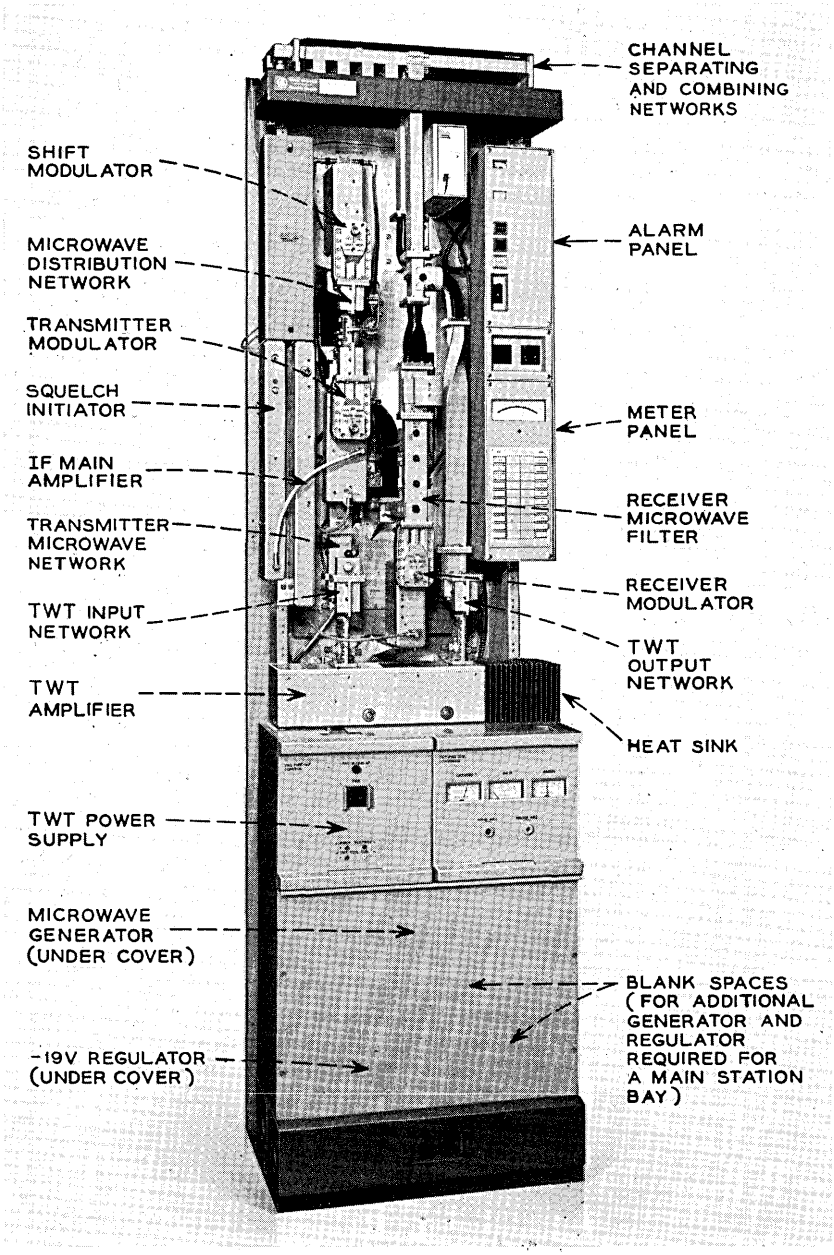

Fig. 1—TH-3 transmitter-receiver bay (repeater bay).

direction without affecting the E-W direction. This improves the overall system reliability and reduces maintenance problems. It also makes receiver- or transmitter-only bays possible. These bays can then be fully equipped at a later time.

In the repeater stations, however, the transmitter and receiver of the same bay serve the same direction of transmission. Since there is no advantage to independence here, some of the circuit functions are combined leading to a simpler radio bay.

A special feature of the bay is the use of directional waveguide filters for channel separation and combination. The use of these filters greatly reduces the number of waveguide components and eliminates the need for hybrids or circulators. Associated with the microwave filtering is another new feature: microwave delay equalization. The equalization of RF filters at RF is more accurate and consistent than the traditional IF equalization.

All modulators are unbalanced (single diode) and with the exception of bias adjustment they contain no tuning adjustments. Two-port access is provided by the use of either a directional filter or a circulator.

Three microwave integrated circuits are used in each radio bay. With the exception of the modulators, TWT, filters, microwave generator, and one isolator, all microwave circuits are contained in these integrated circuits. This contributes greatly to the simplicity of the radio bay.

A new circuit feature called RF squelch is introduced in place of a carrier resupply used in other similar systems. This approach decreases complexity and improves reliability.

The bay can be equipped with some optional components for a frequency-diplexed auxiliary channel which is described in a later paper.

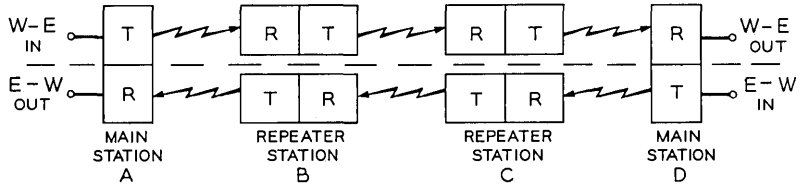

Fig. 2—Simplified radio route.

II. CIRCUIT DESCRIPTION

2.1 *Microwave Transmitter*

The block diagram of the signal portion of the transmitter is shown in Fig. 3. The input is a frequency-modulated 70-MHz signal at −7 dBm, which comes from an FM terminal transmitter or from a preceding radio receiver. This signal is applied to the IF limiter amplifier[2] which removes essentially all amplitude modulation and then drives the transmitter modulator. The limiter amplifier has another output which is used by the squelch initiator unit. The transmitter modulator[2] converts the 70-MHz IF signal into the transmitted microwave signal by modulating the transmitter microwave carrier (TMC)* generated by the microwave generator and associated circuitry as described later. The TMC power applied to the modulator is +18 dBm.

The squelch initiator[2] monitors noise in a narrow slot at 86 MHz. When this noise approaches the noise level corresponding to an open channel (front-end noise amplified by the full gain of the repeater), an offset voltage is applied to the transmitter modulator diode bias. At this new operating point the efficiency of the modulator is decreased so that the transmitter output drops 29 dB, sufficient to prevent adjacent channel interference. The squelch initiator also produces a relay contact closure, delayed by 45 seconds, to indicate the operation of the unit for remote observation. The delay is intended to eliminate any indication which might be associated with normal fading activity, since deep fades are of short duration.[3]

The transmitter modulator output passes through a portion of the microwave distribution network[4] which contains an isolator in the signal path before it connects to the transmitter microwave network. Since the TH-3 microwave carrier is always located 70 MHz below the signal, the circuit function of this network is to pass the upper sideband of the modulator and reflect the lower sideband and all other spurious outputs. This network contains half the total transmitter selectivity. The next active circuit in the signal path is the TWT. Since the TWT can contribute to the repeater distortion by converting amplitude modulation into phase modulation, it is very important to

* In this article the traditional "LO", "BO", "Pump", etc., is called the microwave carrier, since the microwave modulating process produces a suppressed carrier single-sideband output signal. This carrier should not be confused with the signal carrier, which is part of the frequency-modulated signal. For simplification and ease of identification, the transmitter and receiver microwave carriers are abbreviated as TMC and RMC, respectively.

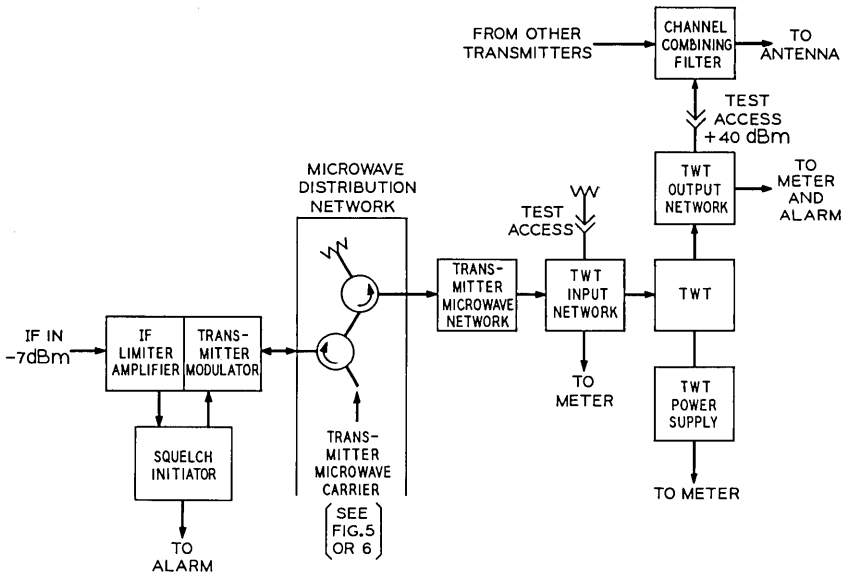

Fig. 3—Microwave transmitter block diagram.

eliminate all sources of AM from the signal.[5] The signal up to this point has negligible AM because of the limiter and the insignificant contribution of the transmitter modulator. The bandpass filter,[6] however, has delay distortion which does introduce AM into the signal. To eliminate this, the delay distortion of the transmitter microwave network is equalized by an RF delay equalizer,[7] which is factory-tuned.

The TWT input network is a microwave integrated circuit[4] which performs a series of functions. First, it provides a good match for the transmitter microwave network by the use of an isolator. It also contains an attenuator for setting the input power of the TWT to +7 dBm. This attenuator consists of a circulator which has one port terminated in an adjustable mismatch and an external waveguide termination. The insertion loss of the attenuator is the return loss of the adjustable mismatch. When the external termination is removed and the mismatch eliminated, the transmitter modulator output is available at that port for testing. Finally, the signal leaves the network through a reduced-height waveguide port which mates with a similar input port of the TWT. A built-in detector serves as a monitor for the transmitter modulator output and is connected to the bay metering panel.

The traveling wave tube is a periodically-focused packaged tube.[8] The tube output is a nominal +40.5 dBm with a minimum gain of 33.5 dB. The tube is used at constant gain by adjusting the helix voltage above the synchronous voltage. This operating point provides lower thermal noise and less AM-to-PM conversion than if the tube were operated at maximum gain, at synchronous voltage. The transmission shape, however, is not flat. The linear slope component is typically −0.01 dB/MHz. This is tolerable since linear slope does not contribute to cross-modulation distortion.[5] The parabolic and cubic components are so slight that the loss that would be involved in flattening the transmission shape would increase the thermal noise more than it would improve the cross modulation. Consequently, the output impedance of the tube is matched by a tuner in the TWT output network to provide maximum output power. This also ensures maximum efficiency.

The TWT power supply[9] is a dc-to-dc converter operating from the −24-volt supply. It generates all the voltages required by the tube. The tube collector current is monitored externally on the bay metering panel.

The TWT output network[4] is a microwave integrated circuit similar to the TWT input network; it performs the same functions with the exception of providing attenuation and test access. A waffle-iron low-pass filter in the network is used to suppress harmonics of the output by at least 30 dB. (The input network also contains this low-pass filter because it is part of the die-cast housing but it serves no function there.) The output power monitor is connected to both the meter and alarm panels for alignment and alarm purposes.

The test access port is a waveguide joint where a precision high-power attenuator can be attached for test purposes. This is the point where the output power is 10 watts (+40 dBm). The signal then enters the channel combining filter.[6] This is a directional filter[10] consisting of a complementary bandpass and bandstop filter. The output signal passes through the bandpass section thus encountering the final selectivity required in the transmitter. The other radio channel signals pass through the bandstop section with a typical loss of 0.1 dB and combine with the bay output at the common output port. The common output port presents a good match at the channel frequencies across the whole radio band and can be connected in tandem with other similar filters tuned to other radio channels or connected to the antenna system. The delay distortion of these filters is equalized in the succeeding receivers.

2.2 *Microwave Receiver*

Figure 4 shows the block diagram of the receiver. The signal enters the receiver from the antenna waveguide or from the preceding bay through the channel separating network.[6] This network consists of a directional filter, similar to the channel combining filter, and a waveguide delay equalizer. This filter has more selectivity than the one in the transmitter to protect the receiver from interference caused by other channels. The delay equalizer equalizes the delay shape of both the channel separating filter and the preceding transmitter channel combining filter. The equalizer is associated with the channel separating filter because this filter has about twice as much delay shape as the channel combining filter. The test access port (a removable waveguide twist) is the reference point where the received signal power on a nominal length path is −23 dBm.

The receiver modulator[2] receives the input signal through an isolator and another directional filter.[6] The purpose of this filter is to combine the received signal and the receiver microwave carrier. The very narrow bandpass filter is tuned to the RMC, thus suppressing the noise sidebands and other spurious signals. The complementary band-reject filter in the signal path attenuates the RMC but does not interfere with the received signal. The receiver modulator converts

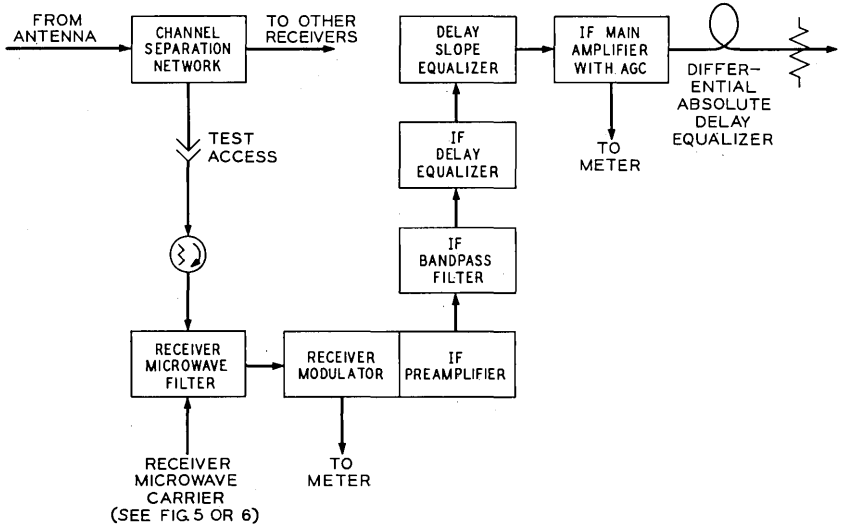

Fig. 4—Microwave receiver block diagram.

the microwave signal into a 70-MHz IF signal. The microwave image signal (2 × 70 MHz below the input signal) generated in the modulator is absorbed by the isolator ahead of the filter. To achieve a low noise figure, the modulator uses a GaAs Schottky barrier diode. The 70-MHz output of the low-noise preamplifier is −1.5 dBm with the nominal RF input and varies with the received signal power. The IF bandpass filter[6] that follows the preamplifier provides additional selectivity at the adjacent channel frequencies and at the IF harmonics. Two filter designs are available for this purpose, the 1044A filter for regular use and the 1009A filter which has greater selectivity at the adjacent channels. This latter filter contributes more to intermodulation noise and is used only when the signal-to-adjacent-channel-signal ratio is less than 22 dB at the bay input. This may occur when both channels are on the same polarization or on converging routes.

The IF delay equalizer equalizes the delay shape of channel separating and combining networks of other channels located between this radio bay and the antenna.[1] The delay slope equalizer is field selected after overall system measurements have been performed. This equalizer is available with five different slopes ranging from −0.5 to +0.5 ns/MHz.

The IF main amplifier[11] operates at a nominal 9-dB gain with a +1.0-dBm output. The built-in AGC circuit varies the gain to follow 40-dB fades or 10-dB upfades without output power variation. The differential absolute delay between the radio channels on the same route can be equalized by the use of appropriate lengths of IF cable at the output of the IF main amplifier. A pad builds out the cable loss to obtain −7-dBm IF output.

2.3 *Microwave Carrier Distribution*

Both the microwave receiver and transmitter modulators require a locally-generated microwave carrier. The TH-3 frequency plan places the receiver and transmitter frequencies 252.04 MHz apart and, by choice,[1] the carrier is always 70 MHz below the signal. As explained earlier in conjunction with Fig. 2, the main station transmitters and receivers operate independently and therefore require independent microwave carrier generators. In the repeaters, however, a single microwave generator is shared between the transmitter and receiver of the same bay. Because of these differences the two types of bays are discussed separately.

2.3.1 *Repeater Bay*

The repeater bay microwave distribution circuit is shown in Fig. 5. The microwave generator[12] is crystal-controlled at about 125 MHz and produces a nominal 1-GHz output at +29 dBm. This output is multiplied by the 6-GHz varactor multiplier[12] to obtain the desired transmitter microwave carrier frequency. The microwave carrier filter attached to the output of the multiplier is required for removing unwanted 500- and 1000-MHz sidebands around the TMC which are generated as harmonics of the lower frequency portions of the multiplier chain.

The output of the microwave carrier filter may pass through the auxiliary channel modulator which phase-modulates the TMC as described in a following paper.[13]

The receiver microwave carrier must be obtained from the TMC since there is only one microwave generator in a repeater bay. The frequency difference between the TMC and RMC is 252.04 MHz (the difference between the transmitter and receiver signals). Whether the TMC or the RMC is higher depends on the bay being a low-high or high-low repeater. This frequency shift is accomplished by a shift modulator.[2]

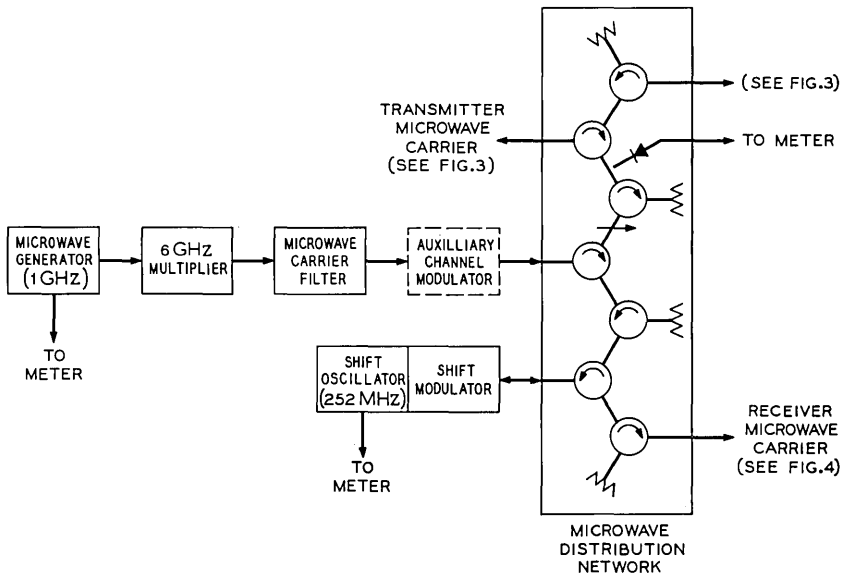

Fig. 5—Microwave carrier distribution (repeater bay).

The distribution of the TMC is performed by the microwave distribution network.[4] The TMC for the transmitter modulator is adjusted for +18 dBm, and the remaining carrier power is applied to the shift modulator. Both the transmitter and shift modulator are single-diode modulators which require a circulator to separate the microwave input and output signals. In addition, other circulators are used as isolators to provide isolation between the transmitter and shift modulator and to terminate the unwanted sidebands of both modulators reflected from their bandpass filters. At the transmitter modulator this filter is the transmitter microwave network, and at the shift modulator the selectivity is provided by the bandpass section of the receiver microwave filter.

Detectors are provided in both the microwave generator and in the microwave distribution network for power monitoring.

2.3.2 *Main Station Bay*

As stated above, the TMC and RMC for the main station transmitter and receiver are generated independently. Each source consists of a 1-GHz generator and a 6-GHz multiplier with the associated microwave carrier filter, as shown in Fig. 6.

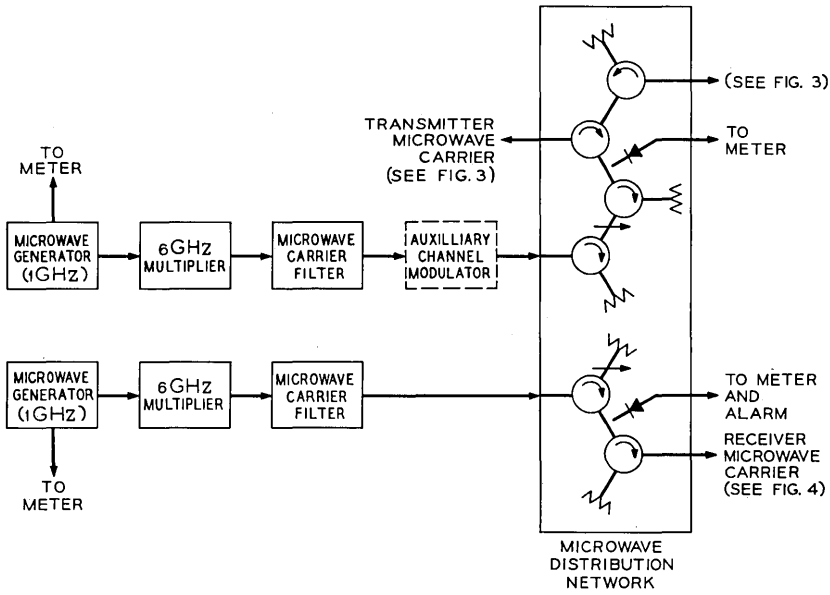

Fig. 6—Microwave carrier distribution (main station bay).

A microwave distribution network accepts the two microwave carriers. The transmitter portion performs as in the repeater bay. On the receiver side a coaxial input is provided in place of the shift modulator port and the circulator at this port is used as an attenuator. This network also contains an additional monitor to meter and alarm the RMC power.

2.4 *Power, Metering, and Alarms*

The radio bay is powered from −24-volt office battery. A −19-volt regulator[14] provides a stable voltage for the solid state circuits in the bay. This choice of voltage provides regulated output even with an emergency battery voltage low limit of −21 volts. The traveling-wave tube has its own power supply, a dc-to-dc converter.

Maintenance is simplified by the use of monitors provided at all significant points in the bay. The centrally located meter panel provides in-service access to these points to allow minor adjustments.

The alarm panel converts certain monitor outputs to alarm and status indications. These may also be used for remote surveillance.

III. PERFORMANCE

3.1 *Thermal Noise*

The thermal noise allocation for the radio line is 36.9 dBrnc0.[1] This noise is contributed by 100 repeaters and 50 main station bays in a typical 4000-mile system. There are two groups of thermal noise sources: the noise figure of the circuits in the transmission path and the carrier-to-noise ratio of the microwave carriers.[12] The typical noise figure and gain of the major blocks of a repeater are shown in Fig. 7.

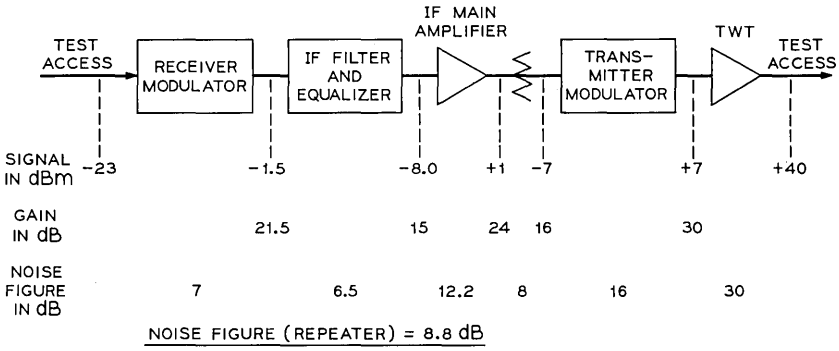

Fig. 7—Repeater noise figure.

The overall repeater noise figure is typically 8.8 dB. Based on the system parameters of Ref. 1, the noise contribution of the transmission circuits can be calculated and it is shown for 150 transmitters and receivers on Fig. 8, Curve A. At the top message circuit this is 36.6 dBrnc0.

The second significant noise contributor is the microwave carrier. FM noise on the carrier is transferred onto the signal in both the receiver and transmitter modulators. In the transmitter modulator this occurs across the full baseband. In the receiver modulator, however, the RMC is filtered by the narrow-band receiver microwave filter. The result is that the scalloping due to the introduction of the same noise at two places in the repeater[15] is noticeably only below 4 MHz, as shown on Fig. 8, Curve B.

The first null occurs at around 3.3 MHz corresponding to a typical value of 300 nanoseconds absolute delay in the receiver.

The total thermal noise (Curve C on Fig. 8) is 36.7 dBrnc0 at 8.524 MHz, which is slightly below the objective.

3.2 *Selectivity*

It was discussed in Ref. 1 that all selectivity is controlled by passive RF or IF networks. In the microwave receiver this is accomplished by the channel separating network and the IF bandpass filter.

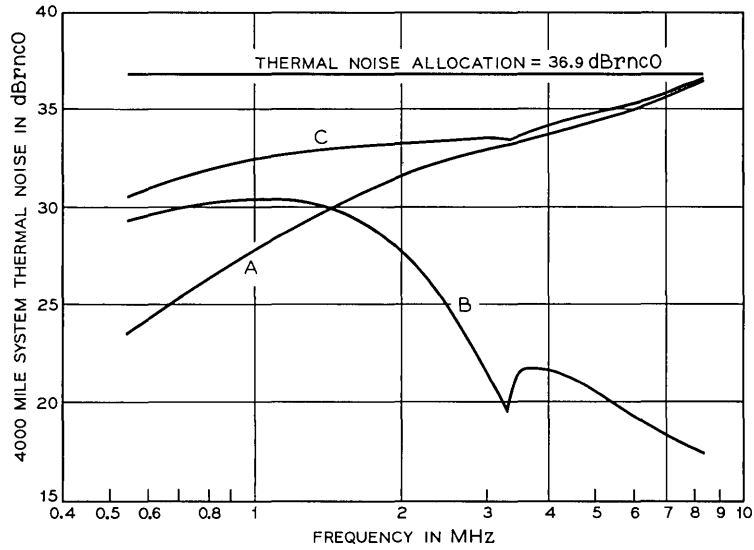

Fig. 8—Radio line thermal noise. Curve A is noise figure, curve B is microwave carrier noise, and curve C is total thermal noise.

In the transmitter there are two RF filters, the transmitter microwave network before the TWT and the channel combining filter at the bay output. It is desirable to have minimum delay distortion, therefore minimum selectivity ahead of the traveling-wave tube due to its AM-to-PM conversion properties. A minimum of 16 dB is required, however, at 40 MHz above the center of the channel to eliminate the interference of the second harmonic of the IF during swept measurements. This and the overall requirement led to splitting the selectivity evenly between the two filters in the transmitter.

The controlling selectivity requirements as explained in Ref. 1 and above are shown in Table I. Typical RF characteristics are shown on Fig. 9. Only one of the transmitter filters is shown on the figure; therefore the full transmitter characteristic is twice the curve shown. The IF characteristics are shown on Fig. 10. Two filters are shown, the 1044A and the optional 1009A. As described earlier, the 1044A filter is normally used.

The IF filters and the transmitter microwave network are delay-equalized units. The channel separating network is over-equalized to compensate for the delay distortion of the previous transmitter channel combining filter.

3.3 *Tone Performance*

There are interferences which do not enter through the antenna, therefore can not be controlled by the selectivity. These interferences are interbay and intrabay leakages, and microwave carrier generator and dc-to-dc converter harmonics.

The most serious interbay interferences can occur from transmitters to receivers. Special care was taken to reduce these leakages: eight screws are used at all waveguide flanges instead of quick-clamps; all

TABLE I—SELECTIVITY REQUIREMENTS RELATIVE TO CHANNEL CENTER FREQUENCY IN dB

Freq (MHz)	Chan Sep Net	IF BPF	Trmtr Mwv Net	Chan Comb Flt
±29.7	9	25		
+40.0			16	
±59.3	47			
±70.0			46.5	46.5
−74.1	45			
−133.4	97			

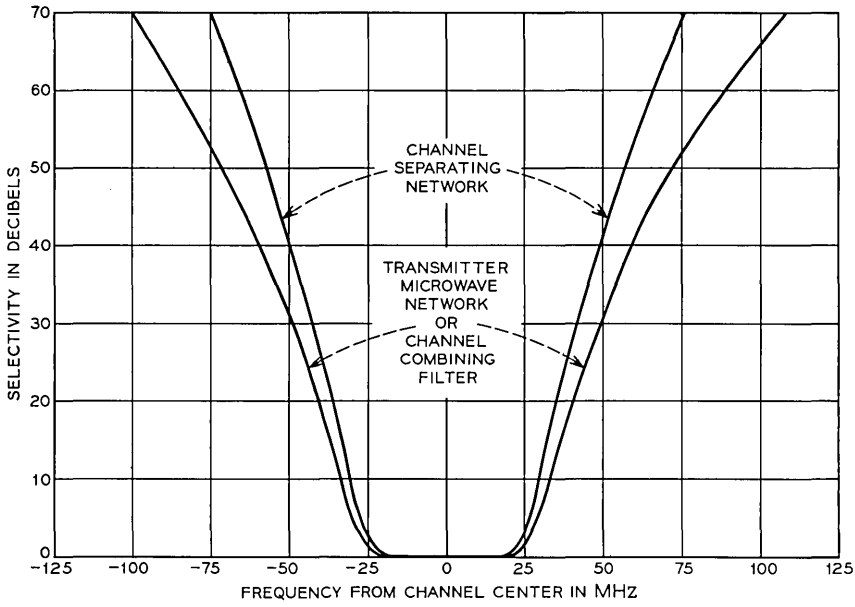

Fig. 9—RF selectivity.

joints are well-machined surfaces or sheet metal covers which seat on gaskets.

Intrabay interference is controlled mainly by the microwave distribution network in the repeater bay which connects the transmitter and receiver together. To avoid interference from the transmitter modulator to the shift modulator, at least 60 dB of isolation is provided, and in the opposite direction more than 68 dB.

A very critical source of potential interference is the dc-to-dc converter used for powering the TWT. This converter operates with a 24-kHz square wave and therefore is very rich in harmonics. If these tones find their way onto the TWT electrodes, they modulate the signal. Special shielded filtering is provided at the interface between the tube and the power supply, and the input leads connecting to the common −24V feeder is also well filtered.

The microwave carrier generator consists of multipliers; therefore it has unwanted harmonics on its output. Due to the last doubler and the sextupler, the output contains tones at approximately ±500 and ±1000 MHz relative to the TMC which could seriously interfere with the signal. For example, a tone occurs at 502 MHz above the TMC

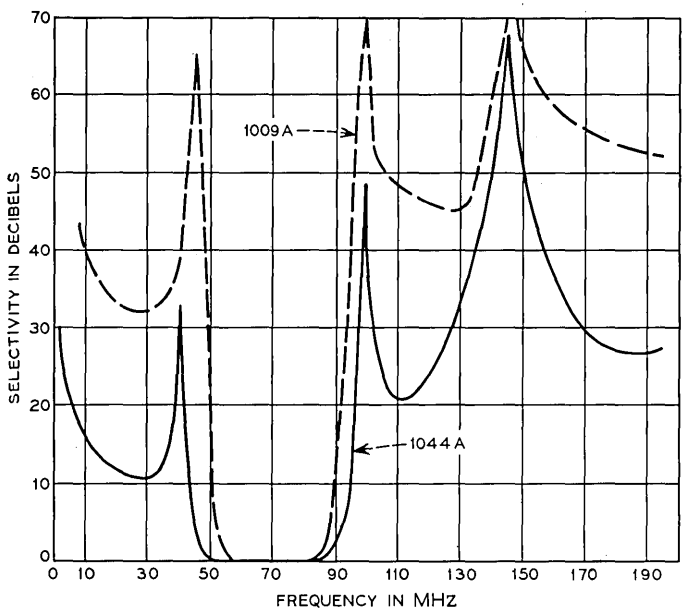

Fig. 10—IF selectivity.

for channel 16T which is shifted 252 MHz by the shift modulator to produce a 2-MHz tone in the RMC of channel 26T. In the transmitter modulator, unwanted TMC tones mix with harmonics of the 70-MHz IF to produce tones in the transmitter output signal. Taking the baseband tone requirements, multiple exposure factors, and conversion losses into account, the requirements shown in Fig. 11 were derived for these tones.

3.4 *Baseband Amplitude Response*

The baseband amplitude response of a radio repeater is shown on Fig. 12. The characteristic is smooth and consistent. The rolloff at 8.524 MHz is about 0.06 dB, at 10 MHz about 0.08 dB, and at 12 MHz about 0.12 dB.

3.5 *Environmental Effects*

The TH-3 transmitter-receiver bay was designed to operate at 75 ±20°F ambient temperature for long-haul 4000-mile systems. Outside these limits the frequency stability and the output power may be

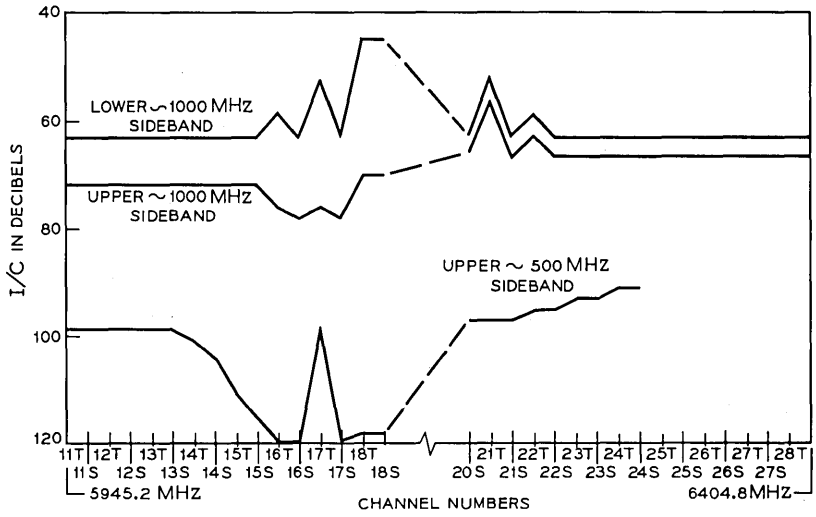

Fig. 11—TMC tone requirements.

affected but the changes are very minor up to the 40 to 120°F limits which are specified for medium haul, up to 1000-mile applications.[16]

One reason for this stability is that the waveguide filters are kept internally at less than 10-percent humidity. This is accomplished by tapping dry air from the station supply feeding the antenna system. The dry air enters the bays through the antenna (indoor) waveguide and leaks through all waveguide components at a slow (one cubic foot per hour) rate.

IV. EQUIPMENT DESCRIPTION

The components of the microwave receiver and transmitter are mounted on a 7-foot or 9-foot, 19-inch unequal flange, duct-type bay framework which is 22½ inches wide and 15½ inches deep. Figure 1 shows the components assembled on a 7-foot bay framework. When a 9-foot framework is used, the components are mounted in the lower 7 feet of the framework and are arranged in the same format used for the 7-foot bay. This leaves the upper 2 feet of the framework open. In general, 7-foot bays will be used in shelters or other low-ceiling buildings[17] whereas 9-foot bays will be used in central offices or other high-ceiling buildings.

All components are accessible and removable from the front of the bay. The bays can, therefore, be mounted back-to-back or against a

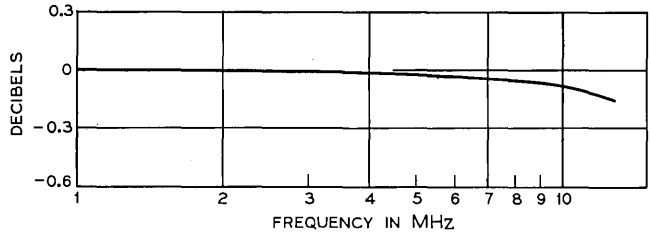

Fig. 12—Baseband amplitude response.

wall. Only one transmitter and one receiver are mounted on a bay framework. This alleviates tight packaging of waveguide components which minimizes use of waveguide spacers and bends, eases assembly during manufacture, eases maintenance by making the test ports more accessible, and minimizes system noise by keeping the waveguide connections between the channel networks as short as possible. Making the test ports more accessible eliminates the need for quick-clamps in that the waveguide screws are easy to remove and reinsert.

Many of the components of the bay are fabricated as die castings. For example, all modulators and the frame for their associated IF circuits, and the microwave integrated circuits, are die castings. This results in manufactured product that is economical and physically and electrically uniform.

Referring to Fig. 1, the −19-volt regulators and microwave generators are mounted in the lower portion of the bay. They are designed as plug-in units for easy removal and are protected by a front cover with quick-release fasteners.

The TWT power supply is mounted above the generators. It consists of two plug-in units arranged such that the left unit must be removed before the right unit can be removed. Removal of the left unit deenergizes the high-voltage right unit making it safe for personnel. The voltages are applied to the TWT amplifier by two cables that pass thru an opening in the top of the power supply framework and connect to two receptacles on the tube.

The TWT amplifier is mounted above the power supply with its receptacles facing the opening in the power supply framework. This arrangement completely encloses the power cable for greatest personnel safety. A test load can be connected to the power supply in place of the amplifier to determine if the amplifier or power supply is faulty in case of a transmitter output failure. To achieve long life for the TWT, the collector electrode is equipped with a finned heat sink cooled by natural convection.

The upper part of the bay supports the modulators, IF circuits, integrated circuits, waveguide networks/filters, miscellaneous waveguide components, and the meter and alarm panels. All waveguide components are mounted by special brackets to minimize physical distortion which degrades the electrical performance. In particular, the channel networks are mounted on a rugged casting which when bolted to the castings of adjacent bays aligns adjacent network ports to within a small fraction of an inch and permits them to be connected by short sections of flexible waveguide with minimum stress.

The meter, alarm, and circuit breaker units are mounted in a single box located at the right side of the bay. The meter unit provides means for monitoring the performance of various circuits in the bay. The alarm unit translates transmitter and receiver alarms into closed relay contacts for operation of external audible and visible alarms. It also has an alarm cutoff key for disabling the external audible alarm and a reset switch for resetting the receiver and transmitter meter relays.

V. SUMMARY

A microwave transmitter-receiver has been developed for providing a high-performance, high-capacity radio facility operating in the 5925 to 6425 MHz common carrier band. Its 10-MHz baseband will carry 1800 frequency division multiplexed voice circuits, one wideband TV channel, or equivalent service.

Its unique features, namely the use of directional waveguide filters for channel separation and combination, microwave delay equalization, microwave integrated circuits, RF squelch, and unbalanced (single-diode) modulators, make it a simple, easily maintained, economical system. The choice of 70-MHz IF and the use of many components common to the TD-3 system make it attractive for sharing routes and facilities with the already existing extensive 4-GHz Bell System network.

VI. ACKNOWLEDGMENTS

The development of the transmitter-receiver bay was the result of the work of a team of individuals. Some of them appear as authors of other papers in this issue while others are acknowledged in those papers. Specifically, the authors wish to acknowledge the physical design effort of T. J. Kelly.

REFERENCES

1. Jansen, R. M., and Prime, R. C., "TH-3 Microwave Radio System: System Considerations," B.S.T.J., this issue, pp. 2085–2116.
2. Giust, O., "TH-3 Microwave Radio System: Modulators," B.S.T.J., this issue, pp. 2155–2173.
3. Vigants, A., "The Number of Fades and Their Durations on Microwave Line-of-Sight Links With and Without Space Diversity," IEEE Int. Conf. Commun., June 9–11, 1969.
4. Dietrich, N. R., "TH-3 Microwave Radio System: Microwave Integrated Circuits," B.S.T.J., this issue, pp. 2175–2194.
5. Cross, T. G., "Intermodulation Noise in FM Systems Due to Transmission Deviations and AM/PM Conversion," B.S.T.J., *45,* No. 10 (December 1966), pp. 1749–1773.
6. Drazy, E. J., Sheehey, R. E., and Wang, H. C., "TH-3 Microwave Radio System: Networks," B.S.T.J., this issue, pp. 2137–2153.
7. Abele, T. A., and Wang, H. C., "An Adjustable Narrow-Band Microwave Delay Equalizer," IEEE Trans. Microwave Theory and Techniques, *MTT-15,* No. 10 (October 1967), pp. 566–574.
8. Bradford, C. E., and Waldron, C. J., "TH-3 Microwave Radio System: The Traveling-Wave Tube Amplifier," B.S.T.J., this issue, pp. 2223–2234.
9. Balicki, J. F., Chun, P. S., and Salvo, F. J., "TH-3 Microwave Radio System: Power System," B.S.T.J., this issue, pp. 2235–2248.
10. Abele, T. A., "A High-Quality Waveguide Directional Filter," B.S.T.J., *46,* No. 1 (January 1967), pp. 81–104.
11. Fenderson, G. L., "TH-3 Microwave Radio System: The IF Main Amplifier," B.S.T.J., this issue, pp. 2195–2204.
12. Bedell, H. R., Judkins, R. W., and Lahlum, R. L., "TH-3 Microwave Radio System: Microwave Generator," B.S.T.J., this issue, pp. 2205–2221.
13. Knapp, J. W., and Seastrand, K. L., "TH-3 Medium-Haul Application: Frequency-Diplexed Auxiliary Channel," B.S.T.J., this issue, pp. 2287–2313.
14. Jewett, W. E., and Mottel, S., "TD-3 Power System," B.S.T.J., *47,* No. 7 (September 1968), pp. 1498–1502.
15. Jensen, R. M., Rowe, R. E., and Sherman, R. E., "TD-3 Microwave Transmitter and Receiver," B.S.T.J., *47,* No. 7 (September 1968), p. 1202.
16. Seastrand, K. L., and Williams, D. S., "TH-3 Medium-Haul Application: System Considerations," B.S.T.J., this issue, pp. 2271–2285.
17. Swift, R. A., and Word, J. A., "TH-3 Medium-Haul Application: Equipment and Building Considerations," B.S.T.J., this issue, pp. 2345–2353.

THE BELL SYSTEM TECHNICAL JOURNAL
Vol. 50, No. 7, September, 1971
Printed in U.S.A.

TH-3 Microwave Radio System:

Networks

By E. J. DRAZY, R. E. SHEEHEY, and H. C. WANG

(Manuscript received March 3, 1971)

This paper describes the filters and networks which provide the frequency selectivity required in the TH-3 microwave transmitter and receiver, and the equalizers, which compensate amplitude and delay distortions introduced by the filters.

I. INTRODUCTION

The frequency selectivity required by the microwave transmitter and receiver of the TH-3 radio system is provided by passive networks. Adjacent-channel selectivity, together with suppression of second and third harmonics of the intermediate frequency (IF) which are generated in the receiving modulator and IF preamplifier, is provided by a loss- and delay-equalized intermediate-frequency filter. Microwave filters and selective networks provide image-frequency and adjoining-channel selectivity, furnish the required discrimination against unwanted tones and noise originating in the microwave generator, and are used for the multiplexing of transmitters and receivers into a common antenna-feed waveguide. Microwave delay equalizers compensate for the envelope delay distortion (EDD) of the selective microwave transmission networks,* so that only a relatively small residue of EDD remains to be mopped up by IF delay equalizers.

II. MICROWAVE TRANSMISSION NETWORKS

The locations and functions of the selective microwave transmission networks are described in another paper in this issue,[1] where overall requirements for the transmitter and receiver selectivities are also pre-

* We define transmission networks and transmission paths as those which carry the modulated signal.

sented. The transmission path of the transmitter contains two such networks, the transmitter microwave network, which precedes the traveling-wave tube (TWT), and the channel combining filter, which follows the TWT and serves the dual functions of multiplexing four transmitters into a common antenna feed waveguide and of providing a substantial part of the required transmitter RF selectivity. The channel separation network serves as the receiver multiplexer and also provides all receiver RF selectivity. The receiver microwave filter adds the receiver microwave carrier (RMC) to the received signal for application to the receiver modulator. It furnishes selectivity in the RMC path, for noise reduction, but none in the transmission path. To minimize transmission and delay irregularities due to reflections, all microwave networks are required to present return losses in excess of 30 dB at all frequencies which must be transmitted.

2.1 *Transmitter Microwave Network*

The transmitter microwave network consists of a bandpass filter, fabricated in WR-159 waveguide, and a one-section microwave delay equalizer of the type developed by T. A. Abele and H. C. Wang.[2]

The electrical requirements for this network evolved from four considerations. These are:

(*i*) This network must provide enough attenuation of the transmitter modulator's carrier leak, at a frequency $f_0 - 70$ MHz,* and unused lower sideband, at $f_0 - 140$ MHz, to prevent overload of the TWT and interference with measurements of the desired sideband.

(*ii*) This network and the channel combining filter, together, must fulfill the overall transmitter RF selectivity requirements.

(*iii*) The EDD of the transmitter microwave network must be less than 0.2 ns over the range $f_0 \pm 9$ MHz. (The importance of minimizing EDD, in this network especially, has been emphasized in another paper in this issue.[1])

(*iv*) The combined selectivity, and therefore the EDD, of the remaining microwave networks of the hop (i. e., channel combining and separating networks) must be such that the EDD can be compensated by a single microwave delay equalizer.

Conflicting implications of these considerations led to equal division of the transmitter out-of-band RF selectivity requirements between the transmitter microwave network and the channel combining filter,

* f_0 is the center frequency of the network's passband.

with resulting requirements for the transmitter microwave network as follows:

Envelope Delay Distortion,	(f_0 to $f_0 \pm 8.5$ MHz)	$\leqq$ 0.2 ns
Envelope Delay Distortion,	(f_0 to $f_0 \pm 15$ MHz)	$\leqq$ 1.0 ns
Insertion loss, in-band	(f_0 to $f_0 \pm 15$ MHz)	unspecified*
Insertion loss, $f_0 - 70$ MHz		$\geqq$ 49.5 dB
Insertion loss, $f_0 - 140$ MHz		$\geqq$ 50.5 dB

The filter of this network is realized as a six-resonator quarter-wave-coupled bandpass structure, based on a lossless maximally-flat-amplitude prototype having a 3-dB bandwidth of 54.2 MHz. Each resonator is bounded by inductive obstacles in the form of arrays of three cylindrical posts. To compensate for the asymmetry of the delay characteristic which results from ohmic losses slight adjustments were made in the lengths of the coupling lines. Figure 1a shows a view of this network and Fig. 1b a sectional view of the delay equalizer. Typical performance characteristics appear in Fig. 2.

2.2 *Channel Combining Filter and Channel Separating Network*

Examples of the channel combining filters and channel separating networks which serve as RF multiplexers for the radio transmitters and receivers, respectively, are shown in Fig. 3. Although the combining filter and separating network differ in details of structure and electrical requirements, similarities in their design principles and physical configurations, together with the facts that they share a common microwave delay equalizer and, to a large extent, complement each other with respect to electrical requirements, make it convenient to describe them together.

The directional filter configuration developed by Abele,[3] consisting of series-connected microwave bandpass and band-rejection filters of equal order, formed the starting point in the design of these multiplexers. The directional filter has the following advantages over the constant-resistance networks[4] used for multiplexing in earlier Bell System microwave equipment:

(*i*) Only two components, a bandpass filter and a band-rejection filter, are required to provide all needed receiver RF selectivity instead of the five (two hybrid junction, two band-rejection filters, and one

* The insertion loss of delay-equalized microwave filters is characteristically very uniform throughout the equalized portion of the passband—of the order of a few hundredths of a decibel for the subject filters. IF mop-up loss equalization compensates these small residual shapes.

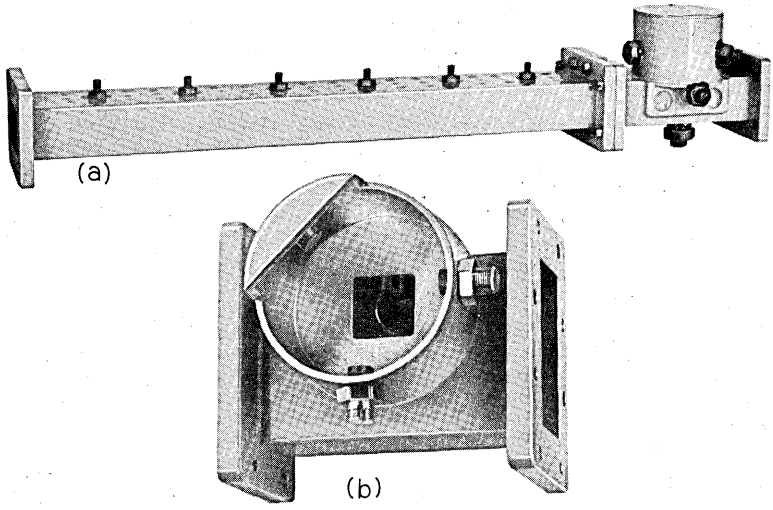

Fig. 1—Transmitter microwave network: (a) complete network; (b) sectional of delay equalizer.

bandpass filter) in the corresponding assembly in constant-resistance form.

(*ii*) The symmetric "T" shape of the directional filter facilitates design of equipment for either "right-handed" or "left-handed" installation.

Abele's directional filter[3] is derived from a true complementary pair, i.e., bandpass and bandstop sections of equal order, necessary if the common-port reflection coefficient of the prototype is to be zero at all frequencies. To conserve space, effect economies in manufacture, and reduce adjacent-channel delay distortion in the "through" paths to physically adjoining bays via the band-rejection section, pseudo-complementary designs were evolved for these filters by programming a digital computer to present the significant transmission and reflection parameters of a complementary prototype, then arbitrarily removing resonators from the band-rejection section, and readjusting the loaded Q's of the remaining ones for optimum performance in terms of system requirements. After satisfactory prototypes were obtained, the microwave elements were synthesized, using essentially the method of W. W. Mumford[5] for the bandpass section and that of Wang[6] for the band-rejection section. The latter entails application of transmission-

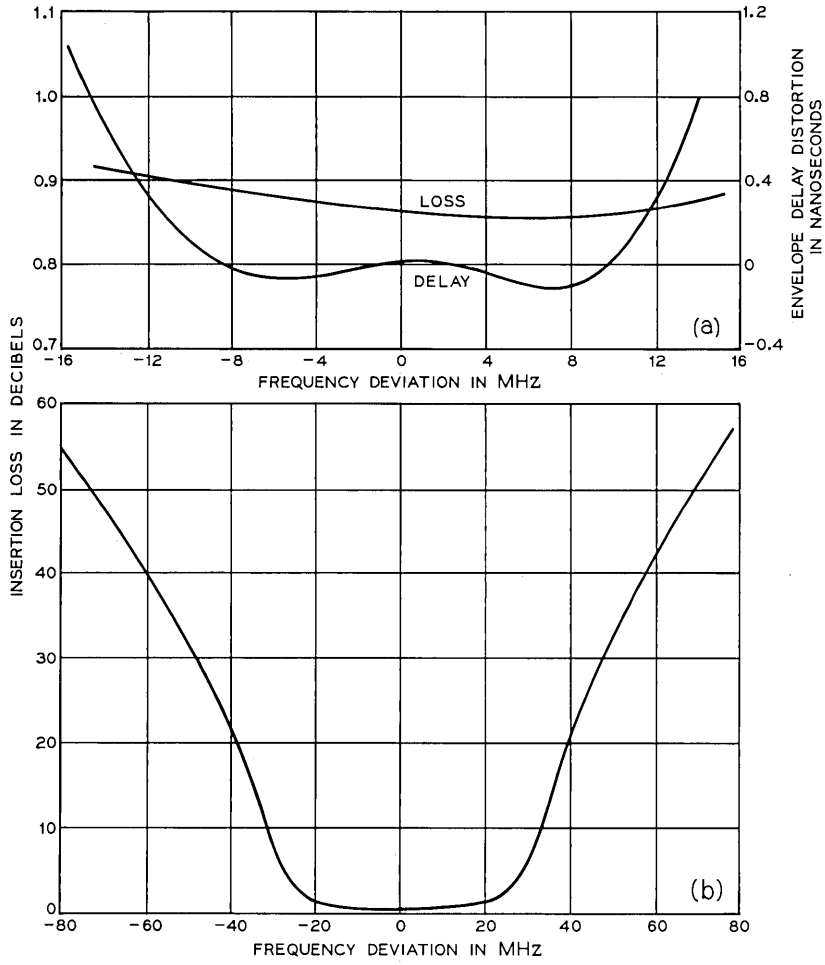

Fig. 2—Typical characteristics of transmitter microwave network: (a) passband EDD and insertion loss; (b) stopband insertion loss.

line synthesis methods and results in a design which has excellent symmetry, required for a satisfactory "fit" with the companion bandpass section, and passband return loss, but requires variations in the characteristic impedances of the coupling lines between resonators. This is achieved by replacing part of the broad wall of the waveguide with a "stepped" plate.

Out-of-band selectivity requirements for the bandpass path of the channel combining network are identical to those of the transmitter

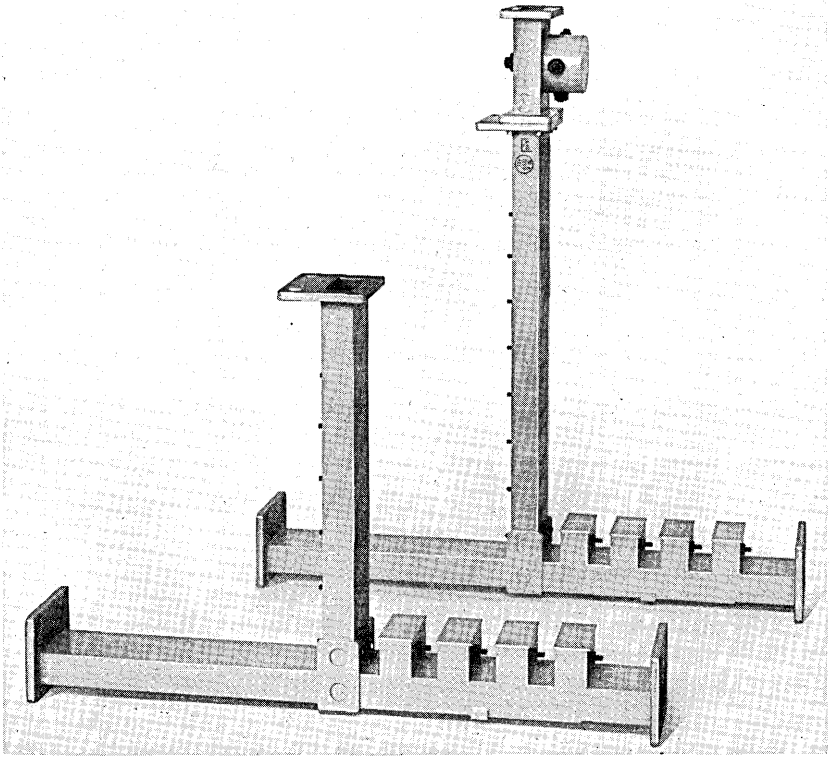

Fig. 3—Channel combining filter (left) and separating network (right).

microwave network as given in Section 2.1. In-band requirements are associated with those of the corresponding channel separating network, and will be covered in a later paragraph.

The microwave realization of the bandpass section of the channel combining network consists of a singly terminated, maximally flat, six-resonator, quarter-wave-coupled assembly, based on a lossless prototype having a 3-dB bandwidth of 54.15 MHz. The section is fabricated in WR-159 waveguide, with resonators bounded by inductive obstacles in the form of transverse arrays of cylindrical posts. The band-rejection section is also fabricated of WR-159 waveguide, and contains four resonators, with parameters determined as described in the preceding paragraph.

The out-of-band selectivity requirements for the bandpass path of the channel separating network are obtained by subtracting from the overall requirements (see Table I of the second paper in this issue)

the sum of (*i*) the insertion loss of the transmitter microwave network, and (*ii*) the insertion loss of the channel combining network at each significant frequency. The governing requirement turns out to be that discrimination of 9 dB is required at a frequency $f_0 \pm 29.7$ MHz.

As in the case of the transmitter microwave network, in-band requirements for the channel combining filter and channel separating network were established on the basis of EDD, with the specific criterion that the EDD of the transmission path between the combining port of a channel combining network and the separating port of the companion separating network be less than 0.4 ns over the frequency range $f_0 \pm 9.0$ MHz, and less than 4.0 ns over the range $f_0 \pm 15$ MHz. With the design, and therefore the EDD, of the channel combining network established, there remained to be determined the order and bandwidth of a bandpass section for the channel separating network which would provide the required out-of-band selectivity, and also, together with the companion combining network, have EDD within the range which could be accommodated by a technically and economically feasible microwave equalizer. An eight-resonator, singly terminated, maximally-flat-amplitude section having a 3-dB bandwidth of 51.8 MHz was found to have the requisite properties, and the separation network is based on this. With the exception of the two additional bandpass resonators, the directional filter of the separation network is similar to that of the combining filter. The delay equalizer is much like the one used on the transmitter microwave filter, and is attached as shown in Fig 3. Insertion loss characteristics of a combining network and a separating network are shown in Figs. 4a and b, respectively, and their combined EDD in Fig. 4c.

2.3 *Receiver Microwave Filter*

The receiver microwave filter combines the signal with the receiver microwave carrier for application to the Schottky-barrier receiving modulator, and also provides selectivity in the RMC path to suppress noise. This is a true complementary directional filter, with three-resonator bandpass and band-rejection sections. Its design is based on a maximally flat, lossless prototype having a 3-dB bandwidth of 4.94 MHz. Since this filter is not required to accommodate large bandwidths in the pass regions of its band-rejection section, the stepped-impedance connecting lines were omitted, with resulting savings in cost. Electrical requirements are:

Insertion loss at f_0, RMC port to modulator port $\leqq 3.8$ dB
Insertion loss at $f_0 \pm 70$ MHz, RMC port to modulator port $\geqq 44.5$ dB

Attenuation slope, signal port to modulator port, $f_0 + 60$ MHz to $f_0 + 80$ MHz, $\leqq 0.65$ dB
(f_0 = RMC frequency)

2.4 *Microwave Generator Tone Suppression Filter*

At the output of the microwave generator, spurious tones were detected and found to be harmful in some cases, since they appeared in the baseband signal frequency. The 5/6, 11/12, 13/12, and 7/6th harmonics of the transmitter modulator carrier frequency are present and can cause unwanted baseband tones. A two-cavity bandpass filter is added at the output of the microwave generator to suppress these tones. Because the output of the generator is in WR-112 waveguide, this size was also chosen for the filter. Because of the narrow separation between the operating frequency and the cutoff frequency of WR-112 guide, special considerations were given to these filters to reduce the passband insertion loss and to avoid possible "holes" in the stop band. It was concluded that for best electrical performance, filters for the low-frequency channels must use capacitive obstacles and filters for high-frequency channels must use inductive obstacles. For cost considerations, there are only four mechanical codes and each code may be tuned electrically to eight different channels (including staggered frequency channels). The three codes for low-frequency channels are designed in the form of two-cavity, maximally flat, direct-coupled bandpass filters with capacitive windows, while the fourth code, for high-frequency channels, has the form of a two-cavity, maximally flat, quarter-wavelength-coupled bandpass filter with inductive posts.

III. IF NETWORKS

3.1 *Function*

The IF networks that are required in the long-haul application of the TH-3 microwave radio system are shown in Fig. 5.

The bandpass filter provides adequate suppression to the adjacent channels which are received along with the desired signal. The bandpass filter also provides attenuation to the second and third harmonics generated in the preamplifier so that echo-like intermodulation noise is sufficiently reduced.

The delay and amplitude equalizers compensate for the delay distortions caused by the band-elimination portion of the directional

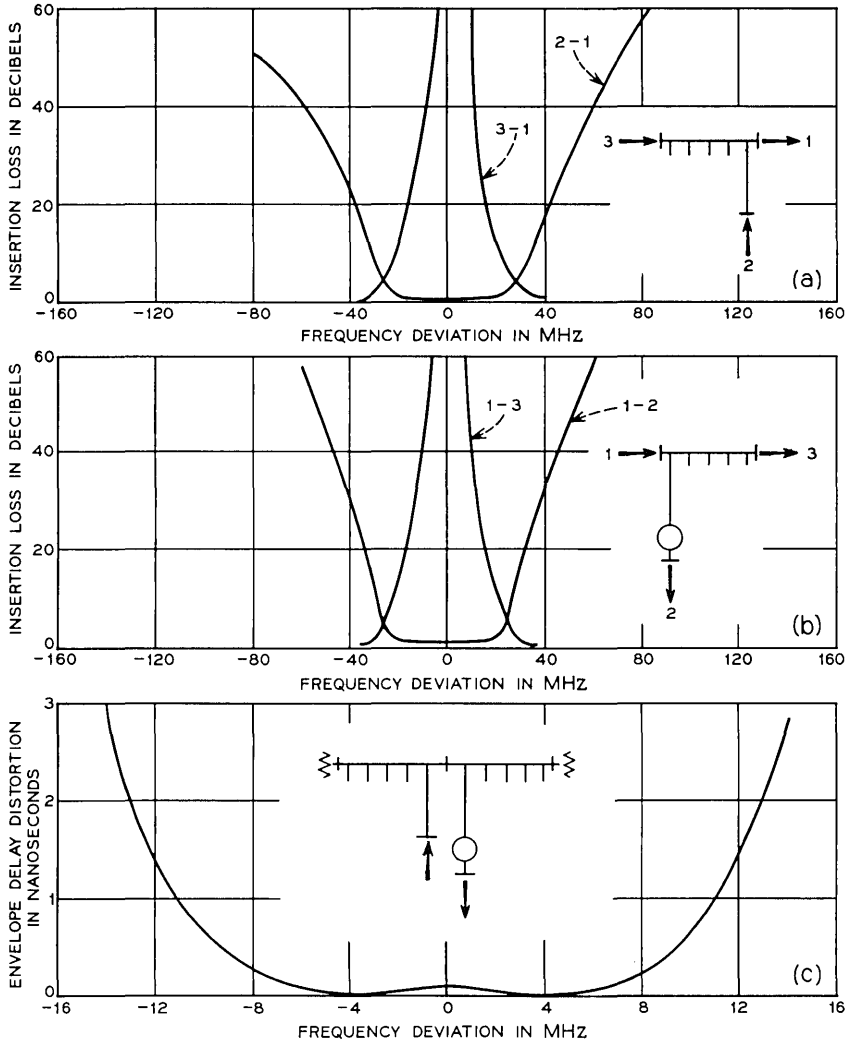

Fig. 4—Typical characteristics of channel combining filter and separating network: (a) insertion losses, combining filter; (b) insertion losses, separating network; (c) EDD, combining filter and separating network together.

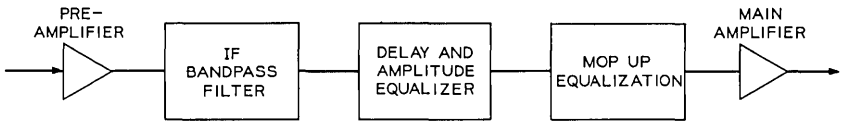

Fig. 5—Location of IF transmission networks in the TH-3 microwave radio system.

filters in the adjacent channels, and for the small residual in-band amplitude distortion of the microwave networks.

The "mop-up" equalizers correct for delay slope that arises due to normal systems variations. This correction is necessary because the intermodulation noise of the radio system is very sensitive to delay slope.

3.2 *IF Bandpass Filter*

Most circuits in the TH-3 repeater that contain active devices are relatively broadband and therefore introduce little transmission distortion. The IF bandpass filter in-band characteristic could be the controlling factor in the intermodulation noise performance of the repeater. Therefore the IF bandpass filter is both delay and amplitude equalized.

3.2.1 *Design Objectives*

The delay and amplitude distortion allowed in the passband is specified as the amount of intermodulation noise, caused by the in-band distortions, contributed by the filter. The transmission requirements for this filter are based on its contributing 0 dBrnc0 or less intermodulation noise per filter. This would be equivalent to a 30-dBrnc0 noise contribution in a 4000-mile system. The calculation of noise is based on an 18.6 log N law of addition, which was found in laboratory measurements on a system containing a similar filter.

Intermodulation noise contributed to the system by the filter is caused by transmission deviations and echoes.

The transmission deviations are the residual delay and amplitude ripples of the filter after it has been equalized. The delay and amplitude tolerances of the filter are based on the worst case peak-to-peak ripple and period of ripple that could occur in the equalized filter. The in-band objectives, based on noise performance, and the out-of-band objectives, based on adjacent channel interference and harmonic rejection, are as follows:

Frequency (MHz)	Delay (ns)	Discrimination (dB) Relative to 70 MHz
66–74	±0.15	
57.5–82.5	±0.25	
60–80		±0.03
56–84		±0.05
39.35–41.35		>20
98.65–100.65		>20
130–150		>25
200–220		>25

In addition, an insertion loss of 4.0 ± 0.2 dB at 70 MHz has been alloted to the filter.

The amplitude shape of the filter passband between 56 and 84 MHz should not have any parabolic component in its characteristic. A parabolic component in the amplitude characteristic would not add to the intermodulation noise, but would cause baseband rolloff.

Impedance mismatches between the filter and the apparatus interfacing the filter can generate echoes. One condition for the generation of an echo is a transmission path over which a fraction of the original signal is reflected and delayed in time from the original signal. Delay and amplitude distortions result from this reflected signal.

In order for the impedance mismatches not to contribute significantly to the intermodulation noise, the level of the echo or reflected signal should be well below the original signal. The measure of impedance mismatch used in this discussion is return loss in dB. To meet the desired echo level, the sum of the return losses at the filter interfaces should be at least 60 dB.

With reference to Fig. 5, the output return loss of the preamplifier is ≧35 dB and the input return loss of the delay and amplitude equalizers is ≧30 dB. In order to meet the 60-dB requirement the input return loss of the filter must be ≧25 dB, and the output return loss ≧30 dB.

3.2.2 *Theoretical Design*

Both the image parameter and insertion loss design of the filter were explored. The insertion loss method[7,8] is a more exact method in that either the passband insertion loss ripple, or the return loss ripple can be specified. Then a circuit configuration realizing these characteristics is synthesized. The design of this filter must be a compromise between the in-band return loss and the delay distortion at the passband edges.

The delay distortion must be kept to a minimum since approximately one-half of the entire configuration consists of delay equalization.

An 8th-order filter was synthesized[9] which has one attenuation pole at zero and one at infinite frequency, and three finite attenuation poles, one below and two above the passband. This filter, shown in Fig. 6a, was synthesized with an equal passband ripple of 0.01 dB, which is equivalent to a return loss of 26.4 dB. It has unequal terminations, i.e., an input impedance of 75 ohms and an output impedance of 66 ohms. Norton and pi-delta transformations were made on this configuration to achieve equal terminations and to get a capacitor to ground from every node of the filter and a capacitor across each inductor. The additional capacitors in the transformed filter, shown in Fig. 6b, are used to compensate for parasitic capacitance.

The input return loss of 26 dB meets the filter requirements; however, the output return loss of 26 dB is 4 dB below the required 30 dB. In order to increase the output return loss, a 2-dB bridged-T loss pad is connected in tandem with the output of the filter. The output return loss is now increased by twice the loss of the pad (4 dB) to the re-

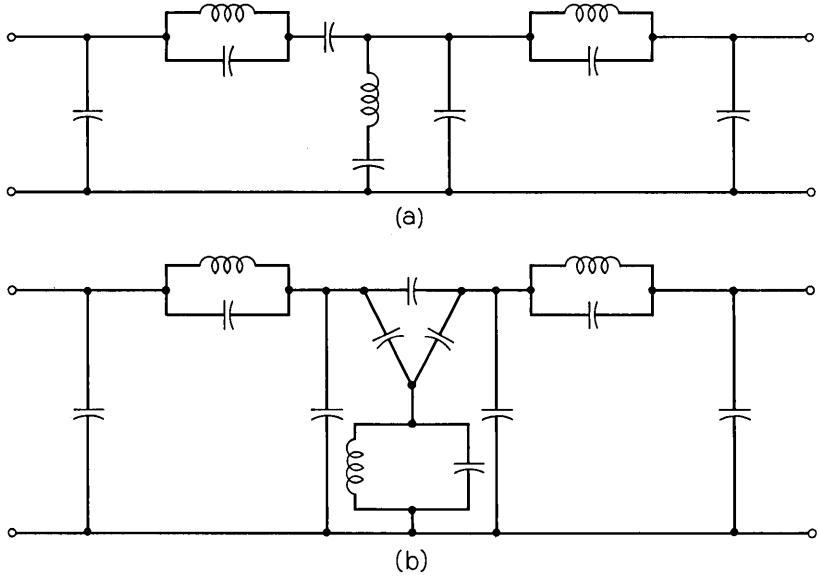

Fig. 6—(a) Schematic of the computed configuration for the filter section of the 1044A filter. (b) Schematic of the transformed configuration for the filter section of the 1044A filter.

quired 30 dB. The pad will also serve as a buffer between the filter section and the delay and loss equalization.

Three bridged-T all-pass sections are used to equalize the delay distortions of the filter to within the design objectives. Since there is a finite Q associated with the elements used in the filter and delay equalizer section, their loss shapes tend to be complementary thus leaving only a positive loss shape to be equalized. The loss equalizer is a bridged-T capacitor section which has an insertion loss with a negative slope. This equalizer is combined with the loss pad to form a single loss section.

Bridged-T configurations are used in order to achieve high return losses.

The complete schematic for the 1044A filter is shown in Fig. 7.

3.2.3 *Measured Performance and Mechanical Assembly*

A typical measured characteristic along with the manufacturing requirements for the 1044A filter are shown in Figs. 8 and 9. The return losses (compared to 75 ohms) meet the requirements previously specified.

Field tests showed that the noise contributed by the filter to the system is less than 0 dBrnc0. These tests also indicate that the baseband rolloff due to the filter meets system requirements.

The 1044A filter is assembled on a printed wiring board and housed in a drawn steel can (see Fig. 10). Sections of the filter are shielded by the use of aluminum cans which are mounted to the printed wiring board.

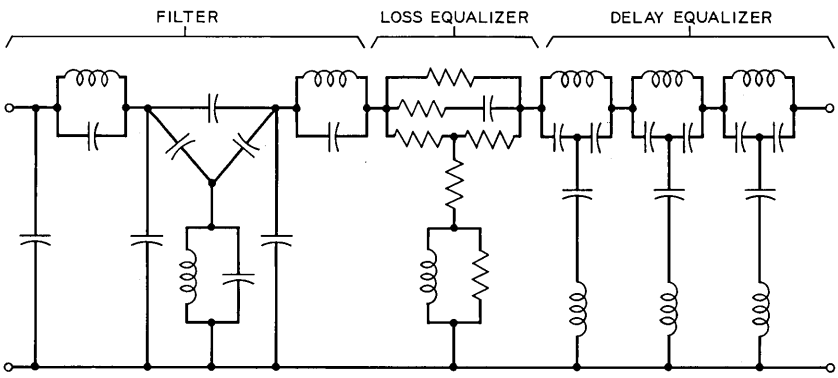

Fig. 7—Schematic diagram of the 1044A filter.

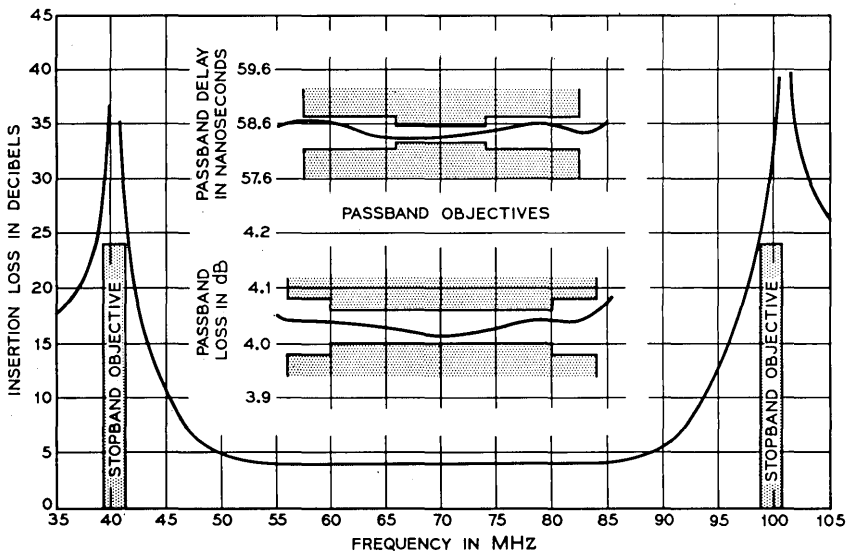

Fig. 8—Passband characteristic of the 1044A filter.

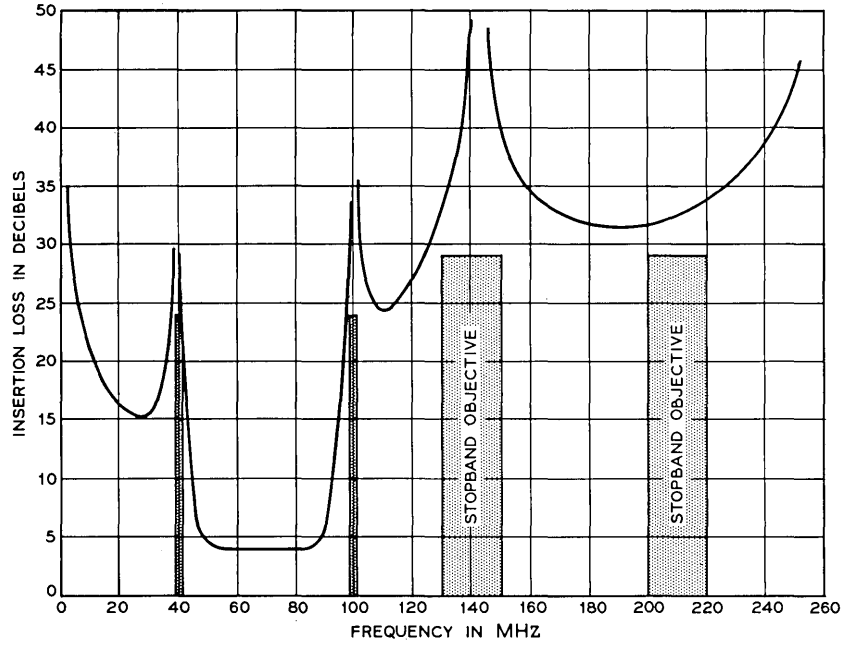

Fig. 9—Stopband characteristic of the 1044A filter.

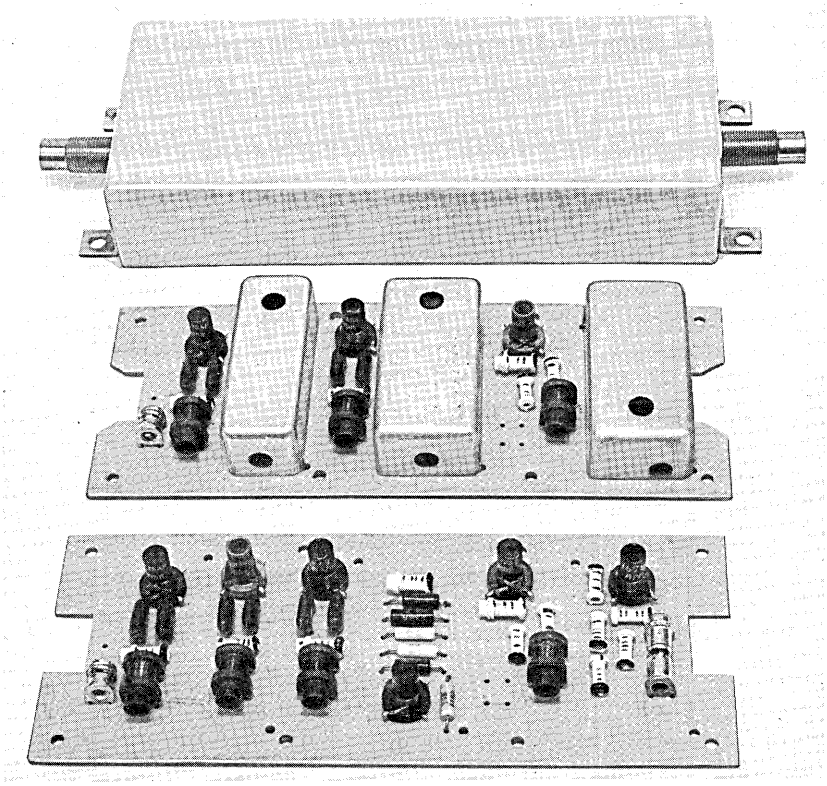

Fig. 10—The 1044A filter.

3.3 *Delay and Amplitude Equalization*

3.3.1 *General*

The microwave channel combining filters and channel separating filters have been designed as directional filters as described earlier in this paper. The bandpass portion of these filters produces a delay distortion in the passband which is equalized at microwave frequencies. The band-elimination portion of these filters produces a delay distortion at the frequencies of the adjacent channels. The shape of the delay distortion caused by this effect depends upon the bay lineup. That is, if a given channel passes only through the directional filter of the adjacent channel at a lower frequency, then only the distortions caused by that directional filter needs to be corrected for. If the signal passes through no adjacent channel filters then no delay correction is

required; however, an amplitude equalizer would be required to compensate for the small residual in-band amplitude shape. Consequently, three different IF delay and amplitude equalizers are necessary to correct for the three possible delay shapes caused by adjacent channel directional filters. A fourth equalizer is needed to correct for amplitude shape only. All four of the equalizers provide the same amplitude shape.

3.3.2 *Requirements*

The three delay shapes are basically a positive slope, a negative slope, and parabolic. The requirements for these equalizers are shown in Fig. 11.

The electrical design for the delay and amplitude section for these networks is of the same type as those used in the 1044A filter.

All requirements that were specified on these networks were met and are as follows:

Frequency (MHz)	Delay Match (ns)	Loss Match (dB)	Return Loss (dB)
55–85	±1.0	±0.10	30 min
58–82	±0.4	±0.05	30 min
61–79	±0.3	±0.03	33 min
70	—	2.2±0.1	—

3.4 *"Mop up" Equalization*

The "mop up" equalization used in the TH-3 radio system is the same as that used in the TD-3 radio system. These equalizers are completely described in Ref. 10 and are only mentioned here for completeness.

IV. ACKNOWLEDGMENTS

The electrical designs for the microwave transmission networks are the work of H. Westphalen, and those for the microwave generator tone suppression filters, of D. A. Vicedomine. The assistance of F. G. Joyal and A. P. Ligor in adjusting and measuring the microwave networks, that of M. Thoma in the numerical optimization of their designs, the contributions of A. J. Alberts and G. A. Tuchen towards their physical realization, and the assistance of A. Albanese and D. H. Klockow, whose knowledge of IF networks proved invaluable, are gratefully acknowledged.

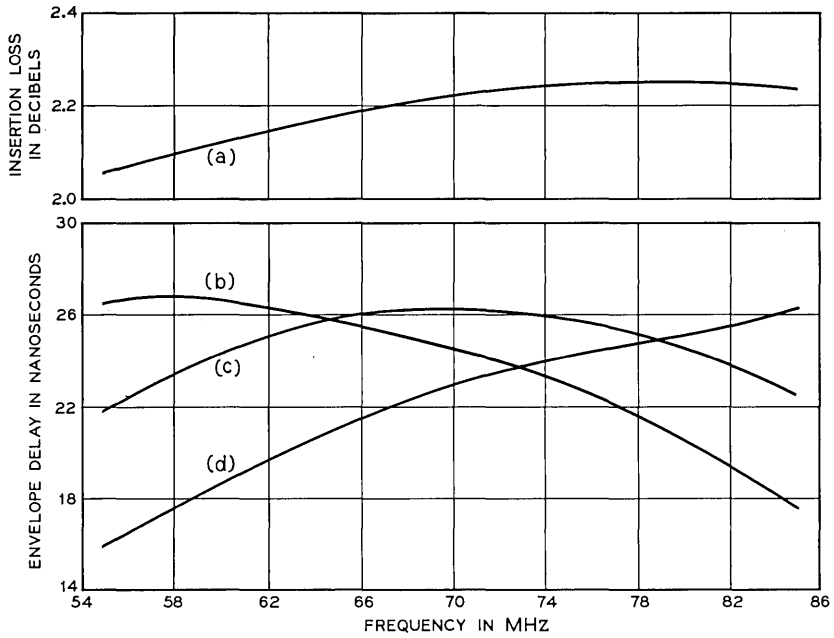

Fig. 11—(a) Insertion loss of the 936A, B, C, and D equalizers and envelope delay of the (b) 936B, (c) 936C, and (d) 936D equalizers.

REFERENCES

1. Hamori, A., and Jensen, R. M., "TH-3 Microwave Radio System: Microwave Transmitter and Receiver," B.S.T.J., this issue, pp. 2117–2135.
2. Abele, T. A., and Wang, H. C., "An Adjustable Narrow-Band Microwave Delay Equalizer," IEEE Trans. Microwave Theory and Techniques, *MTT-15,* No. 10 (October 1967), pp. 566–574.
3. Abele, T. A., "A High-Quality Waveguide Directional Filter," B.S.T.J., *47,* No. 1 (January 1967), pp. 81–104.
4. Lewis, W. D., and Tillotson, L. C., "A Non-Reflecting Branching Filter for Microwaves," B.S.T.J., *27,* No. 1 (January 1948), pp. 83–95.
5. Mumford, W. W., "Maximally-Flat Filters in Waveguide," B.S.T.J., *27,* No. 4 (October 1948), pp. 654–713.
6. Wang, H. C., "An Improved Design of Waveguide Band-Rejection Filters," B.S.T.J., *47,* No. 1 (January, 1968), pp. 1–15.
7. Darlington, S., "Synthesis of Reactance 4-Poles Which Produce Prescribed Insertion Loss Characteristics," J. Math. and Phys., *18,* September 1939, pp. 257–353.
8. Saal, R., and Ulbrich, E., "On the Design of Filter by Synthesis," IRE Trans. Circuit Theory, *CT-5,* December 1958, pp. 284–327.
9. Szentirmai, G., "A Filter Synthesis Program," Chapter 5 in F. F. Kuo and J. F. Kaiser (Eds.), *System Analysis by Digital Computer,* New York: J. Wiley and Sons, 1966.
10. Drazy, E. J., MacLean, R. C., and Sheehey, R. E., "Networks," B.S.T.J., *47,* No. 7 (September 1968), pp. 1397–1422.

THE BELL SYSTEM TECHNICAL JOURNAL
Vol. 50, No. 7, September, 1971
Printed in U.S.A.

TH-3 Microwave Radio System:

Modulators

By O. GIUST

(Manuscript received December 9, 1970)

In a TH-3 repeater the required frequency downconversion, upconversion, and shift is performed by three similar solid state modulators. The choice of an unbalanced design resulted in a simple modulator microwave structure which can be easily tuned and uniformly reproduced. The shift and transmitter modulators use a varactor diode for high pump efficiency while, in the receiver modulator, a Schottky diode is used to achieve a low noise figure and broadband operation.

I. INTRODUCTION

The TH-3 radio repeater makes use of three modulators: a receiver modulator for frequency downconversion, a shift modulator for frequency translation, and a transmitter modulator for frequency upconversion. These are unbalanced solid state modulators having different IF circuits and electrical requirements but similar microwave structures. Each of these modulators consists of two die-cast aluminum parts, one for the microwave structure and the other for the IF circuits.

The receiver modulator is used to downconvert the received microwave signal and to preamplify the 70-MHz IF signal before it is fed to the IF main amplifier for further amplification. Since the receiver modulator is the first active device to act upon the received microwave signal, it was designed primarily to obtain the highest possible carrier-to-noise ratio consistent with good transmission performance and reliability.

The transmitter modulator converts the 70-MHz frequency-modulated IF signal to a microwave signal having an upper and a lower sideband. The upper sideband is selected by an external microwave filter and fed to the TWT amplifier for further amplification prior to

transmission. The transmitter modulator was also designed with special attention toward transmission performance, reliability, and ease of tuning.

In a TH-3 repeater, the frequency plan requires a 252-MHz difference between the received and transmitted signal. As a result, separate local oscillator signals are required for the receiver and transmitter modulators. For reasons of system stability and economy, it is desirable to use a single microwave generator as a source of local oscillator signals. A shift modulator is therefore used to combine a portion of the local oscillator signal with a 252-MHz signal and to produce an output signal having two sidebands, one 252 MHz above and one 252 MHz below the applied local oscillator signal. The desired upper or lower sideband is then selected by an external microwave filter and serves as the local oscillator signal for the receiver modulator. Because of the shift modulator conversion loss, the shift modulator is used in the receiver where the local oscillator signal level required to drive the receiver modulator is considerably lower than the level required to drive the transmitter modulator.

II. THE RECEIVER MODULATOR

The design of the receiver modulator was patterned after an earlier design successfully used in a 4-GHz radio system.[1] As in the case of the other TH-3 modulators, this unit consists primarily of a diode mounted in a reduced-height waveguide structure followed by an IF preamplifier circuit. The local oscillator and received microwave signals are applied to the receiver modulator through an external microwave directional filter. The microwave structure and associated IF circuitry were primarily designed for low noise and therefore use a low-noise Schottky barrier diode (WECo 497A) and input transistor (WECo 45J) respectively.

2.1 *The Microwave Structure*

The receiver modulator uses an unbalanced microwave structure which, because of its simple design, was possible to construct using die-casting techniques which resulted in a uniform product requiring a minimum of machining. As illustrated by Fig. 1, the structure consists of a full-to-reduced-height waveguide step transducer followed by an 8-GHz waffle-iron lowpass filter and a diode mounted in a reduced-height waveguide cavity terminated by a waveguide short. The diode is physically mounted between a coaxial short, which is also the diode holder, and one end of a 5-GHz coaxial lowpass filter.

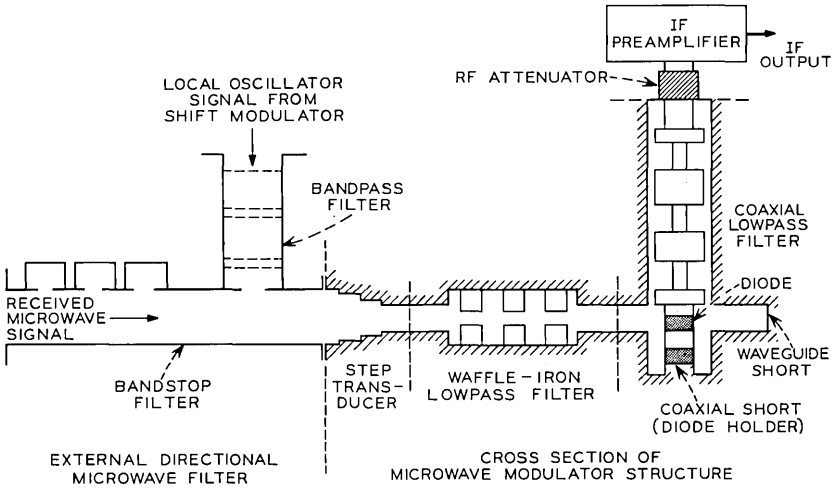

Fig. 1—Basic arrangement of receiver modulator and IF preamplifier assembly.

The coaxial filter has an RF attenuator consisting of a cylindrical bead of microwave lossy material inserted at one end of its center conductor. This attenuator is used to provide additional loss at frequencies above 5 GHz. The combined insertion loss of the coaxial filter and RF attenuator is approximately 3 dB at 0.8 GHz and 50 dB at 6 GHz. The waffle-iron filter has an insertion loss of approximately 3 dB at 8.2 GHz and 40 dB at 12 GHz.

The 5-GHz coaxial lowpass filter presents a high impedance to the input microwave signals thus assuring efficient application of these signals to the diode. The applied microwave frequencies mix in the diode to generate the desired 70-MHz IF difference frequency as well as other products and harmonics of the input signals. Harmonics of the input signals are restricted within the diode cavity by the waffle-iron filter, while the 70-MHz IF signal is applied to the IF preamplifier through the coaxial lowpass filter which is designed to provide a good impedance match to the diode at 70 MHz. The distance which the coaxial short (diode holder) extends into the diode cavity and the position of the waveguide short were experimentally determined to achieve the desired conversion efficiency and in-band stability. DC bias to the diode is applied through the coaxial filter from a network in the IF preamplifier circuit.

The various components required to make up the microwave structure of a transmitter modulator (essentially identical to that of a receiver modulator) are shown in Fig. 2. The structure is precision die

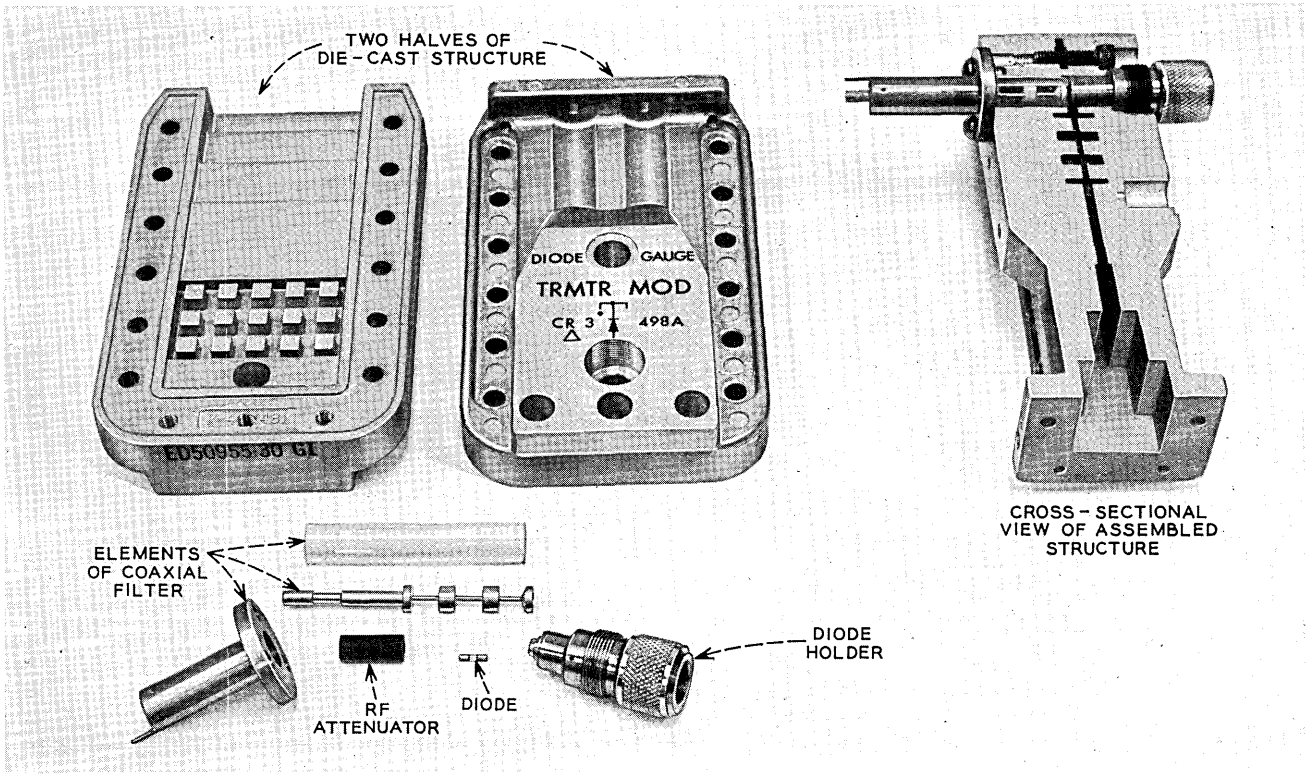

Fig. 2—Sectionalized microwave structure.

cast into two identical halves. It is then machined to accept the diode holder on one side and the coaxial filter on the other. Referring to Fig. 2, a diode gauge hole is machined to a specific depth on the face of one side of the structure. This hole is used to set the distance which the diode protrudes from the diode holder so that when the diode holder is inserted, proper mating of the diode with a small star chuck at the inner end of the coaxial filter is assured.

Typical microwave-to-IF conversion loss of the microwave structure is 4 dB. The nominal local oscillator and received microwave signal levels applied to the structure are +6 and −23 dBm respectively.

2.2 *The IF Preamplifier*

The receiver modulator, shown in Fig. 3, converts the incoming microwave signal into an IF signal with approximately 17 to 27 dB of gain. The IF preamplifier has a noise figure of approximately 2.5 dB and a maximum gain capability of 33 dB. As shown in Fig. 4, it consists of five transistor stages: a common emitter, a common emitter with shunt feedback, and three transformer-coupled common-base stages.

The 70-MHz IF signal taken from the coaxial lowpass filter is applied to inductor L1 or point A depending upon the channel frequency. Inductor L1 is used to improve the impedance match and thus the noise figure of modulators operating in the upper half of the TH-3 band; a wiring option bypasses the inductor in modulators operating in the lower half of the TH-3 band. The LEVEL control is used to set the output power level at −1.5 dBm for the range of inputs

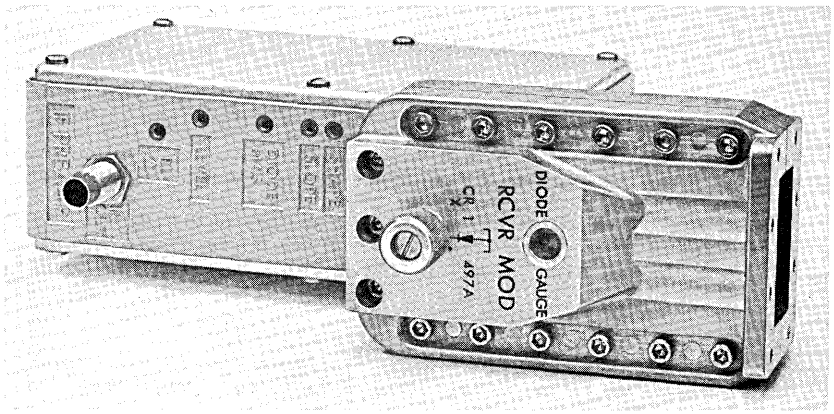

Fig. 3—Receiver modulator.

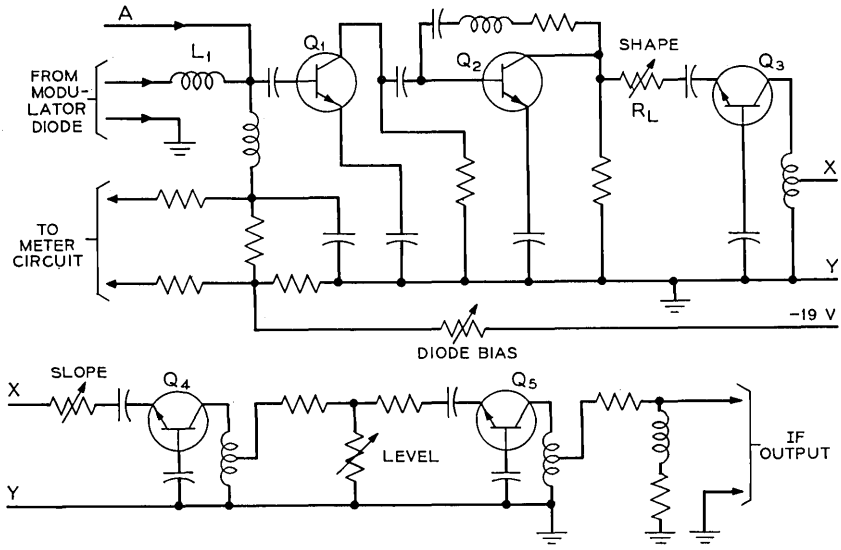

Fig. 4—IF preamplifier schematic.

expected for TH-3 repeater spacings, and has an adjustment range of about 10 dB. SHAPE and SLOPE controls are provided to adjust for flat RF-to-IF transmission. The overall transmission can be made flat to within 0.03 dB peak-to-peak deviation across the 30-MHz signal band. The output return loss is typically better than 30 dB across the same band.

The operation and method of applying the dc bias to the Schottky diode differs from that used in the earlier modulator design. In the earlier design, the diode bias network formed a constant current source. This method had the disadvantage of causing the modulator performance to be very sensitive to variations in local oscillator signal levels. It was found that an optimum bias network source resistance exists which is neither constant current nor constant voltage but which makes the modulator performance relatively insensitive to variations in the modulator local oscillator level. With the optimum source resistance for the bias network, the diode bias current varies with the local oscillator level so that the impedance of the Schottky diode remains relatively constant as the local oscillator level is changed. Measurements on a large number of diodes using this network showed that the optimum diode bias current, once set at the proper level for a given local oscillator level, is independent of the diode characteristics and of the channel frequency.

The DIODE BIAS potentiometer is adjusted to obtain the desired diode current for a given local oscillator level. Once the control is adjusted, changes in local oscillator level cause the diode current to vary as shown by the curve in Fig. 5. Provisions are also made to monitor the diode bias by an external meter circuit. Figure 6 shows the receiver modulator noise figure and IF output level sensitivity to variations in local oscillator level. Once set, the local oscillator level is not expected to vary by more than 1 or 2 dB; this variation is due mainly to temperature variations. However, a level drop as great as 6 dB does not cause an appreciable degradation (typically 0.04 dB) in the shape of the RF-to-IF transmission characteristic over the 30-MHz signal band.

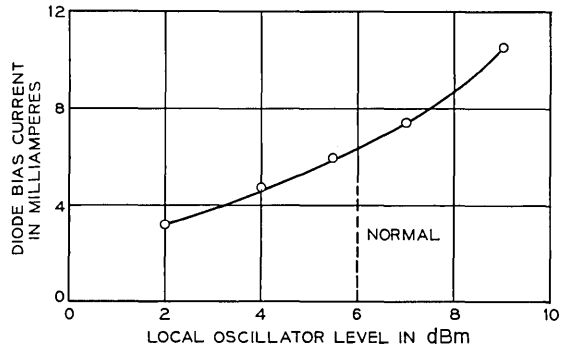

Fig. 5—Optimum diode bias current versus local oscillator level.

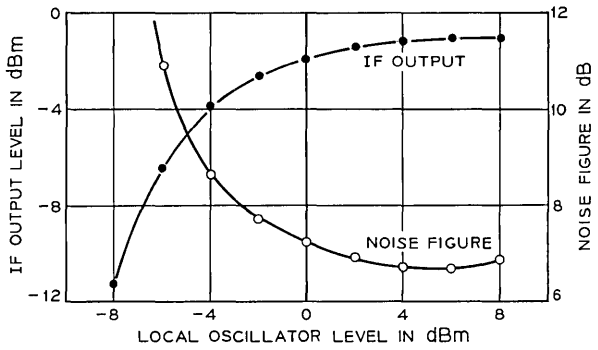

Fig. 6—Typical receiver modulator noise figure and IF output level sensitivity to variations in local oscillator level.

III. THE TRANSMITTER MODULATOR

The transmitter modulator, shown in Fig. 7, consists of an IF limiter amplifier followed by a single varactor diode mounted in a reduced-height waveguide structure. The modulator was designed for a nominal IF input level to the IF limiter amplifier of −7 dBm and a local oscillator microwave signal level of +18 dBm. The modulator was designed as an upper sideband upconverter to translate a 70 ± 15-MHz IF frequency band to any one of sixteen radio channels, each having a bandwidth of 30 MHz and a center frequency in range of 5945 to 6404 MHz. External circulators and a microwave bandpass filter are used to supply the correct local oscillator signal and to select the desired sideband respectively. Tuning to any one of the radio channels is accomplished by selecting the desired output bandpass filter and applying the associated local oscillator signal. The dc bias to the diode is then adjusted to tune the modulator to the desired channel.

An external squelch initiator circuit controls the output signal level of the transmitter modulator. This circuit provides, under extreme fading or absence of microwave carrier conditions, an overriding bias voltage to the varactor diode which detunes the microwave diode cavity and causes a decrease in the modulator output signal level. A more detailed explanation of the squelch function is given in a companion paper.[2]

3.1 *The Microwave Structure*

The transmitter modulator uses an unbalanced microwave structure design, shown in Fig. 8, similar to that used for the receiver modulator.

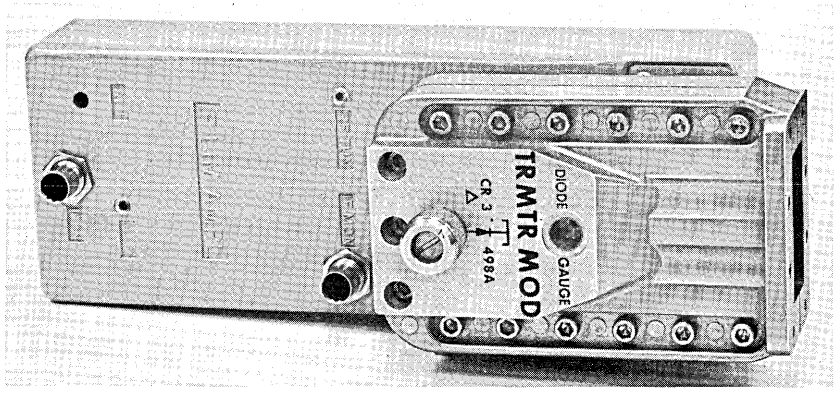

Fig. 7—Transmitter modulator.

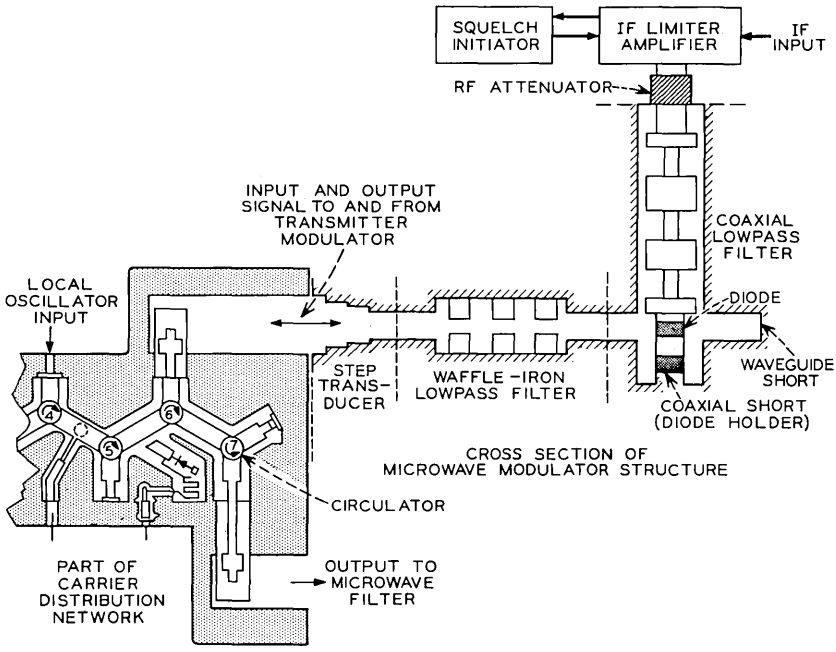

Fig. 8—Basic arrangement of transmitter modulator, IF limiter amplifier, and squelch initiator assembly.

The microwave structures of the two modulators differ only in the position of the waveguide and coaxial shorts and in the characteristic impedance of the coaxial lowpass filter which, in this case, was optimized to match the varactor diode. The WECo 498A varactor diode, rather than a varistor, is used in the transmitter modulator because of its greater upconversion efficiency. In addition, it was desirable to use the upper sideband exclusively for both maximum efficiency and stability, although, from a system viewpoint, it would have been more desirable to use both the upper and the lower sideband.

Referring to Fig. 8, the local oscillator signal is applied to an external carrier distribution network where it is routed to the input of the microwave structure by circulators 4, 5, and 6. The signal finally reaches the diode through the step transducer and waffle-iron lowpass filter. The 70-MHz modulated signal from the output of the IF limiter amplifier is applied to the diode through the coaxial lowpass filter. The waffle-iron structure presents a high impedance to the 70-MHz signal thus assuring efficient application of this signal to the

diode. Similarly, the coaxial lowpass filter presents a high impedance to the microwave signal thus assuring negligible absorption of RF power.

The mixing action of the diode generates frequencies of the type $nf_o \pm mf_i$.* The cavity in which the diode is situated, with its coaxial and waveguide shorts, reflects the RF modulated signal out through the waffle-iron lowpass structure and step transducer to the external carrier distribution network where it is routed to the external microwave filter by circulators 6 and 7. The desired upper sideband ($f_o + f_i$) is routed to the TWT amplifier via the selective microwave bandpass filter. The lower sideband along with other undesired 6-GHz signals ($f_o - f_i$, $f_o \pm 2f_i$, $\cdots$, $f_o \pm mf_i$) are reflected by the microwave filter and terminated by circulator 7 of the carrier distribution network. The harmonics of the 6-GHz signal ($nf_o \pm mf_i$) are restricted to the diode cavity by the waffle-iron and coaxial lowpass structures and are dissipated in the resistive components of the cavity. With the diode at zero bias, the diode cavity is resonated at approximately 5.7 GHz by the waveguide short and the coaxial short. Varying the diode bias from -1 to -4 volts varies the quiescent capacitance of the varactor diode and tunes the structure to any frequency between 5.9 and 6.4 GHz. The nominal local oscillator level is +18 dBm, and the 70-MHz IF level applied to the varactor diode varies from +3 dBM at the low end of the TH-3 frequency band to +5.7 dBm at the high end of the band. This level range was found necessary to reduce the modulator expansion (more than a 1-dB drop in output signal level for a 1-dB drop in local oscillator input level) to a minimum. The pump-to-output-signal loss is less than 9.0 dB. The IF-to-microwave transmission characteristic typically deviates less than 0.02 dB from the output filter characteristic within ± 15 MHz of the channel center frequency. The relative level of the various signal products appearing directly at the output of the transmitter modulator are shown in Fig. 9. The product at the frequency f_o + 70 MHz is the desired upper sideband which is selected by the microwave bandpass filter.

3.2 *The IF Limiter Amplifier*

The IF limiter amplifier is used to suppress the residual AM introduced by nonlinearities in various IF and microwave networks and active devices; it also provides the required IF drive level and dc

* Where f_o = local oscillator frequency, f_i = IF frequency, n = harmonics of f_o, and m = harmonics of f_i.

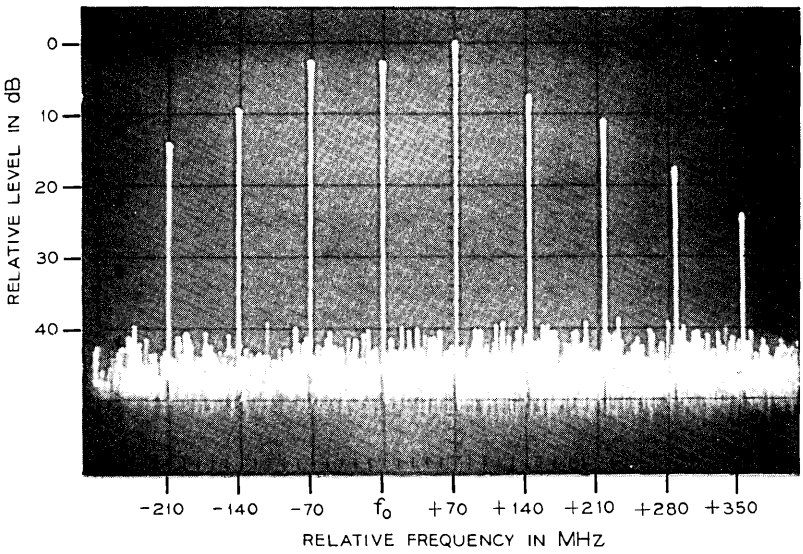

Fig. 9—Relative level of products at the output of the transmitter modulator.

bias for the modulator diode and a monitor signal to operate an external squelch initiator circuit. The IF limiter amplifier consists of a two-stage feedback amplifier at the input, a diode limiting section, and another feedback amplifier pair at the output to drive the varactor diode in the modulator microwave structure. As shown in Fig. 10, it utilizes series-shunt feedback pairs[3] as the basic gain stage for both the input and output amplifiers.

The two-stage input amplifier amplifies the −7-dBm IF input signal by approximately 10 dB. The resulting signal is then fed to the diode limiting section which consists of a series clipper limiter. The limiter was designed to provide a minimum of 20 dB of AM suppression while contributing less than 0.2 degree/dB AM-to-PM conversion. The diodes, CR1 and CR2, are 479A epitaxial silicon Schottky diodes used because of their low capacitance, fast reverse recovery time, and high back-to-forward resistance ratio.

The performance of the limiter is principally dependent upon the diode capacitance which is undesirable because it allows some signal transmission when the diodes are reverse biased. Because this leakage signal is 90 degrees out of phase with the signal transmitted through the diodes, it produces AM-to-PM conversion and degrades the AM suppression. To offset this effect, a balancing signal 180 degrees out

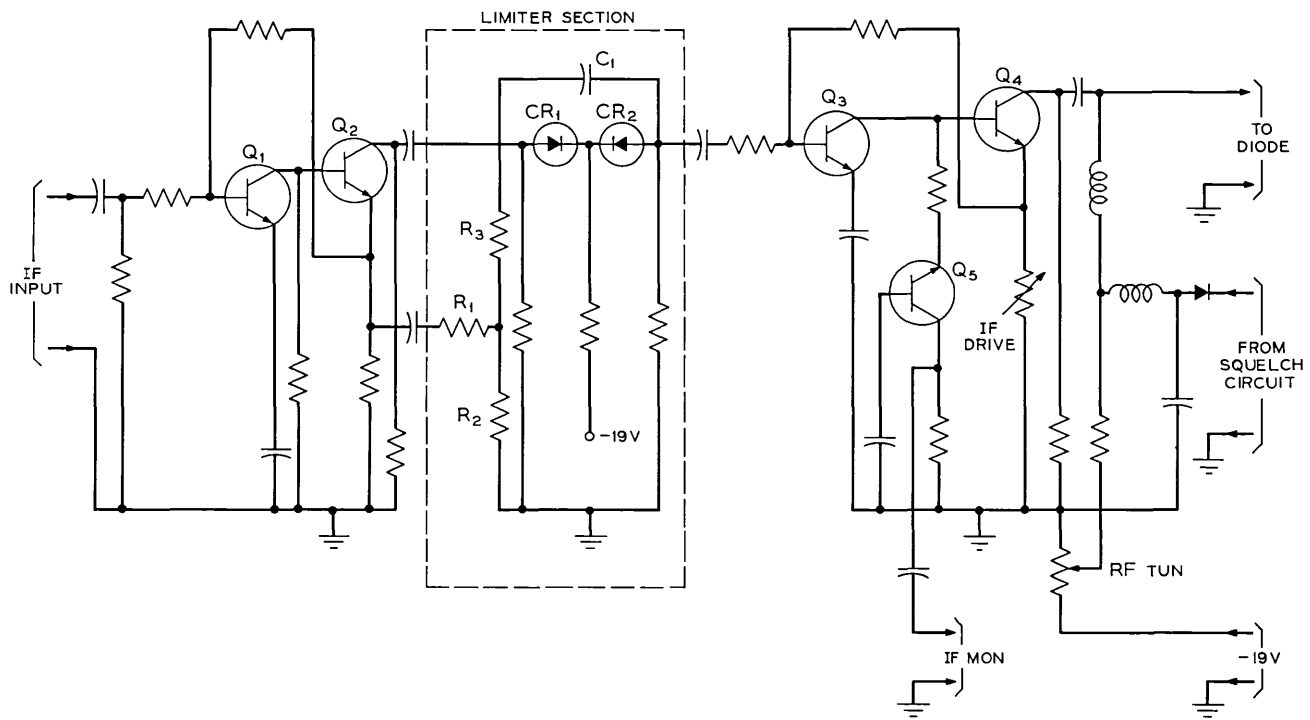

Fig. 10—IF limiter amplifier schematic.

of phase with the leakage signal is taken from the emitter of Q2 and ac-coupled to the resistor divider R1 and R2. These resistors were selected to determine both the ac gain of stage Q2 and the magnitude of the balancing signal. From this point the signal is fed to the output of the limiter through R3 and C1, the values of which were experimentally determined to obtain the desired 180 degrees phase difference. The loss of the 70-MHz signal through the limiter section is approximately 11 dB. The AM suppression and AM-to-PM conversion performance of the IF limiter amplifier are shown in Fig. 11. The output two-stage amplifier has from 10 to 14 dB of gain. The IF DRIVE control adjusts the gain of the output amplifier and is used to drive the modulator diode at the appropriate IF signal level. The RF TUN control is used to set the dc bias to the modulator diode.

The IF monitor delivers a sample of the output signal at approximately −14 dBm to the input of the external squelch initiator circuit. A common base stage provides isolation between the through-trans-

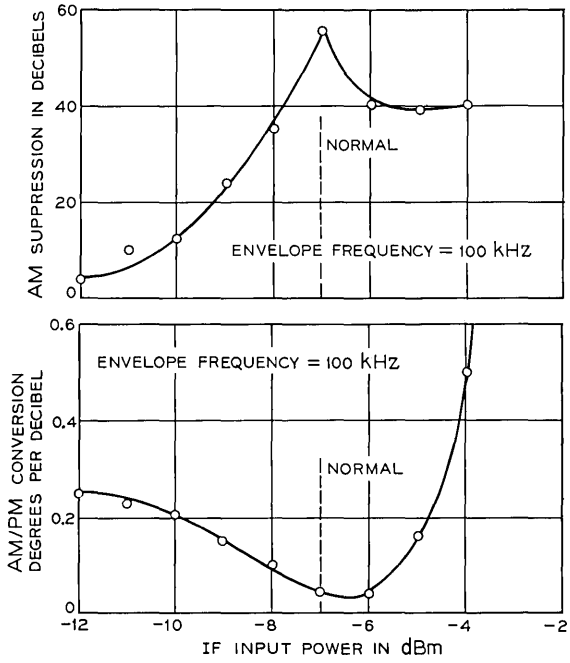

Fig. 11—Limiter AM suppression and AM/PM conversion versus input power.

mission path and the monitor circuit. An access lead is also provided to bias the modulator diode from the squelch initiator circuit.

The overall IF gain and noise figure of the limiter amplifier is approximately 9 to 13 dB and 16 dB respectively. Its transmission characteristic is designed to have a positive slope, typically 0.5 dB, over the 70 ± 15-MHz band.

3.3 *The Squelch Initiator*

The squelch initiator detects the noise level at the IF monitor point of the IF limiter amplifier. When the noise reaches a pre-selected threshold, this circuit generates a negative bias voltage which is fed back to the IF limiter amplifier and applied to the modulator diode.

This voltage is used to override the normal bias to the varactor diode resulting in a detuned diode cavity and a reduction of the microwave signal level at the output of the transmitter modulator, and thus at the output of the TWT amplifier. Figure 12 shows the squelch initiator unit housed in its aluminum casting.

Under normal operating conditions the 70-MHz IF signal from the IF MON jack of the IF limiter amplifier is applied to the input of the squelch initiator circuit at a level of −14 dBm. As shown in Fig. 13, the input signal is filtered by an 86-MHz bandpass filter which has a 3-dB bandwidth of about 2 MHz. The signal or noise appearing in this 2-MHz slot is amplified 73 dB by four series-shunt feedback pairs, each consisting of two high-frequency transistors.[3] The amplified noise is rectified and the resulting dc signal is used to trip a Schmitt trigger circuit. The output of the Schmitt trigger circuit controls the operation of a dc amplifier which provides a negative dc bias voltage for the modulator diode as well as for other alarm functions. The fading range or noise level required to trip the Schmitt trigger circuit is set by the TRIP control.

A 3-dB drop in transmitted signal level normally makes an external meter relay activate an output level alarm. However, when the drop in level is caused by the operation of the squelch circuit, most likely initiated by fading conditions or by a failure of a previous repeater,

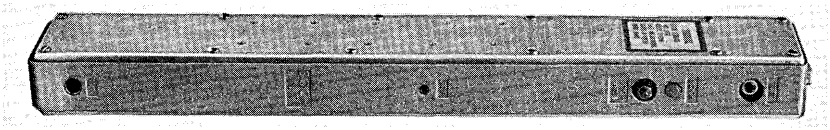

Fig. 12—Squelch initiator.

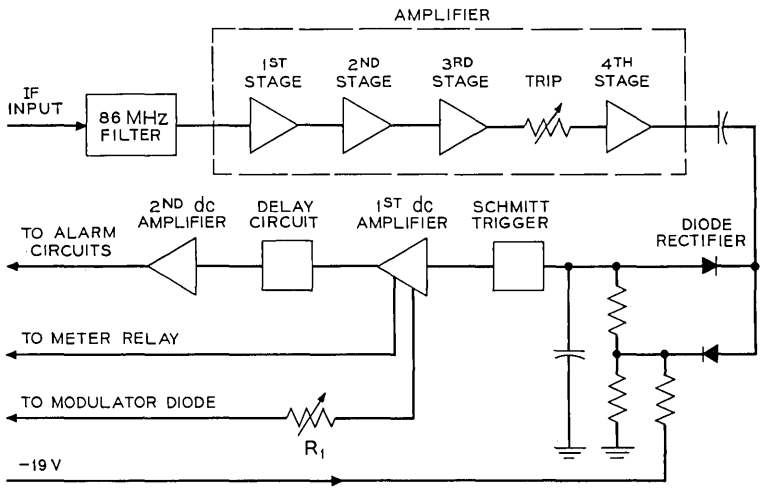

Fig. 13—Squelch initiator simplified schematic.

it is desirable to prevent the operation of the output alarm. This is accomplished by applying a dc bias voltage to the meter relay from the first dc amplifier. When the microwave carrier level is restored, the Schmitt trigger circuit automatically resets resulting in the removal of all dc voltages from the outputs of the dc amplifiers.

Variable resistor R1 is adjusted to provide the overriding bias required to cause a 29-dB drop in transmitted signal level.[2] The delay circuit and the following dc amplifier circuit activate an external alarm circuit 45 seconds after the application of the overriding bias voltage to the modulator diode.

IV. THE SHIFT MODULATOR

The shift modulator consists of an unbalanced microwave structure containing a varactor diode in a reduced-height microwave cavity. This unit is shown in Fig. 14. The unit is used to shift the frequency of a local oscillator microwave signal by ± 252 MHz. The upper or lower sideband output signal is used as the local oscillator signal for the receiver modulator. External circulators and microwave bandpass filters are used to apply the local oscillator signal, route the reflected output signal, and select the desired output sideband. The modulator microwave structure is designed to operate at a local oscillator signal level of +14 to +18.5 dBm and at a 252-MHz level of +6 dBm. This

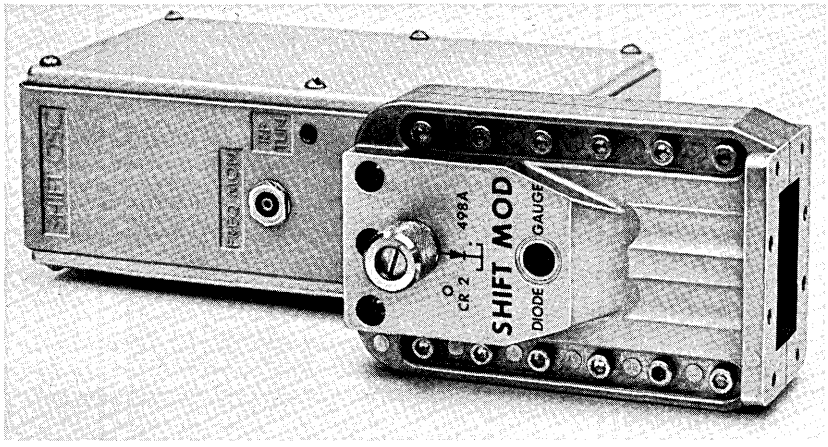

Fig. 14—Shift modulator.

modulator is tuned in the field by the use of a single adjustment which controls the bias applied to the varactor diode.

4.1 *The Microwave Structure*

The microwave structure and principle of operation of the shift modulator are identical to that of the transmitter modulator. As a result, the same structure with its associated diode and coaxial lowpass filter is used in both modulators. However, this structure was designed primarily to meet the more stringent electrical requirements of the transmitter modulator. The routing of the local oscillator signal to the input of the structure and the rerouting of its reflected output signal is accomplished in a manner similar to that illustrated by Fig. 8. Because the principle of operation and the microwave structure is the same in both modulators, the description which follows is kept more general than that given in Section III.

The 252-MHz shift signal from the shift oscillator is applied to the varactor diode through the coaxial lowpass filter. A portion of the local oscillator signal applied to an external carrier distribution network is routed by circulators within the network to the step transducer of the microwave structure. The signal then reaches the diode via the step transducer and waffle-iron lowpass filter. The mixing action of the diode generates two major signal sidebands, one 252 MHz above and one 252 MHz below the applied local oscillator signal, in addition

to other minor sidebands and harmonics of the applied signals. The upper and lower sideband signals are then reflected back out through the waffle-iron filter and step transducer and are routed to the microwave directional filter at the input of the receiver modulator by circulators within the carrier distribution network. The desired sideband, after being selected by the bandpass section of the directional filter, is used as the local oscillator signal for the receiver modulator, while the undesired sideband is reflected by the filter and terminated in a circulator within the carrier distribution network. The pump-to-output-signal loss is less than 9.0 dB.

4.2 *The Shift Oscillator*

The shift oscillator circuit generates a 252-MHz crystal-controlled signal used by the shift modulator to shift the common local oscillator microwave signal. As shown in Fig. 15, this circuit consists of a 126.0200-MHz oscillator, a frequency doubler, and a 252-MHz tuned amplifier.

The oscillator stage uses a seventh overtone crystal which operates at series resonance. The oscillator stability is within ±1 kHz from −10 to +140°F. The FREQ MON jack at the output of the oscillator is used to monitor the frequency while in service. Potentiometer R1, which controls the output level over a 6-dB range, is provided at the output of the multiplier stage. This control is used to set the drive to the varactor diode at +6 dBm. The level of the 252 ± 126-MHz harmonic signal at the output is typically 40 dB down from that of the 252-MHz output signal. Adjustable bias to the varactor diode is provided by the RF TUN potentiometer. A portion of the 252-MHz output level is rectified by diode D1 and used by an external meter circuit for in-service monitoring of the oscillator. As in the case of the transmitter modulator, the shift modulator has only one field adjustment, the RF TUN control, the other controls being factory adjustments.

V. ACKNOWLEDGMENTS

The development of the TH-3 modulators was made possible by the combined effort of many individuals. Specifically, the author wishes to acknowledge the contribution of A. E. Dethlefsen for the initial development of the transmitter and shift modulator microwave structure, F. M. Klisch for the initial development of the receiver modulator microwave structure, D. A. Clark for his early work on the shift oscillator circuit design, G. H. Lentz for the squelch initiator circuit

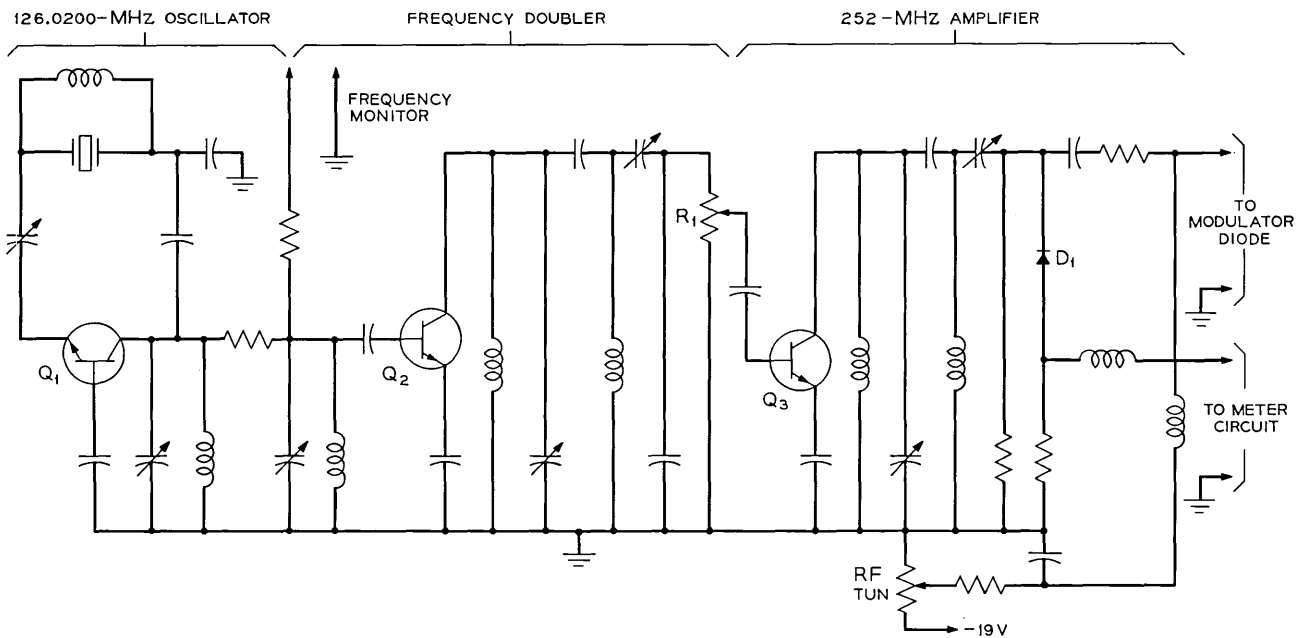

Fig. 15—Shift oscillator schematic.

design, and S. H. Lee for the design of the IF limiter amplifier and IF preamplifier circuits.

REFERENCES

1. Abele, T. A., Alberts, A. J., Ren, C. L., and Tuchen, G. A., "Schottky Barrier Receiver Modulator," B.S.T.J., *47*, No. 7 (September 1968), pp. 1257–1287.
2. Jansen, R. M., and Prime, R. C., "TH-3 Microwave Radio System: System Considerations," B.S.T.J., this issue, pp. 2085–2116.
3. Fenderson, G. L., "TH-3 Microwave Radio System: The IF Main Amplifier," B.S.T.J., this issue, pp. 2195–2204.

THE BELL SYSTEM TECHNICAL JOURNAL
Vol. 50, No. 7, September, 1971
Printed in U.S.A.

TH-3 Microwave Radio System:

Microwave Integrated Circuits

By N. R. DIETRICH

(Manuscript received December 18, 1970)

Microwave integrated circuits have been employed in the Bell System for the first time in the TH-3 radio system. These circuits, using strip transmission lines, provide numerous functions previously achieved with assemblies of individual waveguide components. By utilizing the modern technologies of photolithography, precision die casting, ceramic processing, and tantalum-gold thin films, these circuits provide advantages in size, fabrication, bay "layout," performance, and cost.

I. INTRODUCTION

A series of four high-performance, functionally integrated, microwave circuits has been developed for use in the 6-GHz TH-3 radio system. The circuit designs integrate numerous microwave functions, operating mostly in a strip transmission line medium, into single packages. They replace assemblies of numerous waveguide components used in the design of earlier radio relay systems. The ability to design each function for its specific application and match it to its neighbor allows high performance standards. The resulting reduction in interconnections improves the reliability. Considerable space and cost saving is realized since many common mechanical requirements are satisfied by the same housing. The housings, made of aluminum, are die cast which accounts for a considerable portion of the cost saving. The stripline center conductor and thin film resistors are created by photochemical techniques from a tantalum and gold film. The use of ceramic substrates and thin film technology is important to the achievement of long-term reliability. The inherent precision and low cost of these techniques provide dimensional control and reproducibility and contribute to the overall cost saving.

The circuits, three of which are used in each TH-3 radio bay, are

introduced in a preceding paper[1] by A. Hamori and R. M. Jensen. There are two versions of the carrier distribution circuit. One is for use in a repeater station bay, the other for use in a main station bay. Generally, they perform in the same way in that they distribute microwave carrier power, and provide input and output access to the modulators. Monitoring, testing, and isolation features are included at several points throughout the circuits. The traveling-wave tube input and output circuits operate in the modulated signal path. They provide low transmission loss with negligible slope, high isolation, monitoring, testing, attenuating, filtering, and tuning features within their respective packages. Figures 1 and 2 are photographs of the repeater station carrier distribution circuit and the traveling-wave tube input circuit, schematic drawings are given in Section IV.

Many of the functions integrated into the four circuits are created around one or more circulators as the basic element. A total of seven circulators is included in the repeater station version of the carrier distribution circuit, while the main station version includes six circulators. The traveling-wave tube input and output circuits have two circulators each. All circuits incorporate the necessary transitions between stripline and the transmission modes of the various connecting components. These involve coaxial, waveguide, reduced-height waveguide, and dc connections.

The normal ambient temperature ranges over which the circuits perform are: 80 ± 20°F for the carrier distribution circuits, 90 ± 20°F for the traveling-wave tube input circuit, and 95 ± 20°F for the traveling-wave tube output circuit. The elevated ambient around the TWT circuits is due to the power dissipation of the TWT power amplifier.

II. CIRCUIT DESIGN

2.1 *Circulator and Stripline*

Figures 3a and b show a cross-section view and a top view of the circulator and stripline. The typical circulator admittance as a function of frequency is shown in Fig. 3c. The ground plane spacing is 0.125 inch. A 99.5-percent-pure alumina substrate, 0.024 inch thick, is suspended centrally between the ground planes. The center conductor pattern located on one surface of the substrate is nominally 0.0003 inch thick, about 10 skin depths at 6000 MHz. Since the medium is not homogeneous,[2] the energy does not propagate purely in a TEM mode. There are field components in the direction of

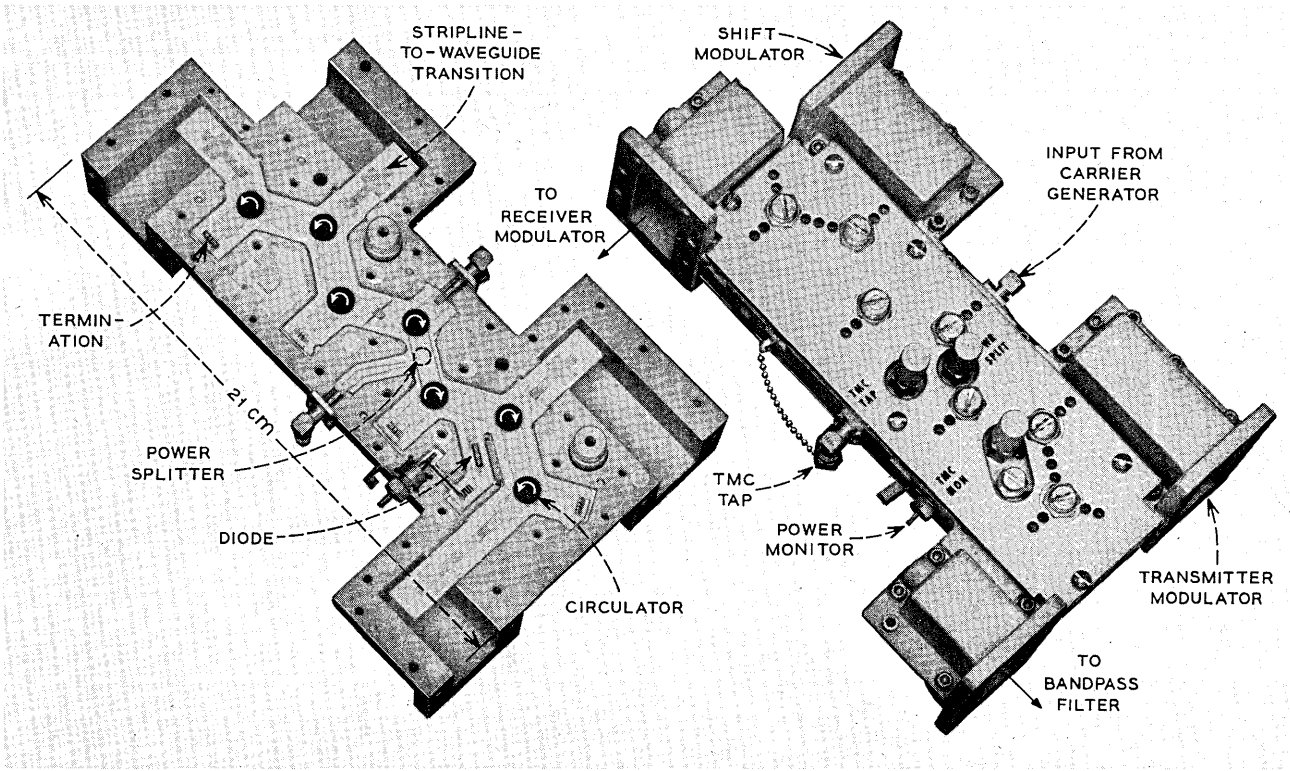

Fig. 1—Open and closed views of the repeater station carrier distribution circuit.

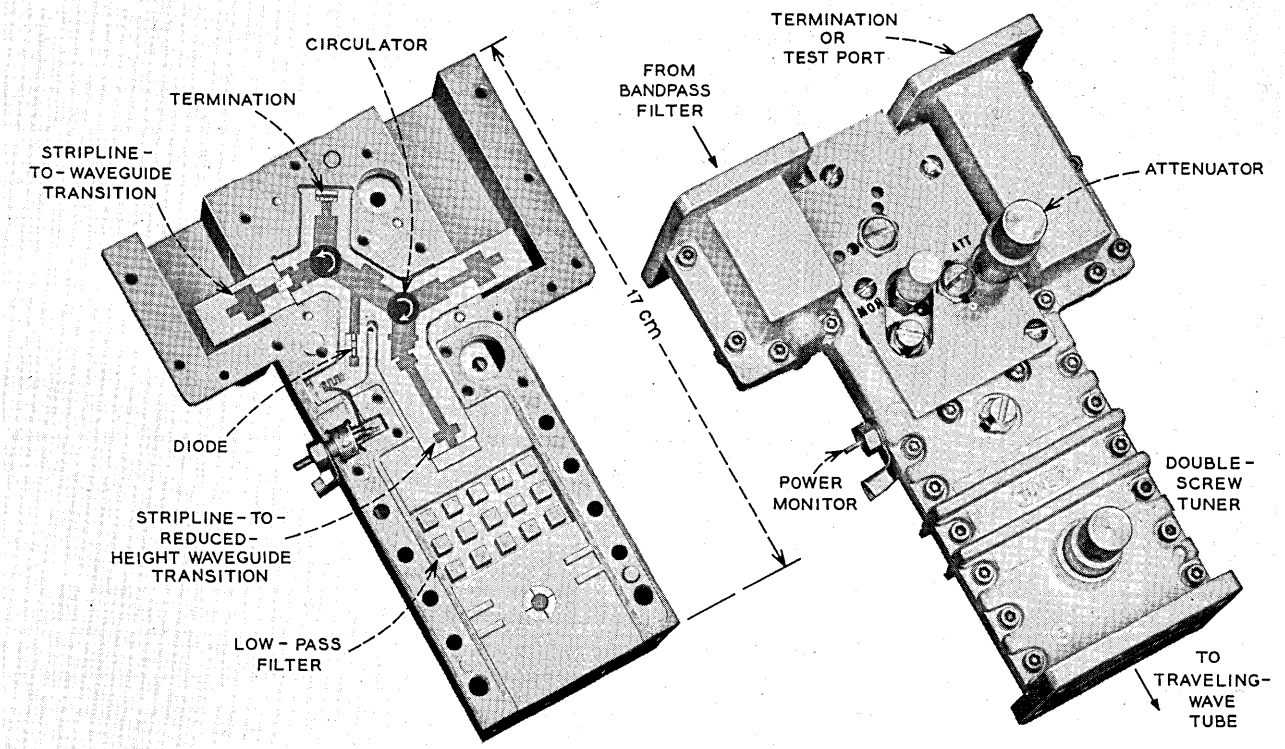

Fig. 2—Open and closed views of the traveling-wave tube input circuit.

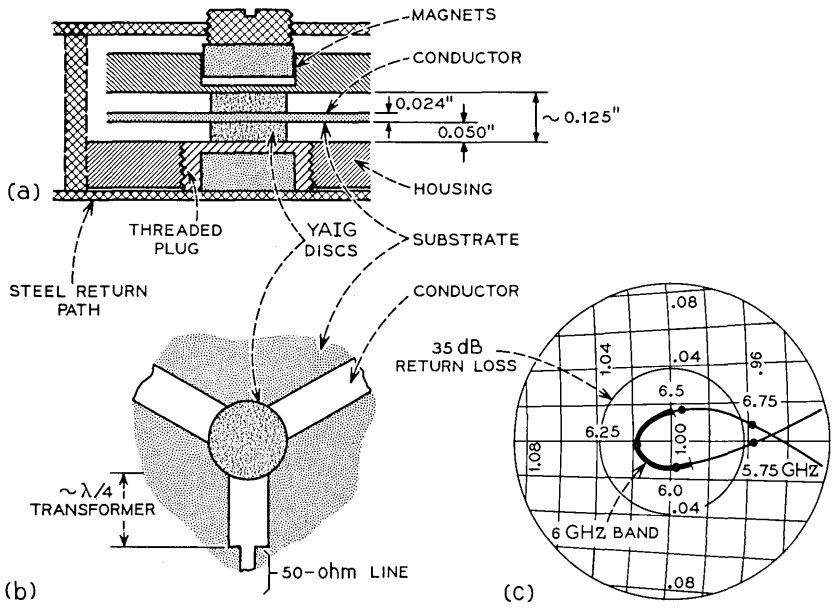

Fig. 3—6-GHz circulator design. (a) Cross-section view (b) Top view of circulator junction. (c) Typical tuned circulator admittance (Smith chart).

propagation. Hence, the medium is dispersive and the propagation constant is a function of frequency and dimensions. This effect, however, is extremely small and may be ignored for practical purposes, and a TEM mode is assumed. The center conductor width required for a characteristic impedance of 50 ohms at 6000 MHz is 0.114 inch. The effective dielectric constant resulting from the presence of the high-dielectric alumina ($\epsilon_r \approx 9.5$) in a small portion of the field region is approximately 1.7 for a 50-ohm line.

The substrate is supported midway between the ground planes by discs of aluminum substituted yttrium iron garnet 0.050 inch thick bonded to both sides of the substrate. The two 0.050-inch-thick discs, plus the 0.024-inch-thick substrate, 0.0003-inch-thick conductor, and two bonds of 0.0002 inch each, stack up to nearly the ground plane spacing. The small difference and the variations due to mechanical tolerances are taken up by tightening a threaded plug located in one ground plane at each circulator junction. Each plug is adjusted individually to contact the circulator discs, thus assuring that no air gap exists. An air gap as small as one thousandth of an inch would change

the impedance of the circulator junction and seriously affect the performance. The dimensions of the discs are adjusted to create a resonant junction at the frequency band of interest. The center conductor pattern on the substrate includes quarter-wave transformers to provide suitable impedance matches into the resonant junction.

The junction impedance is approximately 15 ohms. A quarter-wave impedance transformer of 28 ohms transforms the junction impedance to 50 ohms. Each of the functions included in the integrated circuits was developed individually in its own structure and matched to 50 ohms. After integration the performance is optimized by further tailoring the design to improve interface matches between neighbors. The transformer impedance and length are intentionally chosen to be incorrect for an optimum impedance match. This allows for the incorporation of tuning screws into the matching scheme where performance demands are high. Since mechanical tolerances and ferrimagnetic material properties are difficult and expensive to control to the degree required for consistently high circulator performance, two tuning screws may provide orthogonal fine tuning of the circulator admittance trace so that it may be tuned to the center of the Smith chart. One screw, the ratio screw, effectively changes the transformer admittance and provides fine tuning along the conductance axis. The other screw, the length screw, adjusts the effective length of the transformer and provides tuning along the susceptance coordinate. When such fine tuning is not required, the screws are not included and a correction is made in the center conductor geometry.

The YAIG material upon which the circulator design is based has a saturation magnetization ($4\pi M_s$) of 1160 gauss. This material, which is used in other system components, meets the criteria for avoiding low field losses. The 1300-oersted magnetic biasing field is provided by a pair of barium ferrite permanent magnets at each circulator junction. A threaded screw moves one of the magnets to open or close the air gap in the magnetic circuit and provide tunability for the magnetic flux density at the circulator junction. Tunability is required since the permanent magnet nonuniformity can be 10 percent. There are also variations due to mechanical tolerances and ferrimagnetic materials properties. Each circulator is functionally tuned for best operation by adjusting the magnetic field tuning screw.

A study was made of the temperature dependence of the circulator performance. Generally, the circulator performance degrades at the extremes of the $\pm 20°$F operating temperature range. The degradation is primarily due to changes in the biasing field produced by the perma-

nent magnets. Rather than compensate the magnetic circuit to eliminate the degradation, a margin of performance was added to the room temperature performance objectives. Where isolators and impedance matches are involved, the performance objective was 30 dB reverse loss, or 30 dB return loss per circulator. In order to provide some additional margin to allow for degraded performance over the range of operating temperatures and manufacturing tolerances, the design objective was set at 35–40 dB per circulator. Forward transmission loss is approximately 0.1 dB per pass.

2.2 *Isolator*

The isolation function included in all four circuits is obtained by terminating one arm of a circulator with a thin film resistor in the manner shown in Fig. 4a. The terminating resistor is fabricated by photo-chemical techniques from a film of tantalum nitride. The resistive film is essentially a short section of high-loss transmission

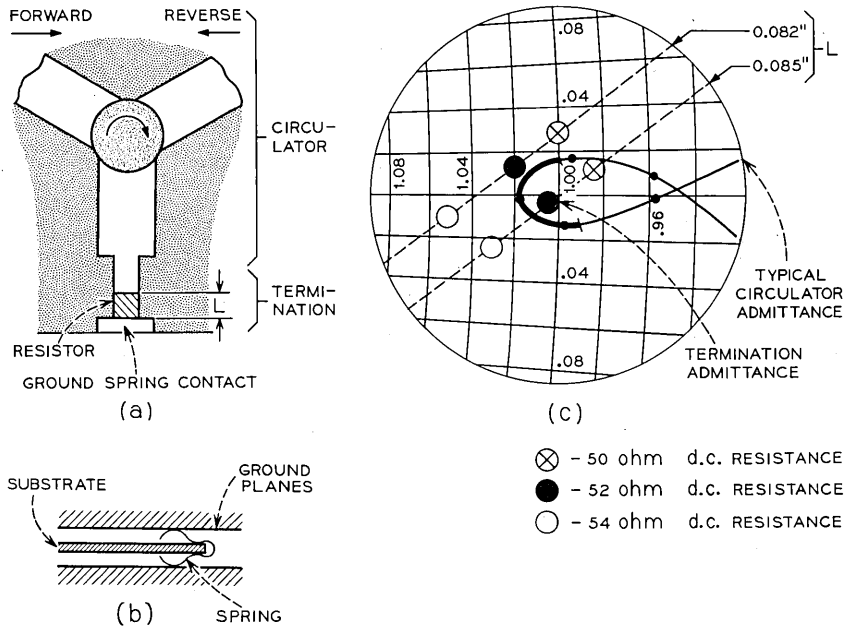

Fig. 4—6-GHz isolator design. (a) Top view of isolator without termination grounding spring. (b) Cross-section view of termination grounding spring. (c) Admittance characteristics of circulator and terminating resistor. The spot size represents the range of admittance variation over the 6-GHz frequency band for each resistor length and dc resistance value indicated.

line. It is connected to the housing through a metal spring clip which slips over the edge of the substrate and contacts a conductor island and the ground planes simultaneously, as shown in Fig. 4b. Thus, each terminating resistor is located close to an edge of the substrate. Various lengths and dc resistances of the resistor were studied. A resistor having a length of 0.085 inch and dc resistance of 52 ohms was chosen as the best termination. This result was based upon the position of the admittance trace on the 1/50 mho admittance chart as shown in Fig. 4c. The spot size represents the range of admittance variation over the 5925–6425-MHz frequency band for the indicated lengths and resistances. Also shown is the typical circulator admittance. It is desired that these two admittances be complex conjugates. The greatest deviation from this relationship is equal to a 0.02 difference in VSWR. This predicts a return loss, and a corresponding reverse loss, for the isolator of 40 dB. The reverse loss of an isolator is determined by the admittance match at the circulator-termination interface. Actual performance of single-stage isolators of this type is: reverse loss consistently in excess of 35 dB and forward loss approximately 0.1 dB.

The power dissipation in the resistor should be limited to 0.5 watt for short time periods and 0.1 watt for extended or continuous periods. These limitations are based on the permanent change in resistance due to elevated temperatures. Tests[3] on resistors show that for 0.1-watt continuous power dissipation, or 10 watts per square inch of film, the change in resistance should be less than 1.0 percent after 20 years. Generally, the limitation on power dissipation is of concern only in the TWT output circuit. Here the signal has been amplified to a power of 10 watts and, should the output of the circuit be severely mismatched, excessive power could be dissipated in the termination of the output isolator.

2.3 *Power Splitter*

The power splitting function[4] used in the repeater station carrier distribution circuit to divide the transmitter microwave carrier (TMC) between the shift modulator and transmitter modulator is shown schematically in Fig. 5a. A tuning screw is located at the common arm junction between two circulators. Various amounts of shunt capacitance may be added to the otherwise matched transmission line by adjusting the screw. Mismatches approaching a short circuit (1–2 dB return loss) can be achieved causing significant portions of the incident power to be reflected. The reflected power is circulated to

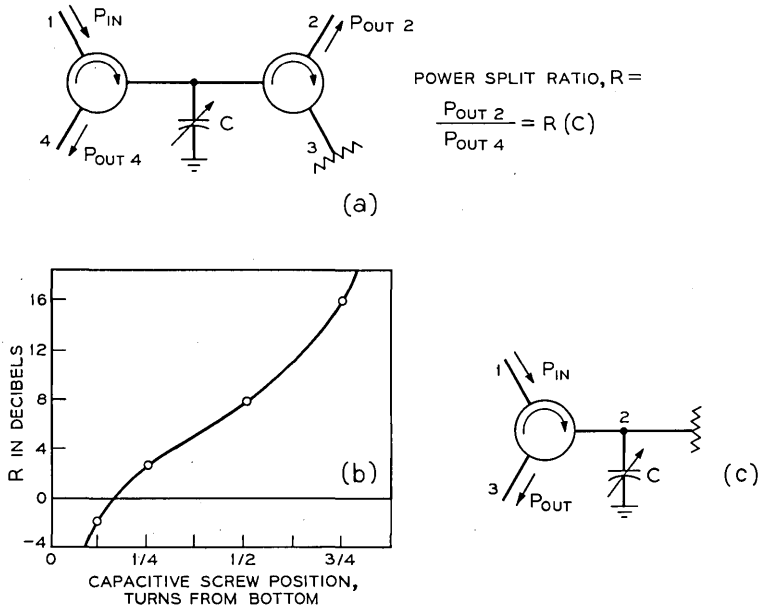

Fig. 5—Variable power splitter and attenuator. (a) Power splitter circuit. (b) Power split ratio vs capacitive screw position. (c) Transmission type attenuator circuit, adjustable from 5 to 30 dB.

port 4, and the power transmitted past the mismatch goes to port 2. Hence, the input power is divided. Note that the input and output impedance matches are not dependent upon the power dividing mismatch. Figure 5b shows the variation of the ratio of the divided powers as a function of the screw position for a frequency in the center of the band.

If the tuning screw reactance is assumed to be purely capacitive and is located at a point on the common arm junction, it is clear that the mismatch will be a function of frequency. The capacitive reactance varies inversely with frequency; hence, the power division ratio will vary as a function of frequency across the 6-GHz band. The ratio varies by 1 dB or more.

2.4 *Attenuator*

Variable attenuation functions are included in the circuits at three places. Each is of slightly different construction in order to satisfy the requirements of the particular application. However, they are similar in operation. The attenuator is created by combining a power

splitter and a terminating resistor–as shown in Fig. 5c. A circulator-mismatch combination divides the incident power as previously described and a terminating resistor is added to dissipate either the transmitted or reflected portion of the power. The transmission type (port 2 terminated) shown in Fig. 5c is more suitable where high ranges of attenuation are required, e.g., 5–30 dB. The reflection type (port 3 terminated) is more suitable for low ranges of attenuation, e.g., 0–5 dB. The attenuator included in the traveling-wave tube input circuit (see Section IV) is somewhat different from these two. It is basically a transmission type. However, it is specially constructed to work in a low attenuation range. Since the circuit is operating in the modulated signal path, the attenuator loss must be relatively insensitive to frequency and it also must be capable of a very low minimum attenuation, 0.1 dB or less. Further, its location in the system makes it a desirable point at which to inject or detect test signals during bay testing. Therefore, the termination is an external, removable, waveguide termination rather than a thin film termination. Removal of the waveguide termination makes the port available for testing, provided the mismatching element of the attenuator can be removed or minimized. A coaxial tuning screw was used. It consists of a metal cylinder sliding inside an axial hole in a metal screw body. The two are separated by a dielectric sleeve several thousandths of an inch thick. The cylinder contacts the center conductor and is spring-loaded to protrude from the screw body. As the screw body is turned, the overlap of the two elements varies to change the area of the coupling capacitance. The close spacing and large areas possible with this design allow a greater range of capacitance variation than that available from the limited area and larger spacing of a plane screw body as used in the power splitter. Two mechanical stops are included in the construction of the screw. When the screw is set fully clockwise the capacitance is high ($\approx$ 50 pF) and the return loss is approximately 0.1 dB. When the screw is set fully counterclockwise the capacitance is reduced to the value necessary to create greater than 20 dB return loss. Hence, the attenuator has a continuous adjustment range from 0.1 dB to 20 dB. The loss slope is less than 0.1 dB across the 5925–6425-MHz frequency band in the low attenuation range. The screw is housed in a collet type locking screw so that it may be locked in position, or adjusted against mechanical drag.

2.5 *Power Monitoring*

Power monitoring features are included at several points throughout the circuits. The power on the main signal path is sampled and

detected. The current output from the detector is indicated on a panel meter where it may be visually monitored for changes. In some cases, alarm circuits indicate failure of some critical component of the system if the current drops below a specified amount.

Generally, sampling is achieved by placing a transmission line close to the main signal path and capacitively coupling a small amount of power to the line. Different sizes of coupling gaps are used depending on the power on the main signal path. A large-diameter tuning screw is located near the coupling gap to allow fine adjustment of the coupling.

The sampled signal is detected by a point contact silicon diode. The operating current for the meter monitor is 14 microamperes into a 6000-ohm load. For the cases where alarm circuits are used the current is 50 microamperes into 1100 ohms. The diode sensitivity is such that these currents are achieved with −6 dBm and 0 dBm of incident power, respectively. Adequate sensitivity is important since the power coupled from the main signal path to the diode may increase the transmission loss through the integrated circuit along the main signal path.

2.6 *Transmitter Microwave Carrier Tap*

A test set used to measure the FM noise figure of the receiver requires a carrier signal to drive its modulator at the same frequency as the transmitter microwave carrier. This signal is provided by the TMC tap, thus eliminating the need for an additional signal generator at each station. A sample of the TMC, approximately +10 dBm, is available at a miniature coaxial connector, which is essentially an open circuit when not in use. The access port is decoupled from the main signal path by nominally 10.7 dB. The coupling is adjustable, and may be set and locked at the desired level during operation.

Since a decoupling of approximately 10 dB is desired, the TMC power must be divided at the coupling junction such that one-tenth the power is coupled to the TMC tap. The impedance looking toward the tap should be approximately 10 times that of the main signal path. Two quarter-wave transformers are used to transform the 50-ohm connecting cable impedance to 500 ohms at the coupling junction while assuring that during periods when the test signal is not utilized, the open circuit of the connector is transformed to the coupling junction as an open circuit. Calculations show that the impedances of the two sections need only be in the proper ratio to achieve the desired coupling. Characteristic impedances of 25 and 75 ohms were

chosen, as these are readily producible. A tuning screw midway along one section provides adjustability of the coupling.

2.7 *Low-Pass Filter and Double-Screw Tuner*

A low-pass filter and double-screw tuner are included in the reduced-height waveguide section of the traveling-wave tube input and output circuits. The filter and the two irises for the tuner can be cast into the housing at little additional cost.

2.8 *Connectors and Transducers*

In addition to the previously mentioned functions, the circuits provide coaxial-to-stripline, waveguide-to-stripline, and reduced-height waveguide-to-stripline transitions that allow interconnection of the integrated circuits with other components in the radio bay.

The coaxial-to-stripline transitions are created by simply providing a mechanical interface since no transmission mode conversion is necessary. To provide the mechanical interface, the center conductor of the miniature connector is extended, by means of a pin, through a bore in the housing. The bore is dimensioned so that it forms a 50-ohm air line with the extending pin. The end of the pin is flattened so that it may be overlapped onto the conductor on the substrate and soldered in position. Greater than 20 dB return loss, which is adequate for the application, is achieved in this manner.

A waveguide-to-stripline transition[5] was developed having greater than 30 dB return loss over the 6-GHz band. The substrate and center conductor are extended through a channel to the broad wall of the waveguide. This extension has a characteristic impedance of 50 ohms. The channel ends at the waveguide wall but the substrate and conductor continue into the waveguide to form an E-field coupling probe as shown in Fig. 6a. The conductor pattern and probe position were varied to optimize experimentally the impedance match relative to a 50-ohm standard. After the incorporation of the transition into the integrated circuits, minor modifications were made to improve the complex conjugate impedance match between the transition and a circulator. Figure 6b shows the typical waveguide port admittance trace obtained from this combination. A special version of this design is used for the bandpass filter port on both carrier distribution circuits. An extra half wavelength of 50-ohm line is included between the circulator and the waveguide. This increases the physical separation between the BPF port and the transmitter modulator port and provides space for the connecting components.

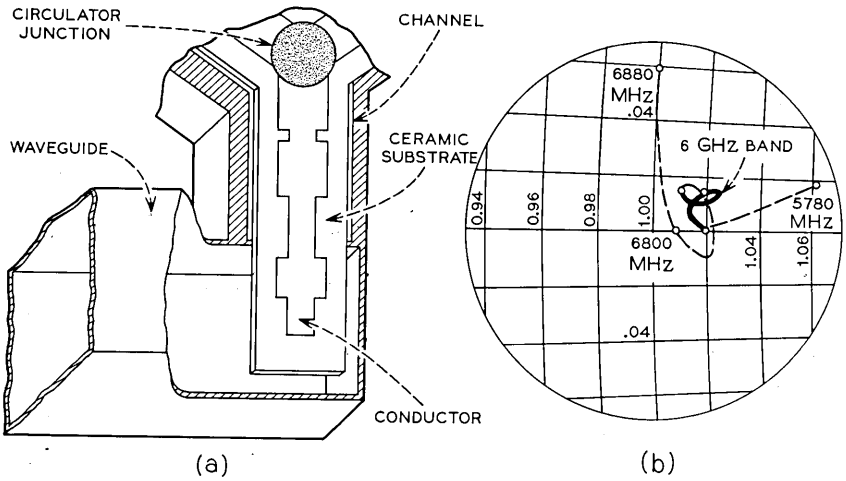

Fig. 6—Stripline-to-waveguide transition. (a) Cut-away view of transition integrated with circulator. (b) Typical waveguide port admittance.

A reduced-height waveguide-to-stripline transition was developed for use in the TWT input and output circuits. In a manner similar to the full-height design, the substrate is extended into the waveguide. However, the substrate enters through the end wall of the guide as shown in Fig. 7. The conductor is shorted to the broad wall to form an H-field coupling loop. The transition has return loss capability of greater than 30 dB.

III. CIRCUIT FABRICATION

3.1 *Substrates*

The substrate material is 99.5-percent-pure aluminum oxide. It is specially processed to a fine grain size before firing. The material was chosen for its low loss tangent and compatibility with processing methods. The fine grain structure allows a finer surface finish to be achieved. A surface finish of 16 microinches, or better, is desirable in order to control the sheet resistivity of the sputtered tantalum nitride film. Excessive surface roughness results in a higher resistivity than expected. For the generation of precision microwave terminating resistors, the objective is usually a low value of resistivity to allow subsequent anodic trimming to the desired resistance.

The shape of the substrates is quite irregular as shown in the photo-

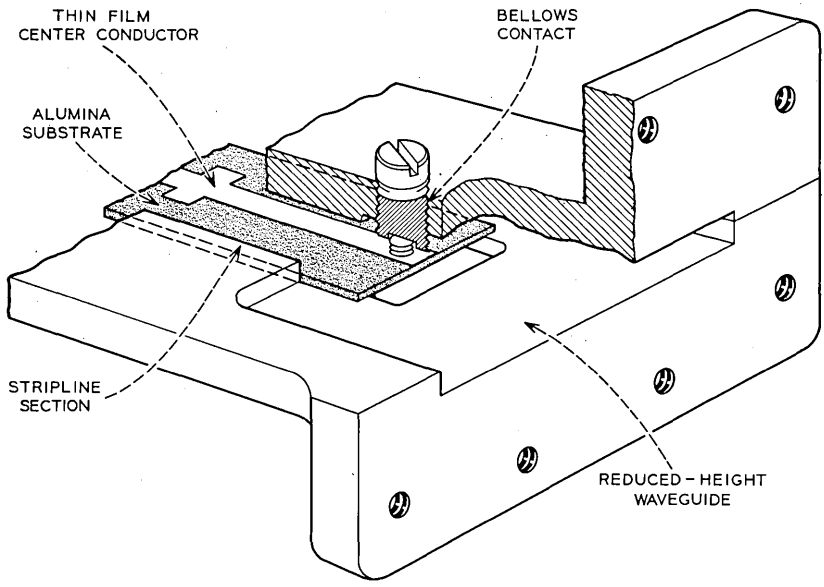

Fig. 7—Stripline-to-reduced-height waveguide transition for interconnection to the traveling-wave tube.

graphs, Figs. 1 and 2. Initially, the center conductor patterns were created on simple rectangular substrates which were placed into housings having large open rectangular areas. This approach was successful in other microwave integrated circuit designs[4,6] at lower frequencies. However, at 6000 MHz, and where isolations as high as 68 dB between ports are required, considerable difficulty was encountered. In this case, the dimensions of the open areas within the housing were large enough to support the propagation of energy through waveguide type modes. This provided shunt paths around the isolators. Consequently, isolations between ports in excess of 40 to 50 dB were not possible. To eliminate this problem, the metal walls in the housings were moved closer to the center conductor pattern to create a channel suitable for the TEM stripline mode, but below the cutoff dimension for the waveguide modes. Channel widths of 0.570 inch were used. Isolations between ports in excess of 80 dB were observed with this configuration. A second consideration also becomes important in the determination of the substrate shape. With the metal housing walls moved closer to the center conductor as described, the dimension of the open areas near the circuit junctions was close to a resonant

dimension in some cases. This allowed cavity type modes to be sustained, affecting couplings, transmission losses, etc. Additional relocation of the metal walls in the troublesome areas shifted the resonant frequencies of these modes out of the band of interest. These two considerations resulted in complex substrate and housing-channel geometries.

In spite of the irregular shape the ceramics industry is capable of supplying finished substrates at a reasonable cost. The shape is die cut from a ribbon of "green" ceramic near the finished thickness. All dimensions are oversize to allow for shrinkage during the firing process. After firing, the substrates are ground to the required thickness and surface finish. Several outside edges of the substrates are also ground to dimension so that they may subsequently be used as referencing edges for registering the pattern relative to the housing.

There are several practical considerations that limit the maximum substrate dimension to approximately four inches. The photographic process capability used in creating the pattern masks is limited to four inches. Also, the substrate manufacturer has similar limitations on size due to process capability and breakage due to handling. Breakage during pattern creation must also be considered. Hence, the conductor patterns are divided into sections, each on its own substrate. The substrate conductor patterns are interconnected with solder-clad ribbon, using solder reflow techniques, at assembly into the housing.

3.2 *Conductor Pattern*

The stripline center conductor geometry is a primary performance-influencing parameter. The width and thickness of the conductor pattern determine the impedance of a transmission line when it is suspended in a medium between two fixed ground planes. Since impedance matching between the various functions is crucial to functional integration, it is essential to control these factors for accuracy and reproducibility. Various linewidths between 0.010 and 0.270 inch are used. These are produced within approximately two-mil tolerances. The photo-chemical techniques lend themselves well to provide the necessary dimensional control at low cost. A suitably cleaned substrate receives several layers of sputtered or evaporated materials. These include: tantalum nitride subsequently used to create the necessary resistors, titanium to provide adherence for following films, palladium[7] to insure long-term adherence of the conductor layers, and gold to prevent oxidation and provide a conductive surface which can subsequently be electroplated to greater thickness.

The conductor pattern and resistor areas are generated from a substrate prepared as described. The undesired materials are selectively etched away using the appropriate photo-chemical techniques. The materials left form the conductor and resistor patterns. The patterns are registered on the substrate by including referencing marks on precision masks to align with the previously mentioned reference edges of the substrates. These reference edges are subsequently positioned against corresponding edges in the housing at assembly to provide proper registration between pattern and housing. The conductor pattern is electroplated with a heavy layer of copper followed by a gold flash to a total thickness of approximately 0.3 mil. The final gold flash prevents oxidation of the conductor surface. The resistor areas are thermally stabilized and trim anodized to proper value at the appropriate stage of processing. The transmission line terminating resistors are 52 ohms. Current limiting resistors in the diode monitor circuits are 1000 ohms.

3.3 *Patterned Substrate Assembly*

The patterned substrate has numerous additional parts added to it before it is ready for assembly into a housing. Circulator discs are bonded to each side of the substrate at each circulator conductor junction. The discs are optically located concentric to the geometric center of the pattern. The center is identified by a cross-hair index mark which is generated along with the pattern. The cross hairs are included in the precision mask which is cut at ten times oversize and reduced to minimize variations due to cutting tolerances. The discs are cemented in position. A fixture is used to align the disc on the unpatterned side of the substrate. At assembly, the brass plug in the housing is turned down against the disc-substrate assembly, placing the stack in compression.

3.4 *Housings*

A precision machined, hardened steel die is used to cast aluminum housings in large quantities to finished dimensions. Where tolerances are tight, or where surfaces must be carefully mated, machining stock is provided for finish cuts with machine tools. Many holes and bores are cast into the housing. Additional reaming and tapping of holes is also required. A small draft is necessary to facilitate release of the part from the die. The effects of this draft and any dimensional variations were determined. These required compensation by changes in the center conductor pattern dimensions or by modifications in the steel

die. This was particularly effective in the area of the waveguide transitions where the location of the probe conductor relative to the waveguide walls is critical. Aluminum housings can be made available in production quantities by the casting and finish machining approach at a fraction of the cost of equivalent machined housings.

Due to the similarity between the repeater station version and main station version of the carrier distribution circuit, the same cast housing is used. Slight machining variations, e.g., the size and location of some holes, and the removal of one waveguide port make the one casting suitable for both circuits. Similarly, a single casting serves for both the traveling-wave tube input and output circuits with minor machining variations. The RF leakage power outside the housing was measured for a large number of assembled circuits. The leakage power was consistently low enough to avoid the generation of interfering tones due to multiple leakage paths within a bay.

IV. CIRCUIT PERFORMANCE

The performance requirements for each circuit are determined by system needs and device capabilities. The isolation requirements are derived from the carrier-to-interference ratio objectives established for the radio bay. Transmission loss is minimized to that which the design is capable of meeting. Any additional loss adds to the microwave generator power output requirements. Impedance match requirements are based on the allowable ripple amplitudes and mismatch losses.

Specific performance requirements for the circuits are discussed in a preceding paper[1] by A. Hamori and R. M. Jensen. The performance of two of the integrated circuits will be described to show the performance capability achieved. Figure 8 lists the important room temperature performance limits over the frequency band of 5925–6425 MHz for a repeater station carrier distribution circuit. Figure 9 shows the traveling-wave tube input circuit.

The realization of some of the isolations is through combinations of isolators and common arm matches. For example, in Fig. 8 the isolation from port 7 to port 1 is due to the impedance match on the common arm between circulators "A" and "B" and the isolator at position "C." Any power reflected from the common arm match passes through circulator "B" to circulators "C" and "D" to port 1. Portions of the modulated signal power returning from the transmitter modulator at port 2 may be reflected from the common arm junction between circu-

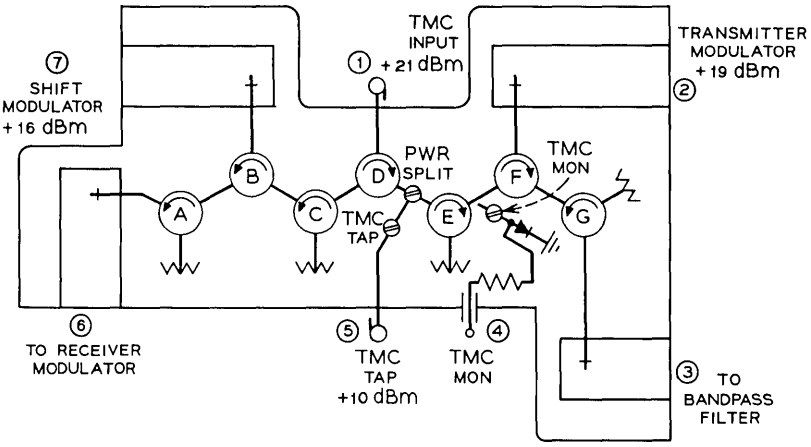

IMPEDANCE MATCHES		ISOLATIONS AND LOSSES		
PORT	RETURN LOSS (MIN. dB)	FROM PORT	TO PORT	dB
1	23	2	7	60 MIN.
2	30	6	1	68 MIN.
3	32	7	1	68 MIN.
6	28	1	2	3 MAX.
7	28	2	3	0.5 MAX.
		7	6	0.5 MAX.

ADJUSTMENTS

PWR SPLIT – SET FOR +3 dB POWER AT PORT 2 RELATIVE TO PORT 7.
TMC TAP – SET FOR –11 dB PORT 5 RELATIVE TO PORT 1.
TMC MON – SET FOR 14 μA. INTO 6-kohm METER LOAD.

Fig. 8—Performance requirements of repeater station carrier distribution circuit.

lators "F" and "G." It then passes through circulator "F" to the line sampled by the power monitor. Since the sampling is nondirective, the diode will detect the sum of the modulated signal power and the desired carrier power. Therefore, tuning screws are included in these common arms so that the matches may be finely adjusted to minimize the reflected signals.

In cases where the common arm match does not enter into a required isolation, circulator tuning screws are not used and an adequate match is achieved by adding fixed tabs to the center conductor geometry. In addition to common arms, several isolators are tabbed where the

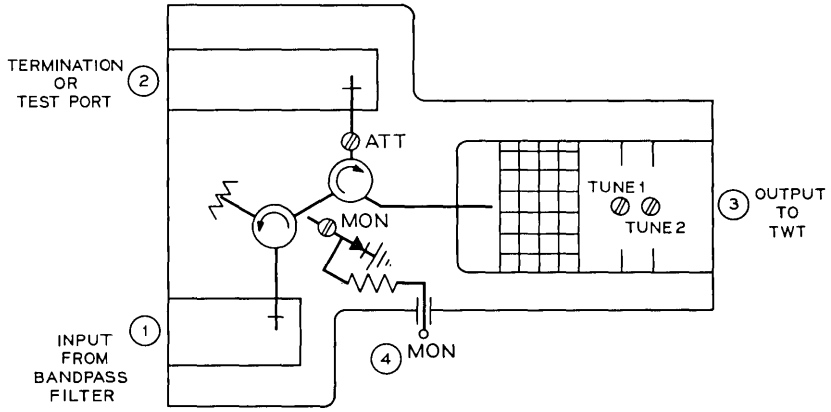

IMPEDANCE MATCHES		ISOLATIONS AND LOSSES		
PORT	RETURN LOSS (MIN. dB)	FROM PORT	TO PORT	dB
1	32	1	3	1*MAX.
2	20	2	3	0.5**MAX.
3	—	3	1	30 MIN.

ADJUSTMENTS

ATT - CONTINUOUSLY VARIES LOSS, PORT (1) TO (3). *FULLY CLOCKWISE, **FULLY COUNTER CLOCKWISE.

MON - SET FOR 14 μA. INTO 6-kohm METER LOAD.

TUNE 1, TUNE 2 - ADJUSTED TO OPTIMIZE INPUT MATCH TO TWT.

Fig. 9—Performance requirements of traveling-wave tube input circuit.

performance demands are not extreme. An isolator using tabs rather than screws is consistently capable of 25 dB reverse loss, or greater. This simplifies the adjusting procedure at the expense of finely tuned performances.

The main station carrier distribution circuit has similar performance to the repeater station version. High isolation between the transmitter and receiver circuits is readily achieved since the two are physically separated by a metal housing insert which separates the channels of the two circuits. Isolation in excess of 80 dB is inherent.

V. CONCLUSIONS

The use of microwave integrated circuits in the TH-3 radio system represents a significant advance in the incorporation of modern tech-

nology into the design of radio bays. By utilizing photolithography, precision die casting, ceramic processing, and tantalum-gold thin films, these circuits provide advantages in size, fabrication, bay "layout," performance, and cost. A carrier distribution circuit constructed with conventional waveguide components would have ten times the weight, fifteen times the volume, and would require three times the number of RF interconnections. The ability to fabricate and test each function to work best with its neighbor results in well-controlled superior overall performance. The reduced number of interconnections improves the reliability and contributes to the cost savings.

The established advantages of this approach have led to the design and application of similar circuits for the 4-GHz TD-3 radio relay system.

VI. ACKNOWLEDGMENTS

The author wishes to express appreciation to numerous people whose contributions were invaluable to the successful completion of this project: R. A. Lippincott, C. C. Shiflett, and E. D. Tidd for supplying thin film circuits and consultation; K. P. Steinmetz for his assistance in securing the die cast housings; M. D. Bonfeld for many technical contributions and continued guidance throughout the project; C. D. Sallada for his diligence and care in assembling, adjusting, and testing circuits and models; and, A. Hamori for his effective liaison between circuit design and system needs.

REFERENCES

1. Hamori, A., and Jensen, R. M., "TH-3 Microwave Radio System: Microwave Transmitter and Receiver," B.S.T.J., this issue, pp. 2117–2135.
2. Brenner, H. E., "Numerical Solution or TEM-Line Problems Involving Inhomogeneous Media," IEEE Trans. Microwave Theory and Techniques, *MTT-15,* No. 8 (August 1967), pp. 485–487.
3. Berry, R. W., Hall, P. M., and Harris, M. T., *Thin Film Technology,* New York: Van Nostrand, Reinhold Co., 1968, pp. 476–478.
4. Aslaksen, E. W., "Integrated Microwave Power Distribution Network," IEEE Trans. Elec. Devices, *ED-15,* No. 9 (September 1968), p. 680.
5. Knerr, R. H., "A New Type of Waveguide-to-Stripline Transition," IEEE Trans. Microwave Theory and Techniques, *MTT-16,* No. 3 (March 1968), pp. 192–194.
6. Saunders, T. E., and Stark, P. D., "An Integrated 4 GHz Balanced Transistor Amplifier," IEEE J. Solid-State Circuits, *SC-2,* No. 1 (March 1967), pp. 4–10.
7. Hall, P. M., and Fisher, J. S., "Termination Materials for Thin Film Resistors," to be published in IEEE Proc., Special Issue on Thin Films.

THE BELL SYSTEM TECHNICAL JOURNAL
Vol. 50, No. 7, September, 1971
Printed in U.S.A.

TH-3 Microwave Radio System:

The IF Main Amplifier

By G. L. FENDERSON

(Manuscript received February 25, 1971)

The IF main amplifier is the output amplifier for the TH-3 microwave radio receiver. The amplifier provides a 3- to 49-dB gain range under control of an associated AGC circuit to compensate for radio signal fading. It was designed to operate with a carrier frequency of 70 MHz with extremely flat transmission characteristics over a 53- to 87-MHz band.

I. INTRODUCTION

The TH-3 IF main amplifier* provides an output of +1 dBm and normally operates at a gain of 9 dB. Under control of an AGC circuit, this gain can be increased to 49 dB or decreased to less than 3 dB. The amplifier uses ten silicon transistors in five gain stages and six silicon transistors in the AGC circuit. Figure 1 shows the block schematic of the amplifier. There are five gain stages in tandem to provide the 49-dB maximum gain. The three intermediate stages are variable gain to provide the 46-dB gain range.

The design objective for the amplifier was a flat transmission and delay characteristic over the 53- to 87-MHz band. Gain deviations of less than 0.03 dB and delay deviations of less than 0.2 ns were desired. In order to meet these objectives a basic gain stage was needed having a very stable broadband transmission characteristic. Other desired characteristics were: (*i*) use of feedback to obtain gain stability, (*ii*) automatic gain control capabilities with the use of a single variable element, and (*iii*) negligible interaction between stages to facilitate cascading. The use of transformers was to be avoided due to the variability of ferrites at these frequencies. This basic gain stage could then be used throughout the radio repeater where IF amplification was required.

* This amplifier is also used in current production of transmitter-receiver bays for the TD-3 system.

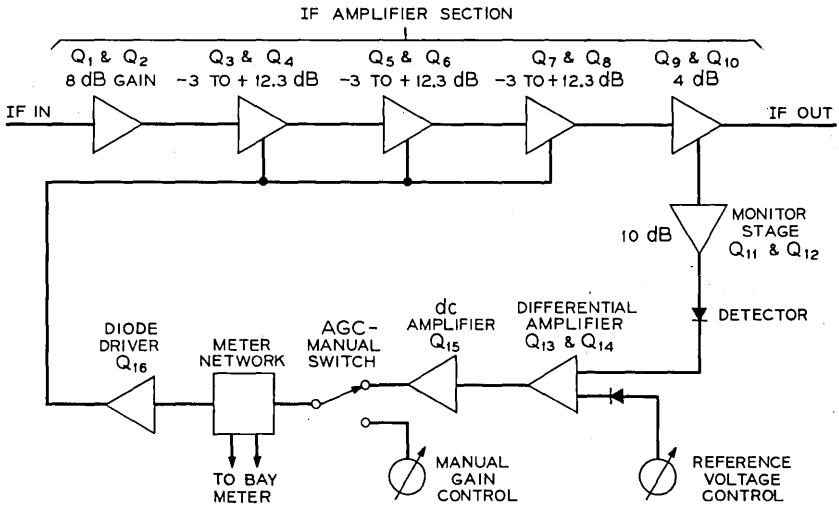

Fig. 1—Block schematic of IF main amplifier.

II. BASIC GAIN STAGE

The basic gain stages developed are shown in Figs. 2 and 3. They are series-shunt feedback pairs having a low input impedance and employing both ac and dc feedback to maintain gain and bias stability. The load may be connected to either the emitter, as shown in Fig. 2, or the collector as shown in Fig. 3. Each connection has a preferred area of usefulness. The emitter-coupled load connection was selected for the IF amplifier section because of its better linearity. The output impedance under this condition is very low due to the shunt feedback. The collector-coupled load connection was selected

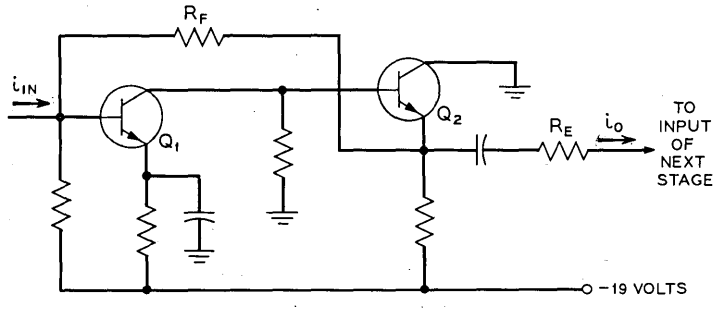

Fig. 2—Emitter-coupled basic gain stage.

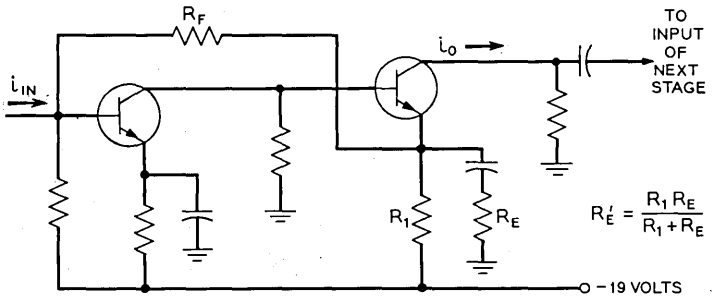

Fig. 3—Collector-coupled basic gain stage.

for the monitor stage because of its greater isolation between input and output. The output impedance under this condition is very large due to the series feedback. Other circuits which use this basic gain stage are the limiter amplifier, the squelch initiator,[1] and the 4A FM terminals.[2]

The transmission response of either the emitter-coupled or the collector-coupled stage is given by a quadratic equation of the form

$$\frac{i_o}{i_{in}} = \frac{k}{s^2 + a_1 s + a_2} \tag{1}$$

where s is complex frequency and k, a_1, and a_2 are constants which depend on the circuit parameters. When $R_F = \infty$, the two open loop poles are real and are located on the negative real axis as shown in Fig. 4. As R_F is decreased the poles move along the axis, finally meet, and then form complex conjugate pairs. Further motion is along a line parallel with the $j\omega$ axis as indicated. When the poles reach points such

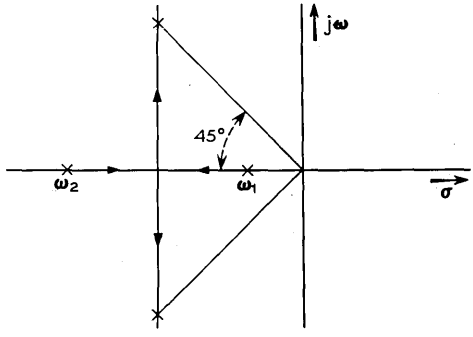

Fig. 4—Root locus plot.

that lines extended to the origin form 45-degree angles with the real axis, a maximally-flat-magnitude response results. If the presence of coupling and bypassing capacitors is ignored, the amplifier is a low-pass structure having a bandwidth equal to the distance between a pole and the origin. For the existing circuit parameters this bandwidth is greater than 200 MHz. Some differences in bandwidth occur between an emitter-coupled and a collector-coupled stage depending on the magnitude of the collector load impedance due to the Miller capacitance effect. These differences, however, are small if the collector load impedance is small, as would be the case in cascaded stages.

Assuming the open-loop gain is large, the closed loop gain for the emitter-coupled stage is

$$\frac{i_o}{i_{in}} = \frac{R_F}{R_E}. \tag{2}$$

Since the collector current contains the shunt feedback current the closed-loop gain for the collector-coupled stage is

$$\frac{i_o}{i_{in}} = 1 + \frac{R_F}{R_E'}. \tag{3}$$

For both circuits R_F is selected for a flat transmission characteristic and R_E is selected for the desired gain. Since the emitter of Q2 is very nearly a zero-impedance point due to the shunt feedback, R_E may be varied without changing the value of the feedback current significantly. This allows variation in gain without affecting the transmission response. R_E may be a fixed resistor for a fixed gain stage or a diode for a voltage-controlled variable gain stage. Thus the basic gain stage has built-in automatic gain control capabilities with the use of a single variable element.

The diode selected for the variable gain stages is the WE474A PIN diode.[3] This diode differs from the standard PN junction diode by a layer of intrinsic silicon between the P and N type silicon. The resistance of the I-layer is controlled by the direct current flowing through it by the process of conductivity modulation, and is independent of the instantaneous variations of the IF signal due to the long transit time and long life time of the injected carriers. Therefore at frequencies above which the junction impedance (which is frequency dependent) is small compared to the I-layer impedance, the PIN diode acts as a frequency independent linear resistance whose value is controlled by the direct current. Figures 5 and 6 show the overall transmission characteristic and the schematic diagram of the

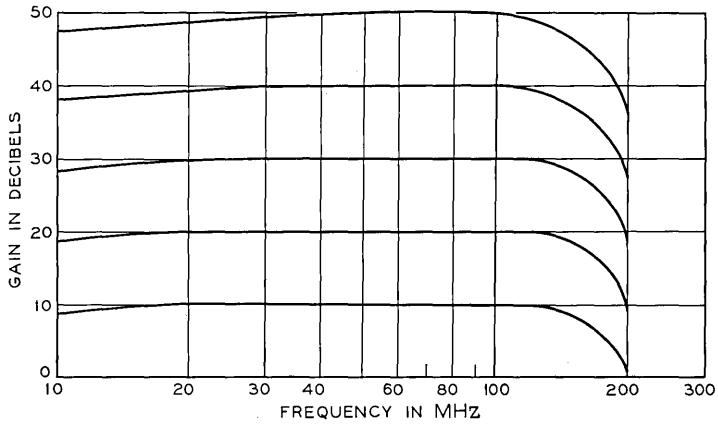

Fig. 5—Transmission characteristic of IF main amplifier.

main amplifier section using the emitter-coupled basic gain stage. Two PIN diodes are used in series for each variable gain stage to minimize the effect of the diode shunt capacitance.

Input and output impedances of 75 ohms are obtained by using a series resistor and shunt capacitor as shown in Fig. 6. The input stage has an additional resistor in series with the capacitor to form a constant resistance network which results in a slightly better return loss. Return losses greater than 30 dB are achieved using this type of matching. Since the emitter impedance of the output stage is fixed by the return loss requirement, the desired gain is obtained by proper selection of the feedback resistor. The value required to obtain 4 dB of gain results in a positive slope across the IF band. An adjustable series R-C network is provided at the input to the stage, as shown in Fig. 6, to correct for this slope and to correct for minor transmission variations in the remainder of the amplifier. With these adjustments the transmission characteristic can be adjusted to be flat within 0.01 dB over the 53- to 87-MHz IF band. The delay is essentially flat (within measuring accuracy of 0.1 ns) over the band with a value of 10.5 ns at normal gain. The delay increases to about 12 ns at 49 dB gain.

The signal levels throughout the amplifier are selected as a compromise between noise figure, AM/PM conversion, and harmonic distortion. For best thermal noise performance the signal levels within the amplifier should be as high as possible. Conversely, AM/PM and harmonic distortion are minimum for low signal levels. For this reason, only a small amount of gain (8 dB) is used ahead of the first variable

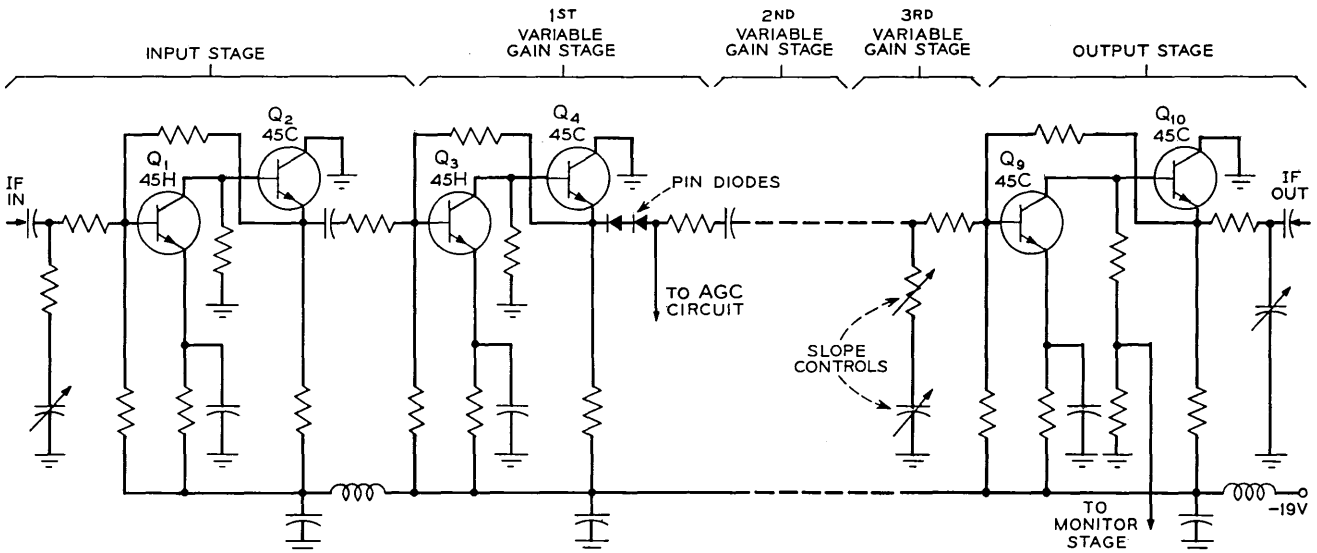

Fig. 6—Schematic of IF amplifier section.

gain stage. This results in an overall noise figure of about 12 dB when the amplifier is operating at normal gain (9 dB). A plot of noise figure versus gain is shown in Fig. 7. Also shown in Fig. 7 is the AM/PM conversion and the second and third harmonic distortion at an output power of +1 dBm. Harmonics cause cross-modulation noise in FM systems by combining in a following nonlinearity to form a delayed fundamental similar to an IF echo. Amplitude modulation, created by previous transmission deviations, causes cross-modulation noise and baseband amplitude distortion when converted to PM by an AM/PM conversion.[4] Design objectives for these parameters were harmonic-to-fundamental power ratios less than −35 dB and AM/PM conversion of less than 0.4 degree/dB measured at normal gain and output power. To meet these objectives for the given signal level conditions, the first and second transistors of each feedback pair were biased at 9 volts, 15 ma and 6 volts, 32 ma respectively.

The 45B, C, and H transistors which are used are part of a family of high-frequency planar, epitaxial, NPN silicon transistors which are characterized by a 1-GHz gain bandwidth product.[3] The 45H is simi-

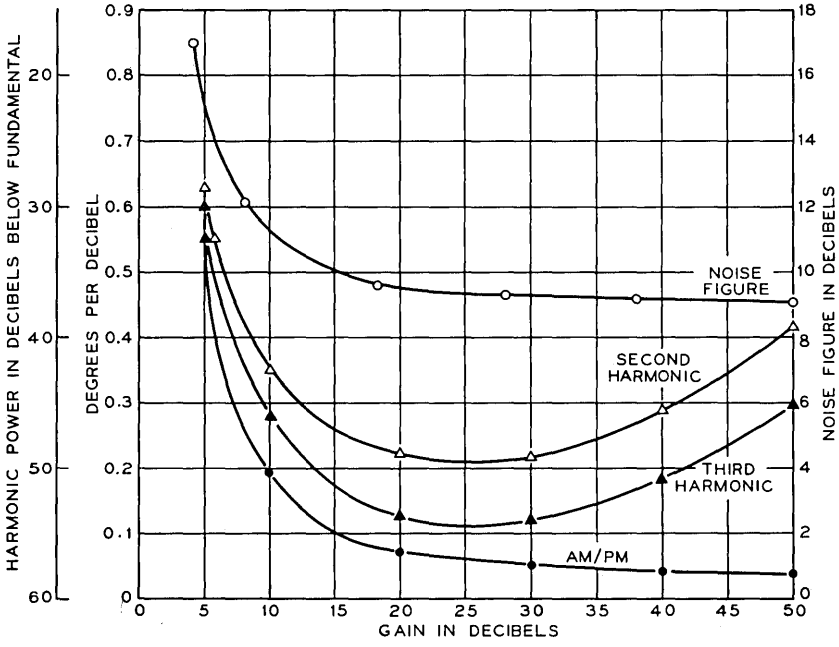

Fig. 7—AM/PM conversion and harmonic distortion of IF main amplifier.

lar to the 45C except for a smaller base resistance which results in a lower noise figure. This transistor is used as the first transistor of the first three feedback pairs to help meet the noise figure objective.

III. AGC CIRCUIT

A schematic of the AGC circuit is shown in Fig. 8. Except for the monitor stage (Q11 and Q12) and the absence of an IF filter, this amplifier is similar to the AGC amplifier described in Ref. 5. The system bandpass filter ahead of the IF main amplifier is relied upon to prevent unwanted tones from affecting the AGC regulation.

The monitor stage is a collector-coupled series-shunt feedback pair. This stage isolates the detector diode from the IF output stage and provides 10 dB of amplification. The IF signal is detected by the detector diode and amplified by a three-stage differential dc amplifier. The IF level control located in the base of Q14 is used to set the output power of the amplifier by adjusting the reference voltage. A diode identical to the detector diode is also used to provide temperature compensation. The metering network at the output of the dc amplifier is used to indicate received signal level. Transistor Q16 provides a high-impedance source with which to drive the PIN diodes. As shown in Fig. 9, the loop gain is large enough to restrict the output level variation over the 40-dB fade range to 0.5 dB. Switch S1 opens the dc feedback loop to allow manual gain adjustment for sweep testing purposes.

Figure 10 shows a photograph of the main amplifier and AGC circuit housed in an aluminum casting, $1\frac{1}{2} \times 2\frac{1}{2} \times 20$ inches.* Three separate printed circuit boards are used for the IF amplifier, AGC circuit and meter network, and supply voltage filter.

REFERENCES

1. Giust, O., "TH-3 Microwave Radio System: Modulators," B.S.T.J., this issue, pp. 2155–2173.
2. Androski, F. J., Lentz, N. E., and Salvage,, R. C., "TH-3 Microwave Radio System: 4A FM Transmitter and Receiver," B.S.T.J., this issue, pp. 2249–2269.
3. Elder, H. E., "Active Solid-State Devices," TD-3 Microwave Radio System, B.S.T.J., *47*, No. 7 (September 1968), pp. 1323–1375.
4. Cross, T. G., "Intermodulation Noise in FM Systems Due to Transmission Deviations and AM/PM Conversion," B.S.T.J., *45*, No. 10 (December 1966), pp. 1749–1773.
5. Fenderson, G. L., Jansen, J. J., and Lee, S. H., "Active IF Units for the Transmitter and Receiver," TD-3 Microwave Radio System, B.S.T.J., *47*, No. 7 (September 1968), pp. 1238–1240.

* The mechanical design was done by R. M. Wheatley.

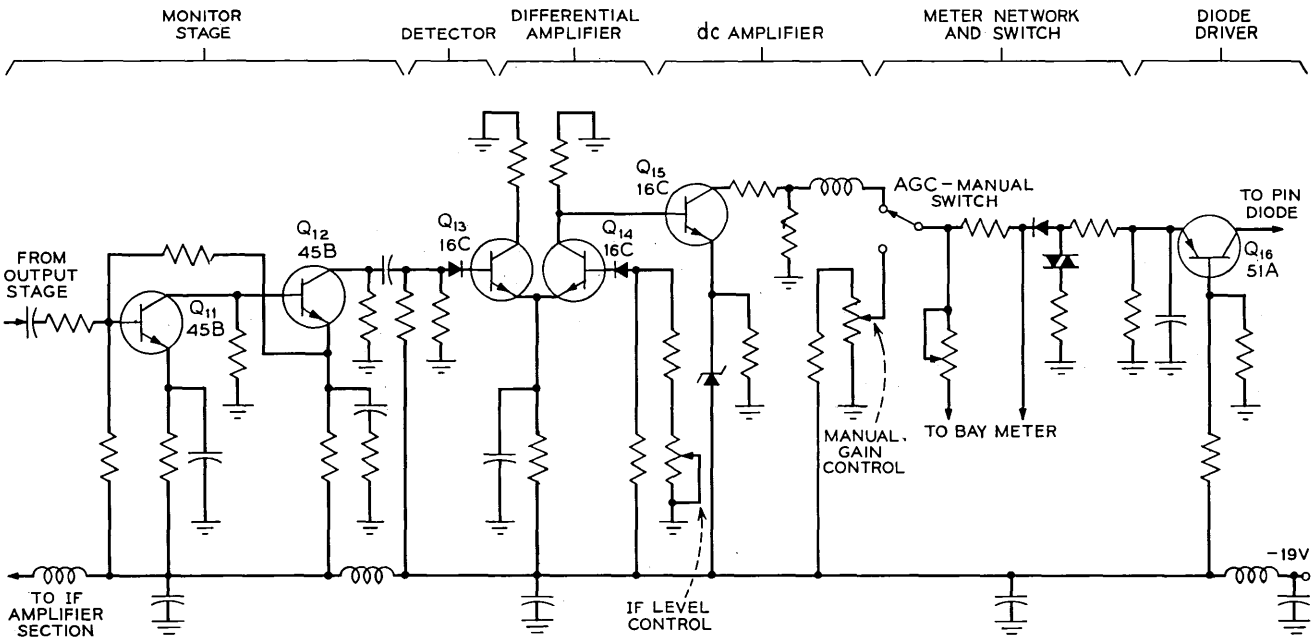

Fig. 8—Schematic of AGC circuit.

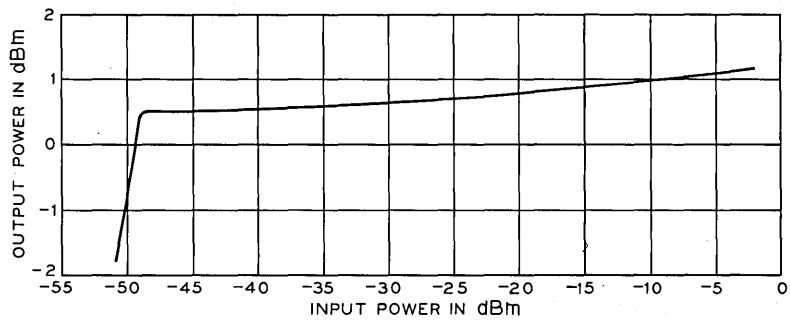

Fig. 9—AGC regulation of IF main amplifier.

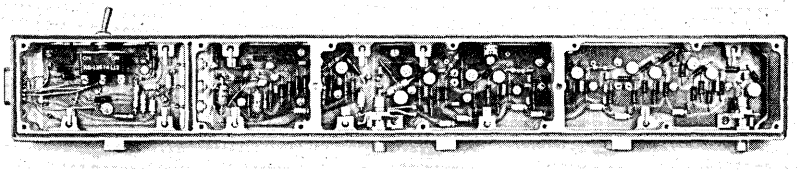

Fig. 10—IF main amplifier.

THE BELL SYSTEM TECHNICAL JOURNAL
Vol. 50, No. 7, September, 1971
Printed in U.S.A.

TH-3 Microwave Radio System:

Microwave Generator

By H. R. BEDELL, R. W. JUDKINS, and R. L. LAHLUM

(Manuscript received March 3, 1971)

The TH-3 microwave generator supplies beat oscillator power for the modulators in the TH-3 radio receiver and transmitter. The design described in this paper provides a reliable low-noise source of microwave power at 6 GHz. Design considerations and performance data are presented.

I. INTRODUCTION

The microwave generator serves as a low-noise, frequency stable source of beat oscillator power for use in the microwave transmitters and receivers of the TH-3 system.[1] It supplies 140 milliwatts of output power, and can be equipped to supply any one of thirty-two different frequencies in the 5875.2- to 6334.8-MHz frequency range.*

A stable crystal-controlled oscillator operates at frequencies between 122.4 and 131.975 MHz. Three tandem transistor frequency doublers are used to multiply the oscillator frequency to 1000 MHz.† The doubler circuits utilize the collector-to-base varactor capacitance of the transistor to enhance the frequency doubling. This results in frequency doubling and power gain simultaneously. A varactor diode sextupler multiplier circuit follows the last transistor doubler to produce the required 6-GHz output power.

II. DESIGN OBJECTIVES

The microwave generator was designed to meet the objectives listed below over the normal station air-conditioned temperature range of

* This equipment is manufactured by the Western Electric Company for Bell System use only.

† In this paper 125, 250, 500, 1000, and 6000 MHz are used to denote any frequency between 122.4 and 131.975 MHz and its second, fourth, eighth, and forty-eighth multiple, respectively.

24°C ± 11°C (75°F ± 20°F) for long-haul systems. Over the range of 4°C to 60°C (40°F to 140°F) some degradation in performance is allowable.

Power Output: The 6-GHz power output must be at least +21.5 dBm (140 milliwatts). The maximum change in output power from 40°F to 140°F must not exceed 3 dB.

Frequency Stability: The frequency of the microwave generator at a main station must be maintained to within 3 parts per million over a four-month period for a constant temperature environment. For temperature variations from 55°F to 95°F and 40°F to 140°F, the frequency must be maintained to within ±4 parts per million and ±50 parts per million, respectively. At a repeater station, a single generator, together with a shift modulator, is used for the radio receiver and radio transmitter. Therefore the generator frequency error cancels, and this error does not affect the transmitted frequency. Since the tight frequency tolerance is needed for main station generators, however, and these constitute about 50 percent of the generator production, the tight frequency requirement is applied to all generators.

Carrier-to-Noise Ratio: The noise requirement for the microwave generator, as shown in Fig. 1, was established on the basis that its

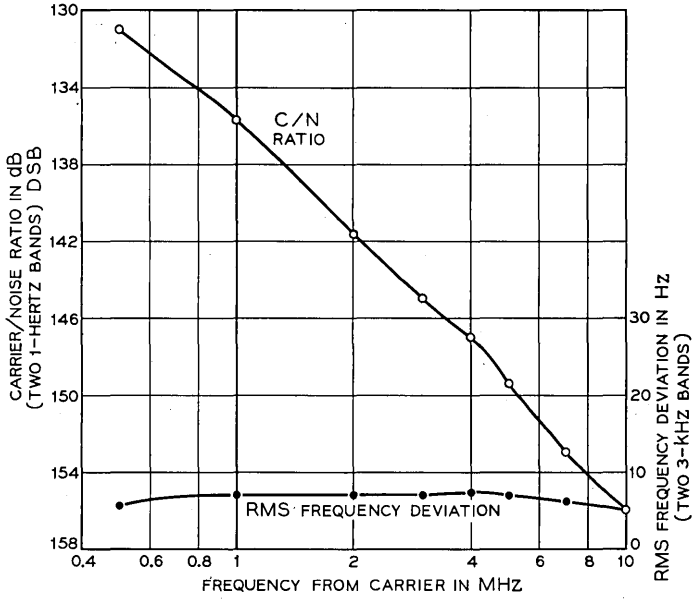

Fig. 1—Microwave generator noise requirement.

noise, when added to the other thermal noise sources, must result in a TH-3 system thermal noise not exceeding 37 dBrnc0.* The requirement is expressed as a ratio of the rms carrier power to the rms noise power in two 1-Hz bands spaced symmetrically about the carrier (DSB) and also as the equivalent rms frequency deviation caused by two 3-kHz noise sidebands.

DC Power Requirement: The microwave generator should operate from a −19-volt supply, regulated to ±0.19 volt.

Tunability: The generator should be tunable to any one of the thirty-two required frequencies. The tuning should be simple to permit easy field alignment.

Common Design: Early in the design stage a decision was made to use a common design (up to 1000 MHz) for both the 6-GHz TH-3 application and the 4-GHz TD-3 application.[2] (The TD-3 generator design uses a quadrupler at the 1000-MHz point to obtain the 4-GHz output.) The common design is feasible since the required crystal oscillator frequencies for TD-3 range from 118.125 to 128.125 MHz and thus overlap the TH-3 crystal oscillator frequencies which extend from 122.4 to 131.975 MHz. By designing the generator circuits through 1000 MHz to have a tunable bandwidth slightly greater than would be required for a TH-3 generator design alone, the same parts may be used for the two applications.

III. OVERALL DESIGN FEATURES

As mentioned above, a crystal-controlled oscillator is used as the frequency determining unit. The frequency was chosen to be as high as possible to minimize the FM noise multiplication factor in reaching the 6-GHz output frequency. About 150 MHz was the highest frequency for which crystals were available to meet the stability requirements needed for TH-3. The oscillator is designed to operate with plug-in crystals having frequencies from 118.125 to 131.975 MHz, with a specific frequency in the range 122.400 to 131.975 MHz being used for each of the channel frequencies of the TH-3 radio system. The oscillator frequency is multiplied by a factor of 48 (125 MHz × 48 = 6 GHz).

The block diagram of Fig. 2 shows the multiplier plan used. The first three circuits following the oscillator-amplifier are frequency doubler stages each using a transistor as the active element. In these

* 150 repeaters, 4000-mile system.

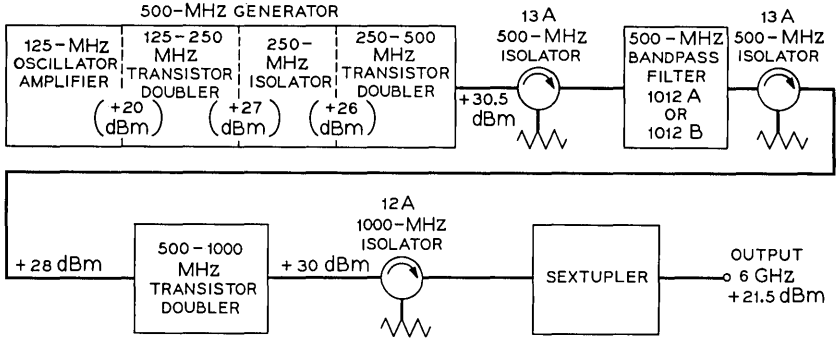

Fig. 2—Microwave generator block diagram.

circuits, the nonlinear collector-base capacitance of the transistor is used as a varactor to improve the multiplication gain over that provided by a conventional transistor doubler. A varactor diode sextupler instead of a transistor multiplier circuit is used to obtain the 6-GHz signal because high power transistors with cutoff frequencies greater than 2 GHz were not available at the time of this development. All units shown in Fig. 2 were designed to operate at a 50-ohm impedance level to facilitate testing in manufacture.

In a microwave generator which uses frequency multiplier stages, the FM index for the noise sidebands increases as 20 $\log_{10} N$ where N is the multiplying factor. Thus the FM noise goes up 6 dB for every doubling action. Also, each transistor and diode frequency multiplier stage contributes noise of its own in addition to increasing the index of modulation of noise from the previous stage. An ideal method of improving the output carrier-to-noise ratio would be to employ a sharp bandpass filter at the 6-GHz output to reduce the noise about the carrier. Noise measurements made on a filterless TH-3 generator (curve A of Fig. 3) show that 9 dB of loss relative to the carrier is needed at 0.5 MHz from the carrier frequency to meet generator noise objectives. Using a single-cavity bandpass filter at the output frequency would require a filter with a loaded Q of 16,800. This Q is so high that use of such a filter becomes impractical because of temperature sensitivity problems.

It was determined that 500 MHz was the highest frequency at which a practical filter, from a size and loss stability standpoint, could be provided. The 500-MHz filter employed uses a capacitively loaded quarter-wavelength cavity. The cavity is made of Invar and the filter has an insertion loss of 2 dB with a loaded Q of 1600. Although locat-

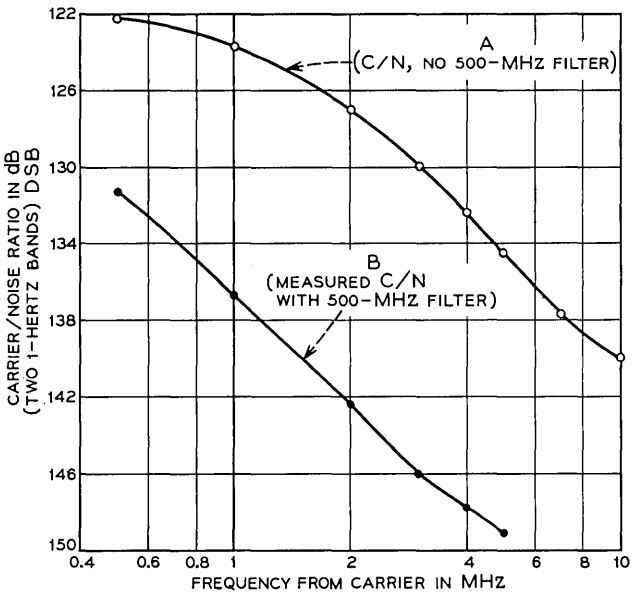

Fig. 3—Microwave generator carrier/noise ratios.

ing the filter at 500 MHz has disadvantages in that noise introduced by subsequent stages is not attenuated, substantial improvement was obtained as shown by curve B of Fig. 3.

IV. CIRCUIT DESIGN FEATURES

4.1 *Oscillator*

The crystal oscillator shown in Fig. 4 is a modified Butler circuit. The base of the oscillator transistor is bypassed to ground at the frequency of oscillation by capacitor C7. The crystal is a 5th overtone unit operating at series resonance. Capacitor C1 is used to adjust the oscillator to exactly the desired frequency. Inductor L1 centers the tuning range of C1. Inductor L3 resonates with the case capacitance of the crystal at the frequency of oscillation and thus the feedback network has two impedance poles which are equally spaced about the impedance zero at the frequency of operation. Capacitors C5 and C6 provide impedance matching to the buffer amplifier stage. The combination of L2, C2, and the transformed input impedance of the second stage provides a parallel tuned circuit at the collector.

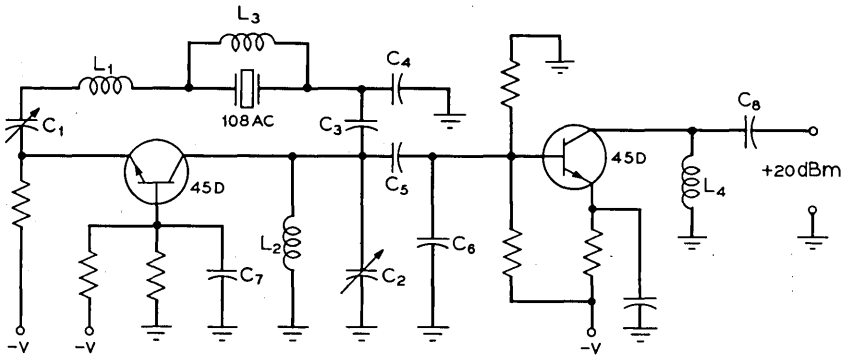

Fig. 4—Oscillator-buffer amplifier circuit.

The carrier-to-noise ratio of the oscillator is limited by the maximum permitted dissipation of the crystal and the noise figure of the transistor. The ratio remains constant as the oscillator output power is varied assuming that the feedback through the crystal is limited by the crystal dissipation. However, it is desirable to have the oscillator output power as high as possible to minimize the noise contribution of the following stages. The oscillator provides approximately +10 dBm of output power to the buffer amplifier. The latter operates as a class A common-emitter amplifier and provides an output of +20 dBm.

4.2 *Transistor Doublers*

Three transistor frequency doubler circuits are used to multiply the 125-MHz output of the oscillator-amplifier to 1000 MHz. Figure 5 shows a circuit diagram which basically is common to all three doublers. The doubling action is enhanced by using the varactor capacitance properties of the transistor collector-to-base junction, C_{bc}.[3] In order to obtain gain in this operating mode, the circuit should

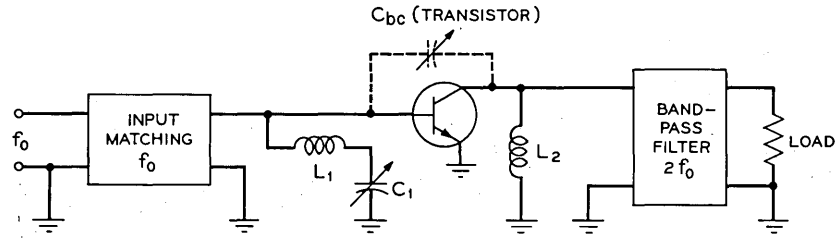

Fig. 5—Typical transistor multiplier circuit.

have at least 3 to 4 dB gain at the input frequency. This requires that a relatively high impedance be presented to the collector at the input frequency, f_o. Since base-to-emitter impedance is small, a high collector-to-ground impedance is provided by selecting L2 to resonate, at f_o, with the collector-to-base capacitance C_{bc}. Thus, a large voltage swing is developed across C_{bc}. Due to the nonlinear action of C_{bc} higher-order currents will flow if a path is provided. Inductor L1 and capacitor C1 series resonate at 2 f_o and provide the base-to-ground path. The load provides such a path in the collector circuits.

The 125- to 250-MHz doubler circuit uses a Western Electric 62C overlay type transistor with 72 emitters and a minimum f_t of 500 MHz. The 250- to 500-MHz doubler uses a Western Electric 62A overlay type transistor with 110 emitters. The 500- to 1000-MHz multiplier circuit has the emitter bypassed by using a quarter-wavelength open circuited transmission line. The 1000-MHz output circuit uses a coaxial cavity with probe coupling to the load. A Western Electric 46F overlay type transistor, which is similar to the 62A except that it does not have a tab type heat sink, is used in this circuit.

4.3 *Sextupler*

This unit, which multiplies the output frequency of the 500- to 1000-MHz transistor doubler to the final output frequency of 6 GHz, uses a varactor diode as the active element. The diode is mounted in a structure comprised of coaxial and waveguide elements as shown by the cross-section view of Fig. 6.

The coaxial transmission line input circuit consists of an impedance transformer in the form of a quarter-wave resonant coaxial cavity tuned to 1000 MHz, a low-pass filter to isolate harmonics of 1000 MHz from the input, a varactor diode, and a shunt resistor for self-bias. The tunable resonant cavity (a) has a loaded Q of 100 and transforms the diode impedance to 50 ohms. The cavity uses magnetic input and capacitive output couplings. The center conductor (b) is made of Invar to achieve the desired degree of temperature stability. The bias resistor (c) is connected between the center conductor of the low-pass filter (d) and ground at a low impedance point to minimize resistor losses at both 1000 MHz and 6 GHz. To insure the proper reflection phase for the 6-GHz signal generated in the diode (e) a suitable length of line (L1) is inserted between the diode and the low-pass filter.

The output circuit, which uses coaxial transmission line and waveguide elements, consists of a tunable coaxial-to-waveguide transducer and a tunable waveguide bandpass filter. The coaxial line (L2) pro-

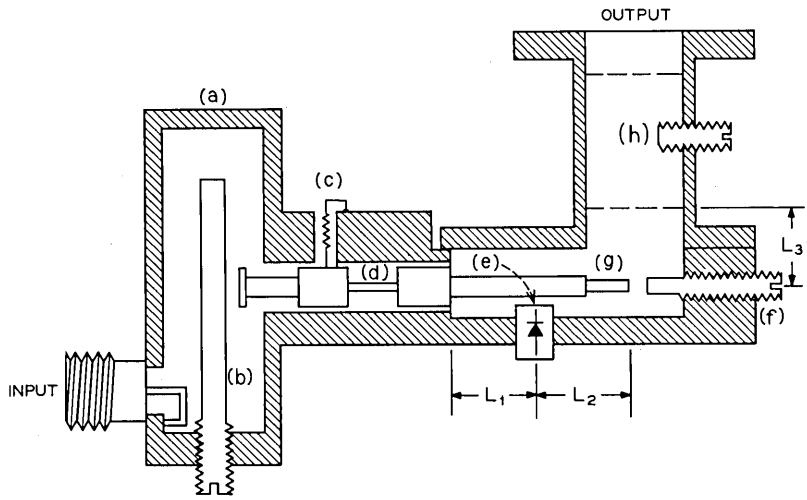

Fig. 6—Sextupler circuit.

trudes into the output waveguide to provide coupling. A capacitive tuning screw (f) opposite the probe (g) in the waveguide optimizes the coupling at the output frequency. A tunable waveguide bandpass filter (h) having a loaded Q of 35 is spaced by a distance (L3) from the probe. It passes the 6-GHz carrier and reactively terminates adjacent harmonics generated by the 1000-MHz drive signal. The output waveguide is used as a high-pass filter to suppress harmonics of the 1000-MHz drive signal at frequencies below the 6-GHz carrier. With an input power of +29 dBm at 1000 MHz, the output power at 6000 MHz is approximately +22 dBm. The varactor diode is a Western Electric 473A diode[4] with typical characteristics as follows: breakdown voltage of 60 volts, series resistance of 1.1 ohms, and capacitance at zero bias of 5 picofarads. This graded junction device is driven into the forward charge storage region and therefore available design theory could not be applied.[5] The multiplier circuit was developed by making use of experimental design techniques to achieve the desired performance. The diode is biased to operate near breakdown. At frequencies between 0.5 and about 3 MHz from the carrier the C/N performance of the multiplier is limited by both the threshold noise associated with the diode breakdown voltage and noise generated in the driving circuit. The selectivity of the input cavity provides some reduction of the noise from the driving circuit.

Additional filtering is provided at the output for tones located ± 500 MHz and ± 1000 MHz from the carrier frequency by a 1349 type bandpass filter.[1] The 500-MHz bandpass filter removes tones which may be present at 125 MHz and 250 MHz from the carrier.

4.4 *Generator Tuning*

To achieve the goal of providing simple alignment procedures, power monitors have been placed in all stages through 500 MHz. Each monitor circuit samples the power output of its corresponding stage, and a diode detector provides a current which may be read on a test meter of the TH-3 transmitter-receiver bay. Thus, these stages may be tuned by observing the response on the bay meter.

Four circulators are used in the generator chain as shown in Fig 2. These circulators were required to obtain coincidence of maximum power and minimum noise. Without the circulators, parametric oscillations occurred under certain tuning conditions.

Tuning of the 500- to 1000-MHz doubler circuit is done by monitoring the transistor collector current. The collector current is adjusted so that the transistor is operated within its dissipation limits.

The sextupler is tuned by adjusting the controls for maximum output power as observed on an external power meter.

The output power of the generator is adjustable over approximately a 5-dB range. The power adjustment is achieved by adjusting the dc bias on the 125- to 250-MHz and the 250- to 500-MHz doublers.

V. PERFORMANCE

5.1 *Power Output Variation with Temperature*

Figure 7 shows the power output as a function of temperature. Curve A gives the performance at the output of the 500- to 1000-MHz stage, curve B at the 6-GHz output frequency. The performance is within the design objectives of 3 dB maximum variation from 4°C to 60°C (40°F to 140°F).

5.2 *Frequency Variation with Temperature*

Figure 8 shows a typical change of crystal oscillator frequency with temperature. The variation in generator frequency is completely dependent on the crystal oscillator stability. The curve indicates that design objectives for frequency stability of the generator are satisfied.

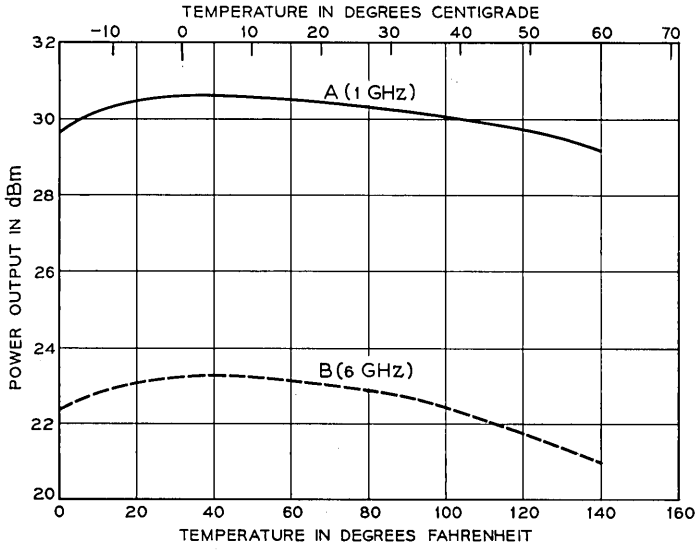

Fig. 7—Microwave power output vs temperature.

5.3 *Carrier-to-Noise Performance*

5.3.1 *Noise Measurement Method*

The carrier-to-noise ratio of the 6-GHz output signal was measured using the equipment shown in Fig. 9. Essentially the arrangement applies the output of the generator being tested to the inputs of two paths, one path (Path A) leading to the signal port of a down converter, the other (Path B) to the beat oscillator port of the converter. The output of the converter, at a frequency of 70 MHz, is applied to an FM receiver which recovers the FM noise at baseband frequencies. The noise is then measured using a tunable, frequency selective, power meter. Since the noise present at the output of the generator is very low, some method must be used to increase it so that it is not masked by the noise of the measuring equipment. This is done by using a highly selective filter to suppress the carrier in the signal path, thus, in effect, degrading the signal-to-noise ratio and increasing the FM index of noise modulation.

The beat oscillator signal for the down converter is supplied in Path B. Path B shifts the frequency of the generator under test by 70 MHz. The output of the shift modulator in Path B is filtered by a sharp

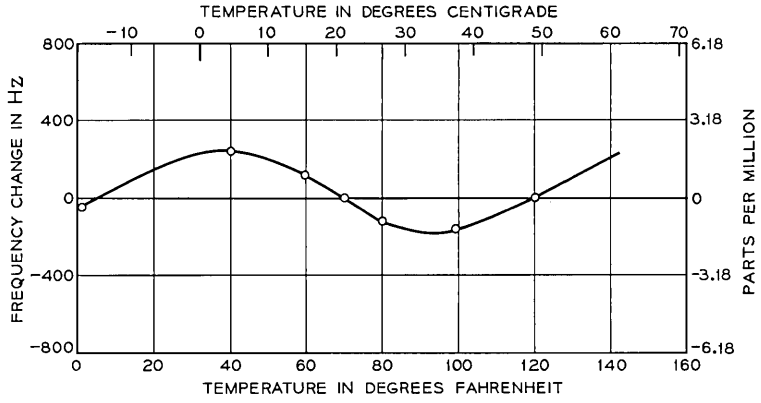

Fig. 8—Crystal frequency vs temperature.

bandpass filter (3-dB points ±0.75 MHz). This filtering essentially removes any noise which might enter the down converter via the beat oscillator port. This test set must be capable of measuring carrier-to-noise ratios as high as 154 dB (1-Hz band, DSB). With the carrier power at +21.5 dBm, the noise power to be measured is −138.5 dBm/Hz. A receiver modulator with a 10-dB noise figure will introduce noise of only −164 dBm/Hz and, therefore, will not produce any significant error.

The FM terminal receiver sensitivity is such that an input carrier-to-noise ratio of 153 dB (DSB) (at a 10-MHz baseband frequency) produces an output equal to the residual FM terminal noise.[6] By increasing the FM index (decreasing the carrier-to-noise ratio) of the signal being measured, the desired output will override the residual noise of the FM receiver. The circulator and sharp bandpass filter, as shown in Path A of Fig. 9, are used to reduce the carrier by approximately 20 dB. The noise at frequencies removed from the carrier suffers little or no attenuation. The carrier-to-noise ratio is decreased by the amount of carrier absorption.

Using the measurement equipment shown in Fig. 9, it can be shown that

$$C/N_{DSB} = -8 + 20 \log FM + 10 \log B - P_{out} + R_1{}^*$$

* The FM terminal receiver measures the FM index which in effect measures the noise on both sides of the carrier (double sideband).

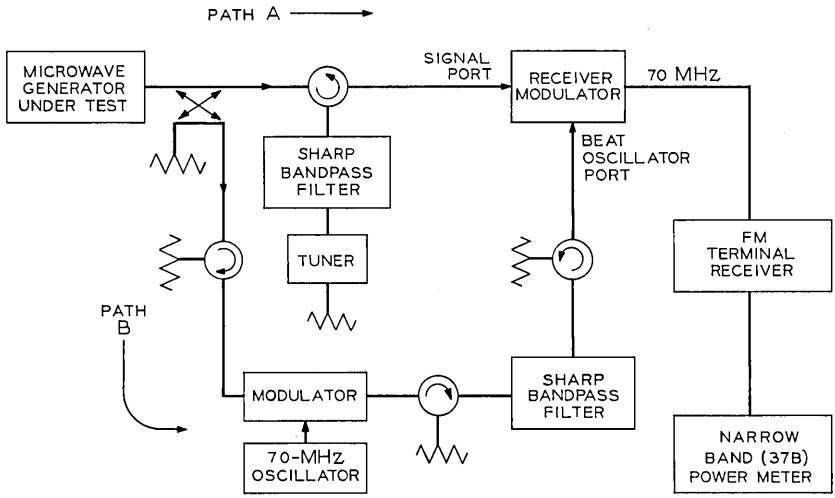

Fig. 9—C/N measurement setup.

where

R_1 = carrier absorption in dB,
FM = baseband frequency (frequency from carrier), in MHz,
B = bandwidth of 37B power meter in Hz, and
P_{out} = baseband output power indicated by the 37B (dBm).

5.3.2 *Carrier-to-Noise Performance*

Curve B of Fig. 3 shows the carrier-to-noise performance of the TH-3 generator.

VI. PHYSICAL DESIGN FEATURES

All units of the microwave generator but the sextupler are mounted in an assembly which measures 21 by 11 by 7 inches. The oscillator-amplifier, the first two transistor multiplier stages, and the 250-MHz isolator are contained in one package, designated the "500 MHz Generator." It and the other major units are shown in Fig. 10. The major components are interconnected using miniature semi-rigid cable (0.141 inch outer diameter), which simplifies the equipment layout and minimizes RF leakage.

The sextupler (designated the "6 GHz Multiplier"), as shown in Fig. 11, is mounted adjacent to the carrier distribution network in the TH-3 bay to minimize cable loss at 6 GHz. The 1000-MHz

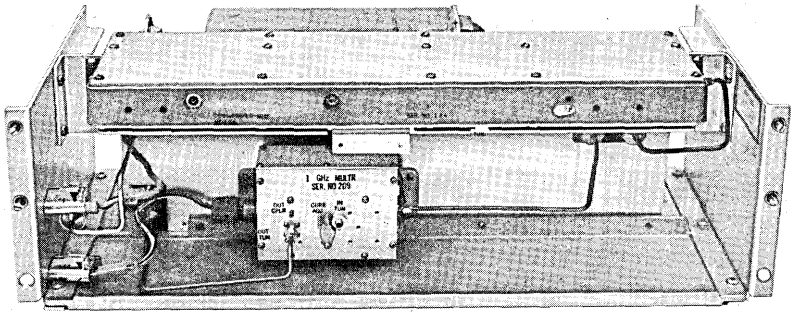

Fig. 10—Microwave generator (without sextupler).

carrier power is fed to the sextupler through a 6-foot low-loss coaxial cable (0.325 inch outer diameter).

The oscillator, two transistor multipliers, and the 250-MHz isolator are housed in the compartmentalized die-cast frame shown in Fig. 12. Printed wiring techniques are employed to achieve controlled wiring essential at these frequencies. Distributed parameters of inductance and capacitance are controlled by path width and length on the printed wiring boards. A separate compartment is provided for decoupling of the power supply leads. Access to the tuning controls and the frequency monitor point is provided on the front surface. The two sheet metal covers and braided gasket material provide complete RF shielding.

A somewhat different approach was employed in the physical design of the 500- to 1000-MHz multiplier, as shown in Fig. 13, because of the higher frequencies at which it operates. At the 500-MHz input end a combination of lumped elements and microstrip was found to provide the required accuracy for control of distributed capacitance and inductance. At the 1000-MHz output end the coaxial cavity approach provided the best realization of the circuit objectives. A small die-cast housing again provides the shielding and decoupling features found in the 500-MHz unit.

The physical embodiment of the sextupler is illustrated by the cross-section diagram of Fig. 6. As indicated in the circuit description of this multiplier each physical part of the structure is an electrical parameter of the circuit. The coaxial transmission line section at the input and the waveguide structure at the output were established by the electrical requirements for the design. Almost every phase of the physical design has a direct bearing on the electrical performance of the end product. The removable diode holder and adjustable tuning

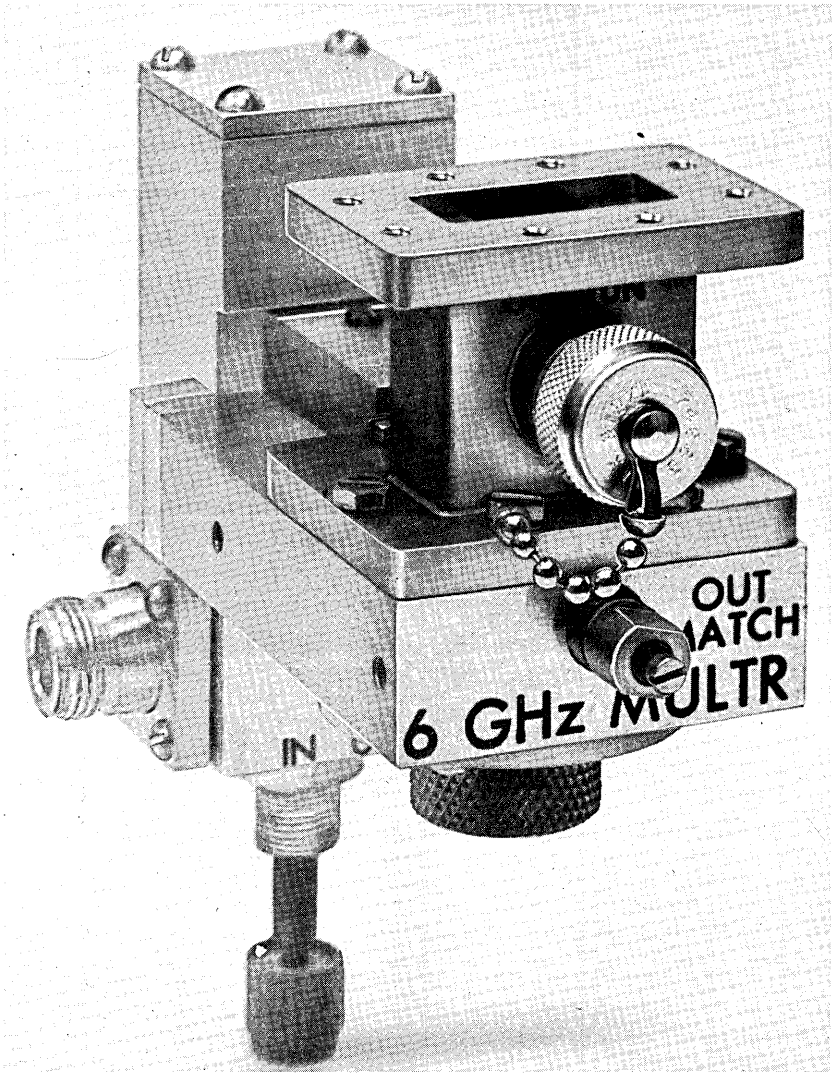

Fig. 11—Sextupler.

screws are specific details that required special design effort to insure good electrical contact pressures and to eliminate RF leakage paths.

During the development of the generator, a great deal of effort was spent to assure that the unit would exhibit high reliability in service. Much of this effort was directed toward achieving high reliability for the transistors. Figure 14 shows a curve of fits (1 failure in 10^9 hours) as a function of junction temperatures for the type of transistor used

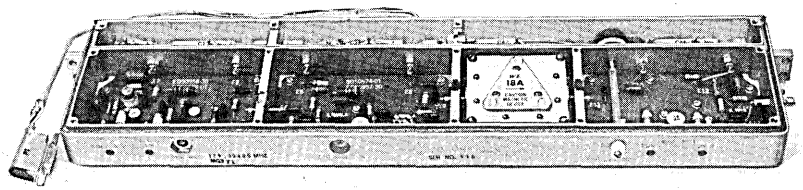

Fig. 12—500-MHz generator.

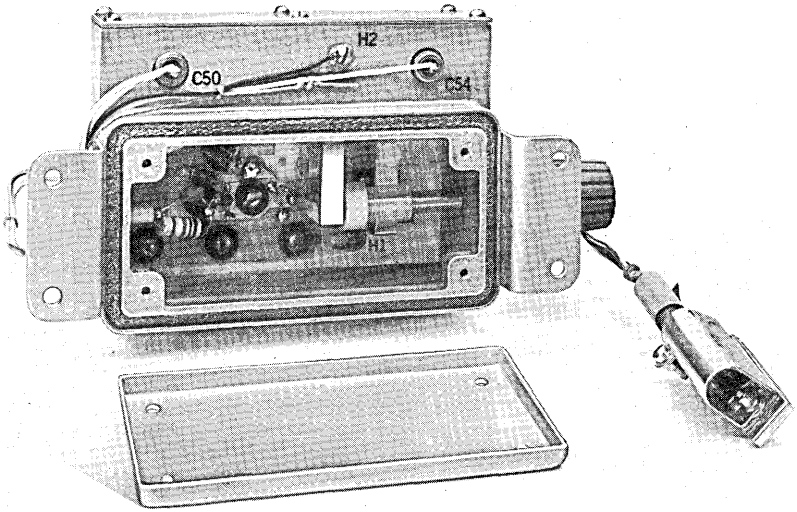

Fig. 13—500-MHz to 1000-MHz multiplier.

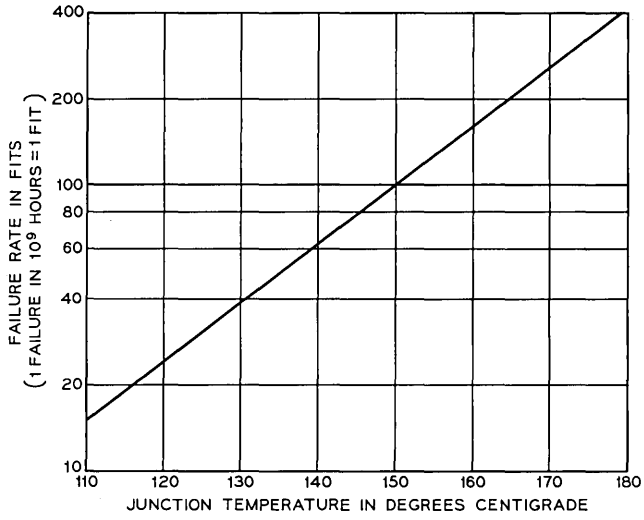

Fig. 14—Failure rate vs junction temperature for 62A, 62C, and 46F transistors.

in the generator. To obtain low junction temperatures, heat sinks were used on the transistors of the frequency multiplier circuits. The 125- to 250-MHz doubler transistor (62A) has a tab-type heat sink which connects to the framework. Use of the tab-type heat sink was desirable as it was compatible with printed circuit boards which were used through 500 MHz. The tab-type heat sink, which was developed by J. E. Clark of the Allentown Laboratory, is shown in a printed circuit board application in Fig. 15. In Fig. 16 the upper curve shows the calculated junction temperature as a function of ambient temperature for the 62C and 62A transistors using the tab-type heat sinks.

In the 500- to 1000-MHz circuit, the transistor is mounted in the wall of the aluminum front plate. This provides low thermal impedance and thus the 46F transistor operates at a junction temperature lower than the 62C and 62A. The calculated values of junction temperature are shown as the lower curve of Fig. 16.

From Figs. 14 and 16 the failure rate at a temperature of 36°C (95°F) for the 62A and 62C is 30 fits each and for the 46F (500 to 1000 MHz) the failure rate is 15 fits. The failure rate for the 125-MHz amplifier transistor is about 30 fits and for the oscillator transistor it is approximately 10 fits. The diode in the sextupler circuit has a failure rate of 30 fits.

The failure rate for those passive components in the generator which would cause loss of service is estimated to be about 900 fits. Since the failure rate for active devices is 145 fits, the total for the generator is 1045 fits which corresponds to a mean time for failure of 109 years.

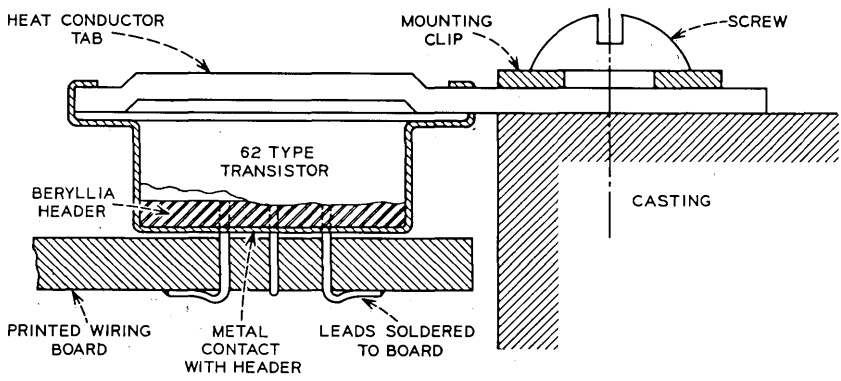

Fig. 15—Tab-type heat sink.

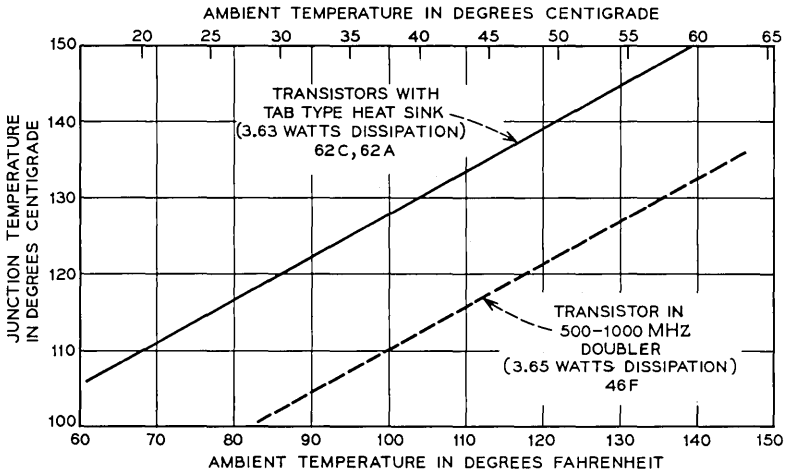

Fig. 16—Junction temperature vs ambient temperature for microwave generator transistors.

VII. ACKNOWLEDGMENTS

The microwave generator could not have been developed without the cooperation and contributions of many people. W. J. Schwarz, J. A. Gerrish, and O. Giust contributed to much of the circuit design. Also, thanks are due to J. Wiley of the Allentown Laboratory for his help with transistors. We also wish to thank R. E. Sherman for encouragement and support.

REFERENCES

1. Hamori, A., and Jensen, R. M., "TH-3 Microwave Radio System: Microwave Transmitter and Receiver," B.S.T.J., this issue, pp. 2117–2135.
2. Jensen, R. M., Rowe, R. E., and Sherman, R. E., "Microwave Transmitter And Receiver," B.S.T.J., *47,* No. 7 (September 1968), pp. 1189–1225.
3. Caulton, M., Sobol, H., and Ernst, R. L., "Generator of Microwave Power by Parametric Frequency Multiplication in a Single Transistor," RCA Review, *XXVI,* June 1965, pp. 286–311.
4. Crigler, F. W., and Decker, D. R., "Harmonic Generator Varactor Diodes For The Microwave Carrier Supply," Section II of "Active Solid-State Devices," B.S.T.J., *47,* No. 7 (September 1968), pp. 1330–1340.
5. Penfield, P., and Rafuse, R. P., *Varactor Applications,* Cambridge, Massachusetts: MIT Press, 1962.
6. Barry, J. F., Gammie, J., Lentz, N. E., and Salvage, R. C., "3A FM Terminal Transmitter And Receiver," B.S.T.J., *47,* No. 7 (September 1968), pp. 1423–1458.

THE BELL SYSTEM TECHNICAL JOURNAL
Vol. 50, No. 7, September, 1971
Printed in U.S.A.

TH-3 Microwave Radio System:

The Traveling-Wave Tube Amplifier

By C. E. BRADFORD and C. J. WALDRON

(Manuscript received March 29, 1971)

The TH-3 radio system employs all solid state components with one exception. Because of the need for output power not obtainable presently from solid state devices, the sole exception is the traveling-wave tube power amplifier. This amplifier furnishes 40.5 dBm output power at 33.5 dB gain over any channel of the 5.925- to 6.425-GHz common carrier band.

This tube employs a long-life cathode made of zirconium-additive nickel. Also, it gives higher power output than traveling-wave tubes previously designed[2] for Bell System radio relay systems. This new tube and periodic permanent magnet circuit are packaged as an integral unit. It does not require focusing or other mechanical adjustments during the life of the tube.*

I. INTRODUCTION

Traveling-wave tubes are used as the transmitting amplifiers for the TH-3 radio system. The 464A traveling-wave tube, manufactured by the Western Electric Company for this application, is designed to provide a power output of 11 watts with 33.5 dB of gain in the linear region.

As is usual for such devices, the tube is operated at 2 to 3 dB below the maximum power output capability of 20 watts in order to keep intermodulation effects low. Also, it has been designed as a completely packaged device to reduce the number of tests and adjustments that are required at the installation site. The package is designed so that the magnet structure can be reclaimed at the end of the tube life for subsequent reuse.

The amplifier, shown in Fig. 1, measures 0.48 × 0.11 × 0.11 meter

* Cathodes made from zirconium-additive nickel were used in the *Telestar*® traveling-wave tube; see Ref. 1.

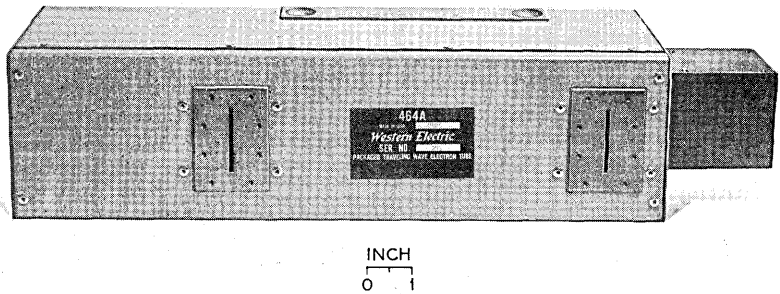

Fig. 1—The 464A traveling-wave tube power amplifier.

and weighs 8.2 kg. The evacuated tube is not visible after it has been packaged. Input and output RF connections are reduced-height (2.54 mm × 40.4 mm) waveguide. Power to run the tube is provided by a solid state regulated high-voltage supply.[3]

Table I summarizes the system requirements upon the 464A tube and typical device performance.

II. ELECTRICAL DESIGN CONSIDERATIONS

Since the power output for which this device is designed is higher than used previously for Bell System radio relay transmission, the internal structure has been changed from that of previous traveling-wave tubes.

TABLE I—464A TWT OPERATION AND PERFORMANCE

Operation	Design Requirement	
Operating frequency, GHz	5.925–6.425	
Operating power output, watts	11.2	
Operating beam current, mA	59.0	
Performance	**Design Requirement**	**Typical Performance**
Saturation power output, watts	~20	20
Gain* at operating power output, dB	31–35	33.5
Amplitude-to-phase modulation conversion at operating power output, degrees per dB	4 max	1.5
Product of gain and noise figure, dB	65 max	63.0

* See Section 2.4

2.1 *Electrode Voltages and Beam Current*

Calculations showed that in order to obtain a saturated power output of 43 dBm it would be necessary to use a beam current of 59 milliamperes, assuming a synchronous helix voltage of 3750 Vdc. The desired power can also be obtained using a somewhat higher helix voltage and lower beam current. However, this would result in a longer helix and more difficult helix intercept problems.

The collector efficiency of this device is 19 percent, typical for tubes of this type. The use of multiple collectors and tapered helix sections had been considered to further increase the efficiency, but it was concluded that such efficiency improvement added costs which were out of proportion to the advantages to be gained.

Thus, the current and voltage were chosen to be a good compromise, which allows for economy in magnet design, while still obtaining satisfactory gain and power output with a reasonable length of helix.

2.2 *Other Parameters*

With the beam voltage and current established, some of the other parameters of interest are:

Cathode current density = 200 mA/cm^2
Beam-to-helix diameter ratio =0.5
Cathode temperature = 740°C (true)

Helix:

mean diameter (wire 0.254 mm dia)	= 2.598 mm
turns per cm	= 9.48
active length	= 17.2 cm*
dielectric loading factor	= 0.782
gain per centimeter	= 3.08 dB
radial propagation constant	= 1.45.

In order to obtain higher operating power, the beam current has been increased as discussed in the previous section. This results in a higher current density in the helix region because the helix diameter is constrained by considerations of the design of the magnetic circuit and its space requirements. This also has the advantage that, without much change in beam convergence, the cathode current density is retained at the same value used in a previous tube,[2] the 461A, resulting in the long cathode life capability demonstrated by these other

* It is necessary to allow sufficient length to overcome losses, such as the loss involved in establishing the wave on the helix.

devices. The beam-to-helix diameter ratio is a conservative value of 0.5; this is in comparison to higher ratios such as 0.8 or 0.9 which result in higher gain per unit length of helix, but can give problems in keeping the beam in focus and could result in requiring readjustment of the tube during operating life. The cathode temperature of 740°C is also a conservative choice; while greater cathode life might be achieved at temperatures closer to the edge of the temperature-limited emission region, 690°C to 710°C, the cathode life of 250,000 hours associated with the chosen operating temperature is more than adequate to meet the design intent, since in practice other factors limit the operating life below this figure.

The helix parameters listed above to complete the description of the tube result from the voltage and current decisions previously discussed.

2.3 *Magnetic Focusing*

To obtain satisfactory focusing (with Alnico-8 magnet material) the magnet period must be somewhat less than 16.13 mm. A value of 15.39 mm was chosen for this design. Calculations of the field required showed that magnetic field densities greater than 0.0970 T (tesla) are required, and a value of 0.1090 T was taken as the design figure.* Experimental values of helix interception current have been found to be below 0.7 percent of the cathode current. Because of the high energy of the electrons which are intercepted and because the helix structure depends on longitudinal conduction for cooling, it is important that this figure be low, preferably below 0.5 mA. Spot heating of the helix structure at helix currents greater than 0.5 mA begins to result in sublimation of helix materials, at these helix voltages.

2.4 *Operation*

The 464A has been designed for operation above the synchronous helix voltage. The advantages of this mode of operation are two: first, the helix voltage becomes a gain control, eliminating the need for the system to accommodate a specific tube gain. Second, the carrier-to-noise ratio is greater by 3 to 7 dB. This carrier-to-noise ratio advantage is gained even though the noise figure at the actual operating point may be above its minimum value. The minimum noise figure occurs at a helix voltage which varies somewhat from tube to tube,

* Criteria arrived at in previous studies[2] have been applied here as well: $\alpha/\beta > 3$, $\beta < 0.06$.

and at a helix voltage greater than that for synchronous operation. The tube is run with the helix voltage increased above synchronous voltage until the output power decreases to 40.5 dBm with a constant input of +7 dBm.

The manner in which the power output varies with helix voltage under conditions of different input power is not very different for this device than for comparable tubes, as shown in Fig. 2. Figure 3 shows the saturation power capability, when calculated under the condition that the tube is run with the helix voltage increased to give 33 dB gain. Figure 4 shows the high-level gain, at midband, calculated from Fig. 2.

III. CONSTRUCTION

3.1 *The Helix*

Ceramic rods support a molybdenum wire helix which is glazed to the rods at each point of contact between rods and wire. When RF power is applied to the input of a medium- or high-power traveling-wave tube, the power output gradually decreases from the initial value over a period of from two to five minutes. This "fade" occurs

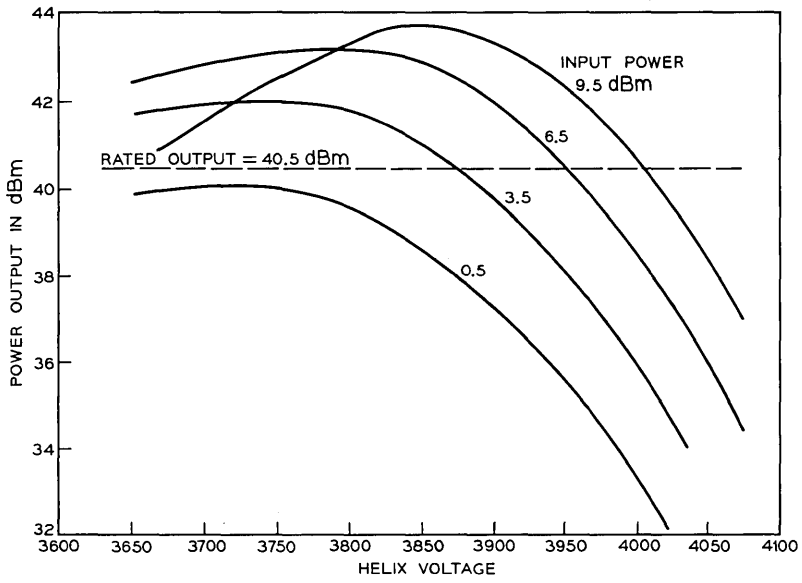

Fig. 2—Power input vs helix voltage curves for the 464A at midband.

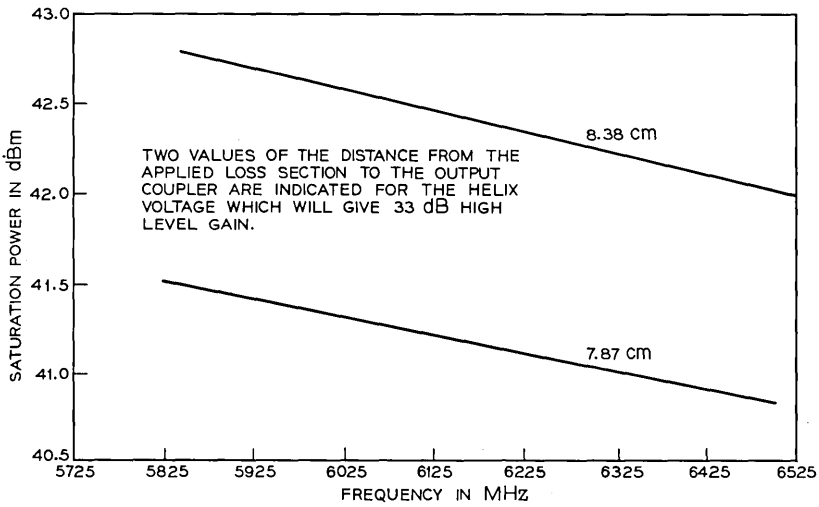

Fig. 3—Effect of loss pattern positioning on power capability.

because the dielectric properties of the helix support rods change as a result of heating of the rods.

Since the 464A has a beam power density 2-1/2 times as high as its predecessors, the degree of fade could become intolerable under some operating conditions. Therefore, fading was reduced by the introduction of a gap of 0.127 mm between the helix wire and ceramic support rods for a distance of ten turns away from the output coupler. The gap is produced by grinding a flat on each rod. This prevents excessive heating of the ceramic rods and associated glaze at the point where the (spot) heating is greatest. At 10 watts output, fade is only 0.2 dB with this provision.

The applied loss is a tantalum film applied by sputtering.[2] Since a loss of about 60 dB is required between the input and output sections to prevent oscillation, greater than 80 dB of loss is applied to provide margin for manufacturing variations and gain changes.

3.2 *The Magnetic Focusing Structure*

Use of a light and compact periodic permanent magnetic (PPM) circuit allows the tube and magnet to be shipped as an integral unit. Thus the beam focus and electrical characteristics can be optimized at the factory. At the end of the useful life of the tube, the entire package is returned to the factory for reuse of the magnetic circuit.

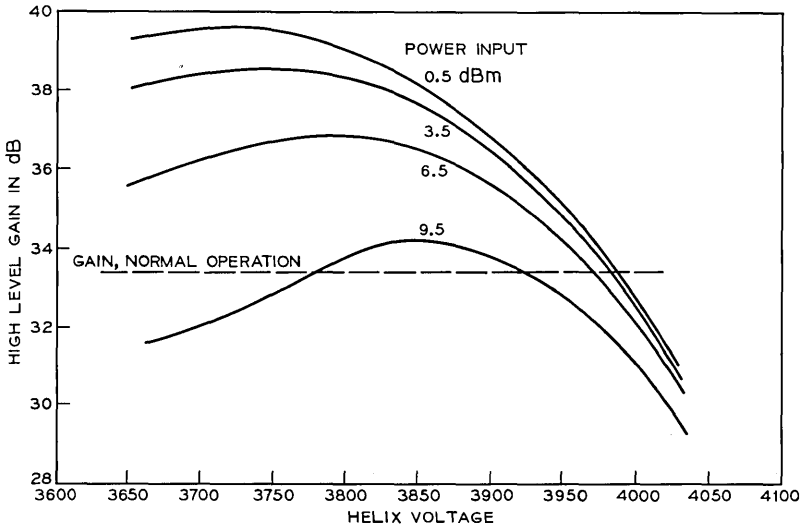

Fig. 4—High-level gain as a function of helix voltage, at midband.

The magnetic circuit consists of 36 Alnico-8 ring magnets stacked alternately with pure iron pole pieces (Fig. 5). The magnets and pole pieces are aligned using a precision mandrel. An epoxy adhesive is used to encapsulate the assembly within an aluminum housing. An RF choke is provided near the input to prevent leakage of the RF through the gun.

To achieve long life it is desirable that the collector be adequately cooled so that critical components of the tube are not overheated. The nominal heat dissipation of the collector is 110 watts. A maximum collector temperature of 150°C occurs for nominal cooling conditions for this dissipation. The collector fits into a hole in the copper cooling

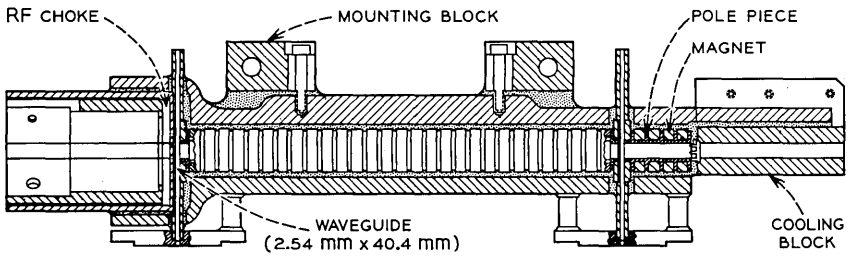

Fig. 5—A cross-sectional view of the 464A magnetic package.

block. The hole in the cooling block is 0.08 mm larger than the collector diameter to allow motion of the collector which in turn permits alignment of the electron beam with the magnetic field. This space is filled with a thermally conductive silicone paste. The collector is held radially (in a single transverse plane) by a reference surface located between the magnetic stack and the cooling block. Two cooling fins are attached to the cooling block during installation of the traveling-wave tube in the radio bay.

The tube is packaged in a sheet steel enclosure for RF shielding, strength, and mechanical protection.

3.3 *Electron Gun*

The 464A uses a convergent Pierce-type electron gun. The gun has a perveance of 0.207×10^{-6} amp/volt$^{3/2}$.

The cathode base material is a high-purity nickel with 0.1 percent zirconium additive. The diffusion rate of the zirconium in this nickel is lower[4] than that of the activating agents in "melt" nickel. Moreover, the arrival rate of zirconium at the nickel-coating interface is more nearly in balance[5] with the rates of the other processes essential to electron emission. The result of substituting the zirconium nickel for "melt" nickel is that the ultimate cathode and cathode coating life is increased and cathode sublimation virtually eliminated as a failure mechanism. Furthermore, the influence of gettering on barium production is decreased. Figure 6 shows the zirconium diffusion rate and coating depletion calculated for this cathode as a function of time.

Field experience with early designs of traveling-wave tubes indicated that one of the failure mechanisms has been associated with the glaze material used in the gun construction. It had been found that the glaze tended to electrolyze during the life of the tube, becoming conductive in high electric fields and leading ultimately to failures. The mechanical design of the 464A gun is such that no glaze material is used in its construction. One ceramic platform is used to support parts at high voltage and this is done so as to permit the use of stud and nut fastening. The basic gun structure is shown in Fig. 7.

IV. TUBE PERFORMANCE

4.1 *Gain and Power*

With an input power of 7 dBm applied, the desired output power of 40.5 dBm is achieved by adjusting the helix voltage to an appropriate value above the synchronous helix voltage. The nominal high-

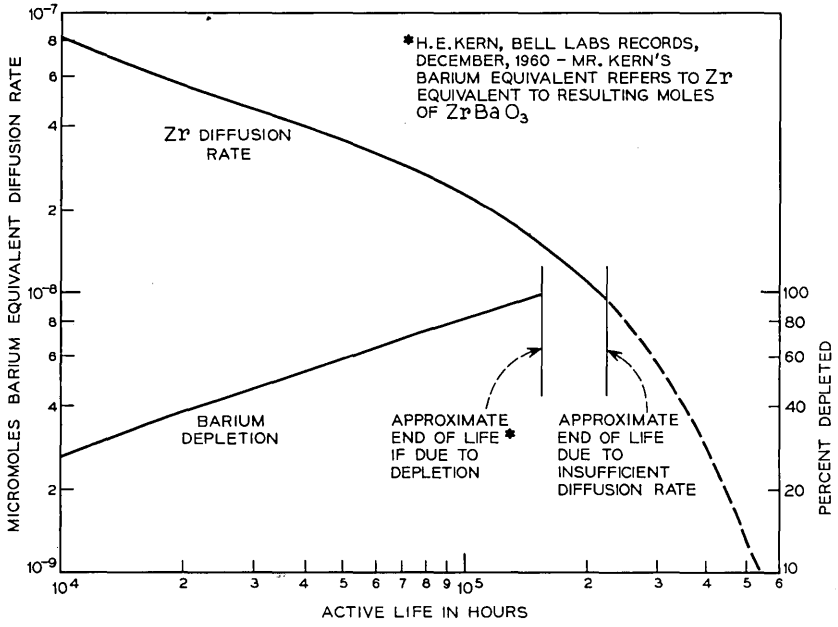

Fig. 6—Diffusion rate and depletion curves for the 464A cathode.

level gain is about 40 db when the helix voltage is set at the synchronous value.

The broadband gain flatness characteristics are optimized during the assembly of the package at the factory. Since the tube is preset for operation over the entire frequency band, complex impedance matching adjustments and measurements are not required for setting up the tube in the radio bay. Tuning adjustments are incorporated in the microwave integrated circuits which attach to the input and output ports of the traveling-wave tube. These are adjusted for maximum output in the particular radio channel in which the transmitter is operated.

4.2 *Noise*

The noise performance of the 464A traveling-wave tube is measured in terms of a noise-gain product (FG). This is defined as

$$FG = \frac{N_o}{kTB},$$

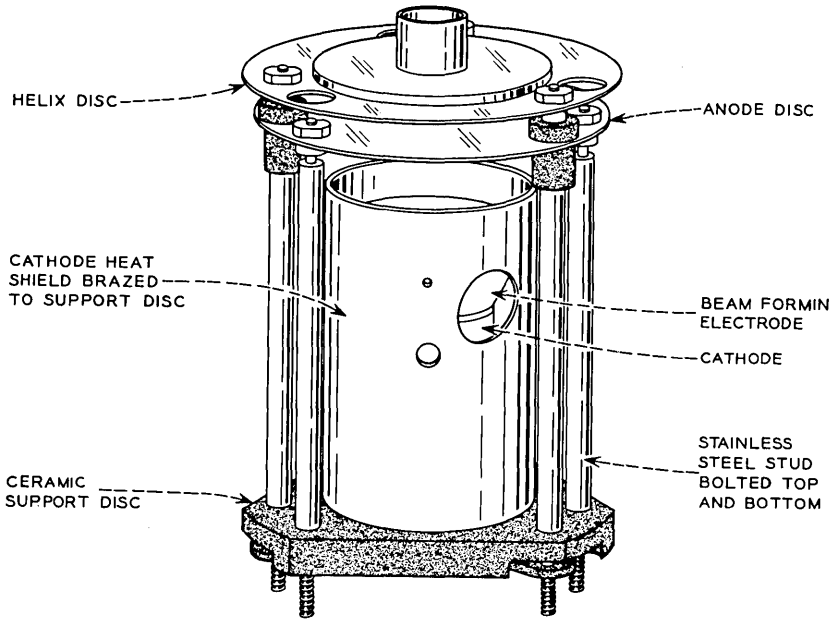

Fig. 7—A view of the electron gun.

where N_o is the thermal noise output of the traveling-wave tube, k is Boltzmann's constant, T is absolute temperature, and B is the bandwidth.

The noise-gain product is measured using an FM detector since FM noise is the important component in an FM system. The measurement is made with the traveling-wave tube driven to an output power of 40.5 dBm. A carrier nulling technique is used to increase the sensitivity of the measuring system.

Best noise performance of the device is achieved by immersing the gun in a small magnetic field. This has the effect of inhibiting the growth of a space-charge wave of noise. This small magnetic field is provided by a coil which surrounds the gun. The noise performance is optimized during the package assembly by adjusting a series resistance in the coil circuit.

4.3 *Life*

Since the reliabilities of other components in the system are designed for the long life achievable with solid state devices, this tube has been designed to be as compatible as possible.

The life of a tube can be discussed from a number of standpoints. In the early days of tubes, the life was most often limited by the cathode. In the present design cathode life no longer limits the life of a tube. In this traveling-wave tube, the zirconium-additive cathode yields an ultimate life greater than 17 years and the environment of the cathode has been kept as pure as possible to take advantage of its potential capability. However, a tube may fail for a number of reasons not directly related to the cathode; such as, foreign particles in the tube, gassy tubes, improper operating conditions, etc. For example, if the loss pattern in a tube degrades, the helix intercept increases causing the glaze to be excessively heated, which in turn increases the level of contaminants arriving at the cathode resulting in tube failure. From experience gained with related tubes, it is reasonable to expect that with the zirconium-additive cathode the median life will be greater than 50,000 hours.[1]

Requirements on the power supply[3] remain substantially the same as for the TD-3 case except for the higher voltage and higher dissipation needed. There is one major change. It has been found that the sequence in which voltages are applied to the tube has a strong effect on tube life. To ensure proper sequencing, the power supply has been designed with automatic turn-on such that the collector voltage has risen to nearly full voltage before the helix voltage is applied; similarly, helix voltage before anode voltage is applied. The same holds for turn-off except that the reverse order is necessary.

V. SUMMARY

The output power of 40.5 dBm required in the TH-3 system is supplied by this traveling-wave tube at a power gain of 33.5 dB. At this power level the noise figure is less than 29 dB and the intermodulation (AM/PM conversion constant) is about 1.5 degrees per dB.

To achieve long life, a cathode with an excellent reliability record in *Telestar*® has been employed.[1] Cathode loading is conservative, 200 mA/cm^2. To retain a favorable environment for the cathode, the gun is constructed without glaze; measures are employed to prevent power fading which would ultimately lead to cathode degradation. To obtain a stable loss pattern, tantalum is used rather than graphite. This reduces the possibility of a degradation[6] in the applied attenuation which in time would result in RF oscillation in the helix. Lastly, the tube-package design is such that focusing or other adjustments are not necessary upon installation or during service; the power supply is

designed to turn the tube on with a minimum of adjustment and in a way most favorable to the tube.

Such measures are expected to result in a median life in excess of 50,000 hours, under operating conditions.

REFERENCES

1. Bodmer, M. G., Laico, J. P., Olsen, E. G., and Ross, A. T., "The Satellite Traveling-Wave Tube," B.S.T.J., *42,* No. 4, Part 3, (July 1963), pp. 1703–1748.
2. Bradford, C. E., "The Traveling-Wave Tube Amplifier for the Microwave Transmitter," B.S.T.J., TD-3 System Issue, *47,* No. 7 (September 1968), pp. 1379–1395.
3. Balicki, J. F., Chun, P. S., and Salvo, F. J., "TH-3 Microwave Radio System: Power System," B.S.T.J., this issue, pp. 2235–2248.
4. Caldwell, C. W., "Thermionic Emission vs Carbon Diffusion in Nickel-Based Oxide Cathodes," Proc. Fifth Annual Nat. Tube Techniques Conf.—1960, pp. 12-1 to 12-6.
5. Kern, H. E., and Graney, E. T., "Thermionic Emission and Diffusion Studies on Zirconium Doped Nickel Cathodes," in *Advances in Electron Tube Techniques,* Vol. 2, New York: Pergamon Press, 1962, pp. 235–239.
6. Anand, R. P., and Morris, R. S., "Applications of Tantalum Films as Traveling-Wave Tube Attenuators," IEEE Conf. Record, 1968-19th Conf. Tube Techniques, September 1968, pp. 162–167.

THE BELL SYSTEM TECHNICAL JOURNAL
Vol. 50, No. 7, September, 1971
Printed in U.S.A.

TH-3 Microwave Radio System:

Power System

By J. F. BALICKI, P. S. CHUN, and F. J. SALVO

(Manuscript received March 8, 1971)

This paper describes TH-3 powering arrangements, particularly the traveling-wave tube dc-to-dc converter.

I. INTRODUCTION

One design goal for the TH-3 radio system was to use or adapt, as much as possible, existing TD-3 powering arrangements. A number of power-related TD-3 facilities, requiring little or no change for TH-3 use, included the −19-volt regulator, the common −24-volt battery plant, and dc distribution and radio-building grounding arrangements. These items will not be discussed here, as they have been detailed in an earlier paper.[1] On the other hand, the 6-GHz, ten-watt, RF output-power objective for TH-3 required a new TWT, coded the 464A,[2] and an associated TWT power supply.

II. TRAVELING-WAVE TUBE DC-TO-DC CONVERTER

2.1 *Circuit Description*

The traveling-wave tube is powered by a dc-to-dc converter which provides all electrode voltages required for the 464A TWT. These requirements, shown in Table I, reflect a general 50-percent increase in electrode high-voltage and current levels over corresponding TH-1 and TD-3 TWTs,[3,4] resulting from a higher unsaturated output-power objective.

The nominal switching frequency of the TWT converter is 23 kHz, whereas 2 kHz is used in TD-3. Concern over possible personnel annoyance and fatigue at the audible frequency, as well as a desire to utilize the existing TD-3 framework and housing to contain the higher-power conversion circuitry of TH-3, required converter operation in the ultrasonic range.

TABLE I—TWT SUPPLY REQUIREMENTS

Electrode	Voltage	Voltage Stability*	Current	Ripple (rms)
Anode	Adjustable, +50 to +850V with respect to the helix voltage	±30V with respect to cathode	0 to 1 mA	25 mV at 40 kHz
Helix	Adjustable, +3600 to +4400V with respect to cathode	±20V with respect to cathode	0 to 4 mA	6 mV at 40 kHz
Cathode	Fixed, −1825V with respect to collector	−1500 to −2000V with respect to collector	59 mA	1.0V
Collector	Connected to ground	—	—	—
Heater†	+7.5V with respect to cathode	±150 mV	0.8 to 0.9A	100 mV
TWT Coil	−24V with respect to ground	−21 to −28V	25 mA	100 mV (p − p)

* Over normal ambient operating range of 55°F to 95°F.
† 9.1 volts during timed, preheat interval.

A block diagram of the dc-to-dc converter is shown in Fig. 1. The nominal −24-volt battery voltage input is regulated and filtered to approximately −17 volts by the heater regulator and applied to the 23-kHz square-wave oscillator. Three square-wave outputs are provided from the 23-kHz oscillator. Of these, two serve as switching transistor base-drive signals to the collector inverter and helix inverter, respectively, while the third output is rectified and filtered to provide 7.5-volt dc heater voltage for the TWT. The heater output voltage is a measure of the voltage impressed on the oscillator, and thus the heater output voltage is regulated. This relationship is used to advantage during the 5-minute cathode preheat interval immediately following supply turn-on, when the heater regulator output voltage is initially held at −20.5 volts, resulting in a heater output voltage of 9.1 volts dc. During this interval, the high heater voltage ensures that (*i*) the TWT cathode is not temperature limited when high voltages are applied, and (*ii*) the high cathode temperature tends to reactivate the surface, thus lengthening the cathode lifetime. At the end of the cathode preheat interval, the electronic time delay relay TD automatically restores the heater regulator output to −17 volts, thereby lowering the TWT heater voltage from 9.1 volts to 7.5 volts. Both heater output voltage levels are adjustable over small ranges, should adjustment become necessary.

The square-wave output voltage from the 23-kHz oscillator cannot be used directly as base drive to the collector and helix inverters. Charge storage in the base region causes power switching transistors to consistently exhibit longer turn-off times than turn-on times. This causes a condition commonly referred to as "switch-through" to occur in an inverter driven by square-wave base drive. "Switch-through" is defined as the overlapping in time of the collector currents of the on-going and off-going switching transistors, and is often the major cause of excessive inverter switching loss and device failure. In order to prevent "switch-through," shaping networks are placed in the base drive paths to the collector and helix inverters.

The base-drive shaping network appearing within the dashed box of Fig. 2 operates in the following manner: Assume that transistor Q1 is off, that Q2 is on, and that the polarity of base-drive winding 5-6-7 on transformer T1 has just commutated, with terminal 5 now positive with respect to terminal 7. A load current, I, will begin flowing as indicated on Fig. 2. Since the core of L1 is not saturated at this time, windings 1-2 and 3-4 are magnetically coupled as a one-to-one transformer. Hence, a current equal to $2I$ must simultaneously flow

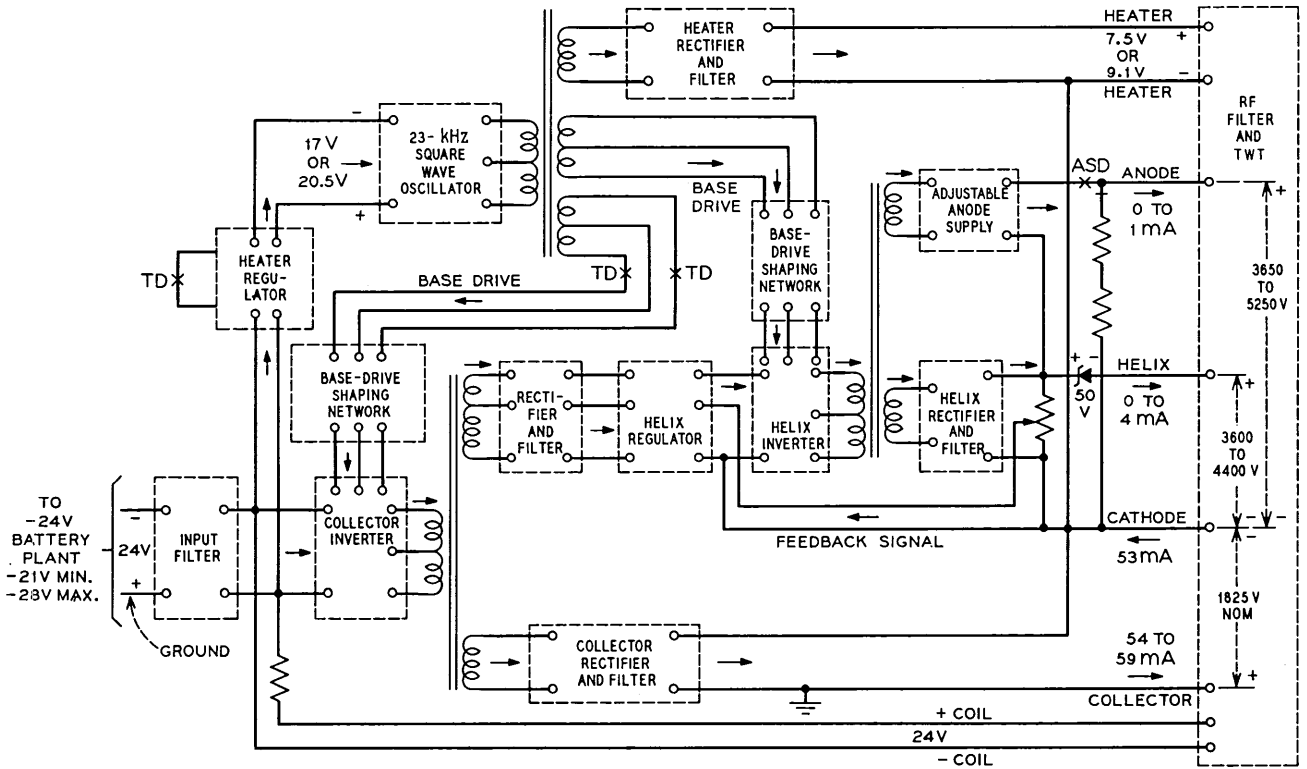

Fig. 1—Block diagram of TH-3 dc-to-dc converter.

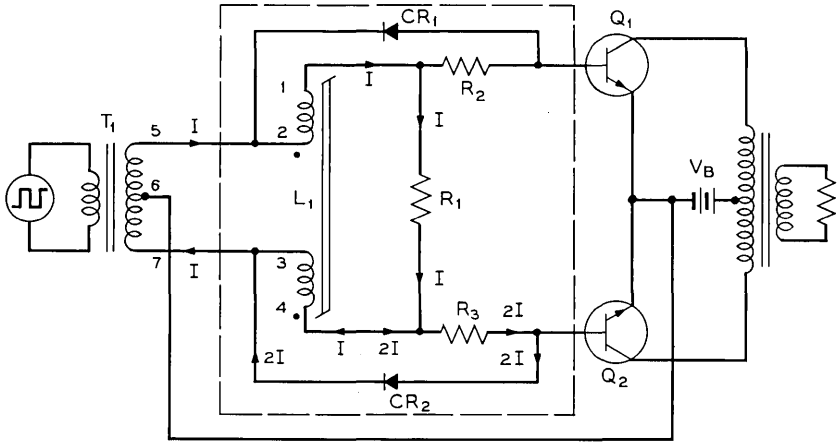

Fig. 2—Base-drive shaping network.

as shown. By transformer action, the sum of the voltage drops across R3 and CR2 appearing across winding 3-4 of L1 will also appear across winding 1-2 of L1, with terminal 2 positive with respect to terminal 1. The polarity of this voltage is such as to reduce the forward voltage appearing across the base-emitter junction of Q1, and in fact, proper choice of circuit parameter values permits this forward voltage to be made less than that necessary to turn Q1 on. In this manner, base-drive current to Q1 can be withheld as long as the core of L1 remains unsaturated, thereby withholding the turn-on of Q1 until after the turn-off of Q2. Upon saturation of L1, however, transformer action ceases and Q1 is driven on, its base drive current level being constrained by resistor R2. To further aid in the prevention of "switch-through," the base region of the off-going transistor is quickly swept free of stored charge by the immediate application of a reverse-bias voltage to its base-emitter junction through a low-impedance path. In Fig. 2, this sweepout current leaves terminal 6 of T1, enters the emitter and leaves the base of off-going transistor Q2, passes through CR2 in the forward direction, and returns to terminal 7 of T1. On alternate half-cycles, the base drive shaping action is reversed, delaying the turn-on of Q2 and accelerating the turn-off of Q1.

As seen in Fig. 1, the −24-volt battery voltage is inverted to yield two 23-kHz square-wave outputs from the collector inverter. The first output, after rectification and filtering, results in the unregulated TWT collector-to-cathode voltage of 1825 volts dc, nominal. Since the TWT collector electrode is operated at ground potential, this collector supply

effectively biases the TWT cathode electrode −1825 volts dc from ground. The second square-wave output, after rectification and filtering, results in an unregulated dc voltage which is isolated from the supply input by virtue of the collector inverter transformer. As such, this dc voltage can be referenced to and precisely regulated above the −1825-volt cathode potential by means of the helix regulator, after which it is inverted by the helix inverter to yield two 23-kHz square-wave outputs.

The first of these is rectified and filtered to produce a nominal helix output voltage of 4000 volts dc, measured with respect to the TWT cathode. Automatic regulation of this voltage is effected by returning a fraction of it to the helix regulator. A potentiometer, accessible from the front panel of the converter, permits continuous adjustment of the returned voltage fraction thus permitting continuous adjustment of the helix output voltage over the range 3600 to 4400 volts dc.

The second 23-kHz output from the helix inverter is delivered to the anode supply which yields a continuously adjustable output voltage between zero and 800 volts dc. This voltage is varied by means of an adjustable auto-transformer accessible from the converter front panel and operated at dc ground in the interest of safety. By stacking this adjustable voltage upon another point clamped at 50 volts dc above the helix output voltage, the anode output voltage is produced. This voltage is continuously adjustable between 50 and 850 volts dc above the helix output voltage, measured with respect to the TWT cathode.

The 464A TWT is provided with a coil in the vicinity of the cathode structure to aid in the improvement of tube noise figure. An unregulated −24 volts, derived from filtered battery, powers this coil.

2.2 *Equipment Design Requirements for TH-3 TWT Converter*

The physical design of the TH-3 TWT converter, shown in Fig. 3, is similar to that of the TD-3 radio system TWT converter (see Ref. 1) despite higher TH-3 voltages and greater heat dissipation. The TH-3 converter design incorporates mechanical operating techniques and dual unit mounting arrangements similar to those of the TD-3 converter.

Several physical design similarities between the TH-3 and TD-3 converters include:

2.2.1 *Use of Die-Cast Panels*

The front panel die castings, which provide for unit latching, component mounting, and carrying, have common usage in present Western

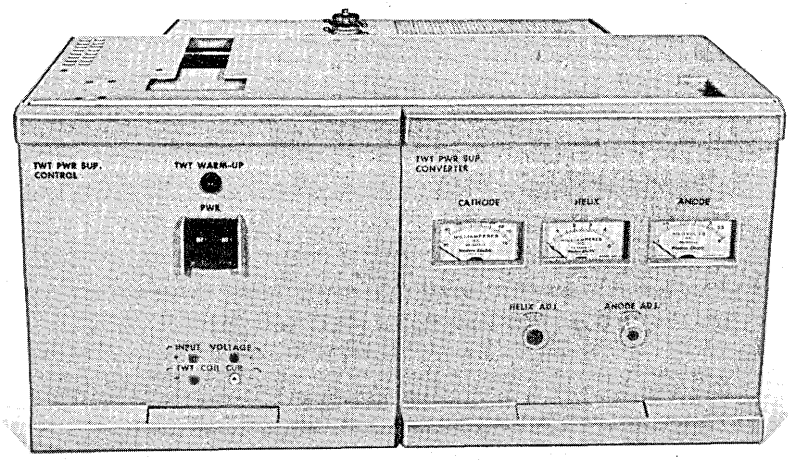

Fig. 3—TH-3 dc-to-dc converter.

Electric production of TD-3 and TH-3 units. The commonality of the front-panel appearance between TD-3 and TH-3 is readily apparent (see Fig. 3 and Ref. 1).

2.2.2 *Placement of High-Voltage Components*

All high-voltage components are mounted on insulated boards or epoxy printed wiring boards. The board and component placement considers not only voltage levels but lead dress for proper circuit operation.

2.2.3 *Personnel Protection Features*

Because of the high potentials present, the mechanical configuration of the supply must ensure personnel protection rather than simply relying on operating instructions. Removal of the left-hand unit will shut down the converter and provide the necessary access to the TWT and supply interconnections. The left-hand unit overlaps the right-hand unit and prevents its sole removal, thereby providing a positive interlock.

Further interlocking is provided by means of a wired interlock loop passing through the associated connectors of the left- and right-hand units and the TWT; consequently all conditions necessary for safety must be fulfilled before the supply can be energized.

Several equipment design requirements unique to the TH-3 TWT converter include:

2.2.4 *New High-Voltage Components*

High-voltage, glass, oil-filled capacitors provide additional output noise suppression and reduce volume requirements. New mica capacitors are used to provide main-unit high-voltage filtering. A miniature high-voltage vacuum relay is used to provide shutdown sequencing.

2.2.5 *Interconnection Grouping Between TWT and Supply*

A single plug-in type connector as used on TD-3 is not appropriate for TH-3 use because of the higher output voltages. The high-voltage outputs of the TH-3 converter are segregated into two voltage groups and the voltage level difference within each group is minimal. Two commercially available quick-disconnect connectors are, therefore, adequate for the application.

2.2.6 *RF Filtering Required to Reduce Converter-Generated Noise*

RF filter components, which are enclosed in a mu-metal housing inside the TH-3 converter framework, provide additional filtering in the converter outputs to the TWT. The leads from the RF box to the TWT are shielded by a mu-metal cover to minimize noise pickup.

III. TWT-CONVERTER INTERFACE

3.1 *Tones*

The gain and phase characteristics of the TWT vary with the helix-to-cathode and anode-to-cathode voltages generated by the converter. Therefore, any ripple or noise present on the helix and anode leads will modulate the microwave carrier being amplified by the TWT. The ripple appears in the TH-3 baseband which spans the 0.3- to 10-MHz range and the auxiliary channel which spans the 11- to 12-MHz range. Tones at harmonics of the normal 23-kHz converter switching frequency were initially found throughout the entire baseband and auxiliary channel. The tone requirements are specified at the ouput of the FM receiver and are shown in Fig. 4.

Two basic methods are employed to reduce converter-generated tones to acceptable levels. First, the helix and anode leads are heavily filtered since these leads directly affect TWT gain. Well over 100 dB of filtering loss throughout the entire baseband frequency range is used between each of these leads and the cathode lead. Second, great care is employed to prevent tones from being induced onto the heavily filtered leads. Magnetic shielding is used at both the source and load. Mu-metal cans are used on all transformers. As discussed in Section

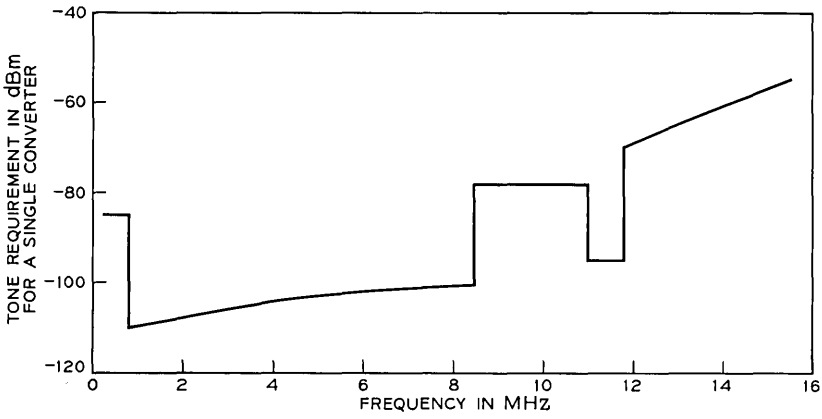

Fig. 4—Tone requirement for a single converter measured at the output of the FM receiver.

2.2.6, the final stages of filtering for all leads are located in a mu-metal box and the output cables which connect to the TWT are shielded with a mu-metal cover. Tests showed that this cover was especially important as tones as high as 16 dB over requirements were found when the cover was removed.

Additionally, induced tones are minimized through the reduction of conducted tones on leads other than the critical helix-to-cathode and anode-to-cathode pairs. While tones on the collector, heater, coil, and interlock leads do not directly modulate the microwave carrier, they can induce tones in more critical leads since they are run in the same cables used for the helix, anode, and cathode leads. For example, rather extensive filtering is required on the interlock loop which is run between the converter and TWT for safety purposes and which carries the timer current. Without this, tones exceeded requirements by as much as 8 dB at 8 MHz, and by as much as 12 dB in the 11- to 12-MHz auxiliary channel band.

3.2 *Negative Resistance Characteristic of the TWT*

The dc-to-dc converter was designed to accommodate the dynamic negative resistance seen looking into the helix-cathode terminals of the TWT. A somewhat typical TWT *I-V* characteristic is shown in Fig. 5. Instability, resulting in a system oscillation, will occur unless the converter output resistance is less than the absolute magnitude of the TWT's dynamic negative resistance.

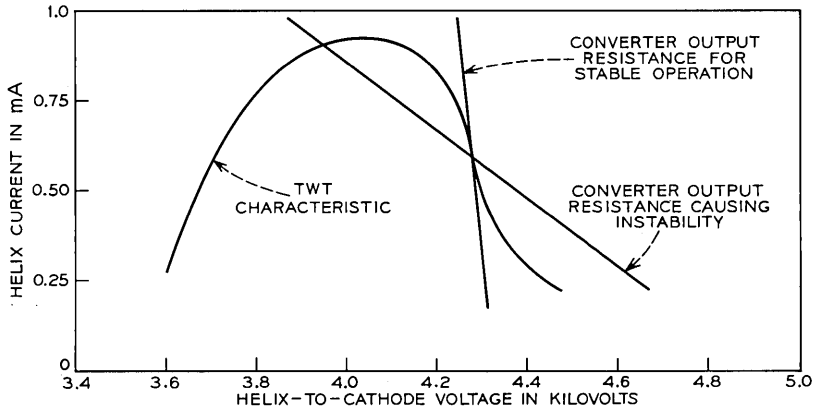

Fig. 5—TWT *I-V* characteristic (with RF drive).

A small-scale linear analysis can be made by defining the reciprocal of the slope of the TWT *I-V* characteristic as a dynamic ac impedance, Z_{HC}. The converter-TWT small-scale linear analysis is made using Fig. 6.

V_R = Reference voltage in helix regulator (8.65-volt voltage regulator diode)
V_{HC} = Helix-cathode voltage at TWT terminals
A = Open-loop gain of helix regulator
Z_O = Open-loop output impedance of the converter
Z_{HC} = AC impedance between the helix-cathode terminals of the TWT

$$B = \frac{R_2}{R_1 + R_2}.$$

Conventional linear feedback analysis of the model shown in Fig 6 yields the following gain equation:

$$\frac{V_{HC}}{V_R} = \frac{A\left(\frac{Z_{HC}}{Z_O + Z_{HC}}\right)}{1 + AB\left(\frac{Z_{HC}}{Z_O + Z_{HC}}\right)}. \tag{1}$$

By Blackman's Impedance[5] Relationship:

$$Z_{OCL} = \frac{Z_O}{1 + AB}, \tag{2}$$

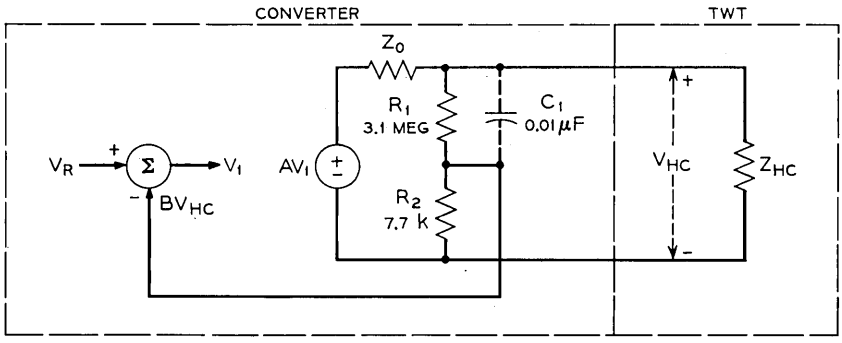

Fig. 6—Linear model of converter-TWT feedback loop (lead capacitor C1 shown with dashed lines).

where Z_{OCL} = closed-loop output impedance of the converter. Substituting (2) into (1) yields, after manipulation:

$$V_{HC} = \frac{AV_R}{(1 + AB)\left(1 + \frac{Z_{OCL}}{Z_{HC}}\right)}. \tag{3}$$

Conventional analysis of (3) indicates that if the open-loop gain $AB = -1$, instability results. However, instability also results if $Z_{OCL}/Z_{HC} = -1$, where Z_{HC} is negative in the region of interest. The latter condition occurs when the converter closed-loop output resistance equals the absolute magnitude of the dynamic negative TWT resistance and the reactive components of the two impedances are equal. Both the converter and TWT impedances have practically negligible reactive components in the frequency range where instability would tend to occur.

Instability is particularly undesirable because the helix-to-cathode voltage oscillation causes the system power level to oscillate, or "bobble," as low-frequency oscillations are called. Even less desirable is the increased helix intercept current which often accompanies this condition.

Bobble is prevented by a lead network in the converter feedback loop. The lead network is formed by capacitor C1 in Fig. 6. Typical converter output impedance curves, with and without the lead network, are shown in Fig. 7. The phase angle of the converter output impedance is less than 10 degrees in this frequency range. The lead network adds a "zero" to the feedback loop at about 0.5 Hz. Thus loop gain is increased significantly in the 2- to 4-Hz range.

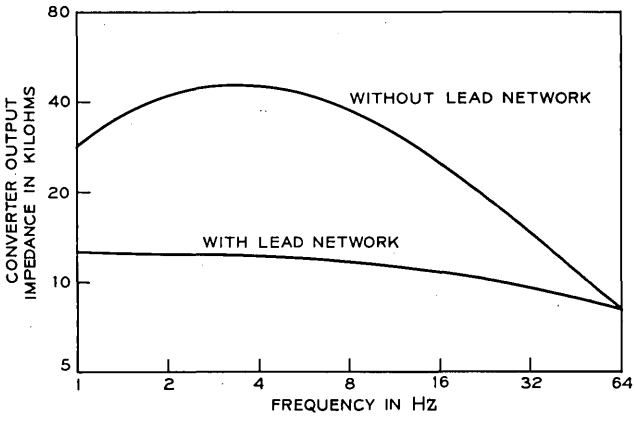

Fig. 7—Typical converter output impedance.

If corrective measures are removed from the converter, a 10-dB peak-to-peak bobble is observed on the RF power meter which monitors TWT output power. The bobble frequency is about 2 to 4 Hz, the frequency range at which the converter output resistance is greatest.

3.3 *Prolonging TWT Cathode Activity*

The 464A TWT is the only vacuum tube used in the TH-3 radio system. As the TWT is the system component with the shortest anticipated lifetime, any improvement made in its reliability will have a corresponding salutary effect on overall system reliability. Since loss of cathode activity is an important cause of TWT failure, several features have been incorporated into the TWT converter to prolong and enhance this activity.

3.3.1 *Cathode Preheat Sequence*

As described in Section 2.1, this 5-minute heater overvoltage interval immediately following converter turn-on is designed to (*i*) prevent temperature-limited operation of the cathode surface, and (*ii*) prolong cathode activity by providing a degree of cathode surface reactivation each time the converter is turned on.

3.3.2 *Automatic High-Voltage Turnup Sequence*

As seen in Fig. 1, timed contact closures, TD, in the base-drive path to the collector inverter insure that no high voltages can be

produced until after the electronic timer TD has timed out. When these base-drive contacts close, enabling the collector inverter, the TWT collector-to-cathode voltage appears rapidly. On the other hand, since the power path for helix and anode output voltages includes several additional tandem blocks, these remaining high voltages lag the appearance of the first by tens of milliseconds. This turn-on voltage sequence prevents the formation of a transient helix-intercept current with attendant reduction in cathode activity due to positive-ion bombardment or reaction with outgassing products.

3.3.3 *Automatic High-Voltage Turn-down Sequence*

Electrically keyed to the input power circuit breaker is a fast, high-voltage vacuum relay ASD arranged as an anode-voltage shorting crowbar. This is shown in Fig. 1. Tripping of the circuit breaker, for any reason, is thereby accompanied by a rapid decay of TWT anode voltage and hence, beam current. An anode crowbar time constant of approximately one millisecond assures rapid beam-current decay with no disruptive intercept currents.

3.3.4 *TWT Positive-Ion Trap*

The converter design, as described in Section 2.1, insures that the anode output voltage is at least 50 or more volts higher than the helix output voltage at all times. The resulting potential gradient established between the TWT helix and anode electrodes inhibits cathode damage due to positive ion bombardment.

IV. SUMMARY

Electrical and physical considerations important to the development of the TH-3 TWT converter have been described. The converter design has been optimized to accommodate the particular characteristics of the 464A TWT which it powers. In particular the converter has been designed (*i*) to hold TWT gain constant through accurate helix and anode voltage regulation, (*ii*) to minimize tones through extensive filtering and shielding, (*iii*) to accommodate the TWT negative resistance characteristic through control of the converter output resistance, and (*iv*) to maximize TWT life and reliability through accurate heater regulation and proper sequence of turn-on and turn-off operations.

V. ACKNOWLEDGMENTS

The authors wish to express their appreciation to the many individuals in the Electronic Power Systems Laboratory who contributed in no small part to the successful development of the TH-3 TWT converter. Among these the authors wish to mention R. E. D. Anderson, R. S. Barton, T. G. Blanchard, E. A. Hake, T. G. Harrigan, W. E. Jewett, P. R. Lantz, S. Mottel, and F. J. Shapiro.

REFERENCES

1. Jewett, W. E., and Mottel, S., "Power System," B.S.T.J., TD-3 System Issue, *47,* No. 7 (September 1968), pp. 1487–1509.
2. Bradford, C. E., and Waldron, C. J., "TH-3 Microwave Radio System: The Traveling-Wave Tube Amplifier," B.S.T.J., this issue, pp. 2223–2234.
3. Laico, J. P., McDowell, H. L., and Moster, C. R., "A Medium Power Traveling-Wave Tube for 6000-Mc Radio Relay," B.S.T.J., *35,* No. 6 (November 1956), pp. 1285–1346.
4. Griffiths, H. D., and Sproul, P. T., "The TH Broadband Radio Transmitter and Receiver," B.S.T.J., *40,* No. 6 (November 1961), pp. 1521–1568.
5. Blackman, R. B., "Effect of Feedback on Impedance," B.S.T.J., *22,* No. 3 (October 1943), pp. 269–277.

THE BELL SYSTEM TECHNICAL JOURNAL
Vol. 50, No. 7, September, 1971
Printed in U.S.A.

TH-3 Microwave Radio System:

4A FM Transmitter and Receiver

By F. J. ANDROSKI, N. E. LENTZ, and R. C. SALVAGE

(Manuscript received February 11, 1971)

FM terminals form an important subsystem of long-haul microwave radio systems as the link between the baseband signal and the 70-MHz FM signal. Designed primarily for use on the TH-3 system, 4A FM terminals are also compatible with the TD-2 and TD-3 long-haul microwave radio systems. Using solid state circuitry throughout, emphasis was placed on reliability and performance consistent with TH-3 objectives with up to sixteen FM terminal pairs in tandem in 4000 miles. The FM transmitter utilizes the capacitance of two voltage-controlled varactor diodes in a resonant circuit of an oscillator operating at an IF frequency of 70 MHz. The diode capacitance is varied by applying a baseband signal across the diodes resulting in a frequency-modulated 70-MHz signal. The FM receiver uses a balanced, parallel resonant type discriminator preceded by two limiter circuits which ensure good AM suppression and a wide dynamic range. The FM terminal pair gain is 16 dB with a balanced baseband input and output impedance of 124 ohms.

I. INTRODUCTION

FM terminals perform the initial and final modulation steps in non-remodulating type microwave radio systems. The 4A FM transmitter converts the baseband signal to a frequency-modulated signal centered at 70 MHz while the 4A FM receiver performs the function of recovering the baseband modulation from the FM signal. The 4A FM terminal equipment will be used to provide improved performance in the TD and TH-3 microwave radio systems.

Design emphasis was placed on: (*i*) improved performance and reliability; (*ii*) reduced cost and size. The 4A FM terminal equipment (see Fig. 1) is capable of carrying up to 1800 message circuits comprising three multiplex mastergroups or one NTSC color television

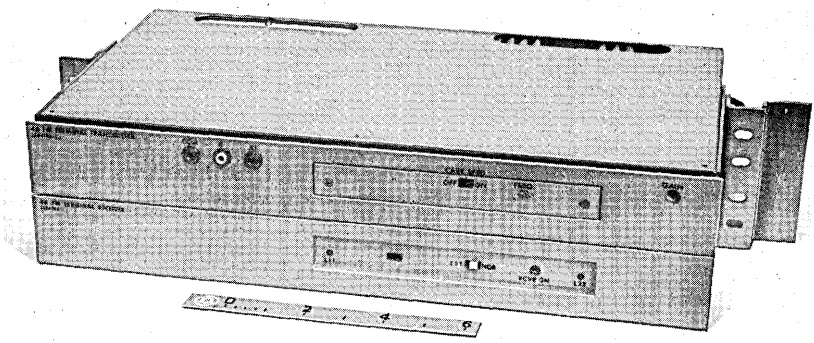

Fig. 1—4A FM terminal pair.

signal. FM terminals are required at each end of a radio route and at intermediate points where some portion or all of the baseband signal must be dropped or added.

II. DESIGN OBJECTIVES

The design objectives assigned to a terminal pair apply with pre-emphasis shapes which are chosen to optimize the overall radio system performance. The pre-emphasis shape used for 1200-circuit loading on TD systems is also used for 1800-circuit loading on TH-3 with little compromise from the ideal shape. With appropriate assumptions about the law of impairment addition, the system allocation to a single pair of terminals is given in Table I.

The modulating signals carried by TH-3 have an upper frequency limit of approximately 8 MHz. However, to minimize the influence of terminals on high-end frequency response and to allow for future applications, the high frequencies are controlled to 12 MHz. Phase distortion of the low-frequency components of the TV signal is satisfactorily controlled by maintaining the transmission response essentially flat down to 6 Hz.

Total FM terminal noise is a combination of fluctuation noise and cross-modulation distortion produced by circuit nonlinearities. In design and maintenance it is the linearity of the facility which is measured and adjusted to control cross modulation. However, since the desired end result is low noise, this is used as a final objective rather than the causative linearity requirements.

Undesired radio signals which leak into a repeatered radio system can cause interfering baseband beat tones at the receiver output. These same spurious signals in earlier radio systems which used klystron

TABLE I—DESIGN OBJECTIVES FOR ONE FM TERMINAL PAIR

Baseband transmission	
Bandwidth (±0.1 dB point)	6 Hz to 10 MHz
(±0.25 dB point)	10 MHz to 12 MHz
Gain stability	±0.25 dB per six-month maintenance interval
Load	1800 message circuits or one NTSC color television signal
Total noise contribution with an 1800-circuit pre-emphasized message load	<17 dBrnc0
Television weighted signal-to-	
low-frequency-noise	>40 dB
high-frequency-noise	>73 dB
Center frequency of FM transmitter	70 MHz ± 100 kHz
Peak frequency deviation	4 MHz
Deviation sense	Positive signal on input tip produces a decrease in transmitter frequency
Transmitter longitudinal suppression	>53 dB up to 1 MHz
Carrier spreading	12 dB reduction of radio frequency interfering tone per 3-kHz band
Change in receiver demodulation sensitivity for a 10-dB reduction in IF input	<0.25 dB
Microphonics	Negligible
Change in transmitter carrier frequency between zero and full-level modulation	<20 kHz
Operating temperature range	0 to 50°C

FM generators were less of an interference problem because the relatively unstable klystron-generated carriers caused the baseband beat frequency to spread randomly over several telephone channels rather than appear as a tone in a single channel. In the 4A transmitter design this same unstable carrier effect is simulated by modulating the carrier at a relatively high index with low-frequency noise when the system is used for telephone message transmission. The carrier is spread or deviated 22 kHz rms to achieve a 12-dB reduction in tone interfering effects in a 3-kHz telephone channel.

The requirement relating to carrier frequency stability as a function of modulation level is associated with the use of the carrier null or Crosby technique to accurately set the transmitter deviation.[1] Since the detection of a carrier null in the presence of adjacent sidebands requires a narrow-band receiver, it is essential that the application of modulation does not shift the carrier outside the receiver passband.

III. FM TRANSMITTER

The block diagram of Fig. 2 shows the general circuit features of the 4A FM transmitter. The balanced input signal is amplified and converted to a low-impedance unbalanced signal which is then applied to the deviator. The signal voltage applied to a pair of hyperabrupt junction varactor diodes modulates the frequency of a 70-MHz oscillator. All circuitry of the deviator, comprising oscillator, varactor diode biasing circuits, and IF buffer amplifier, is located in a controlled temperature environment to maintain the IF output frequency within the prescribed limits of ±100 kHz. The IF is filtered to reduce the harmonic content and amplified to produce the desired output level.

Three peripheral circuits outside the transmission path are included: an oven temperature control circuit, a 0–1-kHz noise generator, and a voltage regulator. The noise is inserted into the baseband signal to spread the carrier slightly and improve radio repeater tone interference performance. The regulator provides −20 volts for each of the units except the oven heater. Primary power for the oven heater and regulator is −24-volt battery.

The individual blocks in Fig. 2 are contained within a single die-cast chassis. Terminal bay cabling plugs into connectors located in the rear of the transmitter unit. Baseband and IF connectors are wired to a patchfield on the terminal bay.

3.1 *Baseband Amplifier*

The baseband amplifier provides a nominal 9 dB of voltage gain controlled to ±0.05 dB in the frequency band of 6 Hz to 10 MHz and ±0.25 dB from 10 MHz to 12 MHz. It also provides 53 dB of low-frequency common mode rejection.

Figure 3 is a simplified schematic diagram of the amplifier. A differential amplifier, Q_1 and Q_2, was selected for the input stages to provide common mode rejection. The emitter resistors of this amplifier provide local feedback for gain stability, but this configuration is inherently noisy. Transformers were not a practical solution to either the transistor noise or the common mode rejection problem because of the prohibitively wide transmission band of 6 Hz to 12 MHz. The noise difficulty was overcome by negative feedback of the combined noise from the collectors of the differential transistors Q_1 and Q_2 through the high-impedance current source of transistor Q_4. This feedback reduces the transistor noise by more than 12 dB. Transverse

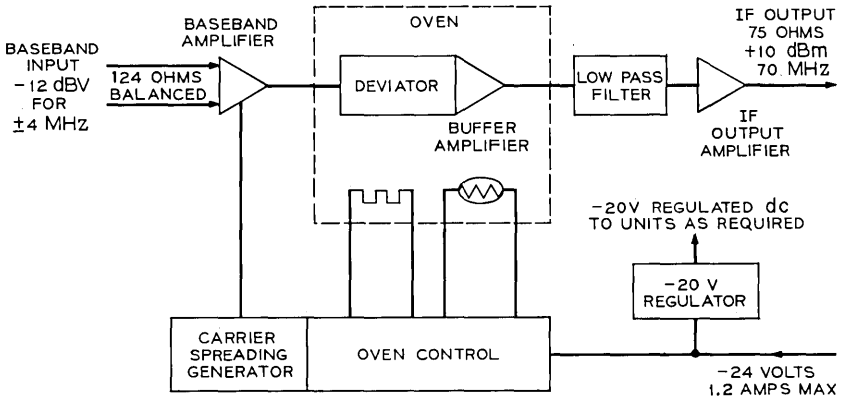

Fig. 2—Block diagram of 4A FM transmitter.

or out-of-phase signals cancel in the resistive combiner. This results in normal applied signals being unaffected by the noise feedback loop.

The gain control potentiometer is connected to equal dc voltage points which eliminates bothersome transients during gain adjustments.

A filter is used to isolate the deviator oscillator circuit from the baseband amplifier circuit. The design of this filter is complicated by the small separation between the 12-MHz upper baseband frequency and the corresponding 58-MHz first-order lower sideband of the deviator output. It would be impractical for this filter to also meet

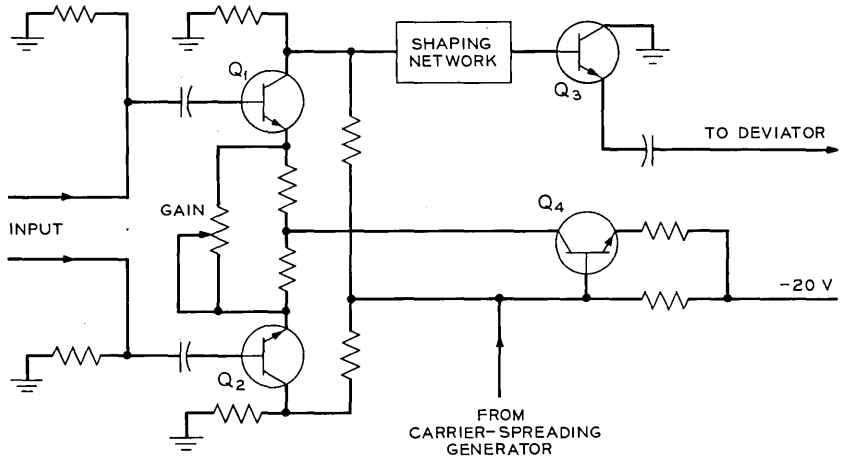

Fig. 3—Simplified schematic diagram of transmitter baseband amplifier.

the baseband frequency response requirements while terminated in the IF resonant circuit of the deviator. Therefore a simple split-apart filter is used for isolation and the resultant baseband transmission is equalized by the shaping network in the baseband amplifier.

3.2 *Deviator*

Frequency modulation in the FM transmitter is performed by the deviator. A direct deviator was used because a new design hyperabrupt junction varactor diode makes it possible to achieve broadband linearity needed in a deviator oscillating at the IF frequency of 70 MHz. Advantages of this approach, relative to the heterodyne deviator, are the absence of any spurious tones from the mixing process, reduced thermal noise problems due to higher oscillating levels, and a greater bandwidth. The principal disadvantage of the direct deviator is the difficulty in separating the oscillator and baseband signals due to their frequency proximity.

To ensure IF frequency stability, temperature control was chosen in preference to automatic frequency control. This was based on economic advantage, the elimination of low-frequency response limitations associated with an automatic frequency control loop, and the general advantages which accrue from temperature stabilization of the semiconductor circuit environment. However, the lack of an automatic frequency control circuit imposes stringent requirements on oscillator frequency stability.

The deviator is essentially a 70-MHz oscillator that is made up of a low-phase-shift amplifier with a variable phase feedback circuit (see Fig. 4). The feedback loop phase shift plus the residual phase

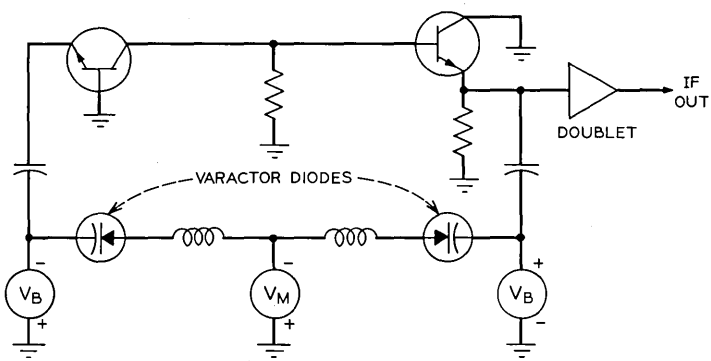

Fig. 4—Basic configuration of transmitter deviator.

shift of the amplifier equals zero degrees at the oscillating frequency.

A new hyperabrupt junction diode coded 511A was developed specifically for this application.[2] Figure 5 shows a typical diode capacitance versus voltage characteristic. Of particular interest from the standpoint of its effect on modulation linearity is the slope of the capacitance-voltage curve in the neighborhood of the operating point.

Assuming that near the operating point the diode capacitance voltage relationship can be written in the form

$$C_d = K_1 V^{-m},$$

a deviator with a single diode and inductor in the feedback path will oscillate at a frequency given by the following relationship:

$$f = \frac{1}{2\pi\sqrt{LC_d}} = \frac{V^{m/2}}{2\pi\sqrt{LK_1}}.$$

This assumes that the oscillator frequency is essentially determined by the resonant frequency of the feedback circuit.

For f to be linearly dependent on V, m must equal 2. In practice, however, a number of factors modify the preceding idealized situation. Stray capacitance for example generally requires m to be higher than the theoretical optimum. In addition, the assumed capacitance law is not accurately descriptive of the real life relationship. This is illustrated in Fig. 6 where $m = [d(\log C)/d(\log V)]$ is plotted versus bias voltage. Only in a very narrow region near the peak of the curve is m approximately constant, corresponding to an operating point in the maximum slope region of the C-V characteristic of Fig. 5. Since the maximum value of m is a diode parameter of special interest, it has been designated m.*

The diode characteristic illustrated in Fig. 6 is too narrow to obtain satisfactory deviation linearity over the desired sweep range. However, the linear operating range can be extended by using a technique analogous to the double-tuned transformer. Two diodes are connected in series as shown in Fig. 4 with individually adjustable biases. When the biases are identical at the value corresponding to m* the series-tuned circuit will behave like the single diode case. If now the biases are offset in opposite directions, the individual m characteristics (Fig. 6) will separate to produce a broadening of the region in which m is reasonably constant. This is illustrated in Fig. 7 where the computed deviation sensitivity has been plotted against oscillator frequency with the bias offset V_B as a parameter. The analogy with undercoupled and overcoupled tuned transformers is evident. The

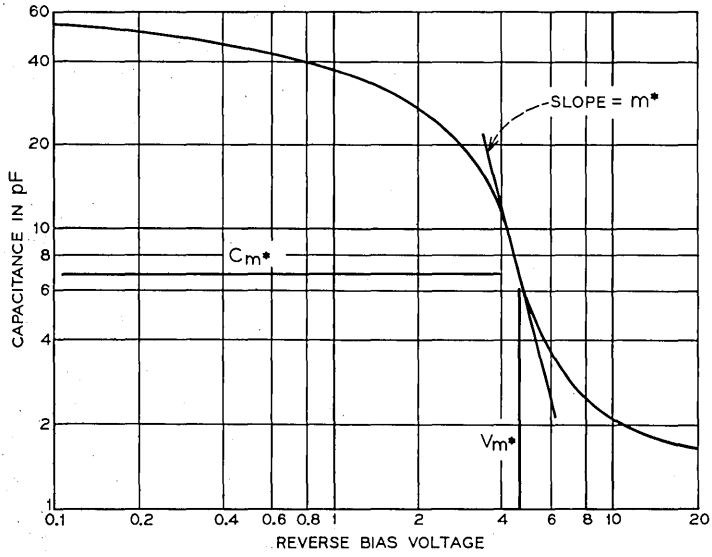

Fig. 5—Hyperabrupt junction diode capacitance vs voltage.

characteristics of Fig. 7 were obtained in a very straightforward manner starting with the capacitance-voltage characteristic of an actual diode. With two such diodes in series, the resonant frequency versus the modulating voltage V_m (Fig. 4) can be determined for each V_B. The derivative of these characteristics gives the deviation sensitivity in MHz/volt which is then plotted against resonant frequency. The deviation sensitivity plot of Fig. 7 is essentially the characteristic that

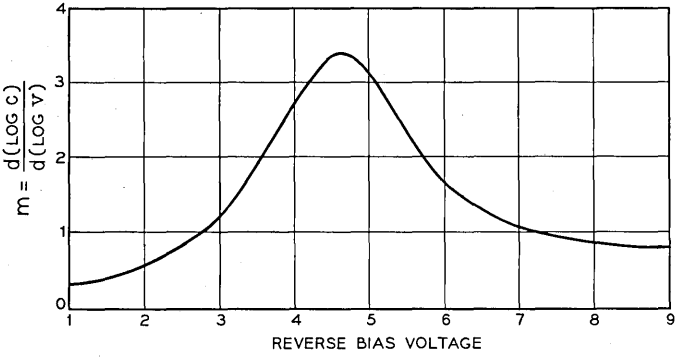

Fig. 6—Hyperabrupt junction diode m vs voltage.

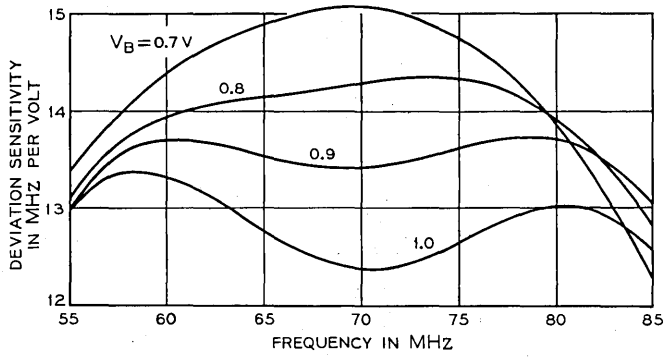

Fig. 7—Deviation sensitivity vs oscillator frequency.

would be seen on a linearity test set. Such a test set usually displays the result in percent of nonlinearity as shown in Fig. 8 for a 4A transmitter. The similarity, at least in shape, of the optimum curve in Fig. 7 with the measured characteristic in Fig. 8 is evident.

A common-base, common-collector amplifier configuration was chosen to complete the oscillator loop. The low amplifier input-output impedances and the high varactor impedances at baseband frequencies provide the required filtering needed to separate the IF and baseband frequencies. This assures that most of the baseband signal voltage drop occurs across the varactors while the IF signal present at the point of insertion is at a minimum. The loop amplifier has a gain slightly greater than unity with the common-collector stage biased to limit the loop oscillating level to a predetermined value. This

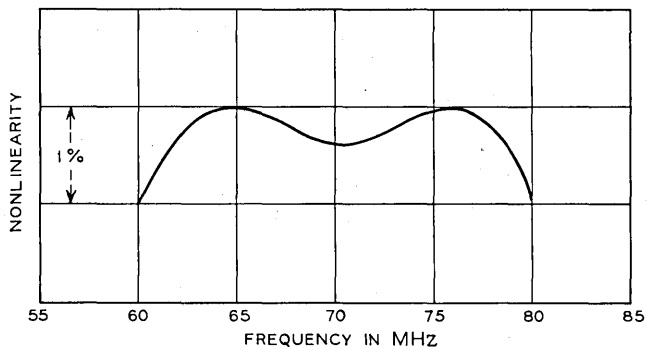

Fig. 8—Typical nonlinearity of a 4A FM transmitter.

limiting action maintains the loop gain at unity and allows for slight variations in amplifier gain and feedback loss. In practice each diode in the feedback network has an independent bias which is adjusted to produce a linear frequency deviation over the range of 62 to 78 MHz.

The oscillator loop is tapped at the amplifier output and fed to a doublet amplifier. This amplifier sets the proper IF operating level for the entire transmitter and also serves to buffer the oscillator from external impedances. A low-pass constant resistance filter at the output of the buffer amplifier reduces the harmonic components of the IF output signal.

The frequency elements most sensitive to temperature are the varactor diodes. The frequency is stabilized by isolating the diodes from heat generated by nearby circuitry. This is accomplished by placing the diodes as far as possible from heat-producing transistors and resistors and by cutting a slot in the printed wiring board between the heat source and the diodes. Also, the biasing circuits are temperature compensated for capacitance changes of the varactor diodes. This approach is good for only the average diode capacitance versus temperature characteristic and produces a stability within ±10 kHz per degree Celsius (Centigrade).

The greatest stabilizing factor is the temperature control of the entire oscillator, including the biasing and buffering circuits. By placing the sensing element for the oven control circuit as close as possible to the varactor diodes, the capacitance changes are reduced considerably. Two factors influence the selection of circuit operating temperature. On the one hand, reliability of components, particularly active ones, makes a low operating temperature desirable; on the other hand, the need for frequency stability up to 50°C ambient makes an oven temperature at least this high a necessity. As a compromise, 50°C was chosen for circuit operation with loss of control at approximately 43°C due to power dissipation of the circuitry within the oven. These factors result in a stability of ±1 kHz per degree within the control range and ±10 kHz per degree above 43°C.

3.3 *Carrier-Spreading Circuit*

The carrier-spreading circuit supplies noise with an upper bandwidth limit of 1 kHz to deviate the FM carrier at a high modulation index. This carrier deviation is analogous to an unstable carrier in spreading the beat frequency of interference-generated baseband tones into random noise interference in several message channels. This

technique using 22 kHz rms deviation results in a 12-dB reduction of the interfering tone level appearing in a disturbed channel.

Noise which originates in a diode back-biased into the noise region is filtered by a 1-kHz low-pass R-C network with 18 dB per octave rolloff. A field effect transistor is used to transform the high impedance of the low-pass filter for insertion into the baseband amplifier. A switch for disabling the noise generator is provided since the low-frequency noise would interfere with television transmission.

3.4 *IF Output Amplifier*

The IF output amplifier consists of a harmonic suppression filter and doublet amplifier with a fixed gain of approximately 8 dB. Harmonic components of the IF signal are reduced by the combined filters of the deviator and amplifier to a level that is lower than that generated in the output amplifier. The doublet is a two-transistor amplifier with series-shunt feedback.[3] The 70, 140, 210, and 280 MHz output levels of the transmitter are +10, −10, −20, and −40 dBm, respectively.

IV. FM RECEIVER

A block diagram of the 4A FM receiver, including the IF and baseband levels, is shown in Fig. 9. In the input amplifier-limiter the 70-MHz signal is amplified and fed to a limiter circuit in order to reduce any amplitude modulation which may be present on the signal. The limiter output is further amplified and applied to a filter-equalizer which attenuates harmonics generated in the limiter. This network also provides envelope delay equalization for the overall receiver. The

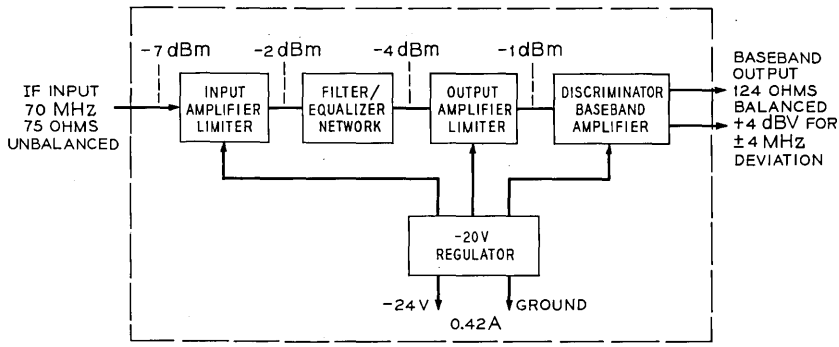

Fig. 9—Block diagram of 4A FM receiver.

signal then passes to a second amplifier-limiter which provides an additional 18 dB of AM suppression. In addition, due to the combined action of the two limiter circuits, the dynamic range of the receiver is extended so that a 10-dB reduction in IF input produces a change of less than 0.25 dB in the receiver baseband output. The signal is then applied to a discriminator where the baseband information is recovered from the frequency-modulated IF signal. After detection, the demodulated baseband signal is amplified by a balanced baseband amplifier. The receiver circuitry is powered from a series transistor regulator which provides a stable output voltage for line voltage variations and changes in temperature. The regulator operates from the −24-volt office battery supply.

4.1 *Input Amplifier-Limiter*

The basic IF amplification stage in the 4A receiver utilizes a doublet amplifier comprised of two transistors with series-shunt feedback. This same amplifier configuration is used in the TH-3 IF main amplifier.[3]

The doublet stage is followed by a limiter circuit. Two series-connected diodes amplitude-clip the frequency-modulated signal to remove any undesired amplitude modulation resulting from residual transmission distortions which may be present on the IF signal. The amplitude modulation suppression exceeds 28 dB for modulating frequencies up to 10 MHz.

In the series-type diode limiter used in the 4A receiver, limiting is accomplished with two forward-biased expitaxial silicon Schottky barrier diodes[4] as shown in Fig. 10. Any amplitude modulation on the FM signal is removed by clipping the signal current when it exceeds the diode bias current. However, the amount of AM suppression is limited by the magnitude of the signal shunted across the diodes

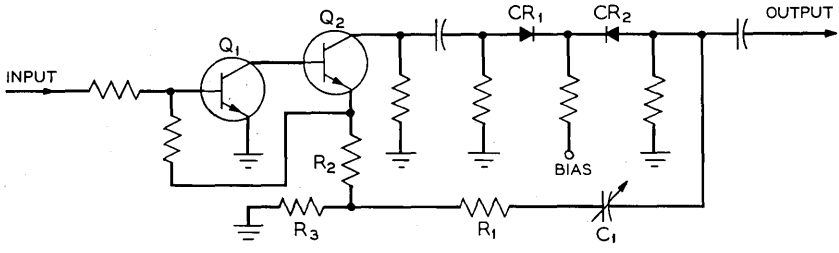

Fig. 10—Compensated limiter circuit of 4A FM receiver.

by the parasitic capacitance of the diodes when in the reverse-biased state. This limitation is overcome by applying a signal at the limiter output which is 180 degrees out-of-phase with the capacitively-bypassed signal. This antiphase signal cancels the leakage current shunted across the diodes thereby increasing the AM suppression and decreasing the amplitude-to-phase conversion.

The compensating circuit used to derive the antiphase signal consists of capacitor C_1 and resistors R_1 through R_3 of Fig. 10. The amplitude of the out-of-phase signal is reduced by the ratio of resistors R_2 and R_3. The R-C network comprised of R_1 and C_1 further reduces the amplitude and adjusts the phase of the compensating signal. The through signal and the antiphase signal are combined at the limiter output resulting in a significant improvement in performance. The efficiency of the balancing technique is illustrated in Fig. 11 which shows the AM suppression and AM-PM conversion as a function of amplifier-limiter input level. The compression characteristic of the input amplifier-limiter is shown in Fig. 12.

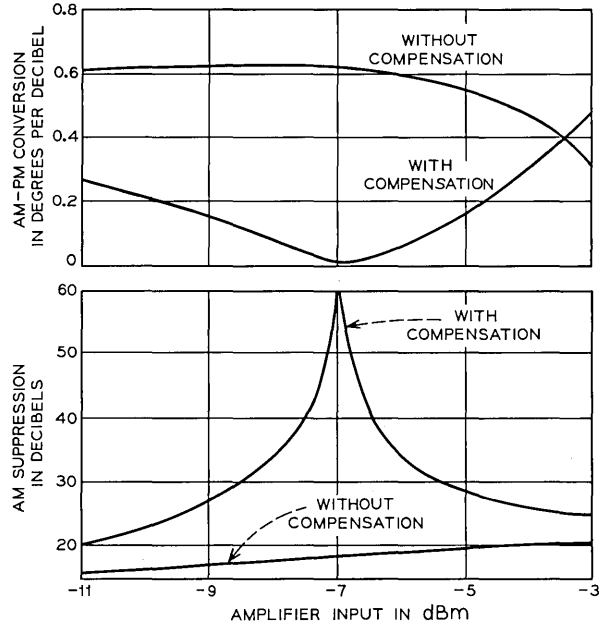

Fig. 11—AM-PM conversion and AM suppression vs amplifier input level of 4A FM receiver input amplifier-limiter (100-KHz modulating frequency).

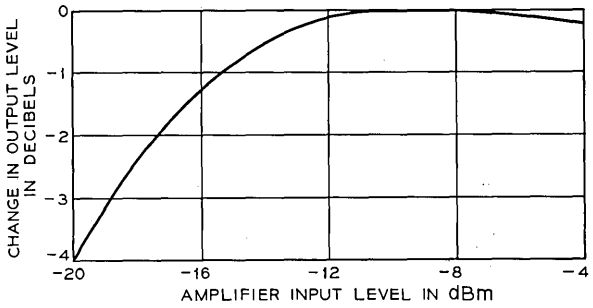

Fig. 12—Output change vs amplifier input level of 4A FM receiver input amplifier-limiter.

Gain and slope adjustments are provided in the doublet stage following the limiter circuit to set the output level and reduce the transmission slope of the input amplifier-limiter over the 60- to 80-MHz band to less than 0.05 dB.

4.2 *Output Amplifier-Limiter*

The output amplifier-limiter consists of a stage of amplification, an uncompensated limiter, and a harmonic filter. Since the amount of amplitude modulation at the input to this limiter will generally be small, compensation is unnecessary. The limiter reduces amplitude modulation by 18 dB for modulating frequencies up to 10 MHz. A constant resistance low-pass filter attenuates harmonic tones generated by the limiter circuit. The nominal input and output levels are −4 and −1 dBm, respectively.

4.3 *Discriminator Baseband Amplifier*

The discriminator consists of a doublet stage, a balanced resonant discriminator, and a baseband amplifier as shown in the simplified sketch of Fig. 13. The high- and low-frequency parallel resonant tank circuits are tuned to specific frequencies thereby eliminating the complexity of simultaneously adjusting receiver sensitivity, crossover frequency, and linearity. The common tank circuit provides an independent receiver linearity adjustment, thereby minimizing the interaction between adjustments. The overall receiver linearity is less than 0.3 percent for a peak-to-peak deviation of 10 MHz.

An R-L-C impedance network at the output of each detector diode provides a constant impedance over the baseband-to-IF frequency band. By controlling the impedance in this region a source of second-

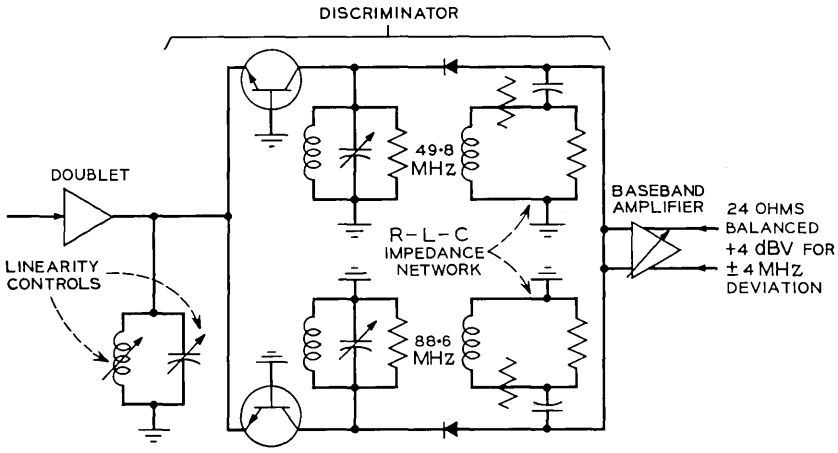

Fig. 13—4A FM receiver discriminator circuit.

order distortion is controlled. Otherwise, the generation of these A − B type products results in excessive modulation noise in the bottom message channels.

The balanced baseband amplifier circuit remains essentially unchanged from its 3A counterpart.[5] Minor modifications were introduced in the shaping network used to adjust baseband frequency response in order to control the flatness of the frequency characteristic to within 0.1 dB out to at least 12 MHz.

V. TANDEM PERFORMANCE

Laboratory experience on the tandem performance of the 4A FM transmitter and receiver has shown a very satisfactory degree of reproducibility.

5.1 *Noise Load Performance*

The most satisfactory measure of terminal performance from the standpoint of message applications is based on the use of bandlimited fluctuation noise to simulate the multichannel speech load. Noise and cross-modulation performance measured in this manner is presented in Figs. 14 and 15 corresponding to 1200- and 1800-circuit message loading, respectively. The performance at reference drive with 1800-circuit loading is well within the objective of 17 dBrnc0.

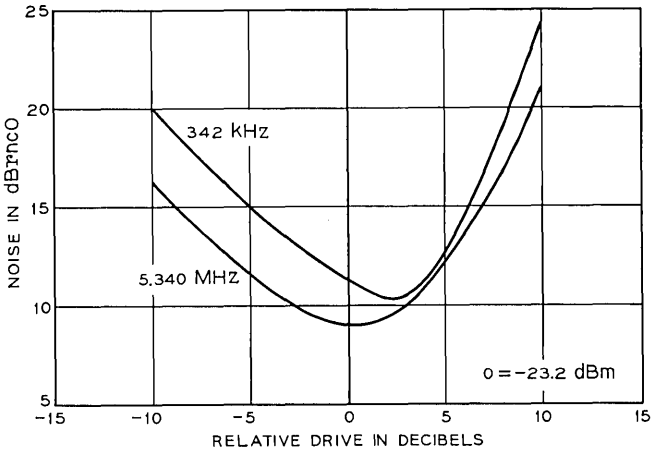

Fig. 14—4A FM terminal pair, 1200-circuit noise load, 457D pre-emphasis.

5.2 *Fluctuation Noise*

Fluctuation noise generated by a tandem transmitter and receiver and measured at the receiver output is shown in Fig. 16. This total noise is made up of several distinguishable contributors as indi-

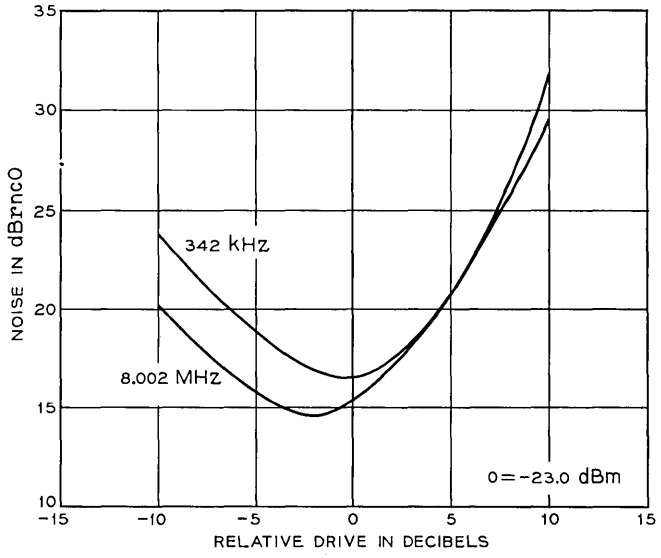

Fig. 15—4A FM terminal pair, 1800-circuit noise load, 457D pre-emphasis.

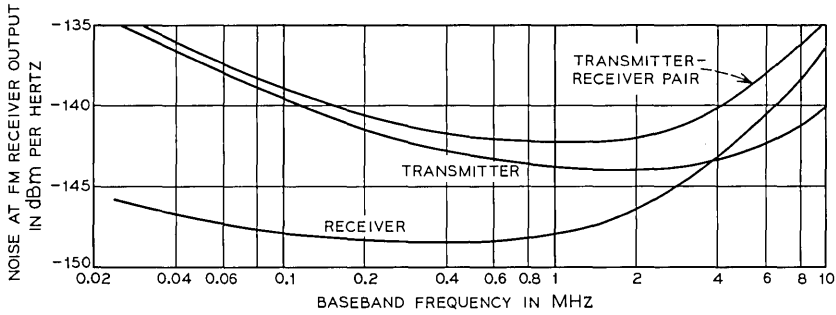

Fig. 16—4A FM terminal pair: fluctuation noise.

cated in the figure. Fluctuation noise at high baseband frequencies is controlled by the noise figure of the receiver input amplifier-limiter which has the lowest signal level of the terminal pair. In the baseband region below about 3 MHz, the main fluctuation noise source is the transmitter baseband amplifier.

For television transmission, the ratio of peak-to-peak video signal to weighted noise is the most meaningful measurement of performance. For this measurement the weighted baseband noise is generally separated into two regions, one encompassing the low-frequency end of the band up to 4 kHz and the other encompassing the range from 4 kHz up to approximately 4.5 MHz. The noise is measured at the FM receiver output following the video de-emphasis network. Typical values for signal-to-weighted low-frequency noise and signal-to-weighted (color) high-frequency noise are 106 and 97 dB, respectively, meeting the corresponding 40- and 73-dB objectives with a comfortable margin.

5.3 *Transmitter Carrier Frequency Shift With Modulation*

When an FM transmitter is modulated there is generally a small shift in the output carrier frequency relative to the unmodulated value. On the 4A transmitter with ±4 MHz sine-wave modulation, this shift is less than 2 kHz.

5.4 *Transmitter Carrier Frequency vs Voltage*

Transmitter performance variations due to −24-volt line changes are minimal. In particular the output frequency changes are small. Typical frequency change over the entire operating range of 21 to 27 volts is less than ±1 kHz per volt.

5.5 *Baseband Amplitude Response*

The baseband response is flat to within ±0.05 dB from 6 Hz to 11 MHz and rolls off gradually beyond those frequencies. The high end at 12 MHz is down less than 0.2 dB relative to 10 MHz.

For television purposes the low-frequency response is frequently characterized by the response to a 60-Hz square wave. Slope on the square wave output expressed as a percentage of the peak-to-peak signal is a measure of the phase fidelity at the fundamental frequency. Typical slope measured at the output of a 4A terminal pair is 2.0 percent which approximates a low-end 3-dB cutoff frequency of 0.7 Hz.

5.6 *Differential Gain, Differential Phase, and Linearity*

The differential gain and phase as measured with pre-emphasis are within 0.02 dB and 0.25 degree for a deviation of ±1.69 MHz. Nonlinearity for the terminal pair with 12 MHz peak-to-peak deviation is less than 0.5 percent.

5.7 *Transmitter Longitudinal Suppression*

Longitudinal suppression is a measure of sensitivity to extraneous signal and transient pickup on balanced shielded cable used for video trunking. Figure 17 shows the suppression achieved over the frequency range useful for television transmission.

VI. EQUIPMENT FEATURES

The physical features of a 4A receiver, which is essentially the same as a transmitter, are shown in Fig. 18. A single die-cast framework containing five shielded sections which house the individual printed wiring boards is used for a transmitter or receiver unit. Each printed wiring board is attached to a metal shield separated by a distance of approximately one-half inch by metal studs. This type of construction provides a good mechanical as well as a good electrical connection between the circuit board and ground. The subassembly is inserted into a compartment and fastened to the framework. Each metal shield performs a second function by serving as a portion of the bottom cover for the unit as well as an individual circuit ground plane. The opposite side of the chassis is enclosed by a single cover as illustrated in the photograph.

Radiation between compartments is prevented by a rubber gasket containing numerous small pieces of wire. The cover is tightened

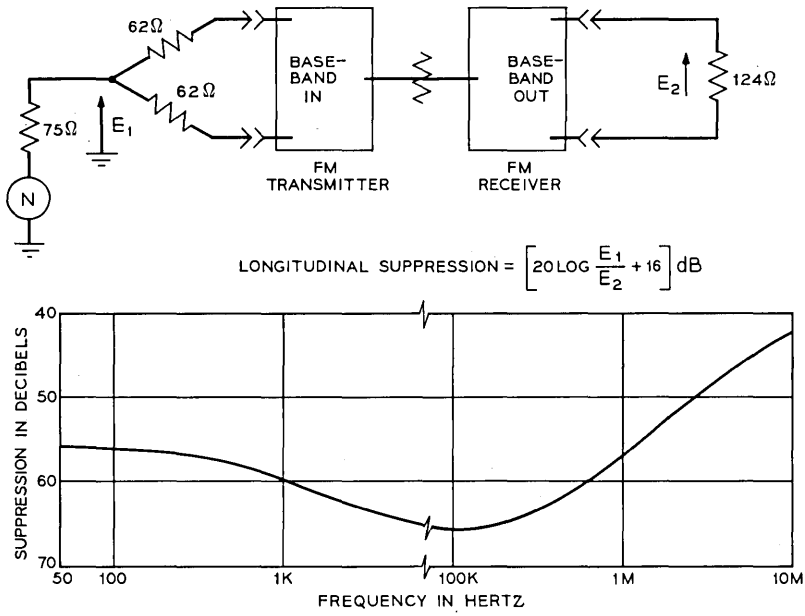

Fig. 17—4A FM terminal pair: longitudinal suppression.

down against the gasket material and inserted into a channel surrounding each compartment, establishing a continuous ground at the junction of the sidewall and the cover.

A transmitter or receiver unit, two inches high and weighing approximately seven pounds, slides on nylon tracks into a special shelf which is designed to mount on a 19-inch bay framework. Three shelf

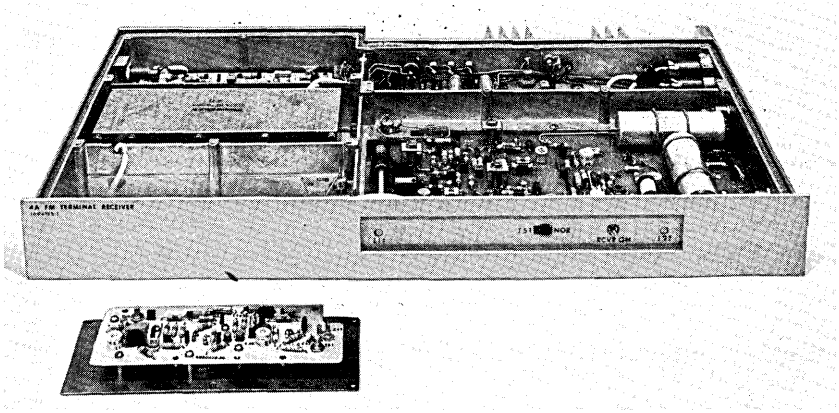

Fig. 18—Assembly features of 4A FM transmitter or receiver.

arrangements are available housing two, three, or five units. Each unit is fastened to the shelf by a special latch arrangement located at the rear of the bay.

The power, IF, and baseband connections are located at the rear and sides of the unit, respectively. The IF and baseband connections are wired to a patchfield on the FM terminal bay to provide access for test purposes. A nine-foot FM terminal bay can be equipped with up to fifteen 4A FM transmitters and fifteen 4A FM receivers.

A portable version of the 4A FM terminal unit, weighing approximately 45 pounds, was also designed. This unit consists of a portable housing with accessories designed to provide a complete portable FM terminal facility. Auxiliary equipment supplied with the housing includes two balanced-to-unbalanced transformers, balanced-to-unbalanced pre- and de-emphasis networks, a pad for the back-to-back terminal interconnections, and a jackfield. For normal usage an associated 117-volt, 60-Hz rectifier unit is available with an output capability of 1.6 amperes at −24 volts. A direct connection to the −24-volt central office battery is also available. A photograph of the portable FM terminal is shown in Fig. 19 with the front cover of the portable housing removed.

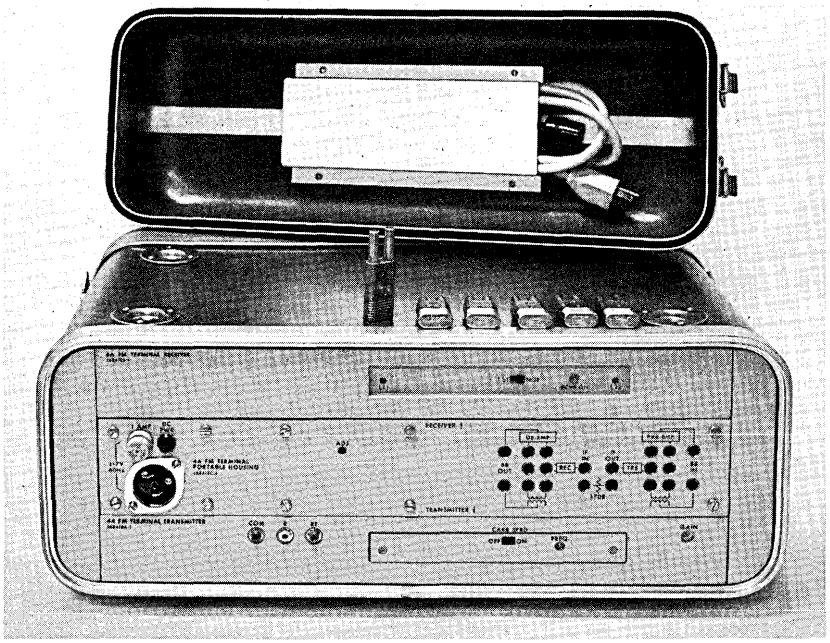

Fig. 19—Portable 4A FM terminal pair.

VII. SUMMARY

The 4A FM terminal pair has been designed to provide a better performing, lower cost, and physically smaller replacement for the 3A FM terminal pair. Operating at an IF center frequency of 70 MHz, the terminal pair can be used on all TD microwave radio system applications as well as on the TH-3 microwave radio system.

VIII. ACKNOWLEDGMENTS

The authors wish to acknowledge the many individuals of the Radio Transmission Laboratory who have contributed to the development of the 4A FM transmitter and receiver.

REFERENCES

1. Crosby, M. G., "A Method of Measuring Frequency Deviation," R.C.A. Review, *4*, No. 4 (April 1940), pp. 473–477.
2. Foxhall, G. F., and Milne, R. A., "Advantages of Ion Implantation in Fabricating Hyperabrupt Junction Diodes," IEEE Int. Electron Device Meeting, October 1969.
3. Fenderson, G. L., "TH-3 Microwave Radio System: The IF Main Amplifier," B.S.T.J., this issue, pp. 2195–2204.
4. Elder, H. E., "Active Solid-State Devices," B.S.T.J., TD-3 System Issue, *47*, No. 7 (September 1968), pp. 1323–1377.
5. Barry, J. F., Gammie, J., Lentz, N. E., and Salvage, R. C., "3A FM Terminal Transmitter and Receiver," B.S.T.J., TD-3 System Issue, *47*, No. 7 (September 1968), pp. 1423–1458.

THE BELL SYSTEM TECHNICAL JOURNAL
Vol. 50, No. 7, September, 1971
Printed in U.S.A.

TH-3 Medium-Haul Application:

System Considerations

By K. L. SEASTRAND and D. S. WILLIAMS

(Manuscript received February 22, 1971)

The medium-haul application of TH-3 was developed to provide an economically attractive system of moderate length and cross section without seriously compromising performance. To achieve high-quality transmission the radio transmitter-receiver bays and FM terminals common to the long-haul plant were used. Supporting equipment was both designed and adapted specifically for the medium-haul application in order to keep overall costs to a minimum.

I. INTRODUCTION

This paper discusses a radio system which has been made available to the Associated Bell System Companies to help meet their demands for high-performance transmission capability. It is made up of the TH-3 IF heterodyne radio bay and 4A FM terminals along with a number of supporting features. This system was formulated to be a flexible package that may be customized to specific transmission needs within the Bell System. Flexibility results from the optional use of a frequency-diplexed auxiliary channel, a one-by-one baseband protection switching system, a single transmitting/receiving antenna, and the use of shelters to house the equipment. These features collectively distinguish the medium-haul concept from that which is typically called long or short haul.

In spite of the difficulty establishing a model for the medium-haul system, since the anticipated applications are so varied, a 1000-mile, 1800-circuit system model (38 hops with 4 baseband switching sections) has been selected. This choice represents a reasonable compromise between the 4000-mile long-haul model and the 250-mile short-haul model and will be used to describe noise and reliability performance. This system will meet the two-way reliability objective

of 0.02 percent and, depending on how the options are exercised, has a noise performance falling within the range from 35.5 to 36.0 dBrnc0. Extrapolation of performance data to other arrangements is relatively straightforward.

II. SYSTEM DESCRIPTION

The development of an overall radio system suitable for medium-length and medium-cross-section applications has resulted in the use of some existing subsystems, the adaptation of others, and some completely new designs. At the heart of the radio system are the TH-3 transmitter-receiver bays[1] and the 4A FM terminals.[2] These are used essentially as originally designed, while the power plant and the buildings are existing designs which require some adaptation for this application. Such items as the 300A protection switching system,[3] the E2 status reporting and alarm system for medium haul,[4] and the frequency-diplexed auxiliary channel[5] involved fundamental design work most of which was stimulated by the medium-haul application.

Figure 1 shows in a simplified manner the essentials of a medium-haul TH-3 system. Main stations, which are the switching section end links, are characterized by the presence of baseband signals. The 300A protection switching system shown in Fig. 1 may be at a main station or it may be physically isolated from the main station by as much as eight miles via wire line entrance links. If the system includes more than one tandem switching section, a back-to-back pair of main stations exists at the junction of the switching sections. Repeaters are characterized by the fact that the through signal does not go through an FM remodulation process; therefore, with the exception of the auxiliary channel signal, only RF and IF signals are present at repeaters.

The following paragraphs briefly cover some of the salient features of the blocks shown in Fig. 1.

2.1 *Basic Transmission Equipment*

This equipment includes the entrance links, FM terminals, and TH-3 transmitter-receiver bays. Standard 3A wire line entrance link gain and equalization equipment and 4A FM terminals are used with medium-haul systems. As with the entrance links and FM terminals, the TH-3 transmitter-receiver bay is identical for both long- and medium-haul applications.

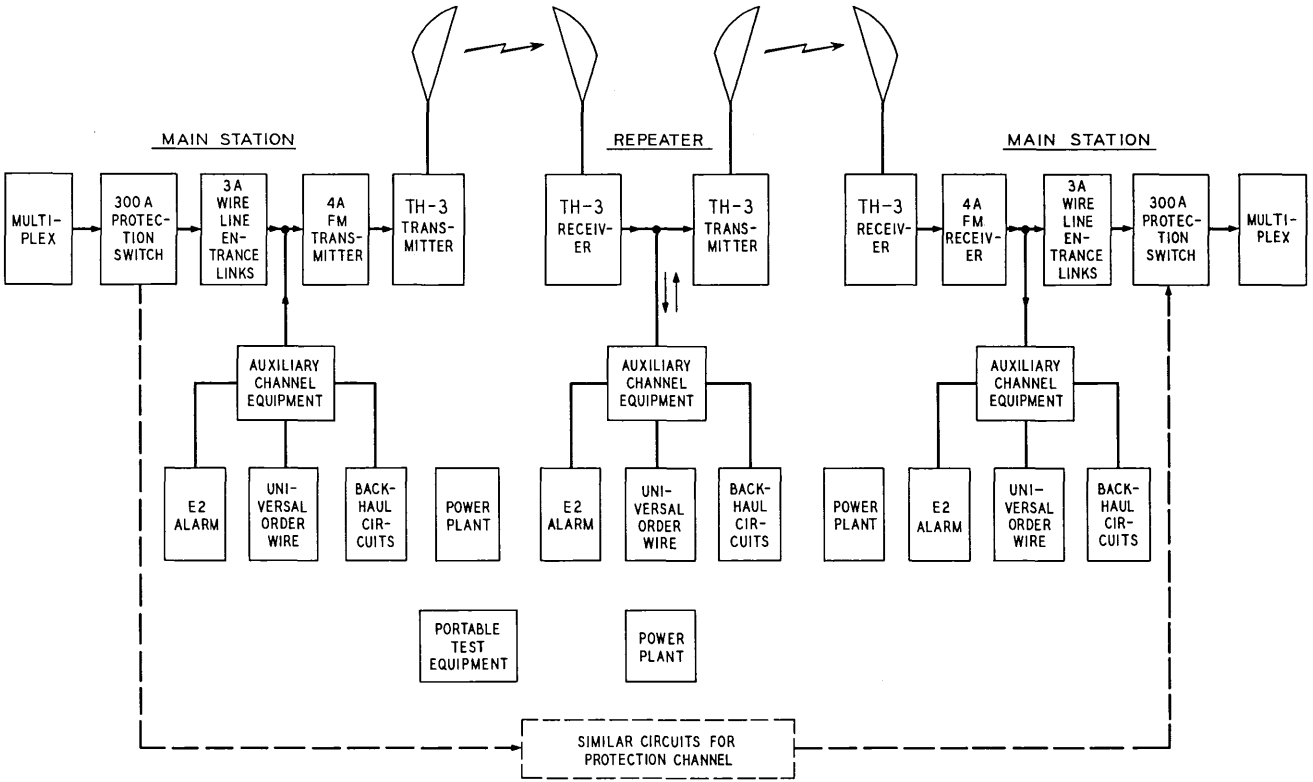

Fig. 1—Typical two-hop medium-haul system providing transmission in one direction. Similar equipment is required for transmission in the opposite direction.

2.2 *Baseband Protection Switch*

A new solid state protection switching system, designated 300A, has been developed to provide a one-for-one baseband switch for the protection of message service. Protection is provided by modulating simultaneously the two radio channels at the transmitting end of the switching section. All switching is done at the receiving end where the channel monitors, automatic logic, and controls are located. The comparatively high signal handling capacity of the switch and its low loss permit the entrance links and FM terminals to be included within the switching section.

2.3 *Auxiliary Circuit Facility*

The frequency-diplexed auxiliary channel is an inband (over the radio) transmission facility with access at each radio station. It operates above the normal 1800-circuit payload signal in a narrow band centered at 11.38 MHz. The basic auxiliary channel arrangement has available three voice-frequency circuits. Two of these would normally be used to carry order wire and alarm information, the third being available for other uses. With additional multiplex, up to 48 circuits for trunking may be provided. These "backhaul" circuits are intended to provide trunking facilities from a relatively remote location, near a repeater station, to a point where they would have access to the Bell System network. When 4A FM terminals are used, the auxiliary channel will have a noise performance roughly equal to that of short-haul radio (35 dBrnc0 for 10 hops).

Access to the auxiliary channel is straightforward at terminal stations since the baseband signal is present. At repeater stations a 4A FM receiver is bridged onto the IF signal path. The FM receiver output then provides a signal which may be utilized without any interference to the 1800 circuits in the through path. To modulate additional 11.38-MHz information onto the system a microwave FM modulator is placed in tandem with the microwave generator signal (local oscillator) driving the repeater transmitter modulator. By this means, access to the radio channel is available at each repeater station.

Since the auxiliary channel carries alarm information, it is important that transmission be highly reliable. For this reason, the auxiliary channel has its own protection switching system. The signal is fed over two RF channels; at each station along the route, the better performing RF channel is selected.

2.4 *E2 Status Reporting and Control System*

At the time the medium-haul concept was being established, an examination of existing alarm reporting systems showed them either to have capacity for too few alarms, indications, and orders, or to be physically too large and expensive for medium-haul purposes. In addition, the dc voltages associated with the power required for these systems was often not readily available at medium-haul installations.

One of the systems considered was the recently developed E1 status reporting and control system. This is a solid state digital system which includes data transmission facilities for use on a standard voice channel. Although in its existing embodiment it was large and costly for the medium-haul purpose, it had been designed using a modular approach. Stimulated by the medium-haul need, a modified version of the E1 system (called E2) was developed. This revised version eliminated the large cross-connect field that previously occupied one-third of the bay, and broke down the groups of alarms, indications, and orders into smaller packages.

The medium-haul needs involve approximately 12 orders and 90 combined alarms and indications at each station. The final remote E2 package handles this capacity with room for limited growth; i.e., a total of 32 orders and 128 combined alarms and indications. Capacity to grow to 256 alarms and indications exists by adding a small amount of hardware. A central E2 station for use with medium haul can control up to 64 remote stations. Each of these remote stations is "polled" by the central station for the status of its alarms.

The E2 package allows medium-haul systems to take advantage of the latest in designs and technology without incurring the large expense associated with status reporting and control systems tailored to larger needs.

2.5 *Portable Test Equipment*

Radio stations housing medium-haul TH-3 systems will frequently have as few as four transmitter-receiver bays along with a limited number of bays of supporting equipment. This is a small fraction of of the total amount of equipment located in a typical long-haul radio station. To minimize the cost of test equipment for medium-haul routes, use of portable test equipment is recommended. This test equipment is composed primarily of commercially available test gear housed in lightweight suitcases which can be easily transported. It may be stored at a central location, such as a maintenance station

or alarm control center, from which it can be taken to any station that requires testing. Use of a limited number of sets of the equipment, depending on the length of the system, can drastically reduce the investment in test equipment compared to maintaining complete fixed test equipment at each radio station. Such a procedure is permissible because of the long test intervals that are expected to apply to both the TH-3 equipment and the supporting gear.

A feature of the TH-3 transmitter-receiver that helps make the portable concept attractive is the ability to replace any component in the bay without requiring immediate alignment with test equipment. This practice, when applied on a limited basis, will result in such slight impairment to system performance that precise alignment can be postponed until convenient.

The photograph in Fig. 2 shows a cart that permits stacking of the test equipment during maintenance. The test gear shown in the photograph is capable of maintaining the TH-3 radio bays with virtually the same accuracy attainable with test equipment dedicated to a station. Several additional commonly available test sets are used in conjunction with the maintenance of the auxiliary channel, order wire, alarm, and power equipment.

2.6 *Equipment Shelters*

An equipment shelter concept developed for short-haul radio may be used for medium-haul TH-3. This concept provides for factory installed and tested radio equipment with a minimum of field installation. Aluminum "truck body" type structures are available to house the radio equipment. Several different lengths are available depending on anticipated growth. For a radio system of this type where a limited amount of equipment is installed with a minimum of special modifications, this type of shelter provides a very economical building. A bay pivoting arrangement was developed to permit mounting the equipment against the shelter wall and still allow maintenance from both sides of the bay.

2.7 *Power*

The main source of power at medium-haul stations is a −24-volt battery reserve plant. Small amounts of power at +24 volts are indirectly supplied from the −24-volt plant by voltage converters. The current drain at a typical repeater station is 65 amperes, with a recommended battery reserve of about 33 hours. The 111A power plant specified for this system permits two alternatives: either a

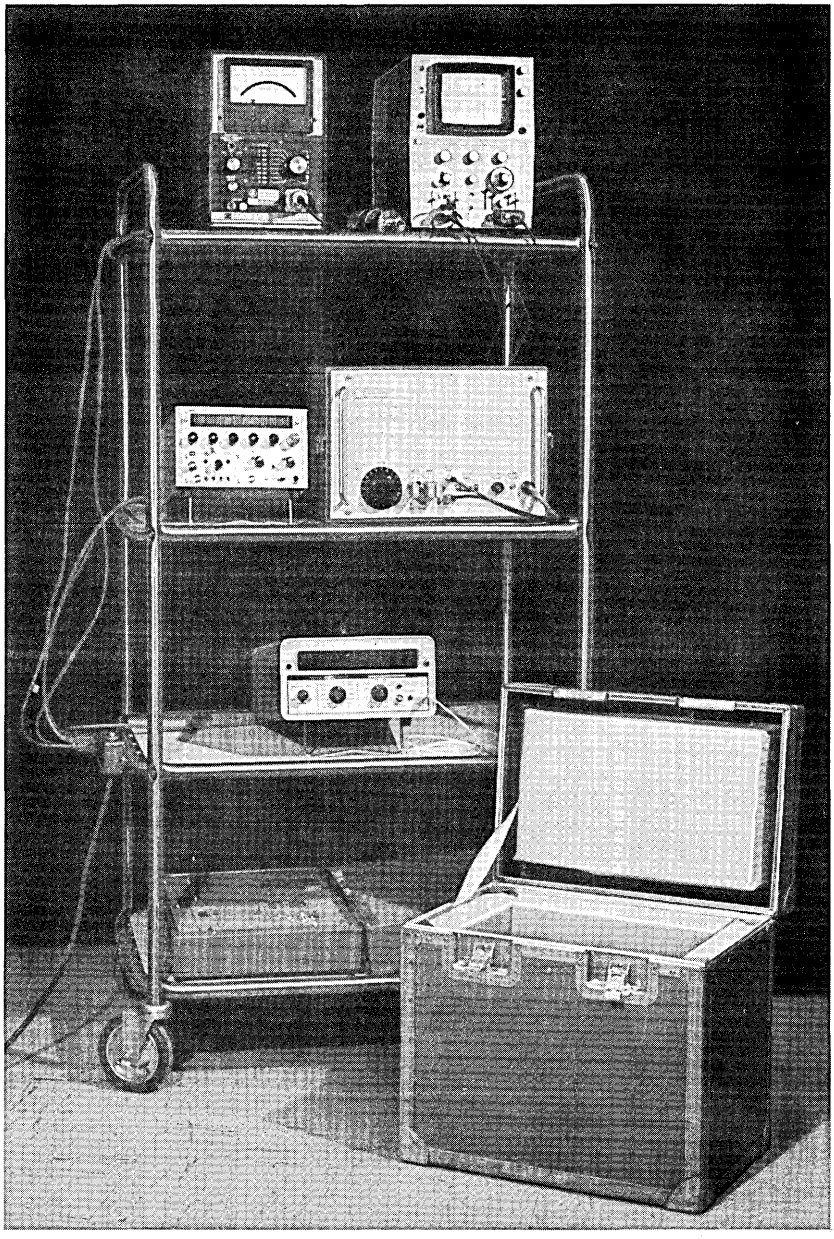

Fig. 2—Portable test equipment on cart.

rectifier which operates from three-phase primary power or a newly developed 100-ampere single-phase rectifier. The single-phase rectifier is necessary since some of the radio stations will be remotely located from three-phase lines.

2.8 *Environmental Limits*

To reduce building costs for medium-haul systems, the equipment shelters (or small buildings for that matter) may not be air conditioned, but fans and heaters might be required depending on local climatic conditions. An environmental temperature range of 40°F to 120°F was established for medium-haul systems, a range which can be maintained without air conditioning in most areas. This will reduce building costs. Performance of the equipment has been established to be satisfactory over this range.

III. BASEBAND MODULATING SPECTRUM

3.1 *General*

TH-3 medium-haul systems provide a usable baseband of up to 10 MHz capable of carrying 1800 message circuits or other broadband services. With the auxiliary channel and 300A protection switching system continuity pilot, the baseband spectrum of medium-haul systems contains signals having frequencies higher than the 1800-circuit message payload. The frequency deviation of medium-haul systems is therefore reduced compared to that of long-haul systems so that the necessary bandwidth* of the RF signal will not exceed the 30-MHz authorized bandwidth as specified by the FCC.

3.2 *Baseband Spectrum*

The composite broadband baseband signal that is applied to the FM transmitter is shown in Fig. 3. Power levels of the components are also shown. Part of the baseband spectrum is the 1800-message circuit load that is identical to that of the long-haul application except for its reduced total power. A continuity pilot which is used by the 300A protection switching system appears at 11.88 MHz. The auxiliary channel, consisting of a double sideband AM signal, occupies the frequency band from 11.09 MHz to 11.67 MHz with the auxiliary channel subcarrier at 11.38 MHz.

---

* Necessary bandwidth (BW) as defined by FCC Rules: $BW = 2X$(highest baseband modulating frequency) $+ 2X$(peak frequency deviation).

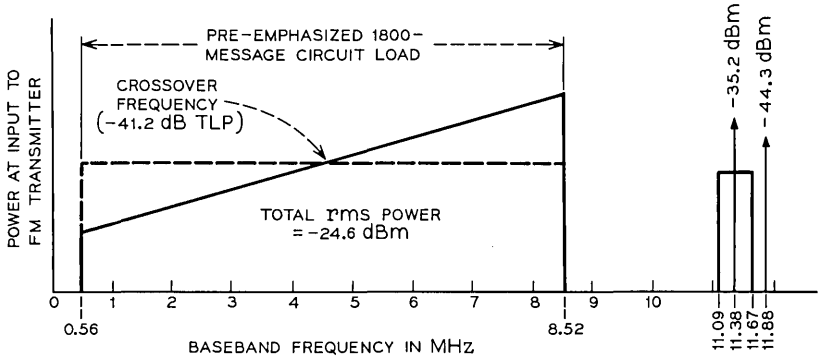

Fig. 3—Composite baseband spectrum at FM transmitter input.

3.3 *Frequency Deviation*

Immediately preceding the FM transmitter, the auxiliary channel signal is combined with the other baseband signals through a resistive combining network as shown in Fig. 4. Because the total power of the 1800-message circuit load is significantly greater than the power of the auxiliary channel signal or of the continuity pilot, the system's total frequency deviation is essentially controlled by the power in the 1800-circuit load. The −23.0 dBm power of the 1800-circuit load at the input side of the combining network is identical to the total baseband power delivered to the FM transmitter for long-haul applications.[6] The insertion loss of this network reduces the frequency deviation of the 1800-circuit load by 1.6 dB.

Based on the levels in Fig. 4 the rms frequency deviation of the

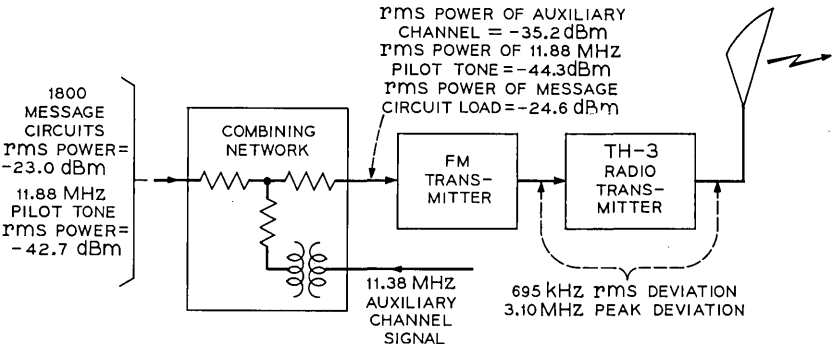

Fig. 4—Signal combining network and power levels.

various components of the baseband signal may be calculated. These are shown in Table I. The component deviations are then added on a root-mean-square basis resulting in a total rms frequency deviation of 695 kHz for the composite medium-haul signal.

Broadband message signals such as considered here have their peak frequency deviation related to the rms frequency deviation by a 13-dB peak-to-rms power factor.* This results in a 3.10-MHz peak frequency deviation for the composite medium-haul signal. Application of the definition for necessary bandwidth yields:

$$BW = 2(3.10 \text{ MHz}) + 2(11.88 \text{ MHz}) = 30 \text{ MHz}.$$

TABLE I—COMPONENT DEVIATIONS

1800-message circuit average busy hour rms deviation	663 kHz
11.88-MHz pilot tone rms deviation	69 kHz
11.38-MHz auxiliary channel rms deviation (carrier and sidebands)	196 kHz
TOTAL RMS DEVIATION	695 kHz

IV. ANTENNA AND FREQUENCY CONSIDERATIONS

Since route economy is a major consideration with the TH-3 medium-haul application, the use of a single antenna for transmitting to and receiving from a given direction is recommended. The horn reflector antenna is preferred because of its high gain and directivity but direct feed dual polarization parabolic radiators may also be used. New routes will generally use the single antenna approach since considerable cost savings result from simplified tower, waveguide, and building arrangements.

TH-3 medium-haul systems may also be added to established 4-GHz long-haul routes where existing buildings, towers, and antennas are available, in which case separate transmitting and receiving antennas would be used.

4.1 *Single-Antenna Frequency Plan*

The channel frequencies available for medium-haul systems are identical to those available for long-haul systems; that is, either a regular or staggered frequency plan may be used.[6] Having a choice

* A 13-dB peak factor is specified in the FCC Rules and Regulations for calculating necessary bandwidth.

of two frequency plans is important to medium-haul applications since, with only the regular plan available, interference might result between the TH-3 system and existing short-haul 6-GHz systems which use the staggered plan. The regular and staggered frequency plans allow a degree of flexibility when planning and designing new medium-haul routes.

Figure 5 shows channel assignments and antenna arrangements of a typical two-hop installation. The transmitters and receivers of a single radio bay are separated in frequency by the standard 252 MHz. This separation minimizes the possibility of the high-level transmitter signal interfering with the low-level receiver signal. Additional coupling loss between transmitters and receivers is achieved by transmitting and receiving on opposite polarities. In Fig. 5 only two frequencies are used for each two-way radio channel which will allow maximum utilization of the available 6-GHz spectrum.

4.2 *Interferences With Single Antennas*

With separate transmitting and receiving antennas, intrasystem interference that might be produced by the transmitted signal leaking into the receiving antenna facing the same direction is limited by the antenna's side-to-side coupling loss (typically 90 dB to 100 dB). Single antenna operation does not provide the high coupling loss of dual antennas; therefore, certain transmitter-receiver channel combinations may result in near-end intrasystem interference. For this reason, additional RF selectivity is available when single antenna operation is chosen.

4.2.1 *Tone Interferences*

The interferences that are attributed specifically to single antenna operation are related to the use of a 70-MHz IF. These are single-frequency (tone) interferences occurring at 4.13 MHz or 6.6 MHz in the baseband, depending on the channel combinations as discussed in Ref. 6.

4.2.2 *Additional Selectivity*

Additional selectivity, in the form of a nine-inch band-rejection filter located in the indoor waveguide runs (external to the bays), is specified to eliminate the interferences discussed above. The selectivity of these filters is such that system tone objectives will be satisfied.[6] Use of these filters will introduce a minimal amount of delay slope into some channels but the standard mopup equalization

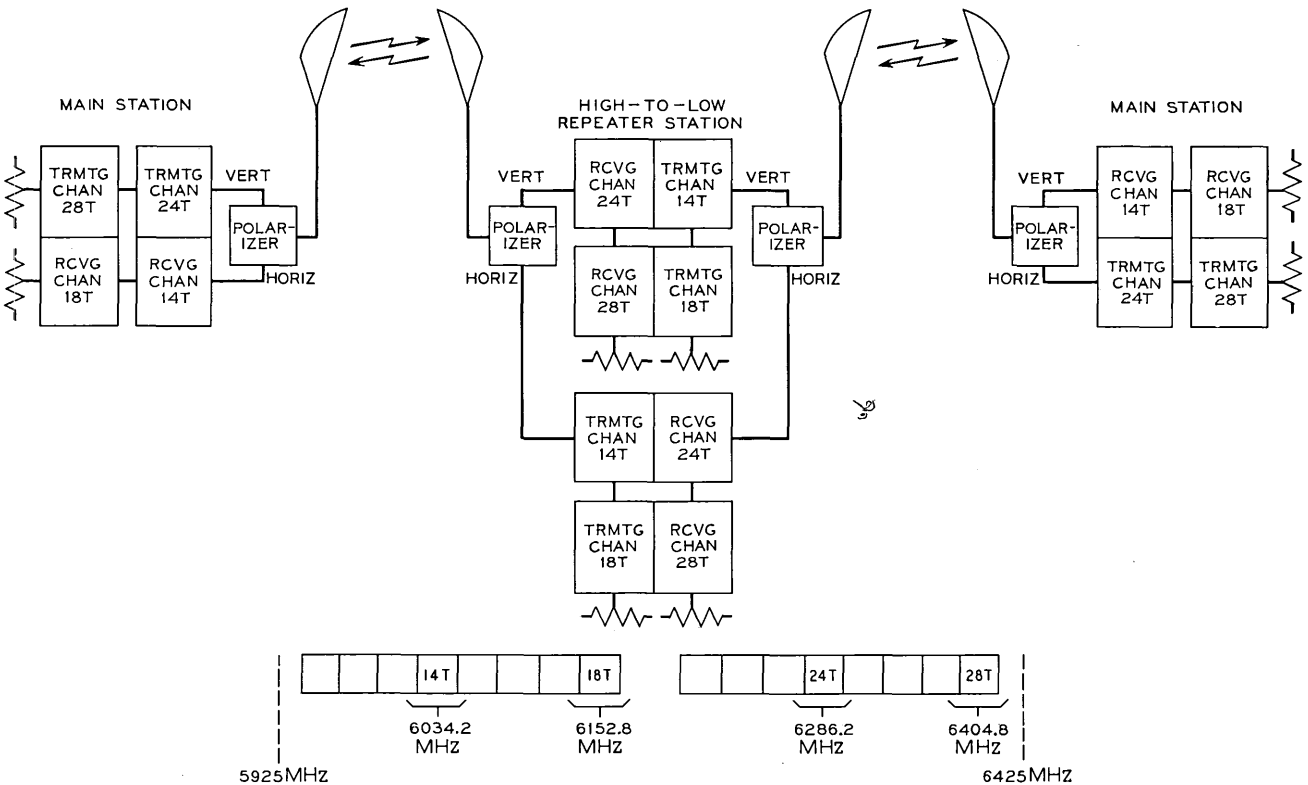

Fig. 5—RF channels and connections for a typical two-hop medium-haul system.

procedures remove this distortion. The reduction of interference level that is provided by the 4A FM transmitter's carrier-spreading circuit is not assumed in the selectivity requirements.[2] Routes using the 4A FMT will have additional margin from these interferences.

V. PERFORMANCE

The noise performance of a medium-haul TH-3 system is primarily determined by the noise performance of the FM terminals and the transmitter-receiver bays. Since these same items essentially determine the noise performance of long-haul radio routes, it is not surprising that the noise performance of medium-haul systems is approximately equal to long-haul systems scaled to the same length. Some of the features unique to medium haul, such as the auxiliary channel, reduced frequency deviation, and extended temperature limits, do have a small modifying effect on the overall system noise performance.

5.1 *Effect of Auxiliary Channel*

Since the auxiliary channel and broadband payload signals are jointly carried over these facilities, some intermodulation effects may occur. The message circuit showing the largest effect due to this noise is the top payload circuit. The noise in that circuit increases about 0.2 dB when the auxiliary channel signal is applied to a ten-hop system.

5.2 *Effect of Reduced Frequency Deviation*

The rms frequency deviation of the 1800-circuit load is reduced by 1.6 dB in order to satisfy FCC rules. To compensate for the lower signal level at the FM receiver output, the gain of the receiving wire line entrance link is increased by a corresponding amount. The reduced deviation results in a slight decrease in intermodulation noise and a small increase in idle noise. Field measurements indicate an increase in total noise of less than 1 dB with the reduced frequency deviation.

5.3 *Effect of Extended Temperatures*

The system noise performance is affected very little over the temperature range 40°F to 120°F. A small increase in system noise due to reduced transmitter power occurs at the high temperature extreme. At temperatures above 100°F, the reduced efficiency of the microwave circuits results in a small reduction of transmitter output

power. The corresponding system noise is expected to degrade less than 1 dB, even when the overall route is exposed to these high temperatures. No significant changes in system performance occur at the low temperature extreme. Since the effects of these extended temperatures are slight, no special concern is required in engineering systems. The advantages of reduced building costs far outweigh the effects of the extended environmental range.

VI. APPLICATIONS OF MEDIUM-HAUL TH-3

6.1 *Morgan City-New Orleans System*

The first medium-haul application of TH-3 radio consisted of three hops installed by South Central Bell Telephone Company between Morgan City and New Orleans, Louisiana. The route layout and frequency plan are shown in Fig. 6. This system largely fulfills the description of the medium-haul application as covered in this article.

Existing VF landlines were readily available for carrying order wire and alarm signals. Therefore the frequency-diplexed auxiliary channel was not used. Single horn reflector antennas were installed at all stations.

At the Thibodaux repeater, potential interferences with other nearby routes did not allow a 252-MHz frequency shift for the through channels. Main station radio bays, each having independent transmit and receive frequencies, were installed to permit an appropriate shift of the RF frequencies.

Since the Morgan City-New Orleans route was the first medium-haul installation, particular attention was given to installation problems and overall system tests. No serious problems were encountered.

6.2 *Great Falls–Shelby System*

The second medium-haul TH-3 system was established by the Mountain Telephone Company on a route between Great Falls and

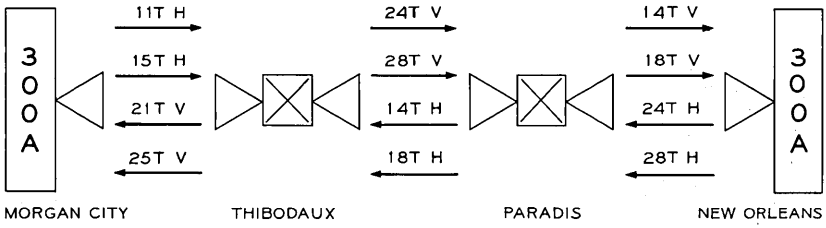

Fig. 6—Morgan City-New Orleans medium-haul installation.

Shelby, Montana. This system parallels an existing TJ microwave radio route, allowing the use of existing buildings, towers, and antennas. Figure 7 shows the variety of antenna systems employed. Careful choice of RF frequencies allowed the use of these existing facilities without creating any intrasystem interference problems.

This route also served as the first installation of the frequency-diplexed auxiliary channel. Details of the auxiliary channel performance are covered elsewhere in this issue.[5]

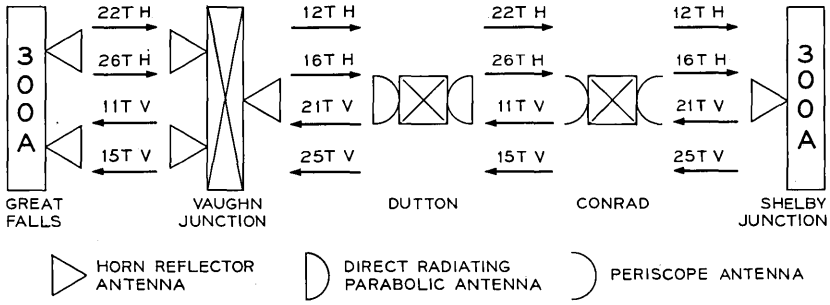

Fig. 7—Great Falls–Shelby Junction medium-haul installation.

VII. ACKNOWLEDGMENT

The medium-haul concept has been developed as the result of efforts by many people. The authors wish to acknowledge all those who contributed to the project. Cooperation from both Mountain Telephone Company and South Central Bell Telephone Company enabled us to measure the success of the medium-haul application.

REFERENCES

1. Hamori, A., and Jensen, R. M., "TH-3 Microwave Radio System: Microwave Transmitter and Receiver," B.S.T.J., this issue, pp. 2117–2135.
2. Androski, F. J., Lentz, N. E., and Salvage, R. C., "TH-3 Microwave Radio System: 4A FM Transmitter and Receiver," B.S.T.J., this issue, pp. 2249–2269.
3. Cooney, R. T., Griffiths, H. D., and Lanigan, F. H., "TH-3 Medium-Haul Application: Protection Switching," B.S.T.J., this issue, pp. 2315–2343.
4. Swift, R. A., and Word, J. A., "TH-3 Medium-Haul Application: Equipment and Building Considerations," B.S.T.J., this issue, pp. 2345–2353.
5. Knapp, J. W., and Seastrand, K. L., "TH-3 Medium-Haul Application: Frequency-Diplexed Auxiliary Channel," B.S.T.J., this issue, pp. 2287–2313.
6. Jansen, R. M., and Prime, R. C., "TH-3 Microwave Radio System: System Considerations," B.S.T.J., this issue, pp. 2085–2116.

THE BELL SYSTEM TECHNICAL JOURNAL
Vol. 50, No. 7, September, 1971
Printed in U.S.A.

TH-3 Medium-Haul Application:

Frequency-Diplexed Auxiliary Channel

By J. W. KNAPP and K. L. SEASTRAND

(Manuscript received February 22, 1971)

This paper describes a means of economically adding up to fifty VF circuits to a microwave radio system in addition to the regular payload signal. One feature of this system is its ability to add or extract information at IF repeaters without either bringing the payload signal to baseband or adding additional circuitry in the payload path.

I. INTRODUCTION

Point-to-point microwave radio systems require surveillance and maintenance to insure high-quality performance and reliability. This is accomplished by having access at each of the radio stations to an order-wire facility and a surveillance and control system, as well as other various special purpose circuits. The electrical signals associated with these circuits are typically carried to and from the radio stations over 3-KHz voice-frequency circuits. Three possible ways of transmitting these signals are to carry them over voice-frequency land lines, on a separate microwave channel, or directly on the payload microwave channel.

Land lines have been widely used in the past, but have two major disadvantages. Often the land lines between radio stations may follow a long circuitous route over a wide variety of transmission facilities. Secondly, they are relatively costly, especially if construction of new lines is required to provide access at a remote radio station. The question of cost is particularly important when one talks about low- or medium-density routes where the cost of the equipment required to perform these functions is spread over a limited number of telephone circuits.

The use of a separate microwave channel (auxiliary channel) has gained popularity in recent years. It frequently provides transmission

over a much more highly controlled medium than does connection through miscellaneous land lines and consequently is much more reliable and of uniformly good performance quality. In addition to the associated multiplex, this type of auxiliary channel requires separate radio transmitting and receiving equipment at each radio station, consequently it is also fairly costly.

The third alternative of using the payload microwave radio channel to carry the surveillance and control signals is reliable, has good quality transmission, and is the most modest in cost. Using the existing radio as the transmission vehicle not only permits economic advantages but also simplifies maintenance since no separate radio transmitters and receivers are required. This paper concerns itself with the development and performance of an auxiliary channel of this type (the frequency-diplexed auxiliary channel) for use with the medium-haul application of TH-3 radio.

II. SYSTEM OBJECTIVES

2.1 *Capacity*

The medium-haul radio systems require two or three VF transmission circuits (service circuits) to accomplish the necessary maintenance and control functions. The surveillance and control system requires one of the VF circuits, the radio order circuit (order wire) another VF circuit, and, if equipped with an express radio order circuit, a third.

In addition to the service circuits, another category of circuit is sometimes useful. Frequently radio repeater stations are located near small population centers which are distant from larger cities where toll switching centers would be located. If a limited number of commercial trunk circuits could be inexpensively carried over the radio from a radio station to another along the route, substantial economic savings could be had. The frequency-diplexed auxiliary channel provides this facility (up to forty-eight VF circuits) without incurring the cost and noise penalty of demodulating the overall payload signal and equipping this station with master group multiplex equipment. The only multiplex required is that necessary to accommodate the forty-eight circuits.

2.2 *Performance*

These questions of system length, noise performance, and reliability are closely related; slight sacrifices in one sometimes yield substantial

added margin in another. The forty-eight circuit backhaul facility is similar in many respects to other short-haul microwave radio systems such as TL and TM microwave radio.[1] It is therefore logical to consider performance objectives similar to those set for such systems. This corresponds to a maximum length of 250 miles and a noise objective of 35 dBrnc0. The TH-3 medium-haul radio system performance model is based on a system length of 1000 miles.[2] While the backhaul may be limited to 250 miles, the circuits used to carry order-wire and alarm signals may be required to traverse the full 1000-mile length. Therefore, on a system meeting the backhaul noise objective, the worst case noise performance of the service circuits would be 41 dBrnc0. This performance is more than adequate for the order-wire and surveillance and control circuits.

2.3 *Reliability*

Another measure of auxiliary channel performance is its reliability. Since the microwave radio itself carries the auxiliary channel, an outage of the basic radio system will affect not only the payload, but the auxiliary channel as well. The need for good auxiliary channel reliability exists since the backhaul circuits are carrying commercial circuits and the service circuits are used both for maintenance and alarm reporting. The two-way end-to-end outage objective for a 250-mile short-haul system is 0.02 percent. A 0.02-percent end-to-end reliability objective therefore is not unreasonable for a 250-mile backhaul trunk. This would also be acceptable for the order-wire and alarm circuits.

Another consideration, however, which does not apply to initial medium-haul installations, but may in the near future, is the necessity of the auxiliary channel to carry control tones for the payload protection switching system. Initial medium-haul applications are protected on a one-for-one basis and do not require control tones for head end switching. Future application of some type of 1-for-n protection switching would however require the auxiliary channel to carry this type of signal. On systems of this type reliability objectives typically allocate 2.0 percent of the total radio system outage time to joint outages of the auxiliary channel. Probability studies indicate this objective can be achieved if the auxiliary channel outage is not greater than 0.02 percent for 250 miles two-way. This grade of reliability can be achieved on the auxiliary channel if it is carried simultaneously over two RF channels and the better channel selected automatically.

Assuming such a one-for-one protection switching arrangement, the fade margin of the auxiliary channel must be at least 35 dB.

2.4 *Payload Interaction*

The above system objectives all center around the auxiliary channel performance itself. The effect of the auxiliary channel on the noise performance of the payload signal must also be considered. The presence of the auxiliary channel must not cause excessive distortion to the payload signal. Since the auxiliary channel signals and the broadband payload signals are jointly carried over a common facility intermodulation effects can and do exist. To realize the benefits afforded by using a frequency-diplexed auxiliary channel, a 1-dB increase in the payload noise due to the presence of the auxiliary channel was judged to be an acceptable tradeoff. Thus for an 1800-channel, 1000-mile radio system equipped with a fully loaded auxiliary channel along the entire route, the noise in a payload circuit could increase from the nominal objective of 35.5 dBrnc0[2] to 36.5 dBrnc0. As will be seen however, the performance ultimately realized degrades the worst offended payload channel by less than 0.5 dB.

III. DESIGN CONSIDERATIONS

Several modulation techniques, such as AM, FM, or PM, might be employed to modulate the auxiliary channel information onto the payload radio channel. The use of an FM or PM modulation process makes it possible to meet the noise performance demanded by the backhaul circuits. Since the baseband signal is also FM modulated onto the radio channel, the VF auxiliary channel signals must first be shifted to an unused portion of the baseband spectrum and then mixed or diplexed with it.

3.1 *Auxiliary Channel Spectrum*

The choice of the shift or diplexing frequency is dependent on many factors, the most important of which is the baseband frequency spectrum occupied by the 1800-circuit payload signal. For TH-3 medium-haul systems the baseband spectrum of the payload and related signals is shown in Fig. 1. The signal from mastergroup multiplex equipment typically used in conjunction with the radio system occupies a band spectrum 0.564 to 8.524 MHz. In some medium-haul applications of TH-3 such as video the baseband spectrum is occupied essentially to dc. To allow the auxiliary channel to be used with any

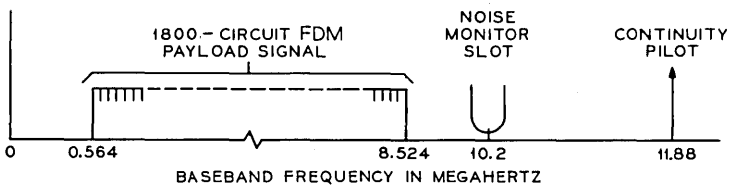

Fig. 1—TH-3 medium-haul baseband frequency assignments without auxiliary channel.

of these applications, a diplexing frequency above the payload is required. A diplexing frequency greater than 10 MHz is also desirable. Although TH-3 has a usable baseband bandwidth out to about 12 MHz, Fig. 1 shows that portions of the spectrum between 10 and 12 MHz are occupied or used for other purposes. The 1 × 1 protection switch for the radio system utilizes a 17-kHz noise slot at 10.2 MHz and a pilot at 11.88 MHz to control switching logic. In addition, the spectrum at 10.7 ± 0.150 MHz must be avoided since a spurious tone can arise in this region under certain combinations of radio channel frequencies. Based on these restrictions and the need for an absolute minimum bandwidth of 200 kHz for the service and backhaul circuits, the spectrum between 10.7 and 11.88 MHz must be used. Although the available bandwidth in this region is about 1 MHz, the usable portion is less than this. The bandwidth of the auxiliary channel signal should be less than 564 kHz to keep A − B intermodulation products[3] due to second-order nonlinearities below the lower end (564 kHz) of the payload.

The final frequency choice depends on the modulator techniques used to diplex the signal. In this case, a two-step modulation process is used to translate the individual VF circuits to the 11-MHz region. The first step of modulation utilizes conventional SSB suppressed carrier modulators to shift the VF circuits to an intermediate frequency range. To accomplish the second step of modulation i.e., shifting the 8- to 284-kHz SSB multiplex spectrum to the 11-MHz region, a double sideband suppressed carrier* process was selected. The decision to use DSB-AM was influenced by the ability to achieve the diplexing process within the available spectrum with a minimum of circuitry and easily realized filters. With this modulation process the signal also carries its own frequency reference, ensuring end-to-end frequency stability.

* As will be discussed later, some carrier is transmitted along with the sidebands for synchronization purposes, but the modulation process retains all the characteristics of the DSBSC process.

It is necessary to select the exact carrier frequency of the DSB-AM modulator with some care. To eliminate tone interference into the normal 1800-circuit payload (0.564 to 8.524 MHz), the difference between the 11.88-MHz switching pilot and the subcarrier should be less than 0.564 MHz. Also for those applications using multiplexed 4-kHz signals in the spectrum below 564 kHz, the same (A − B) product should fall in the guard band between the 4-kHz slots. Finally, to minimize interference into a video signal, the product should be an odd multiple of the half-line rate (i.e., 15734/2 Hz).[4] Considering all these factors a subcarrier frequency of 11.384379 MHz evolves.

Figure 2 shows the DSB-AM spectrum generated by the two-step modulation process used. This is the signal which is ultimately diplexed onto the radio channel.

3.2 *Noise Performance Factors*

This section develops the relationships between the frequency deviation of the radio carrier due to the auxiliary channel signal and the auxiliary channel noise performance. This provides the basis for selecting the auxiliary channel drive. Having determined this drive, further considerations such as noise contributions of the diplexing circuits and the effects of the auxiliary channel on the 1800-circuit payload are examined.

3.2.1 *Deviation Requirement*

The noise performance of the auxiliary channel (W_{n0}) in dBrnc0 is directly related to the noise power measured at the output of the individual VF circuits. This relationship is:

$$W_{n0} = [N_0 + 88] \text{ dBrnc0}, \tag{1}$$

where N_0 is the rms noise in dbm at the output of the VF channel as measured with C-message weighting and referenced to zero transmission level. The noise, N_0, can be expressed as a function of the signal-to-noise ratio ($S_0 - N_0$):

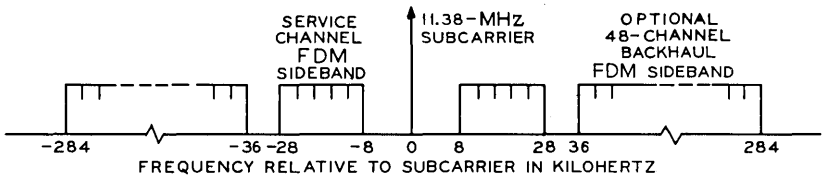

Fig. 2—Auxiliary channel 11-MHz DSB-AM spectrum.

$$N_0 = S_0 - [S_0 - N_0]. \tag{2}$$

The signal S_0 is the rms power in a single message circuit during the average busy hour as measured at the output of the VF channel relative to zero transmission level. The character of the signals carried by the auxiliary channel (i.e., primarily nondata signals) results in S_0 being equal to -17 dBm0. The noise performance can then be expressed as:

$$W_{n0} = [71 - (S_0 - N_0)] \text{ dBrnc0}. \tag{3}$$

When the auxiliary channel is carried over a ten-hop radio system, the noise performance objective is 35 dBrnc0. The signal-to-noise ratio will then be:

$$(S_0 - N_0)_{\text{VF}} \geqq 71 - 35 = 36 \text{ dB}.$$

Since a signal-to-noise ratio is being considered, the reference to zero transmission level may be disregarded. Therefore, in terms of a signal-to-noise ratio, directly at the demodulated VF output, the objective is:

$$(S - N)_{\text{VF}} \geqq 36 \text{ dB}. \tag{4}$$

The auxiliary channel is diplexed onto the radio system by a double-sideband AM process; therefore, the post-detection signal-to-noise ratio is ideally 3 dB greater than the double-sideband predetection signal-to-noise ratio.* Therefore, the per circuit signal-to-noise objective at a point ahead of the DSB demodulation process in the 11-MHz spectrum is:

$$(S - N)_{11 \text{ MHz}} \geqq 33 \text{ dB}. \tag{5}$$

The minimum signal level that will give this signal-to-noise ratio can be determined once the magnitude of the noise has been established. The auxiliary channel signal goes through two distinct tandem transmission paths: the multiplexing and diplexing part of the path which carries only the auxiliary channel signals and the basic radio transmission path which carries both the auxiliary channel signals and the 1800-circuit payload signals. The diplexing circuits were custom designed for the auxiliary channel signal and therefore it was possible to keep their noise contribution to a minimum. Consequently the noise performance of the auxiliary channel is limited primarily

* This assumes that the noise contribution by the DSB and SSB demodulating equipment is negligible.

by noise introduced by the radio system at 11 MHz. The following development of an expression for the required auxiliary channel deviation will initially neglect the effects of the circuit dedicated exclusively to the diplexing of the auxiliary channel. The secondary noise contributions by the diplexing equipment will be considered separately.

The model of the radio system being considered includes one FM terminal pair and ten radio transmitter-receiver pairs (hops). Both the FM terminals and the radio transmitter-receiver pairs are significant noise contributors. Each of these add several basic types of noise:

(*i*) *Idle noise independent of signals carried by the system.* This can be due to shot noise, front end noise, etc. Let p_1 be the noise power contributed by this mechanism from the FM terminals and p_2 be the corresponding contribution of a radio hop.

(*ii*) *Intermodulation products generated from within the 1800-circuit payload signal which fall in the auxiliary channel spectrum.* This will also appear as a contributor to the idle noise floor of the auxiliary channel. Let p_3 be the noise power contributed by this mechanism from the FM terminals and p_4 be the corresponding contributions of a radio hop.

(*iii*) *Intermodulation products generated by the presence of the auxiliary channel signal* (either by itself or interacting with the 1800-circuit signal) *which fall in the auxiliary channel spectrum.* This is conventionally called the intermodulation noise. Let p_5 and p_6 be the noise power contributed by this mechanism for the FM terminals and radio hop, respectively.

The bandwidth and total power of the auxiliary channel signal is sufficiently limited that noise due to contributions from within the third category (p_5 and p_6) are of secondary importance. Therefore only contributions from the first two types of noise will be considered. The measured results reported later in the paper will show this to be a valid approximation.

Since the noise contributions being considered are generated independently, it is reasonable to assume they add to each other on a power basis. Further, the noise p_2, contributed by individual radio hops in a multihop system, will accumulate on a power basis since no correlation exists between hops. The noise contribution p_4, however, may exhibit some correlation between hops. Based on these factors the overall auxiliary channel noise p_N is:

$$p_N = p_1 + np_2 + p_3 + n^k p_4 , \tag{6}$$

where n is the number of radio hops, k is a correlation coefficient with a range from 1.0 (power addition) to 2.0 (voltage addition).

In order to appreciate the full significance of the term n in equation (6) one must realize that the noise performance of the auxiliary channel is almost completely dependent on the noise performance of the basic radio system. The noise as shown will result from the collective number of hops between the transmitting terminal in the switching section and the station being measured. If one is not in the center of a switching section this number will differ depending on the direction of transmission.

The absolute magnitude of each of the noise powers in equation (6) is dependent upon where they are measured in the system. In an FM radio system a convenient way to express noise levels for comparison purposes is to use the equivalent rms frequency deviation of the radio carrier produced by each noise contributor. Since power is proportional to the square of the frequency deviation, equation (6) may be rewritten as:

$$\bar{f}_N^2 = \bar{f}_1^2 + n\bar{f}_2^2 + \bar{f}_3^2 + n^k \bar{f}_4^2 , \tag{7}$$

where $\bar{f}^2$ is the rms frequency deviation corresponding to p. Similarly the signal power is proportional to a frequency deviation, $\bar{f}_S^2$. Therefore the signal-to-noise ratio at a point such as the output of the FM receiver can be expressed as:

$$(S - N)_{11\ \mathrm{MHz}} = 10 \log [\bar{f}_S^2/\bar{f}_N^2], \tag{8}$$

where $\bar{f}_S$ and $\bar{f}_N$ are the rms frequency deviations produced by equal bands of signal and noise in the auxiliary channel 11-MHz DSB-AM spectrum. Substituting this into equation (5) yields:

$$10 \log [\bar{f}_S^2/\bar{f}_N^2] \geqq 33 \text{ dB}$$

or

$$\bar{f}_S \geqq 44.6\ \bar{f}_N . \tag{9}$$

Equation (9) is the desired result. The auxiliary channel per circuit rms deviation of the radio carrier ($\bar{f}_S$) required to meet the 35-dBrnc0 objective may be determined using equation (7) once the corresponding value of $\bar{f}_N$ is determined.

To obtain the data necessary to calculate $\bar{f}_N$ a series of noise measurements were made. The noise in a 3-kHz slot at 11 MHz at the FM receiver output was measured with and without an 1800-circuit noise

load signal applied. The contributions for the FM terminals were found to be:

$$\bar{f}_1 = 123.5 \text{ Hz (for 3-kHz band centered at 11 MHz)}$$
$$\bar{f}_3 = 67.0 \text{ Hz.}$$

The measurements also indicated the idle noise contributed by a radio hop ($\bar{f}_2$) to be 47.5 Hz. Since these measurements were made on a radio system having 1 dB higher idle noise than the objective,[5] a correspondingly lower value for $\bar{f}_2$ is used here, i.e.,

$$\bar{f}_2 = 42.3 \text{ Hz.}$$

To determine $\bar{f}_4$ and the law of addition (k), the noise measurements were repeated with the number of hops a variable. Two possible radio system configurations were considered. The 1044A IF bandpass filter is normally used at each repeater. For this case:

$$\bar{f}_4 = 44.9 \text{ Hz}$$
$$k = 1.0.$$

For certain possible radio interference conditions a narrower IF bandpass filter (1009A) may be required. For systems using this filter:

$$\bar{f}_4 = 60.5 \text{ Hz}$$
$$k = 1.25.$$

Since the use of the 1044A filter is the normal case, the corresponding values for $\bar{f}_4$ and k will be used in this analysis. Therefore, with the following values inserted in equation (7):

$$\bar{f}_1 = 123.5 \text{ Hz}$$
$$\bar{f}_2 = 42.3 \text{ Hz}$$
$$\bar{f}_3 = 67.0 \text{ Hz}$$
$$\bar{f}_4 = 44.9 \text{ Hz}$$
$$n = 10$$
$$k = 1.0,$$

$\bar{f}_N$ = 239.5 Hz in a 3-kHz band at 11 MHz, and

$\bar{f}_S$ = 10,700 Hz* per 3-kHz sideband at 11 MHz.

* For comparison purposes the deviation level of the top (8.5 MHz) circuit in the 1800-circuit payload on a medium-haul system is 20,000 Hz. At this deviation level a ten-hop noise performance, including a 3A FM transmitter and a 4A FM receiver, of about 30 dBrnc0 is achievable.

Thus, based on the idle noise floor at 11 MHz due to the radio system alone, each 11-MHz VF sideband must be impressed on the radio carrier with at least 10,700 Hz rms frequency deviation. If no other noise sources were present this is the deviation required to just meet the 35-dBrnc0, ten-hop objective. Two additional factors must be taken into consideration to determine the actual frequency deviation. The first of these involves the secondary noise sources previously mentioned. The total noise from the auxiliary channel diplexing and multiplexing circuits may be quantatively expressed as follows:

SSB-AM Multiplex Equipment	23 dBrnc0
11-MHz DSB-AM Diplexing Equipment	16 dBrnc0
	Total—23.8 dBrnc0

The composite of these noise contributions must be considered a part of the overall 35-dBrnc0, ten-hop auxiliary channel noise objective. Increasing the auxiliary channel drive 2 dB (i.e., to a frequency deviation of 13,350 Hz per sideband) will allow sufficient margin to insure meeting the overall 35-dBrnc0 objective.

3.2.2 *Noise Introduced into 1800-Circuit Payload*

As indicated in Section 2.4, the objective for noise introduced into the 1800-circuit payload signal by the presence of the auxiliary channel signal is 1 dB or less. This interaction noise is primarily due to intermodulation effects. Intermodulation products between the 1800-circuit payload and the 11-MHz auxiliary channel signals, and products generated from within the auxiliary channel signal itself, may fall back into the payload spectrum. Of these contributors only the first type involving product formation between the auxiliary channel and payload signals are of importance. The spectral width and location of the 11-MHz DSB-AM signal were carefully chosen to keep intermodulation products generated from within the auxiliary channel signal out of the payload spectrum. However intermodulation between the two signals can result in products (A − B and A + B for example) which fall into the payload occupied spectral region between 2.576 and 8.524 MHz. The noise produced by these products, which are generated as a result of radio system nonlinearities, will be uncorrelated with the intrinsic payload channel noise. Therefore power addition between the intrinsic and auxiliary channel induced noise may be assumed. With a nominal ten-hop FM-terminal-to-FM-terminal payload performance of about 30 dBrnc0, the noise introduced into the payload by a fully loaded auxiliary channel signal

(48 backhaul circuits and 3 service circuits) traversing the same hops may be as much as 24 dBrnc0 without exceeding the 1.0-dB degradation objective. Analysis of the results of the measurements mentioned earlier indicated that this would not be a difficult requirement to meet at the 13,350 Hz per circuit deviation level. A worst case ten-hop terminal-to-terminal value of 13.5 dBrnc0 was indicated by the measurements. Thus the degradation can be expected to be about 0.1 dB.

3.3 *Repeater Deviation Process and Modulator Requirements*

3.3.1 *Deviation Process*

The 11-MHz DSB-AM auxiliary channel signals must be diplexed onto the radio channel at each radio site. At a terminal station, where access to the baseband signal exists, the diplexing process is relatively simple, requiring only a direct addition of the 1800-circuit payload and 11-MHz auxiliary channel signals ahead of the FM terminals. At an IF radio repeater where access to the baseband signal is not available, the diplexing process is more involved. The desired end result is the same, however. The local 11-MHz auxiliary channel signal must be applied in such a manner that the resulting FM on the outgoing radio carrier is the same as if the baseband signal causing the existing FM on the incoming IF signal were added linearly with the new 11-MHz signal and the composite then used to frequency modulate the outgoing radio carrier. What is desired in this case is a process obeying the following equations:

Given the radio signal coming into a repeater station:

$$v_i(t) = A_i \cos [\omega_c t + \phi_i(t)],$$

where ω_c = carrier radian frequency (RF or IF), $\phi_i\ (t)$ = instantaneous phase argument due to existing payload frequency modulation. The desired output radio signal after adding the new auxiliary channel information is:

$$v_0(t) = A_0 \cos [\omega_c t + \phi_a(t) + \phi_i(t)],$$

where ω_c and $\phi_i(t)$ are as previously described and $\phi_a(t)$ = instantaneous phase argument due to the auxiliary channel. Since both frequency and phase modulation produce complex spectrums, it is difficult to realize the desired output signal without introducing excessive distortion into both modulation arguments as well as interaction between them. One technique however which has been used to accomplish this without these pitfalls involves modulating the converter beat oscillator signal before combining it with the through path signal.

Figure 3 shows how this process is used at a TH-3 repeater to modulate the 11-MHz auxiliary channel signal onto the outgoing radio carrier. The locally generated DSB-AM 11-MHz auxiliary channel signal, $v_a(t)$, is applied as phase modulation on the transmitter microwave carrier, ω_{BO}, via a varactor type phase modulator (16A modulator). Therefore, at the output of the 16A, the microwave carrier signal is of the form:

$$v_{BO}(t) = \cos [\omega_{BO}t + \phi_a(t)],$$

where $\phi_a(t) = kv_a(t)$.

This phase-modulated signal and the already frequency-modulated IF signal,

$$v_{IF}(t) = \cos [\omega_{IF}t + \phi_i(t)],$$

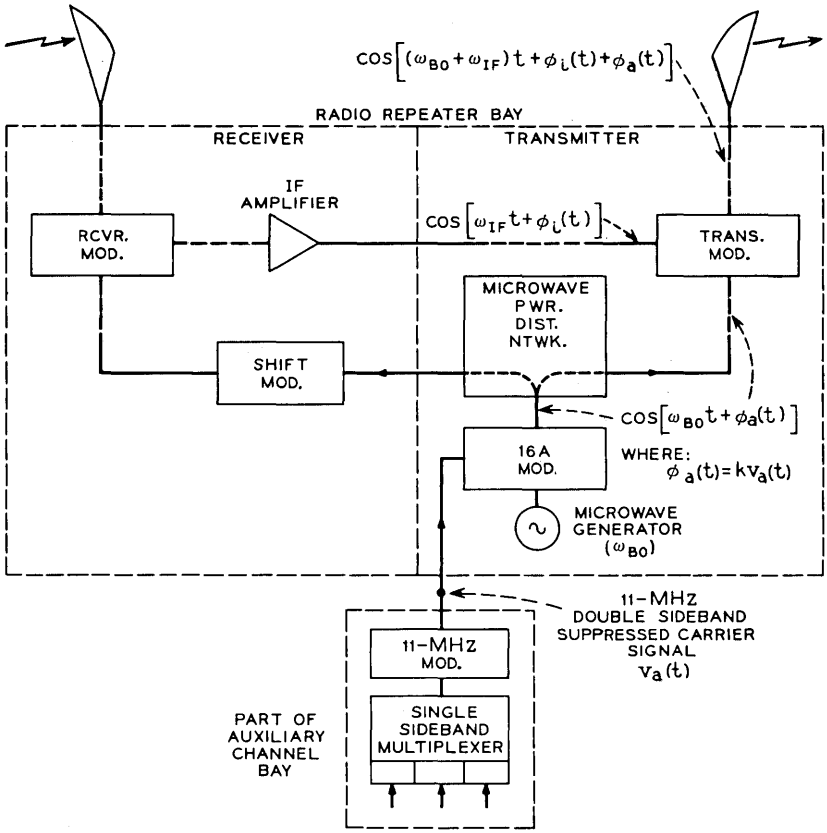

Fig. 3—Auxiliary channel transmitter.

are applied as inputs to the transmitter upconverter. The upconverter forms the product of these inputs, thus generating sum and difference frequencies. RF filtering is used to select the sum frequency:

$$v_0(t) = \cos [\omega_c t + \phi_i(t) + \phi_a(t)],$$

where $\omega_c = \omega_{IF} + \omega_{BO}$,
which is the desired result.

Note that Fig. 3 also shows that a shifted version of modulated microwave carrier is used in the receiver downconverter. The 11-MHz modulation is stripped off the receiver microwave carrier before it reaches the downconverter by the normal selectivity included in this path. This avoids the problem of double modulation.

It should also be noted that phase modulation is used to modulate the 11-MHz auxiliary channel signal onto the transmitted carrier even though a frequency demodulator is used at subsequent points to recover this information. Because of the relatively narrow band involved with the 11-MHz modulating signal, the difference between PM and FM is negligible. No shaping is used to account for the fact that the modulation is ultimately recovered with an FM demodulator. An advantage of this type of modulator is that it is in tandem with the microwave generator. This preserves the inherent frequency stability of the microwave carrier.

3.3.2 *Phase Modulator Requirements*

Figure 4 shows a simplified schematic of the 16A phase modulator. The unmodulated 6-GHz signal appearing at the coaxial input port (RF IN) is routed by a circulator to port 2 and into the reflecting coaxial side arm containing a reverse-biased varactor diode. The 11-MHz modulating signal is superposed on the dc reverse bias and causes the junction capacitance and therefore the equivalent electrical length

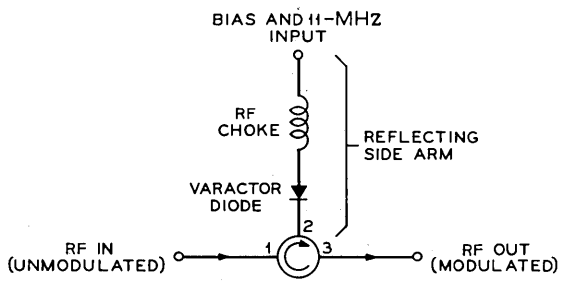

Fig. 4—Simplified schematic of 16A phase modulator.

of the reflecting side arm to vary. The reflected 6-GHz signal which ultimately leaves port 3 of the circulator (RF OUT) is thus phase modulated by this process.

This type of phase modulator is extremely reliable and economical but is limited to relatively low modulation indices due to the inherent nonlinear relationship between junction capacitance and applied voltage. However, careful design and choice of operating parameters coupled with a low modulation index permitted a modulator design meeting linearity constraints.

With a full complement of service and backhaul circuits, the deviation required to meet noise performance requirements dictate that the 16A must be capable of producing a 10-degree peak deviation (index = 0.174) without appreciable modulation distortion products due to overload.[6] With a modulating spectrum of 568 kHz centered at 11.38 MHz, the main products of concern are the second-order (2A), (A − B), and third-order (A + B − C) types.[3] With approximately 30-MHz RF channel spacing, excessive (2A) products (22.76 MHz modulation) could result in interference in an adjacent TH radio channel or another system using the same frequency plan. The (A − B) products, on the other hand, will generate interference which generally falls below the lower end of the normal 1800-circuit payload spectrum (564 kHz). For those applications using this lower portion of the baseband however, this interference must be kept to tolerable levels. Finally, the third-order (A + B − C) products fall back into the auxiliary channel itself and these must also be controlled if noise objectives are to be met. Analysis and testing showed that to meet the noise objectives dictated by the above considerations, a modulator meeting the following linearity requirements was required.

For ± 10-degree peak deviation by a single sine wave at 11.38 MHz:

$$20 \log [v_{1f}/v_{2f}] = 20 \text{ dB},$$

$$20 \log [v_{1f}/v_{3f}] = 25 \text{ dB},$$

where v_f = voltage at frequency f at the output of an FM receiver detecting modulation and

$$v_{2f}, v_{3f} = \text{2nd, 3rd harmonics of } v_f.$$

After considerable design effort and optimization of modulator parameters such as diode type, diode location, and operating bias, a modulator meeting the above objectives was achieved. Other important constraints such as a nominal deviation sensitivity of 2.6 degrees/volt and an RF insertion loss less than 1 dB were also met. Further, only

a single modulator configuration was required for all the possible TH-3 microwave carrier frequencies. (5.875–6.335 GHz)

Figure 5 is a photograph of a TH-3 repeater bay equipped with a 16A modulator.

IV. SYSTEM DESCRIPTION

The first step of the two-step modulation process utilizes conventional SSB suppressed carrier modulators to shift the VF circuits to an intermediate frequency range. The service circuits are shifted to a band of 4-kHz slots between 8 and 28 kHz. Similar multiplex equipment is available to provide the optional backhaul feature. The spectrum between 36 and 284 kHz is allocated for this purpose.

In most multiplex systems, the oscillators used for demodulation at the receiving end of a multiplex link are synchronized to those used at the transmitting end. This is the technique used with the backhaul circuits; however, its use with the three service circuits would result in a relatively high cost per circuit. To eliminate the need for synchronization in this case, the service channel transmit and receive units are each equipped with independent crystal controlled oscillators. The stability of these oscillators is adequate to hold the end-to-end VF error due to this source to ± 2 Hz. This stability is more than adequate for all service channel uses.

Unlike the first step of modulation, where existing equipment was used, the shift to 11 MHz required the development of new equipment. Except for the synchronization technique the modulators and demodulators involved are quite conventional. Both use standard balanced ring modulators and filter configurations to generate and demodulate the DSB signal. A local crystal oscillator is used in each case to produce the diode switching necessary for product formation. For synchronization purposes the modulator at a terminal radio station is deliberately unbalanced to allow a small amount of properly phased local carrier to leak out with the sidebands. At subsequent demodulators this carrier is picked off and a local voltage-controlled crystal oscillator is locked to it by a phase lock loop circuit.* The free-running stability of the 11-MHz crystal oscillators used and the gain of the phase loop is such that under worst case "pull-in" the

* If as is used here a product demodulator is used to demodulate the DSBSC signal, the local carrier used at the demodulator must be of the same phase that the original carrier used for modulation would be at the point of demodulation; otherwise quadrature distortion results and the amplitude of the detected signals roll off as the cosine of the phase error.

maximum phase error of the regenerated carrier is less than 5 degrees. When the oscillator is locked the frequency is exactly that of the leaked carrier and therefore the frequency error introduced by the shift to 11 MHz and back is zero. To insure the proper phasing of auxiliary channel information launched at a repeater, the 11-MHz modulators are also phase and frequency synchronized to the leaked

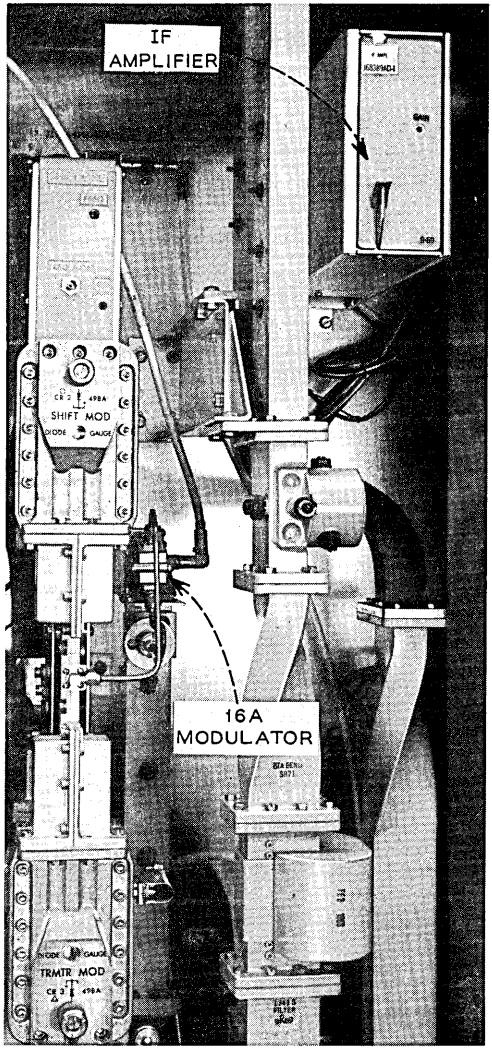

Fig. 5—TH-3 equipped for auxiliary channel.

carrier by utilizing a similar scheme. Figure 6 is a photograph of the DSB-AM modulator/demodulator panel.

4.1 *Terminal Station*

After being DSB-AM modulated to the 11-MHz region, the auxiliary channel information must be impressed on the radio signal as FM. Figure 7 shows an auxiliary channel terminal station. At a terminal radio station where there is access to the baseband signal, the existing baseband and the locally generated DSB 11-MHz auxiliary channel signal are added linearly in a resistive combining network. The composite is then used to deviate the 70-MHz IF signal via the FM terminal. Note also that it is at this point that the 11.38-MHz subcarrier required for synchronizing subsequent 11-MHz modulators and demodulators is launched.

Recovery and demodulation of the 11-MHz auxiliary channel signal from other stations is also a simple matter at a terminal station. At the output of the terminal FM receiver, the desired 11-MHz band along with the synchronizing 11.38-MHz carrier launched at the other end of the system is separated from the composite signal by a resistive splitting network and the appropriate filter. The filter in this case is built into the 11-MHz demodulator which synchronously demodulates the DSB-AM signal to recover the 8- to 284-kHz SSB multiplexed spectrum of the service and backhaul information.

4.2 *Repeater Station*

At a radio repeater access to the baseband signal is not available since IF repeaters are employed. Therefore the process of adding new and recovering existing auxiliary channel information is more difficult.

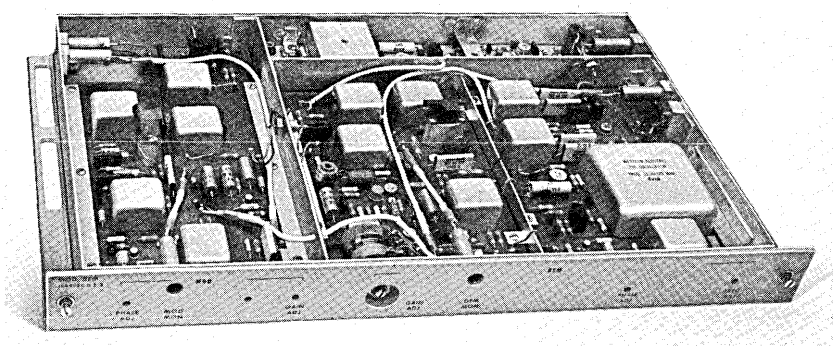

Fig. 6—DSB-AM repeater modulator/demodulator panel.

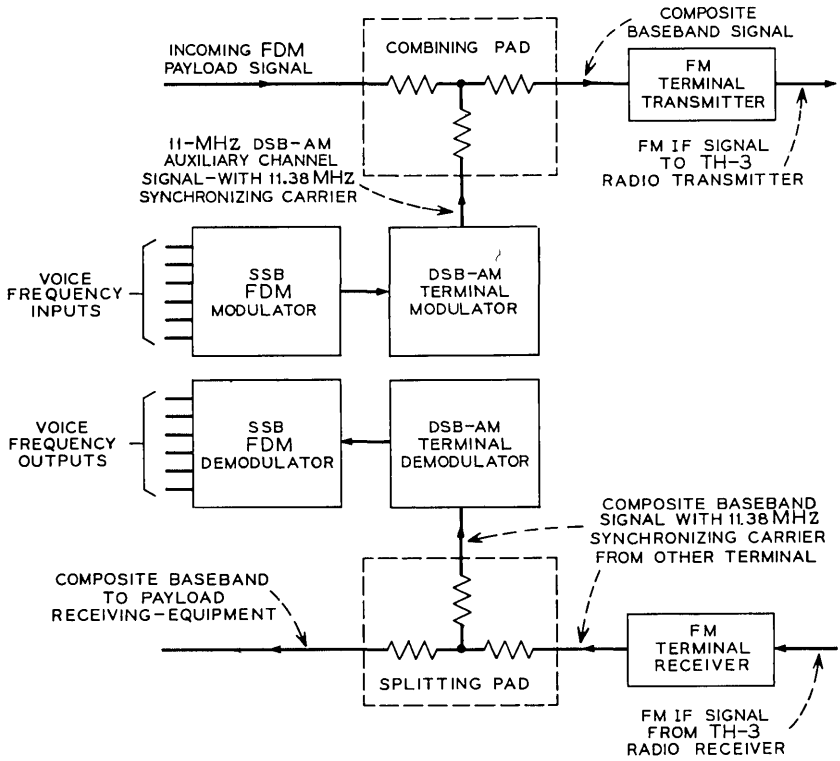

Fig. 7—Auxiliary channel diplexing process at a terminal radio station.

4.2.1 *Receiver*

Figure 8 shows how the recovery process is achieved at a repeater. A portion of the frequency-modulated 70-MHz IF signal is picked off the thru path at point "A," amplified, and FM demodulated to gain access to the composite baseband. At this point the auxiliary channel signal is synchronously demodulated by a circuit identical to the terminal receiver. Since this process adds no active circuitry to the transmission path, it is possible for the existing IF signal to continue through the repeater undistorted.

4.2.2 *Transmitter*

Modulating the 11-MHz auxiliary channel information onto the FM radio signal at a repeater is more involved. For subsequent 11-MHz DSB demodulators to properly demodulate the 11-MHz

sidebands launched at a repeater, the sidebands added at a repeater must have the correct phase relationship to the existing 11.38-MHz synchronizing subcarrier. If this phase relationship is not achieved, quadrature distortion will result. The 11-MHz sidebands added at a repeater must have the same phase relationship to the 11.38-MHz carrier as if they were launched via the terminal modulator. Just

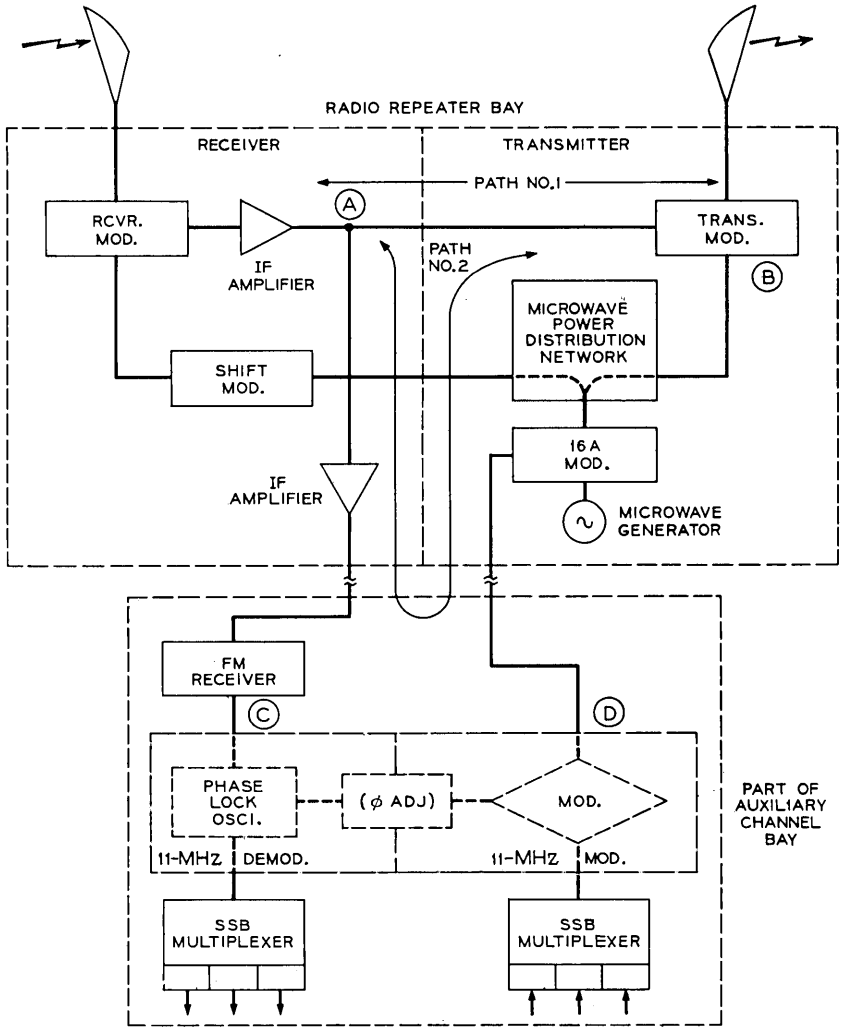

Fig. 8—Repeater auxiliary channel modulator synchronization.

as with the demodulator, this requires that the local 11.38-MHz carrier used to generate the 11-MHz DSBSC signal at a repeater also be phase synchronized to the existing 11.38-MHz subcarrier. Figure 8 shows how the required synchronization and absolute phase angle of the modulator carrier is achieved by using a portion of the demodulator phase-locked carrier.

Relative to the phasing problem, the points in the radio thru path marked "A" and "B" are of critical concern. Point "A" is the point at which the IF signal for the auxiliary channel receiving equipment is bridged from the main thru path signal. Point "B" is the point in the upconverter where the newly added 11-MHz DSBSC information, now existing as FM on the microwave carrier, finally mixes with the existing 11-MHz DSB-AM information from the preceeding station. Point "C" is another important point relative to this discussion. This is the point at which the local phase-locked oscillator is synchronized to the existing 11.38-MHz subcarrier.

As the thru signal travels from "A" to "B" over path 1, the 11.38-MHz carrier, existing as FM sidebands on the IF signal, undergoes a phase shift. The phase of the local 11.38-MHz phase-locked oscillator, on the other hand, is synchronized to the detected 11.38-MHz carrier existing at point "C" in path 2. The phase shift in the carrier from "A" to "C" also depends on the delay and absolute phase shift associated with the equipment and variable length cabling in this path. Similarly there is a variable amount of delay or phase shift associated with the circuits and cabling between the output of the 11-MHz DSBSC modulator, point "D", and the mixing point "B" over the remaining part of path 2. This latter phase shift affects the modulated sidebands only since the carrier is fully suppressed in this case. The phase of the 11.38-MHz carrier is contained in the sidebands however and it is this equivalent phase that is important when the new sidebands ultimately join the thru path signal (at point "B"). To avoid quadrature distortion when the signal is demodulated, the phase angle of the equivalent 11.38-MHz carrier relative to the existing carrier should be zero or 180 degrees (polarity of signals added at a repeater relative to other auxiliary channel signals is not important for the type information being carried). To compensate for the variable phase shift over path 2 relative to that over path 1, an adjustable phase shifter (ϕ ADJ in Fig. 8) is used in the carrier path between the output of the 11.38-MHz phase-locked oscillator and the ring modulator used to generate the repeater 11-MHz DSBSC signal. Once set, the delays and phase shifts associated with the various

circuit elements involved in the two paths are stable enough to hold the phase error within a few degrees. This is more than adequate for the applications involved.

4.3 *Auxiliary Channel Switching*

Auxiliary channel transmission outages may be the result of either equipment failures or propagation disturbances. Since the auxiliary channel is carried over the basic radio, when a radio channel on a particular hop experiences a transmission outage, so will the auxiliary channel on that radio channel. This could represent somewhat of a problem since alarms and order wire are always most needed during outage periods. The outgrowth is the need for a protection switching arrangement for the auxiliary channel. Conceptually this is straightforward. The auxiliary channel signals are simultaneously carried over two separate RF channels and the better performing is automatically selected for use. The outage time of the auxiliary channel can then be reduced to a matter of only minutes per year.

The reasons why information introduced at a repeater must be phase synchronized with the information coming from the preceding stations has already been discussed. This requirement has a strong influence on the design of the auxiliary channel protection switching system. It means that the terminal station and all the repeater stations must have their auxiliary channel switch on the same RF channel. This in turn suggests that the quality of auxiliary channel transmission be established at the receiving terminal station and a choice made. The repeater switches can then be slaved to the switch at the receiving terminal station. Figure 9 shows this relationship. The switch at the receiving terminal station includes a control oscillator panel which generates one of two VF tones depending on the status of that switch. The tone is sent back over the system, in the opposite direction, to the repeater stations where it causes the repeater switches to operate to the same RF channel.

This figure shows transmission in only one direction. There exists a mirror image (not shown in Fig. 9) for transmission in the opposite direction. The photograph in Fig. 10 shows an overall repeater auxiliary channel bay.

V. SYSTEM PERFORMANCE

The overall performance objective for the auxiliary channel is that it be capable of carrying the required service circuits and up to forty-eight backhaul circuits. While extensive laboratory testing and analyt-

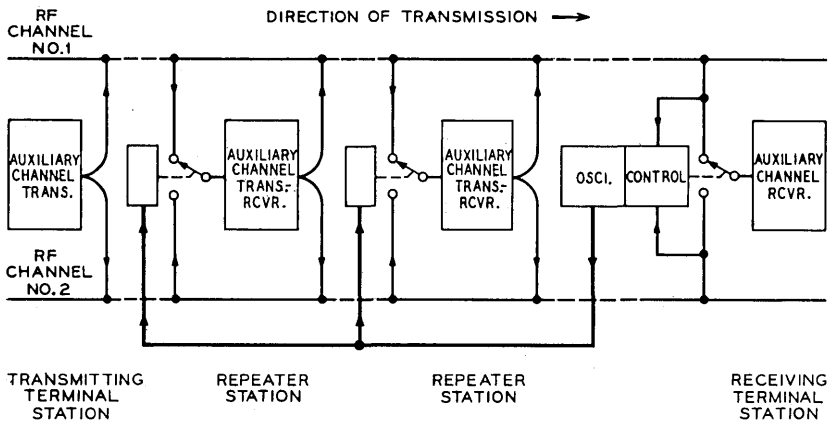

Fig. 9—Slaved protection switching.

ical work was done during all phases of development to insure meeting objectives, final evaluation ultimately requires statistical data from the field. Field testing of the initial installation, a four-hop TH-3 medium-haul route between Great Falls and Shelby, Montana, indicates that noise and reliability objectives are being met.

5.1 *Backhaul Noise Performance*

The technique of noise loading is typically used to evaluate the noise performance of broadband systems. As mentioned earlier the noise performance of the auxiliary channel is dominated by the radio system which carries the composite 1800-circuit payload plus the auxiliary channel (3 service and 48 backhaul circuits). The noise contribution of the auxiliary channel equipment carrying only the 51-circuit FDM signal is small enough to be neglected. Therefore it is possible to ignore the statistical considerations associated with the narrowband 51-circuit signal itself. This permits the use of conventional noise loading for evaluating overall auxiliary channel noise performance.

Figure 11 shows some typical noise loading results under the above loading conditions over the Great Falls to Shelby route. Curve A shows the noise load result thru a typical 11-MHz DSB-AM modulator and demodulator connected back-to-back. Curve B shows the results with the same units thru a 3A FM terminal transmitter and 4A FM terminal receiver connected back-to-back at IF. In this case a noise-simulated 1800-circuit payload is also present at the input to

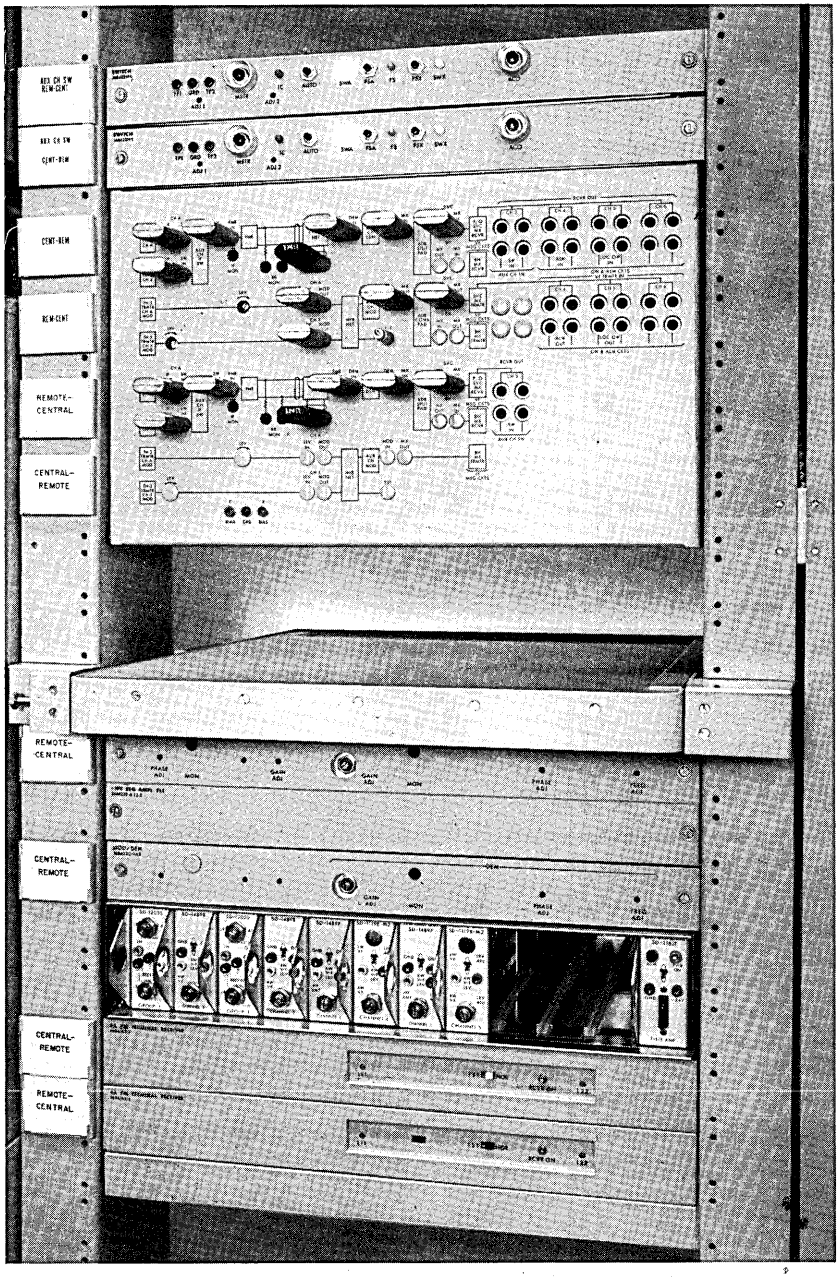

Fig. 10—Repeater auxiliary channel bay.

the 3A FMT at the average busy hour reference drive level. The 11.88-MHz switching pilot was also present to create essentially normal operating conditions. Curve C shows the results, under the same conditions, over the four-hop Great Falls to Shelby route. For comparison purposes, curve D shows the results at the end of the same four hops with the auxiliary channel signal applied via a 16A modulator at a repeater station (three hops away from the measuring end). The simulated 1800-circuit payload signal remained on the system during this measurement.

A four-hop noise performance of 33 dBrnC0 at reference drive was determined from the measurements. It should be noted that when these measurements were made, the radio system was equipped with 1009A IF bandpass filters. Using the appropriate rms noise deviations given in Section 3.2, equation (7) predicts a four-hop performance which agrees within 0.2 dB of this measured result.

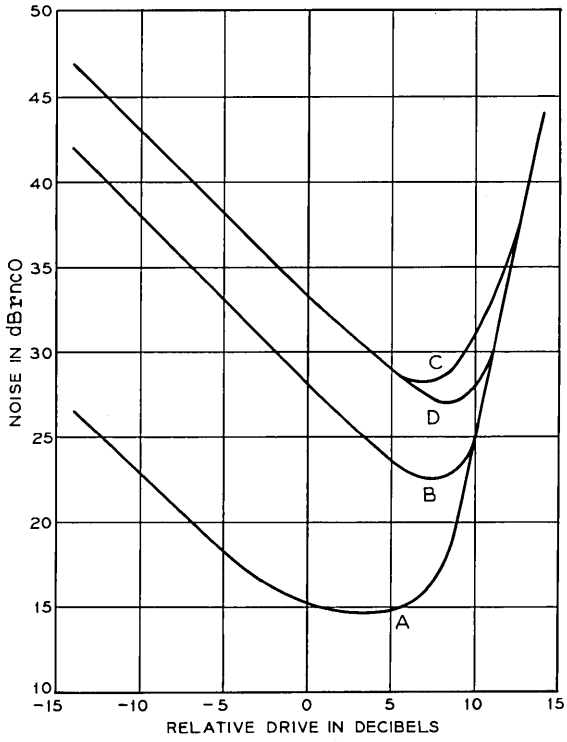

Fig. 11—Forty-eight channel noise loading results (70 KHz).

Note also from curve D that the noise contribution of the 16A modulator to the auxiliary channel noise performance is negligible compared to the rest of the system.

5.2 *Fade Margin*

To meet reliability objectives, the auxiliary channel performance should insure that in the presence of a 35-dB RF fade, the noise will not exceed 55 dBrnc0. For a hop with a nominal received RF signal of −23 dBm at the radio bay, this requirement was met at the 13,350 Hz per 3-kHz sideband deviation level. Analysis indicates nominal hops will have about 37 dB fade margin.

5.3 *Measurement of Payload Interaction*

Since the primary interference into the 1800-circuit payload is due to intermodulation products between the 11-MHz auxiliary channel signal and the payload, the noise performance of the payload signal was also studied by noise loading techniques. Several slots within the normal 0.564- to 8.524-MHz payload spectrum were carefully measured with and without 48-circuit noise load applied. This was done with the auxiliary channel signal applied via the 3A FMT as well as via the 16A modulator at a repeater. The measurements showed that the top payload circuit experienced the greatest noise increase. The degradation easily met the 1-dB objective (typically 0.1 to 0.2 dB).

Measurements in a slot below the normal payload spectrum were also made to evaluate the (A − B) noise from the auxiliary channel spectrum itself. Again this was done with the noise loaded auxiliary channel signal launched via the 3A FMT as well as the 16A modulator. For a slot at 70 kHz the increase in noise due to the auxiliary channel on the Montanna four-hop system was 2 dB. This was for the case where the auxiliary channel was applied via the 3A FMT. With the auxiliary channel signal applied via each of several 16As at repeaters, the increase was less than 0.5 dB. The predominant source of the direct interfering (A − B) products was the 3A FMT. Therefore, for a ten-hop system, the increased noise should be even less than 2 dB. The lower payload channels are generally less noisy than those at higher frequencies, therefore this interference level should be acceptable even for those special applications using the spectrum below 564 kHz.

An improved FM terminal (4A FMT) further reduces the noise due this source.

5.4 *Operational Performance*

Many other facets of system performance besides noise performance were studied. Such factors as system operation and stability during switching activity were also studied. In all cases the system functioned properly without loss of synchronization or communication between stations. In addition, stability measurements over a period of several months indicate that the system and propagation characteristics are stable enough to achieve the desired reliability. Thus, considering all factors, the frequency-diplexed auxiliary channel system should prove to be a useful and economical means of providing the surveillance, control, and other functions required for the maintenance of the radio system. The established noise performance should also make the backhaul feature an attractive option.

VI. ACKNOWLEDGMENTS

The frequency-diplexed auxiliary channel has been developed as the result of efforts by many members of Bell Telephone Laboratories. The cooperation of the American Telephone and Telegraph Company, Western Electric Company, and Mountain Bell Telephone Company was also important to the success of this undertaking.

REFERENCES

1. Friis, R. W., Jansen, J. J., Jensen, R. M., and King, H. T., "The TM-1/TL-2 Short Haul Microwave Systems," B.S.T.J., *45,* No. 1 (January 1966), pp. 1–95.
2. Seastrand, K. L., and Williams, D. S., "TH-3 Medium-Haul Application: System Considerations," B.S.T.J., this issue, pp. 2271–2285.
3. Members of the Technical Staff, Bell Telephone Laboratories, *Transmission Systems for Communications,* 4th ed., Winston-Salem, N. C.: Western Electric Company, 1970, Chapter 10.
4. Fink, D. G., *Television Engineering Handbook,* New York: McGraw-Hill Book Company, 1957.
5. Jansen, R. M., and Prime, R. C., "TH-3 Microwave Radio System: System Considerations," B.S.T.J., this issue, pp. 2085–2116.
6. Holbrook, B. D., and Dixon, J. T., "Load Rating Theory for Multi-Channel Amplifiers," B.S.T.J., *18,* No. 4 (October 1939), pp. 624–644.

THE BELL SYSTEM TECHNICAL JOURNAL
Vol. 50, No. 7, September, 1971
Printed in U.S.A.

TH-3 Medium-Haul Application:

Protection Switching

By R. T. COONEY, H. D. GRIFFITHS, and F. H. LANIGAN

(Manuscript received March 15, 1971)

This paper describes the 300A and the auxiliary channel protection switching systems which provide continuity of service on TH-3 medium-haul radio systems. Both protection switching systems operate on a one-by-one frequency diversity basis. The 300A is a baseband-to-baseband system and protects the message circuit load. The auxiliary channel switching system protects the order-wire and alarm circuits and operates at both IF and baseband frequencies. System design considerations and circuits of special interest, including solid state switches and integrated circuit modules, are discussed in some detail.

I. INTRODUCTION

Protection switching systems providing continuity of message service are a necessary part of many radio communication systems. For long-haul applications, the TH-3 radio system uses the 100A IF-to-IF protection switching system for the radio portion of the system and the 200A IF-to-baseband and baseband-to-IF protection switching system for the FM terminal and entrance link portion of the system.[1] Two separate switching systems are required since switching sections are often connected in tandem and converging radio routes are often interconnected at IF frequencies. For medium-haul applications, the TH-3 system is generally comprised of a single switching section with FM terminals at each end. Therefore, baseband-to-baseband switching encompassing both the radio and baseband portions of the radio system is a more optimum arrangement. In addition, since the growth of service on most medium-haul installations is expected to be relatively slow, a single radio channel of the message capacity of TH-3 should be adequate for many years. Therefore, a system having one regular channel carrying service and one protection channel serving

as a backup is appropriate. To meet these needs, the 300A, one-by-one, baseband-to-baseband, protection switching system was developed.

In this system, the two radio channels are permanently bridged at the transmitting end of the switching section and are switched at the receiving end of the system. The receiving end equipment includes a non-revertive switch, channel monitors, and control functions. A detailed description of the 300A system is given in Section II.

The auxiliary radio channel is part of the total message load carried by the TH-3 medium-haul system and has a protection switching system which is separate from the 300A system.[2] The auxiliary channel provides circuits for use within the switching section to carry order-wire, alarm, and control information. These circuits have appearances at each of the radio stations along the route. For reliability of service, the auxiliary channels are inserted on both the regular and protection channels of the radio system. The auxiliary channel protection switching equipment at the receiving main station determines whether the auxiliary channel demodulating equipment is connected to the regular or the protection channel. The repeater station protection switching is slaved to the main station equipment and operates in synchronism with it. The auxiliary channel switching system is described in Section III.

II. 300A PROTECTION SWITCHING SYSTEM

2.1 *System Considerations*

A one-way switching section utilizing the 300A system is shown in Fig. 1. The section includes one or more radio hops with FM terminals and wire line entrance links at each end. The entrance links may be connected external to the switching system if desired. The transmitting end of the 300A system feeds the baseband signal over both channels by means of a hybrid transformer. The hybrid also couples a continuity pilot oscillator to both channels. A switch provides access to the protection channel for emergency restoration or for other purposes. The function of the receiving end is to monitor the quality of the channels, perform the required logic and control functions, and to switch between the two channels.

An innovation of this system is that the channel monitors used to determine channel quality are located after the receiving switch. The advantage of this arrangement is that the switch in the 300A system is protected by the switching system. As a consequence of this arrangement, the channel monitors are not associated with a particular radio

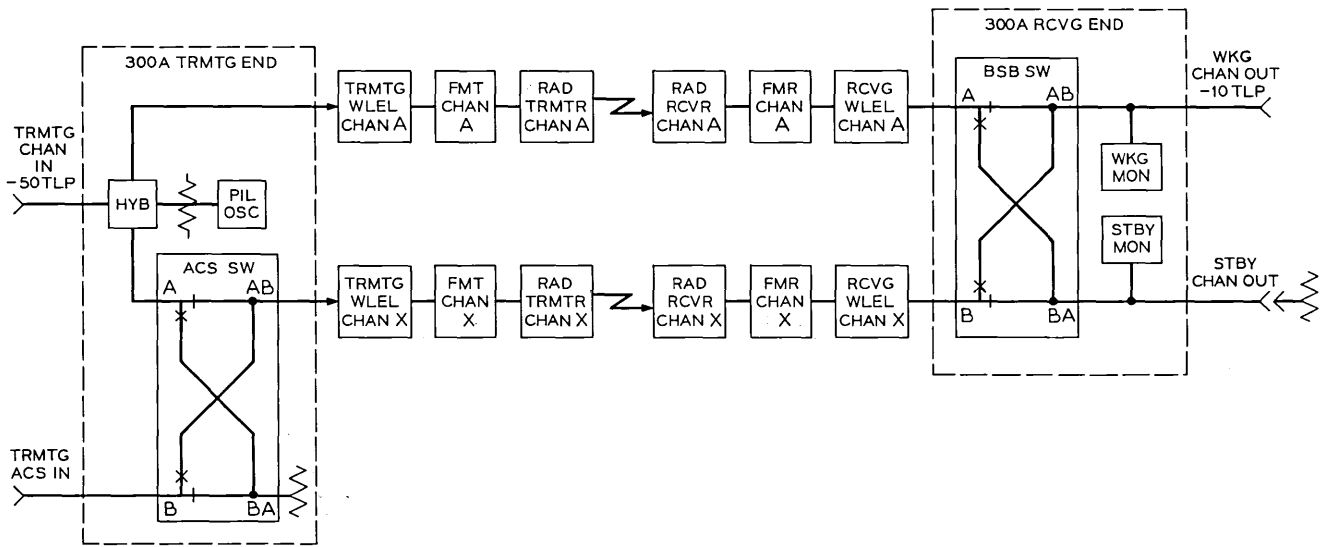

Fig. 1—Typical switching section block diagram.

channel, but may be connected to either one depending on the position of the switch. The working monitor is connected to the output of the system that is carrying service, and therefore will indicate failure every time service is lost. Of course, if the standby channel is available, the failure should not last longer than it takes to complete a switch, which is about one millisecond. The standby monitor is connected to the channel not carrying service.

Channel quality is determined on the basis of the presence or absence of the continuity pilot and on the level of noise in a slot located at 10.2 MHz. Either loss of pilot or excessive noise is considered a channel failure which, if emanating from the working monitor, will initiate a switch. Failures from the standby monitor will initiate alarms. The noise threshold at which a noise failure indication is given from the working channel monitor corresponds to a noise level of 55 dBrnc0 in the top message circuit. The standby monitor is set at a noise level of 53 dBrnc0 to insure positive switching action.

The continuity pilot frequency of 11.880229 MHz was chosen for the following reasons:

(*i*) It can be used on systems carrying video or digital signals whose transmission requirements preclude the use of low-frequency pilots.

(*ii*) The frequency spectrum in the vicinity of 11.88 MHz is clear of any interference from the radio system and a tone at that frequency does not cause interference into the radio system or into the 300A noise slot.

(*iii*) When frequency modulated on the radio carrier, the second-order sidebands of the 11.88-MHz pilot fall between mastergroups on the adjacent channel signal. This reduces the possibility of adjacent channel interference.

(*iv*) Modulation products related to the frequency difference between the pilot and the auxiliary channel carrier (11.384379 MHz) fall at a location which causes minimal interference.

The transmitted pilot level of −7 dBm0 corresponds to a frequency deviation of 69 kHz rms on the pre-emphasized TH-3 system, which is within CCIR recommendations for this type of pilot. This level was determined after consideration of several interrelated system characteristics and circuit limitations. It was desirable to insert the pilot at the lowest possible level to minimize interference and modulation problems and to load the message channel as little as possible. On

the other hand, high pilot levels would allow wider pilot detector bandwidths for a required pilot-to-noise ratio, thereby enabling the detector to operate with greater speed. The above level was a compromise between these effects.

The pilot detector trip point (where the channel monitor indicates loss of pilot) was chosen to be −17 dBm0 or 10 dB below the level of the transmitted pilot. Allowing 5 dB for misalignment and for 11.88-MHz rolloff in the radio system, a minimum pilot-to-trip-point ratio of 5 dB remains. This margin is considered necessary for reliable detector operation.

A detector bandwidth of 1.2 kHz was chosen to insure that noise cannot simulate the pilot until a failure due to noise has occurred. This bandwidth is sufficiently wide to allow relatively loose requirements on the frequency stability of the pilot oscillator and on the selectivity of the pilot detector filter. With these characteristics, the pilot detector reacts to loss of pilot within one millisecond at noise levels exceeding 55 dBrnc0.

The noise slot is located at 10.2 MHz and has a bandwidth of 20 kHz. Considerations which led to this selection are as follows:

(*i*) This frequency is above the 10-MHz baseband and is below a potential source of interference from system tones at 10.55 MHz. It is also low enough to allow good correlation between noise in the slot and noise in the message circuits.

(*ii*) The bandwidth is as large as possible consistent with realistic selectivity requirements on the noise detector filter. The bandwidth is sufficiently wide to provide reasonable speed of recognition of high noise levels. Speed of recognition of excess noise is dependent upon the time constants of the detector circuit, the rate of change of noise level, and the actual noise level. With this bandwidth and the detector parameters chosen, the detector will indicate channel failure in about 10 milliseconds for a sudden change in noise level from no noise to noise 2 dB greater than the noise fail point. Since the fastest fades rarely exceed 1 dB per 10 milliseconds, this speed of response is adequate. It should be noted that equipment failures are detected much more rapidly by the continuity pilot detector.

The switching element used in the 300A system is a solid state baseband switch arranged in the configuration shown in Fig. 1. It functions as a make before break switch to insure continuity of service when a transfer between the regular and protection channels is made, provided that the two channels have been equalized for absolute delay.

The operate time of the switch is approximately one millisecond. The switch is controlled directly from the logic circuits.

One of the inherent properties of a solid state switch is that when power is lost, transmission through the switch is lost. To prevent transmission loss through the 300A switch, the switch is powered from two separate +24-volt feeders and the circuit is arranged to maintain transmission to the working channel output should one of the feeders fail.

The 300A system handles baseband message signals from 60 kHz to 12 MHz with the following transmission characteristics:

Receiving End

Insertion Loss—Less than 1 dB
Frequency Response—Within 0.3 dB, 60 kHz to 12 MHz
Within 0.1 dB, 300 kHz to 10 MHz
Return Loss—Greater than 26 dB
Isolation—Greater than 90 dB
Transfer Time—1 millisecond, make before break

Transmitting End

Insertion Loss—Less than 4 dB
Frequency Response—Within 0.3 dB, 60 kHz to 12 MHz
Return Loss—Greater than 26 dB

Integrated circuits are used exclusively to realize logic and control functions and are used to a limited extent in the linear circuits. The logic and control circuits use Western Electric's 4-volt RTL series of integrated circuits. Interfacing between the 4-volt and the 24-volt circuits is accomplished with relay driver integrated circuits. Integrated operational amplifiers are used as dc amplifiers and as modified Schmitt triggers. All integrated circuits used in the 300A system are standard hybrid integrated circuits. Each integrated circuit consists of a silicon chip mounted on a ceramic substrate having a lead frame to allow application to standard printed wiring boards. A typical printed board is shown in Fig. 2.

Field maintenance of the 300A system is accomplished with standard test equipment generally available in radio stations in conjunction with two oscillators and a split pad built into the 300A package. The two oscillators, one at 10.2 MHz and the other at 11.88 MHz, are used to adjust the noise and pilot trip points of the monitor units. Spare plug-in units are provided to allow quick repair of the 300A system.

Power sources of +24 volts and −24 volts are required by the 300A

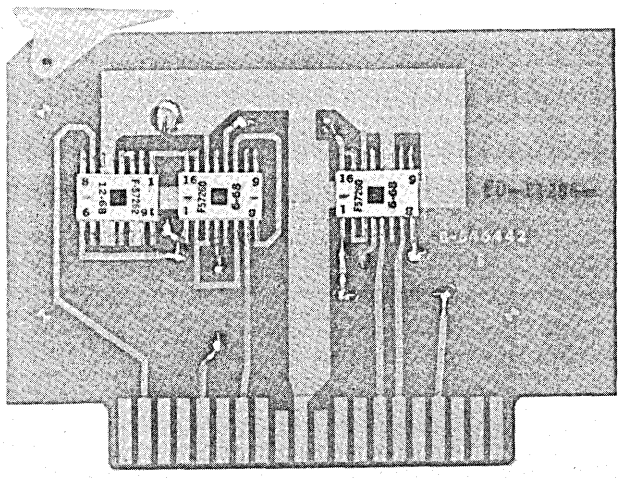

Fig. 2—Typical printed wiring board with integrated circuits.

system. The +24-volt source may be obtained from the −24-volt supply using dc-to-dc converters or directly from a battery plant. Suitable filtering of these supplies to reduce noise and transients is accomplished with power supply filters mounted in the same bay as the 300A equipment.

Additional voltages required for operation of the integrated circuits and for operation of units requiring regulated voltages are obtained with diode regulators associated with the individual units. These voltages include +4.3, +12, and −6.2 volts for the integrated circuits and +18 and −18 volts for the monitor units. Redundant power feeders are provided and fusing is arranged to preclude loss of transmission when a single fuse or feeder fails.

2.2 *Overall System Operation*

2.2.1 *Block Diagram of Receiving End*

An expanded block diagram of the receiving end of a 300A switching system is shown in Fig. 3. The "ON" and "OFF" gates in the diode switch are shown symbolically as "break" and "make" contacts, respectively. With the switch set as shown, channel A is the working channel and channel X is the standby channel. The working and standby pilot and noise monitors are connected to the respective channels through resistive bridging taps. These monitors supply the necessary information about the condition of both channels to the automatic logic, the pilot and noise fail indicating circuit, and the

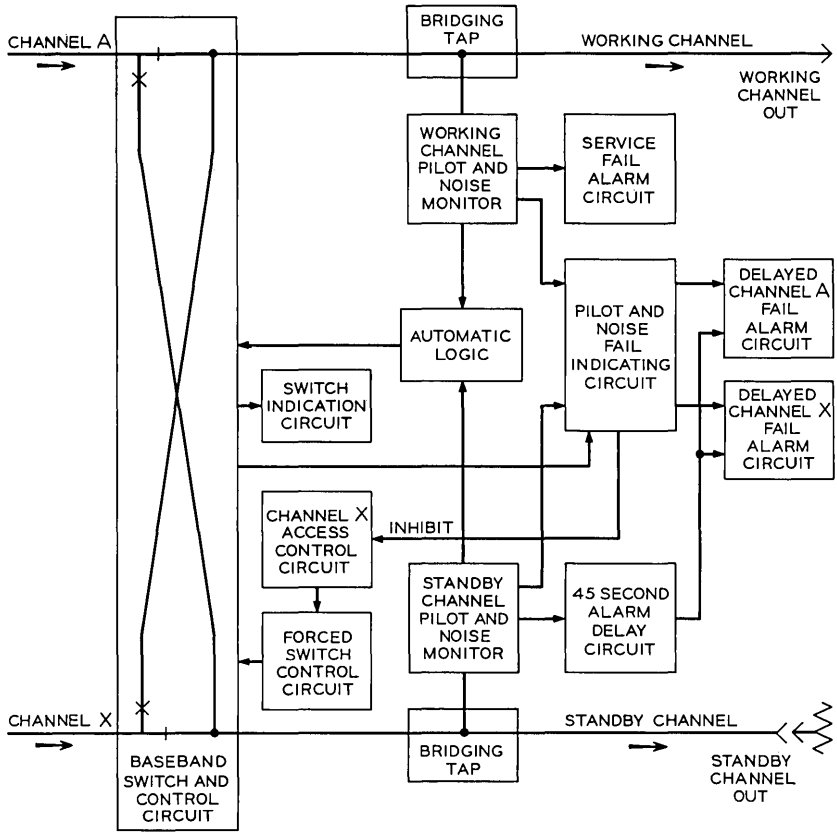

Fig. 3—Receiving end block diagram.

alarm circuits. Forced switch and channel X access controls are provided which operate directly into the baseband switch control circuit for manual control. The switch indication circuit identifies the working channel at all times.

2.2.2 *Automatic Switching*

With the control set for the automatic mode of operation, the baseband switch will operate whenever the working monitor indicates a failure while the standby monitor indicates good. Immediately following the switch operation the working monitor indicates good and the standby monitor indicates a failure.

For example, if channel A is the working channel and it fails while

channel X is good, automatic operation of the switch immediately makes channel X the working channel and the failed channel A becomes the standby. If the failure was due to fading, channel A will recover as the fade clears out but the switch will not revert. Channel X will continue to be working channel and channel A the standby until X fails while A is good. Then the switch will automatically operate again to make A the working channel and X the standby.

2.2.3 *Manual Switching*

The receiving switch can be forced to make either of the channels the working channel by manual operation of the forced switch controls. When the forced switch controls are operated, the automatic logic loses control of the baseband switch. Automatic operation is resumed when the forced switch controls are reset to automatic.

2.2.4 *Access Switching*

A means of disassociating channels A and X so that channel A can carry the regular message service while channel X is being used for emergency restoration or some other special service is available as an optional feature. When it is furnished, operation of the access control at the transmitting end causes the transmitting access switch to operate. This disconnects channel X from the splitting hybrid and connects the access trunk through the switch to channel X. At the receiving end, operation of the access control forces the receiving switch to make A the working channel and X the standby channel, providing channel A is not failed at the time. A safety inhibit feature is provided which prevents the receiving access control circuit from operating if channel A is failed.

2.2.5 *Alarms*

A service failure alarm is generated whenever the working channel fails and cannot be made good immediately by automatic switch operation.

A delayed channel A or channel X failure alarm is generated whenever the standby channel fails and remains failed for 45 seconds. When the access controls are operated, an immediate service failure alarm is generated if either channel fails.

2.2.6 *Indications*

Front panel lamps are provided to indicate which channel is the working channel, whether channels A and X are failed due to noise

or loss of pilot, and whether a channel failure is simply a prolonged failure of the standby channel or a more serious service failure. Lamps are also provided to indicate whether the system is operating in the automatic mode or whether one of the forced switch or access switch controls has been operated.

2.3 *Unit Descriptions*

2.3.1 *Baseband Switch*

This unit is comprised of four switching elements and a control circuit incorporated in one package. As shown in Fig. 1, it has two inputs (A and B) and two outputs (AB and BA). The switch is a bilateral device and the input and output designations are used for descriptive purposes only. In its normal state, the A input is connected to the AB output and the B input is connected to the BA output. In the switched state, the connections are reversed. Adjacent elements of the switch are always in opposite states, a characteristic which is taken advantage of in the design as described below.

Each switch element consists of two diodes, two transistors, and their associated components. As shown in Fig. 4, each element is identical. Operation of the element consisting of Q3, Q4, CR2, and CR3 will now be described.

To establish a low-loss connection between A and AB, transistor Q3 is turned on, and transistor Q4 is turned off, thereby forward biasing diodes CR2 and CR3. To open the connection between A and AB, transistor Q3 is turned off and Q4 is turned on. Diodes CR2 and CR3 are now reverse biased by the ground on the anode side provided by Q4 and by a positive voltage on the cathode sides provided by current from adjacent switch elements flowing through resistors R1 and R2. The two diodes and transistor Q4 form a controlled loss tee pad and transistor Q3 serves as a current valve to reduce the current drawn by the switch.

Simplified equivalent circuits of a switching element in the "ON" and "OFF" states are shown in Fig. 5. From Fig. 5, the insertion loss of an "ON" switching element is given by:

$$\text{I.L. (ON)} = 20 \text{ Log} \left[\frac{(R_o + R_f)(R_o + 2R_s)}{2R_oR_s} \right] \text{dB},$$

where

R_o = source impedance = 75 ohms,
R_f = diode forward impedance = 1 ohm, and
R_s = shunt impedance of biasing network = 3,000 ohms.

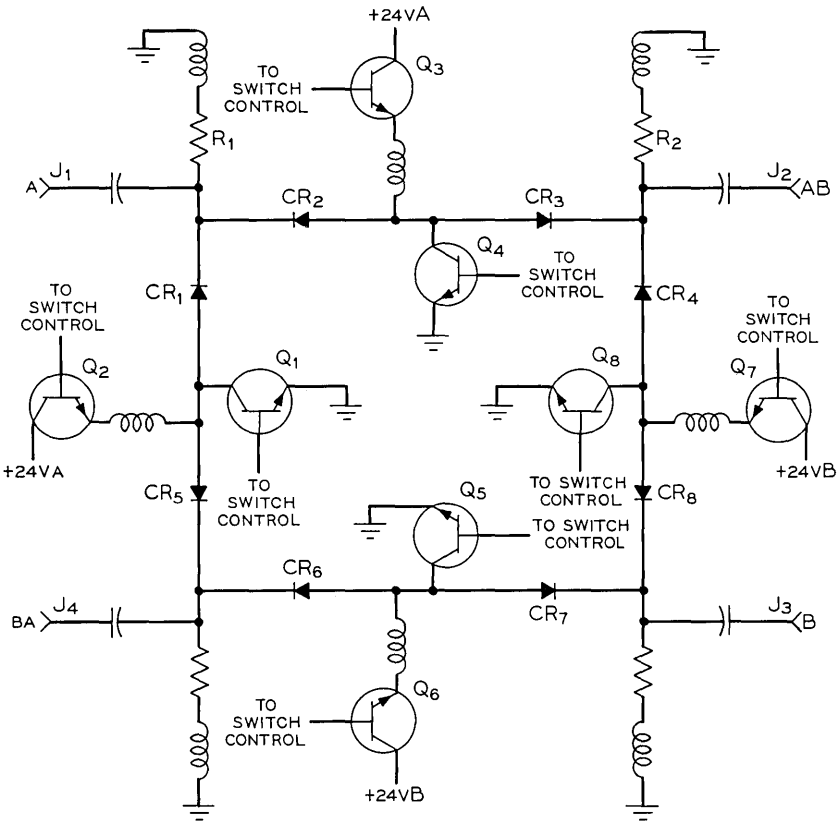

Fig. 4—Baseband switch schematic.

The impedance of the biasing network is designed to optimize the return loss of the switch for a particular diode impedance. The "ON" insertion loss is thereby controlled entirely by the diode impedance. With the above values, the insertion loss is 0.22 dB which is within the factory specified limits of from 0.1 to 0.3 dB. The insertion loss of an "OFF" switching element is given by:

$$\text{I.L. (OFF)} = 20 \text{ Log} \left[\frac{2}{R_o R_t (2\pi f C_r)^2} \right] \text{dB},$$

where

R_t = impedance of shunt transistor = 9 ohms,
f = frequency in Hz, and
C_r = reverse capacitance of the diode = 2.5 pF.

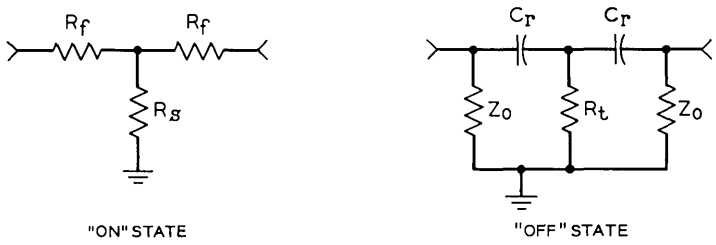

Fig. 5—Switching element equivalent circuits.

At a frequency of 10 MHz, using these nominal values, the "OFF" insertion loss is 101 dB. In practice, the insertion loss is about 95 dB, being limited by ground loops and by power supply coupling.

The operation of the switch elements is controlled to achieve a make before break type of operation. The switching action is also controlled to minimize the transient inherent in changing the bias of the diodes in the switching elements. The switching action is shown in Fig. 6. After the input control lead changes state, there is a delay of about

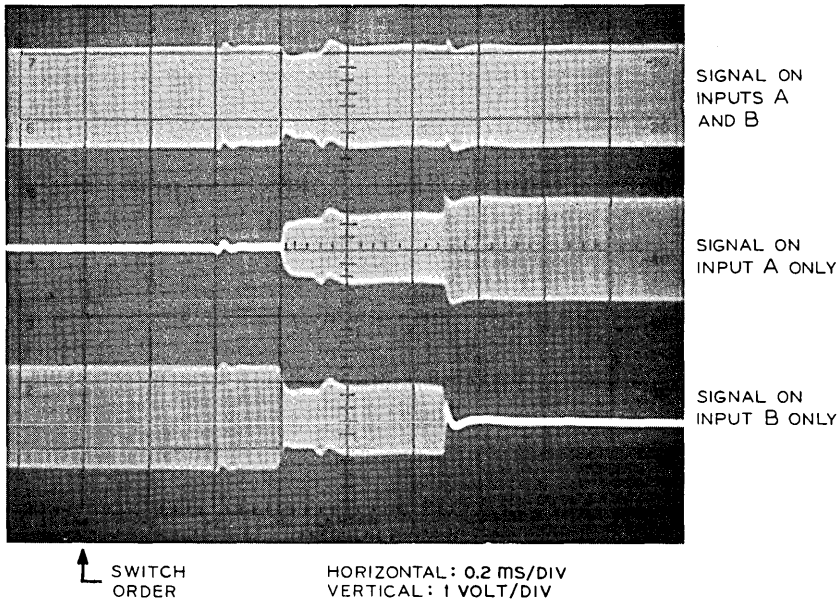

Fig. 6—283B switch transfer action as seen at output AB.

0.6 millisecond before the temporary period when both inputs are connected to the output. The double connection lasts for about 0.5 millisecond, after which the switch is completed. The switching transient has negligible energy above 60 kHz, and therefore does not affect signals carried by the 300A system.

The power handling capability of the switch is +20 dBm of sine wave power. This is the required capability for operation at a −10-dB transmission level point. When operated at this level, the switch contributes less than 5 dBrnc0 of noise.

A photograph of the switch, coded the 283B switch, is shown in Fig. 7. It is housed in a shielded unit with reduced size jacks used for signal connections and a 15-pin connector used for power and control leads. Its dimensions are 4.25 inches long, 3.8 inches wide, and 1.375 inches deep.

2.3.2 *Channel Monitor*

The channel monitor continuously monitors the quality and continuity of the working and standby channels by measuring noise in a

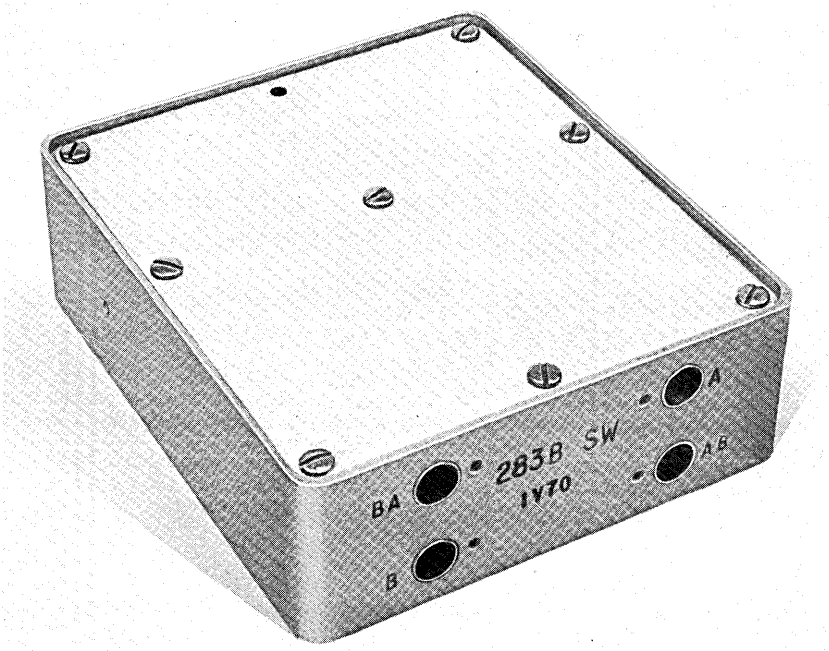

Fig. 7—283B baseband switch.

20-kHz slot centered at 10.2 MHz and by detecting the presence of a continuity pilot. A block diagram of the monitor circuit is shown in Fig. 8.

The sensitivity of the monitor is determined by the lowest level of pilot and noise which must be detected, which occurs when the entrance links are not included within the switching section. Under this condition, the BSB input of the monitor is a −64-dB TLP taking into account the 30-dB loss of the bridge tap. At this point, the pilot level at the trip point is −79 dBm and the power in the noise slot at the trip point is −88 dBm. Allowing a 10-dB margin, the sensitivity of the monitor must be sufficient to detect noise signals as low as −98 dBm. Since the detectors require signal levels of approximately 0 dBm, 98 dB of gain must be provided for the noise signal and 89 dB for the pilot signal. This gain is broken up into several blocks as shown in Fig. 8. Sufficient adjustment range is provided to enable the monitor to be used when the entrance links are included within the switching section.

Four filters provide the necessary selectivity in the monitor circuit. The first is a high-pass LC filter which attenuates the payload signal thereby preventing overloading of the following amplifier stages. Two monolithic crystal filters are used to separate the noise and pilot

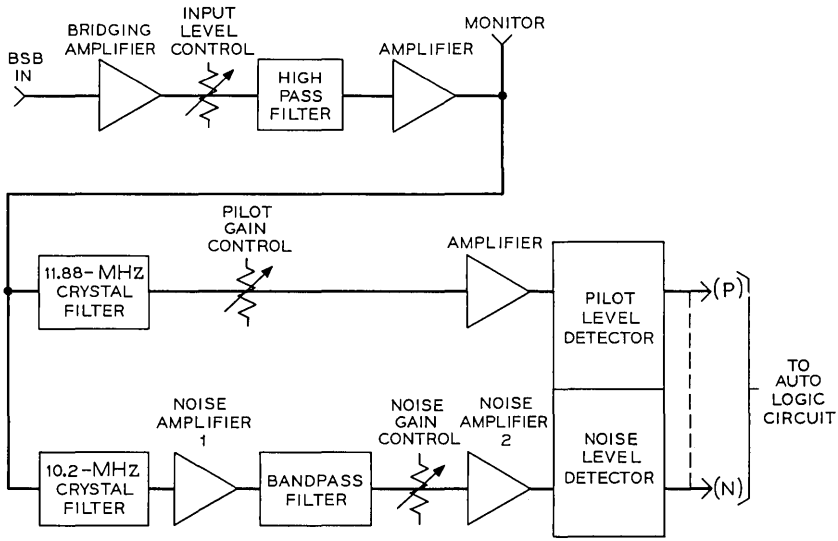

Fig. 8—Monitor circuit block diagram.

signals into two different paths. The selectivity of the crystal filter in the noise path is shown in Fig. 9. The pilot filter has a similar characteristic, but with reduced bandwidth. An additional bandpass LC filter is provided in the noise path to increase the selectivity, primarily to attenuate the auxiliary channel carrier located at 11.38 MHz.

Detection is accomplished with a pair of diodes followed by an integrated circuit operational amplifier as shown in Fig. 10. The operational amplifier functions as a Schmitt trigger to provide well defined switch and restore settings. It features a restore setting control which does not interact with the switch setting. With no noise present, the output of the OP AMP is held to −0.7 volt by the forward bias on diode CR1. A reference voltage of −0.6 volt on the non-inverting (NI) input of the OP AMP is provided by R4 and R5. Under these conditions, negligible current is drawn through the restore control R3, thereby preventing its setting from affecting the switch point. When the detected noise on the inverting (I) input reaches −0.6 volt, the output of the OP AMP becomes positive. Fast switching action is enhanced by positive feedback provided by resistor R2. The positive voltage at the output is limited to +4.3 volts by breakdown diode CR1. The voltage on the non-inverting input of the OP AMP becomes more positive and may be controlled by adjusting potentiometer R3. The setting of R3 will therefore determine the noise

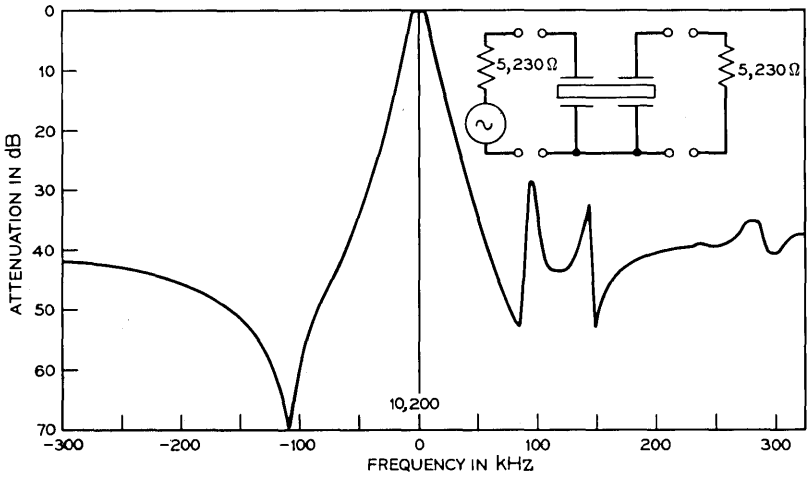

Fig. 9—Selectivity of noise crystal filter.

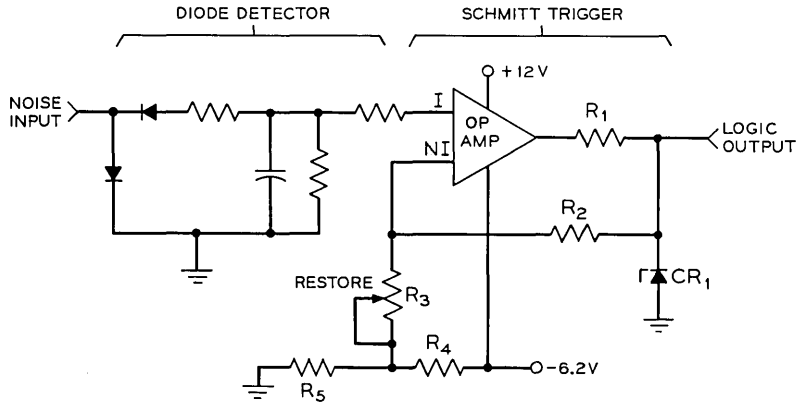

Fig. 10—Noise detecting circuit.

level at which the detector will restore to its no noise state. The pilot detection is done with a similar circuit except no restore adjustment is provided.

The monitor is housed as a shielded package as shown in Fig. 11. Its overall dimensions are 6.825 inches long, 3.75 inches wide, and 2.75 inches high.

2.3.3 *Automatic Logic*

The logic for automatic control of the system is shown as a single block in Fig. 3 and in more detail in Fig. 12. The logic levels shown on the interconnecting leads in Fig. 12 are the normal levels when the working and standby channels are both good, with channel A as the working channel, and the controls set for the automatic mode of operation.

The working and standby monitors each furnish two inputs to the automatic logic. Loss of pilot on the working channel causes a logic level change from 1 to 0 on the PW input. Failure of the working channel due to noise causes a logic level change on the NW input from 0 to 1. Either type of failure on the working channel causes the W input to the sequential logic to change from 1 to 0.

Similarly, a failure of the standby channel due to noise or loss of pilot causes the S input to the sequential logic to change from 1 to 0.

Whenever the working channel fails while the standby channel is good, the logic level on the T input to the flip-flop (FF) in the sequential logic changes from 1 to 0 causing the flip-flop to change

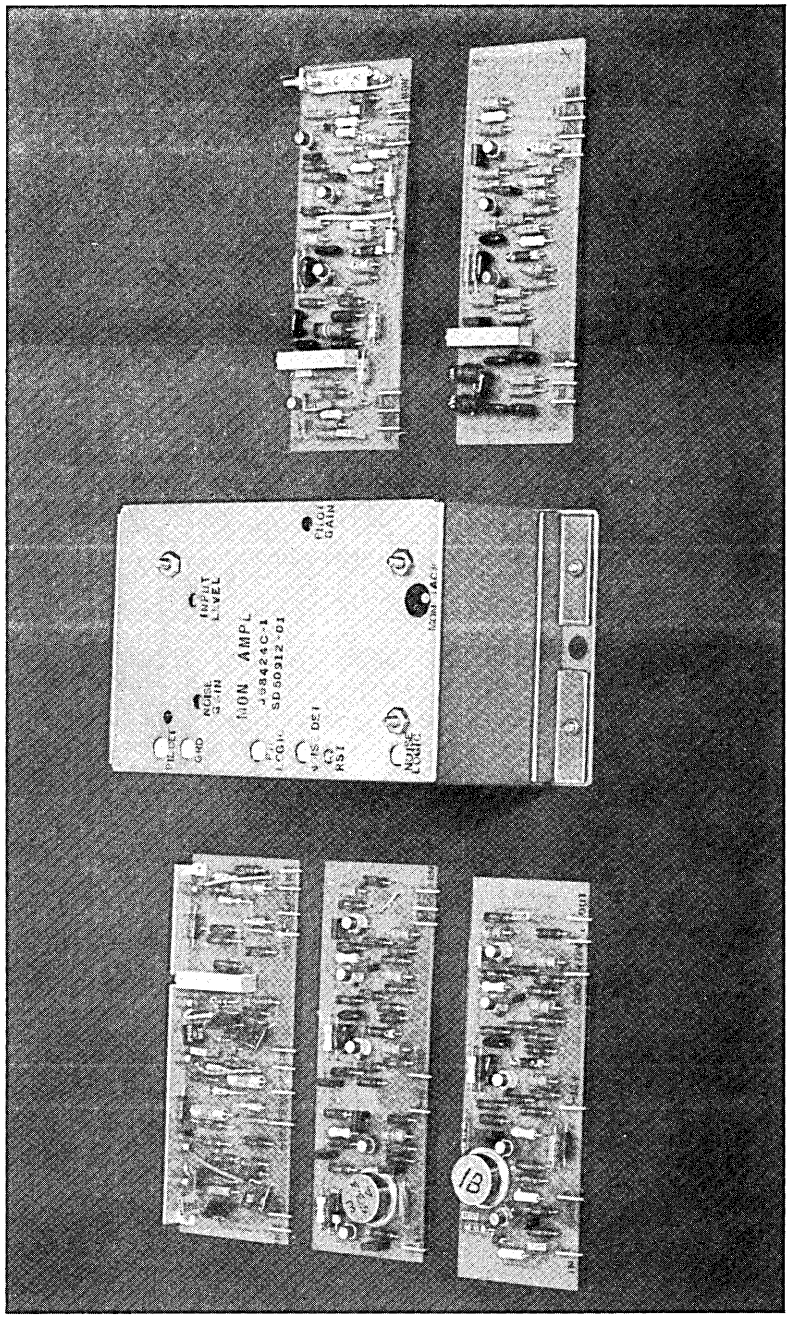

Fig. 11—Channel monitor.

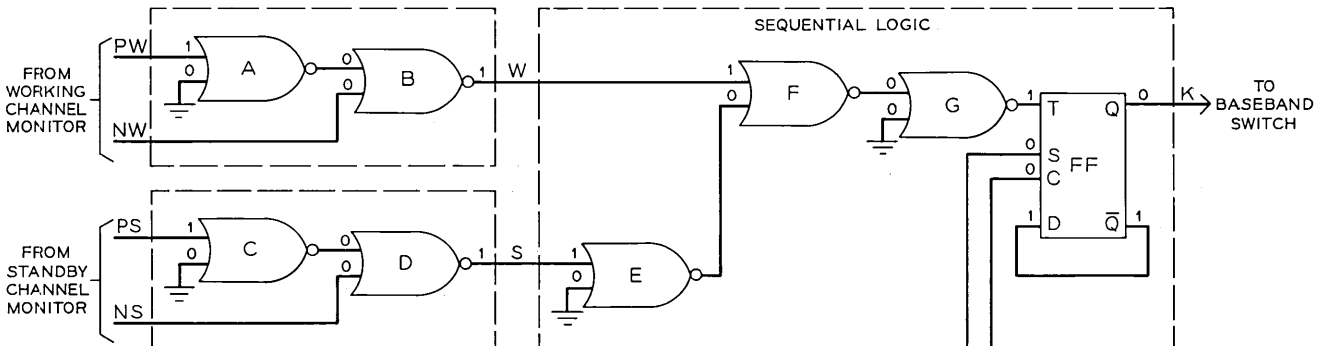

TRUTH TABLES

A

PW	NW	W
0	0	0
0	1	0
1	0	1
1	1	0

B

PS	NS	S
0	0	0
0	1	0
1	0	1
1	1	0

STATE TABLE

W-S	00	01	11	10	K
5	2	(1)	4		0
7	(2)	6	3		1
7	8	6	(3)		1
5	2	1	(4)		0
(5)	2	1	4		0
7	8	(6)	3		1
(7)	8	6	3		1
5	(8)	1	4		0

Fig. 12—Automatic logic circuit.

state. A change on the T input from 0 to 1 does not cause the flip-flop to change state.

The K output of the sequential logic controls the baseband switch. When K = 0, channel A is the working channel and channel X is the standby channel. When K = 1, channel X is the working channel and channel A is the standby channel.

Truth table A in Fig. 12 defines the input-output functions of gates A and B. Truth table B defines the input-output functions of gates C and D. The state table defines the input-output functions of the sequential logic composed of gates E, F, and G, and the flip-flop (FF).

The first stable (circled) state in the state table is taken as the condition when inputs W and S are both 1 and output K is 0. This means that the working and standby channels are both good and channel A is the working channel. If the working channel (A) fails while the standby (X) remains good, the inputs change from 11 to 01, causing the output to change from 0 to 1. This is the second stable (circled) state in the state table. When output K changes from 0 to 1, the baseband switch changes state reversing the roles of channels A and X, making X the working channel and A the standby channel. The working channel then becomes good again and the failed channel (A) becomes the standby channel. This changes the W and S inputs to the sequential circuit from 01 to 10 and the circuit assumes the third stable (circled) state, and the output K remains 1. If next the standby channel (A) becomes good while the working channel (X) is still good, the W and S inputs change from 10 to 11 and the circuit assumes stable state 6 (circled), with the output remaining at 1.

The next time the working channel (X) fails while the standby (A) remains good, the stable state changes will be from 6 to 8 to 4, with the output changing from 1 to 0. Subsequently, when the standby channel again becomes good, the inputs will again change from 10 to 11 and the circuit will return to stable state 1, holding the 0 output.

All other possible input-output changes are similarly defined by the state table.

There are two manual control inputs to the sequential logic (K1 and K2) that originate in the forced switch control circuit. These go to the set (S) and clear (C) inputs of the flip-flop. The forced switch control circuit operates directly into the baseband switch for manual control. The K output of the automatic logic is made to follow the forced switching operation by the K1 and K2 inputs. Otherwise an undesired automatic switch operation may take place just after the system is returned from manual control to automatic operation.

2.3.4 *Pilot and Test Oscillators*

Pilot, pilot test, and noise test oscillators are identical except for frequency. They are conventional solid state crystal-controlled oscillators designed for operation at either 10.2 or 11.88 MHz, followed by a two-stage amplifier and a low-pass output filter.

2.3.5 *Controls, Indications, and Alarms*

The controls, indications, and alarms circuit provides the sources required to generate alarms to the office and C1 or E-type alarm systems, and the operating keys and relays required to control the system locally or remotely.

The following features are provided:

(*i*) Local and remote indicating lamps to indicate the status of the system at all times

(*ii*) Local and remote alarm lamps to indicate the source of each alarm

(*iii*) Connections to office alarms, C1 or E-type alarm facilities, and aisle pilot lamps for alarms in the system

(*iv*) Operating keys and relays for making forced switches to either channel A or X or making an access switch to channel X

(*v*) An alarm cutoff (ACO) key to silence the audible alarm and to extinguish the appropriate aisle pilot lamps.

2.4 *Relay Interface and Wiring Considerations*

To protect the integrated circuits against noise and other voltage transients which might be coupled in from the office wiring, all alarm, indicating, and control connections between the 300A system and the office alarm system or remote alarm and control systems are made through interfacing relays. Integrated circuit relay drivers operate the relays which provide the outgoing alarms and indications. Incoming control orders operate relays in the 300A which in turn operate integrated circuit flip-flops to provide clean, non-bouncing inputs to the logic and control circuits. Diodes across each relay winding suppress the transients generated by the relays in the 300A. All wiring associated with relays and front panel lamps and controls is carefully segregated from the wiring associated with logic circuit interconnections.

2.5 *Equipment Features*

The 300A switch unit, shown in Fig. 13, contains the units for the receive end of a switching section for one direction of transmission

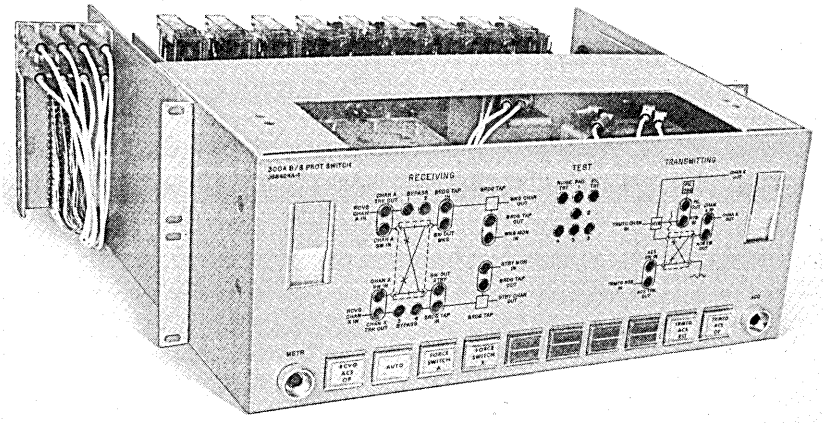

Fig. 13—300A switch unit.

and the units for the transmitting end of a switching section for the opposite direction of transmission. The test oscillators and split pad are also incorporated in the unit and have front panel jack appearances. The 300A unit occupies the space of four 1-3/4 inch mounting plates in a 19-inch bay. Its shipping weight is 42 pounds.

The unit consists of a drawer and drawer housing, which, when extended, allows access to all plug-in units and wiring. All active circuits are packaged as plug-in units for ease of maintenance and trouble shooting.

All controls and indications are mounted on the front panel and provision is made to multiple these functions to a remote control panel within the station. Connections for C-type or E-type alarm systems are also provided for control from distant alarm centers.

Access jacks are provided on the front panel for test purposes and to permit manual patches to be made during trouble conditions. As shown in Fig. 13, a simplified diagram of the transmission circuit is imprinted on the front panel jack field to indicate the function of each jack. Connections between the jacks are made by means of patch plugs. For normal operation the patch plugs are oriented in the vertical position, for test or trouble conditions the patch plugs are oriented in the horizontal position.

2.6 *Testing*

The 300A system is designed to be tested with the test oscillators provided in the 300A unit in conjunction with standard test equip-

ment normally available in radio stations. Front panel jack appearances are provided to allow easy access to the pilot oscillator, baseband switches, and monitors. Special jack appearances are provided to allow patches to bypass service around the switch without interrupting service. The only adjustments required are the level and frequency of the pilot and test oscillators and the noise and pilot trip points of the monitors. Test points are provided within the 300A drawer for voltage measurements for use in trouble shooting procedures. When a trouble is located, it is generally repaired by replacing a defective plug-in unit with a spare unit.

III. AUXILIARY CHANNEL SWITCHING

3.1 *System Considerations*

The auxiliary channel carries the order-wire and alarm signals as well as providing additional voice channels for the TH-3 medium-haul system. Its signals are diplexed above the message load on the two radio channels in each direction of transmission, with modulating and demodulating equipment at each of the repeaters and main stations. It is a facility that is complete within itself and is independent of the 1800-message circuit load.

The auxiliary channel signal is inserted on and removed from the two radio channels within the protection switching system protecting the broadband message load, normally the 300A system. The auxiliary channel circuits receive no protection from, and are independent of the 300A system, except for the use of the 11.88-MHz pilot as described below. Protection is provided by the auxiliary channel switching system on a one-by-one basis.

Since the auxiliary channel circuits appear at each repeater, the switching system must operate switches at each repeater. As explained in Ref. 2, the main station and all repeater station switches must be operated in synchronism to either channel A or channel X. The control point of the auxiliary channel switching system is at the receiving main station of the switching section. Repeater station switches are controlled by the main station equipment by means of a voice-frequency control line operating over the auxiliary channel system in the opposite direction to that being protected, as shown in Fig. 14.

The main station portion of the auxiliary channel protection switching system is very similar in operation and physical make up to the 300A equipment. Therefore, the description of the main station equipment is limited to a discussion of its differences from the 300A equip-

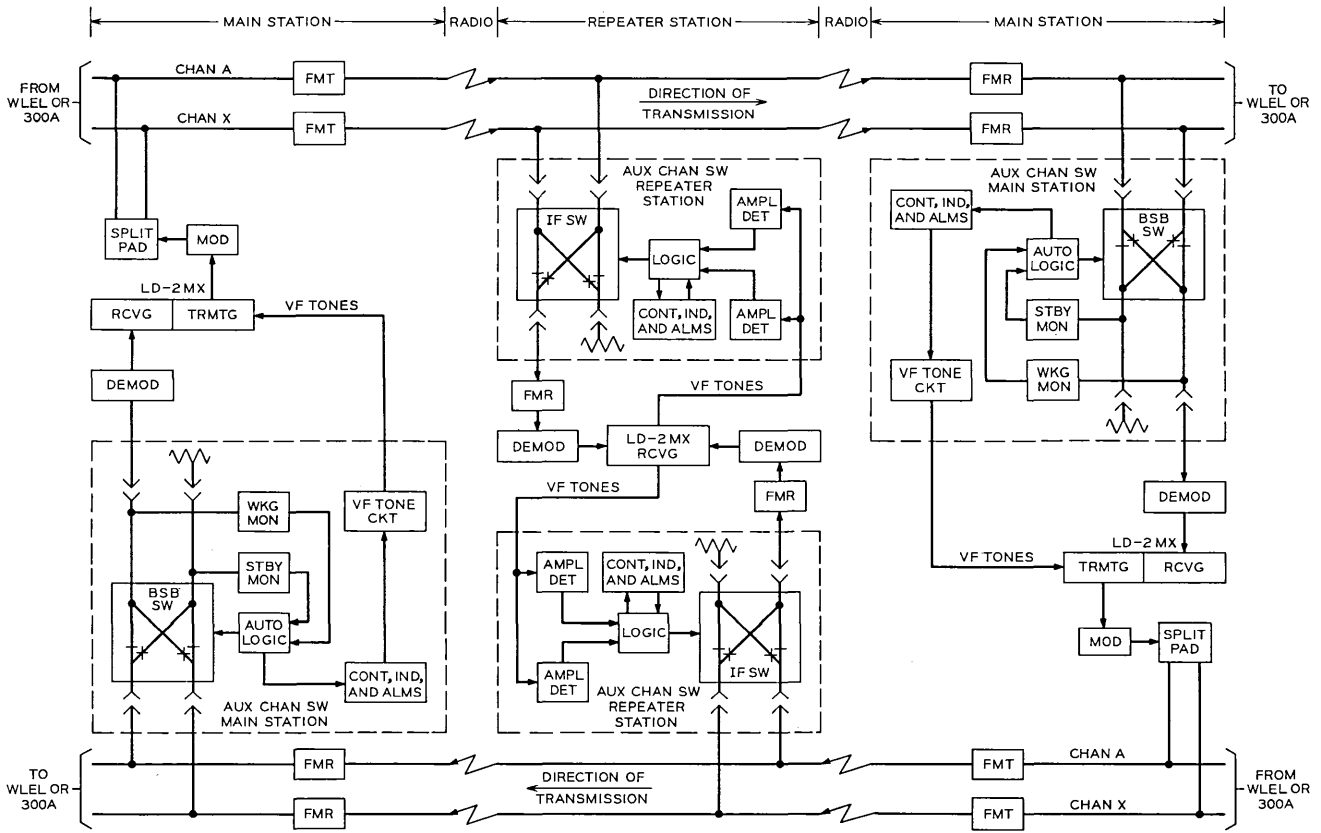

Fig. 14—Auxiliary channel switching system block diagram.

ment. The major differences are: no transmitting equipment is required for the auxiliary main station switch, the access feature is not provided, and a voice-frequency tone unit consisting of two tone oscillators is required for the main station unit. Other differences include a low-loss bridge tap and different monitor settings. These latter differences are required because the signal levels in the auxiliary main station switch are lower than in the 300A switch.

The repeater station equipment is bridged on both radio channels at IF, and connects one of the IF signals to the auxiliary channel FMR as shown in Fig. 14. The connection is made by a solid state IF switch similar to the 300A baseband switch. Operation of the switch is controlled by the tones being sent from the main station equipment. The tones are converted to a digital signal by bandpass filters and amplifier-detector circuits.

At both the main station and repeater station, controls, alarms, and indications are provided for use by station personnel. These functions can also be remotely monitored and controlled through connection to E-type alarm and status reporting systems.

The voice-frequency tone signaling code used to control the repeater station switches consists of two tones, one present and the other absent. With a 1615-Hz oscillator turned on, the switches are connected to channel A; with a 2295-Hz oscillator on, the switches are connected to channel X. If no tones or both tones are present at the repeater station, no switching takes place and an invalid code alarm is generated by the repeater station equipment.

As shown in Fig. 14, the control tones are carried to the repeater stations via the auxiliary channel in the opposite direction, which is in turn protected by its auxiliary channel protection switching system. This arrangement provides a reliable transmission path for the control tones. However, it is important that the repeater station be capable of recognizing the signaling tones in the presence of noise at least up to the switch point of the auxiliary channel. The tones are carried at a level of -25 dBm at 0 dB TLP which is sufficiently low to represent only a small portion of the auxiliary channel load handling capacity. The sensitivity of the repeater station switching equipment to noise on the control line is such that no false switching activity takes place until the noise level is about 70 dBrnc0, which is well above the critical point of 55 dBrnc0 where the channel is considered bad.

Power requirements for the main station equipment are approximately the same as for the 300A system. The repeater station units

require +24 volts and −24 volts which is provided by the power supply for the auxiliary channel equipment.

3.2 *Repeater Station Unit Descriptions*

3.2.1 *IF Switch*

The IF switch, coded the 283A switch, is outwardly identical to the 283B baseband switch used in the 300A system (see Fig. 7). However, electrically it operates over the frequency range of 50 MHz to 100 MHz. This high frequency range, and a maximum signal power handling capability of +10 dBm, permit low diode bias current of about 5 milliamperes to be used in this switch compared to 40 milliamperes in the baseband switch. The high frequency of operation also allows the use of 10-microhenry instead of 1-millihenry chokes, thus permitting greater speed of operation.

The circuit of the switching elements is the same as that of the baseband switching elements (see Fig. 4), with the exception that the current limiting transistors (Q2, Q3, Q6, and Q7) are not required because of the low current levels in the IF switch. Low values of inductance and capacitance are used since the signal frequencies are in the IF range.

The switching action as seen at the output of the switch on an oscilloscope is shown in Fig. 15. The top line is with identical signals present on inputs A and B, the next line is with a signal on input A, and the last line is with a signal on input B. The transfer from A to B is completed within about 0.4 microsecond with no loss of transmission.

Other characteristics of the switch are:

Frequency Range—50 MHz to 100 MHz
Insertion Loss—"ON" State <0.3 dB
Insertion Loss—"OFF" State >90 dB
Return Loss—>30 dB
Power Supply—+24 volts at 60 mA.

3.2.2 *Logic and Control*

The logic and control for the repeater station IF switch is shown as single blocks in Fig. 14 and in more detail in Fig. 16. The logic levels shown on the interconnecting leads in Fig. 16 are the normal levels when: tone 1 is present, tone 2 is absent, the system is operating in the automatic mode, and the IF switch is set so that the FMR is connected to channel A.

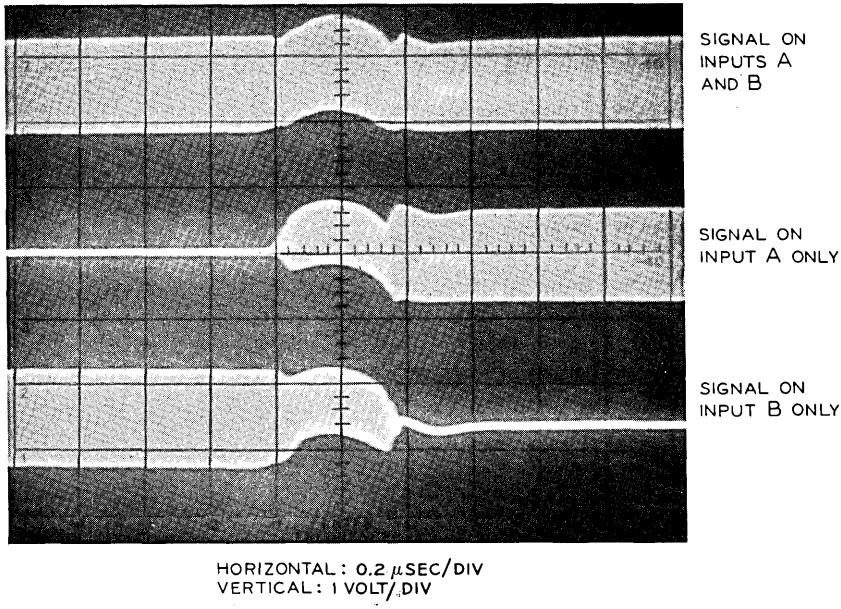

Fig. 15—283A switch transfer action as seen at output AB.

When an order is received to switch the FMR to channel X, tone 1 disappears and tone 2 becomes present, causing inputs T1 and T2 to change state (T1 = 0, T2 = 1). This causes the set-reset flip-flop (FF) to change state, and, after a 5-millisecond delay, the IF switch control lead (OP) changes to 1. A 1 on the IF switch control lead makes the IF switch change state thus switching the FMR to channel X. The 5-millisecond delay at the output of the automatic logic is bi-lateral, that is, the output to the OP lead is delayed 5 milliseconds for either a positive or a negative input transition. This prevents momentary operations of the IF switch if short transient input changes occur.

If the T1 and T2 inputs both become 1 or both become 0, the flip-flop (FF) will not change state. Either two ones or two zeros from the tone detectors is an invalid code. If the invalid code condition exists for more than 175 milliseconds, an invalid code alarm is generated by the invalid code logic circuitry.

Inputs A and B are used for manual control of the IF switch. When A and B are 1 and 0, respectively, the IF switch control lead (OP) is forced to become 0. When A and B are 0 and 1, respectively, the

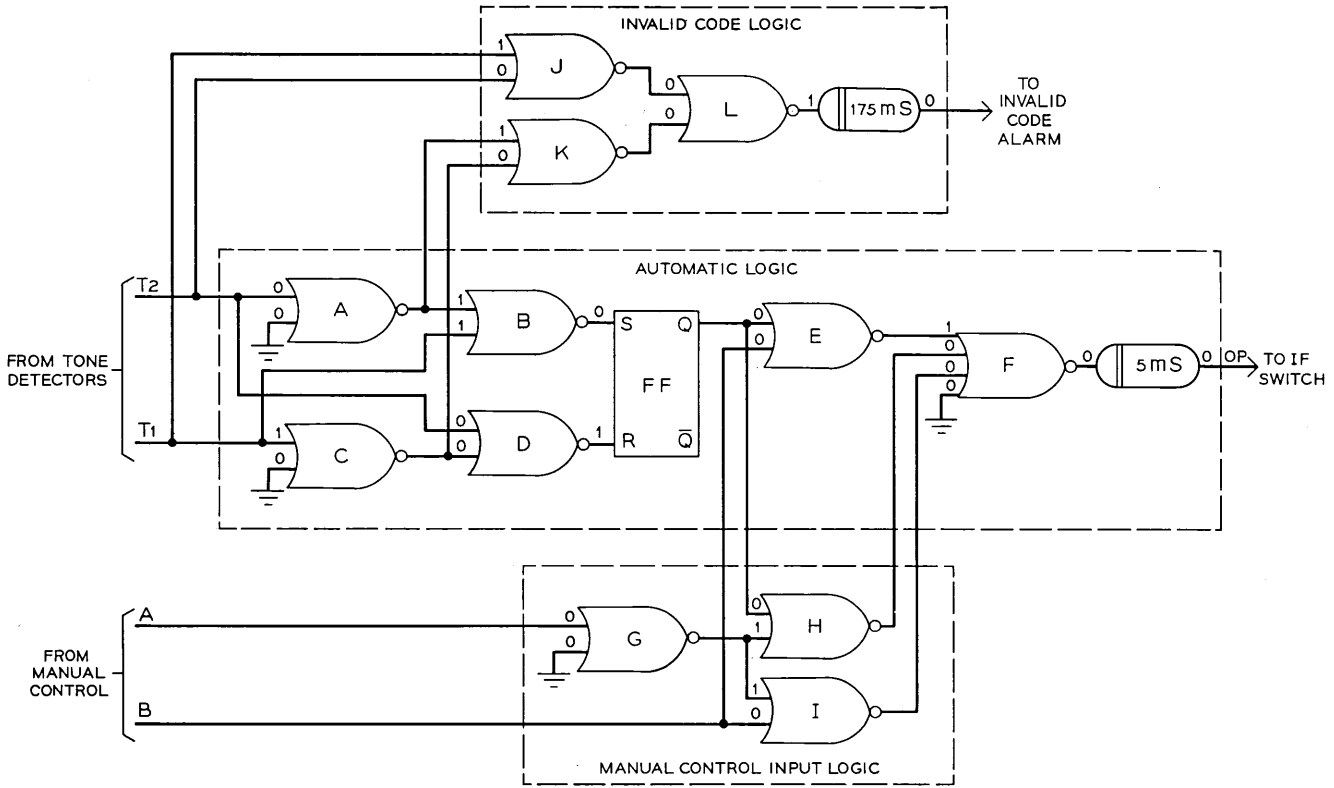

Fig. 16—Repeater station logic.

IF switch control lead is forced to become 1. When A and B are both 0, the circuit is under automatic control.

3.2.3 *Amplifier-Detector*

The amplifier-detector circuit detects the presence or absence of a VF tone that is originated at the main station switching equipment. There are two amplifier-detectors in each repeater station switch unit, one associated with the 1615-Hz tone and one associated with the 2295-Hz tone. The appropriate VF tone is picked off the VF line by a bandpass filter and applied to the amplifier-detector, which in turn supplies a logic signal to the logic circuit.

The amplifier detector is composed of two integrated circuit operational amplifiers and a diode detector. The first operational amplifier is used to amplify the VF tone and includes a gain control for setting the operate point. The tone is then detected by the diode detector and the resultant dc voltage is applied to the second operational amplifier. This operational amplifier functions as a Schmitt Trigger and is similar to the detector used in the monitor circuit (see Fig. 10). The Schmitt Trigger supplies the logic with a logic level 1 for tone present and a 0 for tone absent.

3.3 *Equipment Features*

The auxiliary channel main station switching unit consists of a 300A type drawer and a VF tone unit containing the two oscillator units. These units occupy the space of six 1-3/4 inch mounting plates in a 19-inch bay. The repeater station switch panel, shown in Fig. 17, contains the IF switch, two voice-frequency filters, two amplifier-detector units, logic, and control circuits. It occupies the space of one 1-3/4 inch mounting plate in a 19-inch bay.

IV. SUMMARY

Two independent switching systems have been described that provide automatic switching for the TH-3 medium-haul microwave radio system. The 300A system is a one-by-one baseband switching system that insures adequate reliability of the payload signal. The auxiliary channel switching system insures adequate reliability of the frequency-diplexed auxiliary channel circuits that carry order-wire and alarm information. Although protecting circuits that may be carried simultaneously on the TH-3 radio system, these two protection switching systems are functionally and physically independent. Considerable

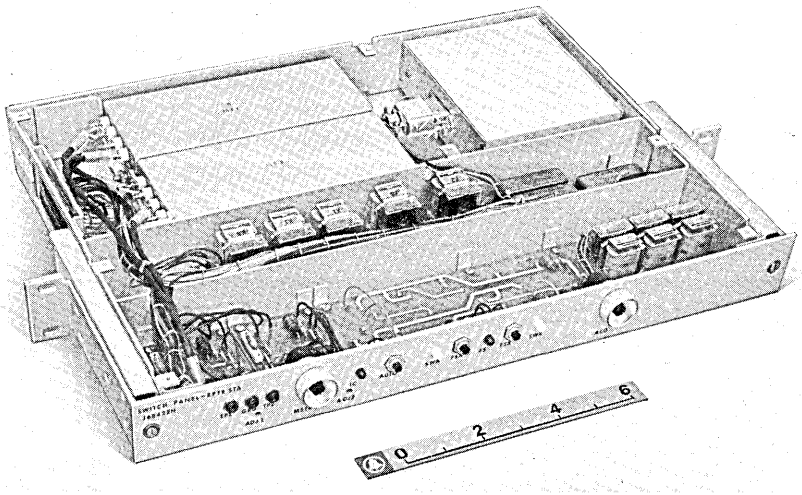

Fig. 17—Repeater station switch panel.

effort was taken to achieve high reliability, ease of maintenance, and simplicity of operation in both systems.

V. ACKNOWLEDGMENTS

Many members of the Radio Transmission Laboratory have contributed to the development of the TH-3 medium-haul protection switching systems. Among them the authors wish to mention R. O. Davidson, P. A. Pearson, and J. D. Wiidakas. The mechanical design was the responsibility of A. D. Boren, J. W. Sponsler, and L. F. Travis.

REFERENCES

1. Griffiths, H. D., and Nedelka, J., "100A Protection Switching System," B.S.T.J., *44*, No. 10 (December, 1965), pp. 2295–2336.
2. Knapp, J. W., and Seastrand, K. L., "TH-3 Medium-Haul Application: Frequency-Diplexed Auxiliary Channel," B.S.T.J., this issue, pp. 2287–2313.

THE BELL SYSTEM TECHNICAL JOURNAL
Vol. 50, No. 7, September, 1971
Printed in U.S.A.

TH-3 Medium-Haul Application:

Equipment and Building Considerations

By R. A. SWIFT and J. A. WORD

(Manuscript received January 4, 1971)

This paper points out the salient equipment and building considerations peculiar to the TH-3 radio system with emphasis on the ability to combine TH-3 with existing radio systems.

I. INTRODUCTION

TH-3 radio in its overall systems equipment concept for 4000-mile long-haul radio is almost identical to TD-3 radio.[1] The primary difference is in the frequency band, the circuit capacity, and the number of radio channels per route. All of the supporting equipments, such as power plants, FM terminals, radio line protection switching, entrance link and FM terminal protection switching, patching and access and emergency restoration equipment as well as test equipment, are essentially identical in their application to TD-3 and TH-3. Some of of the supporting items will handle broadband channels of both TD-3 and TH-3 on a direct intermix basis whereas others require only minor changes.

The largest application of TH-3 will be in the addition of TH-3 radio at 6 GHz to already established fully loaded TD-2 and TD-3 radio routes operating at 4 GHz (overbuilding); this involves using existing buildings and common facilities, including antennas and waveguide insofar as possible.

Two TH-3 radio systems have been developed; a version for use on 4000-mile long-haul routes and a simplified version for use on medium-haul routes where only one working broadband channel is required. This capacity restriction for medium-haul usage permits the protection switching to be greatly simplified and the use of a single antenna for transmitting and receiving in each direction. This medium-haul system should have considerable application in meeting

operating company needs for microwave radio systems on other than major routes.

II. BUILDINGS AND FACILITIES

The Central Office Layouts and Design Committee of the Long Lines Department of the American Telephone and Telegraph Company has initiated the design of a Type 1260 building (see Fig. 1) which is proposed as a standard for repeater station applications and can also apply to small "through"* main switching stations. This building, having a floor area of 1260 square feet, can contain 16 TH-3 T/R bays (8 two-way broadband channels), 24 TD-3 T/R bays (12 two-way broadband channels), and the necessary supporting equipment for a through route. Provision is made for a third module addition to provide for additional side-leg routes or additions such as terminal facilities.

The use of a systems combining network in the vertical run of waveguide enables the simultaneous use of antennas and vertical circular waveguides for both 4- and 6-GHz signals for long-haul applications. Separate horizontal rectangular waveguides are required to accommodate 4 and 6 GHz from the separation networks into the station.

A new dehydrator provides dry air to both the external waveguides and antennas and to the indoor waveguides to stabilize the performance of the Transmit-Receive filters. This dehydrator combines a refrigerating element plus a desiccant (drying agent) chamber to remove the air moisture. It can provide 100 cubic feet per hour of −40°F dewpoint air at a pressure of approximately 7 inches of water which is adequate to supply a combined TD-3/TH-3 through repeater station. A relief valve is incorporated in this unit to avoid over-pressure on low loads.

When TH-3 is used to overbuild on a 4-GHz TD-2 system, the problem becomes more complicated. The dc power required in an existing TD-2 station is at voltages of −12, +130, +250, and −24. The basic voltage for TH-3 and its latest supporting equipments is −24. Since the −24 V requirements for a TD-2 station are small, TH-3 additions to a TD-2 station in most instances will require either additions to or a larger −24 V power plant. A further problem is that of building additions since the initial station planning may not have considered this extent of expansion.

* Non-junction stations.

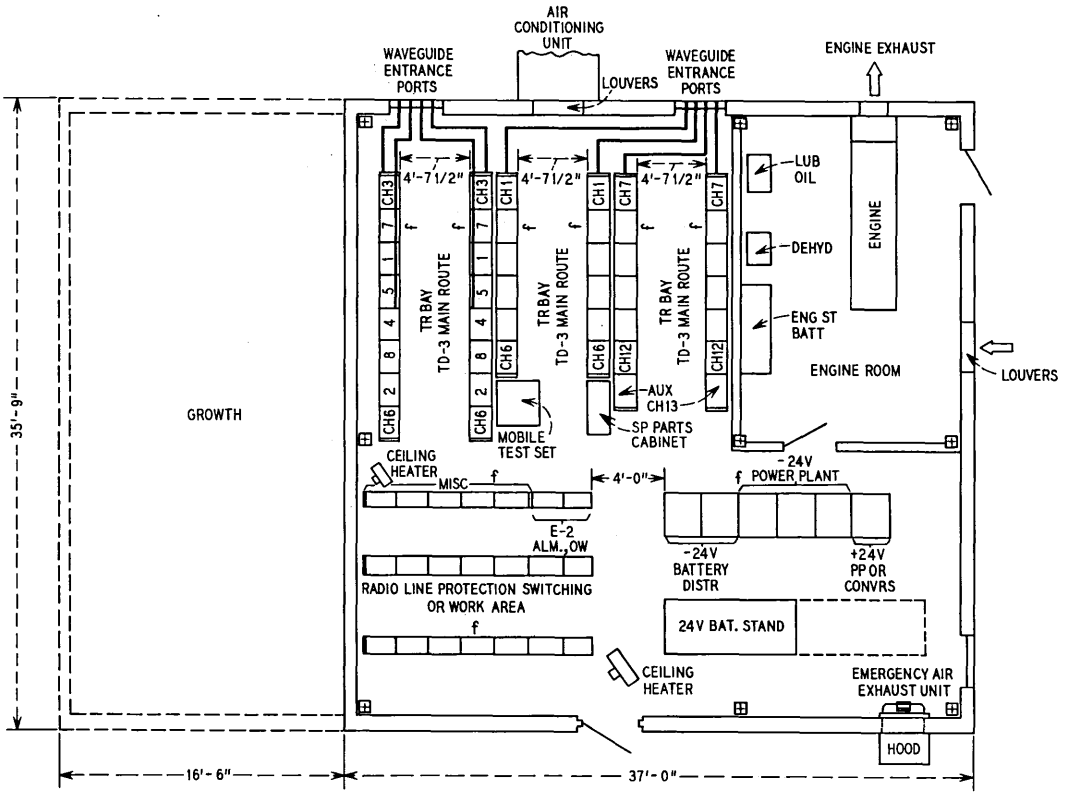

Fig. 1—Standard 1260 radio repeater building.

In the first installations of TD-3 certain power supply leads feeding into noisy loads such as dc-to-dc converters were put in metallic ducts to avoid the possibility of unwanted coupling into critical circuits. Through use of additional filtering in the input to such loads the noise has been reduced to acceptable levels and isolation of these power leads is no longer required in TD-3 and TH-3 installations.

III. TH-3 MEDIUM HAUL

In addition to its use for long-haul and major routes, a specific application of TH-3 is for medium-haul routes, where the protection system is 1 × 1 utilizing a single working radio channel protected by a second identical channel. Protection is from baseband at one terminal to baseband at the far terminal, encompassing the total radio facility from end to end. In this medium-haul system the stations will be either small buildings or factory-equipped transportable shelters. The shelter is an aluminum structure similar in appearance to a truck trailer body. It provides an economical alternative to small buildings, deriving savings through reduced first costs, standardized engineering, and factory installation and test. Two typical floor plans (Figs. 2 and 3) show the placement of equipment in a small building and in a shelter, respectively. Although the medium-haul system is presently protected by a one for one switching system, plans for growth include a one for three system. Table I lists the basic elements required in a TH-3 medium-haul radio station.

It is anticipated that applications of the TH-3 medium-haul system also will be in existing telephone company buildings. The repeater station at Dunbarton, New Hampshire, shown in Fig. 4, is an example where the TH-3 system has been installed in a small building which houses a TJ 11-GHz microwave radio system.[2]

Some relaxation in requirements is allowed in medium-haul systems. In the case of the environmental station temperature, limits of 40°F to 120°F are permissible whereas 55°F to 95°F is a requirement for TH-3 long haul. No requirements are placed on humidity in either case because of the dry air in the microwave networks and filters.

IV. ALARMS AND MAINTENANCE ORDER CIRCUITS

The office alarm system for TH-3 stations is basically the same as that provided for TD-3. The individual audible and visual alarm equipment is decentralized with individual alarm relay circuits and lamps located in the equipment where the alarms originate. The alarm

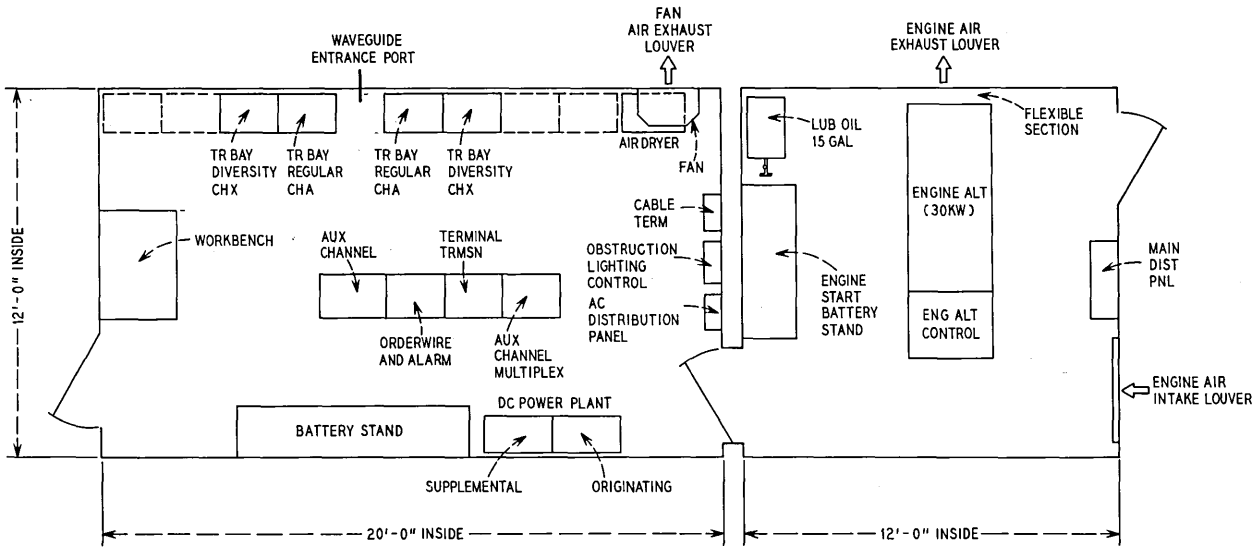

Fig. 2—Standard floor plan layout for a TH-3 repeater station in a small building.

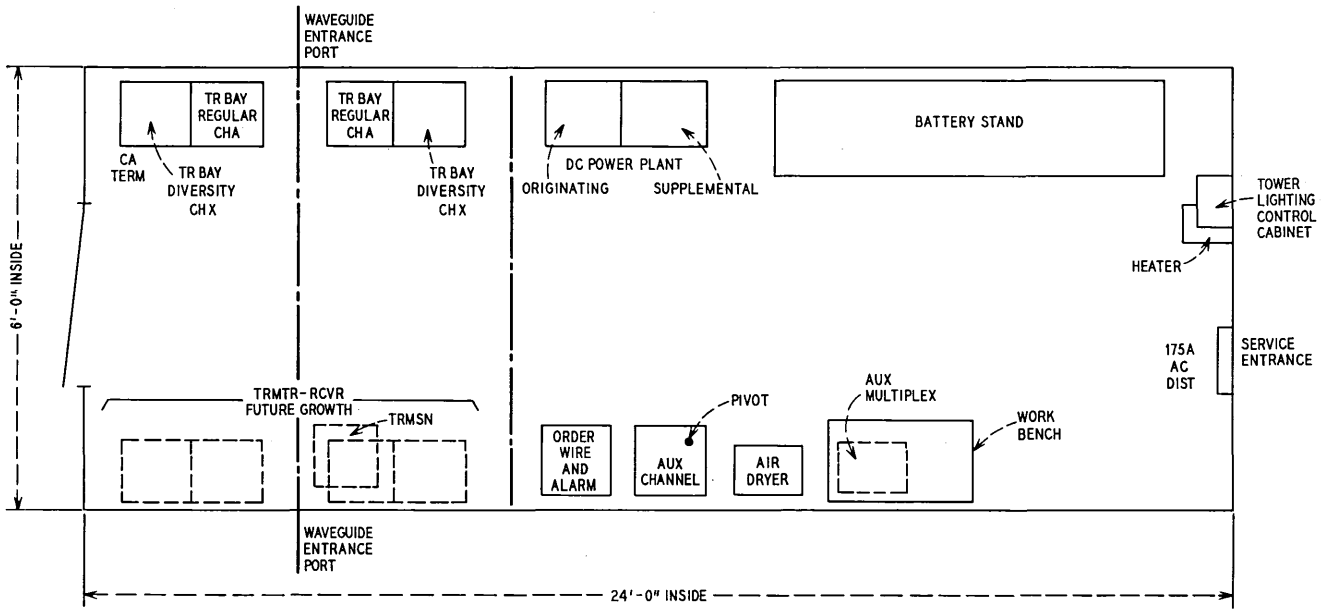

Fig. 3—Floor plan layout for a TH-3 repeater station in a standard shelter.

TABLE I—EQUIPMENT IN TH-3 MEDIUM-HAUL RADIO STATIONS (1 × 1 SYSTEM)

Equipment	Station	
	Terminal	Repeater
1. Transmitter-receivers	Two per station	Four per station
2. Frequency-diplexed auxiliary channel (optional)	One per station	One per station
3. 48-circuit backhaul multiplex applied to auxiliary channel	As required	As required
4. E-type status and control system	One central bay at an alarm center or one remote unit if the terminal is not an alarm center	One remote unit per station
5. General pupose order wire	One per station	One per station
6. 300A protection switch* (1 × 1)	One per station	None required
7. 4A FM terminals	Two transmitters and two receivers per station	Two receivers required in each auxiliary channel
8. 3A wire line entrance link	Two gain and equalization panels and a maximum of four auxiliary gain and equalization panels as required	
9. Test equipment and spare parts	One set of portable test equipment and spare parts to be stored at one terminal or as required	
10. Dehydrator for dry air supply to antenna system and to the transmitter-receiver bays	One per station	One per station
11. Tower obstruction light control panel	One per station if required	One per station if required
12. AC power distribution panel	One per station	One per station
13. Emergency engine alternator	One recommended per station	One recommended per station
14. −24-volt power plant	Two 100-ampere rectifiers (one redundant for reliability) per station	Two 100-ampere rectifiers (one redundant for reliability) per station
15. −24-volt battery	One string per station	One string per station
16. +24-volt power plant	3.5-ampere, −24 V to +24 V converters provided where required	3.5-ampere, −24 V to +24 V converters provided where required
17. Heating and air conditioning equipment	As required for personnel comfort or battery reserve capacity and life	As required for personnel comfort or battery reserve capacity and life
18. Antennas and associated waveguide	Single antenna required for transmitting and receiving	Single antenna in each direction required for transmitting and receiving

* Normally located at the multiplex end of the wire line entrance link. The 300A protection switch may or may not be located in the radio station.

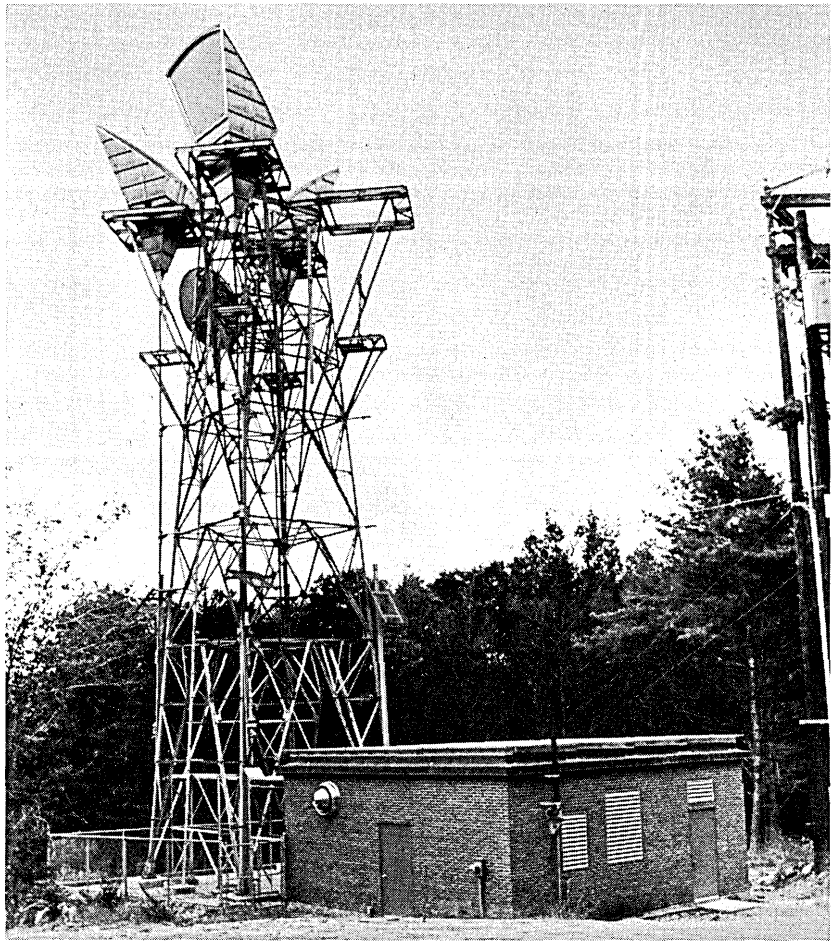

Fig. 4—Dunbarton, New Hampshire, combined TH-3 and TJ radio repeater station.

system directs maintenance personnel by means of main and cross-aisle lights to the failed equipment. Relays and indicating lamps for miscellaneous common office equipment including the waveguide pressure, dehydrator, open door, and tower navigation lighting are located together in a common unit.

The new E2 status reporting and control system is a digital alarm system used to transmit alarm and status information from unattended stations to the attended control station and to transmit orders from

the control station. The E2 system has a maximum capacity of 4096 alarms and indications and 4096 orders per unattended station. It also offers greater speed of operation, space reduction, and flexibility than previous alarm reporting and control systems.

The increased capacity and flexibility of the E2 system has made it economical to prepare a standard arrangement of the indications and alarms, reducing the effort required to engineer a particular office. In addition, the maintenance operator at the control station requires fewer records to interpret the signals he receives from the unattended stations because his display is identical for a particular piece of equipment for all offices.

The E2 system, in conjunction with certain additional equipment, also has the capability to gather analog readings from unattended stations and the potential to provide automatic surveillance under control of a computer at the control stations. With these two features, the frequency of routine visits to the unattended offices could be reduced resulting in reduced maintenance expenditures for these offices.

The new general purpose order wire is used for voice communications between the TH-3 offices. Both local and express order wires may be furnished. The equipment is solid state and provides direct station-to-station *Touch-Tone*® dialing and selective signaling. In a repeater station all of the equipment, including the handset, dial, and electronics, is housed in a 6-inch-high unit in a 23-inch bay.

REFERENCES

1. Skrabal, R. J., and Word, J. A., "Equipment and Building Considerations," B.S.T.J., TD-3 Issue, *47,* No. 7 (September 1968), pp. 1511–1530.
2. Gammie, J., and Hathaway, S. D., "The TJ Radio System," B.S.T.J., *39,* No. 4 (July 1960), pp. 821–877.

THE BELL SYSTEM TECHNICAL JOURNAL
Vol. 50, No. 7, September, 1971
Printed in U.S.A.

On the Intersymbol Interference Problem for the Gaussian Channel

By A. D. WYNER

(Manuscript received March 31, 1971)

In this paper we are concerned with the Holsinger–Gallager model for the continuous-time Gaussian channel. Gallager[1] proved a coding theorem for this channel, and Cordaro and Wagner[2] showed that the theorem remains valid when the effect of intersymbol interference from previous channel uses is taken into account. We show here that the Cordaro–Wagner result holds under somewhat weaker hypotheses. Further, the proof here is more elementary, since it does not depend on reproducing kernel Hilbert space theory. Finally we pose what we feel is an important open problem concerning the stability of the model.

I. INTRODUCTION

In this paper we are concerned with the Holsinger-Gallager model of the continuous-time Gaussian channel. Gallager[1] proved a coding theorem for this channel, and Corado and Wagner[2] showed that this theorem remains valid when the effect of intersymbol interference from previous channel uses is taken into account. We show here that the Cordaro-Wagner result holds under somewhat weaker hypotheses. Further, our proof is more elementary, since it does not depend on reproducing kernel Hilbert space theory. Finally, we pose what we feel is an important open problem concerning the stability of the model.

In the Holsinger-Gallager[1] model, the channel output is

$$y(t) = \int_{-\infty}^{t} h_1(t - \tau)x(\tau)\, d\tau + z(t), \qquad -\infty < t < \infty, \tag{1}$$

where $x(t)$ is the channel input, $h_1(t)$ is the impulse response of a causal linear filter, and $z(t)$ is a sample from a stationary Gaussian process with two-sided spectral density $N(f)$. A *code* (M, T, S, λ) for this channel is a set of M functions $\{x_i(t)\}_{i=1}^{M}$ with support on the interval $[0, T]$ which satisfy

$$|| x_i ||^2 = \int_0^T x_i^2(t)\, dt \leqq ST \tag{2}$$

(thus S is the allowable average signal "power"), together with a set of M disjoint Borel sets $\{B_i\}_1^M$ of functions defined on $[0, T]$, such that the error probabilities

$$P_{ei} \triangleq \Pr\{y_i \notin B_i\} \leqq \lambda, \qquad 1 \leqq i \leqq M. \tag{3}$$

The random function $y_i(t) (0 \leqq t \leqq T)$ is given by (1) with $x(t) = x_i(t)$.

Gallager made the following assumptions

$$\int_{-\infty}^{\infty} N(f)\, df < \infty,$$

$$\int_{-\infty}^{\infty} |\, H_1(f)\, |^2\, df < \infty, \qquad \int_{-\infty}^{\infty} \frac{|\, H_1(f)\, |^2}{N(f)}\, df < \infty, \tag{4}$$

where $H_1(f) = \int_0^\infty h_1(t) e^{-i2\pi ft}\, dt$ is the Fourier transform of $h_1(t)$. Subject to these conditions, Gallager shows that the capacity of the channel with allowable average signal power S is

$$C = C_S = \int_{-\infty}^{\infty} \max\left\{\log \frac{B_S\, |\, H_1(f)\, |^2}{N(f)}\, , 0\right\} df, \tag{5a}$$

where the number B_S is defined (uniquely) by

$$S = \int_{-\infty}^{\infty} \max\left\{B_S - \frac{N(f)}{|\, H_1(f)\, |^2}\, , 0\right\} df. \tag{5b}$$

Equations (5) are justified by the following:

Theorem 1 (Gallager): Let $E(R, S)$ be the error-exponent given by Gallager (Ref. 1, Section 8.5). $E(R, S) > 0$ and continuous, for $S > 0$, and $0 \leqq R < C_S$. Then for arbitrary $\epsilon > 0$, $S > 0$, $0 \leqq R < C_S$, there exist codes (M, T, S, λ) where (as $T \to \infty$)

$$M \geqq e^{RT} \quad \text{and} \quad \lambda \leqq \exp\{-(E(R, S) - \epsilon)T + o(T)\}.$$

Now suppose that we wish to use the channel in successive T-second intervals. If $\{x_i(t)\}_{i=1}^M$ are a set of M code functions with support on $[0, T]$, then the channel output for $0 \leqq t \leqq T$ will be given by

$$y_i^*(t) = \int_0^t h_1(t - \tau) x_i(\tau)\, d\tau + z(t)$$

$$+ \sum_{n=-\infty}^{-1} \int_{nT}^{(n+1)T} h_1(t - \tau) x_{i_n}(\tau - nT)\, d\tau, \tag{6}$$

where $1 \leqq i, i_n \leqq M$ $(n = -1, -2, \cdots)$. The term

$$\hat{r}(t) = \sum_{n=-\infty}^{-1} \int_{nT}^{(n+1)T} h_1(t - \tau) x_{i_n}(\tau - nT)\, d\tau$$

represents intersymbol interference in the interval $[0, T]$ due to signals corresponding to previous intervals. We use $y_i^*(t)$ instead of $y_i(t)$ to indicate the presence of intersymbol interference. With the channel output given by (6) we can redefine a code (M, T, S, λ) as a set of M pairs $\{(x_i(t), B_i)\}_{i=1}^{M}$ exactly as above. Here, however, we require [instead of (3)] that

$$\Pr\{y_i^*(t) \notin B_i\} \leqq \lambda, \qquad 1 \leqq i \leqq M, \tag{7}$$

for *all possible* $\hat{r}(t)$. The random function $y_i^*(t)$ is given by (6).

Cordaro and Wagner[2] succeeded in establishing the validity of Gallager's Theorem for this modified model by making the following additional assumptions. The first is that

$$\int_{-\infty}^{\infty} [|\log N(f)|/(1 + f^2)]\, df < \infty, \tag{8}$$

so that $N(f) = |G_1(f)|^2$ for some $G_1(f)$ with inverse Fourier transform $g_1(t) = 0$, $t < 0$. The second assumption is that $k_1(t)$, the inverse Fourier transform of $H_1(f)/G_1(f)$, is bounded by

$$|k_1(t)| \leqq Ae^{-ct}, \tag{9}$$

for some $A, c > 0$.

In Section II we show that the Cordaro-Wagner result holds with condition (9) replaced by the following essentially weaker condition: By (8) we can find a $G(f)$ such that $N(f) = |G(f)|^2$ and the linear filters corresponding to $G(f)$ and its inverse are causal.[3] Let $k(t)$ be the inverse Fourier transform of $H_1(f)/G(f)$. Then the new condition is that for t sufficiently large

$$|k(t)| \leqq \frac{A}{t^{1+\beta}}, \tag{9'}$$

for some $A, \beta > 0$. Note that by (4)

$$\int_{-\infty}^{\infty} [|H_1(f)|^2/N(f)]\, df = \int_0^{\infty} k^2(t)\, dt < \infty,$$

so that (9') is not a very strong additional assumption.

An Open Problem: In order to achieve the error probability guaranteed by Theorem 1 or in fact simply a vanishing error probability (as $T \to \infty$) for $R < C_S$, Gallager's proof requires the receiver to make arbitrarily precise measurements (see for example Lemma 8.5.1 in Ref. 2). A

practical system, however, imposes certain limitations on the accuracy with which we can make measurements. Therefore a reasonable requirement for the decoding regions $\{B_i\}_1^M$ is the following:

$$y_1 \in B_i\ ,\ y_2 \in B_j \qquad (i \neq j) \Rightarrow \frac{1}{T}\int_0^T [(y_1(t) - y_2(t))]^2\, dt > \nu, \tag{10}$$

for some $\nu > 0$. Thus ν is a measure of the accuracy of the measurements at the decoder. The channel capacity will therefore depend on ν, say $C_S(\nu)$. A quantity of interest might be $\lim_{\nu \to 0} C_S(\nu)$. Whether or not this quantity is the same as C_S in (5) is an open question.

II. PROOF OF THE MAIN RESULT

Let us consider first the problem with no interference from previous channel uses when the input $x(t)$ has support on the interval $[0, T]$. Gallager (Lemma 8.5.1, p. 413) shows that knowledge of the function $y(t)$, $0 \leqq t \leqq T$, is equivalent to knowledge of a certain vector $\mathbf{v} = (v_1\ ,\ v_2\ ,\ \cdots)$. This vector $\mathbf{v}$ can be represented by

$$\mathbf{v} = \mathbf{u} + \mathbf{z}, \tag{11}$$

where $\mathbf{z}$ is a sequence of statistically independent standard Gaussian variates, and the vector $\mathbf{u}$ is defined as follows. Let

$$u(t) = \int_0^T k(t - \tau)x(\tau)\, d\tau, \qquad t \geqq 0, \tag{12}$$

where $k(t)$ is defined in Section I and $x(t)$ is the channel input. Let $\mathcal{S}$ be the subspace of $\mathcal{L}_2(-\infty, \infty)$ spanned by the orthonomal functions $\{\theta_i(t)\}_1^\infty$ defined on p. 416 of Ref. 2. Let $P_{\mathcal{S}}(u)$ be the projection of $u(t)$ on the subspace $\mathcal{S}$. Then $\mathbf{u} = (u_1\ ,\ u_2\ ,\ \cdots)$, where u_k is the coefficient of $\theta_k(t)$ in the expansion of $P_{\mathcal{S}}(u)$ in the basis $\{\theta_i(t)\}_1^\infty$.

We will not need any properties of the $\theta_i(t)$ except for the fact [which follows from the causality of the filters corresponding to $G(f)$ and $H_1(f)/G(f)$] that $\theta_i(t)$ has support on the interval $[0, T]$.

Let $\{x_i(t)\}_1^M$ be a set of code signals with parameters $S = S_1$ and $T = T_1$. Let $\mathbf{u}_i$ be the $\mathbf{u}$ corresponding to $x(t) = x_i(t)$, and let $\mathbf{v}_i = \mathbf{u}_i + \mathbf{z}$. Then if the minimum-distance decoder is used,

$$\begin{aligned} P_{ei} = \Pr\{y_i \notin B_i\} &= \Pr \bigcup_{j \neq i} [|| \mathbf{v}_i - \mathbf{u}_i || \geqq || \mathbf{v}_i - \mathbf{u}_j ||] \\ &= \Pr \bigcup_{j \neq i} [|| \mathbf{z} || \geqq || \mathbf{z} - (\mathbf{u}_j - \mathbf{u}_i) ||] \\ &= \Pr \bigcup_{j \neq i} [\langle \mathbf{z}, \mathbf{u}_j - \mathbf{u}_i \rangle \geqq \tfrac{1}{2} || \mathbf{u}_j - \mathbf{u}_i ||^2], \end{aligned} \tag{13}$$

where "|| ||" denotes Euclidean norm and "⟨ , ⟩" denotes inner product. In particular,

$$P_{ei} = \Pr\{y_i \notin B_i\} \geqq \Pr\{\langle \mathbf{z}, \mathbf{u}_j - \mathbf{u}_i \rangle \geqq \tfrac{1}{2} ||\mathbf{u}_j - \mathbf{u}_i||^2\}$$
$$= \Phi_c(\tfrac{1}{2} ||\mathbf{u}_j - \mathbf{u}_i||), \qquad j \neq i, \tag{14}$$

where $\Phi_c(\xi) = \int_\xi^\infty (2\pi)^{-\frac{1}{2}} e^{-\eta^2/2}\, d\eta$, the complementary error function.

Now, let us suppose that we are given a code (M, T_1, S_1, λ_1), $\{(x_i(t), B_i)\}_1^M$ for the no-interference model. We can assume that the B_i correspond to the minimum-distance decoder. We now form a new code $\{(x_i^*(t), B_i^*)\}_1^M$ with parameters $T = T_2 = (1 + \delta)T_1$ and $S = S_2 = \alpha S_1/(1 + \delta)$ for use on the channel with intersymbol interference (6). We set

$$x_i^*(t) = \begin{cases} \alpha x_i(t), & 0 \leqq t \leqq T_1, \\ 0, & T_1 < t \leqq (1 + \delta)T_1 = T_2, \end{cases} \tag{15}$$

where $\alpha > 1$ and $\delta > 0$ are arbitrary. Note that we have allowed a guard band of width δT_1 between channel inputs. We will specify the decoding sets B_i^* below, mentioning here only that the decoder will observe the received waveform $y^*(t)$ only for $0 \leqq t \leqq T_1$.

We can discretize the channel exactly as above and consider the channel output (when $x_i^*(t)$ is the input) to be given by the vector

$$\mathbf{v}_i^* = \alpha \mathbf{u}_i + \mathbf{z} + \hat{\mathbf{u}}, \tag{16}$$

where $\mathbf{u}_i$ and $\mathbf{z}$ are exactly as in (11) and $\hat{\mathbf{u}}$ (which represents the effect of previous channel uses) is the vector whose coordinates are the coefficients in the expansion of $P_S(\hat{u}(t))$ in the $\{\theta_i(t)\}$, and

$$\hat{u}(t) = \sum_{n=-\infty}^{-1} \int_{nT}^{(n+1)T} k(t - \tau) x_{i_n}^*(\tau - nT)\, d\tau = \sum_{n=-\infty}^{-1} \hat{u}_n(t), \tag{17}$$

where $1 \leqq i_n \leqq M$.

The decoding regions B_i^* will correspond to the minimum-distance decoder, i.e., $y^* \in B_i^*$ if the corresponding $\mathbf{v}$ is closer in Euclidean norm to $\alpha \mathbf{u}_i$ than to all $\alpha \mathbf{u}_j$ $(j \neq i)$. Thus for a given $\hat{\mathbf{u}}$,

$$\Pr\{y_i^* \notin B_i^*\} = \Pr \bigcup_{j \neq i} \{||\mathbf{v}_i^* - \alpha \mathbf{u}_i|| \geqq ||\mathbf{v}_i^* - \alpha \mathbf{u}_j||\}.$$

Now let ϵ, $S_1 > 0$, and $R (0 \leqq R < C_{S1})$ be given, and let the (M, T_1, S_1, λ_1) code $\{(x_i, B_i)\}_1^M$, discussed above, be a set of codes which satisfy Theorem 1; that is,

$$M \geqq e^{RT_1} \quad \text{and} \quad \lambda_1 \leqq \exp\{-(E(R, S_1) - \epsilon)T_1 + o_1(T_1)\}.$$

We will show that for T_1 sufficiently large, the derived code has parameter $\lambda \leqq \lambda_1$. Thus we will have found a set of codes (M, T_2, S_2, λ) for the model with intersymbol interference with

$$S_2 = \frac{\alpha^2 S_1}{(1+\delta)}, \qquad M \geqq \exp\left\{\frac{R}{(1+\delta)} T_2\right\},$$

and

$$\lambda \leqq \exp\left\{-\frac{(E(R, S_1) - \epsilon)}{(1+\delta)} T_2 + \frac{o_1(T_2)}{(1+\delta)}\right\}.$$

Since $E(R, S)$ is continuous and α may be chosen arbitrarily close to 1 and δ arbitrarily close to zero, we will have established Theorem 1 for the intersymbol interference case which is our main result. Thus it remains to establish that the error probability for the derived code $\leqq \lambda_1$. We will do this by showing that (for T_1 sufficiently large) for each $i = 1, 2, \cdots, M$ and all possible $\hat{r}(t)$,

$$\Pr\{y^*(t) \notin B_i^*\} \leqq \Pr\{y(t) \notin B_i\}. \tag{18}$$

Inequality (18) will follow directly from the following lemmas (the proofs of which conclude this section).

Lemma 1: Inequality (18) is satisfied, if

$$||\hat{\mathbf{u}}|| \leqq \frac{(\alpha - 1)}{2} \min_{i \neq j} ||\mathbf{u}_i - \mathbf{u}_j||. \tag{19}$$

Lemma 2: For the codes $\{(x_i, B_i)\}_{i=1}^{M}$, as $T_1 \to \infty$,

$$\min_{i \neq j} ||\mathbf{u}_i - \mathbf{u}_j||^2 \geqq O(T_1).$$

Lemma 3: As $T_1 \to \infty$, $||\hat{\mathbf{u}}||^2 \leqq O(T_1^{1-2\beta})$.

From Lemmas 2 and 3, condition (19) in Lemma 1 will be satisfied for T_1 sufficiently large. Thus so will (18) be satisfied for T_1 sufficiently large.

Proof of Lemma 1: Since B_i and B_i^* are the minimum-distance decoders, the left member of (18) is

$$\Pr\{y_i^* \notin B_i^*\} = \Pr \bigcup_{j \neq i} \{||\mathbf{v}_i^* - \alpha \mathbf{u}_i|| \geqq ||\mathbf{v}_i^* - \alpha \mathbf{u}_j||\}. \tag{20}$$

The right member of (18), $\Pr\{y_i \notin B_i\}$ is given by (13). Consider the event

$$\{||\mathbf{v}_i^* - \alpha \mathbf{u}_i|| \geqq ||\mathbf{v}_i^* - \alpha \mathbf{u}_j||\}$$
$$= \left\{\langle \mathbf{z} + \hat{\mathbf{u}}, \mathbf{u}_j - \mathbf{u}_i \rangle \geqq \frac{\alpha}{2} ||\mathbf{u}_j - \mathbf{u}_i||^2\right\}. \tag{21}$$

But by the hypothesis of Lemma 1 (19),

$$| \langle \hat{\mathbf{u}}, \mathbf{u}_j - \mathbf{u}_i \rangle | \leqq || \hat{\mathbf{u}} || \cdot || \mathbf{u}_j - \mathbf{u}_i || \leqq \frac{(\alpha - 1)}{2} || \mathbf{u}_j - \mathbf{u}_i ||^2.$$

Thus the event in (21)

$$\subseteq \left\{ \langle \mathbf{z}, \mathbf{u}_j - \mathbf{u}_i \rangle \geqq \frac{\alpha}{2} || \mathbf{u}_j - \mathbf{u}_i ||^2 - \frac{(\alpha - 1)}{2} || \mathbf{u}_j - \mathbf{u}_i ||^2 \right\}$$

$$= \{ \langle \mathbf{z}, \mathbf{u}_j - \mathbf{u}_i \rangle \geqq \tfrac{1}{2} || \mathbf{u}_j - \mathbf{u}_i ||^2 \},$$

Lemma 1 now follows from (20), (13) and the above.

Proof of Lemma 2: For the codes $\{(x_i , B_i)\}_1^M$,

$$\Pr \{ y_i \notin B_i \} \leqq \exp \{ - (E(R, S) - \epsilon) T_1 + o(T_1)) \},$$

so that from (14)

$$\Phi_c(\tfrac{1}{2} || \mathbf{u}_j - \mathbf{u}_i ||) \leqq \exp \{ - (E(R, S) - \epsilon) T_1 + o(T_1) \}.$$

Since, as $\xi \to \infty$, $\Phi_c(\xi) = e^{-(\xi^2/2)(1+o(1))}$, we have

$$|| \mathbf{u}_j - \mathbf{u}_i ||^2 \geqq 8(E(R, S) - \epsilon) T_1 + o(T_1),$$

which implies Lemma 2.

Proof of Lemma 3: Let $\hat{\theta}(t) \in \mathcal{S}$ be the function colinear with $P_{\mathcal{S}}(\hat{u}(t))$ with unit length in $\mathcal{L}_2$ norm. That is $\hat{\theta}(t) = P_{\mathcal{S}}(\hat{u}) / || P_{\mathcal{S}}(\hat{u}) ||$, where "$|| \; ||$" applied to functions is the $\mathcal{L}_2$ norm. Then

$$|| \hat{\mathbf{u}} || = || P_{\mathcal{S}} \hat{u} || = \left| \int_{-\infty}^{\infty} \hat{\theta}(t) \hat{u}(t) \, dt \right|$$

But since all functions in $\mathcal{S}$ and therefore $\hat{\theta}(t)$ have support on $[0, T_1]$,

$$|| \hat{\mathbf{u}} || = \left| \int_0^{T_1} \hat{\theta}(t) \hat{u}(t) \, dt \right| \leqq || \hat{\theta} || \left[\int_0^{T_1} \hat{u}^2(t) \, dt \right]^{\frac{1}{2}}$$

$$= \left[\int_0^{T_1} \hat{u}^2(t) \, dt \right]^{\frac{1}{2}} \leqq \sum_{n=-\infty}^{-1} \left[\int_0^{T_1} \hat{u}_n^2(t) \, dt \right]^{\frac{1}{2}}, \tag{22}$$

where $\hat{u}_n(t)$ is defined in (17).

Consider first the $n = -1$ term in the above summation. For $0 \leqq t \leqq T_1$,

$$| \hat{u}_{-1}(t) |^2 = \alpha^2 \left| \int_{-T_2}^{-\delta T_1} k(t - \tau) x_{i-1}(\tau + T_2) \, d\tau \right|^2$$

$$\leqq \alpha^2 \int_{-T_2}^{-\delta T_1} k^2(t - \tau) \, d\tau \int_{-T_2}^{-\delta T_1} x_{i-1}^2(\tau + T_2) \, d\tau$$

$$\leqq \alpha^2 S_1 T_1 \int_{-T_2}^{-\delta T_1} k^2(t - \tau) \, d\tau.$$

Changing the variable of integration to $w = t - \tau$, we have

$$= \alpha^2 S_1 T_1 \int_{t+\delta T_1}^{t+T_2} k^2(w)\, dw.$$

From condition (9′), for sufficiently large T_1,

$$\leqq \alpha^2 S_1 T_1 \int_{t+\delta T_1}^{t+T_2} \frac{A^2}{w^{2(1+\beta)}}\, dw \leqq \alpha^2 S_1 T_1 \int_{\delta T_1}^{\infty} \frac{A^2}{w^{2(1+\beta)}}\, dw$$

$$= \frac{\alpha^2 S_1 T_1 A^2}{1+2\beta} (\delta T_1)^{-1-2\beta} = \frac{\alpha^2 A^2 S_1}{(1+2\beta)(\delta)^{1+2\beta}} T_1^{-2\beta},$$

and therefore

$$\int_0^{T_1} \hat{u}_{-1}^2(t)\, dt \leqq \frac{\alpha^2 A^2 S_1}{(1+2\beta)\delta^{1+2\beta}} T_1^{1-2\beta}. \tag{23}$$

Next consider $-2 \geqq n > -\infty$. For $0 \leqq t \leqq T_1$, paralleling the above steps we obtain

$$|\, \hat{u}_n(t)\, |^2 \leqq \alpha^2 \int_{nT_2}^{(n+1)T_2} k^2(t-\tau)\, d\tau \int_{nT_2}^{(n+1)T_2} x_{i_n}^2(\tau - nT_2)\, d\tau$$

$$\leqq \alpha^2 S_1 T_1 \int_{t+n'T_2}^{t+(n'+1)T_2} k^2(w)\, dw,$$

where $n' = -n$. Again applying condition (9′), we have

$$|\, \hat{u}_n(t)\, |^2 \leqq \alpha^2 S_1 T_1 \int_{n'T_2}^{(n'+1)T_2} \frac{A^2}{w^{2(1+\beta)}}\, dw$$

$$= \frac{\alpha^2 S_1 T_1 A^2}{1+2\beta} \left[\frac{1}{(n'T_2)^{1+2\beta}} - \frac{1}{[(n'+1)T_2]^{1+2\beta}} \right]$$

$$= \frac{\alpha^2 S_1 T_1 A^2}{(1+2\beta)(1+\delta)^{1+2\beta} T_1^{1+2\beta}} \left[\frac{1}{(n')^{1+2\beta}} - \frac{1}{(n'+1)^{1+2\beta}} \right]$$

$$= \frac{\alpha^2 S_1 A^2}{(1+2\beta)(1+\delta)^{1+2\beta} T_1^{2\beta}} b_{n'}.$$

The important fact here is that as $n' \to \infty$, $b_{n'} = O(n'^{-(2+2\beta)})$. Therefore, the integral

$$\int_0^{T_1} \hat{u}_n^2(t)\, dt \leqq \frac{\alpha^2 S_1 A^2}{(1+2\beta)(1+\delta)^{1+2\beta}} T_1^{1-2\beta} b_{n'}. \tag{24}$$

Substituting (23) and (24) into (22) we have,

$$|| \hat{\mathbf{u}} || \leqq T_1^{\frac{1}{2}-\beta} \alpha A \left(\frac{S_1}{1 + 2\beta} \right)^{\frac{1}{2}} \left[\delta^{-\frac{1}{2}-\beta} + (1 + \delta)^{-\frac{1}{2}-\beta} \sum_{n'=2}^{\infty} b_{n'}^{\frac{1}{2}} \right].$$

Since the summation converges, we have $|| \hat{\mathbf{u}} ||^2 \leqq O(T_1^{1-2\beta})$, which is Lemma 3.

REFERENCES

1. Gallager, R., *Information Theory and Reliable Communication,* New York: John Wiley, 1968, Chapter 8.
2. Cordaro, J. T., and Wagner, T. J., "Intersymbol Interference on a Continuous-Time Gaussian Channel," IEEE Trans. Inform. Theory, *IT-16,* July 1970, pp. 422–429.
3. Zadeh, L., and Desoer, C., *Linear System Theory,* New York: McGraw-Hill, 1963, pp. 423–428.

THE BELL SYSTEM TECHNICAL JOURNAL
Vol. 50, No. 7, September, 1971
Printed in U.S.A.

Time-Varying Spectra and Linear Transformation

By S. C. LIU

(Manuscript received February 9, 1971)

One of the most important prerequisites for defining the spectrum of a nonstationary process is that the spectrum should transform simply and reasonably when the process is transformed linearly, and should lead to information about the important response statistics. Presented in this paper are some useful transform relationships for linear causal systems in terms of C. H. Page's time-varying spectra. Expressions suitable for direct analysis or numerical computation of the time-history of the response process and its bounds, the response power spectrum, the total energy of the system, and the upper bounds on the response shock spectra are given.

I. INTRODUCTION

R. M. Loynes[1] recently established a list of desirable properties for the spectrum of nonstationary processes. The elementary properties include: (*i*) a nonstationary spectrum should be rigorously defined, (*ii*) it should describe in some sense the energy distribution over frequency and time, and (*iii*) it reduces to the ordinary spectrum when the process is stationary (Loynes' properties A1, A2, and A5). Both Page's instantaneous power spectrum[2] and M. B. Priestley's evolutionary spectrum[3] satisfy these basic requirements. Another spectrum definition based on the notions of two-dimensional spectra arising in the consideration of harmonizable processes[4,5] also satisfy these basic requirements with some qualifications. However, from the practical point of view, especially when the filtering and convolution of a random process is involved the most important requirement is the existence of simple transform relationships for linear systems. A spectrum should transform simply and reasonably when the process is transformed linearly (property A3, Loynes). In other words, input-output relationships are required so that a knowledge of the spectrum of a process determines the spectrum of the transformed process. In addition, these

relationships must be suitable for numerical computations. This is because most vibration data are available in the discrete form and the analytical solution of most nonstationary problems is difficult to obtain. Presented in this paper are some useful transform relationships for nonstationary processes using Page's time-varying spectra.

II. BACKGROUND

Consider a real function $x(t)$ in $(-\infty, \infty)$, which may be either a sample function of a random process, or a shock function which is zero outside the range $t \in [a, b]$ for finite a and b and is Riemann integrable in this same range. The function $x(t)$ is assumed to have finite energy. The running spectrum of $x(t)$ is defined as[2]

$$X(t, \omega) = \int_{-\infty}^{t} x(\tau) \exp(-i\omega\tau)\, d\tau, \tag{1}$$

where "i" is the imaginary unit. The instantaneous power spectrum is defined as

$$\begin{aligned} \rho_x(t, \omega) &= \frac{\partial}{\partial t} \mid X(t, \omega) \mid^2 \\ &= 2x(t)\ \mathrm{Re}\,[\exp(i\omega t) X(t, \omega)] \end{aligned} \tag{2}$$

which is even in ω. If $x(t)$ is a random process having a time-dependent autocorrelation function $R_x(t, \tau) = E[x(t)x(t - \tau)]$ where E denotes expectation, the instantaneous power spectrum of the process is understood to be the average of the spectra of all its sample functions. Let $S_x(t, \omega) = E[\rho_x(t, \omega)]$ and take the expectation of both sides of (2), we obtain

$$S_x(t, \omega) = 2 \int_0^{\infty} R_x(t, \tau) \cos \omega\tau\, d\tau. \tag{3}$$

The above relation shows that $S_x(t, \omega)$ is completely defined by $R_x(t, \tau)$. When $x(t)$ is stationary, (3) reduces to the ordinary relation as $R_x(t, \tau) = R_x(\tau)$ and $S_x(t, \omega) = S(\omega)$, both independent of t.

Some important properties of $X(t, \omega)$ and $\rho(t, \omega)$ as evident from their definitions are in order.

(*i*) $X(t, \omega)$ is Hermitian, i.e., $X(t, -\omega) = X^*(t, \omega)$. The symbol * denotes the complex conjugate.

(*ii*) Let $E(t)$ be the energy of $x(t)$ up to time t. The function $\rho_x(t, \omega)$ can be regarded as the energy density in the (t, ω) plane as seen by

$$E(t) = \int_{-\infty}^{t} |\, x(\tau)\,|^2\, d\tau = \frac{1}{2\pi}\int_{-\infty}^{\infty} |\, X(t, \omega)\,|^2\, d\omega$$

$$= \frac{1}{2\pi}\int_{-\infty}^{t}\int_{-\infty}^{\infty} \rho_x(\tau, \omega)\, d\omega\, d\tau. \tag{4}$$

(*iii*) Both $X(t, \omega)$ and $\rho_x(t, \omega)$ depend on the past history of $x(t)$, but not on the future.

(*iv*) The function $\rho_x(t, \omega)$ may take negative values (see Ref. 2, p. 106) but the integral $\int_{-\infty}^{t} \rho_x(\tau, \omega)\, d\tau$, the energy spectral density of frequency ω, is always positive.

(*v*) The time derivative of $X(t, \omega)$ relates to the signal $x(t)$ itself by

$$x(t) = \exp(i\omega t)\, \partial X(t, \omega)/\partial t$$

$$= \exp(-i\omega t)\, \partial X^*(t, \omega)/\partial t. \tag{5}$$

We will now proceed to derive from some input-output relations for a simple causal linear system in terms of $X(t, \omega)$ and $\rho_x(t, \omega)$.

III. INPUT-OUTPUT RELATIONS

Consider a simple, second-order causal linear system whose equation of motion is given by

$$\ddot{y} + 2\lambda\omega_o\dot{y} + \omega_o^2 y = x(t) \tag{6}$$

with homogeneous initial conditions $y(0) = \dot{y}(0) = 0$, where $\lambda < 1.0$ and ω_o are positive constants representing respectively the damping and natural frequency of the system. This system has a transfer function between the output y and input x given by $H(\omega) = (\omega_0^2 - \omega^2 + 2i\lambda\omega\omega_o)^{-1}$ and a corresponding impulse response $h(t) = [\exp(-\lambda\omega_o t) \sin pt]/p$ for $t > 0$, where $p = (1 - \lambda^2)^{\frac{1}{2}}\omega_o$. We obtain the following results for different response parameters.

3.1 *Time-Varying Spectra of Response Process*

Using the convolution integral and the casual property of the system, i.e., $h(t) = 0$ for $t < 0$, and assuming the excitation begins at $t = 0$, the response $y(t)$ in (6) is given in terms of $X(t, \omega)$ by

$$y(t) = \int_0^t x(\tau)h(t - \tau)\, d\tau$$

$$= \frac{1}{2\pi}\int_{-\infty}^{\infty} H(\omega)X(t, \omega) \exp(i\omega t)\, d\omega. \tag{7}$$

Following the definition of (1), the running spectrum of $y(t)$ is

$$Y(t, \omega) = X(t, \omega)H(\omega) - e_Y(t, \omega), \tag{8}$$

where

$$e_Y(t, \omega) = \int_0^t x(\tau_1) \exp(-i\omega\tau_1) \int_{t-\tau_1}^{\infty} h(\tau_2) \exp(-i\omega\tau_2)\, d\tau_2\, d\tau_1 \tag{9}$$

is the error involved in the approximation $Y(t, \omega) \simeq X(t, \omega)H(\omega)$. Notice from (8) and (9) that $Y(t, \omega)$ is given by the double integral in the $\tau_1 - \tau_2$ plane of a function $f(\tau_1, \tau_2) = x(\tau_1)h(\tau_2) \exp(-i\omega\tau_1 - i\omega\tau_2)$ over an area of an equal-sided triangle formed by the line $\tau_1 + \tau_2 = t$ in the first quadrant. The value of $X(t, \omega)H(\omega)$ is given by the same integral over an extended area from 0 to t along the τ_1 axis and from 0 to ∞ along the τ_2 axis. The error e_Y is given by the difference of these two integrals.

Let $F\{x_t\}$ be the Fourier transform of x_t, the part of $x(t)$ from t on, and $F\{y_t\}$ be the Fourier transform of y_t, the part of $y(t)$ from t on. It can be shown that the error $e_Y(t, \omega)$ in (9) is also given by

$$e_Y(t, \omega) = H(\omega)F\{x_t\} - F\{y_t\}. \tag{10}$$

It follows from (8) that the instantaneous power spectrum of $y(t)$ is

$$\begin{aligned}\rho_y(t, \omega) &= \left(\frac{\partial X}{\partial t} H - \frac{\partial e_Y}{\partial t}\right)(X^*H^* - e_Y^*) + (XH - e_Y)\left(\frac{\partial X^*}{\partial t} H^* - \frac{\partial e_Y^*}{\partial t}\right) \\ &= \rho_x(t, \omega) \mid H(\omega) \mid^2 + e_\rho(t, \omega),\end{aligned} \tag{11}$$

where

$$e_\rho(t, \omega) = \frac{\partial}{\partial t} \mid e_Y \mid^2 - He_Y^* \frac{\partial X}{\partial t} - H^*e_Y \frac{\partial X^*}{\partial t} \tag{12}$$

is the error involved in the approximation $\rho_y(t, \omega) \cong \rho_x(t, \omega) \mid H(\omega) \mid^2$.

Some interesting remarks can now be made about e_Y, and subsequently about e_ρ which is closely related to e_Y through (12). The energy bound in ω for $e_Y(t, \omega)$ can be considered as follows. Let the norm of an arbitrary function $Q(\omega)$ be defined as $\| Q \|_\omega = [\int_{-\infty}^{\infty} \mid Q(\omega) \mid^2 d\omega]^{\frac{1}{2}}$, then from Parseval's Theorem $\| F\{x_t\} \|_\omega = \| x_t \|_\tau = [\int_t^\infty \mid x(\tau) \mid^2 d\tau]^{\frac{1}{2}}$, and similarly $\| F\{y_t\} \|_\omega = \| y_t \|_\tau = [\int_t^\infty \mid y(\tau) \mid^2 d\tau]^{\frac{1}{2}}$. Suppose $h(t)$ is integrable so that $\mid H(\omega) \mid \leqq A$ is bounded, then it follows from (10) that

$$\| e_Y(t, \omega) \|_\omega \leqq A\left[\int_t^\infty \mid x(\tau) \mid^2 d\tau\right]^{\frac{1}{2}} + \left[\int_t^\infty \mid y(\tau) \mid^2 d\tau\right]^{\frac{1}{2}}$$

which $\to 0$ as $t \to \infty$. If furthermore $x(t)$ is integrable, from which $\mid F\{x_t\} \mid \leqq \int_t^\infty \mid x(\tau) \mid d\tau$ which $\to 0$ with t and consequently $\mid F\{y_t\} \mid$

also $\rightarrow 0$ with t, then (10) indicates $| e_Y(t, \omega) | \rightarrow 0$ in t, uniformly in ω. This result can also be concluded from (9) because in which the function $f(\tau_1, \tau_2) = x(\tau_1)h(\tau_2) \exp(-i\omega\tau_1 - i\omega\tau_2)$ is integrable in two dimensions.

For a more practical purpose, we now consider the familiar first- and second-order simple linear systems. The running spectrum of the response $y(t)$ and other pertinent quantities are given in Table I, in which $\alpha^{-1} = \tau_o =$ decay time of the impulse response $h(t)$ of the first-order system and $\tau_o = (\lambda\omega_o)^{-1}$ decay time of $h(t)$ of the second-order system. From this table, it can be seen that for large t/τ_o ratio the error $e_Y(t, \omega)$ for both systems [given by the second term in the expression for $Y(t, \omega)$] will be small. In general at the same time t, the error for a system having short decay time (broad bandwidth) is smaller than that having long decay time (narrow bandwidth). Therefore $e_Y(t, \omega)$ for systems with a flat spectrum (high damping) is smaller compared with that for high resonant systems (low damping). This observation is also evident from the damping term appearing in the expression of $Y(t, \omega)$ for the second-order system in Table I.

In many cases the impulse responses and the input are both bounded functions defined on positive t axis such that $|h(t)| \leqq A_1 \exp(-a_1 t)$ and $|x(t)| \leqq A_2 \exp(-a_2 t)$ for some positive A_1, A_2, and $a_1 > a_2$. Then from (9) $|e_Y(t, \omega)| \leqq A_1 A_2 [\exp(-a_2 t) - \exp(-a_1 t)]/a_1(a_1 - a_2)$. Therefore the error $|e_Y(t, \omega)|$ approaches zero as the time t increases; and for a certain time $t > t_o$ the error can be regarded as negligibly small.

From (8) another useful pair of equations relating to the time derivatives of the input and output running spectra can be obtained:

$$\left.\begin{aligned} \frac{\partial Y(t, \omega)}{\partial t} &= \frac{\partial X(t, \omega)}{\partial t} H(\omega) - \frac{\partial e_Y(t, \omega)}{\partial t} \\ \frac{\partial Y^*(t, \omega)}{\partial t} &= \frac{\partial X^*(t, \omega)}{\partial t} H^*(\omega) - \frac{\partial e_Y^*(t, \omega)}{\partial t} \end{aligned}\right\} \tag{13}$$

which in turn will lead to the following relationship between the input and output time histories.

3.2 *Response Time-History and Some Bounds*

Using (13) and the analogous relation for $y(t)$ as $x(t)$ in (5), we obtain

$$\begin{aligned} y(t) &= x(t)H(\omega) - \frac{\partial e_Y}{\partial t} e^{i\omega t} \\ &= x(t)H^*(\omega) - \frac{\partial e_Y^*}{\partial t} e^{-i\omega t} \end{aligned} \tag{14}$$

TABLE I—RESPONSE RUNNING SPECTRUM AND RUNNING FREQUENCY RESPONSE SPECTRUM

	First-order system	Second-order system†
$h(t),\ t > 0$	$a \exp(-at)$	$\frac{1}{p} \exp(-\lambda\omega_o t) \sin pt$
$H(\omega)$	$\frac{a}{a + i\omega}$	$\frac{1}{\omega_o^2 - \omega^2 + 2i\lambda\omega_o\omega}$
$H(t, \omega)$	$H(\omega)[1 - e^{-(a+i\omega)t}]$	$H(\omega)[1 - g(t)e^{-(\lambda\omega_o+i\omega)t}]$
$Y(t, \omega)$	$H(\omega)\left[X(t, \omega) - e^{-(a+i\omega)t} \int_0^t x(\tau)e^{-(a+2\omega)\tau}\, d\tau\right]$	$H(\omega)\left[X(t, \omega) - e^{-(\lambda\omega_o+i\omega)t} \int_0^t x(\tau)g(t-\tau)e^{-\lambda\omega_o\tau}\, d\tau\right]$

† $g(t) = \cos pt + \frac{\lambda\omega_0 + i\omega}{p} \sin pt.$

which relates the input and output time histories in terms of the transfer function of the system and the error function in (9). The time-history of the response function $y(t)$ can also be related to the time-history of the input function $x(t)$ through the simple expression

$$x(t)y(t) = \frac{1}{\pi}\int_0^\infty \mathrm{Re}\,[H(\omega)]\rho_x(t,\omega)\,d\omega. \tag{15}$$

Notice that the above relation is advantageous when the direct multiplication of input and output functions is involved. We prove (15) in the following. Consider the integral

$$\int_0^t x(\tau)y(\tau)\,d\tau = \frac{1}{2\pi}\int_{-\infty}^\infty H(\omega)\int_0^t x(\tau)X(\tau,\omega)\exp(i\omega\tau)\,d\tau\,d\omega.$$

It follows from the causal property of the system and Parseval's theorem that

$$\int_0^t x(\tau)y(\tau)\,d\tau = \frac{1}{2\pi}\int_{-\infty}^\infty H(\omega)\mid X(t,\omega)\mid^2 d\omega.$$

Differentiating both sides with respect to t, (15) immediately follows.

We now establish the upper bound for $|y(t)|$ and $|y(t)|^2$ in terms of transfer characteristics of the system and input spectrum. From (7), Schwarz's inequality yields

$$\mid y(t)\mid^2 \leqq E(t)N, \tag{16}$$

$$\mid y(t)\mid \leqq E(t)^{\frac{1}{2}}N^{\frac{1}{2}}, \tag{17}$$

where $E(t)$ is the total energy of the input function $x(t)$ up to the time t and is given by (4), and $N = \int_{-\infty}^{\infty}\mid h(\tau)\mid^2 d\tau > 0$. Equations (16) and (17) are also valid if $x(t)$ is a random process. In this case the left-hand side quantities $\mid y(t)\mid^2$ and $\mid y(t)\mid$ are replaced by $E[\mid y(t)\mid^2]$ and $E[\mid y(t)\mid]$ respectively. For our simple system, $N = (4\lambda\omega_o^3)^{-1}$, and

$$E[\mid y(t)\mid^2] \leqq \frac{1}{8\pi\lambda\omega_o^3}\int_{-\infty}^t\int_{-\infty}^\infty S_x(t,\omega)\,d\omega\,d\tau. \tag{18}$$

3.3 *Total Energy of the System*

The total energy $E_s(t)$ of the system described by (6) at time t is given by

$$E_s(t) = \tfrac{1}{2}\mid Z(t,p)\mid^2 \exp(2\lambda\omega_o t), \tag{19}$$

where $Z(t,p)$ is the running spectrum of $z(t) = x(t)\exp(\lambda\omega_o t)$ at the frequency p. The relation (19) can be proved as follows. Taking, according to (1), the running Fourier transform of both sides of (6) and integrating by parts, we have

$$[\dot{y} + (i\omega + 2\lambda\omega_o)y] \exp(-i\omega t) + [\omega_o^2 + 2i\lambda\omega\omega_o - \omega^2]Y(t, \omega) = X(t, \omega)$$

in which the initial conditions have been used. The second term on the left-hand side of the above equation vanishes when setting $\omega = \theta_1 = i\lambda\omega_o + p$ or $\omega = \theta_2 = i\lambda\omega_o - p$. Thus

$$[\dot{y} + (i\theta_1 + 2\lambda\omega_o)y] \exp(-i\theta_1 t) = X(t, \theta_1) = Z(t, p), \tag{20}$$

$$[\dot{y} + (i\theta_2 + 2\lambda\omega_o)y] \exp(-i\theta_2 t) = X(t, \theta_2) = Z^*(t, p). \tag{21}$$

Multiplying (20) and (21) and dividing the result by 2, we have

$$\tfrac{1}{2}[\dot{y}^2 + 2\lambda\omega_o y\dot{y} + \omega_o^2 y^2] = \tfrac{1}{2} \mid Z(t, p) \mid^2 \exp(2\lambda\omega_o t).$$

But the left-hand side is the total energy of the system and therefore (19) is proved.

Taking expectation of both sides of (19), we obtain the expected energy of the system subjected to the random excitation $x(t)$

$$E[E_s(t)] = \frac{1}{2} \int_{-\infty}^{t} \int_{-\infty}^{t} R_x(\tau_1, \tau_1 - \tau_2) \cdot \exp[\lambda\omega_o(\tau_1 + \tau_2) - ip(\tau_1 - \tau_2)]\, d\tau_1\, d\tau_2 . \tag{22}$$

For the undamped system, i.e., at the limit when $\lambda \to 0$, (19) reduces to $\tfrac{1}{2}(\dot{y}^2 + y^2) = \tfrac{1}{2} \mid X(t, \omega_o) \mid^2$ which agrees with the principle of energy conservation. It is also interesting to note that a simple manipulation of (20) and (21) can lead to the familiar convolution relation between input and output

$$y(t) = \frac{1}{p} \int_{-\infty}^{t} x(\tau) \exp[-\lambda\omega_o(t - \tau)] \sin p(t - \tau)\, d\tau$$

as given by (7).

3.4 *Bounds on the Shock Spectrum*

The shock spectrum of $x(t)$, $t \in [a, b]$ is the maximum absolute response defined as $S_d(\omega_o, \lambda) = \sup_t \mid y \mid$ = the displacement spectrum or $S_v(\omega_0, \lambda) = \sup_t \mid \dot{y} \mid$ = the velocity spectrum. We establish the following upper bounds to them:

$$S_d(\omega_o, \lambda) \leqq \sup_t \left[\frac{1}{p} \mid Z(t, p) \mid \exp(-\lambda\omega_o t)\right] \leqq \sup_t \frac{1}{p} \mid Z(t, p) \mid , \tag{23}$$

$$S_v(\omega_o, \lambda) \leqq \sup_t \left[\frac{1}{(1 - \lambda^2)^{\frac{1}{2}}} \mid Z(t, p) \mid \exp(-\lambda\omega_o t)\right] \leqq \sup_t \mid Z(t, p) \mid . \tag{24}$$

The proof of these relations is straightforward. Write $Z(t, \omega) = |Z(t, \omega)| \exp [-i\phi_z(t, \omega)]$ in which the phase angle $\phi_z(t, \omega) = \tan^{-1} [-S_z(t, \omega)/C_z(t, \omega)]$, S_z and C_z are the running sine and cosine transform of $z(t)$ respectively. It follows from (20) or (21) that

$$\dot{y} + \lambda\omega_o y + ipy = | Z(t, p) | \exp \{-\lambda\omega_o t + i[pt - \phi_z(t, p)]\}.$$

The above relation leads to

$$\dot{y} + \lambda\omega_o y = | Z(t, p) | \exp (-\lambda\omega_o t) \cos [pt - \phi_z(t, p)],$$

$$py = | Z(t, p) | \exp (-\lambda\omega_o t) \sin [pt - \phi_z(t, p)],$$

and (23) and (24) follow directly.

For the undamped system ($\lambda \to 0$), $p = \omega_o$, $Z(t, p) = X(t, \omega_o)$; therefore (23) and (24) reduce to

$$\omega_o S_d(\omega_o, 0) \leqq \sup_t | X(t, \omega_0) | \quad \text{and} \quad S_v(\omega_o, 0) \leqq \sup_t | X(t, \omega_o) |,$$

respectively.

IV. ILLUSTRATIONS

We now consider the following nonstationary processes for their time-varying spectra.

4.1 *Multiplicative Process*

$$x(t) = n(t)\phi(t),$$

where $n(t)$ is a stationary process with an autocorrelation function $R_n(\tau)$ and spectral density $S_n(\omega)$, and $\phi(t)$ is a causal deterministic function. The time dependent correlation function and power spectrum are

$$R_x(t, \tau) = R_n(\tau)\phi(t - \tau),$$

$$S_x(t, \omega) = 2\phi(t) \int_0^t R_n(\tau)\phi(t - \tau) \cos \omega\tau \, d\tau.$$

When $n(t)$ is a white noise with $R_n(\tau) = R_o\delta(\tau)$, $R_o > 0$, then $S_x(t, \omega) = S(t) = 2R_o\phi^2(t)$ becomes frequency independent. When $\phi(t)$ is slowly varying such that $\phi(t - \tau/2) \simeq \phi(t + \tau/2)$, then $R_x(t, \tau) = \phi^2(t)R_n(\tau)$ and $S_x(t, \omega) = \phi^2(t)S_n(\omega)$. This implies that $x(t)$ is locally stationary and its power spectrum changes with respect to time not in the general shape but in its area covered with the ω-axis only.

4.2 *Periodic Nonstationary Process*[6,7]

In this class of processes, the time dependent autocorrelation function is given as $R_x(t, \tau) = \Sigma\psi_k(\tau)\ exp\ (2\pi ikt/T)$ for a constant T. It can be readily shown that

$$S_x(t, \omega) = \frac{1}{2\pi} \sum_k \Psi_k(\omega) \exp(2\pi ikt/T),$$

where $\Psi_k(\omega)$ is the Fourier transform of $\Psi_k(\tau)$ and has the property that $\Psi_o(\omega) \geqq 0$ and $\Psi_k(\omega) = \Psi_k(2\pi k/T - \omega)$. Moreover, it is easy to show that the time-varying power spectral density of the response process $y(t)$ is also periodic with the same period T:

$$S_y(t, \omega) = \frac{1}{2\pi} \sum_k q_k(\omega) \exp(2\pi ikt/T)$$

in which $q_k(\omega) = \Psi_k(\omega)H(\omega)H(2\pi k/T - \omega)$.

The application of the rest of the input-output relations of Section III to these two types of nonstationary processes for either direct analysis or numerical computation is a straightforward exercise.

V. ACKNOWLEDGMENT

The author is indebted to H. J. Landau for helpful discussions.

REFERENCES

1. Loynes, R. M., "On the Concept of the Spectrum for Nonstationary Processes," J. Royal Statist. Soc. B, *30*, No. 1 (1968), pp. 1–30.
2. Page, C. H., "Instantaneous Power Spectrum," J. App. Phys., *23*, No. 1 (January 1952), pp. 103–106.
3. Priestley, M. B., "Evolutionary Spectra and Nonstationary Processes," J. Royal Statist. Soc. B, *27*, No. 2 (1965), pp. 204–237.
4. Dubman, M. R., "The Spectral Characterization and Comparison of Nonstationary Processes," U. S. Dept. of Commerce Clearinghouse Document AD619178, August 1965.
5. Hurd, H. L., "Some Remarks on the Spectrum for Nonstationary Processes," unpublished work.
6. Hurd, H. L., "An Investigation of Periodically Correlated Stochastic Processes," Ph.D. Thesis, Duke University, Durham, N. C., 1969.
7. Gudzenko, L. I., "On Periodically Nonstationary Processes," Radio Eng. and Electronics, *4*, No. 6 (1959), pp. 1062–1064.

THE BELL SYSTEM TECHNICAL JOURNAL
Vol. 50, No. 7, September, 1971
Printed in U.S.A.

Multiple-Path Fading on Line-of-Sight Microwave Radio Systems as a Function of Path Length and Frequency

By C. L. RUTHROFF

(Manuscript received March 22, 1971)

Transmission over line-of-sight microwave radio paths is analyzed with the aid of a piece-wise linear approximation of the atmospheric index of refraction. The simple model is adequate; it predicts published experimental results.

A short path is defined on which no deep fading can occur and the maximum length of such a path is estimated from measured data for New Jersey. Expressions are presented for the worst-case amplitude-frequency response and for the maximum echo delay for short paths. It is shown that if the normal Fresnel-zone clearance is maintained on short paths, no fading will occur due to substandard conditions of propagation.

W. T. Barnett's result is also predicted from this model: the distribution of attenuation on long paths is a function of L^3/λ where L is the path length and λ is the free space wavelength.

The distribution of deep fades on long paths is predicted by this model to have the same slope as the Rayleigh distribution, the slope normally found in measurements of attenuation distributions on long paths.

I. INTRODUCTION

Terrestrial and satellite radio systems for common carrier applications at frequencies above 10 GHz have been proposed recently.[1,2] For terrestrial systems the lengths of transmission paths may be limited to a few kilometers by the attenuation caused by rain.[3–5] A similar limitation holds for satellite systems—for that part of the transmission path which is contained in earth's atmosphere.

For both terrestrial and satellite systems, it is anticipated that economies can be achieved if the information can be transmitted as sequences of short pulses. But O. E. DeLange has shown that pulses with durations of a few nanoseconds can suffer serious degradation

during transmission over a 22.8-mile path at a frequency of 4 GHz; in his experiment, the degradation occurred during conditions of frequency-selective fading.[6,7] For the proposed systems, this result raises an important question—for the path lengths of interest, can pulses of a few nanoseconds duration be transmitted without suffering intolerable degradation due to frequency-selective fading? No answer to this question has been found in the literature; one of the purposes of this paper is to answer it.

In pioneering work on the propagation of microwaves, A. B. Crawford, DeLange, W. C. Jakes, and W. M. Sharpless have shown that severe frequency-selective fading on line-of-sight transmission paths can be explained in terms of multiple-path transmission.[6-9] Their results have been confirmed by others and it is generally accepted that the mechanism of multiple-path transmission is responsible for most severe frequency-selective fading.[10-15]

In this paper, fading due to multiple-path transmission and fading due to substandard refraction are discussed with emphasis on short transmission paths. In the model used, signal power from the transmitter travels to the receiver over two or more paths.[13] Multiple-paths are caused by a layer of atmosphere above the transmission path which has a negative gradient in the index of refraction. Generally the energy traveling over the separate paths will undergo unequal phase shifts; if the received signal, which is the vector sum of the signals received from these paths, is reduced substantially below its free-space value by this mechanism, multiple-path fading is said to occur.

Multiple-path fading, then, is a function of the magnitude of the gradient in the index of refraction of the refracting layer. It is reasonable to assume that there is a maximum value of this gradient which occurs in a climatic region. Based on this assumption, it will be shown that a path length L_0 exists such that for any path of length $L \leqq L_0$—called a short path—deep multiple-path fading cannot occur. The length L_0 is estimated for New Jersey from transmission measurements made by Crawford and Jakes.[7] For example, at 30 GHz, $L_0 \approx$ 4.8 km in New Jersey.

Expressions are also derived for the frequency selectivity, maximum echo delay, and the path clearance required to eliminate fading due to substandard refraction.

Fading on long paths is also discussed and it is shown that the path attenuation distribution is a function of L^3/λ where L is the path length, and λ is the wavelength. This agrees with Barnett's result

which is based on extensive measurements. The correct slope of the distributions of deep fades on long paths is also predicted from this model.

II. REFRACTION IN A SINGLE LAYER

Most severe selective fading occurs during clear summer nights when temperature inversions and associated meteorological effects produce negative gradients in the index of refraction of the atmosphere.[7,10,13] Figure 1 illustrates a simple profile of the index of refraction which can produce two or three transmission paths between transmitter and receiver; two transmission paths are shown.[7] As is usual, the index of refraction is assumed to change only in the vertical dimension. From geometric optics, the position of the elevated negative gradient in the index of refraction allows a direct ray between trans-

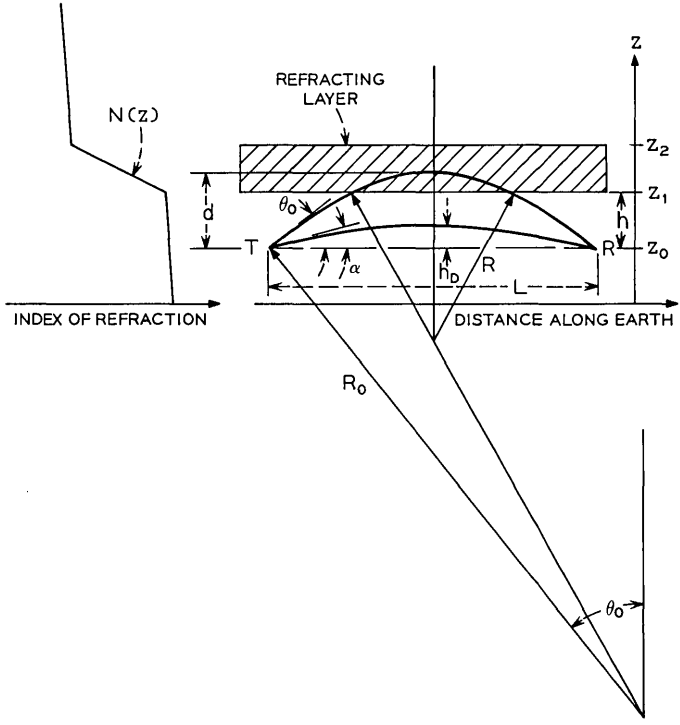

Fig. 1—Refraction from a single layer.

mitter and receiver as shown in Fig. 1, and causes another ray, launched upward at a small angle, θ_0, to be refracted into the receiver.

The magnitudes of the gradients in the index of refraction are small and only those rays which are launched at small angles to the horizontal can be refracted into the receiver. For small angles it has been shown that if the gradient in the index of refraction is constant the refracted ray follows the arc of a circle with radius R, where[13]

$$\frac{1}{R} \approx -\frac{dn(z)}{dz} = -10^{-6}\frac{dN(z)}{dz}. \tag{1}$$

The height above earth is z, $n(z)$ is the index of refraction, and $N(z) \equiv [n(z) - 1]10^6$. The dispersion in the index of refraction is known to be small so we assume $n(z)$ and R are independent of frequency.[13]

The model of Fig. 1 is a simple approximation to the actual variations in the index of refraction which occur on transmission paths. The model is not used because it is simple but because it does all that can be asked of a model—the results predicted from it agree with the results measured in corresponding experiments:

(*i*) Either one, two, or three discrete rays are predicted by the model and all of these combinations of rays have been observed.[7] Four or more discrete rays have not been observed.

(*ii*) Frequency-sweep measurements, which heretofore have been approximated by more than three and as many as eleven distinct signals, are easily approximated by three distinct signals if time variations are assumed in the height, thickness, and index of refraction of the refracting layer.[7,10]

(*iii*) Barnett has determined the dependence of attenuation distributions on path length and wavelength from measurements on many paths at several frequencies; the same result is predicted by this model.

(*iv*) The correct slope of deep-fading distributions on long paths is also predicted from this model.

2.1 *Phase-Shift Along a Ray—General Case*

The geometry for a single refracting layer is shown in Fig. 1. The direct ray has radius R_0 and an angle of departure $\alpha \approx L/2R_0$. A refracted ray leaves the transmitter at angle θ_0 and follows the arc of a circle with radius R_0 until the ray reaches height Z_1. At this point the slope of the index of refraction changes and in the region $Z_1 \leqq z \leqq Z_2$ the ray follows an arc of a circle with radius R. When the ray

passes into the region $Z_0 \leqq z \leqq Z_1$, it again follows an arc of a circle with radius R_0 and arrives at the receiver at the angle θ_0 above the horizontal axis.

The phase shift, ϕ, between the transmitter and receiver is given by

$$\phi = \frac{2\pi}{\lambda} \int n(z)\, ds, \tag{2}$$

where, $n(z)$ is the index of refraction,

λ is the free-space wavelength, and

ds is the element of length along the ray.

The integral in (2) is the optical length of the ray.

It is possible for a refracted ray to rise above the refracting layer and still reach the receiver. To include this case we use the geometry of Fig. 2 to derive the phase shift along a refracted ray. There are three regions to consider.

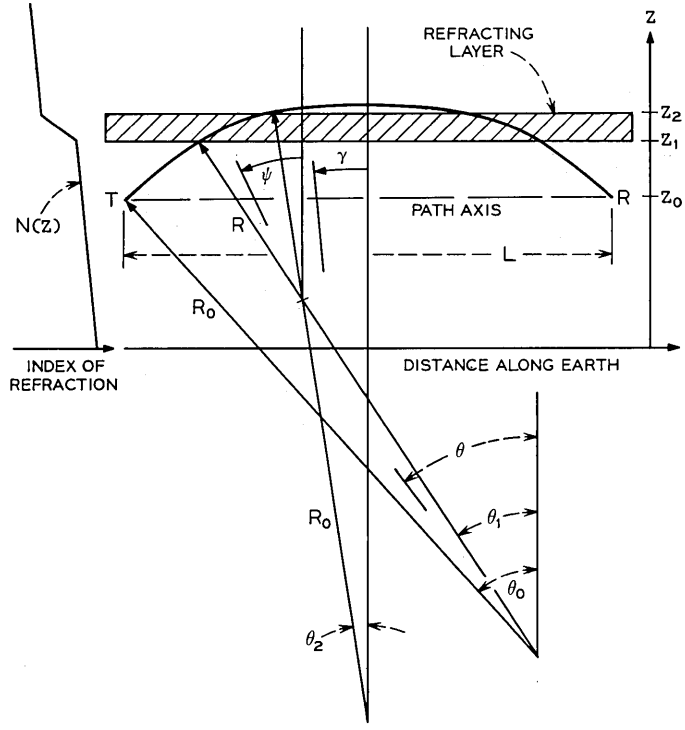

Fig. 2—Single-layer refraction with a ray rising above the refracting layer.

Region I

In the region below Z_1, $n = n_0 - m_0 z$, and a point on the ray is given by $z = Z_0 + R_0(\cos\theta - \cos\theta_0)$, $\theta_1 \leqq \theta \leqq \theta_0$. Substituting for z in n and noting that $dn/dz = -m_0 = -1/R_0$,

$$n = n_0 - m_0 Z_0 - \cos\theta + \cos\theta_0, \qquad \theta_1 \leqq \theta \leqq \theta_0. \tag{3}$$

The element of length along the arc in this region is $ds = R_0 d\theta$.

Region II

In the refracting layer, $n = n_0 - m_0 Z_1 - m(z - Z_1)$, and a point on the ray is given by $z = Z_1 + R(\cos\psi - \cos\theta_1)$, $0 \leqq \psi \leqq \theta_1$. From Fig. 2, $\cos\theta_1 = \cos\theta_0 + (Z_1 - Z_0)/R_0$. Substituting for $\cos\theta_1$ in z, for z in n and noting that $dn/dz = -m = -1/R$,

$$n = n_0 - m_0 Z_0 - \cos\psi + \cos\theta_0, \qquad \theta_2 \leqq \psi \leqq \theta_1. \tag{4}$$

In the refracting layer, $ds = R d\psi$.

Region III

Above the refracting layer, $n = n_0 - m_0 z + m_0(Z_2 - Z_1) - m(Z_2 - Z_1)$ and a point on the ray is given by $z = Z_2 + R_0(\cos\gamma - \cos\theta_2)$, $0 \leqq \gamma \leqq \theta_2$. From Fig. 2, $\cos\theta_2 = \cos\theta_0 + (Z_1 - Z_0)/R_0 + (Z_2 - Z_1)/R$. Substituting for $\cos\theta_2$ in z, for z in n and noting that $dn/dz = -m_0 = -1/R_0$,

$$n = n_0 - m_0 Z_0 - \cos\gamma + \cos\theta_0, \qquad 0 \leqq \gamma \leqq \theta_2. \tag{5}$$

In this region $ds = R_0 d\gamma$.

Since $m_0 Z_0 \ll n_0$, it will be omitted from (3), (4), and (5). By substituting these equations into (2) the optical length of the refracted ray can be written.

$$\begin{aligned}\frac{\lambda\phi}{2\pi} \approx\ & 2\int_{\theta_1}^{\theta_0} (n_0 - \cos\theta + \cos\theta_0) R_0\, d\theta \\ & + 2\int_{\theta_2}^{\theta_1} (n_0 - \cos\psi + \cos\theta_0) R\, d\psi \\ & + 2\int_{0}^{\theta_2} (n_0 - \cos\gamma + \cos\theta_0) R_0\, d\gamma \qquad (6) \\ \approx\ & 2R_0[(n_0 + \cos\theta_0)(\theta_0 - \theta_1) - \sin\theta_0 + \sin\theta_1)] \\ & + 2R[(n_0 + \cos\theta_0)(\theta_1 - \theta_2) - \sin\theta_1 + \sin\theta_2] \\ & + 2R_0[(n_0 + \cos\theta_0)\theta_2 - \sin\theta_2]. \qquad (7)\end{aligned}$$

Only those rays which reach the receiver are of interest. For a ray to be refracted into the receiver the geometry of Fig. 2 requires that the following two relations be satisfied.

$$R_0 \sin \theta_0 - (R_0 - R)(\sin \theta_1 - \sin \theta_2) = L/2, \tag{8}$$

$$0 \leqq \theta_2 \leqq \theta_1 \leqq \theta_0 . \tag{9}$$

The launch angle, θ_0, and the angles θ_1 and θ_2 are related to the height, h, of the refracting layer above the path axis and its vertical thickness, v, by the following equations.

$$h \equiv Z_1 - Z_0 = R_0 \cos \theta_1 - R_0 \cos \theta_0 , \quad \text{and} \tag{10}$$

$$v \equiv Z_2 - Z_1 = R \cos \theta_2 - R \cos \theta_1 . \tag{11}$$

In principle, θ_0, θ_1 and θ_2 can be found from (8), (10), and (11) in terms of the path length, gradient of the index of refraction, and the height and thickness of the refracting layer. These values of θ_0, θ_1 and θ_2 can then be substituted into (7) to determine the optical length of the refracted ray. Our purpose is better served, however, by specializing the solution.

2.2 *Phase-Shift Along a Ray—Special Case*

The worst case of interference, that is, the largest difference in phase between the direct and refracted rays, occurs when the layer it thick enough that no ray which reaches the receiver rises above the layer. This can be demonstrated by the usual methods and the proof is not reproduced here.

The rest of this paper will be concerned primarily with the worst case interference, for which $\theta_2 = 0$.

When $\theta_2 = 0$, (8) and (9) become

$$R_0 \sin \theta_2 - (R_0 - R) \sin \theta_1 = L/2, \quad \text{and} \tag{12}$$

$$0 \leqq \theta_1 \leqq \theta_0 . \tag{13}$$

The limits on the launch angle, θ_0, are found by substituting (13) into (12).

$$L/2R_0 \leqq \sin \theta_0 \leqq L/2R. \tag{14}$$

We introduce a normalizing parameter k such that

$$k \equiv \frac{2R_0}{L} \sin \theta_0 , \quad \text{then, from (14),} \qquad 1 \leqq k \leqq R_0/R. \tag{15}$$

Now,

$$\theta_0 \approx \frac{kL}{2R_0} + \frac{1}{6}\left(\frac{kL}{2R_0}\right)^3, \tag{16a}$$

$$\cos\theta_0 \approx 1 - \frac{1}{2}\left(\frac{kL}{2R_0}\right)^2, \quad \text{and} \tag{16b}$$

$$\theta_1 \approx \frac{L(k-1)}{2(R_0 - R)} + \frac{1}{6}\left(\frac{L(k-1)}{2(R_0 - R)}\right)^3. \tag{16c}$$

With (14), (15), and (16) and recalling that $\theta_2 = 0$, the optical length of the refracted ray is

$$\frac{\lambda\phi_R}{2\pi} \approx n_0 L + \frac{L^3}{24R_0^2}\left[(n_0+1)k^3 - \frac{(n_0+1)(k-1)^3}{(1-R/R_0)^2} - 3k^2\right]. \tag{17}$$

The index of refraction $n_0 \approx 1$, so (17) can be written

$$\frac{\lambda\phi_R}{2\pi} \approx L + \frac{L^3}{24R_0^2}\left[2k^3 - \frac{2(k-1)^3}{(1-R/R_0)^2} - 3k^2\right], \tag{18}$$

for

$$1 \leqq k \leqq R_0/R.$$

The interference between the direct and refracted rays will be determined from (18). First, however, we need expressions for the departure angle and the distance a ray rises above the path as functions of the height of the refracting layer.

2.3 *The Relation Between the Angle of Departure and the Height of the Refracting Layer*

The distance of the refracting layer above the path axis is $h = Z_1 - Z_0$. From Fig. 1,

$$h = R_0(\cos\theta_1 - \cos\theta_0).$$

It is convenient to express h in terms of the maximum distance, h_D, that the direct ray rises above the path axis,

$$h_D = R_0(1 - \cos\alpha).$$

Substituting from (16) and noting that $\alpha \approx L/2R_0$,

$$h_D \approx L^2/8R_0, \quad \text{and} \tag{19}$$

$$\frac{h}{h_D} \approx k^2 - \frac{(k-1)^2}{(1-R/R_0)^2}. \tag{20}$$

2.4 *The Distance a Ray Rises above the Path*

From Fig. 1, the maximum distance, d, that a ray rises above the path axis is

$$d = R(1 - \cos \theta_1) + h.$$

Substituting from (16), (19), and (20),

$$\frac{d}{h_D} \approx k^2 - \frac{(k-1)^2}{(1 - R/R_0)}. \tag{21}$$

2.5 *The Optical Length of the Direct Ray*

If $\theta_1 = 0$ the refracting layer is too high to affect transmission. In this case, transmission is normal and a single ray, launched at an angle $\alpha = \sin^{-1} L/2R_0$, will reach the receiver. This is the direct ray and its optical length is given by setting $\theta_1 = \theta_2 = 0$ and $\theta_0 = \alpha = \sin^{-1} L/2R_0 \approx L/2R_0 + 1/6(L/2R_0)^3$ in (7).

$$\frac{\lambda \phi_D}{2\pi} \approx n_0 L + \frac{(n_0 - 2)}{24R_0^2} L^3. \tag{22}$$

The index of refraction $n_0 \approx 1$ and (22) can be written

$$\frac{\lambda \phi_D}{2\pi} \approx L - \frac{L^3}{24R_0^2}. \tag{23}$$

2.6 *Three-Path Transmission*

The height of the refracting layer above the path axis, the maximum height that a refracted ray rises above the path axis, and the phase shifts, ϕ_R, along the refracted rays are shown in Fig. 3 as functions of k for $R_0/R = 4$. The abscissa is approximately proportional to the angle of departure of a ray because θ_0 is small and $k = (2R_0/L) \sin \theta_0$. The curves in Fig. 3 were computed from (18), (20), and (21).

From Fig. 3 it can be seen that either one, two, or three rays can reach the receiver depending upon the height of the refracting layer; several examples are shown in Fig. 4. In Fig. 4a the layer height is 2.2 h_D. In addition to the direct ray, two rays are refracted into the receiver. As the layer height decreases the vertical separation between the two refracted rays increases as indicated in Figure 4b.

When the height of the layer equals the height of the direct ray, $h = h_D$ and the direct ray coincides with one refracted ray; two rays reach the receiver. And finally, when the layer height is less than h_D, only one ray, refracted from the layer, reaches the receiver as shown in Figure 4d.

The direct ray exists when the height of the layer equals or exceeds h_D, that is, when $h \geqq h_D$. As illustrated in Figure 4c, the direct ray and one refracted ray coincide when $h = h_D$. This occurs when $k = 1$ for the refracted ray.

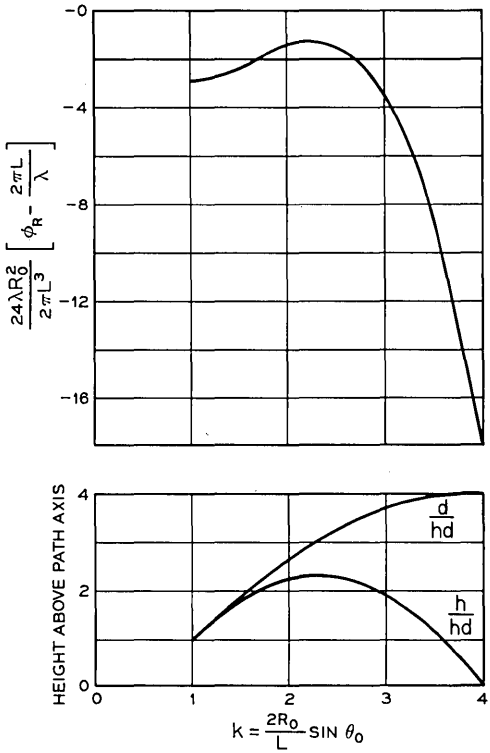

Fig. 3—Phase and height relations in single-layer refraction for $R_0 = 4R$.

III. SHORT PATHS

It has been known by many people for a long time, and it is intuitively obvious, that if a path is short enough, no deep fading will occur. Apparently no quantitative analysis of short paths has been published; therefore, we present a definition of a short path, estimates of short path lengths in New Jersey for several frequencies of interest, and an analysis of transmission over short paths.

3.1 *Definition of a Short Path*

The largest phase difference between rays occurs when $h/h_D = 1$. In this case the direct ray and one refracted ray coincide, reducing the number of rays to two. The corresponding values of k are

$$k_1 = 1, \quad \text{and}$$

$$k_2 = \frac{1 + (1 - R/R_0)^2}{1 - (1 - R/R_0)^2}.$$

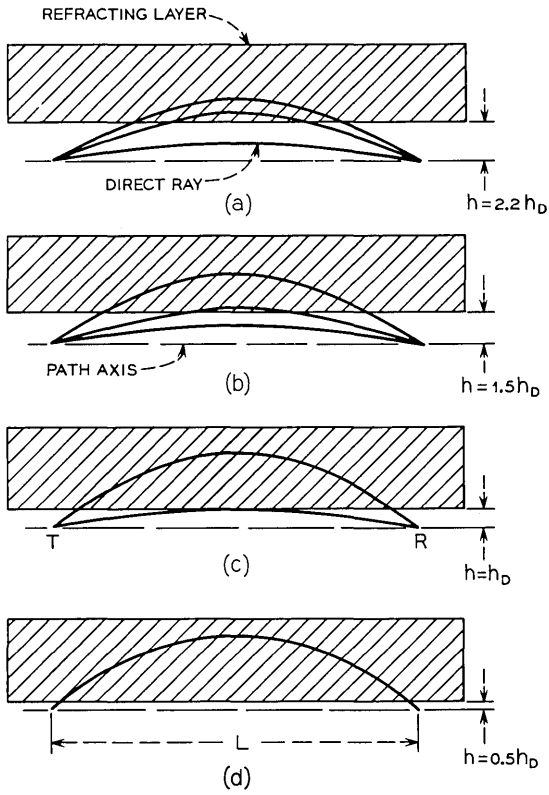

Fig. 4—Single-layer refraction.

The phase difference between these two rays is $\beta \equiv \phi_D - \phi_R$. From (18) and (23),

$$\frac{\lambda\beta}{2\pi} \equiv \frac{\lambda}{2\pi}(\phi_D - \phi_R) \approx \frac{L^3}{24R^2}\frac{(1 - R/R_0)^4}{(1 - R/2R_0)^2}. \tag{24}$$

The direct and refracted rays arrive at the receiver out of phase as shown in Fig. 5. The total received signal, E_R, is the vector sum of the signals received along the two rays.

$$\mathbf{E}_R = \mathbf{E}_0 + \mathbf{E}e^{j\beta},$$

where $\beta \equiv \phi_D - \phi_R$. The magnitude of the received signal is found to be

$$|E_R| = [E_0^2 + 2EE_0 \cos\beta + E^2]^{\frac{1}{2}}. \tag{25}$$

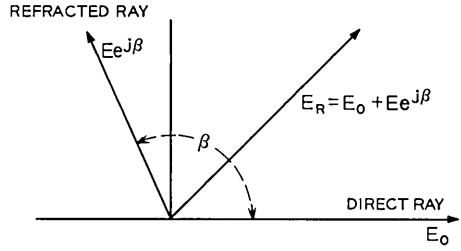

Fig. 5—Phase relations between the signals received via the direct and refracted rays.

A deep fade occurs if $|E_R| \ll E_0$, where E_0 is the amplitude of the received signal during normal transmission.

It may be seen from (25) that deep fading cannot occur unless $\cos \beta$ is negative. Now suppose that the path length is chosen so that, for the maximum negative gradient which occurs in the index of refraction, $|\beta|$ does not exceed a maximum value $|\beta_{\max}| \leqq \pi$. Then the deepest fade—the minimum value of $|E_R|$—can be computed from (25). For instance, if $|\beta_{\max}| \leqq \pi/2$ the minimum value of $|E_R|$ is E_0 and occurs when $E = 0$, and if $|\beta_{\max}| > \pi/2$ the minimum value of $|E_R|$ is given by $|E_R|_{\min} = E_0 \sin |\beta_{\max}|$ which occurs when $E = -E_0 \cos |\beta_{\max}|$. The minimum received signal amplitude is plotted in Fig. 6 as a function of the maximum difference in phase between the two rays.

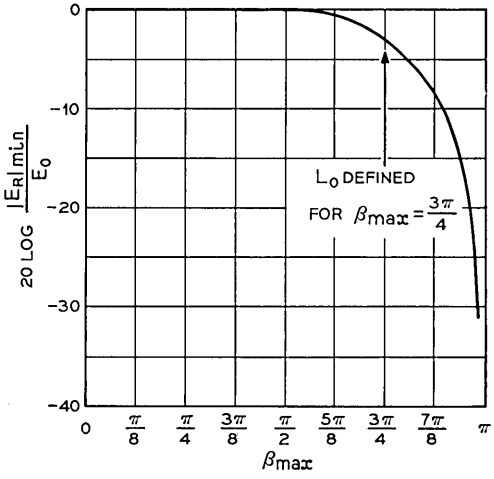

Fig. 6—The minimum amplitude of the received signal as a function of the maximum phase angle between the two received rays.

We now define a path length, L_0, such that for any path of length $L \leqq L_0$, there is no deep fading. L_0 is chosen arbitrarily as the path length for which $|\beta_{max}| = (3\pi)/4$ radians. The deepest fade which can occur on a path of length L_0 is 3 dB as may be seen in Fig. 6. L_0 can be computed from (24) with $\beta = (3\pi)/4$ radians.

$$L_0^3 = 9\lambda R^2 \frac{(1 - R/2R_0)^2}{(1 - R/R_0)^4}. \tag{26}$$

The definition has been made for the largest phase difference which can occur between the direct ray and a refracted ray. This situation occurs when the layer is tangent to the direct ray in which case only two rays exist. If the layer rises a third ray will be refracted into the receiver. The maximum phase difference between any two rays will be less than $3\pi/4$ radians in this situation and the maximum fade will be less than 3 dB. It should be noted that no restriction has been put on the magnitude of the signal received via the refracted rays; for a short path the maximum fade is 3 dB regardless of the magnitude of the sum of the refracted rays as illustrated in Fig. 7.

3.2 *An Estimate of* L_0

Crawford and Jakes, and Sharpless, measured angles of arrival for several years on a 22.8-mile transmission path at a frequency of 24 GHz.[7-9] The maximum difference in the angle of arrival between rays arriving at the receiver was 0.65 degree, the rays arriving at angles of 0.05, 0.35, and 0.7 degree above the normal angle of arrival. From this data, L_0 has been computed for several frequencies of interest and listed in Table I. The details of the computations are given in the

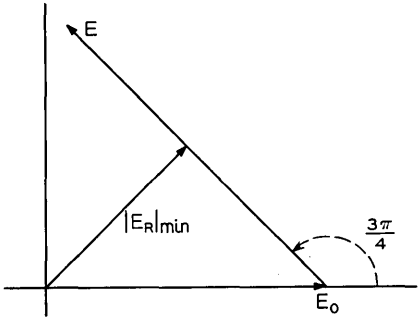

Fig. 7—Phase diagram showing V_{min} independent of refracted signal amplitude E for a short path where $\beta_{max} = 3\pi/4$.

TABLE I—THE LENGTH OF SHORT PATHS IN NEW JERSEY

Frequency in GHz	λ in cm	L_0 in km
4	7.5	9.37
6	5.0	8.20
10	3.0	6.93
20	1.5	5.5
30	1.0	4.8
60	0.5	3.8

Appendix. A reasonable interpretation of this result is that for path lengths less than those given in the table, in similar climatic regions, a deep fade would be a rare event. Paths of length $L \leqq L_0$ will be called short paths.

Since the values of L_0 in Table I were computed from data taken on a 22.8-mile path in New Jersey at 24 GHz, they should be regarded as approximate. More accurate values can be determined from measurements on shorter paths.

3.3 *The Slope of the Amplitude as a Function of Frequency*

Recalling that β is a function of frequency it follows from (25) that the magnitude of the received signal is also dependent upon frequency. Now,

$$\frac{d \ln |E_R|}{d\beta} = \frac{1}{|E_R|} \frac{d|E_R|}{d\beta}$$

and performing the indicated operations using (25), we get

$$\frac{d|E_R|}{|E_R|} = -\left[\frac{(E/E_0)\sin\beta}{1 + 2(E/E_0)\cos\beta + (E/E_0)^2}\right] d\beta.$$

The maximum value of the quantity in the brackets for a path of length L_0 occurs for $E = E_0$ and is

$$\left.\frac{d|E_R|}{|E_R|}\right|_{\max} = -\frac{d\beta}{2(\sqrt{2} - 1)}.$$

Now, after substituting $d\beta = \beta df/f$ we have

$$\left.\frac{d|E_R|}{|E_R|}\right|_{\max} = -\frac{\beta}{2(\sqrt{2} - 1)} \frac{df}{f}. \tag{27}$$

Example:

For a path of length L_0, $\beta = (3\pi)/4$ and (27) becomes

$$\left.\frac{d|E_R|}{|E_R|}\right|_{\max} = -\frac{3\pi}{8(\sqrt{2} - 1)} \frac{df}{f} = -2.85 \frac{df}{f}.$$

For a 500-MHz bandwidth at 20 GHz, the maximum change in amplitude across the band is approximately 7 percent or 0.6 dB.

3.4 *The Maximum Echo Delay*

The received signal is the sum of the signals transmitted over the direct and refracted paths. From the definition of a short path the maximum phase difference between the received signals is $\beta_{max} = (3\pi)/4$ radians corresponding to a difference in path length $\Delta L = \frac{3}{8}\lambda$. The maximum time delay τ is

$$\tau = \frac{\Delta L}{c} = \frac{3}{8f} \text{ seconds.} \tag{28}$$

At a frequency of 20 GHz the maximum echo delay on a short path is 0.01875 nanosecond. Pulses with a duration of one nanosecond would suffer little degradation on a short path at this frequency.

IV. LONG PATHS

Radio systems at 4 and 6 GHz normally have paths much longer than L_0. Consider a path at 6 GHz of length $L = 5L_0 \approx 41$ km. For the same negative gradient of the index of refraction used to derive L_0, the path difference between the direct and refracted rays is

$$\beta = \frac{3\pi}{4}\left(\frac{L}{L_0}\right)^3 = \frac{3\pi}{4} \times 125 \text{ radians.}$$

On the phase plane the phase difference between the direct and refracted waves corresponds to 46 complete revolutions plus an angle of $7\pi/4$ radians. This situation is illustrated in Fig. 8. Small changes in the

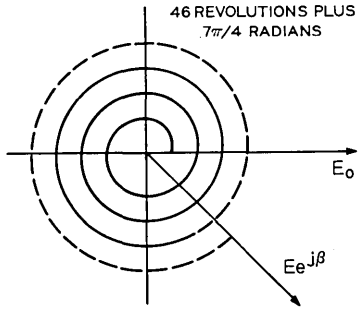

Fig. 8—The phase between signals received via the direct and refracted rays on a 41-km path at 6 GHz for the gradient in the index of refraction corresponding to $L_0 = 8.20$ km.

gradient of the index of refraction will cause the vector $\mathbf{E}e^{j\vartheta}$ to make a complete revolution—and pass through one of the phases $(2n - 1)\pi$, $n = \pm 1, \pm 2, \cdots$, where it is possible for deep fading to occur. Similarly, changes in frequency can cause $\mathbf{E}e^{j\vartheta}$ to rotate through large angles, a mechanism reflected in the frequency selectivity of this type of fading on long paths.

4.1 *Effect of Small Changes in the Gradient of the Index of Refraction on Interference*

From (1) and (24) the fractional change in β as a function of the fractional change in the gradient of the index of refraction can be derived.

$$\frac{d\beta}{\beta} = \frac{2}{(1 - R/R_0)(1 - R/2R_0)} \frac{d(dN/dz)}{dN/dz}. \tag{29}$$

For the 6-GHz, 41-km path, the fractional change in dN/dz required to produce a rotation of $\mathbf{E}e^{j\vartheta}$ through 2π radians is, for $R_0/R = 4$,

$$\frac{d(dN/dz)}{dN/dz} = 0.7 \text{ percent}.$$

Thus, small changes in the gradient of the index of refraction can produce large changes in the amplitude of the received signal on long transmission paths.

4.2 *Effect of Changes in Frequency on Interference*

Taking the derivative of β with respect to frequency in (24), we get $d\beta = \beta df/f$. For the 6-GHz, 41-km path, the change in frequency required to cause a change in β of 2π radians is

$$df = f \frac{d\beta}{\beta} = \frac{6 \times 10^3 \times 2\pi}{3\pi \times 125/4} = 128 \text{ MHz}.$$

During such fading conditions a frequency-sweep experiment would show minima separated by approximately 128 MHz.

Swept-frequency measurements have been reported in the literature and the results have been approximated by adjusting the amplitudes and phases of a number of sinusoidal signals to obtain a good fit to the experimental amplitude-frequency response.[7,10] Each sinusoid represented a discrete ray with constant amplitude and delay. In all cases, more than three sinusoids—rays—were required to obtain a satisfactory fit to the measured data.

The apparent contradiction between these results and the three-ray theory disappears when time-variations in the height, the thickness, and the gradient of the index of refraction of the refracting layer are

included. All of the approximations were made with the tacit assumption that the optical lengths of the rays remained constant during the time of a single sweep. This assumption does not hold in practice; the best evidence of this is the sequence of amplitude-frequency responses shown in Fig. 10 of Ref. 7. Each frequency-sweep took one second and sweeps are shown at ten-second intervals. The substantial changes in response which occur in ten seconds imply that non-negligible changes in response may occur during the one-second sweep time. Instead of postulating additional rays to approximate the measured frequency-swept response of the path, it is reasonable to postulate appropriate time variations in the height, the thickness, and the gradient of the index of refraction of the refracting layer.

There is another argument in support of this view. Four or more distinct rays have never been observed in measurements of angle-of arrival although two-ray or three-ray transmission has been observed on many occasions.[7] And while transmission with four or more rays is conceivable—for instance, with two layers like those in Fig. 2—the incidence of such conditions is apparently much less than the incidence of two-path or three-path transmission.

4.3 *The Onset of Fading on Long Paths*

It is reasonable to suppose that the negative gradient of the index of refraction develops slowly on clear summer nights. At some time a second ray may form and interfere with the direct ray at the receiver. For a small gradient the received signal may increase initially since β is small. As the negative gradient increases in magnitude the angle β will increase and cause the received signal to decrease when β approaches π radians. The angle β will continue to increase as the magnitude of the gradient increases. When β is large, rapid fading may occur due to small variations in the magnitude of the gradient as described previously. Small changes in the height or thickness of the layer may have a similar effect.

Now, smaller inversions of the index of refraction occur more often than do larger ones. Therefore, for a relatively small inversion, a long path may have fading whereas a shorter path may not. We may expect, then, that the fading distribution is a function of β and hence, of path length L and wavelength λ.

4.4 *Distribution of Attenuation as a Function of Path Length and Frequency*

The attenuation distribution is usually written as the probability—fraction of time—that the received signal amplitude, $|E_R|$, is less than a specified value, V_0.

$$\text{ATTENUATION DISTRIBUTION} \equiv P(|E_R|/E_0 \leqq V_0/E_0). \tag{30}$$

In the present model, the amplitudes of the signals received via the refracted rays are nominally equal to the amplitude of the signal received in the absence of the refracting layer. Since the probability of three rays of equal amplitude combining to form a deep fade is much less than the probability of two rays of equal amplitude combining to form a deep fade, we conclude that the distribution of attenuation is dominated by two-ray interference. The received signal is written

$$E_R/E_0 = 1 + (E/E_0)e^{i\beta},$$

where, from (18) and (23),

$$\beta = \phi_D - \phi_R \approx \frac{2\pi L^3}{24\lambda R_0^2}\left[2k^3 - \frac{2(k-1)^3}{(1-R/R_0)^2} - 3k^2 + 1\right].$$

By virtue of (1), (11), (15), (16), and (20), β can be written

$$\beta \approx \frac{2\pi L^3}{24\lambda R_0^2} F(dN/dz, h, v). \tag{31}$$

Although E and E_0 are nominally equal, there are always small variations in their magnitudes due to small inhomogeneities in the atmosphere. The ratio E/E_0 may therefore be expected to have a rather narrow probability density function which has a mean value of unity and which changes very little in the interval $1 - V_0/E_0 \leqq E/E_0 \leqq 1 + V_0/E_0$, where $V_0 \ll E_0$. On long paths the model suggests that E/E_0 and β are statistically independent. Then,

$$P(|E_R|/E_0 \leqq V_0/E_0) = \iint p_1(E/E_0)p_2(\beta)\, d\beta\, d(E/E_0)$$

and the integral is evaluated over a circle of radius V_0/E_0 centered at the origin of the phase plane.

For deep fades, $V_0 \ll E_0$ and the distribution can be written

$$\begin{aligned} P(|E_R|/E_0 \leqq V_0/E_0) &= \int p_1(E/E_0)\, d(E/E_0) \int p_2(\beta)\, d\beta \\ &\approx P(1 - V_0/E_0 \leqq E/E_0 \leqq 1 + V_0/E_0) \\ &\quad \cdot \sum_{n=0}^{\infty} P((2n+1)\pi - V_0/E_0 \leqq \beta \leqq (2n+1)\pi + V_0/E_0) \\ &\approx p_1(1)\frac{2V_0}{E_0}\sum_{n=0}^{\infty} P((2n+1)\pi - V_0/E_0 \\ &\quad \leqq \frac{2\pi L^3}{24\lambda R_0^2} F(dN/dz, h, v) \leqq (2n+1)\pi + V_0/E_0). \end{aligned} \tag{32}$$

The probability density function of $F(dN/dz, h, v)$ is not a function of path length or frequency, hence, the relationship in (32) agrees with Barnett's results which were obtained from measured distributions on long paths; the attenuation distribution is independent of path length, L, and wavelength, λ, as long as the ratio L^5/λ remains constant.[16]

Most of the time the sum in (32) is zero. During periods of heavy fading on long paths β may be regarded as being uniformly distributed in the interval $0 \leqq \beta \leqq 2\pi$. In this case, (32) may be written

$$P(|E_R|/E_0 \leqq V_0/E_0) \propto \frac{2}{\pi} p_1(1)\left(\frac{V_0}{E_0}\right)^2. \tag{33}$$

The slope of the distribution in (33) is the same as that of the Rayleigh distribution normally resulting in measurements of deep fading on long paths.

V. THE EFFECT OF SUBSTANDARD CONDITIONS ON SHORT PATHS

On long transmission paths fading can also be caused by an unusually large positive gradient in the index of refraction of the atmosphere.[7,13] During such conditions the rays from the transmitter bend away from the earth. If the gradient is large enough, a ray which is tangent to the earth in the direction of the receiver will be bent upward enough to miss the receiving antenna. This means that no direct ray will reach the receiver; the receiver is therefore in the diffraction region and the received signal amplitude will be substantially reduced below the level received when the conditions of propagation are normal. This type of fading is said to be caused by substandard refraction.[7,13]

We assume that the gradient in index of refraction is in the vertical direction only and extends over the length of the path. The radius of curvature of a ray is computed as described in Section II; in this case the center of curvature is above the transmission path. The geometry is shown in Fig. 9a, and the substandard gradient is illustrated in Fig. 9b. As long as the gradient in the index of refraction results in a bending radius $R \geqq R_{\min}$, a ray can reach the receiver. If the gradient increases further, the bending radius is reduced and there is no ray which can reach the receiver; the ray with radius R_x in Fig. 9a illustrates this condition.

The geometry is shown in Fig. 10 for the tangent and normal rays for a flat earth approximation. The clearance between the direct ray and the surface of the earth is d, and from the geometry of Fig. 10.

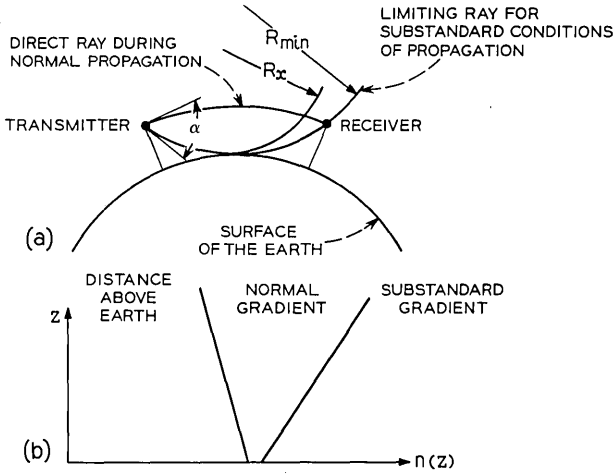

Fig. 9—(a) Ray bending during substandard conditions. (b) The index of refraction of the atmosphere during normal and substandard conditions.

$$d \approx \frac{L\theta_{max}}{4} \approx \frac{L^2}{8R_{min}}. \tag{34}$$

If the smallest value of R_{min} can be determined, a path clearance, d, can be computed from (34) such that no fading of this type is possible on a path whose clearance exceeds d. It is not possible to guarantee a value of R_{min} but a useful estimate can be made.

Crawford and Jakes observed no such fading on a 22.8-mile path during several years of measurement.[7] The path clearance was 280 feet. The radius of the limiting ray for this path, computed from (34), is $R_{min} \approx 2 \times 10^8$ cm. Since no fading due to substandard refraction was observed, a ray with a radius this small probably did not occur. For any path, in a similar climatic region, with a clearance d, com-

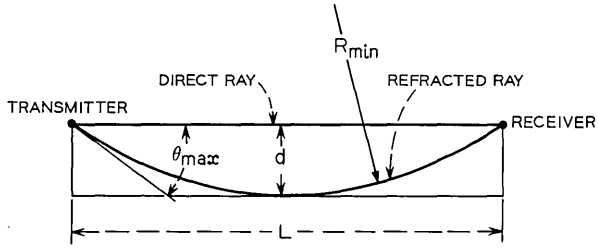

Fig. 10—Ray bending during conditions of substandard propagation.

puted from (34) with $R_{min} = 2 \times 10^8$ cm, such a fade would be a rare event.

Since no fading due to substandard refraction was observed the radius $R_{min} = 2 \times 10^8$ cm may be conservative. However, Crawford and Jakes did observe such fading on another path of length 12.6 miles and with a clearance of 63 feet.[7] Fading due to substandard refraction on this path could occur for rays with radii less than 2.84×10^8 cm. Evidently rays with radii less than 2.84×10^8 cm did occur but there were no rays with radii less than 2×10^8 cm. The use of $R_{min} = 2 \times 10^8$ cm to determine path clearances in similar climates is therefore not unduly pessimistic.

Path clearances, d_0, sufficient to eliminate fading due to substandard refraction on short paths can be computed from (34) using the lengths of short paths in Table I. These are shown in Table II.

It is of interest that d_0, for short paths, is always less than $\sqrt{\lambda L_0}/2$. Therefore, if a short path meets the usual Fresnel-zone clearance objective of $\sqrt{\lambda L_0}/2$, such a fade would be a rare event.

VI. CONCLUSION

Negative gradients in the index of refraction of the atmosphere are believed to be the cause of most severe fading on line-of-sight transmission paths operated at microwave frequencies. It has been shown in this paper that if the gradient has a maximum value, there is a length of transmission path, L_0, below which there is no deep multiple-path fading. Paths of length less than L_0 are called short paths. This path length has been estimated for New Jersey from measurements, reported by Crawford and Jakes, of the angle-of-arrival of microwave energy during conditions of severe multiple-path fading. The path length L_0 depends upon the maximum difference in the angles-of-arrival measured, and the largest difference recorded in

TABLE II—CLEARANCE REQUIRED TO PREVENT FADING DUE TO SUBSTANDARD REFRACTION ON SHORT PATHS

Frequency in GHz	λ in cm	L_0 in km	d_0 in cm
4	7.5	9.37	548
6	5.0	8.20	420
10	3.0	6.93	300
20	1.5	5.5	189
30	1.0	4.8	144
60	0.5	3.8	90.4

several years of measurement was used to compute L_0 at several frequencies of interest. These are shown in Table I. A reasonable interpretation of this result is that for short paths a deep fade would rarely, if ever, occur.

It is also shown that for short paths—paths shorter than L_0—the transmission is insensitive to bandwidth; pulses with durations of the order of one nanosecond will not suffer severe degradation on short paths.

The distribution of attenuation of fading on long paths is predicted from this model to be independent of the path length, L, and the wavelength, λ, as long as the ratio L^3/λ remains constant. This result is in agreement with Barnett's result which was obtained by other means.

The frequency-selectivity of long paths was also derived from the model. Using the values of L_0 presented in Table I, the minimum frequency separation between adjacent minima in a frequency-sweep measurement on a long path can be computed. The frequency separation between adjacent minima is inversely proportional to the third power of the path length.

The lengths of short paths were computed from measurements made in New Jersey and probably apply to regions with similar fading experience. The negative gradients in the index of refraction are functions of meterological parameters including temperature and humidity, and these may vary substantially in different climates. We may expect, for instance, that path length L_0 may be different in desert regions than it is in New Jersey.

VII. ACKNOWLEDGMENTS

This work was done in response to E. F. O'Neill's question about the transmission of short pulses over short-hop radio systems. The estimates of the lengths of short paths in New Jersey could not have been made without the experiments of A. B. Crawford and W. C. Jakes—experiments which were beautifully conceived, executed, and reported. Finally, I am grateful to T. L. Osborne, V. K. Prabhu, M. V. Schneider, and L. C. Tillotson for their comments and advice.

APPENDIX

In the experiments of Crawford and Jakes, the maximum difference in the angle of arrival between rays arriving at the receiver was 0.65 degree. This event occurred in the month of August and three rays

were present, arriving at angles of 0.05, 0.35, and 0.7 degree above the normal angle of arrival.

The index of refraction at the surface of the earth, N_s, and its gradient dN_s/dz, vary from season to season as described by B. R. Bean and E. J. Dutton.[17] In our notation,

$$-\frac{dN_s}{dz} = 7.32\, e^{(0.005577N_s)}, \tag{35}$$

where the unit of height is a kilometer. In the month of August, $N_s \approx 360$ in New Jersey. From (1) and (35),

$$\frac{dN_s}{dz} = -54.5N \text{ units/km}, \quad \text{and}$$

$$R_0 = 1.83 \times 10^9 \text{ cm}. \tag{36}$$

We assume that the normal angle of arrival during non-fading conditions is determined by this value of R_0. In addition to seasonal variations in N_s and dN_s/dz, there are diurnal variations.[17] It is assumed here that such a variation increased the angle of arrival of the direct ray by 0.05 degree for the event described above. A new value of R_0, corresponding to the new angle of arrival will now be computed.

The angle of arrival of the direct ray during nonfading conditions is computed using (36),

$$\alpha_0 = \frac{L}{2R_0} = 0.001 \text{ radian} = 0.0573 \text{ degree}.$$

During the fading event, α_0 increased to a new value

$$\alpha_1 = 0.0573 + 0.05 = 0.1073 \text{ degree}.$$

The new radius of curvature is $R_0 = L/(2\alpha_1) = 0.98 \times 10^9$ cm. The angles of arrival of the two refracted rays are

$$\theta_1 = 0.35 + 0.0573 = 0.4073 \text{ degree} \quad \text{and}$$

$$\theta_2 = 0.7 + 0.0573 = 0.7573 \text{ degree}.$$

From (16a),

$$k_1 \approx \theta_1/\alpha_1 = 3.8, \quad \text{and}$$

$$k_2 \approx \theta_2/\alpha_1 = 7.05.$$

These values of k occur for the same layer, that is, for the same h/h_D. Then, from (20),

$$k_2^2 - \frac{(k_2 - 1)^2}{(1 - R/R_0)^2} = k_1^2 - \frac{(k_1 - 1)^2}{(1 - R/R_0)^2}.$$

Solving for $(1 - R/R_0)^2$,

$$(1 - R/R_0)^2 = \frac{k_1 + k_2 - 2}{k_1 + k_2} = 0.815,$$

for which

$$R_0/R = 10.3.$$

After substitution into (23) we get,

$$L_0 = 4.8\lambda^{\frac{1}{3}} \text{ kilometers, } \lambda \text{ in cm.}$$

REFERENCES

1. Tillotson, L. C., "Use of Frequencies above 10 GHz for Common Carrier Applications," B.S.T.J., *48,* No. 6 (July–August 1969), pp. 1563–1576.
2. Tillotson, L. C., "A Model of a Domestic Satellite Communication System," B.S.T.J., *47,* No. 10 (December 1968), pp. 2111–2137.
3. Hathaway, S. D., and Evans, H. W., "Radio Attenuation at 11 KMC," B.S.T.J., *38,* No. 1 (January 1959), pp. 73–97.
4. Semplak, R. A., and Turrin, R. H., "Some Measurements of Attenuation by Rainfall at 18.5 GHz," B.S.T.J., *48,* No. 6 (July–August 1969), pp. 1745–1756.
5. Ruthroff, C. L., "Rain Attenuation and Radio Path Design," B.S.T.J., *49,* No. 1 (January 1970), pp. 121–135.
6. DeLange, O. E., "Propagation Studies at Microwave Frequencies by Means of Very Short Pulses," B.S.T.J., *31,* No. 1 (January 1952), pp. 91–103.
7. Crawford, A. B., and Jakes, W. C., "Selective Fading of Microwaves," B.S.T.J., *31,* No. 1 (January 1952), pp. 68–90.
8. Sharpless, W. M., "Measurement of the Angle of Arrival of Microwaves," Proc. IRE, *34,* No. 11 (November 1946), pp. 837–845.
9. Crawford, A. B., "Further Observations of the Angle of Arrival of Microwaves," Proc. IRE, *34,* No. 11 (November 1946), pp. 845–848.
10. Kaylor, R. L., "A Statistical Study of Selective Fading of Super-High Frequency Radio Signals," B.S.T.J., *32,* No. 9 (September 1953), pp. 1187–1202.
11. Durkee, A. L., "Results of Microwave Propagation Tests on a 40-Mile Overland Path," Proc. IRE, *36,* No. 2 (February 1948), pp. 197–205.
12. Friis, H. T., "Microwave Repeater Research," B.S.T.J., *27,* No. 2 (April 1948), pp. 183–246.
13. Kerr, D. E., *Propagation of Short Radio Waves,* New York: McGraw-Hill, 1951.
14. Desirant, M., and Michiels, J. L., *Electromagnetic Wave Propagation,* New York: Academic Press, 1960, pp. 471–478.
15. Saxton, J. A., *Radio-Wave Propagation in the Troposphere,* New York: Elseviere Publishing Co., 1962, pp. 3–15.
16. Barnett, W. T., unpublished work.
17. Bean, B. R., and Dutton, E. J., *Radio Meteorology,* National Bureau of Standards Monograph 92, Washington: U. S. Government Printing Office, March 1, 1966.

THE BELL SYSTEM TECHNICAL JOURNAL
Vol. 50, No. 7, September, 1971
Printed in U.S.A.

Data Transmission by Combined AM and PM

By J. SALZ, J. R. SHEEHAN, and D. J. PARIS

(Manuscript received March 2, 1971)

This paper presents theoretical analysis and experimental verification of the performance of a digital data modem which uses combined amplitude and phase modulation (AM–PM). The theoretical model assumes operation over the bandlimited additive Gaussian channel. The receiver used in the experiment, and for which theoretical results are presented, uses an envelope detector in parallel with a phase detector to recover the data. The criteria of error rate and communication efficiency (measured in bits per cycle of bandwidth) as functions of average signal-to-noise ratio (S/N) are used to make comparisons with other modulation schemes. The theory predicts a performance from 1 to 4 dB poorer than what can be realized from single sideband (SSB) modulation. We present experimental results which indicate excellent agreement with the theory.

I. INTRODUCTION

Theoretical investigations of the performance of combined amplitude and phase modulation systems have been reported on by C. R. Cahn[1] (1960), J. C. Hancock and R. W. Lucky[2] (1960), Lucky and Hancock[3] (1962), and more recently by M. Leiter and M. P. Talbot[4] (1967). These investigators found that, on the additive white Gaussian channel, combined AM and PM yields a better error rate at fixed signal-to-noise ratio than PM or AM alone when the number of total levels is $\geqq 8$.

Here we rigorously establish these claims for a practical system. Instead of using linear matched filter detection (Ref. 2), we use differential or coherent phase detection to estimate the phase and a conventional envelope detector to estimate the amplitude. While theoretically optimum signal locations in two-dimensional space are generally not quantized but subject only to fixed power limitation, we consider practical signal sets which are quantized.

The questions we answer in this paper are the following: Given an N-level system and the facility to use L amplitudes and M phases such that $N = LM$, what is the value of L, and consequently M, such that the error rate is smallest for a fixed amount of S/N when signaling over the bandlimited additive Gaussian channel? How does this combined modulation scheme compare with only PM or AM at fixed S/N? How efficient is this modulation scheme in terms of attainable bits per cycle of bandwidth at fixed error rate? And finally how close can these theoretical results be realized in the laboratory with actual hardware?

II. THE MATHEMATICAL MODEL

We represent the transmitted signal by the time series

$$S(t) = \sum_n (V + Ab_n) \cos [\omega_0 t + \theta_n] g(t - nT) \tag{1}$$

where $b_n = \pm(2k - 1), k = 1, 2, \cdots, L/2$, for all n are the amplitude symbols and $\{\theta_n\}$ is a set of M equally spaced phases. The signal $g(t)$ is a bandlimited ideal pulse such that $g(nT) = 1$, when $n = 0$ and $g(nT) = 0$ for all other n. For the calculations that follow we take $g(t) = \sin [(\pi t)/T]/[(\pi t)/T]$ without loss of generality. The positive constants V, A, and ω_0 are so far arbitrary. The total amount of information carried by $S(t)$ is $1/T$ $(\log_2 L + \log_2 M) = 1/T$ $(\log_2 N)$ b/s, $N = ML$. We regard the amplitude symbols $\{b_n\}$ and the phase symbols $\{\theta_n\}$ as independent random variables. By introducing a uniformly distributed phase in the argument of the cos $(\cdot)$ function in equation (1) and also randomizing the epoch of $g(t)$ renders the signal $S(t)$ stationary. A straightforward calculation* reveals that the total average power in $S(t)$ is

$$P_S = \langle S^2(t) \rangle = \left(\frac{V^2}{2} + \frac{A^2}{2} \frac{L^2 - 1}{3} \right) \tag{2}$$

where $\langle \cdot \rangle$ denotes the ensemble average.

For the added noise we use the standard representation

$$W(t) = x(t) \cos \omega_0 t + y(t) \sin \omega_0 t$$

where $x(t)$ and $y(t)$ are stationary zero mean independent baseband Gaussian processes possessing identical variance σ^2.

The data receiver processes the sum signal $S(t) + W(t)$ to obtain estimates of $\{b_n\}$ and $\{\theta_n\}$. Reception is accomplished in two parallel

* Detailed calculations of power in data signals may be found in Ref. 5, pp. 51–55.

detectors. These detectors will be denoted respectively by E—the envelope detector and ϕ—the phase detector.

The E detector operates by first computing the envelope of $S(t) + W(t)$ and then synchronously sampling the result at every T seconds. The ϕ detector computes the phase of signal plus noise (see Ref. 5 for a detailed discussion of phase modulation and demodulation) which is then synchronously sampled to derive estimates of $\{\theta_n\}$. In all these operations we assume that correct timing information is available at the receiver.

We begin by analyzing the E detector first. The envelope of the sum signal is

$$E^2(t) = [\sum_n (V + Ab_n) \cos \theta_n g(t - nT) + x(t)]^2 + [\sum_n (V + Ab_n) \sin \theta_n g(t - nT) + y(t)]^2 \quad (3)$$

and a sample taken at $t = 0$ gives

$$E^2 = \{(V + Ab_0) \cos \theta_0 + x\}^2 + \{(V + Ab_0) \sin \theta_0 + y\}^2 \quad (4)$$

where we have used some obvious notational shorthands. In order that a genuine envelope exist we must have $V + Ab_0 > 0$ for all values of b_0. This results in the condition

$$V > (L - 1)A \quad (5)$$

since max $b_0 = (L - 1)A$. Our task in the next section will be to evaluate the error rate in the E detector from estimates of the probability distribution of E^2.

The ϕ detector computes either the phase differential of $S(t) + W(t)$ or the actual phase. As long as $S(t)$ has a nonvanishing envelope these measurements are unambiguous.

III. ERROR RATE ANALYSIS

The error rate of the E detector is determined from the conditional tail probabilities of E^2 [equation (4)]

$$F_\alpha = P_r[E^2 \leqq \alpha^2 \mid \bar{x}, \bar{y}]$$

and

$$F_\beta = P_r[E^2 \geqq \beta^2 \mid \bar{x}, \bar{y}]$$

where

$$\bar{x} = (V + Ab_0) \cos \theta_0$$

and

$$\bar{y} = (V + Ab_0) \sin \theta_0 .$$

It is difficult to analyze the exact representation of these probabilities and therefore we resort to exponentially tight upper bounds.

The lower tail probability is upper bounded by

$$F_\alpha = \int_0^\infty u(\alpha^2 - E^2)\, dP(E^2) \leqq \int_0^\infty e^{\lambda\alpha^2} e^{-\lambda E^2}\, dP(E^2)$$
$$= e^{\lambda\alpha^2} M_{E^2}(-\lambda), \qquad \lambda \geqq 0 \tag{6}$$

where $u(\cdot)$ is the unit step function, P is the probability distribution of E^2, and $M_{E^2}(\lambda) = \langle e^{\lambda E^2} \rangle$ is the moment generating function of E^2. In a like manner an upper bound to the upper tail probability is

$$F_\beta \leqq e^{-\beta^2\lambda} M_{E^2}(\lambda). \tag{7}$$

Since E^2 [equation (4)] is the sum of squares of two independent Gaussian random variables with means $\bar{x}$, $\bar{y}$ and identical variance σ^2 the moment generating function is readily calculated (see Ref. 5, p. 270). The result is

$$M_{E^2}(\lambda) = \frac{1}{1 - 2\lambda\sigma^2} \exp\left\{\lambda \frac{\bar{x}^2 + \bar{y}^2}{1 - 2\lambda\sigma^2}\right\} \tag{8}$$

where

$$\bar{x}^2 + \bar{y}^2 = (V + Ab_0)^2 = a^2.$$

Using equation (8) in equations (6) and (7) gives

$$F_\alpha \leqq \frac{1}{1 + 2\lambda\sigma^2} \exp E_+(\lambda),$$

$$F_\beta \leqq \frac{1}{1 - 2\lambda\sigma^2} \exp E_-(\lambda) \tag{9}$$

where

$$E_+(\lambda) = \lambda\alpha^2 - \lambda \frac{a^2}{1 + 2\lambda\sigma^2}$$

and

$$E_-(\lambda) = -\lambda\beta^2 + \lambda \frac{a^2}{1 - 2\lambda\sigma^2}.$$

The upper bounds just derived hold for only positive λ. As is usual in these calculations there exists an optimum λ for each of these bounds

which makes them exponentially tightest. To find these λ's we set the derivative of E_+ and E_- to zero to obtain:

$$\frac{d}{d\lambda} E_+(\lambda) = 0 \rightarrow \frac{-a^2 + \alpha^2}{4\alpha^2} + \lambda\sigma^2 + (\lambda\sigma^2)^2 = 0$$

yielding the two roots

$$\lambda = \frac{1}{2\sigma^2}\left(-1 \pm \frac{a}{\alpha}\right).$$

For a positive root to exist it is necessary that $a^2 > \alpha^2$ (a physically reasonable condition) and the optimum λ is therefore

$$\sigma^2\lambda = \frac{1}{2}\left(\frac{a}{\alpha} - 1\right).$$

When this value of λ is substituted into (9) we get the final result

$$F_\alpha \leqq \frac{\alpha}{a} \exp\left\{-\frac{1}{2\sigma^2}(a - \alpha)^2\right\}. \tag{10}$$

Similarly when $d/d\lambda\ E_-(\lambda)$ is set to zero we obtain two roots for λ namely $\lambda\sigma^2 = 1/2\ (1 \pm a/\beta)$. Here the physically reasonable condition is that $a/\beta < 1$ giving rise to two positive roots. When both of these roots are substituted into $E_-(\lambda)$ it is found that $\lambda\sigma^2 = 1/2\ (1 - a/\beta)$ yields the smallest value. Using this root in equation (9) results in the final answer for an upper bound on the upper tail probability.

$$F_\beta \leqq \frac{\beta}{a} \exp\left\{-\frac{1}{2\sigma^2}(\beta - a)^2\right\}. \tag{11}$$

We now have all the ingredients to perform error rate calculations.

Symbol detection is obtained by comparing the received envelope to fixed thresholds. The received envelope in the absence of noise is $V + Ab_0 = V \pm A(2k - 1)$, $k = 0, 1, 2, \cdots, L/2$ and the thresholds are set to $V \pm 2Ak$. We see from equations (10) and (11) that the exponents of both upper and lower tail probabilities depend on the difference between the received amplitude value and the threshold. The maximum of the difference is simply A. Consequently when only adjacent errors are considered, the error rate is upper bounded by

$$P_E \leqq C \exp\left\{-\frac{A^2}{2\sigma^2}\right\} \tag{12}$$

where the constant C is of minor importance. More general techniques[5] for studying the behavior of tail probabilities of arbitrary Gaussian

quadratic forms show that equation (12) is also an asymptotic formula, approaching the actual error rate as $\sigma^2 \to 0$. We therefore use $\exp(-A^2/2\sigma^2)$ as a good estimate for the error rate in subsequent calculations.

The probability of error for phase detectors is well known (see Ref. 5). The explicit formula for differential phase detection is

$$P_{\phi d} = \exp\left\{-\frac{D^2}{2\sigma^2} 2\sin^2\frac{\pi}{2M}\right\} \tag{13}$$

while for coherent phase detection

$$P_{\phi c} = \exp\left\{-\frac{D^2}{2\sigma^2}\sin^2\frac{\pi}{M}\right\} \tag{14}$$

holds where D is the minimum value of the envelope in the absence of noise.

$$D = V - A(L-1). \tag{15}$$

It is reasonable to require that the error rates in the E and ϕ detectors be exponentially identical. This requirement leads to the condition

$$A^2 = \begin{cases} 2(V - AL + A)^2 \sin^2\frac{\pi}{2M}, & \text{differential detection (D. D.)} \\ (V - AL + A)^2 \sin^2\frac{\pi}{M}, & \text{coherent detection (C. D.).} \end{cases} \tag{16}$$

Solving for V explicitly gives

$$V = \begin{matrix} Af_d(L, M), & \text{D.D.} \\ Af_c(L, M), & \text{C.D.} \end{matrix} \tag{17}$$

where

$$f_d(L, M) = L - 1 + \frac{1}{\sqrt{2}} \frac{1}{\left|\sin\frac{\pi}{2M}\right|}, \text{ D.D.}$$

and

$$f_c(L, M) = L - 1 + \frac{1}{\left|\sin\frac{\pi}{M}\right|}, \quad \text{C.D.}$$

These formulas indicate how the power is to be partitioned between the signal that carries phase information and the signal that carries

the amplitude information and consequently determine the threshold levels in the E detector.

Using equation (17) in equation (2) we obtain a formula for the total average transmitted power as a function of the number of amplitude levels L and the number of phases M

$$P_S = \frac{A^2}{2}\left[f_i^2(L, M) + \frac{L^2 - 1}{3}\right] \tag{18}$$

where f_i is either f_d or f_c depending on the type of phase detector employed.

IV. THEORETICAL COMPARISONS

We now wish to compare the probability of error exponents of the mixed modulation system with that of pure phase and pure amplitude modulation at fixed signal-to-noise ratio. For the mixed modulation system we first express $A^2/2$ as a function of the power using equation (18) and then substitute into equation (12). Neglecting the constant coefficient we obtain

$$P_{E\phi} \sim \exp\left\{-\frac{P_S}{\sigma^2}\frac{1}{g_i^2(L, M)}\right\} \tag{19}$$

where

$$g_i^2(L, M) = f_i^2(L, M) + \frac{L^2 - 1}{3}.$$

When only phase modulation is used with total number of levels $N = ML$, the error rates become

$$P_\phi \sim \begin{cases} \exp\left\{-\frac{P_S}{\sigma^2} 2\sin^2\frac{\pi}{2ML}\right\}, & D.D. \\ \exp\left\{-\frac{P_S}{\sigma^2}\sin^2\frac{\pi}{ML}\right\}, & \text{C.D.} \end{cases} \tag{20}$$

When only amplitude modulation* is used, $V = 0$ and $\{\theta_n = 0\}$ in equation (1), the error rate for $LM = N$ levels is[5]

$$P_a \sim \exp\left\{-\frac{P_S}{\sigma^2}\frac{3}{(LM)^2 - 1}\right\}. \tag{21}$$

We have thus far ignored the front-end filter which precedes the detectors. Since the data spectrum is flat across the band, no distortion

* We assume that coherent demodulation is used.

will result if the transfer function of the front-end filter is also flat. We therefore use the characteristic

$$H(f) = \begin{cases} 1, & f_0 - \frac{1}{2T} \leqq |f| \leqq f_0 + \frac{1}{2T} \\ 0, & \text{elsewhere} \end{cases} \tag{22}$$

where $\omega_0 = 2\pi f_0$.

Assuming that the added noise has a flat double-sided spectral density N_0, the variance σ^2 is

$$\sigma^2 = \frac{2N_0}{T} \tag{23}$$

and the common factor in all the error-rate expressions becomes

$$\Lambda = \frac{P_S}{\sigma^2} = \frac{TP_S}{2N_0} = \frac{\text{energy/bit}}{\text{watts/cycle}}.$$

The factors multiplying Λ in equations (19), (20), and (21) are all equal to or less than unity and therefore may be regarded as a degradation over binary systems. (These factors reduce to unity for binary systems.)

Comparisons between these systems can conveniently be made by noting the relative sizes of these coefficients as functions of L and M such that $N = LM$. Toward this end the following definitions are made.

$$\begin{aligned} D_{E\phi i} &= 10 \log_{10} g_i^2(L, N), \qquad i = c \quad \text{or} \quad d \\ D_\phi &= -10 \log_{10} \left(2 \sin^2 \frac{\pi}{2N}\right) \\ D_{\phi c} &= -10 \log_{10} \left(\sin \frac{\pi}{N}\right) \\ D_a &= 10 \log_{10} \left(\frac{N^2 - 1}{3}\right). \end{aligned} \tag{24}$$

A natural question which now arises is the following: for fixed N is there an L which minimizes $D_{E\phi i}(L, N)$? The answer is yes and the comparisons we present are based on this optimum choice of L — the number of amplitude levels.

Our first results are summarized in Table I for typical values of N. For instance, in a 4-level system all phase modulation yields better performance than a combined system since D_ϕ is less than $D_{E\phi i}$ by 1.7

TABLE I—TABULATION OF PERTINENT PARAMETERS

N	Optimum L (For combined systems only)	Optimum M (For combined systems only)	$D_{E\phi l}$ in dB	$D_{E\phi c}$ in dB	D_{ϕ} in dB	D_{a} in dB	$D_{\phi c}$ in dB
4	2	2	7.0	7.0	5.3	7.0	3.0
8	2	4	9.6	8.3	11.2	13.2	8.3
16	2	8	13.5	11.5	17.3	19.3	14.2
32	4	8	16.9	15.6	23.2	25.3	20.2
64	4	16	20.4	18.5	29.2	31.3	26.2
128	8	16	23.5	22.2	35.2	37.4	32.2

dB. There is no advantage here in splitting the levels. On the other hand for an 8-level system, 2 amplitudes and 4 phases appears preferable than just 8 phases or 8 amplitudes and the advantages gained are 1.6 dB when 8 phases are used and 3.6 dB when 8 amplitudes are used. It is always advantageous to mix the levels when $N \geqq 8$. The advantage becomes more pronounced as N becomes large.

We now turn attention to the communication efficiency of the various modulation schemes considered. The figure of merit used is the attainable number of bits per cycle for a given signal-to-noise ratio and fixed error rate. The rate R in bits per cycle attained by these systems is

$$R = \frac{\log_2 N}{TB} = \frac{\rho}{B} \log_2 N \tag{25}$$

where ρ is the symbol signaling rate and B is the required bandwidth. For ideal double-sideband systems such as PM and AM-PM, ρ/B is equal to unity while for baseband and single sideband systems, ρ/B is equal to two. We therefore have

$$\begin{aligned} (R)_{\text{D SB}} &= \log_2 N \quad \text{bits/cycle} \\ (R)_{\text{S SB}} &= 2 \log_2 N \quad \text{bits/cycle.} \end{aligned} \tag{26}$$

Since we are comparing systems operating over unequal bandwidths, it is appropriate to give an alternative interpretation of the constant

$$\Lambda = \frac{P_S}{2N_0} = \frac{P_S}{2N_0\rho}. \tag{27}$$

It is tempting to call Λ the signal-to-noise ratio. However the quantity $2N_0\rho$ is not necessarily the noise power in the physical bandwidth. The harmful noise power can only be determined once a relationship be-

tween the signaling rate and the physical bandwidth is given. For double sideband systems Λ is in fact the actual signal-to-noise ratio, since $\rho = B$. However for baseband and SSB, $\Lambda = \frac{1}{2}(S/N)$. We dwell on this point because often the parameter Λ is used to make comparisons and it is very easy to overlook the 3-dB factor when what is often of interest is the actual S/N. For example, we see from Table I that 4-level AM is 1.7 dB worse than 4-level PM. We must bear in mind however that the AM system for which the figures are given in the table are double sideband AM. If, however, the comparison is sought for baseband AM or SSB-AM then 3 dB more must be added to the 7 dB.

We see from equations (20) or (21) that in order to maintain a fixed error rate in PM and AM the signal-to-noise ratio must vary as the square of the number of levels when the latter is large. When S/N is expressed in dB it then is directly proportional to the logarithm of the number of levels and hence to the efficiency expressed in bits per cycle. Plots of efficiency vs S/N in dB for AM and PM will therefore appear linear with identical slopes. (The intercepts may be different.) A similar argument applies to SSB modulation but the resulting slope is twice as large compared with PM and AM. This is evident from the fact that in SSB twice as many bits per cycle can be attained as in PM or double sideband AM with the same number of levels.

We shall now show that the efficiency of combined AM and PM as a function of S/N expressed in dB is also linear and follows the same slope as the efficiency of SSB. In order to prove this claim we must demonstrate that in combined AM and PM S/N varies linearly with the number of levels to maintain a fix error rate. This variation can be deduced by considering the asymptotic behavior of $g_i^2(L, N)$ [equation (19)]. Disregarding all multiplicative factors of L and N and dropping the additive constants we see that

$$g_i^2(L, N) \sim \left(L + \frac{N}{L}\right)^2 + L^2$$

$$\sim L^2 + N + N^2L^{-2}. \tag{28}$$

The optimum L is proportional to $\sqrt{N}$ since

$$\frac{\partial g_i^2(L, N)}{\partial L} \sim L - \frac{N^2}{L^3} = 0 \tag{29}$$

implies that

$$g_i^2(N) \sim N. \tag{30}$$

The various relationships using similar calculations as above are briefly summarized below

SSB or AM Baseband

$$(\mathrm{S/N})_{\mathrm{dB}} \sim 20 \log_{10} N = \frac{20}{\log_2 10} \log_2 N$$

and since

$$(R) \text{ bits/cycle} = 2 \log_2 N$$

we have that

$$R \sim \frac{\log_2 10}{10} (\mathrm{S/N})_{\mathrm{dB}} .$$

Combined AM and PM

$$(\mathrm{S/N})_{\mathrm{dB}} \sim 10 \log_{10} N = \frac{10}{\log_2 10} \log_2 N$$

and since

$$(R) \text{ bits/cycle} = \log_2 N$$

we have that

$$R \sim \frac{\log_2 10}{10} (\mathrm{S/N})_{\mathrm{dB}} .$$

PM and Double Sideband AM

$$(\mathrm{S/N})_{\mathrm{dB}} \sim 20 \log_{10} N = \frac{20}{\log_2 10} \log_2 N$$

and since

$$(R) \text{ bits/cycle} = \log_2 N$$

we have that

$$R \sim \frac{\log_2 10}{20} (\mathrm{S/N})_{\mathrm{dB}} .$$

To complete the picture we find from Shannon's capacity formula that

$$\begin{aligned} (R)_{\text{capacity}} &\sim \log_2 (\mathrm{S/N}) \\ &= \tfrac{1}{3}(\mathrm{S/N})_{\mathrm{dB}} \end{aligned} \tag{31}$$

and since $\frac{1}{3}$ is very close to $\frac{1}{10}\log_2 10$ we see that SSB and combined AM and PM follow the capacity slope.

It now remains to uncover how far these curves are from one another. The results appear in Fig. 1. A most interesting picture is revealed; combined AM and PM is indeed only 3–4 dB worse than SSB when differential phase detection is used. When coherent phase detection is employed only 1–2 dB is given up.

V. SYSTEM IMPLEMENTATION

We now discuss the implementation of a combined AM-PM modem which was used to evaluate the performance of the various signal formats analyzed in the previous sections. For convenience a basic signaling rate of 1200 symbols per second was used operating over an ideal linear channel in the frequency range of 600-3000 Hz. The signaling elements were designed to have raised cosine shapes with 100-percent excess bandwidth.[5] In order to optimize performance in the presence of additive Gaussian noise, signal shaping was divided between transmitter and receiver.

The transmitter was designed to have the capability of generating the signal vectors shown in Fig. 2. For noncoherent (differential) demodulation of PM, the generated signal phases were spaced at odd

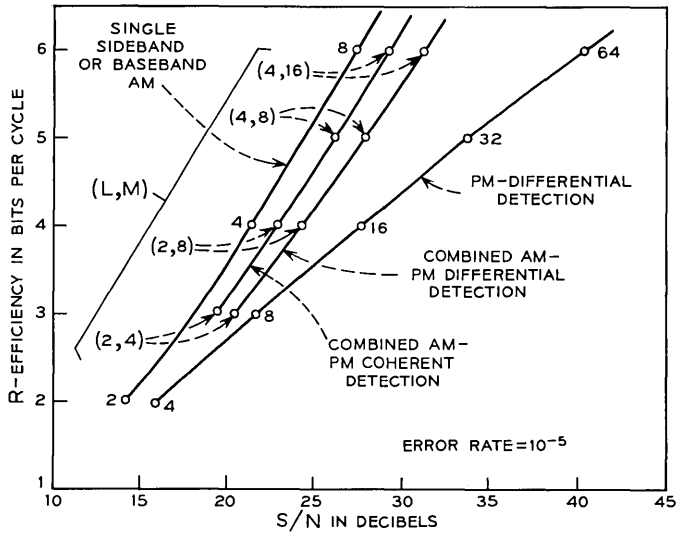

Fig. 1—Theoretical efficiency vs S/N for various modulation systems.

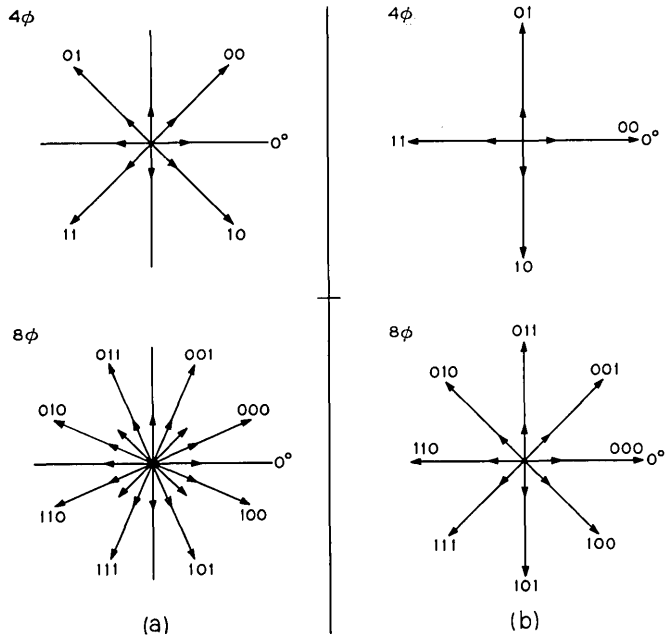

Fig. 2—Tail-to-head phase shifts: (a) noncoherent (differential) demodulation of PM; (b) coherent demodulation of PM.

multiples of 45 degrees and 22-1/2 degrees for 4ϕ and 8ϕ, respectively. For coherent PM demodulation, the spacing was multiples of 90 degrees and 45 degrees, respectively.

Generation of the amplitude levels was accomplished in a balanced amplitude modulator according to the formulas given in equation (17) and repeated on Fig. 3.

The receiver is shown in block diagram form in Fig. 4. The receiving filter eliminates out-of-band noise and provides signal shaping. Amplitude and phase demodulation was accomplished in separate parallel paths.

The phase detector was designed to operate in either a coherent mode or in a differentially coherent mode. For differential demodulation the signal from the receiving filter was multiplied with delayed and phase-shifted versions of itself. Low-pass filtering of these products produced in-phase (I) and quadrature (Q) baseband eye patterns. Analog arithmetic performed on I and Q at the sampling instants yielded the recovered data which was fed out in serial form. For coherent demodulation, everything was done in the same manner except that a coherent

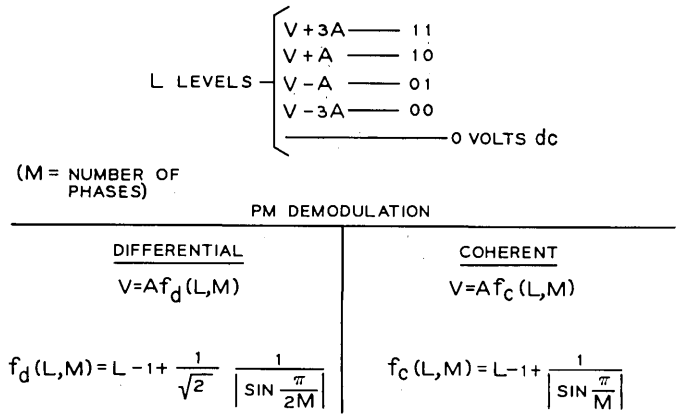

Fig. 3—Definition of amplitude levels.

local carrier signal was used to multiply the phase-shifted delay line outputs.

Amplitude demodulation was performed by extracting the envelope of the signal from the receiving filter. The coded information contained in the envelope (E) was obtained by slicing the envelope and folded envelope. The AM data was then fed out in serial form.

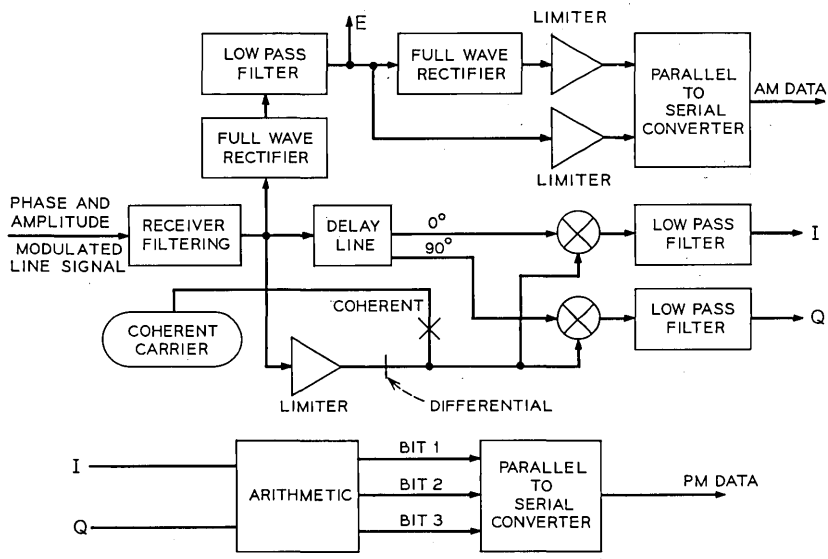

Fig. 4—Receiver block diagram.

Figures 5 thru 8 show baseband eye patterns of some of the signal formats generated for the experiments. Also shown are polar plots, generated by attaching the I and Q signals to the horizontal and vertical inputs of an oscilloscope. Z-axis intensification at the sampling instant produced the points in signal space.[6] Note that the coherent polar plots are rotated 45 degrees from this position in Fig. 2*b*. This 45-degree rotation eliminates a zero-voltage level which would otherwise appear in the eye patterns.

VI. EXPERIMENTAL RESULTS

The configuration shown in Fig. 9 was used to evaluate the error performance of various signal formats in the presence of additive band-limited Gaussian noise. The various signal formats generated in the experiments are summarized below:

	Differential (D)
4ϕ	Coherent (C)
8ϕ	D, C
$2L$, 4ϕ	D, C
$2L$, 8ϕ	D, C
$4L$, 8ϕ	D, C

Since timing jitter and phase off-set are not included in the theory, timing phase and coherent carrier phase were adjusted manually at the receiver.

The experimental results are shown in Fig. 10. These results were used to generate the efficiency curve of Fig. 11. The theoretical results are again repeated (properly scaled) on this curve.

Correspondence between predicted and measured performance is seen to be quite good. For example, the predicted difference in performance between 8ϕ differential and (4ϕ, $2L$) differential is 1.6 dB. The measured difference is found to be 1.5 dB.

Another indicator of how closely the implementation and the theoretical model match can be seen from Fig. 10. The measured performance of 4ϕ differential departs from theory by only 0.8 dB.

VII. ACKNOWLEDGMENT

We wish to acknowledge R. J. Tracy for making significant design contributions to the experimental modem.

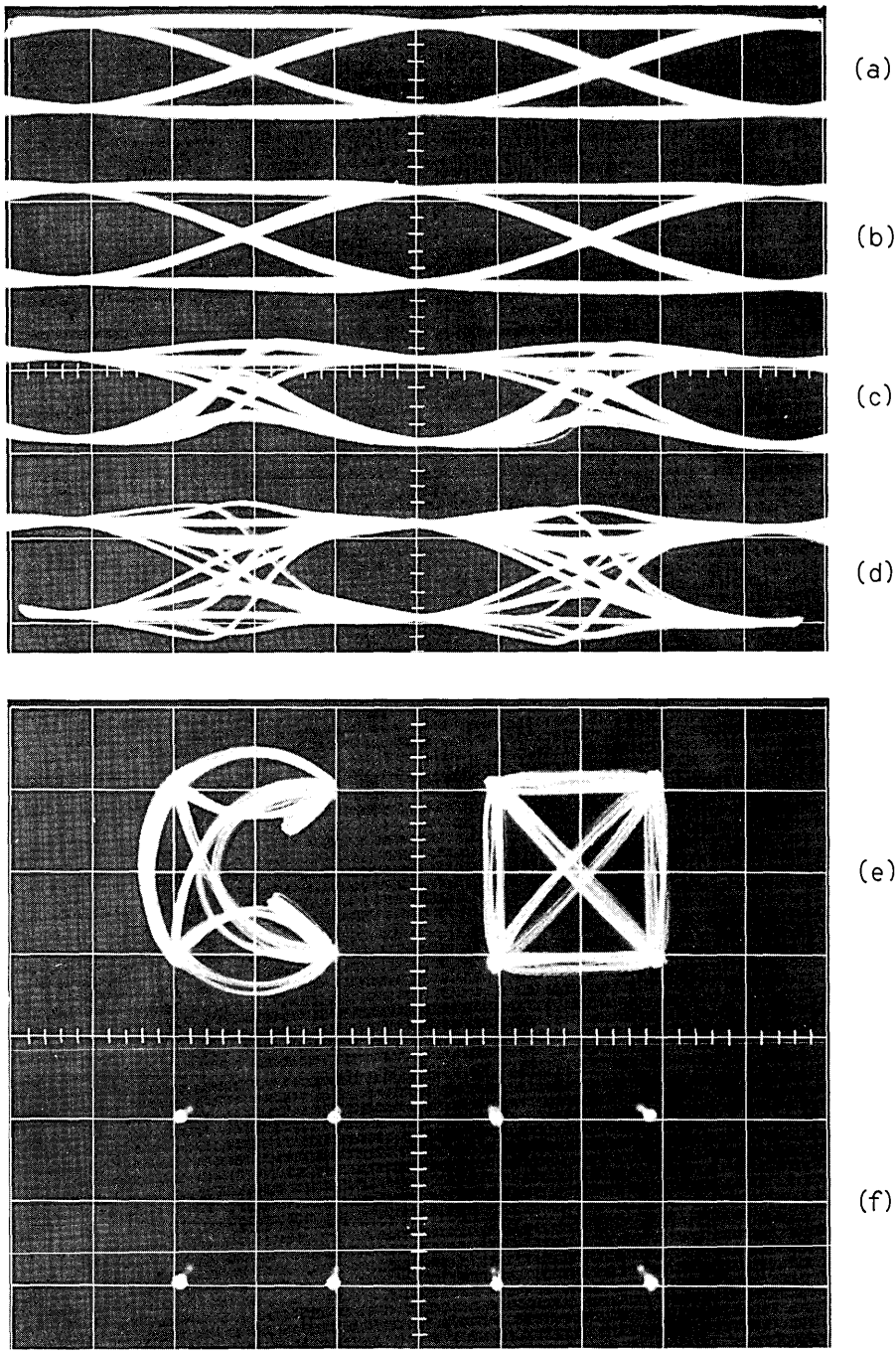

Fig. 5—Four-phase eye patterns: (a) Q coherent; (b) I coherent; (c) Q differential; (d) I differential; (e) polar plots, l. to r., differential, coherent; (f) polar plots intensified at sample time.

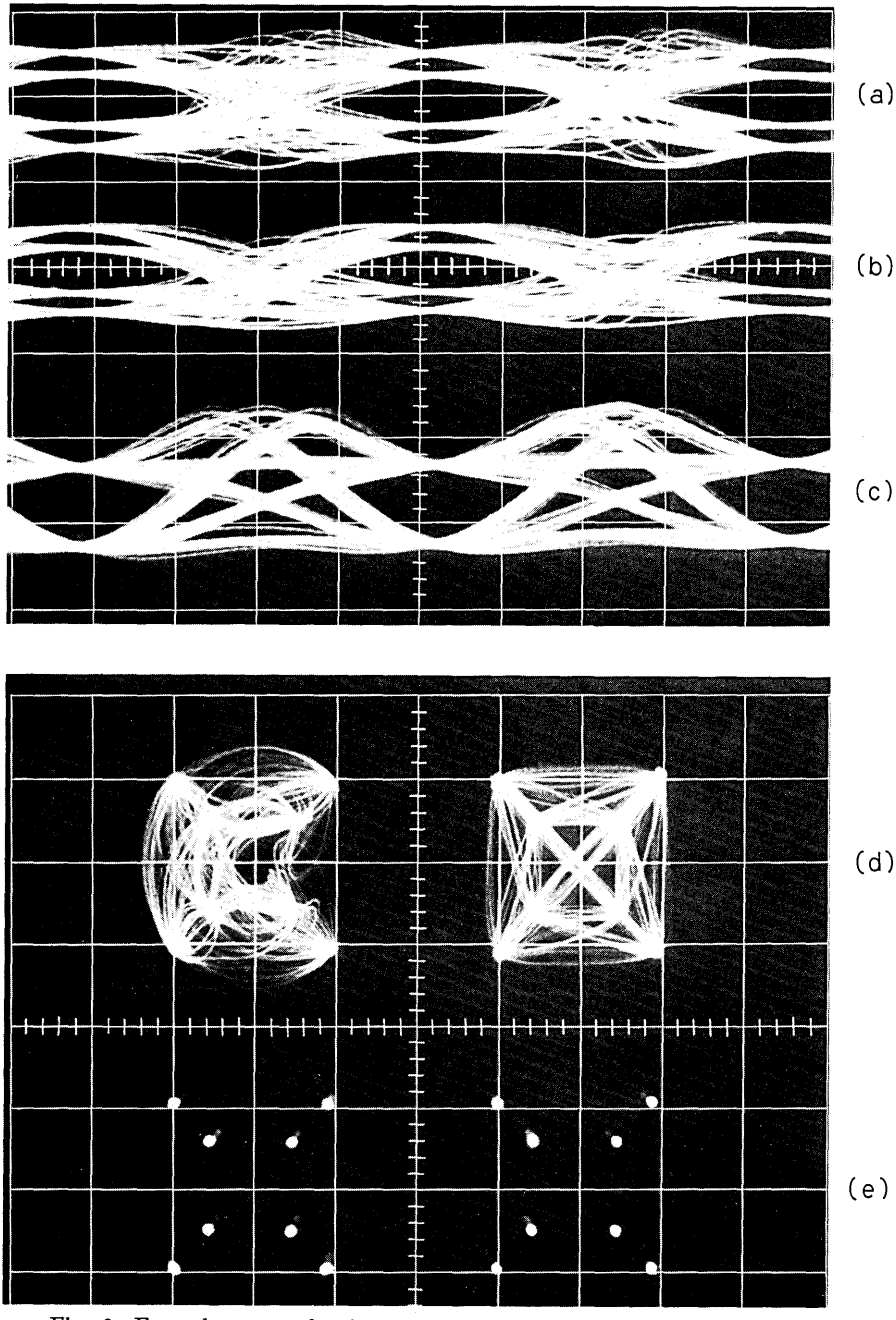

Fig. 6—Four-phase, two-level eye patterns: (a) I differential; (b) Q differential; (c) AM envelope; (d) polar plots, l. to r., differential, coherent; (e) polar plots intensified at sample time.

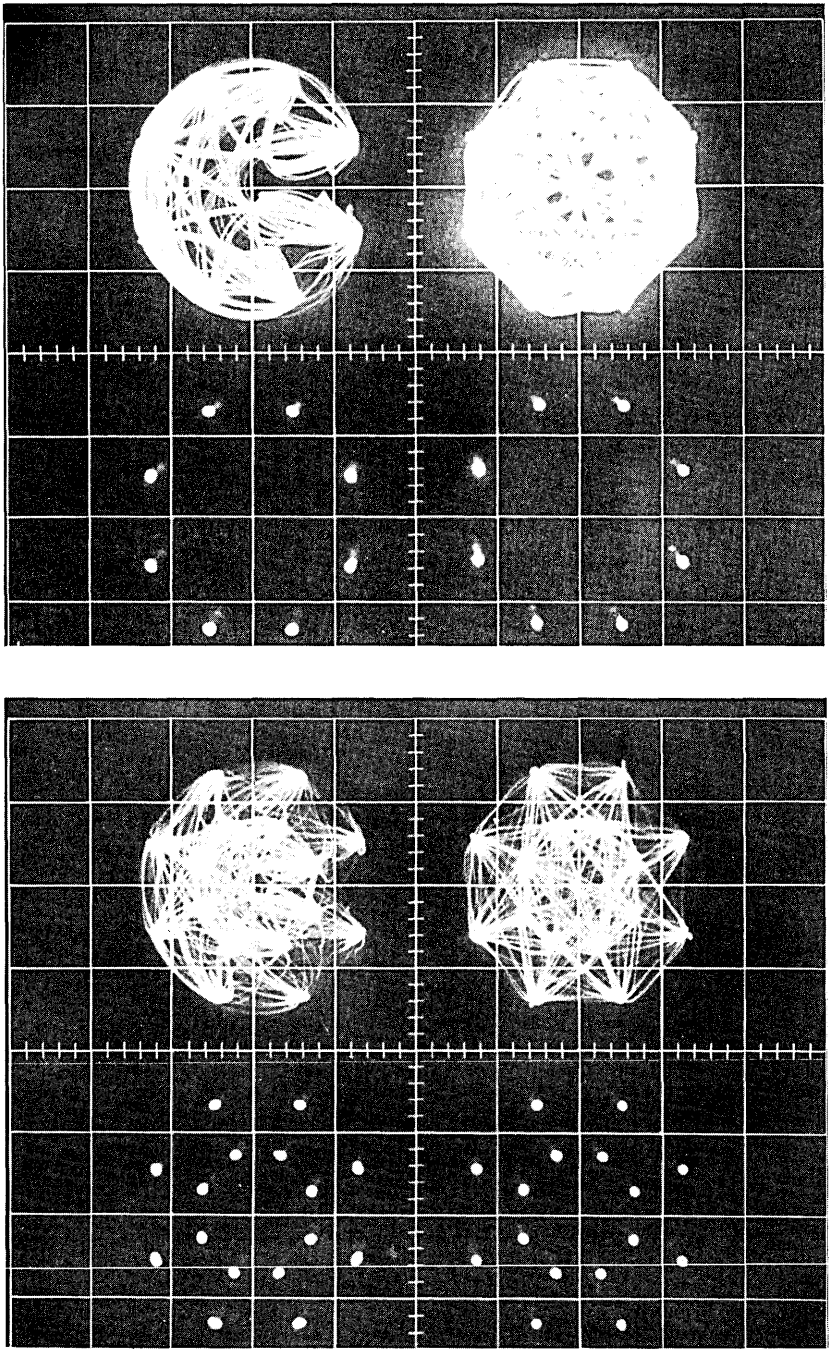

Fig. 7—(a) Eight-phase eye patterns; (b) Eight-phase, two-level eye patterns.

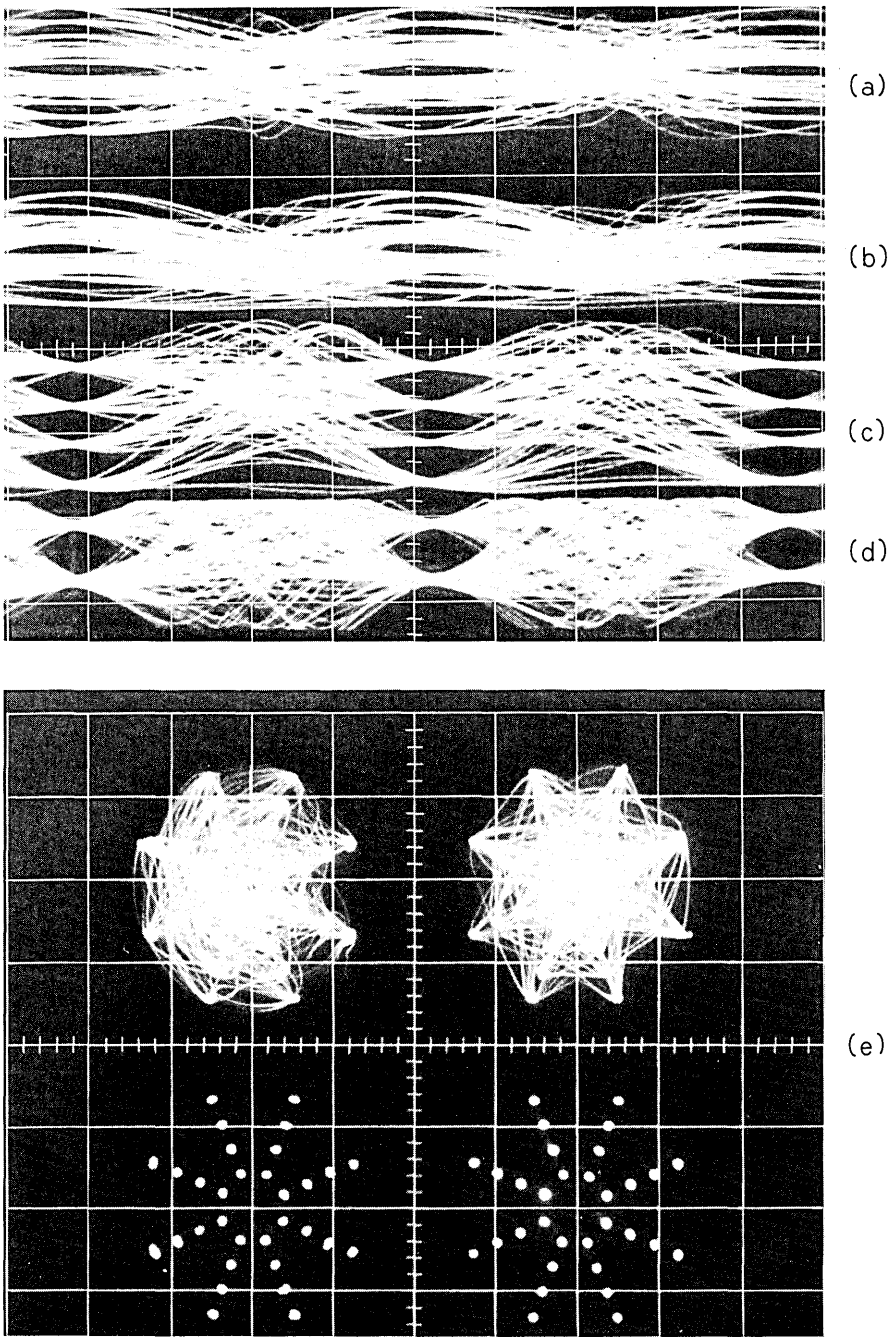

Fig. 8—Eight-phase, four-level eye patterns: (a) I differential; (b) Q differential; (c) AM envelope; (d) folded envelope; (e) polar plots.

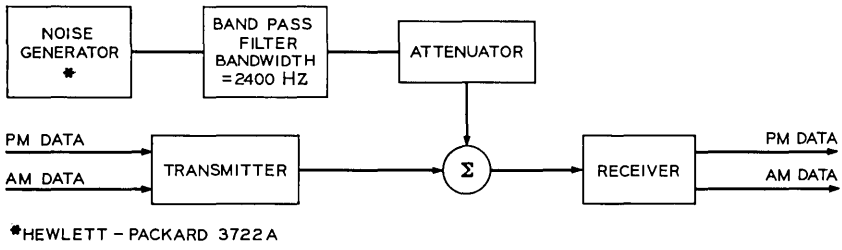

Fig. 9—Experimental configuration.

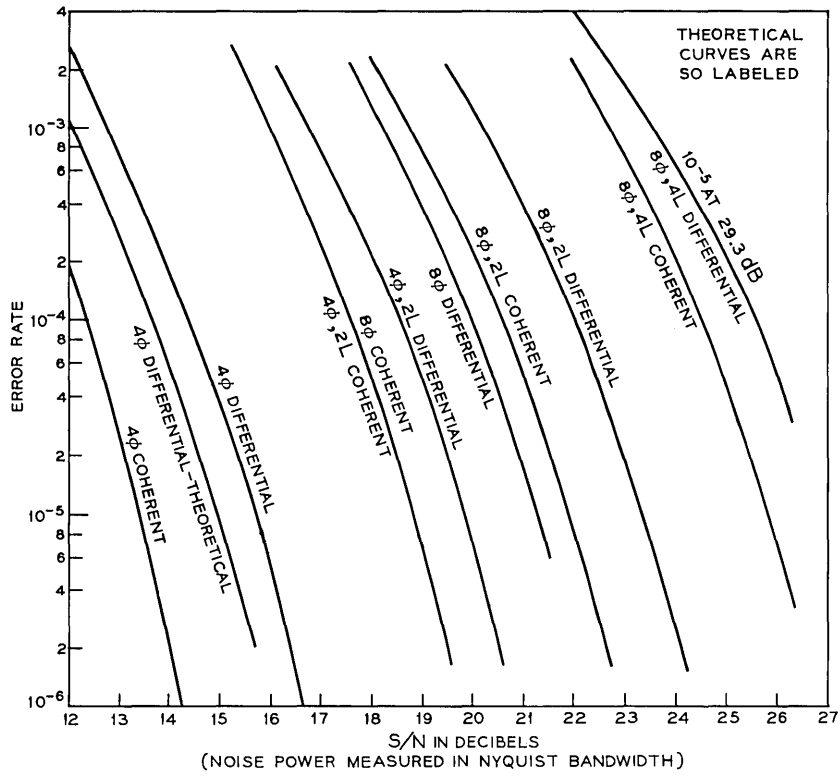

Fig. 10—Performance curves.

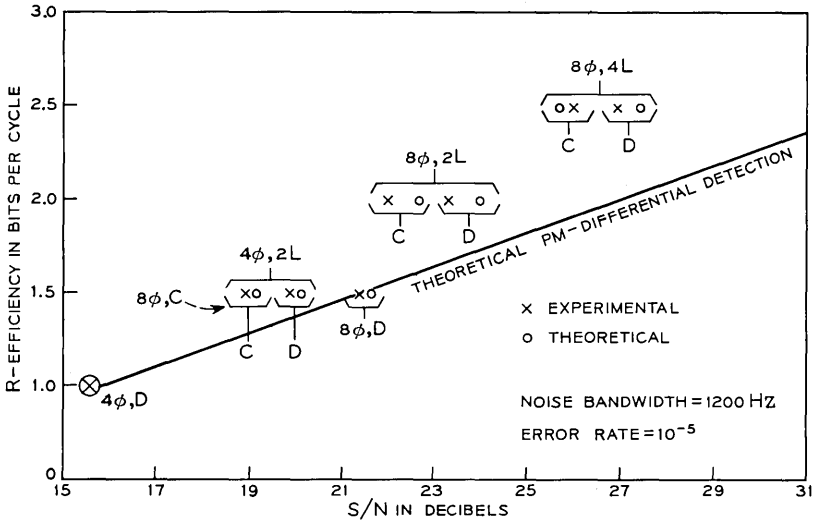

Fig. 11—Performance comparisons for noise impairment.

REFERENCES

1. Cahn, C. R., "Combined Digital Phase and Amplitude Modulation System," IRE Trans. Commun. Syst., *CS-8,* No. 3 (September 1960), pp. 150–155.
2. Hancock, J. C., and Lucky, R. W., "Performance of Combined Amplitude and Phase Modulated Communication Systems," IRE Trans. Commun. Syst., *CS-8,* No. 4 (December 1960), pp. 232–237.
3. Lucky, R. W., and Hancock, J. C., "On the Optimum Performance of N-ary Systems Having Two Degrees of Freedom," IRE Trans. Commun. Syst., *CS-10,* No. 2 (June 1962).
4. Leiter, M., and Talbot, M. P., Jr., "The Performance of Combined Phase and Amplitude Digital Data Communication Systems," MITRE Report MTP-65, September 1967.
5. Lucky, R. W., Salz, J., and Weldon, E. J., Jr., *Principles of Data Communication,* New York: McGraw-Hill Book Co., 1968.
6. Davey, J. R., "Digital Data Signal Space Diagrams," B.S.T.J., *43,* No. 6 (November 1964), pp. 2973–2983.

THE BELL SYSTEM TECHNICAL JOURNAL
Vol. 50, No. 7, September, 1971
Printed in U.S.A.

Crosstalk in Outside Plant Cable Systems

By G. J. FOSCHINI

(Manuscript received February 4, 1971)

A transmission model of outside plant wire pair cable systems is given. The model includes direct crosstalk within cable units and has been adapted for computer manipulation in the form of a voice-frequency simulation program. The program can simulate the terminal behavior of any coterminous system composed of a cascade of mixed gauges of pulp and PIC cables, load coils, and bridged taps. There is evidence that the simulation capability can provide useful estimates of direct, within unit, FEXT at least up to the high kilohertz frequency region. Factory data on capacitance unbalance are the essential data source for the crosstalk portion of the simulation program.

For many systems studies a nominally specified cable should be represented stochastically. In this development a Brownian motion process is used to model the stochastic behavior of the capacitance unbalance. The diffusion constants for the various pair-to-pair combinations of capacitance unbalance can be expressed in terms of cable geometry. The development of this expression using capacitance unbalance data forms a basis for selecting pair twist lengths.

I. INTRODUCTION

A transmission model of outside plant wire pair cable systems which includes direct crosstalk is developed here. We begin by presenting a deterministic model of outside plant systems by means of matrix representations of the various elements. The perturbation technique for handling pair-to-pair coupling is developed in detail. An adaptation of the model in the form of a simulation program is discussed and comparisons between simulations and experiments are made. A stochastic treatment of pair-to-pair capacitive coupling is given which is shown to lead to a method of optimal twist length selection.

We stress that the theory we present here has its origin in the work of others (see, for example, Ref. 1 through 4). The ideas of direct crosstalk and of treating capacitance unbalance as random functions with

a delta function covariance are familiar to those who have worked on crosstalk. We organize and extend available techniques in the direction of furnishing a suitable systems engineering model of crosstalk. The transformation of our model into a practical engineering tool extends the use of routine data on pair-to-pair capacitance unbalance that are taken at Western Electric's cable manufacturing locations on a daily basis.

II. OUTSIDE PLANT SYSTEMS—GENERAL

For simplicity we limit the discussion to an idealized version of the outside plant. We assume that a plant system is comprised of a cascade of passive n-port networks as depicted in Fig. 1.

These networks are primarily wire pair cables, although we include load coils, splices, and open circuited bridged taps. The objective is to be able to simulate the response of a broad class of outside plant systems to single-frequency excitations. We seek a programmed simulation capability that will enable the evaluation of crosstalk performance. The crosstalk performance (near end or far end) is usually expressed in the form of the cumulative distribution function of pair-to-pair crosstalk values. These cumulative distributions form the basis for answering a large class of systems engineering questions concerning crosstalk.

At this point in the development of this work only the stochastic nature of pair-to-pair capacitance unbalance is included. The effects of moisture, temperature, aging, externally generated noise, or manufacturing variability of other cable parameters are not considered. Active devices are also not included. For many problems involving active devices it is important to characterize the behavior of the passive portions of the plant that interconnect these devices. Furthermore, the technique we present for handling crosstalk appears to be extend-

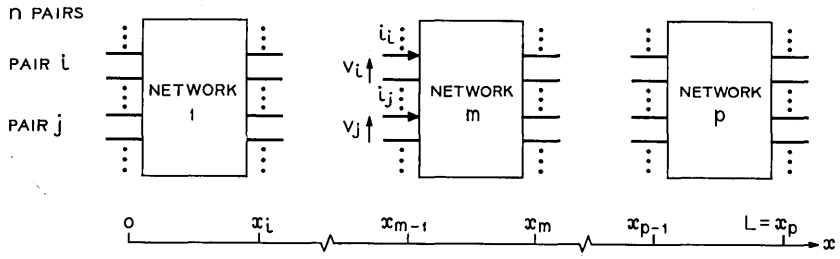

Fig. 1—A cascade of passive n-port networks.

ible to the problem of modeling variations in other cable parameters as will be indicated in the next section. However, the available data on the variability of other cable parameters is sparse and it is therefore premature to attempt to include these at this time in a numerical model.

The mathematical representation of the terminal behavior of these systems is generated from the solutions to the differential equations that characterize the physical laws that the constituent sybsystems obey, and the boundary relations that characterize the interaction between contiguous subsystems. In our model the system is characterized at each point in space (x) and time (t) by the vector of pair voltages $\mathbf{v}(x, t)$ and pair currents $\mathbf{i}(x, t)$. Thus longitudinal symmetry is implicitly assumed, that is, metallic mode propagation is not affected by any series or shunt primary constant unbalance. Each of the networks is described by a mathematically well behaved first-order homogeneous system of linear differential equations. We make the standard simplification of suppressing the time variable by restricting the excitations to be of the same frequency and in phase. The solution matrices to these differential equations with initial value equal to the identity matrix are ideally suited to cascaded structures. Following the terminology in 2-port network theory, we call this solution the *ABCD* chain matrix of the subsystem where

$$\begin{bmatrix} \mathbf{v}(x_m) \\ \mathbf{i}(x_m) \end{bmatrix} = \begin{bmatrix} A_m & B_m \\ C_m & D_m \end{bmatrix} \begin{bmatrix} \mathbf{v}(x_{m-1}) \\ \mathbf{i}(x_{m-1}) \end{bmatrix}.$$

It then follows that

$$\begin{bmatrix} \mathbf{v}(L) \\ \mathbf{i}(L) \end{bmatrix} = \prod_{k=1}^{p} \begin{bmatrix} A_{p+1-k} & B_{p+1-k} \\ C_{p+1-k} & D_{p+1-k} \end{bmatrix} \begin{bmatrix} \mathbf{v}(0) \\ \mathbf{i}(0) \end{bmatrix}$$

where the order of multiplication is important.

Generally when a system is specified there is some degree of uncertainty concerning its behavior. This uncertainty is modeled by assuming any chain matrix to be of the form $\mathsf{D} + \epsilon\mathsf{S}(\omega)$* where D is deterministic and $\mathsf{S}(\omega)$ is a matrix random process with zero mean. The parameter ϵ, which is called the perturbation coefficient, will be needed to facilitate our analysis. Since different system elements have different physical constants we unify the theory by treating these constants as parameters in the chain matrices. Thus the chain matrices are indexed over a set of parameter values and so they are stochastic processes.

* Here ω is used to indicate a random sample point not an angular frequency.

First we deal with the deterministic features of our systems. That is, we discuss features that are common to all realizations of these stochastic systems. Therefore, in the next section the fact that we are really dealing with stochastic subsystems is unimportant and is neglected.

III. THE PERTURBATION COEFFICIENT—ϵ

We express here the known fact that unwanted coupling between wire pairs in a cable system produces low-level interference on all pairs in proximity to an energized pair. The parameter $\epsilon > 0$ can be thought of as a scale to measure just how close a system is to an ideal one ($\epsilon = 0$) in which the pairs are uncoupled. We shall develop some simplifications that occur as ϵ tends to zero.

We begin by showing the central role of the perturbation coefficient in reducing the size of a cable crosstalk computation. An n-pair cable of length L is a linear passive bilateral $2n$-port network, and at any frequency it has a chain matrix ($ABCD$) characterization which we shall denote by $T(L)$

$$\begin{bmatrix} \mathbf{v}(L) \\ \mathbf{\imath}(L) \end{bmatrix} = T(L) \begin{bmatrix} \mathbf{v}(0) \\ \mathbf{\imath}(0) \end{bmatrix}, \tag{1}$$

where the v's and the $\imath$'s are the voltages and currents at the $2n$ ports of the network. We assume that $T(x)$ is defined by the matrix initial value problem

$$\frac{dT(x)}{dx} = -\begin{bmatrix} 0 & \mathbf{Z}(x) \\ \mathbf{Y}(x) & 0 \end{bmatrix} T(x) \quad \text{and} \quad T(0) = I, \tag{2}$$

where I is the identity matrix. The matrix $\mathbf{Z}(x)$ is a symmetrical $n \times n$ impedance matrix with entries that are continuous complex functions of the real variable x and whose diagonal terms are all equal and are denoted by z, which is a constant. Similarly for the admittance matrix $\mathbf{Y}(x)$. We write $\mathbf{Z}(x) = zI + \epsilon\boldsymbol{\zeta}(\mathbf{x})$ and $\mathbf{Y}(x) = yI + \epsilon\mathbf{n}(\mathbf{x})$ where $\boldsymbol{\zeta}(\mathbf{x})$ and $\mathbf{n}(\mathbf{x})$ have zero diagonals and z and y are constants with positive real and imaginary parts. Recall that ϵ is the perturbation coefficient.

We shall be interested in making crosstalk computations of the type where one pair in a cable is energized and the near-end voltages and far-end voltages on the other pairs are to be solved for. Using $T(L)$, the chain matrix characterization of the cable, and the boundary conditions, we obtain $2n$ equations with $2n$ unknowns. If there are 100 pairs in the cable we must invert a 200×200 complex matrix to solve for the crosstalk voltages. Practical considerations in inverting a

matrix of this size places the problem out of reach of the computer. We shall develop an approximation whereby the computation is decomposed into the inversion of 99, 4 × 4 matrices. This enables the calculation to be handled quite easily by the computer.

For simplicity in what follows we shall assume that at both ends the cable pairs are terminated in their "characteristic impedance" $Z_0 = \sqrt{z/y}$. Also we shall normalize by assuming that the energized pair is impressed with a voltage generator of voltage V ($\approx$ 2 volts) and an internal impedance Z_0 so that one volt is established across the terminals of the energized pair. We shall follow the convention that the near-end crosstalk $NEXT(i, j) = [v_j(0)/v_i(0)]$ and the far-end crosstalk $FEXT(i, j) = [v_j(L)/v_i(L)]$ denote the ratios of the voltage on pair j due to the disturbing voltage on pair i at the cable terminals.

Using the boundary relations and substituting into equation (1) we can obtain the equations for $NEXT(i, j)$ and $FEXT(i, j)$.

Consider the hypothetical cable containing only two pairs whose defining equation is

$$\frac{d\hat{T}(x)}{dx} = -\begin{bmatrix} 0 & 0 & z & \epsilon\zeta_{ij}(x) \\ 0 & 0 & \epsilon\zeta_{ij}(x) & z \\ y & \epsilon\eta_{ij}(x) & 0 & 0 \\ \epsilon\eta_{ij}(x) & y & 0 & 0 \end{bmatrix} \hat{T}(x) \quad \text{and} \quad \hat{T}(0) = I.$$

If pair i is energized the equation for the crosstalk on pair j becomes

$$v_i(L)\begin{bmatrix} 1 \\ F\hat{E}XT(i, j) \\ 1/Z_0 \\ F\hat{E}XT(i, j)/Z_0 \end{bmatrix} = \hat{T}(L)\begin{bmatrix} 1 \\ N\hat{E}XT(i, j) \\ (V - 1)/Z_0 \\ -N\hat{E}XT(i, j)/Z_0 \end{bmatrix}. \tag{3}$$

The hatted variables $N\hat{E}XT(i, j)$ and $F\hat{E}XT(i, j)$ are called direct crosstalks. The direct crosstalk which considers only the existence of pairs i and j in the cable and the crosstalk which considers the existence of all n-pairs in the cable are asymptotically equivalent as is shown in the appendix. That is,

$$\lim_{\epsilon \to 0} \frac{N\hat{E}XT(i, j)}{NEXT(i, j)} = 1.$$

There is strong experimental evidence that in the systems of interest ϵ is so small that for most practical purposes asymptotic equivalence can be interpreted as equality.

Next we decompose the problem of determining a 4×4 matrix T into a problem of determining two 2×2 matrices. To accomplish this we introduce some artificial voltages and currents $V_1(x)$, $V_2(x)$, $I_1(x)$, and $I_2(x)$, via the following transformation, which we shall call P

$$\begin{bmatrix} V_1(x) \\ V_2(x) \\ I_1(x) \\ I_2(x) \end{bmatrix} = \begin{bmatrix} 1 & 1 & 0 & 0 \\ -1 & 1 & 0 & 0 \\ 0 & 0 & 1 & 1 \\ 0 & 0 & -1 & 1 \end{bmatrix} \begin{bmatrix} v_1(x) \\ v_2(x) \\ i_1(x) \\ i_2(x) \end{bmatrix}.$$

The above transformation maps the problem of two uniform coupled pairs to that of determining the chain matrices for two nonuniform but uncoupled pairs. The dependence of T on ϵ will be important now. So, since x is understood to be fixed at $L > 0$, we shall write $T(\epsilon)$ instead of $T(L)$. Letting $\tilde{T}(\epsilon)$ denote the chain matrix of the system of two uncoupled pairs we have $T(\epsilon) = P^{-1}\tilde{T}(\epsilon)P$. As a consequence $T(\epsilon)$ has the following form:

$$T(\epsilon) = \tfrac{1}{2}\begin{bmatrix} \mathsf{A}_1(\epsilon) + \mathsf{A}_2(\epsilon) & \mathsf{A}_1(\epsilon) - \mathsf{A}_2(\epsilon) & \mathsf{B}_1(\epsilon) + \mathsf{B}_2(\epsilon) & \mathsf{B}_1(\epsilon) - \mathsf{B}_2(\epsilon) \\ \mathsf{A}_1(\epsilon) - \mathsf{A}_2(\epsilon) & \mathsf{A}_1(\epsilon) + \mathsf{A}_2(\epsilon) & \mathsf{B}_1(\epsilon) - \mathsf{B}_2(\epsilon) & \mathsf{B}_1(\epsilon) + \mathsf{B}_2(\epsilon) \\ \mathsf{C}_1(\epsilon) + \mathsf{C}_2(\epsilon) & \mathsf{C}_1(\epsilon) - \mathsf{C}_2(\epsilon) & \mathsf{D}_1(\epsilon) + \mathsf{D}_2(\epsilon) & \mathsf{D}_1(\epsilon) - \mathsf{D}_2(\epsilon) \\ \mathsf{C}_1(\epsilon) - \mathsf{C}_2(\epsilon) & \mathsf{C}_1(\epsilon) + \mathsf{C}_2(\epsilon) & \mathsf{D}_1(\epsilon) - \mathsf{D}_2(\epsilon) & \mathsf{D}_1(\epsilon) + \mathsf{D}_2(\epsilon) \end{bmatrix},$$

where the matrices

$$\begin{bmatrix} \mathsf{A}_i(\epsilon) & \mathsf{B}_i(\epsilon) \\ \mathsf{C}_i(\epsilon) & \mathsf{D}_i(\epsilon) \end{bmatrix} \qquad i = 1, 2$$

are the $ABCD$ matrices for the nonuniform lines without coupling. Figures 2a and 2b portray the transformation in detail. So $\mathsf{A}_2(\epsilon) = \mathsf{A}_1(-\epsilon)$, $\mathsf{B}_2(\epsilon) = \mathsf{B}_1(-\epsilon)$, $\mathsf{C}_2(\epsilon) = \mathsf{C}_1(-\epsilon)$, and $\mathsf{D}_2(\epsilon) = \mathsf{D}_1(-\epsilon)$. Using the definition of derivative we obtain that for ϵ sufficiently small

$$T(\epsilon) \approx \begin{bmatrix} \mathsf{A}_1(0)I & \mathsf{B}_1(0)I \\ \mathsf{C}_1(0)I & \mathsf{D}_1(0)I \end{bmatrix} + \epsilon \begin{bmatrix} \mathsf{A}_1'(0)J & \mathsf{B}_1'(0)J \\ \mathsf{C}_1'(0)J & \mathsf{D}_1'(0)J \end{bmatrix},$$

where

$$J = \begin{bmatrix} 0 & 1 \\ 1 & 0 \end{bmatrix}.$$

This formula is particularly useful for generating the linear approximation to the $T(\epsilon)$ matrix for the case of constant coupling, that is, the case when $\eta(x)$ and $\zeta(x)$ are constant functions. The matrix is as follows, with $\Gamma = \sqrt{zy}$,

$$\begin{bmatrix} \cosh \Gamma L & -\epsilon \dfrac{(Z_0\eta + Z_0^{-1}\zeta)L}{2} \sinh \Gamma L & -Z_0 \sinh \Gamma L & \epsilon Z_0 \left(\dfrac{(Z_0^{-1}\zeta + Z_0\eta)L}{2} \cosh \Gamma L - \dfrac{(\eta Z_0 - Z_0^{-1}\zeta)L}{2\Gamma L} \sinh \Gamma L \right) \\ -\epsilon \dfrac{(Z_0\eta + Z_0^{-1}\zeta)L}{2} \sinh \Gamma L & \cosh \Gamma L & \epsilon Z_0 \left(\dfrac{(Z_0^{-1}\zeta + Z_0\eta)L}{2} \cosh \Gamma L - \dfrac{(\eta Z_0 - Z_0^{-1}\zeta)L}{2\Gamma L} \sinh \Gamma L \right) & -Z_0 \sinh \Gamma L \\ -\dfrac{1}{Z_0} \sinh \Gamma L & \epsilon \dfrac{1}{Z_0} \left(\dfrac{(Z_0\eta + Z_0^{-1}\zeta)L}{2} \cosh \Gamma L + \dfrac{(\eta Z_0 - Z_0^{-1}\zeta)L}{2\Gamma L} \sinh \Gamma L \right) & \cosh \Gamma L & -\epsilon \dfrac{(Z_0\eta + Z_0^{-1}\zeta)L}{2} \sinh \Gamma L \\ \epsilon \dfrac{1}{Z_0} \left(\dfrac{(Z_0\eta + Z_0^{-1}\zeta)L}{2} \cosh \Gamma L + \dfrac{(\eta Z_0 - Z_0^{-1}\zeta)L}{2\Gamma L} \sinh \Gamma L \right) & -\dfrac{1}{Z_0} \sinh \Gamma L & -\epsilon \dfrac{(Z_0\eta + Z_0^{-1}\zeta)L}{2} \sinh \Gamma L & \cosh \Gamma L \end{bmatrix} \cdot \tag{4}$$

For the case when $\eta(x)$ and $\zeta(x)$ are arbitrary continuous functions we obtain the following linear approximation to $T(\epsilon)$

$$\begin{bmatrix} \cosh \Gamma L & 0 & -Z_0 \sinh \Gamma L & 0 \\ 0 & \cosh \Gamma L & 0 & -Z_0 \sinh \Gamma L \\ -\dfrac{\sinh \Gamma L}{Z_0} & 0 & \cosh \Gamma L & 0 \\ 0 & -\dfrac{\sinh \Gamma L}{Z_0} & 0 & \cosh \Gamma L \end{bmatrix}$$

$$\cdot \begin{bmatrix} 1 & -\epsilon \displaystyle\int_0^L \frac{(\eta(x)Z_0 - \zeta(x)Z_0^{-1})}{2} \sinh 2\Gamma x \, dx & 0 & \epsilon Z_0 \displaystyle\int_0^L (Z_0\eta(x) \sinh^2 \Gamma x - Z_0^{-1}\zeta(x) \cosh^2 \Gamma x) \, dx \\ -\epsilon \displaystyle\int_0^L \frac{(\eta(x)Z_0 - \zeta(x)Z_0^{-1})}{2} \sinh 2\Gamma x \, dx & 1 & \epsilon Z_0 \displaystyle\int_0^L (Z_0\eta(x) \sinh^2 \Gamma x - Z_0^{-1}\zeta(x) \cosh^2 \Gamma x) \, dx & 0 \\ 0 & -\dfrac{\epsilon}{Z_0} \displaystyle\int_0^L (Z_0\eta(x) \cosh^2 \Gamma x - Z_0^{-1}\zeta(x) \sinh^2 \Gamma x) \, dx & 1 & \epsilon \displaystyle\int_0^L \frac{(\eta(x)Z_0 - \zeta(x)Z_0^{-1})}{2} \sinh 2\Gamma x \, dx \\ -\dfrac{\epsilon}{Z_0} \displaystyle\int_0^L (Z_0\eta(x) \cosh^2 \Gamma x - Z_0^{-1}\zeta(x) \sinh^2 \Gamma x) \, dx & 0 & \epsilon \displaystyle\int_0^L \frac{(\eta(x)Z_0 - \zeta(x)Z_0^{-1})}{2} \sinh 2\Gamma x \, dx & 1 \end{bmatrix}. \tag{5}$$

Substituting this evaluation of $T(\epsilon)$ into equation (3) and solving for the linear approximations to the crosstalks yields the classical formula

$$N\hat{E}XT(i, j) \approx -\epsilon \int_0^L \frac{(Z_0\eta(x) - Z_0^{-1}\zeta(x))}{2} e^{-2\Gamma x}\, dx$$

$$F\hat{E}XT(i, j) \approx -\epsilon \int_0^L \frac{(Z_0\eta(x) + Z_0^{-1}\zeta(x))}{2}\, dx.$$

In this section we have achieved a canonical representation of coupled pairs in a cable. Our representation is complete enough to permit pair-to-pair crosstalk calculations to be made, but our representations are approximate. We have not developed any analytical relationships between the magnitude of errors involved and ϵ. Pragmatically we have not had any need for such relationships as we have been able to rely on experimental verification of our assumptions.

The structure of the cable chain matrix that we have developed expedites the determination of the chain matrix experimentally using

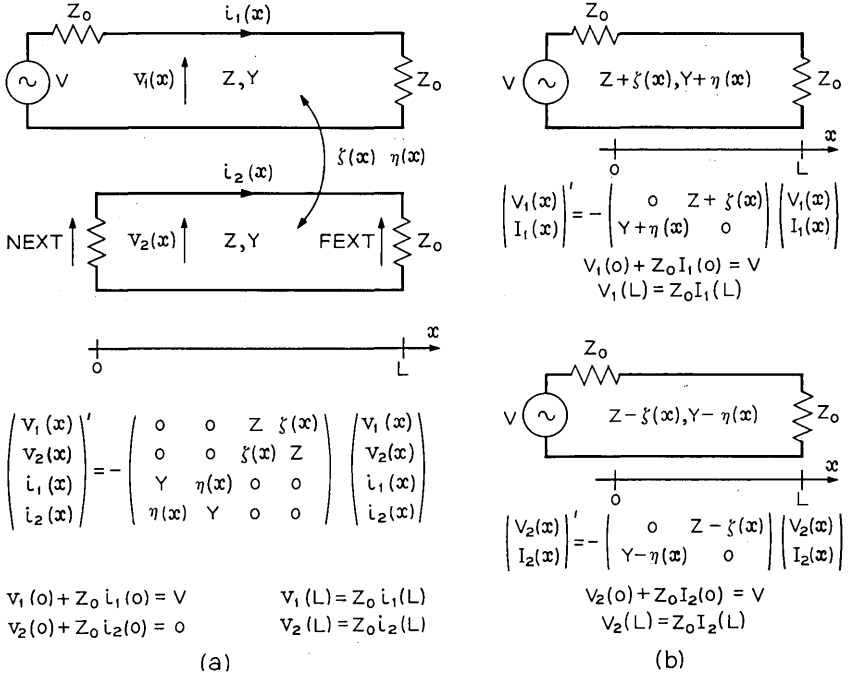

Fig. 2a—Two identical coupled transmission lines and their characterizing equations.

Fig. 2b—Two nonuniform uncoupled transmission lines and their characterizing equations.

a generalized open circuit–short circuit technique. Specifically each of the A, B, C, and D matrices has the form of a perturbation of some nonzero multiple of the identity. A straightforward generalization of the classical open circuit–short circuit technique, capitalizing on the approximation that can be made in inverting a matrix of the aforementioned form, makes for a simple determination of the A, B, C, and D matrices. Since the experimental technique is straightforward we shall not discuss it further.

In this section we have discussed crosstalk computations for a single cable. The extension to a cascade of cables is straightforward. We need only modify (3) by replacing $T(L)$ by the ordered product $\prod_{k=1}^{p} T_{p-k+1}$ and Z_0 can be replaced by possibly distinct impedances at $x = 0$ and $x = L$. In the Appendix we have proven asymptotic equivalence in a special case of a single cable. (We spare the reader the general proof for cable systems.) We shall use asymptotic equivalence of crosstalk and direct crosstalk for cable systems in the sections that follow. We note that if bridged taps are excluded the extension of the asymptotic equivalence to cable systems is immediate.

IV. SIMULATING THE PLANT AT VOICE FREQUENCIES

The first phase of the computer simulation of the outside plant has been limited to voice frequencies. The program generates the subsystem chain matrices and multiplies them together to get a realization of the $ABCD$ matrix for the system. The program can simulate an extensive class of coterminous systems; specifically, the loop can be comprised of any cascade of PIC cables, pulp cables, load coils, and bridge taps. Thus, given the termination impedances and excitations we can solve for any of the terminal voltages and currents. The important feature of the program is that it provides the capability to make crosstalk computations.

There were a number of reasons why we began the simulation effort with the voice plant. First the very vastness of the overall project of outside plant cable simulation dictates that one should begin by handling a somewhat self-contained portion of the project that could form the basis for future effort. The simplification that arises in dealing with voice plant makes it an attractive starting place as we now show.

Ostensibly the basis for the simulation of individual cables is equation (5). The chain matrices for load coils and bridge taps can be obtained from the matrix for the cable. We note that the entries of the

ABCD matrix depicted in equation (5), that involve pair-to-pair unbalances have the following form

$$\int_0^L [H_1(f, x)Z_0\eta(x) + H_2(f, x)Z_0^{-1}\zeta(x)]\, dx,$$

where the H_i are continuous complex hyperbolic functions. For any common set of cable parameters the $\zeta(x)$ term is negligible at voice frequencies ($f < 4000$ Hz). To help see why inductance unbalance can be neglected at voice frequencies we first note that for any of the cable pairs simulated, the absolute value of the characteristic impedance decreases by an order of magnitude in changing from its dc value to its high-frequency asymptote. Then by looking at the manner in which Z_0 appears in (5), or (4), we see that the capacitive coupling effect is accentuated while the inductive coupling effect is de-emphasized at voice frequencies. Hence in the voice band we need only consider

$$\int_0^L H_1(f, x)\eta(x)\, dx.$$

Replace the continuous function $H_1(f, x)$ by its average value $L^{-1}\int_0^L H_1(f, x)\, dx$ in the integral. By continuity we shall lose negligible accuracy so long as L is sufficiently small. For values of f in the voice band the actual cable section lengths between splices are sufficiently small. Hence the integral becomes

$$\int_0^L \left[\frac{1}{L}\int_0^L H_1(f, y)\, dy\right]\eta(x)\, dx = \left[\frac{1}{L}\int_0^L \eta(x)\, dx\right]\int_0^L H_1(f, y)\, dy.$$

So in effect we have replaced $\eta(x)$ by its average value. That is to say we can treat $\eta(x)$ as if it were a constant function. So equation (4) with $\zeta(x) = 0$ becomes the basic representation of cables in the voice band.

The function $\eta(x)$ has the form

$$\eta(x) = \sqrt{-1}\, 2\pi f c(x),$$

where $c(x)$ is the distributed capacitance unbalance. In an idealized situation where only two pairs are present, let 1′, 1″ and 2′, 2″ denote the wires in the first and second pairs, respectively; then we have from Ref. 1,

$$c(x) \approx \tfrac{1}{4}[c_{1'2'}(x) - c_{2'1''}(x) + c_{1''2''}(x) - c_{2''1'}(x)].$$

At voice frequencies the numerical values of a cable chain matrix can be obtained if the values of Γ, Z_0, and $\int_0^L c(x)\, dx$ are known. For quality

assurance, Western Electric undertakes a bridge measurement of $|\int_0^L c(x)\,dx|$ for various pair combinations in the cables that it manufactures. Thus we have the data necessary to compute these chain matrices at voice frequencies.

Another important reason for beginning with the simulation of voice plant is that there are several systems engineering studies for which voice plant crosstalk data is an essential ingredient. For example, the comparison of unigauge plant with existing plant, determining gain limitations for station sets, and evaluating the performance of PBX trunk circuits are some of the topics of interest where crosstalk performance, particularly near-end crosstalk performance, is important.

To test the program two 3000-foot sections of cable and a bank of load coils were measured for unbalance of capacitance and inductance respectively. The cables were spliced together first with and then without the load coils at the splice. The near-end crosstalk distributions were measured in both cases. The unbalance data along with the nominal values of primary constants for the cables and coils were fed to the program. Figures 3 and 4 depict the success of the simulation.

In most systems engineering studies, a cable's behavior is evaluated

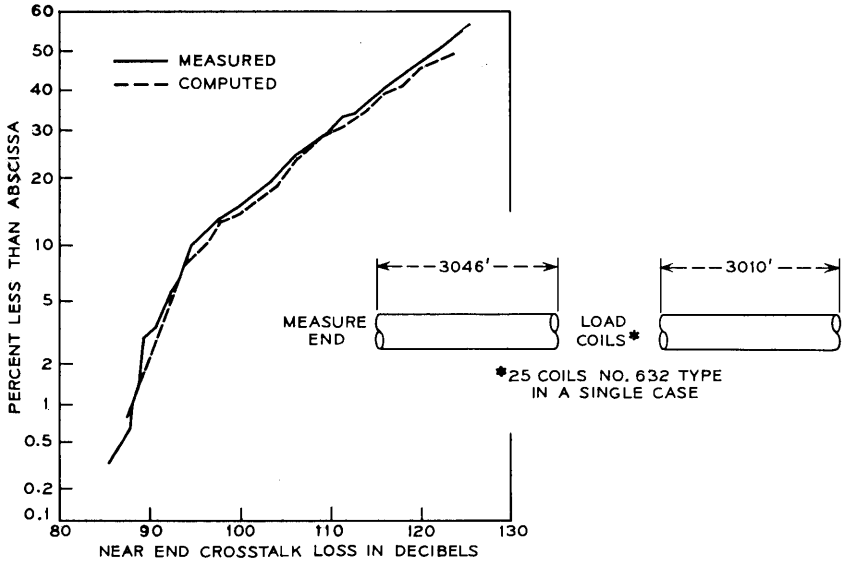

Fig. 3—Comparison of measured and computed distributions of 1-kHz within unit (25 pair) near-end crosstalk on 6065 feet of 26-gauge polyethylene cable (loaded, 600 Ω termination). (On normal probability paper.)

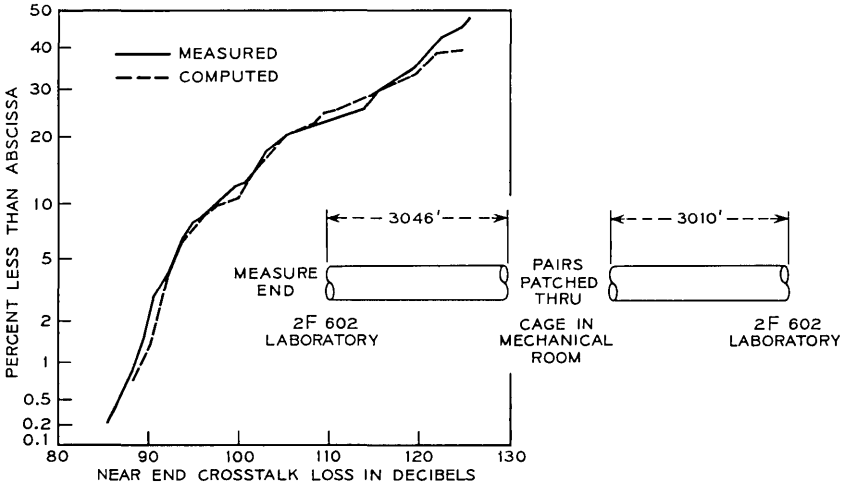

Fig. 4—Comparison of measured and computed distributions of 1-kHz within unit (25 pair) near-end crosstalk on 6065 feet of 26-gauge polyethylene cable (non-loaded, 600 Ω termination). (On normal probability paper.)

from a combination of nominally specified transmission constants and empirically derived crosstalk estimates. We are striving to utilize more of a cable's inherent communication capacity and so a more detailed description of cable crosstalk behavior is needed. By modeling the stochastic nature of cable crosstalk we get a pertinent refinement of the crosstalk evaluation capability. In this section we indicate the reason why crosstalk should be treated stochastically. We give a heuristic technique for simulating this stochastic behavior at voice frequencies.

For convenience we order the array of pair-to-pair capacitance unbalances $\{\int_0^L c_{ij}(x)\,dx;\ i = 2, 3, \cdots, n,\ i < j\}$ to form a vector $\mathbf{C}(L)$. We have limited $i < j$ since $c_{ii}(x) = c_{ji}(x)$. Ample Western Electric quality assurance data on capacitance unbalance are on file. Data are available on all types of cables from all Western cable manufacturing plants going back many years.

To provide a voice plant crosstalk simulation capability we need data on $\mathbf{C}(L)$ for all the kinds of cable involved in the outside plant. The information concerning a cable that is usually available to the systems engineer is the pair size, gauge, mutual capacitance, insulation, and length. A review of quality assurance capacitance unbalance data shows that the values of $\mathbf{C}(L)$ for cables meeting the same nominal specification are not identical. Thus we see the need to treat $\mathbf{C}(L)$ as a stochastic process $\mathbf{C}(L, \omega)$ where ω indexes the sample space Ω.

Next we discuss how representative quality assurance data were selected for simulation purposes.

The vector $\mathbf{C}(L, \omega)$ has signs associated with its components as will be explained in the next section. The quality assurance samples of $\mathbf{C}(L, \omega)$ are unsigned. Some special measurements on signed values of $\mathbf{C}(L, \omega)$ were made and it was concluded that $\mathbf{C}(L, \omega)$ could be assumed to have mean $\mathbf{0}$. For simulation purposes the quality assurance data were randomly signed with equal probability of being positive or negative. (Thus we are implicitly assuming that the components of $\mathbf{C}(L, \omega)$ are symmetrically distributed. This assumption is consistent with the detailed model of capacitance unbalance in the sequel. Of course the accuracy of the simulation ultimately tests our assumptions.)

Another shortcoming of the quality assurance data is that for cable units in excess of 25 pairs a biased sampling of the capacitance unbalance values is taken. Only certain pair combinations that are prone to high capacitance unbalance are measured. So the data needed for simulation are incomplete. Techniques can be developed for determining the parameters of the true distributions from the biased samples. Because of the difficulty involved with such techniques it was decided to approximate units of 50 and 100 pairs as combinations of 25-pair units. Because of this approximation the pair combinations prone to high crosstalk loss are not correctly modeled. This is of no consequence since it is the distribution of the values of low crosstalk loss that we seek. The degree of success of a simulation of one of the field experiments on in-place cables in Scranton, Pennsylvania, is depicted by Fig. 5. Finally, to use the data, the individual capacitance values are adjusted for length according to a square-root correction factor. The square-root correction factor is well known; it has been verified experimentally and will be discussed further in the next section.

For each type of cable several capacitance unbalance matrices are necessary since several sections of a single type of cable may be used in one system. Capacitance unbalance data on 19-, 22-, 24-, and 26-gauge pulp insulated cable and 22-, 24-, and 26-gauge PIC cable were obtained. The data spanned a 1-year period at the Western Electric Plant in Hawthorne, Illinois, and at least 25 reels of each type of cable were represented in the data. The annual interval is particularly significant for pulp data since the capacitance unbalance is sensitive to the humidity at the time of manufacture. An analysis of the data substantiated the view that the pulp capacitance unbalance is not a function of gauge.

To use a square-root length correction on the data means that, given

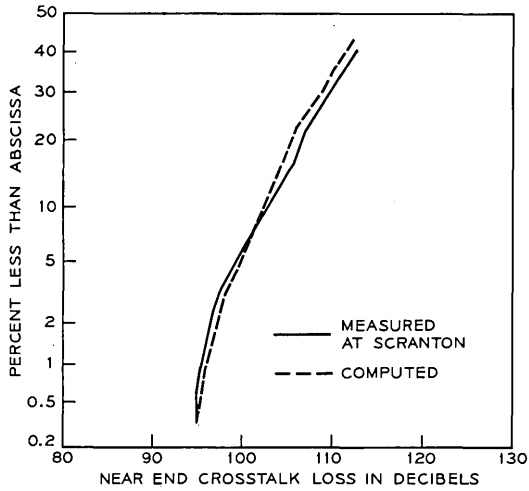

Fig. 5—Comparison of measured and computed 1-kHz within unit (50 pair) near-end crosstalk on 2800 feet of 22-gauge pulp cable (600 Ω termination). Two 19-gauge, 25-pair pulp units were used in the computer simulation of the 50-pair unit. (On normal probability paper.)

a sample $\mathbf{C}(L, \omega)$, to get a sample of $\mathbf{C}(l, \omega)$ we multiply $\mathbf{C}(L, \omega)$ by $\sqrt{l/L}$. As we mentioned, the data was randomly signed and a pulp, PIC distinction was maintained while a gauge distinction within pulp was not acknowledged. The problem remained of providing separate sequences of capacitance tables for pulp and for PIC cables. The problem was resolved differently for pulp than for PIC. In both cases a distribution, called a universal distribution, was constructed by pooling accumulated data from over 25 cables. For pulp a typical cable was modeled by using a set of 300 pair-to-pair capacitance unbalance values whose distribution matched the universal distribution. Numerous shuffled copies of the list of 300 values were prepared to enable modeling of randomly spliced pulp sections. Since PIC is spliced color to color the procedure used to represent pulp was not valid for PIC. For each PIC gauge the tables were sequenced to give the most representative distributions priority in selecting tables for a simulation study. In comparing the individual distributions to the universal distribution particular emphasis was given to the fit of the high capacitance tail. The simulation scheme provides for placing the most representative distributions at the near end in order to assure the most representative estimates of near-end crosstalk.

The formulas used for *NEXT* and *FEXT* were obtained as follows. Let $\{T_i\}$ $i = 1, 2, \cdots, k$ represent the chain matrices of k subsystems ordered so that T_1 is at what we shall arbitrarily call the near end and T_k is at the far end. Thus the terminal behavior of the system is described by $T = T_k T_{k-1} \cdots T_1$. Let $\mathbf{n} = (\eta_1, \eta_2, \cdots, \eta_k)^t$ be a vector such that η_i is the coupling in the ith subsystem. Recall that the A, B, C, and D submatrices of T_i contain η_i in the off-diagonal positions only. Neglecting quadratic terms and higher in the η_i variables we obtain

$$T \approx \begin{bmatrix} a_1 & a_2 & b_1 & b_2 \\ a_2 & a_1 & b_2 & b_1 \\ c_1 & c_2 & d_1 & d_2 \\ c_2 & c_2 & d_2 & d_1 \end{bmatrix} \triangleq$$

$$\prod_{i=1}^{k} \begin{bmatrix} a_1^{(i)} I & b_1^{(i)} I \\ c_1^{(i)} I & d_1^{(i)} I \end{bmatrix}$$

$$+ \sum_{i=1}^{k} \eta_i \left(\prod_{m=1}^{i-1} \begin{bmatrix} a_1^{(m)} I & b_1^{(m)} I \\ c_1^{(m)} I & d_1^{(m)} I \end{bmatrix} \right) \begin{bmatrix} a_2^{(i)} J & b_2^{(i)} J \\ c_2^{(i)} J & d_2^{(i)} J \end{bmatrix} \left(\prod_{m=i+1}^{k} \begin{bmatrix} a_1^{(m)} I & b_1^{(m)} I \\ c_1^{(m)} I & d_1^{(m)} I \end{bmatrix} \right).$$

Let us assume that the near end is terminated in an impedance z_S and that the far end is terminated in an impedance z_R . Using the boundary conditions we obtain

$$v_1(L) \begin{bmatrix} 1 \\ FEXT \\ \dfrac{1}{z_R} \\ \dfrac{FEXT}{z_R} \end{bmatrix} = T \begin{bmatrix} 1 \\ NEXT \\ \dfrac{V-1}{z_S} \\ \dfrac{-NEXT}{z_S} \end{bmatrix}.$$

Solving and neglecting quadratic terms in the variable with a subscript 2 we obtain

$$NEXT \approx \left[\frac{b_2 - z_R d_2}{b_1 - z_R d_1} - \frac{z_S a_2 - b_2 - c_2 z_S z_R + d_2 z_R}{z_S a_1 - b_1 - c_1 z_S z_R + d_1 z_R} \right]$$

and

$$FEXT \approx \left[(a_1 d_2 - a_2 d_1 - b_2 c_1 - b_1 c_2) - \frac{z_S a_2 - b_2 - c_2 z_S z_R + d_2 z_R}{z_S a_1 - b_1 - c_1 z_S z_R + d_1 z_R} \right].$$

If the system does not contain bridged taps then the parenthetic term in the expression for *FEXT* can be neglected. Since we have neglected higher order terms both *NEXT* and *FEXT* are linear in **n**. We are led to introduce **N** and **F** such that

$$NEXT = \langle \mathbf{n}, \mathbf{N} \rangle \quad \text{and}$$

$$FEXT = \langle \mathbf{n}, \mathbf{F} \rangle.$$

In our simulation studies the system description yields the information necessary to determine **N** and **F** and the sample space of **n**. We randomly select enough **n** vectors and form the scalar products to determine the statistics of *NEXT* and *FEXT*.

V. THE STOCHASTIC NATURE OF A CABLE AND OPTIMAL TWIST LENGTH SELECTION

In the previous section it was mentioned that the nominal specification of a cable leaves its behavior somewhat uncertain. It followed that the class of cables that meet a nominal specification has different chain matrix representations. Here we present a model for this stochastic behavior of the chain matrices. Specifically we deal only with the coupling terms in these matrices and the other terms are assumed to be constants.*

A Gaussian process $X(t, \omega)$ with zero mean and covariance $k^2 \times \min(t_1, t_2)$ is called a Brownian Motion or Wiener Process. If $X(0, \omega) = 0$ with probability one the process is said to be centered.

The process was first used to model the motion of a particle in a fluid where $X(t, \omega)$ is one of the displacement coordinates after time t and ω indexes over all particles. The number k is called the diffusion constant. This constant is a measure of the tendency of a particle to stray from its initial position.

In what follows we shall concentrate on capacitance but analogous statements are to be applied to inductance as well. Let $c_{ij}(x, \omega)$ represent the capacitance coupling function between pair i and pair j. Let $C_{ij}(x, \omega)$ represent the accumulated capacitance, that is, let

$$C_{ij}(x, \omega) = \int_0^x c_{ij}(\xi, \omega)\, d\xi.$$

*The model we present is intended for standard PIC and pulp cable designs and should not be applied to highly precision engineered cables wherein determinism would play a more significant role than we allow here.

Here ω indexes over all realizations of a cable of a particular type. We shall model the accumulated capacitance unbalance $C_{ij}(x, \omega)$ by treating it as a sample function of a Brownian Motion process. This is an approximation that was reached after considering the manufacturing process and after reviewing quality assurance records on accumulated capacitance unbalance data. The model is in agreement with the empirically established correction of a 10-dB translation of *FEXT* distributions for a tenfold increase in cable length.

In our application, distance plays the role of time. Therefore, the coupling terms in the cable matrix can be viewed as stochastic integrals of the form $\int_0^L H(x)\, dC(x, \omega)$. When $\int_0^L c(x, \omega)\, dx$ is a Brownian Motion process the stochastic integral* is called a linearly conditioned Brownian Motion process. The matrix of stochastic integrals is a multivariate, centered, linearly conditioned Brownian Motion process.

The capacitance unbalance function $c_{ij}(x, \omega)$ represents an effective distributed capacitance. It is a mathematically simple idealization which attempts to include the effects of all the capacitive coupling between pair i and pair j. The strongest contribution to this coupling function is believed to arise from the capacitances between each wire of pair i and each wire of pair j. The net effect of these four capacitances is expressed as a difference of nearly equal quantities. This difference can be positive or negative at x depending on the geometric relationship of the pairs at x. The pairs are twisted with different twist lengths in an attempt to cause the coupling capacitance to be positive as much as it is negative.

Presently available data is in the form of samples of $\left| \int_0^L c(x, \omega)\, dx \right|$ where only one value of L is associated with each ω. This provides no information pertaining to the covariance of $c(x, \omega)$ and so we make an assumption. Pair twist lengths are short (a few inches long) in comparison with the cable lengths of interest (thousands of feet). Thus in the light of our previous statements, it is reasonable to suggest that $c(x, \omega)$ be modeled as having a delta function covariance and this assumption is consistent with the Brownian motion model. From equation (5) we see that the coupling interacts with hyperbolic functions of Γx so that the assumption of a delta function covariance is most reasonable at voice frequencies where for the cables of interest the wavelengths are of the order of at least tens of miles.

There are many reasons to suspect that the capacitance unbalance function is an extremely irregular function when considered over thou-

* For a treatment of Brownian Motion and the stochastic integral concept see Ref. 5.

sands of feet. There are random disturbances that can change the function drastically over inches. For example, the vibrations of the cable manufacturing machinery, impurities or eccentricities in the insulation, tertiary coupling paths, slipping of the twist, etc. Furthermore the twist lengths are not precisely maintained. Thus, for cable lengths of interest (a thousand feet or so), it is quite reasonable to treat $\int_0^x c_{ij}(\xi, \omega)\, d\xi$ stochastically.

We are assuming that Var $C_{ij}(x, \omega) = k_{ij}^2 x$, where k_{ij} is a constant and x is the cable length. If we let $C(x, \omega)$ denote the random variable whose sample space is all pairs in cables of a particular type then Var $C(x, \omega)$ is simply the average of the individual variances, that is,

$$\text{Var } C(x, \omega) = \frac{1}{(n^2 - n)/2} \sum_{i<j} EC_{ij}^2 = \frac{L}{(n^2 - n)/2} \sum_{i<j} k_{ij}^2 .$$

So by pooling data on accumulated capacitance for all the different i, j combinations the data should still exhibit a variance which is linear with length.

Following the work reported here W. N. Bell has explored the accuracy and effectiveness of this Brownian motion model utilizing factory data. His conclusions (unpublished) are positive. Extensive data at two different lengths verified the linear dependence of Var $C(x, \omega)$ with length [Var $C(0, \omega) = 0$ at the third point]. Thus the use of the $\sqrt{L}$ correction of the data that was mentioned previously is indicated. The $C(x, \omega)$ are shown to be normal in the tails while in the neighborhood of the mean (0) the density is lower than normal and this is compensated for by an excess at zero. The departure from normality may be due to the measurement technique but the departure is unimportant since tail behavior is what concerns us. Furthermore if there really is an excess of zero capitances unbalances then the Brownian motion model is a slightly pessimistic one and hence useful in bounding system performance.

The diffusion constant k_{ij} appears to be an excellent way to express the capacitance unbalance of the pair combination. Furthermore, $\text{maximum}_{i,j}\, k_{ij}$ is a good measure of the capacitance unbalance of a cable. A statistical analysis of the quality assurance data reveals the relationship between k_{ij} and the twist lengths of pair i and pair j (t_i and t_j). The uncovering of this relationship provides a basis for optimal twist length selection. To demonstrate this idea W. N. Bell used quality assurance data on 145 25-pair PIC cable units to estimate the diffusion constants for the neighboring pair combinations. As suspected, the data revealed a strong relationship between the diffusion

constants and cable geometry. An extensive statistical analysis of this relationship was undertaken by A. K. Jain who determined that the formula

$$k_{ij}^2 L = \left[0.090 \times \frac{t_i^{0.62} t_j^{0.62}}{|\, t_i - t_j \,|^{0.23}}\right]^2 L \qquad (t_i \neq t_j)$$

(k_{ij} has dimensions of $pf/(ft)^{1/2}$.)

explained 79 percent of the total variation in the data. Besides establishing the relationship between the cable geometry and crosstalk performance, statistical analysis also provides an alternate means for simulating capacitance unbalance distributions for standard PIC and pulp cable designs.

As in the motion of particles in a liquid the mathematical model of Brownian motion is an approximation of the physical situation that must be applied discriminately. We stress this point since the continuity of $c_{ij}(x, \omega)$ was used to solve the differential equations that lead to the chain matrix while the mathematical model of Brownian motion does not account for this continuity. Thus while $c_{ij}(x, \omega)$ is sufficiently irregular so as to model its integral as Brownian Motion, it is smooth enough to be called continuous when expressing the physical laws that a cable must obey.

The inductance unbalance process ($\int_0^L l_{ij}(x, \omega)\, dx$) has not been studied. A small appreciation for how the inductance unbalance relates to the capacitance unbalance enables us to speculate that it is also a Brownian Motion process that is correlated with the capacitance process. Since both forms of unbalance derive from the cable geometry, it is reasonable to attempt to relate these unbalances. In our simulation program we neglect inductance unbalance since this neglect causes negligible error at voice frequencies. The frequency at which inductance unbalance causes an appreciable contribution to crosstalk remains to be determined.

A computer simulation of Scranton, Pennsylvania, field measurements of far-end crosstalk was made. In this case the distribution tails were nearly reproduced up to 775 kHz. At the higher frequencies it appears that the inductance unbalance is the cause of the departure between the measured and computed tails (see Fig. 6). Another simulation was made of three sets of factory far-end crosstalk measurements (3.15 MHz). In each case the computed tails were about 5 dB different from the measured tails due to inductance unbalance (see Fig. 7 where one of these cases is depicted). Figures 6 and 7 do indicate a significant correlation between 1 kHz capacitance unbalance and the crosstalk at

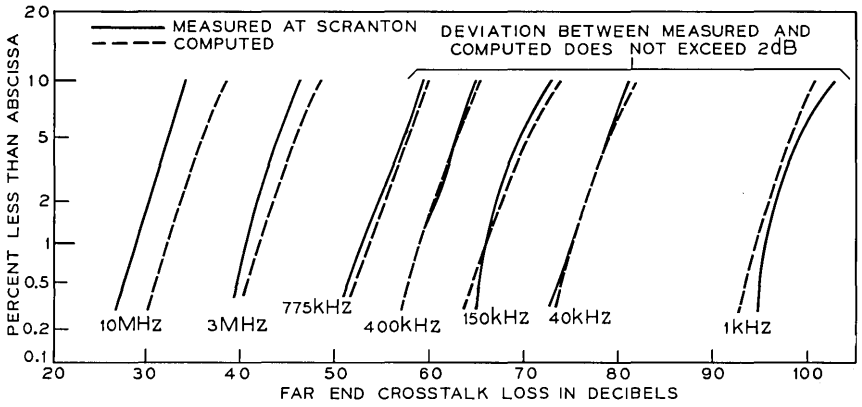

Fig. 6—Comparison of measured and computed distribution tails of within unit (50 pair) far-end crosstalk. The system is 2702 feet long, it has 4 splices, and is composed of 22-gauge pulp cable. The measured tails are based on measurements of in-place cable in Scranton, Pennsylvania. The computed tails are based on a random selection of 1-kHz factory capacitance unbalance data. (On normal probability paper.)

higher frequencies. In conclusion it seems that voice-frequency capacitance data can be used as a basis for simulating the crosstalk performance of a system up to at least the high kHz frequency range.

We are now in a position to give an abstract definition of the outside plant. Let L index over $[0, \infty)$. Let $(\Omega, \mathcal{A}, p)$ be a probability space. By an outside plant subsystem we mean any $2n \times 2n$ complex matrix stochastic process $X_L(\omega)$ of the form

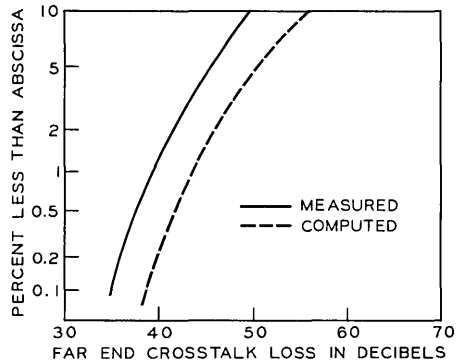

Fig. 7—Comparison of measured and computed distribution tails of 3.15-MHz within unit (50 pair) far-end crosstalk on 1000 feet of 22-gauge pulp cable. The computed distribution is based on 1-kHz capacitance unbalance data. (On normal probability paper.)

$$X_L(\omega) = \begin{bmatrix} \mathsf{a}(L)I & \mathsf{b}(L)I \\ \mathsf{c}(L)I & \mathsf{a}(L)I \end{bmatrix} (I + \epsilon Y(L, \omega)),$$

where $\begin{pmatrix} \mathsf{a}(L) & \mathsf{b}(L) \\ \mathsf{c}(L) & \mathsf{a}(L) \end{pmatrix}$ is the chain matrix characterization of a physically realizable, linear, passive, bilateral, symmetric two port and $Y(L, \omega)$ has a multivariate Gaussian distribution with mean 0. Let χ denote an independent set of all such $X_L(\omega)$. Let X^α and X^β belong to χ. By $X^\alpha \cdot X^\beta$ we mean the ordinary matrix product with the ϵ^2 term neglected. Since the product of 2×2 symmetric matrices with determinant one is again a symmetric matrix with determinant one and since the sum of independent Gaussian matrices with mean zero is again a Gaussian matrix with mean zero it follows that χ is closed under this multiplication. We note that χ clearly contains the identity matrix and that the multiplication we have defined is associative. A collection of elements closed under an associative multiplication rule and containing the multiplicative identity element is called a semigroup. Our definition of χ is a bit too general so we present the characters of interest: the cables, the bridged taps, and the load coils.

Cable Representation

Equation (5) defines the cable. The integrals involving capacitance and inductance unbalance are to be considered as stochastic integrals with respect to the Brownian motion process. The statistics of the capacitance portion of the cable process are known if the statistics of the matrix $(\int_0^L c_{ij}(x, \omega)\, dx)$ are known. Recall the way the stochastic integral was defined. The cable matrix has mean

$$\begin{bmatrix} \cosh \Gamma LI & -z_0 \sinh \Gamma LI \\ -z_0^{-1} \sinh \Gamma LI & \cosh \Gamma LI \end{bmatrix}.$$

The dispersion matrix involves terms of the form

$$\int_0^L \frac{(\phi(x)\bar{\psi}(x) + \bar{\phi}(x)\psi(x))}{2}\, dx k_{lm,rs},$$

where $\phi(x)$ and $\psi(x)$ are deterministic hyperbolic functions of the primary constants and

$$k_{lm,rs} = E\left\{\left[\int_0^L dC_{lm}(x, \omega) \int_0^L dC_{rs}(x, \omega)\right]\right\}$$

which can be determined from capacitance unbalance data.

Given Γ, Z_0, f, and capacitance unbalance data the chain matrix can be sampled. For example, to get a sample of

$$-\epsilon Z_0 \int_0^L \sinh 2\Gamma x \; \eta_{ij}(x, \omega)\, dx$$

merely multiply the sample of $\int_0^L c_{ij}(x, \omega)\, dx$ by

$$\Theta = \sqrt{\frac{\epsilon^2 \mid 2\pi f Z_0 \mid^2}{L}} \int_0^L \sinh 2\Gamma x \, \overline{\sinh 2\Gamma x}\, dx.$$

This follows from the fact that if $X(\omega)$ is normally distributed with mean zero and variance V and Θ is a constant then $\Theta X(\omega)$ is normally distributed with mean zero and variance $\mid \Theta \mid^2 V$ and from the definition of stochastic integral.

The Representation of a Cable in the Open Bridged Tap Arrangement

Let $\left(\begin{smallmatrix} A & B \\ C & D \end{smallmatrix}\right)$ be a cable matrix. By the representation of an open-circuited bridged tap we mean the first two terms in the power series in ϵ for $\left(\begin{smallmatrix} I & 0 \\ A^{-1}C & I \end{smallmatrix}\right)$.

The Representation of a Load Coil

By the representation of a load coil we mean the random matrix

$$\begin{bmatrix} [1+(R+i2\pi fL)(G+i2\pi fC)]I & -(R+i2\pi fL)I \\ -(G+i2\pi fC)[R-i2\pi fL)(G+i2\pi fC)+2]I & [1+(R+i2\pi fL)(G+i2\pi fC)]I \end{bmatrix}$$

$$-\sqrt{-1}\,\epsilon 2\pi f \begin{bmatrix} & & & & 0 & \\ & & & & 0 & M_{ij}(\omega) \\ & & \circ & & \ddots & \\ & & & & M_{ij}(\omega) & 0 \\ 0 & & & & & \\ & 0 & M_{ij}(\omega) & & & \\ & & \ddots & & \circ & \\ M_{ij}(\omega) & & 0 & & & \end{bmatrix},$$

where M_{ij} is Gaussian with mean zero.

Let $X(\omega) = \left(\begin{smallmatrix} a & b \\ c & a \end{smallmatrix}\right)$ $(I + \epsilon Y(\omega))$ be a system. Let $\mathbf{V}_S$ and $\mathbf{V}_R$ denote voltage stimuli and let $\mathbf{v}_S$ and $\mathbf{v}_R$ denote voltage responses. Let $(y_{S1}, y_{S2}, \cdots, y_{Sn})^t = \mathbf{y}_S$ and $(y_{R1}, y_{R2}, \cdots, y_{Rn})^t = \mathbf{y}_R$ denote the vector terminal admittances. The basic relation is

$$\begin{bmatrix} \mathbf{v}_R \\ (\mathbf{v}_R - \mathbf{V}_R)^t, \mathbf{y}_R) \end{bmatrix} = X(\omega) \begin{bmatrix} \mathbf{v}_S \\ (\mathbf{V}_S - \mathbf{v}_S)^t, \mathbf{y}_S) \end{bmatrix}.$$

For ϵ sufficiently small we can solve for the random variables $\mathbf{v}_R$ and $\mathbf{v}_S$. It is easy to show that these random variables are asymptotic to a multivariate normal distribution as ϵ tends to zero.

Consider the problem of characterizing the near-end crosstalk performance of a certain loop. Here $\mathbf{V}_R = \mathbf{0}$, $\mathbf{V}_S = (0, 0, \cdots 0, 2, 0, \cdots 0)^t$ where the 2 is in the ith position. $v_{R1}, v_{R2}, \cdots, v_{R(i-1)}, v_{R(i+1)}, \cdots, v_{Rn}$ are the far-end crosstalks and $v_{S1}, v_{S2}, \cdots, v_{S(i-1)}, v_{S(i+1)}, \cdots, v_{Sn}$ are the near-end crosstalks. There is a set of these random variables for each i. For each $\omega \epsilon \Omega$ there corresponds a distribution of near-end and far-end crosstalk. The set of all these distributions characterize the crosstalk behavior of the system. We illustrate the stochastic nature of systems. To accomplish this, capacitance unbalance data on nine 22-gauge PIC cables was selected at random from Western Electric's cable manufacturing plant at Hawthorne, Illinois. In an unbiased manner, this data was used to simulate three 9-kft systems having two splices each. The three far-end crosstalk distributions are shown in Fig. 8. There were only twenty-five pairs in this system. Apparently, as the number of splices and/or the number of pairs is increased the distributions of different realizations of the same system tend to look more and more alike. Further study of the implication of the stochastic nature of outside plant systems is needed.

VI. CONCLUSIONS

A mathematical model of outside plant wire pair cable systems that includes crosstalk is given. The voice-frequency version of the model has been used to develop a computer simulation capability. It appears that this simulation capability can be extended to at least high kHz frequencies. Quality assurance data is the key to this simulation effort. This same data can be used to provide the basis for optimal twist length selection.

VII. ACKNOWLEDGMENTS

The work presented in this paper is an outgrowth of the many discussions the author had with the late F. L. Schwartz. Thanks are also due to S. F. Stumpf and Mrs. R. E. Parris who did the computer programming and to M. F. Veverka who did most of the experimental work.

S. O. Rice urged the author to investigate V. R. Saari's work[6] in the light of matrix techniques. The development of the analogs between coupled lines and nonuniform, uncoupled lines originated from such an investigation. The cooperation of W. N. Bell and A. K. Jain who

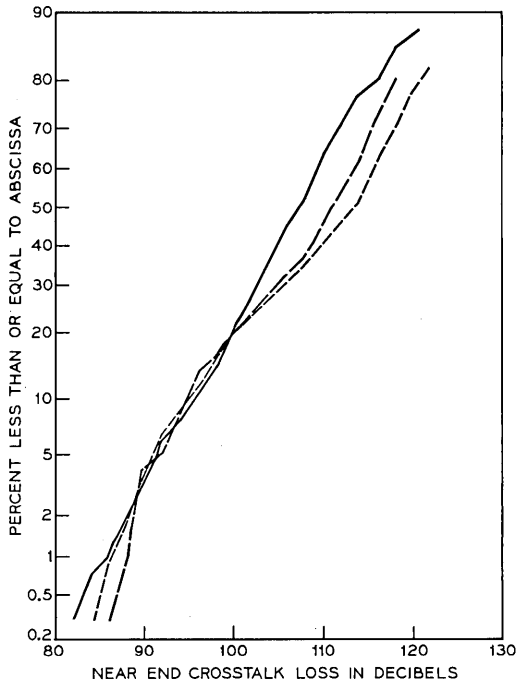

Fig. 8—Three separate realizations of the 1-kHz near-end crosstalk distribution of a nominally specified system. The nominal specification is a 25-pair, 22-gauge PIC system which is composed of three 3000-foot sections. The terminations are 600 Ω. (On normal probability paper.)

pursued the ideas concerning the statistical model and kindly permitted me to mention their unpublished results is greatly appreciated.

In closing, the author expresses his thanks to numerous individuals who planned, executed, or relayed the measurements used here.

APPENDIX

We shall give a detailed proof that $NEXT(i, j)$ and $N\hat{E}XT(i, j)$ are asymptotically equivalent. In what follows we shall lose no generality by assuming that $i = 1$ and $j = 2$. The solution to equation (2) is given by

$$T(x) = \exp\left[-\begin{bmatrix} 0 & zI \\ yI & 0 \end{bmatrix} x\right] \cdot \Omega_0^x \left[\epsilon \exp\left[+\begin{bmatrix} 0 & zI \\ yI & 0 \end{bmatrix} \xi\right] \begin{bmatrix} 0 & \eta(\xi) \\ \zeta(\xi) & 0 \end{bmatrix} \exp\left[-\begin{bmatrix} 0 & zI \\ yI & 0 \end{bmatrix} \xi\right]\right]. \quad (6)$$

(See Ref. 7 for the definition and basic properties of $\Omega_0^x(\cdot)$ and the proof that (6) is the solution. Equation (6) offers another method from which equations (4) and (5) can be obtained.) Because of the way ϵ appears in $\Omega_0^x(\cdot)$ and because $\Omega_0^x(\cdot)$ converges we can view $\Omega_0^x(\cdot)$ and hence $T(x)$ as a convergent power series in ϵ. From elementary considerations it can be shown that

$$\exp\left[-\begin{bmatrix} 0 & zI \\ yI & 0 \end{bmatrix} L\right] = \begin{bmatrix} \cosh \Gamma LI & -z_0 \sinh \Omega LI \\ -\frac{1}{z_0} \sinh \Gamma LI & \cosh \Gamma LI \end{bmatrix}.$$

For the manipulations we shall do here it will be convenient to partition $T(\epsilon)$ into square matrices, namely,

$$T(\epsilon) = \begin{bmatrix} A' & z_0 B' \\ \frac{C'}{z_0} & D' \end{bmatrix} = \sum_{i=1}^{\infty} \epsilon^i \begin{bmatrix} A_i' & z_0 B_i' \\ \frac{C_i'}{z_0} & D_i' \end{bmatrix}.$$

We are now prepared to determine the relation between $N\hat{E}XT(1, 2)$ and $NEXT(1, 2)$. Note we have

$$\begin{bmatrix} \mathbf{v}(L) \\ \frac{\mathbf{v}(L)}{z_0} \end{bmatrix} = T'(\epsilon) \left(\begin{bmatrix} \mathbf{v}(0) \\ -\frac{\mathbf{v}(0)}{z_0} \end{bmatrix} + \begin{bmatrix} 0 \\ \vdots \\ 0 \\ \frac{V}{z_0} \\ \cdot \\ 0 \end{bmatrix} \right). \tag{7}$$

It will suffice to deal with (7) which we can rewrite as

$$(A' + D' - (B' + C'))\mathbf{v}(0) = (D' - B') \begin{bmatrix} V \\ 0 \\ \vdots \\ 0 \end{bmatrix}.$$

Since $\lim_{\epsilon \to 0} (D' - B') = e^{\Gamma L} I$ is nonsingular, we conclude that for ϵ sufficiently small, say $\epsilon < \epsilon_1$, the matrix $(D' - B')$ is nonsingular. Thus for $\epsilon < \epsilon_1$, we can write

$$(I + (D' - B')^{-1}(A' - C'))v(0) = \begin{bmatrix} V \\ 0 \\ \vdots \\ 0 \end{bmatrix}.$$

Now $\lim_{\epsilon \to 0} (I + (D' - B')^{-1}(A' - C')) = 2I$ thus for ϵ sufficiently small, say $\epsilon < \min(\epsilon_1, \epsilon_2)$ we can write

$$v(0) = (I + (D' - B')^{-1}(A' - C'))^{-1} \begin{bmatrix} V \\ 0 \\ \vdots \\ 0 \end{bmatrix}.$$

Since D' and B' are convergent power series, we can write

$$D' - B' = e^{\Gamma L}[I + \epsilon(e^{-\Gamma L}[(D_1' - B_1') + \epsilon(D_2' - B_2') + \cdots])].$$

Thus for ϵ sufficiently small, say $\epsilon < \min(\epsilon_1, \epsilon_2, \epsilon_3)$ the inversion of $D' - B'$ is essentially the inversion of the identity plus an operator small enough to permit the Neumann inversion, see Ref. 8. Hence

$$\begin{aligned}(I + (D' - B')^{-1}(A' - C')) &= I + e^{-\Gamma L}(I - \epsilon e^{-\Gamma L}((D_1' - B_1') + \cdots) \\ &\quad + \epsilon^2 e^{-\Gamma L}((D_1' - B_1') + \cdots)^2 + \cdots) \\ &\quad \cdot e^{\Gamma L}(I + \epsilon e^{-\Gamma L}(A_1' - C_1') + \epsilon^2 e^{-\Gamma L}(A_2' - C_2') + \cdots) \\ &= 2I - \epsilon e^{-\Gamma L}(D_1' - B_1' + A_1' - C_1') + 0(\epsilon^2).\end{aligned}$$

Once again if we assume that ϵ is sufficiently small, say $\epsilon < \min(\epsilon_1, \epsilon_2, \epsilon_3, \epsilon_4)$ we can use the Neumann inversion to obtain

$$v(0) = \tfrac{1}{2}(I + 2\epsilon e^{\Gamma L}(A_1' + D_1' - B_1' - C_1') + 0(\epsilon^2)) \begin{bmatrix} V \\ 0 \\ \vdots \\ 0 \end{bmatrix}. \tag{8}$$

Now we note that (8) can be viewed as a $2n \times 2n$ system resulting from (7) or a 2×2 system corresponding to (6), in the latter case, all quantities needed to be hatted. Evidently $\lim_{\epsilon \to 0} V(\epsilon) = 2$. Since $\hat{A}_1'$, $\hat{D}_1'$, $\hat{B}_1'$, and $\hat{C}_1'$ are merely the 2×2 upper right-hand corner submatrices in A_1', D_1', B_1', and C_1' it follows from (8) that the power

series expressions for $N\hat{E}XT(i, j)$ and $NEXT(i, j)$ have identical coefficients of ϵ, (but not of ϵ^n, $n \geqq 2$). Thus $N\hat{E}XT(i, j)$ and $NEXT(i, j)$ are asymptotically equivalent.

An analogous proof goes through for $FEXT(i, j)$ and $F\hat{E}XT(i, j)$.

REFERENCES

1. "Dr. Campbell's Memoranda of 1907 and 1912," B.S.T.J., *14,* No. 4 (October 1935), pp. 558–572.
2. Carson, J. R., and Hoyt, R. S., "Propagation of Periodic Currents Over a System of Parallel Wires," B.S.T.J., *6,* No. 3 (July 1927), pp. 495–545.
3. Kaden, H., "Das Nebensprechen Zwischen Parallelen Koaxialen Leitungen," Electrische Nachrichten Technik, Band 13, Heft 11 (1936).
4. Cravis, H., and Crater, T. V., "Engineering of T1 Carrier System Repeatered Lines," B.S.T.J., *42,* No. 2 (March 1963), pp. 431–486.
5. Doob, J. L., *Stochastic Processes,* New York: John Wiley and Sons, 1962.
6. Saari, V. R., "Coupled Mode Theory, With Applications to Distributed Transformers," 1962 IRE Int. Conv. Rec., *10,* Part 2, p. 61.
7. Gantmacher, F. R., *The Theory of Matrices,* Vol. II, New York: Chelsea Publishing Company, 1959, p. 126.
8. Friedman, B., *Principles and Techniques of Applied Mathematics,* New York: John Wiley and Sons, 1962, p. 36.

THE BELL SYSTEM TECHNICAL JOURNAL
Vol. 50, No. 7, September, 1971
Printed in U.S.A.

Performance of a System of Mutually Synchronized Clocks

By J. P. MORELAND

(Manuscript received March 18, 1971)

This paper is concerned with mutual sychronization—a scheme for synchronizing a nationwide network of clocks for an integrated digital transmission and switching communications system. Described is an approach to the problem of determining values for the design parameters of a one-sided, linear phase averaging scheme with no filters. Two different sets of performance objectives are considered. The primary results concern the bounds which the effects of delay change force on the parameters which describe the inherent clock stability. Specifically, if a performance objective is no slips, and a limit is imposed on the amount of buffer storage, then an upper bound is forced on the allowable random drift in the free-running frequencies of the clocks. Alternatively, if an objective is that the slip rate not exceed some specified rate, again with a limited buffer size, then an upper bound is forced on the rate of random drift. Both bounds depend on the network configuration with the so called "dumbbell" configuration representing the worst case. A numerical example is included.

I. INTRODUCTION

This paper is concerned with mutual synchronization—a scheme for synchronizing a nationwide network of clocks for an integrated digital transmission and switching communication system. The clock at a switching center in such a system determines the rate of flow of data bits through the switch and to the output links. Buffer stores can make allowances for small, temporary differences in the received rate (determined by a distant clock and delay change) and the local switch clock rate. However, if a frequency difference persists then a buffer will occasionally overflow (or underflow) causing deletion (or repetition) of data bits from the output stream. Either such error is referred to as a slip. In this paper a synchronous network is one in which there are either no slips or, alternatively, in which the slip rate does not exceed some given rate.

Mutual synchronization was conceived about 10 years ago[1] as an

alternative to a master-slave synchronous timekeeping plan for large telephone networks. This new plan aimed at eliminating the possible need to reorganize a master-slave network in the event of failure of a timing link or the master clock. Previous analyses have been largely concerned with questions of stability,[2] equilibrium frequency,[3] dynamic response,[4,5] and control strategies.[6]

Questions relating to the system's ability to meet specific performance objectives, e.g., no slips, have been largely ignored. It has been noted that since changes in phase differences between clocks remain finite, sufficiently large buffers could be placed in each communications link to avoid such slips. However, the relationships between required buffer size and clock stability, delay changes, network configuration, and control parameters have not been established. It is to this question that this paper is addressed. A simple control strategy is considered, viz., one-sided, linear phase averaging with no filters. Two different sets of performance objectives are considered and the results are expressed as bounds which are forced on parameters which describe the inherent clock stability. A statement of these performance objectives and a description of the network model follow.

II. ALTERNATIVE PERFORMANCE OBJECTIVES

2.1 *Performance Objective #1*

Let a performance objective be no slips. Assume, also, a given amount of buffer storage (of sufficient size to account at least for changes in link delay). As an additional objective, the variation of system frequency (i.e., that common frequency at which all clocks operate in equilibrium) must not exceed the bandwidth limitations of transmission and switching equipment (which might typically be of the order of one part in 10^5). To meet the first objective, changes in phase difference between any pair of clocks must not exceed a given value. Due to the effect of delay change on clock phase and system frequency, this requirement will be seen to force an upper bound on the allowable random drift in a clock's free-running frequency (i.e., that frequency at which it would operate in the absence of a control input). The second objective forces an upper bound on the allowable total drift of a clock's free-running frequency.

2.2 *Performance Objective #2*

As an alternative, suppose slips are permitted to occur but at no more than a given rate. In addition, assume the same objective, as in

Section 2.1, on variations of system frequency. Again, a given amount of buffer storage is assumed. In this case frequency differences between pairs of clocks (that persist long enough for several slips to actually occur) must not exceed some preset value. This value will depend on the slip rate requirement and the amount of buffer storage and might typically be of the order of one part in 10^9. Due to the effects of delay change, this requirement will be seen to force an upper bound on the allowable rate of random drift of any clock's free-running frequency.

Changes in equilibrium phase differences occur as a result of changes in the free-running frequencies of the clocks or the transmission delays between clocks. Frequency differences between pairs of clocks are nonequilibrium effects which occur while the free running frequencies or the transmission delays are changing. The magnitude of both these effects depends critically upon the network configuration. The "dumbbell" configuration, consisting of two equal size groups of mutually synchronized clocks with full interconnection within a group but only a single intergroup link (Fig. 1), appears to represent the worst case.

It is assumed that performance objectives must be met without knowledge of network configuration; specifically, all clocks and timing links are to be considered "equal," regardless of their location in the network. Design parameters are determined, then, so that objectives are met in the dumbbell configuration.

III. CONTROL MODEL

In one-sided phase averaging the frequency of each office clock is controlled by an average of the observed phases of signals received from distant clocks, as measured with reference to the phase of the local clock. The frequency of each clock responds then to both a change

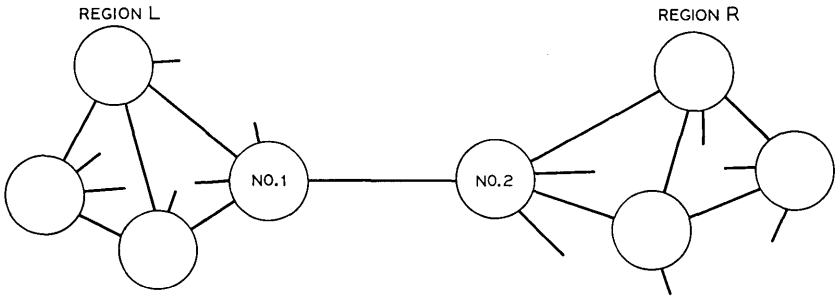

Fig. 1—Dumbbell configuration.

in the phase of a distant clock and to a change in the transmission delay from a distant clock. (Two-sided controls, in which the results of phase comparisons are transmitted back, on a special data link, to control the distant clocks, can eliminate the effect of delay on frequency.[5,6]) The general control equation is

$$f_i(t) = F_i(t) + K_i \sum_{j=1}^{N} a_{ij}\{p_j[t - \tau_{ij}(t)] - p_i(t) + \phi_{ij}\}. \qquad (1)$$

In this equation: N is the number of clocks; f_i is the frequency of the ith clock; F_i is the free-running frequency of the same clock (frequency in the absence of a control input); K_i is a control gain with the dimensions of reciprocal time; a_{ij} are averaging coefficients such that

$$a_{ij} \geqq 0, \qquad \sum_{j=1}^{N} a_{ij} = 1 \qquad i = 1, 2, \cdots, N;$$

p_i is the phase of the ith clock, related to frequency by

$$\frac{dp_i}{dt} = f_i ;$$

τ_{ij} is the transmission delay encountered by a pulse arriving at the ith office, from the jth, at time t; and ϕ_{ij} is a reference phase whose value depends upon initial conditions.

IV. SYSTEM FREQUENCY

Previous studies[3] have shown that if the system parameters remain constant and there exists at least one clock which distributes timing control to every other clock (either directly or indirectly via some intermediate clocks) then the system will asymptotically approach an equilibrium state in which all clocks run at a common frequency—called the system frequency. Under these conditions the system equations can be solved algebraically for the system frequency; the result is[3]

$$f = \frac{\sum_{i=1}^{N} b_i\left(F_i + K_i \sum_{j=1}^{N} a_{ij}\phi_{ij}\right)}{\sum_{i=1}^{N} b_i\left(1 + K_i \sum_{j=1}^{N} a_{ij}\tau_{ij}\right)}, \qquad (2)$$

where the weighting coefficients b_i depend upon the gains and the averaging coefficients. In the general case b_i is the cofactor of any

element in the ith row of the matrix $K(I-A)$, where K is the diagonal matrix with diagonal elements K_i, I is the identity matrix, and A is the matrix of the averaging coefficients a_{ij}. The proof of these results is found in Ref. 3.

The effects of delay change and free-running frequency drift on the system frequency will be considered separately, allotting to each one-half the maximum-allowable variation.

V. EFFECTS OF DELAY CHANGE ON SYSTEM FREQUENCY (BOUND ON GAIN)

To obtain some feel for the effects of delay change on the system frequency consider first a network of two clocks with equal control gains and suppose that the transmission delay between them increases by an amount $\Delta\tau$. By symmetry each clock is subjected to the same influence and, hence, signals will arrive $\Delta\tau$ seconds later at *both* clocks. The corresponding change in both observed phases is, then, $f\tau - (f + \Delta f)(\tau + \Delta\tau) \approx -(f\Delta\tau + \tau\Delta f)$, where Δf is the (as yet undetermined) change in the system frequency. But this change is equal to the gain K times change in observed phase; hence,

$$\Delta f \approx \frac{-Kf\Delta\tau}{1 + K\tau}.$$

To estimate the effects of delay changes in a more general network suppose that all gains K_i are equal and that identical delay changes $\Delta\tau$ occur on all links at the same time. The above reasoning, with the identical conclusion, applies also to this case as may be verified from equation (2). That is, with $K_i = K$ and $\tau_{ij} = \tau$,

$$f + \Delta f = \frac{1}{1 + K(\tau + \Delta\tau)} \frac{\sum_{i=1}^{N} b_i(F_i + K\phi_i)}{\sum_{i=1}^{N} b_i},$$

from which

$$\Delta f \approx \frac{-Kf\Delta\tau}{1 + K\tau} = -\frac{K\tau}{1 + K\tau} f \frac{\Delta\tau}{\tau}.$$

Since the fractional change in delay, $\Delta\tau/\tau$, is typically several orders of magnitude greater than the allowable fractional change in f, it follows that K must be chosen so that $K\tau$ is much less than unity; hence, neglecting the sign of the change,

$$\Delta f \approx Kf\Delta\tau. \tag{3}$$

If the maximum allowable variation of system frequency (due to delay change) is $\frac{1}{2}\Delta f_s$, then K must satisfy the upper bound

$$K \leqq K_s = \frac{1}{2\Delta\tau_s}\frac{\Delta f_s}{f_o}, \tag{4}$$

where $\Delta\tau_s$ is the maximum delay change (assumed to occur at the same time on all links) and f_o is the nominal system frequency. This is one of two upper bounds on the gain which will lead to an upper bound on either the total random drift or rate of random drift in a clock's free-running frequency.

VI. EFFECT OF CLOCK DRIFT ON SYSTEM FREQUENCY

With $K\tau \ll 1$, the change in the system frequency is, approximately,

$$\Delta f \approx \frac{\Sigma b_i \Delta F_i}{\Sigma b_i}.$$

Thus, if the drifts are systematic, i.e., all in the same direction, then (assuming a simple average over N clocks) each clock must have the property that its total free-running frequency drift does not exceed the allotted variation in the system frequency (i.e., $\frac{1}{2}\Delta f_s$). If, however, the drifts are not correlated then the standard deviation of the system frequency is (again assuming a simple average over N clocks) inversely proportional to the square root of the number of clocks. In this case the allowed drift can, for large networks, be somewhat greater than $\frac{1}{2}\Delta f_s$.

VII. DUMBBELL CONFIGURATION

The magnitude of the effects of delay and clock drift on the phase and frequency differences between pairs of clocks, unlike their effects on system frequency, depends critically upon the network configuration. The "dumbbell" configuration, illustrated in Fig. 1, appears to represent the worst case. In this configuration the N offices are divided into two equal groups, with a direct timing link from every clock to every other clock in the same group, but only one timing link (the bar of the dumbbell) connecting one group to the other. In this configuration changes in the free-running frequencies or the delays can force a relatively large change in the phase difference between clocks in opposite halves. An intuitive feeling for such an effect may be

obtained by supposing that each bar clock has but one "vote" out of $N/2$ in determining the common frequency of the clocks in its half of the dumbbell, while signals on the bar link have but one of $N/2$ votes in determining the frequency of a bar clock. On this basis one might guess then that a given change $\Delta\phi$ in the phase difference between the bar clocks would tend to produce a change of magnitude $K/(N/2)^2\ |\Delta\phi|$ in the common frequency of the clocks in each half (one half up, the other down). Assuming this to be true, suppose then that all the delays in one half should increase by an amount $\Delta\tau$, thus tending to decrease the frequency of the clocks in that half by $Kf\Delta\tau$ [equation (3)], while the opposite occurs in the other half. By symmetry the system frequency will not change. Hence, to compensate for the tendency of each half to change frequency by an amount $\pm Kf\Delta\tau$, the phase change $\Delta\phi$ must be such that

$$\frac{K}{(N/2)^2} \mid \Delta\phi \mid = Kf\Delta\tau, \quad \text{or}$$

$$\mid \Delta\phi \mid = \frac{N^2}{4} f \mid \Delta\tau \mid.$$

This result will be formally verified below. The dumbbell is not the only configuration which can give rise to the factor N^2. For example, the phase difference between the end clocks in a bilateral chain also grows, under similar conditions, as the square of the number of clocks. However, the dumbbell is worse in the sense that this dependence on network size holds for any two clocks in opposite halves.

The conclusions pertaining to the dumbbell configuration are based on the following assumptions:

(*i*) The gain K_i at each clock has the same value K.

(*ii*) Each control link (shown in Fig. 1) is assigned the same weight; hence, for $N/2 \gg 1$, all (nonzero) a_{ij} are approximately equal to $2/N$.

(*iii*) The delays on all links within region R and within region L (see Fig. 1) are approximately equal, respectively, to τ_R and τ_L and the difference $\mid \tau_R - \tau_L \mid$ changes at a constant rate $\dot{\tau}_D$ for $t_{\dot{\tau}}$ seconds. The maximum change $\Delta\tau_D$ persists for $t_{\Delta\tau}$ seconds at which point the difference returns to its original value (Fig. 2). Such a situation might reflect an effect of a cold front moving successively through the two regions.

(*iv*) The free-running frequency of each clock drifts at a constant rate of $\pm\dot{F}$ for $t_{\dot{F}}$ seconds, with the maximum drift $\pm\Delta F$ per-

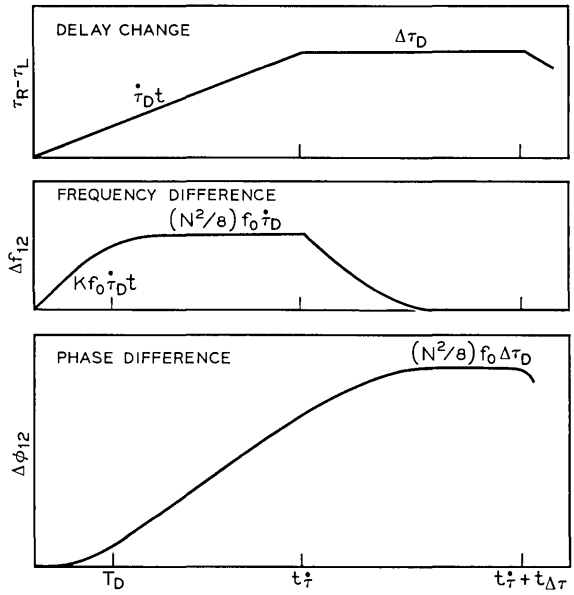

Fig. 2—Response of dumbell to delay change.

sisting for $t_{\Delta F}$ seconds. The drifts are uncorrelated and hence the standard deviation of the difference $| F_R - F_L |$ of the numerical averages of the free-running frequencies in each half grows at a rate $2\dot{F}/\sqrt{N}$ up to maximum change of $2\Delta F/\sqrt{N}$.

To gain some insight into the results to be presented, the effects of a step change in delay will be considered first. Thus, suppose that the delay on each link within region R suddenly increases by an amount $\Delta\tau$, while the opposite occurs on each link within region L—with no change in the bar-link delay. By symmetry there will be no change in the system frequency nor in the phase differences between any pair of clocks both within region R or both within region L (*Note:* R and L excludes the bar clock). Consider then, any one of the clocks within region R; the following statements apply:

(*i*) Signals from each of the other $(N/2 - 2)$ clocks within R arrive later by an amount $\Delta\tau$, thus tending to make this clock run slower.

(*ii*) To balance this tendency, signals from bar clock #2 must arrive earlier by an amount $(N/2 - 2)\Delta\tau$; i.e., the phase of bar clock

#2 must advance with respect to that of each clock within R by an amount $(N/2 - 1)f\Delta\tau$.

Next consider bar clock #2; the following statements apply:

(*i*) Signals from each of the $(N/2 - 1)$ clocks within R arrive later by an amount $(N/2)\Delta\tau$, thus tending to make this clock run slower.

(*ii*) To balance this tendency, the signal from bar clock #1 must, then, arrive earlier by an amount $(N/2 - 1)(N/2)\Delta\tau$, i.e., the phase of bar clock #1 must advance with respect to that of bar clock #2 by approximately $(N^2/4)f\Delta\tau$ as suggested above.

An estimate of the time required to reach equilibrium may be obtained by noting that the initial effect of the step change is to decrease the frequency of bar clock #2 by $Kf_o\Delta\tau$ and to increase that of bar clock #1 by the same amount—resulting in an initial frequency difference of $2Kf_o\Delta\tau$. If this difference persisted, an interval of duration $N^2/8K$ would be required to reach equilibrium. The actual approach to equilibrium is an exponential with time constant $T_D = N^2/8K$.

The response to a ramp change in delay could, if the system equations were linear, be derived directly from the response to a step change. That is, a ramp change is the integral of a step change and hence, were the system linear, the response to a ramp change would be the integral of the response to a step change. Although the systems equations are not linear in the delays, it is assumed that changes are slow enough so that a linear approximation is justified. The frequency difference Δf_{12} between the bar clocks is then shown, in the Appendix, to be given by the solution of the following linear differential equation:

$$\ddot{\Delta f}_{12} + K\dot{\Delta f}_{12} + \frac{8K^2}{N^2}\Delta f_{12} = K(\dot{F}_R - \dot{F}_L) - Kf_o(\dot{\tau}_R - \dot{\tau}_L), \qquad (5)$$

where f_o is the nominal value of the system frequency.

In what follows, the effects of delay and free-running frequency changes will again be considered separately.

VIII. EFFECT OF DELAY CHANGE (ADDITIONAL BOUNDS ON GAIN)

The solution of equation (5), while the delay difference $\tau_R - \tau_L$ is changing at a constant rate $\dot{\tau}_D$, is shown in the Appendix to be

$$\Delta f_{12} \approx \frac{N^2}{8} f_o\dot{\tau}_D(1 - e^{-t/T_D}), \qquad (6)$$

where $T_D = N^2/8K$ is the previously suggested time constant. The complete solution for Δf_{12} and for the change $\Delta\phi_{12}$ in the phase difference between the bar clocks is sketched in Fig. 2 (for the case when both t_τ and $t_{\Delta\tau}$ are large compared with T_D).

If the "equilibrium" frequency difference

$$\Delta f \mid \max = \frac{N^2}{8} f_o \dot{\tau}_D \tag{7}$$

does not exceed the maximum allowable difference $\frac{1}{2}\Delta f_D$, i.e., if

$$N \leqq N_f = \left(\frac{4\Delta f_D}{f_0 \dot{\tau}_D}\right)^{\frac{1}{2}} \tag{8}$$

then no restriction need be placed on the gain K. However, if $N > N_f$ then an upper bound, determined from equation (6) with $t = t_\tau$, is forced on K. For $(N^2/8)f_o\dot{\tau}_D \gg \frac{1}{2}\Delta f_D$ the bound is

$$K \leqq K_f = \frac{\Delta f_D}{2f_o\Delta\tau_D} \; ; \quad \text{for} \quad N \gtrsim 3N_f \; . \tag{9}$$

Similarly, if the "equilibrium" change in phase difference

$$\Delta\phi \mid \max = \frac{N^2}{8} f_o \Delta\tau_D \tag{10}$$

is less than the allowable change $\frac{1}{2}\Delta\phi_D$, i.e., if

$$N \leqq N_\phi = \left(\frac{4\Delta\phi_D}{f_o\tau_D}\right)^{\frac{1}{2}} \tag{11}$$

then K may be chosen arbitrarily. However, if N exceeds N_ϕ an upper bound must be placed on K. When the equilibrium value is much larger than the allowable change, the least upper bound is easily determined. For, then, the time constant $T_D = N^2/8K$ must be made long compared with the interval over which the delay disturbance persists. The phase difference grows then nearly as if the two halves were not connected and hence approaches the value $Kf_o t_D \Delta\tau_D$, which will not exceed the maximum allowable value provided K meets the upper bound

$$K \leqq K_\phi = \frac{\Delta\phi_D}{2f_o t_D \Delta\tau_D} \; ; \quad \text{for} \quad N \gtrsim 3N_\phi \tag{12}$$

where $t_D = t_\tau + t_{\Delta\tau}$.

IX. BOUNDS ON CLOCK STABILITY

It is assumed that the stabilities of the clocks under consideration are such that performance objectives would not be met if the halves of the dumbbell were not joined by the bar link (for small numbers of clocks this is nearly equivalent to assuming that objectives would not be met with all clocks operating independently). Thus, the interval during which the free-running frequencies drift and that for which the maximum drift persists must both be long compared with the dumbbell time constant T_D. Hence, the frequency difference between the bar clocks approaches $(N^2/8K) \mid \dot{F}_R - \dot{F}_L \mid$, while the change in phase difference approaches $(N^2/8K) \mid \Delta F_R - \Delta F_L \mid$. For the assumed model these numbers are random variables; however, for purposes of further discussion they will be replaced by the values of their standard deviation, i.e.,

$$\Delta f \mid \max = \frac{N^{\frac{3}{2}}}{8K} \dot{F} \tag{13}$$

and

$$\Delta\phi \mid \max = \frac{N^{\frac{3}{2}}}{8K} \Delta F. \tag{14}$$

If the performance objective is no slips then $\Delta\phi$ must not exceed $\frac{1}{2}\Delta\phi_D$ and hence, from equation (14), the random drift in each clock's free-running frequency must satisfy the bound

$$\Delta F < \frac{4K}{N^{\frac{3}{2}}} \Delta\phi_D ,$$

where K must not exceed K_s, as given by equation (4), and further, if $N \gtrsim 3N_\phi$, must not exceed K_ϕ as given by equation (12). Assuming $K_\phi < K_s$ (see Section X), the maximum value of $\Delta F/f_o$ is

$$\Delta F/f_o \mid \max = \begin{cases} \dfrac{2}{N^{\frac{3}{2}}\Delta\tau_s} \dfrac{\Delta\phi_D}{f_o} \dfrac{\Delta f_s}{f_o} & N < N_\phi \\ \dfrac{2}{N^{\frac{3}{2}} t_D \Delta\tau_D} \left(\dfrac{\Delta\phi_D}{f_o}\right)^2 & N \gtrsim 3N_\phi , \end{cases} \tag{15}$$

where

$$N_\phi = \left(\frac{4\Delta\phi_D}{f_o\Delta\tau_D}\right)^{\frac{1}{2}}.$$

Similarly, if the performance objective is expressed as a maximum slip rate then Δf must not exceed $\frac{1}{2}\Delta f_D$ and hence, from equation (13), the rate of random drift in the free-running frequency of each clock must satisfy the bound

$$\dot{F} < \frac{4K}{N^{\frac{1}{2}}} \Delta f_D ,$$

where K must not exceed K_s and further, if $N \gtrsim 3N_f$, must not exceed K_f as given by equation (9). Assuming $K_f < K_s$ (see Section X) the maximum value of $\dot{F}/f_o$ is

$$\dot{F}/f_o \mid \max = \begin{cases} \dfrac{2}{N^{\frac{1}{2}}\Delta\tau_s} \dfrac{\Delta f_D}{f_o} \dfrac{\Delta f_s}{f_o} & N < N_f \\ \dfrac{2}{N^{\frac{1}{2}}\Delta\tau_D} \left(\dfrac{\Delta f_D}{f_o}\right)^2 & N \gtrsim 3N_f , \end{cases} \tag{16}$$

where

$$N_f = \left(\frac{4\Delta f_D}{f_o \dot{\tau}_D}\right)^{\frac{1}{2}}.$$

X. NUMERICAL EXAMPLE

Assume that all links are approximately 300 miles in length with a nominal delay of 6.5 microseconds per mile and a delay variation of 0.035 percent per degree Fahrenheit (these values apply to pulp-insulated cable). In considering the effect of delay change on the system frequency assume a temperature variation of $\pm 40°$F, leading to $(\Delta\tau)_s \approx$ 30 μs. As the worst case condition in the dumbbell configuration, assume that the temperature difference between the two halves changes at a rate of about 2°F per day for about 1 week, leading to $\dot{\tau}_D \approx 2 \times 10^{-11}$ and $\Delta\tau_D \approx 10$ μs; and assume that the maximum difference persists for about 1 week.

Assume, also, that the system frequency corresponds to the digital sampling rate in D-type PCM channel banks, viz., 8×10^3 frames/second, and that it is to vary by no more than one part in 10^5 (which sets the total allowable free-running frequency drift). Furthermore, assume that $\Delta\phi_D = 1$ frame (which is ample allowance for the link delay change $f_o\Delta\tau_s \approx 1/4$ frame) and that Δf_D is not to exceed one part in 10^9.

Under these conditions, the various upper bounds on K are

$$K_s = 1/6\ s^{-1},$$

$$K_\phi = 5 \times 10^{-6}\, s^{-1},$$

$$K_f = 5 \times 10^{-5}\, s^{-1}.$$

If there are to be no slips (performance objective #1), then the maximum allowable random drift in any clock's free running is

$$\Delta F/f_o \mid \max = \begin{cases} \dfrac{4 \times 10^{-5}}{N^{\frac{3}{2}}} & N < 7 \\ \dfrac{2 \times 10^{-9}}{N^{\frac{3}{2}}} & N \gtrapprox 21. \end{cases}$$

The first bound corresponds roughly to the performance obtainable from relatively inexpensive crystal oscillators. However, the second bound, which must be met if the number of clocks exceeds about 20, implies atomic standards.

Alternatively, if it is the slip rate that is to be bounded (performance objective #2) then the rate of random drift in any clock's free running must not exceed

$$\dot{F}/f_o \mid \max = \begin{cases} \dfrac{6 \times 10^{-5}}{N^{\frac{3}{2}}} \Big/ \text{day} & N < 14 \\ \dfrac{2 \times 10^{-8}}{N^{\frac{3}{2}}} \Big/ \text{day} & N \gtrapprox 42. \end{cases}$$

Again, the first bound is met by relatively inexpensive crystal oscillators while the second, which applies if there are more than about 40 clocks, implies either the best present day crystals or atomic standards.

XI. CONCLUDING REMARKS

It should not be concluded that a mutually synchronized system must be designed as described above. For example, although the dumbbell configuration represents a worst case, it is perhaps too unlikely a case on which to base parameter specifications. Furthermore, the dependence of clock frequency on delay can be eliminated with two-sided controls[5] (which, however, requires a special data link). Alternatively, sufficient reliability without the problems associated with a large-dumbbell network might be obtainable from some type of hierarchical system—composed, for example, with clocks of varying degrees of stability[7] or of a small number of mutually synchronized clocks at a top level with lower levels consisting of a number of similar small groups each redundantly slaved to higher levels. Finally,

it should be noted that the relatively large phase shift which may occur between the bar clocks in the dumbbell configuration could be reduced by increasing the "weight" given to the bar link (i.e., by increasing the averaging coefficients associated with this link). This, however, is not really in the original spirit of mutual synchronization, as it requires that the system configuration be known and used in determining the averaging coefficients. This introduces administrative complications comparable to those involved in reorganizing a master-slave network.

XII. ACKNOWLEDGMENTS

I am grateful for the numerous suggestions made during the preparation of this paper by M. B. Brilliant and C. R. Clinesmith.

APPENDIX

Phase and Frequency Difference in the Dumbbell

It is assumed that the solutions of equation (1) are continuous functions of the delays and that frequency changes are slow enough so that the approximations

$$p_i(t - \tau_i) \approx p_i(t) - f_i\tau_i$$

are justified. Furthermore, changes in $f_i\tau_i$ are assumed dominated by changes in delay (i.e., doppler shift) so that f_i, in this product, may be replaced by the nominal frequency f_o. Since the delay τ is small compared with the response time $1/K$, i.e., $K\tau \ll 1$, these approximations appear reasonable.

The control equation [equation (1)] for the left-hand bar clock may, then, be written in the form

$$\dot{f}_1 = \dot{F}_1 - Kf_o\dot{\tau}_L + K\{f'_L - f_1\} + \frac{K}{N/2}\{f_2 - f_1\}, \tag{17}$$

where f'_L is the arithmetic average of clock frequencies in region L (which excludes the bar clock) and, from equation (1), satisfies

$$\dot{f}'_L = \dot{F}'_L - Kf_o\dot{\tau}_L + \frac{K}{N/2}\{f_1 - f'_L\}. \tag{18}$$

Similarly, for the right-hand bar clock

$$\dot{f}_2 = \dot{F}_2 - Kf_o\dot{\tau}_R + K\{f'_R - f_2\} + \frac{K}{N/2}\{f_1 - f_2\}, \tag{19}$$

where

$$\dot{f}'_R = \dot{F}'_R - Kf_o\dot{\tau}_R + \frac{K}{N/2}\{f_2 - f'_R\}. \tag{20}$$

The network shown in Fig. 3 is equivalent in that it is described by the above set of equations.

With x and y denoting, respectively, the frequency differences $f_1 - f_2$ and $f'_L - f'_R$, it follows from equations (17) through (20) that

$$\dot{x} + K\left(1 + \frac{4}{N}\right)x = Ky + \dot{F}_1 - \dot{F}_2 - Kf_0(\dot{\tau}_L - \dot{\tau}_R) \tag{21}$$

and

$$\dot{y} + \frac{2K}{N}y = \frac{2K}{N}x + \dot{F}'_L - \dot{F}'_R - Kf_o(\dot{\tau}_L - \dot{\tau}_R). \tag{22}$$

Eliminating y from equation (21) it follows that x satisfies (for $N \gg 1$)

$$\ddot{x} + K\dot{x} + \frac{8K^2}{N^2}x = K(\dot{F}_L - \dot{F}_R) - K^2f_o(\dot{\tau}_L - \dot{\tau}_R) \tag{23}$$

and its solution, subject to the initial conditions $x(t = 0) = 0$ and $y(t = 0) = 0$ which implies $\dot{x}(t = 0) = (\dot{F}_1 - \dot{F}_2) - Kf_o(\dot{\tau}_L - \dot{\tau}_R)$, is

$$\begin{aligned} x(t) \approx{}& \frac{N^2}{8}f_o(\dot{\tau}_L - \dot{\tau}_R)(1 - e^{-t/T_D}) + \frac{N^2}{8K}(\dot{F}_L - \dot{F}_R) \\ &+ \frac{(\dot{F}_L - \dot{F}_1) - (\dot{F}_R - \dot{F}_2)}{K(1 - 8/N^2)}e^{-Kt} \\ &+ \frac{(\dot{F}_1 - \dot{F}_2) - \frac{N^2}{8}(\dot{F}_L - \dot{F}_R)}{K(1 - 8/N^2)}e^{-t/T_D}, \end{aligned}$$

where $T_D = N^2/8K$.

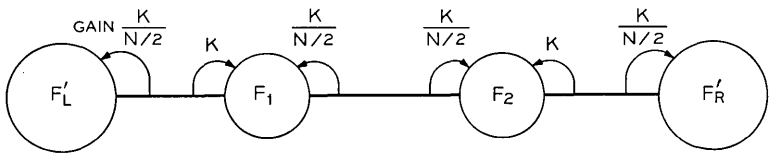

Fig. 3—Equivalent dumbbell configuration.

REFERENCES

1. Runyon, J. P., "Reciprocal Timing of Time Division Switching Centers," U. S. Patent No. 3,050,586, August 21, 1962.
2. Karnaugh, M., "A Model for the Organic Synchronization of Communications Systems," B.S.T.J., *45,* No. 10 (December 1966), pp. 1705–1736.
3. Brilliant, M. B., 'The Determination of Frequency in Systems of Mutually Synchronized Oscillators," B.S.T.J., *45,* No. 10 (December 1966), pp. 1737–1748.
4. Brilliant, M. B., "Dynamic Response of Systems of Mutually Synchronized Oscillators," B.S.T.J., *46,* No. 2 (February 1967), pp. 319–356.
5. Sandberg, I. W., "Some Properties of a Nonlinear Model of a System for Synchronizing Digital Transmission Networks," B.S.T.J., *48,* No. 9 (November 1969), pp. 2975–2997.
6. Candy, J. C., and Karnaugh, M., "Organic Synchronization: Design of the Controls and Some Simulation Results," B.S.T.J., *47,* No. 2 (February 1968), pp. 227–259.
7. Pierce, J. R., "Synchronizing Digital Networks," B.S.T.J., *48,* No. 3 (March 1969), pp. 615–636.

THE BELL SYSTEM TECHNICAL JOURNAL
Vol. 50, No. 7, September, 1971
Printed in U.S.A.

A Combinatorial Analysis of the Main Distributing Frame: Spare Requirements for Conversion to Preferential Assignment from Random Assignment

By M. A. SCHUMER

(Manuscript received September 24, 1970)

This paper presents a combinatorial analysis of a mathematical model of the Main Distributing Frame (MDF). Results are found concerning the amount of additional spare needed to convert a randomly connected MDF to a preferentially assigned mode of operation. The analysis is first performed for an MDF having two sections and serving one class of service. The results are subsequently extended to an MDF with multiple sections and several classes of service.

I. INTRODUCTION

The Main Distributing Frame (MDF) is that equipment in a central office building whose main function is to permit the flexible interconnection of cable from outside the building to central office equipment inside the building. This primary function accounts for most of the terminal capacity of a typical MDF. The remaining capacity serves a wide variety of other cross-connecting functions ranging from tying together two outside plant cable pairs to cross-connecting two or more pieces of central office equipment.

The conventional MDF is a double-sided steel structure with protectors or terminal strips mounted on one side, and terminal strips on the other. These are referred to as the "verticals" and "horizontals" due to their mounting orientation. The vertical side is the part of the MDF where the outside cable is terminated. The horizontal side is the part of the MDF where cables, which connect to the equipment of a central office (mainly line and trunk equipment), are usually terminated. To provide the maximum capacity of interconnections as well as complete flexibility in the connection of any outside plant equipment to any central office equipment, administration of the MDF must result in small numbers of long cross-connections. This can only

be accomplished by having the outside plant terminals opposite or nearly opposite the central office equipment terminals. The MDF at present is handled on a completely manual basis by framemen and framewomen who connect and disconnect the large number of wires which terminate on the MDF.

Cables terminated on the vertical side of the MDF are connected to the horizontal side by wires referred to as "cross-connections" or "jumpers." Where the outside plant terminals are not directly opposite the central office equipment terminals, these wires are run along horizontal shelves in order to connect these vertical and horizontal terminals together. Presently, assignment of outside plant terminals to central office equipment terminals is on a random basis, i.e., no attempt is made to make assignments so that jumper lengths are kept to a practical minimum. Therefore, when cross-connections become too numerous or too long they accumulate excessively, become unmanageable, and exceed the capacity (jumper volume) of the horizontal shelves.

One proposed method of keeping cross-connections short is the use of preferential assignment. In this mode of operation the MDF is divided into several zones, and records are kept which show in which zones cables and central office equipment are terminated. When connections are to be made, for example, between a cable pair and line circuit, a cable pair is first selected based on outside plant economics and availability. Then, line equipment is selected which is located in the same zone as the cable pair or in the closest zone to it. This method reduces jumper pileup and increases the MDF capacity. There arises the question of how many additional spare terminals and, therefore, how much central office equipment is required to convert from a randomly connected MDF to a preferentially assigned mode of operation. Although some people may feel that a prohibitive amount of spare would be needed, the following sections show that under the specified conditions a relatively small amount of spare is required by this conversion.

The approach used in this analysis is the following. Initially, it is assumed that there is a single class of service on the MDF. Given the initial number of wires which cross from one zone to another, and a model for the introduction of preferential assignment, the probability of exhausting spare in at least one zone can be found exactly for a 2-zone MDF and bounded for the general case. Since running a few jumpers between zones is not considered a problem, this probability is an upper bound on the probability of the MDF encountering trouble

while converting to preferential assignment. For a given probability of MDF trouble, we can, therefore, find an upper bound on the amount of spare equipment required by conversion. If the number of zone crossings is not known for a randomly connected MDF, the probability of exhausting spare can be averaged over the joint probability of the number of crossovers of each kind.

When dealing with several classes of service,* each service can be treated as a separate MDF with its own zone structure. To do this we make a simplifying assumption about the manner in which changes in service occur.

It should be noted that the analysis performed here finds the additional spare required initially for conversion to preferential assignment. However, once the conversion is completed, all that is needed is some small amount of spare to effectively administer service changes.

II. DISTRIBUTION OF CROSSOVERS IN A 2-ZONE MDF

In this section and in the next section, a model is developed for a 2-zone MDF. This model can be used to determine how much spare is required for conversion to preferential assignment. In later sections the more general and more useful case of multizone MDF is considered.

As illustrated in Fig. 1, zone 1 and zone 2 of the MDF terminate N_1 and N_2 outside plant cable pairs (side O) respectively. On the inside plant side (side I) there are $N_1 + S_1$ and $N_2 + S_2$ terminals

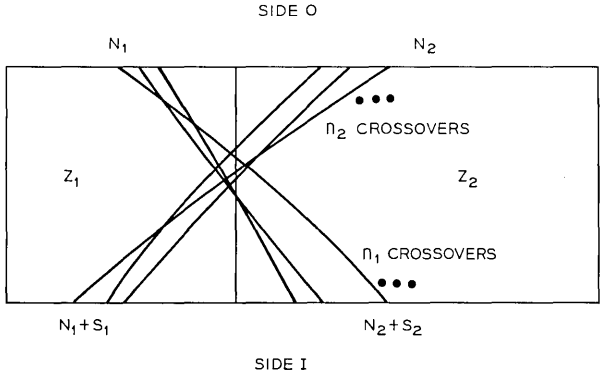

Fig. 1—Model of a 2-zone MDF.

* This term usually refers to the class of subscriber's line. Here this term will be used in a more general sense and will refer to various classes of all equipment or cable pairs terminated on the MDF.

respectively. S_1 and S_2 are the nominal number of spare equipment terminals available for each zone of the MDF.

First, assume that the MDF is used to capacity (i.e., all $N_1 + N_2$ outside plant terminals are connected to equipment or inside plant terminals). Further, assume that the terminals are randomly connected. We wish to find the probability $p(n_1, n_2)$ of having exactly n_1 jumpers crossing from side O of zone 1 to side I of zone 2, and exactly n_2 jumpers crossing from side O of zone 2 to side I of zone 1. This situation is illustrated in Fig. 1. After finding a suitable model to account for preferential assignment, the probability of exhausting spare at any time during the implementation of preferential assignment will be found using $p(n_1, n_2)$. This will be done in Section III.

In order to calculate $p(n_1, n_2)$ we assume all possible ways, W_0, to wire the MDF are equally likely (random connections). $p(n_1, n_2)$ is, then, the ratio of $W(n_1, n_2)$, the total number of ways to connect the MDF with n_1 and n_2 crossovers of the respective types, to W_0.

First, let us find W_0. As a first step, we choose at random $N_1 + N_2$ terminals of side I to be used. We can do this in $C(T, N)$* ways where $T = N_1 + S_1 + N_2 + S_2$ and $N = N_1 + N_2$. In addition, we will use the following notation: $S = S_1 + S_2$, $T_1 = S_1 + N_1$, and $T_2 = S_2 + N_2$. Now let us permute the N terminals we are using; there are $N!$ ways. Since the two operations of choosing and permuting are independent, the total number of ways to connect the MDF is the product of the separate enumerations, or

$$W_0 = N!\, C(T, N) = T!/S!. \tag{1}$$

Next, $W(n_1, n_2)$ is found as follows. First, let us choose n_2 terminals from side I of zone 1, which will accommodate jumpers from side O of zone 2. There are $C(T_1, n_2)$ distinct ways to make this choice. Likewise, there are $C(T_2, n_1)$ distinct ways of making the analogous choice for zone 2. Now zone 1 has $N_1 - n_1$ unused terminals on side O which will require direct connection to the remaining terminals of side I of zone 1. There are $T_1 - n_2$ unused terminals on side I of zone 1 (n_2 have been used to connect to side O of zone 2). Therefore, there are $C(T_1 - n_2, N_1 - n_1)$ possible ways to make direct connection in zone 1. Similarly, the direct connection in zone 2 can be made in any of $C(T_2 - n_1, N_2 - n_2)$ ways. Thus far, N_1 terminals from side I ($N_1 - n_2$ from zone 1 and n_2 from zone 2) have been chosen for con-

* $C(n, k) = \binom{n}{k} = n!/k!(n-k)!$

nection to the N_1 terminals on side O of zone 1. Upon choosing the N_1 terminals, each permutation of the chosen terminals corresponds to a unique configuration. There are N_1 ! such permutations. Similarly, there are N_2 ! permutations for the N_2 terminals of side O of zone 2. Since each of the enumerations listed above is independent of the others, the total number of configurations, $W(n_1, n_2)$, is the product of each of the individual enumerations or

$$W(n_1, n_2) = C(T_1, n_2)C(T_2, n_1)C(T_1 - n_2, N_1 - n_1) \cdot C(T_2 - n_1, N_2 - n_2)N_1!\, N_2!.$$

Upon expanding into factorials, simplifying, and regrouping, we have

$$W(n_1, n_2) = C(N_1, n_1)C(N_2, n_2)C(S, S_1 + n_1 - n_2)\frac{T_1!\, T_2!}{S!}. \quad (2)$$

$p(n_1, n_2)$ is the ratio $W(n_1, n_2)/W_0$ or

$$p(n_1, n_2) = C(N_1, n_1)C(N_2, n_2)C(S, S_1 + n_1 - n_2)/C(T, T_1). \quad (3)$$

III. PROBABILITY OF EXHAUSTING SPARE IN A 2-ZONE MDF

Now suppose that a 2-section MDF has n_1 and n_2 crossovers of the two types discussed above; and that it is decided to begin using preferential assignment. Note that simplifying assumptions are made that the MDF is filled to capacity (i.e., all $N_1 + N_2$ outside plant terminals are connected to equipment or inside plant terminals) and that all lines have the same class of service.*

With preferential assignment, the desire is to keep all jumpers within the zone, i.e., not to have crossovers from one zone to another. Suppose a change occurs for a jumper which does not cross the boundary. If no spare is available in that zone, the change cannot occur (unless the boundary is crossed, which we will assume is not allowed). However, if a spare is available, there will be just as much spare available after the change. Clearly then, a change for such a line does not affect the total amount of available spare. Therefore, since our goal is to find the probability of running out of spare while implementing preferential assignment, we need only consider the $n_1 + n_2$ lines that cross the boundary between sections.

Since we start with n_1 crossovers from side O of zone 1 to side I of

* It is shown in a later section that under certain restricting conditions, the results for a single class of service can be extended to the case of many classes of service.

zone 2 and with n_2 crossovers from side O of zone 2 to side I of zone 1, the number of remaining spare terminals (on side I) is $S_1 + n_1 - n_2$ for zone 1 and $S_2 + n_2 - n_1$ for zone 2. The process of changing service for the $n_1 + n_2$ lines can be described as a random walk starting at (0, 0) with $n_1 + n_2$ epochs. At each epoch (corresponding to a change for one of the $n_1 + n_2$ lines) we move to the right and one step up if one of the n_1 lines has a change, and a step down if one of the n_2 lines has a change. We denote the location of a point on the path by (h_r, r) where h_r is the height at epoch r. This situation is described in Fig. 2. The final point of the random walk will, in all cases, be $(n_1 - n_2, n_1 + n_2)$ as illustrated in Fig. 2. Each step up in the random walk brings zone 1 one step closer to running out of spare and zone 2 one step further from running out of spare, and conversely for steps down. The probability of exhausting spare, $\Pr\{\text{exhaust}/n_1, n_2\}$, is then the probability that a randomly chosen path from (0, 0) to $(n_1 - n_2, n_1 + n_2)$ (there are $C(n_1 + n_2, n_1)$ such paths) touches or crosses one or both of the boundaries at height $S_1 + n_1 - n_2$ and height $-S_2 + n_1 - n_2$.

More precisely stated, our problem is to determine the probability

$$\Pr\{\text{exhaust}/n_1, n_2\} = 1 - \Pr\{-S_2 + n_1 - n_2 < h_r < S_1 + n_1 - n_2 \quad \text{for} \quad r = 1, 2, \cdots, n_1 + n_2\}. \tag{4}$$

As discussed in Appendix A, this problem is equivalent to a form of the ballot problem[1] and the solution to our problem becomes

$$\Pr\{\text{exhaust}/n_1, n_2\} = 1 - \sum_k [C(n_1 + n_2, n_2 - kS) - C(n_1 + n_2, S_1 + n_1 + kS)]/C(n_1 + n_2, n_1) \tag{5}$$

where the summations are over all integers (positive, negative, and zero) for which the summands exist.

If we know n_1 and n_2 in advance this is the desired result. However, if we do not have this knowledge (e.g., if we do not wish to count all of the crossovers) this result should be weighted by the joint probability of n_1 and n_2. Now let us assume that we have no *a priori* information about n_1 and n_2. To find the probability of exhausting spare, equation (5) is weighted by $p(n_1, n_2)$, i.e.,

$$\Pr\{\text{exhaust}\} = 1 - \sum_{n_1} \sum_{n_2} \Pr\{\text{exhaust}/n_1, n_2\} p(n_1, n_2). \tag{6}$$

Substituting equations (3) and (4) into equation (6) and simplifying yields

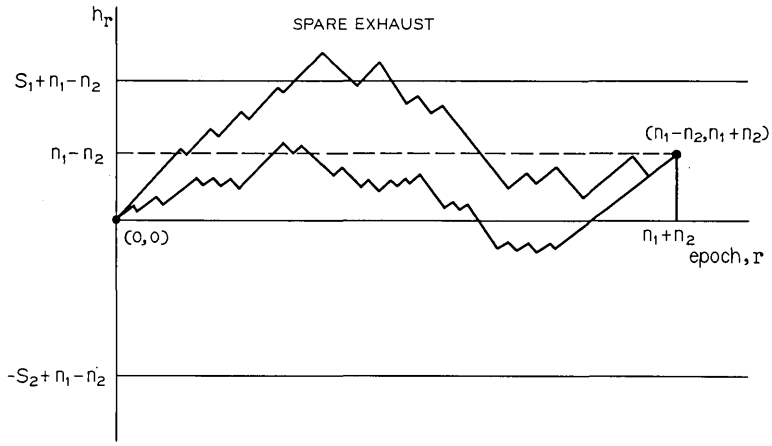

Fig. 2—Random walk model for a 2-zone MDF.

$$\Pr\{\text{exhaust}\} = 1 - \sum_{n_1}\sum_{n_2}\left\{\sum_{k}[C(n_1+n_2, n_2-kS) - C(n_1+n_2, S_1+n_1+kS)] \times \frac{C(N_1, n_1)C(N_2, n_2)C(S, S_1+n_1-n_2)}{C(n_1+n_2, n_1)C(T, T_1)}\right\}. \quad (7)$$

Expanding binomial coefficients in terms of factorials, simplifying, and regrouping yields

$$\begin{aligned}\Pr\{\text{exhaust}\} &= 1 - \frac{1}{C(N_1+N_2, N_1)C(T, T_1)} \\ &\times \sum_{n_1}\sum_{n_2}\sum_{k}[C(N_1+N_2, N_1+kS)C(S, S_1+n_1-n_2) \\ &\times C(N_2-kS, n_2-kS)C(N_1+kS, N_1-n_1) \\ &- C(N_1+N_2, T_1+kS)C(S, S_1+n_1-n_2) \\ &\times C(T_1+kS, N_1-n_1)C(N_2-S_1-kS, n_2-S_1-kS)]. \quad (8)\end{aligned}$$

At this point the order of summation is interchanged, summing first with respect to n_1 then with respect to n_2. In each case the basic combinatorial identity of Appendix B [equation (23)] is used with the final result:

$$\Pr\{\text{exhaust}\} = 1 - \frac{\sum_{k} [C(T, T_1 - kS)C(N, N_2 - kS) - C(T, N_1 - kS)C(N, T_1 + kS)]}{C(T, T_1)C(N, N_1)}. \tag{9}$$

As an example of the result of this equation, see Fig. 3. The curves are plots of Pr{exhaust} versus nominal percent spare, s ($s = S/N$), for 2-zone (equal size) MDFs with 10^4, 10^5, and 10^6 lines* and one class of service.

Equation (9) gives the probability of exhausting spare in one or both of the two zones. To find the probability of exhausting in a single zone, say zone 1, we wish to find the probability

$$\Pr\{Z_1 \text{ exhausts}\} = \sum_{n_1} \sum_{n_2} \Pr\{Z_1 \text{ exhausts}/n_1, n_2\} p(n_1, n_2).$$

The probability conditioned on n_1 and n_2 can be written

$$\Pr\{Z_1 \text{ exhausts}/n_1, n_2\} = 1 - \Pr\{h_r < S_1 + n_1 - n_2 \quad \text{for} \quad r = 1, 2, \cdots, n_1 + n_2\}. \tag{10}$$

As discussed in Appendix A this is a one-sided ballot problem[1] with solution

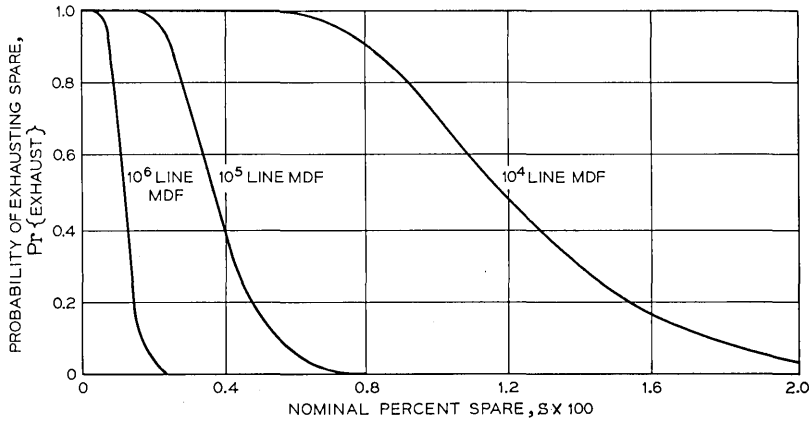

Fig. 3—Probability of exhausting spare vs nominal percent spare for a 2-zone (equal size) MDF.

* Note that "line" is being used here to mean cable termination of any kind on the MDF.

$$\Pr\{Z_1 \text{ exhausts}/n_1, n_2\} = \frac{C(n_1 + n_2, S_1 + n_1)}{C(n_1 + n_2, n_1)}.$$

Again, if we know n_1 and n_2 exactly, then this is the desired solution. However, we assume no such *a priori* knowledge, and upon multiplying by $p(n_1, n_2)$ and summing over n_1 and n_2 (as we did for Pr{exhaust}), the result is

$$\Pr\{Z_1 \text{ exhausts}\} = \frac{C(T_2 + N_2, N_2 - S_1)}{C(T_2 + N_2, N_2)}. \tag{11}$$

Figure 4 shows plots of equation (11) for zones which comprise one-half of an MDF with 10^4, 10^5, and 10^6 lines and one class of service.

In the case of a 2-zone MDF, an exact solution has been found for the probability of exhausting spare in the entire MDF and for the probability that a particular zone exhausts spare. As will be shown in the next two sections, the general solution for the probability for exhausting spare in an M-section MDF is difficult to find. Instead, the result [equation (11)] for a particular section can be used to find upper and lower bounds on the desired probability.

IV. DISTRIBUTION OF CROSSOVERS IN AN M-ZONE MDF

In this section the distribution of crossovers for an M-zone MDF with a single class of service is found in much the same way as it was found for a 2-zone MDF in Section II.

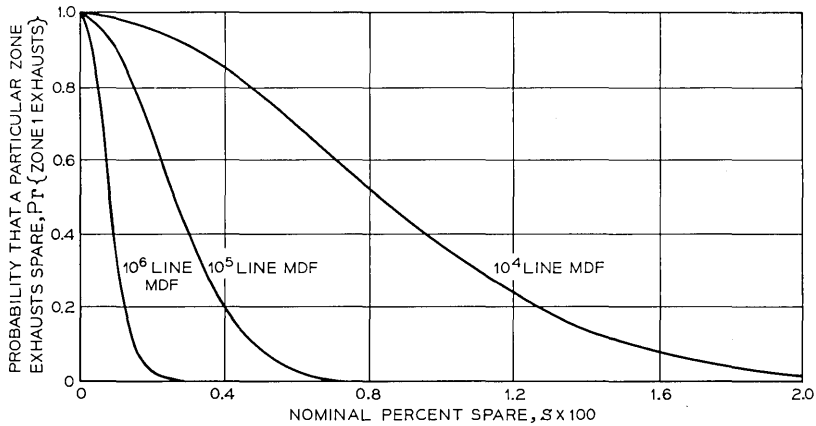

Fig. 4—Probability that a particular zone exhausts spare vs nominal percent spare for a 2-zone (equal size) MDF.

The configuration of the M-zone MDF is illustrated in Fig. 5. For simplicity, the following notation will be used:

$$T_i = N_i + S_i ,$$

$$S = \sum_{i=1}^{M} S_i ,$$

$$T = \sum_{i=1}^{M} T_i .$$

In addition, we define n_{ij} to be the number of crossovers from side O of zone i to side I of zone j with $n_{ii} = 0$ by definition. In this case the number of distinct ways to wire the MDF is again given by W_0 of equation (1), using the more general definitions of T and S above.

Now we must determine for a given matrix $\{n_{ij}\}$ of crossovers the number, $W(\{n_{ij}\})$, of distinct connections of the MDF that have $\{n_{ij}\}$ crossovers of each type. Let us concentrate on the ith zone. Side I of this zone must supply the other zones with $\Sigma_k n_{ki}$ terminals to connect to side O of those zones. The number of ways to do this is

$$(T_i ; n_{1i} , n_{2i} , \cdots , n_{Mi} , T_i - \sum_k n_{ki})^*$$

where the summation is from $k = 1$ to $k = M$. As far as direct connections are concerned, $N_i - \Sigma_k n_{ik}$ terminals must be chosen from the $N_i + S_i - \Sigma_k n_{ki}$ terminals remaining on side I. This may be done in $C[T_i - \Sigma_k n_{ki} , N_i - \Sigma_k n_{ik}]$ ways. In addition, after choosing the particular terminals to be connected, the N_i terminals on side O of zone i can be permuted in $N_i!$ ways. Each of the choices mentioned above

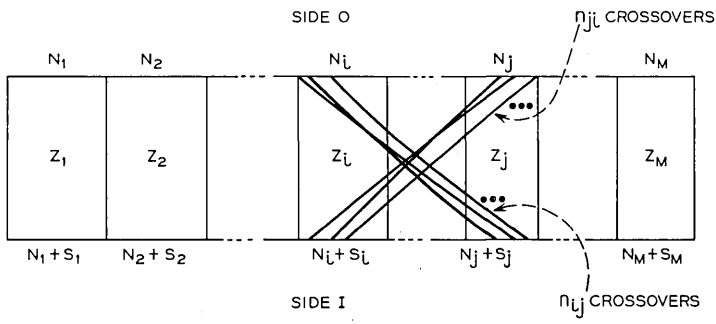

Fig. 5—Model of an M-zone MDF.

* $(a; a_1 , a_2 , \cdots , a_n) = a!(a_1 ! \, a_2 ! \cdots a_n !)^{-1}$.

is independent for each zone. Therefore, the number of ways to connect the MDF with $\{n_{ij}\}$ crossovers is the product of the three numbers enumerated above for each zone, viz.,

$$W(\{n_{ij}\}) = \prod_{i=1}^{M} C(T_i - \sum_k n_{ki}\ ,\ N_i - \sum_k n_{ik})N_i\ !$$
$$\cdot(T_i\ ;n_{1i}\ ,n_{2i}\ ,\ \cdots\ ,n_{Mi}\ ,T_i - \sum_i n_{ki}).$$

The probability, $p(\{n_{ij}\})$, of having $\{n_{ij}\}$ crossovers is equal to the ratio $W(\{n_{ij}\})/W_0$ or upon regrouping

$$p(\{n_{ij}\})$$
$$= \frac{(S;\ S_1+\sum_k (n_{1k}-n_{k1}),\ S_2+\sum_k (n_{2k}-n_{k2}),\ \cdots\ ,\ S_M+\sum_k (n_{Mk}-n_{kM}))}{(T;\ T_1\ ,\ T_2\ ,\ \cdots\ ,\ T_M)}$$
$$\times \prod_{i=1}^{M} (N_i\ ;n_{i1}\ ,n_{i2}\ ,\ \cdots\ ,n_{iM}\ ,N_i - \sum_k n_{ik}). \qquad (12)$$

Equation (12) is, then, the distribution of crossovers for an M-zone MDF. Equation (12) reduces to equation (3) for $M = 2$, in which case $n_{12} = n_1$ and $n_{21} = n_2$.

V. PROBABILITY OF EXHAUSTING SPARE IN AN M-ZONE MDF

The remarks about the random walk model of Section III can be generalized in the following way. Let there be a random walk for each zone starting at (0, 0). The number of epochs is equal to the total number of crossovers, viz., $\Sigma_i\ \Sigma_j\ n_{ij}$. For zone i, the height of the random walk at epoch r is h_{ir}. Each of the M random walks moves one step to the right at each epoch. In addition, each random walk moves up each time spare is reduced and down when spare is increased in its corresponding zone. Thus, at each epoch one walk moves up, one moves down, and the others exhibit no change in height. Each random walk has associated with it a boundary, $S_i + \Sigma_j\ n_{ij} - \Sigma_j\ n_{ji}$, and there is a further restriction that each walk reach the final point $[\Sigma_i\ \Sigma_j\ n_{ij}$, $\Sigma_j\ n_{ij} - \Sigma_j\ n_{ji}]$. The probability that the MDF exhausts is

$$\Pr\{\text{exhaust}\} = 1 - \Pr\{h_{ir} < S_i + \sum_i (n_{ij} - n_{ji})$$
$$\text{for all}\quad i = 1, 2, \cdots, M$$
$$\text{and for all}\quad r = 1, 2, \cdots, \sum_i \sum_j n_{ij}\}. \qquad (13)$$

This problem is equivalent to an M candidate ballot problem as described in Appendix C. This problem, unlike the simpler ballot problems of Appendix A, is as yet unsolved. However, upper and lower bounds for equation (13) can be found, as shown in the next section.

VI. BOUNDS ON THE PROBABILITY OF EXHAUSTING SPARE IN AN M-ZONE MDF

In this section, the result [equation (11)] for the probability of exhausting spare in a single zone is used to find upper and lower bounds on the probability of exhausting spare in an M-zone MDF.

If we denote the M zones by $Z_1, Z_2, \cdots, Z_M$, we have

$$\Pr\{\text{exhaust}\} = \Pr\{Z_1 \text{ or } Z_2 \text{ or } \cdots \text{ or } Z_M \text{ exhausts}\}. \tag{14}$$

For simplicity let us assume that zones are indistinguishable,* i.e., that $N_1 = N_2 = \cdots = N_M$ and that $S_1 = S_2 = \cdots = S_M$. Now equation (14) can be rewritten as[2]

$$\begin{aligned}\Pr\{\text{exhaust}\} = {} & M \Pr\{Z_1 \text{ exhausts}\} - C(M, 2) \Pr\{Z_1 \text{ and } Z_2 \text{ exhaust}\} \\ & + C(M, 3) \Pr\{Z_1 \text{ and } Z_2 \text{ and } Z_3 \text{ exhaust}\} + \cdots \\ & + (-1)^{M-1} \Pr\{Z_1 \text{ and } Z_2 \text{ and } \cdots \text{ and } Z_M \text{ exhaust}\}. \end{aligned} \tag{15}$$

Successive partial sums of equation (15) oscillate about $\Pr\{\text{exhaust}\}$ and in particular

$$M \Pr\{Z_1 \text{ exhausts}\} \geqq \Pr\{\text{exhaust}\} \geqq M \Pr\{Z_1 \text{ exhausts}\} - \frac{M(M-1)}{2} \Pr\{Z_1 \text{ and } Z_2 \text{ exhaust}\}. \tag{16}$$

Given a randomly wired MDF, a zone is less likely to exhaust if it is known that another zone has exhausted, i.e.,

$$\Pr\{Z_1 \text{ exhausts}/Z_2 \text{ exhausts}\} \leqq \Pr\{Z_1 \text{ exhausts}\}$$

and so

$$\Pr\{Z_1 \text{ and } Z_2 \text{ exhaust}\} \leqq \Pr\{Z_1 \text{ exhausts}\} \Pr\{Z_2 \text{ exhausts}\}.$$

Substituting into equation (16) and recalling that $\Pr\{Z_1 \text{ exhausts}\} = \Pr\{Z_2 \text{ exhausts}\}$ (since the zones are of equal size) yields

$$M \Pr\{Z_1 \text{ exhausts}\} \geqq \Pr\{\text{exhaust}\} \geqq M \Pr\{Z_1 \text{ exhausts}\}$$

* This assumes an even spread of equipment, which is not necessarily true in practice but can be approximately achieved through retermination of equipment. Retermination to achieve spreading has been done to enhance the effectiveness of preferential assignment.

$$- \frac{M(M-1)}{2} (\Pr \{Z_1 \text{ exhausts}\})^2. \qquad (17)$$

Equation (11) gives $\Pr\{Z_1 \text{ exhausts}\}$ for a 2-zone MDF. One can consider the M-zone MDF as having two zones, one with N_1 terminals and S_1 spares and the second with $(M-1)N_1$ terminals and $(M-1)S_1$ spares. Thus, in equation (17),

$$\Pr \{Z_1 \text{ exhausts}\} = \frac{C((M-1)(T_1+N_1), (M-1)N_1 - S_1)}{C((M-1)(T_1+N_1), (M-1)N_1)} \qquad (18)$$

and with the substitution, equation (17) gives the resulting upper and lower bounds for the probability of exhausting spare in any section of a multizone MDF with a single class of service.

As an example of the results that can be obtained from equation (17), Fig. 6 shows plots of the upper and lower bounds on Pr{exhaust} for 10-section MDFs having 10^4, 10^5, and 10^6 lines. The upper bound is shown as a solid line and the lower bound is shown as a dashed line and is incompletely drawn. Figure 7 shows plots of bounds on Pr{exhaust} for 10^4-, 10^5-, and 10^6-line MDFs with 10^3-line zones. Pr{exhaust} for a 10^5-line MDF with 5, 10, and 20 zones is plotted in Fig. 8. The meaning of these results will be discussed in greater detail in Section VIII.

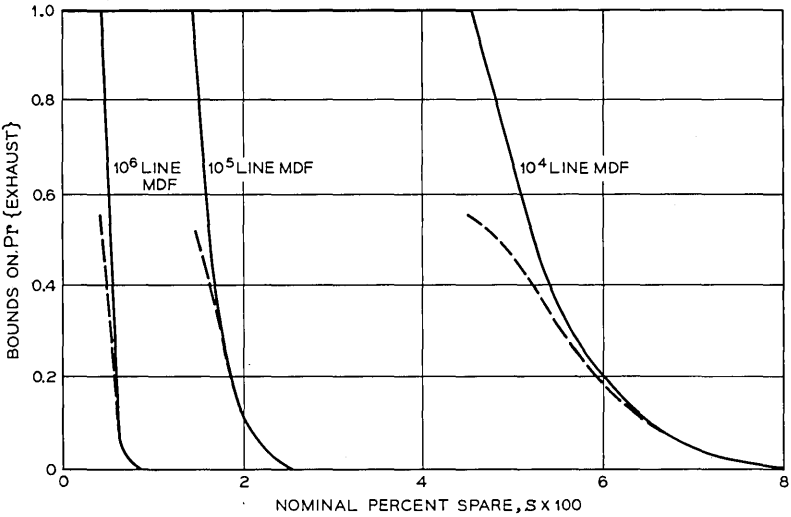

Fig. 6—Bounds on probability of exhausting spare for a 10-zone MDF, for 10^4, 10^5, and 10^6 lines (solid line—upper bound, broken line—lower bound).

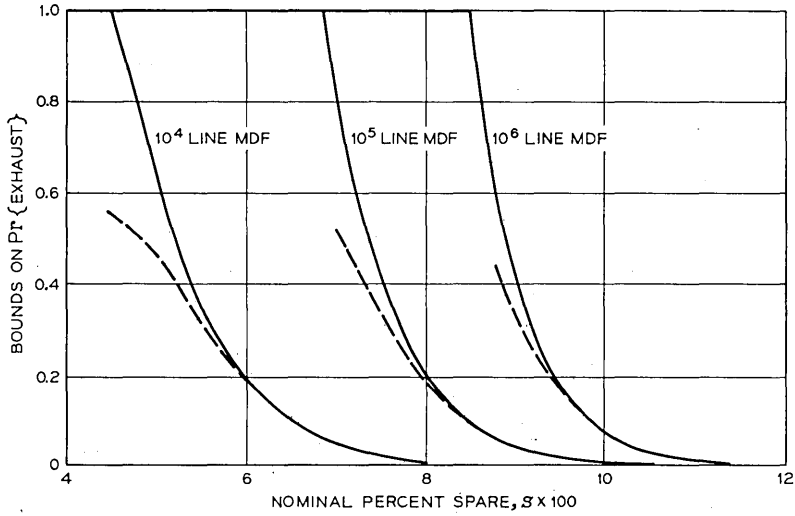

Fig. 7—Bounds on probability of exhausting spare for 10^4-, 10^5-, and 10^6-line MDFs with 10^3-line zones (solid line—upper bound, broken line—lower bound).

VII. SEVERAL CLASSES OF SERVICE

The analysis up to this point has considered a single class of service. The results for one class of service can be extended to the case of several classes of service, CS_1, CS_2, $\cdots$, CS_P, if we assume that a cable pair is always used for the same class of service. Then each class of service can be considered to comprise its own sub-MDF. This is also true for the less restrictive assumptions which follow.

Assume first that the working and spare equipment for each service is evenly distributed throughout the M zones of the MDF. In addition, assume that whenever a customer in zone Z_i requests a change in service from CS_j *to* CS_k, another customer in Z_i makes the symmetric request for change from CS_k to CS_j.*

With these assumptions, we can consider the single M-zone MDF with P classes of service to consist of P sub-MDFs each with a single class of service and M zones. Side O of each of the P sub-MDFs is comprised of the terminals equipped for that particular class of service. At any time, side I of each of the P sub-MDFs consists of all side I terminals of the total MDF which are connected to equipment of the particular class of service for that sub-MDF.

* This is unlikely to always be true in an instantaneous sense. However, it is reasonable in an average sense if the make-up of services on the total MDF is stationary.

As an example of the use of this analysis, consider the following case. A 100,000-line MDF has three classes of service. Class A serves 70,000 lines, class B serves 25,000 lines, and class C serves 5,000 lines. As described above, each class of service can be assumed, for the purpose of analysis, to comprise its own sub-MDF. Suppose a 10-zone preferential assignment procedure is introduced. After considering each class of service as having its own sub-MDF and applying the analysis of Section VI, we find the results illustrated in Fig. 9.

To assure negligible Pr{exhaust} during conversion to preferential assignment class A needs about 3 percent spare (2100 equipped spare terminals), class B requires about 5 percent spare (1250 equipped spare terminals), and class C requires about 12 percent spare (600 equipped spare terminals). Further, if there were only one class of service, Fig. 6 shows that about 2.5 percent spare would be required or 2500 equipped spare terminals as compared to 3950 for our example with three classes of service.

Thus, we can conclude that for a given MDF size, multiple classes of service require more spare equipment to convert to preferential assignment. Furthermore, just as a small MDF requires more percent spare than a larger MDF, a class of service provided to a small number of lines in an MDF requires more percent spare than a class serving

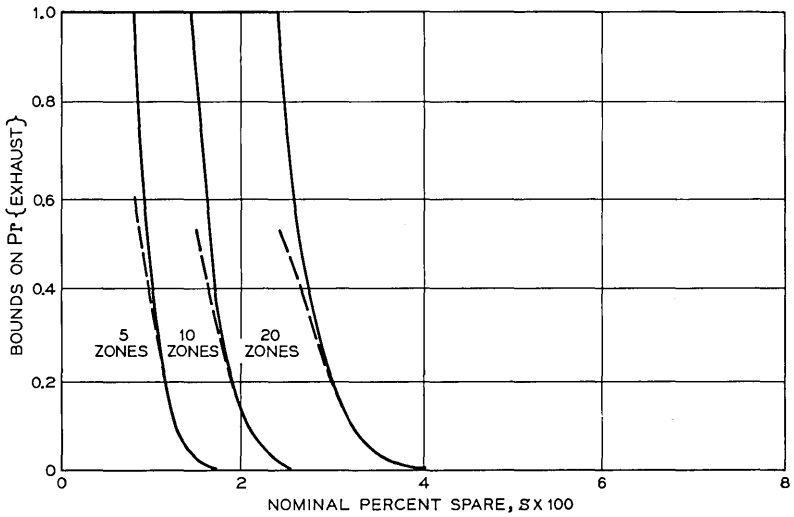

Fig. 8—Bounds on probability of exhausting spare for a 10^5-line MDF with 5, 10, and 20 zones (solid line—upper bound, broken line—lower bound).

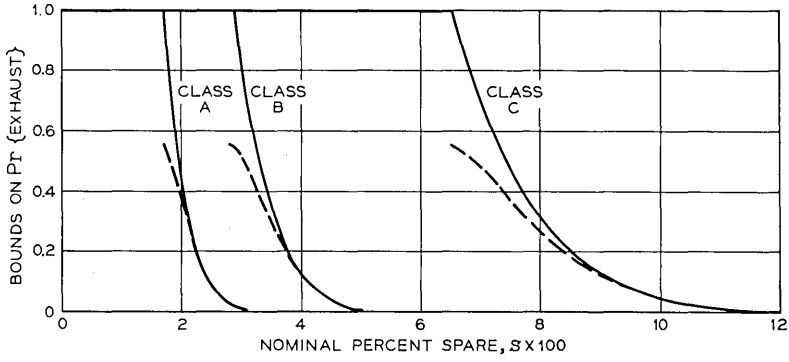

Fig. 9—Bounds on probability of exhausting spare in an MDF with three classes of service (solid line—upper bound, broken line—lower bound).

more lines. Thus, there is an economy of scale for spare equipment during conversion to preferential assignment.

VIII. DISCUSSION OF RESULTS

From Fig. 6 we see that for an MDF serving lines with the same class of service, Pr{exhaust} is negligible in a 10-zone, 10^6-line MDF if we have about 1 percent spare. For a 10-zone, 10^5-line MDF about 2.5 percent spare is sufficient and for a 10-zone, 10^4-line MDF about 8 percent spare is required. Thus, if we fix the number of zones, the required percent spare decreases as the size of the MDF increases. On the other hand, if, as in Fig. 7, zone size is fixed at say 10^3 lines, larger MDFs require more percent spare to attain the same value of Pr{exhaust}.

Figure 8 illustrates the effect of zone size on an MDF of a given size. For a 10^5-line MDF, 5 zones require about 1.75 percent spare for negligible Pr{exhaust}. If we have 10 zones, about 2.5 percent spare is required, while about 4 percent spare is required for 20 zones.

It should be remembered that an MDF will not be in trouble simply because spare has exhausted. Running a "few" jumpers across the boundary between zones is not considered a problem. Trouble occurs when this happens too often. Thus, the spare requirements stated above, based on Pr{exhaust}, are really upper bounds on the spare required for conversion to preferential assignment. We can heuristically say that the tightness of Pr{exhaust} as an upper bound on the prob-

ability of trouble increases with the size of the MDF. This is due to the fact that running jumpers between zones is more detrimental to larger MDFs.

In addition to analyzing a single class of service, a method for analyzing the case of multiple classes of service has been discussed. The results indicate that multiple classes increase the need for increased spare, since smaller classes require more percent spare than larger classes. It should be noted that the remark that Pr{exhaust} is a better upper bound for larger MDFs carries over to multiple classes of service. Specifically, Pr{exhaust} is a tighter upper bound for the probability of getting into trouble for a class of service which serves many lines rather than a few lines.

The example for the case of multiple classes of service treated three relatively small classes of service. In practice central offices employ thirty or more subscriber classes of service, and several hundred other classes of cross-connections. If all classes of service were of equal size, then spare requirements could become quite large. Usually, however, a few classes of service account for most of the terminations on the MDF, while the many remaining classes of service have a relatively small number of terminations. These less widely used classes would require a disproportionate amount of spare equipment. However, if less spare were provided for these classes, the resulting number of long cross-connections would be small if such classes constitute a small percentage of MDF terminations.

IX. CONCLUSIONS

Preferential assignment is a method to reduce the volume of wire in the MDF and thus increase the effective MDF capacity. The analysis presented here investigates the spare requirements for conversion of an MDF to preferential assignment from random assignment. Starting with a fully loaded, randomly connected MDF, conversion to preferential assignment first requires an even distribution of circuit types over the MDF. When, as discussed above, a few classes of service account for most of the terminations on the MDF, the overall percent spare required for conversion to preferential assignment is in the order of a few percent. If this assumption is not valid, then spare requirements may become relatively large. In either case the analysis presented here provides a useful method for estimating spare requirements.

X. ACKNOWLEDGMENTS

The author wishes to express his appreciation to P. J. Burke for his suggestions and, in particular, for pointing out Takács' solution to the 2-candidate ballot problem. The author is also grateful to C. W. Zebe for numerous discussions and suggestions. Thanks are also due to the reviewers for their constructive criticism of the original manuscript.

APPENDIX A

Ballot Problems and the Solution for a 2-Zone MDF

As stated in Section III, the problem of finding Pr{exhaust/n_1 , n_2} is equivalent to the ballot problem (Ref. 1, problem 4) which states: In a ballot, candidate A scores a votes and candidate B scores b votes, and all the possible voting records are equally probable. Let $c - d < b - a < c$ where $0 < c < d$ are integers. Denote by α_r and β_r the number of votes registered for A and B, respectively, among the first r votes recorded. Find the probability

$$P = \Pr\{c - d < \beta_r - \alpha_r < c \quad \text{for} \quad r = 1, 2, \cdots, a + d\}. \quad (19)$$

Takács[1] shows the solution to be

$$P = \sum_k [C(a + b, a - kd) - C(a + b, a + c + kd)]/C(a + b, a). \quad (20)$$

To apply this solution to the problem at hand, let $b = n_1$, $a = n_2$, $c = S_1 + n_1 - n_2$, $d = S_1 + S_2$. Also, let β_r be the number of upward steps and α_r be the number of downward steps after r epochs in the random walk model of Fig. 2. Therefore, in the notation of Section III,

$$h_r = \beta_r - \alpha_r .$$

Making these substitutions, we have

$$\Pr\{-S_2 + n_1 - n_2 < h_r < S_1 + n_1 - n_2 \quad \text{for} \quad r = 1, 2, \cdots, n_1 + n_2\}$$
$$= \sum_k [C(n_1+n_2 , n_2-kS) - C(n_1+n_2 , S_1+n_1+kS)]/C(n_1+n_2 , n_1).$$

This is the result reported in equations (4) and (5).

The problem of finding Pr{zone 1 exhausts/n_1 , n_2} is equivalent to the one-sided ballot problem (Ref. 1, problem 3) which states: In a ballot, candidate A scores a votes and candidate B scores b votes, and all the possible voting records are equally likely. Let $b < a + c$ where c is a positive integer. Let α_r and β_r be the number of votes registered

for A and B, respectively, among the first r votes recorded. Find the probability

$$Q_c(a, b) = \Pr \{\beta_r < \alpha_r + c \quad \text{for} \quad r = 1, 2, \cdots, a + b\}.$$

The solution is shown to be

$$Q_c(a, b) = 1 - \frac{C(b, c)}{C(a + c, c)}.$$

Upon making the substitutions that were made for the two-sided ballot problem, we have

$$\Pr \{h_r < S_1 + n_1 - n_2\} = 1 - \frac{C(n_1 , S_1 + n_1 - n_2)}{C(S_1 + n_1 , S_1 + n_1 - n_2)}.$$

After expanding binomial coefficients and regrouping, the result is

$$P\{h_r < S_1 + n_1 - n_2\} = 1 - \frac{C(n_1 + n_2 , S_1 + n_1)}{C(n_1 + n_2 , n_1)}$$

as reported in equations (10) and (11).

APPENDIX B

A Basic Combinatorial Identity

The basic combinatorial identity

$$\sum_i \begin{bmatrix} r \\ i \end{bmatrix} \begin{bmatrix} s \\ m - i \end{bmatrix} = \begin{bmatrix} r + s \\ m \end{bmatrix} \tag{21}$$

(where r, s, m, and i are integers and the sum is over all integers for which the summand exists) is easily proven[3] by considering the equation

$$(1 + x)^r(1 + x)^s = (1 + x)^{r+s}.$$

Expansion of each term in a binomial series yields

$$\sum_i \begin{bmatrix} r \\ i \end{bmatrix} x^i \sum_j \begin{bmatrix} s \\ j \end{bmatrix} x^j = \sum_m \begin{bmatrix} r + s \\ m \end{bmatrix} x^m. \tag{22}$$

Equating terms on each side of equation (22) with exponent m results in equation (21).

Equation (22) can be expressed in another, more general form. If we let $i = k + j$ with k and i integers, equation (22) becomes

$$\sum_i \binom{r}{k+j}\binom{s}{m-k-j} = \binom{r+s}{m},$$

where the sum is again for all integers for which the summand exists. If we further let $n = m - k$ the result is

$$\sum_i \binom{r}{k+j}\binom{s}{n-j} = \binom{r+s}{k+n}. \tag{23}$$

APPENDIX C

An M-Candidate Ballot Problem

In a ballot there are M candidates, viz., $C_1, C_2, \cdots, C_M$. Each of N voters casts a ballot which contains a vote in favor of one candidate and a vote against another candidate. Let b_i and a_i be the total pro and con votes for C_i. Let k_{ij} be the total number of ballots which have a vote for C_i and a vote against C_j. Thus $b_i = \Sigma_j k_{ij}$ and $a_i = \Sigma_j k_{ji}$. It is assumed that all possible voting records are equally probable. Let β_{ir} and α_{ir} be the number of pro and con votes, respectively, registered for C_i among the first r ballots recorded. Find the probability

$$P = \Pr\{\beta_{ir} - \alpha_{ir} < d_i \text{ for each } i = 1, 2, \cdots, M \text{ and for each } r = 1, 2, \cdots, \sum_i a_i\}. \tag{24}$$

Note that $\Sigma_i \alpha_i = \Sigma_i b_i$.

This problem is equivalent to the random walk model of Section V if we let $h_{ir} = \beta_{ir} - \alpha_{ir}$, $d_i = S_i + \Sigma_j (n_{ij} - n_{ji})$, and $\{k_{ij}\} = \{n_{ij}\}$.

This problem is much more complex than the ballot problems of Appendix A, and has not, as far as the author knows, been solved.

REFERENCES

1. Takács, L., *Combinatorial Methods in the Theory of Stochastic Processes*, New York: John Wiley and Sons, 1967, pp. 7, 212–213.
2. Feller, W., *An Introduction to Probability Theory and Its Applications*, 2nd Edition, New York: John Wiley and Sons, 1957, Chapter 4.
3. Hall, M., Jr., *Combinatorial Theory*, Waltham Mass.: Blaisdell Publishing Co., 1967, p. 6.

Contributors to This Issue

FRANK J. ANDROSKI, A.E.E., 1961, Wentworth Institute; Bell Telephone Laboratories, 1961—. Mr. Androski has worked on the TL-1, TL-2, and TM-1 short-haul microwave radio systems, the TH-1 long-haul microwave radio system, and the 4A FM terminal receiver. He is presently working on the 3A wire line entrance link.

JAMES F. BALICKI, B.E.E., 1960, University of Detroit; M.E.E., 1962, New York University. Mr. Balicki has worked for Michigan Bell Telephone Company as a Student Engineer in 1957 and 1958, and for Bell Telephone Laboratories as a Member of Technical Staff from 1960 to 1970. At Bell Laboratories he planned power systems and developed power supplies for station, PBX, special customer, carrier, coaxial, multiplex, and microwave systems. He joined American Telephone and Telegraph Company in July, 1970, as an Assistant Engineering Manager in the Special Customer Systems group of the Engineering Department, where he is responsible for power systems on customer premises and for emergency reporting systems, including private line telephone systems, group alerting systems, and answering bureau equipment for the universal emergency number (911) system. Member, Public Fire Service Communications Committee of the National Fire Protection Association, Eta Kappa Nu, Tau Beta Pi.

HARRY R. BEDELL, B.S.E.E., Northeastern University; Bell Telephone Laboratories, 1953—. Mr. Bedell completed the Bell Laboratories Communications Development Training Program in 1956 and worked on telephone answering equipment in the station apparatus area. In 1958 he transferred to the transmission systems area to work on the development and physical design of the cable repeater for the T1 carrier system. In 1963 he began work in the Radio Laboratory on the physical design of microwave generators for the TD-3 and TH-3 systems. His current responsibilities include the physical design of the TH-3 transmitter-receiver bay, associated equipment components, and test equipment. Member, Eta Kappa Nu.

C. E. Bradford, B.S. (E.E.), 1942, Worcester Polytechnic Institute; M.S. and Ph.D. (Nuclear Physics), 1954, Illinois Institute of Technology; Bell Telephone Laboratories, 1954—. Mr. Bradford started in Bell Laboratories with an investigation of the effect of manufacturing tolerances on electron guns, and has been involved in designing and developing Bell System and military traveling-wave tubes, Bell System masers, and military magnetrons. For a number of years he was responsible for design engineering for traveling-wave tubes in production by the Western Electric Company. He is presently engaged in developing the characterization of millimeter-wave diodes for the millimeter waveguide system. Member, IEEE, A.I.P., Sigma Xi.

Ping S. Chun, B.A. (Chemistry), 1955, University of Hawaii; B.S.E.E., 1962, University of Pennsylvania; M.E.E., 1964, New York University; Bell Telephone Laboratories, 1962—. Mr. Chun has been principally engaged in the development of electronic power conditioners for military and microwave radio systems. His present responsibilities include energy systems planning for data communications, waveguide, carrier, and digital transmission systems. Member, IEEE, Eta Kappa Nu, Tau Beta Pi.

Richard T. Cooney, B.S.E.E., 1959, University of Rhode Island; M.S.E.E., 1962, Northeastern University; Bell Telephone Laboratories, 1959—. Mr. Cooney's work has included designing and developing analog portions of the 100A protection switching system, developing the TD-3 transmitter-receiver test set, and a noise reduction program on the TH radio system. Since 1967 he has been concerned with the design of new protection switching systems including the 300A and auxiliary channel switching systems. Member, IEEE, Eta Kappa Nu, Tau Beta Pi, Phi Kappa Phi.

N. R. Dietrich, Electronic Technology, 1959, RCA Institutes; B.S.E.E., 1966, Lafayette College; Graduate studies, 1968—, Lehigh University; Bell Telephone Laboratories, 1959—. Mr. Dietrich has been active in the development of traveling-wave maser amplifiers for the *Telstar*® project, and microwave ferrite devices and integrated circuits for radio relay applications. He is currently working on the development of lumped element circulators for the high-capacity mobile telephone system. Member, IEEE, Tau Beta Pi, Eta Kappa Nu.

Elbert J. Drazy, B.S.E.E., 1942, Purdue University; Bell Telephone Laboratories 1942—. Mr. Drazy has been concerned with de-

veloping test equipment for microwave radar and for microwave radio relay and video transmission systems, as well as developing carrier supplies for the L-type multiplex equipment, and FM terminals for long-haul microwave radio relay systems. Since 1964 he has supervised a group developing microwave networks for radio systems. Member, Tau Beta Pi, Eta Kappa Nu, Sigma Xi.

GERALD L. FENDERSON, B.S.E.E., 1960, University of Maine; M.S.E.E., 1963, Northeastern University; Bell Telephone Laboratories, 1960—. Mr. Fenderson has been primarily concerned with the development of IF amplifiers for solid state microwave radio systems.

GERARD J. FOSCHINI, B.S.E.E., 1961, Newark College of Engineering; M.E.E., 1963, New York University; Ph.D. (Mathematics), 1967, Stevens Institute of Technology; Bell Telephone Laboratories, 1961—. Mr. Foschini initially worked on real-time program design. Since 1965 he has mainly engaged in analytical work concerning the transmission of signals over stochastic channels. Member, Sigma Xi, Mathematical Association of America, American Men of Science, New York Academy of Sciences.

O. GIUST, Assoc. E.E., 1959, Franklin Technical Institute; Bell Telephone Laboratories, 1959—. Initially Mr. Giust worked on the TH-1 radio system and has since contributed to the design of the 100A protective switching system and the microwave generator for the TD-3 and TH-3 radio systems. Currently he is doing development work on the TH-3 radio system.

HERBERT D. GRIFFITHS, B.S., 1949, University of Western Ontario; M.S., 1950, McGill University; Bell Telephone Laboratories, 1954—. Mr. Griffiths has been involved in the development of microwave radio and its associated protection switching systems. In recent years he has been supervising a group responsible for the design of new protection switching systems including the 100A, the 300A, and the auxiliary channel switching systems. His group is now designing the 400A protection switching system.

ANDRAS HAMORI, Dipl. Eng., E.E., 1955, Technical University of Budapest, Hungary; Bell Telephone Laboratories, 1957—. Mr. Hamori was initially concerned with the final development of the D1 channel bank and the line repeater for the T1 carrier system. Later he worked

on the development of the 100A protection switching system and the TD-3 radio relay system. He was the supervisor of the group responsible for the circuit development of the TH-3 radio transmitter and receiver bay. Presently, his group is developing digital terminals for radio systems.

ROBERT M. JANSEN, B.E.E., 1966, Villanova University; M.S.E.E., 1967, Stanford University; Bell Telephone Laboratories, 1966—. Mr. Jansen's first assignment was in system and test equipment analysis for the TD-3 radio system. Later he transferred to system analysis work on the TH-3 radio system. Currently, he is also teaching the Transmission Systems Design course at the Merrimack Valley Laboratory. Member, IEEE, Tau Beta Pi, Eta Kappa Nu.

R. M. JENSEN, B.S. in E.E., 1937, Purdue University; Bell Telephone Laboratories, 1937—. Mr. Jensen first was engaged in developing audio equipment, and then worked in quality assurance. In 1938 he began developing L-type multiplex networks, and during World War II he was concerned with tuned amplifiers, coaxial filters, and crystal-controlled oscillators. In 1956 Mr. Jensen was assigned to develop microwave networks, and in 1959 he became a supervisor. In 1964 he began supervising a group designing equipment for TL-2/TM-1 radio relay, FM terminals, wire line entrance link, TD-3 radio relay, and then TH-3 radio. Now his group is designing digital radio relay equipment. Member, Sigma Pi Sigma.

ROBERT W. JUDKINS, Bell Telephone Laboratories, 1954—. Mr. Judkins' early work was directed towards design and development of microwave ferrite non-reciprocal devices and microwave switches. Since 1960, he has been engaged in design and development of microwave circuits, such as upconverters, frequency multipliers, and waveguide networks, for use in the TD-3 and TH-3 radio systems.

J. W. KNAPP, B.S.E.E., 1963, University of Massachusetts; M.S.E.E., 1965, Northeastern University; Bell Telephone Laboratories, 1963—. Since joining Bell Laboratories, Mr. Knapp has been involved in both circuit and system design work for short-haul and long-haul microwave radio systems. He is currently developing circuits for application on a frequency-diplexed auxiliary channel for long-haul radio systems. Member, Tau Beta Pi, Eta Kappa Nu, Phi Kappa Phi.

ROBYE L. LAHLUM, B.S., 1963, North Dakota State University; M.S.E.E., 1965, Northeastern University; Bell Telephone Laboratories, 1963—. Mr. Lahlum has worked on IF amplifiers for the TD-3 system and on the microwave generator for the TD-3 and TH-3 systems. At the present time, he is working on digital circuits for a millimeter-wave radio system called digital radio. Member, Tau Beta Pi.

FREDERICK H. LANIGAN, Bell Telephone Laboratories, 1952—. After early work on the automatic protection switching system for TD-2 radio channels (TDAS), Mr. Lanigan was involved for several years with the current engineering problems of the automatic protection switching system of TH radio (THAS). He was then assigned to work on the development of the logic and control circuits for the 100A protection switching system. More recently he has been engaged in the development of the logic and control circuits of the 300A protection switching system, and at present is assigned to the development of logic and control circuits for the 400A protection switching system.

N. E. LENTZ, B.S.E.E., 1952, Washington State University; Bell Telephone Laboratories, 1952—. Mr. Lentz completed Bell Laboratories' Communications Development Training Program in 1955, and worked on video amplifiers and test equipment for the TD-2 radio system. Mr. Lentz holds several patents for the timing circuits he designed for the T-carrier PCM system. He developed circuits for the 3A and 4A FM terminals and a squelch circuit for the 3A wire line entrance link. He is now designing circuits for the radio digital terminal.

S. C. LIU, B.S.C.E., 1960, National Taiwan University; M.S., 1964, and Ph.D., 1967, University of California at Berkeley; Bell Telephone Laboratories, 1967—. Mr. Liu has been working in the areas of mechanical vibrations, random processes, structural dynamics, and earthquake engineering. Member, American Society of Civil Engineers, Seismological Society of America.

JAMES P. MORELAND, B.S.E.E., 1964, M.Sc., 1964, and Ph.D., 1967, The Ohio State University; Instructor, 1961–64, Research Associate, Electro Science Laboratory, 1964-68, and Assistant Professor, 1967–68, The Ohio State University; Bell Telephone Laboratories, 1968—. Mr. Moreland has worked on optical communications systems and, since

1968, has been primarily concerned with systems engineering problems associated with digital communications. Member, IEEE, Sigma Xi, Tau Beta Pi, Eta Kappa Nu.

DAVID J. PARIS, B.S.E.E., 1966, Drexel University; M.S.E.E., 1968, Columbia University; Bell Telephone Laboratories, 1966–1971. Mr. Paris has concentrated on the development of multiphase data sets for commercial applications. Member, IEEE, Tau Beta Pi, Eta Kappa Nu, Phi Kappa Phi.

RONALD C. PRIME, B.Sc. in E. E., 1958, University of Southampton (England); M.S.E., 1961, Princeton University; Bell Telephone Laboratories, 1961—. Mr. Prime's first assignment with Bell Laboratories was to design the receiving logic for the 100A switching system which is used to protect TD and TH-3 radio. Later he transferred to systems analysis work on the TD-3 radio relay system. He is now supervisor of the Systems Planning and Applications Group, responsible for TH-3 radio. Graduate member, IEE.

CLYDE L. RUTHROFF, B.S.E.E., 1950, and M.A., 1952, University of Nebraska; Bell Telephone Laboratories, 1952—. Mr. Ruthroff has published contributions on the subjects of FM distortion theory, broadband transformers, FM limiters, threshold extension by feedback, and microwave radio systems for satellite and terrestrial use. He is interested in the extension of radio communication into the millimeter and optical wavelengths. Member, IEEE, Sigma Xi, American Association for the Advancement of Science.

ROBERT C. SALVAGE, Associate degree in E.E., 1955, Newark College of Engineering; Western Electric Co., 1953–1955; Bell Telephone Laboratories, 1955—. Mr. Salvage started work on the TD-2 microwave system and has since contributed to designs for the TJ, TL, and TM short-haul microwave systems. He has worked on developing FM terminals since 1963, completing the first solid state terminal in 1967. Currently he is working on in-service testing of radio transmission systems.

FRANK J. SALVO, B.S.M.E., 1968, Polytechnic Institute of Brooklyn; Bell Telephone Laboratories, 1953—. Since 1962, Mr. Salvo has been a member of the Power Systems Physical Design Department with equipment design responsibilities for dc/dc converters used in micro-

wave, carrier, and submarine cable systems. He is presently involved in the design of general-use power supplies for Central Office *Picturephone*® trunk services and waveguide transmission systems.

J. SALZ, B.S.E.E., 1955, M.S.E., 1956, and Ph.D., 1961, University of Florida; Bell Telephone Laboratories, 1961—. Mr. Salz first worked on the remote line concentrators for the electronic switching system. He has since engaged in theoretical studies of data transmission systems, and is currently a supervisor in the data theory department. During the academic year 1967–68 he was on leave as Professor of Electrical Engineering at the University of Florida. Member, IEEE, Sigma Xi.

MICHAEL A. SCHUMER, B.E. (E.), 1964, City College of New York; M.A., 1966, and Ph.D., 1968, Princeton University; Raytheon Research Division, 1967–1969; Bell Telephone Laboratories, 1964–1965 and 1969—. In his earlier association with Bell Laboratories, Mr. Schumer was engaged in the design of diagnostic tests for No. 1 ESS. He has been involved in research in communication theory and optimization techniques. He is presently engaged in switching systems planning for the local area. Member, IEEE, Eta Kappa Nu.

K. L. SEASTRAND, B.S.E.E., 1959, Worcester Polytechnic Institute; M.S.E.E., 1961, Northeastern University; Bell Telephone Laboratories, 1959—. Mr. Seastrand was engaged in developing test equipment associated with the T1 carrier repeatered line. Later he also worked on the development of the TL-2 and TM-1 radio systems. He presently supervises a group which had the responsibility for developing the frequency-diplexed auxiliary channel and the medium-haul application of TH-3. Member, IEEE.

JOHN R. SHEEHAN, B.S.E.E., 1962, Drexel University; M.E.E., 1964, New York University; Bell Telephone Laboratories, 1962—. Mr. Sheehan has been concerned with problems in data transmission. His work has included problems relating to signal design, modem design, and automatic equalization techniques. He currently supervises a group concerned with modem development.

R. E. SHEEHEY, E.E., Assoc., 1960, Wentworth Institute; Bell Telephone Laboratories, 1960—. Mr. Sheehey has been involved in devel-

oping various types of electrical networks, and is now designing and developing networks for radio systems.

R. A. SWIFT, B.S.E.E., 1943, Union College; Bell Telephone Laboratories, 1946—. Mr. Swift has been engaged in the mechanical and equipment design aspects of Bell System and military systems. He supervised the groups responsible for the mechanical design and evaluation of missile-borne guidance equipment for the Titan and Thor-Delta Missiles and the *Telstar*® satellite. At present, he supervises a group responsible for the equipment design of microwave radio systems.

C. J. WALDRON, B.S. (Mathematics), 1970, Albright College; Bell Telephone Laboratories, 1957—. Mr. Waldron has worked on development of reflex klystrons for application in the TH and TJ microwave systems. Since 1961 he has been involved in the development of traveling-wave tubes for Bell System applications.

HAN-CHIU WANG, B.S.E.E., 1955, Cheng-kung University, Taiwan, China; M.S.E.E., 1960, University of Notre Dame; Ph.D., 1965, Polytechnic Institute of Brooklyn; Chinese Government Radio Adm., 1956–1958; Polytechnic Institute of Brooklyn, 1964–1965; Bell Telephone Laboratories, 1965—. Mr. Wang is currently engaged in developing millimeter wave components for the waveguide transmission system.

DONALD S. WILLIAMS, B.S.E.E., 1966, University of Washington; M.S.E.E., 1968, Northeastern University; Bell Laboratories, 1966—. Mr. Williams was involved in the initial system planning and development of the TH-3 radio system and has worked on various system problems. He is now concerned primarily with TH-3 medium-haul applications and system problems unique to the Telephone Operating Companies. Member, IEEE, Tau Beta Pi.

JOHN A. WORD, B.S., 1930, University of California (Berkeley); Bell Telephone Laboratories, 1930—. Prior to World War II, Mr. Word worked on the design of toll terminal room equipment. During World War II, he worked on sonar, communications countermeasures, and microwave radio. At present, he supervises a group in the equipment design of short- and long-haul microwave radio systems. Member,

Tau Beta Pi, Eta Kappa Nu; associate member, Sigma Xi; senior member, IEEE; registered professional engineer in the State of New York.

AARON D. WYNER, B.S., 1960, Queens College; B.S.E.E., 1960, M.S., 1961, and Ph.D., 1963, Columbia University; Bell Telephone Laboratories, 1963—. Mr. Wyner has been doing research on various aspects of information theory. He spent the year 1969–1970 visiting the Department of Applied Mathematics, Weizmann Institute of Science, Rehovot, Israel and the Department of Electrical Engineering, the Technion, Haifa, Israel on a Guggenheim Foundation Fellowship. He has also been a full- and part-time faculty member at Columbia University and the Polytechnic Institute of Brooklyn. He has been Chairman of the Metropolitan New York Chapter of the IEEE Information Theory Group, and is presently a member of the National Administrative Committee. He is also Associate Editor for the Shannon Theory of the IEEE Transactions on Information Theory. Member IEEE, SIAM, AAAS, Tau Beta Pi, Eta Kappa Nu, Sigma Xi.

CONTENTS

(Continued from front cover)

GENERAL ARTICLES

Bell System